COLD ACTIVE ENZYME BOOSTER TECHNOLOGY (ENBOOT) FOR BIODEGRADATION OF P-XYLENE

SABA MIRI

A DISSERTATION SUBMITTED TO
THE FACULTY OF GRADUATE STUDIES
IN PARTIAL FULFILLMENT OF THE REQUIREMENTS
FOR THE DEGREE OF
DOCTOR OF PHILOSOPHY

GRADUATE PROGRAM IN CIVIL ENGINEERING
YORK UNIVERSITY
TORONTO, ONTARIO

July, 2022

ABSTRACT

p-xylene is used as a solvent in medical technology, the leather, paint, and rubber industries. The principal pathway of human contact to p-xylene is via soil and groundwater contamination. Bioremediation offers potential advantages such as being cost-effective and environmentally friendly with lesser undue damage to environments. The main aim of this project is to find an enzyme mixture for biodegradation of p-xylene contaminated sites. In this regard, screening of indigenous bacteria, identification of involved enzymes, and biodegradation tests were carried out. The results showed that xylene monooxygenase (XMO) and catechol 2,3-dioxygenase (C2,3D) have a matching end product, they acted in symphony to degrade p-xylene. The mixture of these enzymes confirmed the complete degradation of p-xylene within 48 h in groundwater (initial concentration of 200 mg/L), 7 days in soil tests (initial concentration of 10,000 -12,000 mg/kg of soil) at 15°C, which is revolutionary for the industrial sector. In soil column tests, different concentrations of the enzyme mixture were used (1x, 5x, and 10x dilution). In this test, 92-94% p-xylene removal was achieved in the treated soil with a 5x diluted enzyme mixture (contained 10 U/mL of XMO and 20 U/mL of C2,3D). Our results showed that biodegradation is a scale-dependent phenomenon and the maximum degradation rate decreased from ~90% to 68% from the soil column to tank tests. It is due to limited access of enzymes to trapped p-xylene in soil pores, low dissolved oxygen, soil heterogeneity, and free phase contaminant. In addition, one of the major challenges in the practical and commercial application of these enzymes is their inherent instability. Our results showed that immobilization improved the stability of enzymes. For example, micro/nano biochar-chitosan matrices increased the stability of enzymes with more than 50% residual activity after 30 days at 4±1 ºC, while the free enzymes had less than 10% of its activity. Overall, this cold-active enzyme mixture can be applied for the biodegradation of all BTEX compounds (benzene, toluene, ethylbenzene, and xylenes). This study could set the guideline for the enzymatic bioremediation of mono-aromatic pollutants in contaminated soil and groundwater under cold conditions.

DEDICATION

TO MY PARENTS

For raising me to believe that anything was possible

TO MY HUSBAND

For making everything possible

TO MY TEACHERS

For giving me invaluable educational opportunities

ACKNOWLEDGEMENT

I would like to express my humble gratitude to my Ph.D. supervisor, **Professor Satinder Kaur Brar** for her guidance, suggestions, and valuable feedback during my doctoral training. And during the most difficult times when developing the project and writing this thesis, she gave me the moral support and the freedom I needed to move on. I want to equally express my regards to my co-supervisor, **Professor Richard Martel** who helped me in solving essential problems with multi-approach ideas. His constant motivation, support, and encouragement helped me to work with more freedom and passion. I would like to especially thanks to **Dr. Thomas Robert** for his constant guidance and technical support. I am sincerely thankful to TechnoRem for financing the project work. I would like to thank **Mr. Jean-Marc Lauzon** for his constant support through this project. I am very grateful to **Dr. Tarek Rouissi** for the time he dedicated to this research and for his constant support.

I would like to thank **Prof. Yi Sheng** and **Prof. Ahmed Eldyasti** for their constant support throughout my Ph.D. program. I would also like to thank my examiners, , **Prof. Rania Hamza** whose suggestions and recommendations helped in improving the quality of my thesis.

A much and special thanks to my research partner **Mr. Seyyed Mohammadreza Davoodi** for his valuable feedback and for a cherished time spent together in the lab. I would like to thank all the laboratory personnel from INRS, especially **Mr. Stephane Moise** for the instrument training. I would like to express my humble gratitude and genuinely like to thank my teammates and colleagues who supported me throughout my Ph.D. study, especially, **Dr. Lecka Joanna, Dr. Carlos Osorio Gonzalez, Dr. Mehrdad Taheran, Dr. Rama Pulicharla, Dr. Pratik Kumar, Mr. Rahul Saini, Dr. Agnieszka Cupryś, Dr. Naghdi Mitra, Dr. Joseph Sebastian, Mr. Mohammad Hossein Karimi Darvanjooghi, Mrs. Gurpreet Kaur, Mrs. Noha Hasaneen, Mrs. Pratishtha Khurana, Mr. Xuhan Shu, Dr. Krishnamoorthy Hegde, Mrs. Mariana Valdez, Dr. Bikash Tiwari, Mr. Behnam Nayebi, Mrs. Shiva Akhtarian.** It would be incomplete without thanking my interns, **Mrs. Anupriya Ravula**, **Dr. Dheeraj Sharma,** and **Mr. Jose Alberto**, who assisted me during the project.

Finally, I would like to give my sincerest thanks to my parents, my spouse, my sisters, my aunt, and my parent-in-law who constantly supported and motivated me.

TABLE OF CONTENTS

LIST OF TABLES

LIST OF FIGURES

GRAPHICAL ABSTRACT

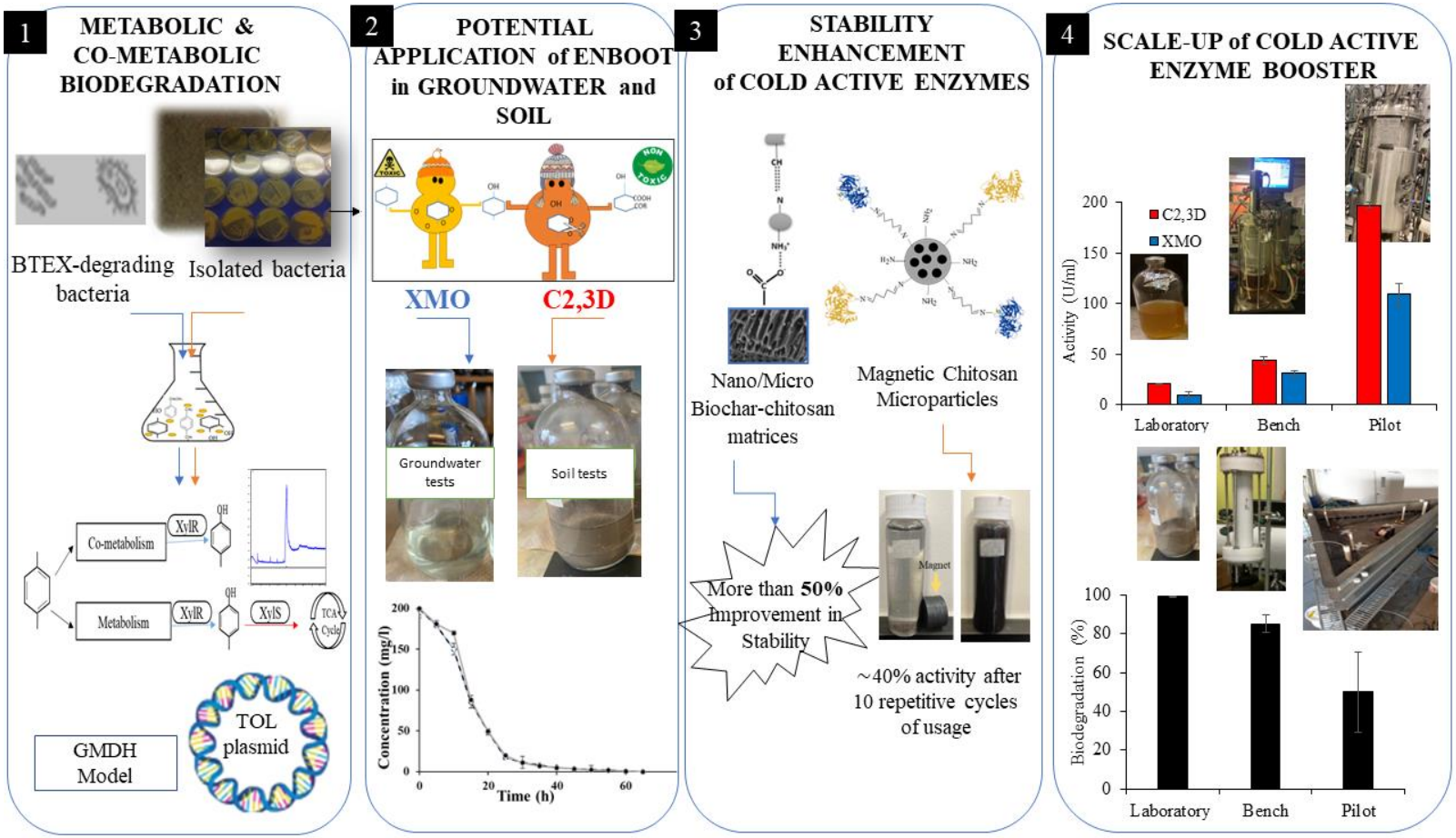

LIST OF PUBLICATIONS OF THIS THESIS

- **Patent and invention disclosure**

1. **Miri S.**, Brar SK., Martel R. Scale-up Procedures to Enzymatic Biodegradation: Pilot-scale bioreactor and Soil tank test. Invention disclosure submitted to TechnoRem Inc. (Industrial partner of this project).

- **Peer-reviewed scientific articles**

1. **Miri S.**, Naghdi M., Rouissi T., Brar SK., Martel R. (2018). Recent biotechnological advances in petroleum hydrocarbons degradation under cold climate conditions: Review. CREST-D-18-00135R2. **Critical Reviews in Environmental Science and Technology**, 1-34.

2. Miri S., Davoodi SM., Rouissi T., Karimi Darvanjooghi MH, Brar SK., Martel R. (2021). Precision Modelling of Co-metabolic Biodegradation of Recalcitrant Aromatic Hydrocarbons in conjunction with experimental data. **Process Biochemistry**, 105, 113-127.

3. **Miri S.**, Rasooli A., Rouissi T., Brar SK., Martel R. (2021). Biodegradation of p-xylene—a comparison of three psychrophilic *Pseudomonas* strains through the lens of gene expression. **Environmental Science and Pollution Research**. 1-15.

4. **Miri, S**., Perez, J. A. E., Brar, S. K., Rouissi, T., & Martel, R. (2021). Sustainable production and co-immobilization of cold-active enzymes from *Pseudomonas* sp. for BTEX biodegradation. **Environmental Pollution**, *285*, 117678.

5. **Miri S.**, Davoodi SM., Rouissi T., Brar SK., Sheng Y., Martel R. (2021). Psychrozymes as novel tools to biodegrade p-xylene and potential use for contaminated groundwater in the cold climate. **Bioresource Technology**, 124464.

6. **Miri, S.,** Davoodi, S. M., Robert, T., Brar, S. K., Martel, R., & Rouissi, T. (2021). Enzymatic biodegradation of highly p-xylene contaminated soil using cold-active enzymes: A soil column study. **Journal of Hazardous Materials**, 127099.

7. **Miri, S**., Ravoula, Akhtarian, S., A., Brar, S. K., Rouissi, T., & Martel, R. Immobilized Cold-Active Enzymes onto Magnetic Chitosan Microparticles as a Highly Stable and Reusable Carrier for p-xylene Biodegradation in Soil. **Submitted to Process Biochemistry**.

LIST OF CONFERENCES

1. **Miri S.**, Brar S.K, Rouissi T., Martel R. (2022). Microbial community dynamic in understanding the fate of bioremediation of oil-contaminated environments. 44rd AMOP technical seminar on environmental contamination and response, Government of Canada. June 8th -10th.

2. **Miri S.**, Davoodi, S. M., Brar S.K, Kadri T. (2021). Enzymes: Catalysts to remediate Conventional and Unconventional Oils. 71st Canadian Chemical Engineering Conference, Montreal, Canada. October 24th – 27th.

3. Brar S.K, **Miri S**. (2021). Bioremediation and Microorganisms: It takes two to Tango. F-EIR Conference 2021. Chandigarh, India. October 18th – 22nd.

4. **Miri S.**, Brar S.K, Martel R. Rouissi T. (2021). Bacterial and Fungal Enzyme Cocktail for the Biodegradation of p-Xylene Spill in Groundwater. 43rd AMOP technical seminar on environmental contamination and response, Government of Canada. June 8th -10th.

5. **Miri S.**, Brar S.K, Rouissi T., Martel R. (2020). Potential use of paper-solid waste for production of cold-active enzymes for monoaromatic hydrocarbons spill clean-up in groundwater. Canadian Symposium on Water Quality Research, Nov. 6th, 2020.

6. **Miri S.**, Brar S.K, Rouissi T., Martel R. (2020). Biodegradation of Central Intermediates Produced from Biodegradation of Xylene Isomers Spill in Groundwater. SETAC North America 41st Annual Meeting. Nov 15th, 2020, Texas, United states.

7. **Miri S.**, Brar S.K, Rouissi T., Martel R. (2020). Gene expression of *Pseudomonas* strains triggered by p-xylene spill in groundwater. 1st virtual Canadian Symposium on Water Quality Research, July 24th, 2020.

8. **Miri S.**, Rouissi T., Brar S.K (2019). Microbial or enzymatic biodegradation in contaminated groundwater? Poster competition of the CentrEau Quebec Students Day, March 22 th, 2019, Laval University, Quebec city, Quebec, Canada

9. **Miri S.**, Kuknur P.R., Rouissi T., Brar S.K (2019). Production and immobilization of *Bacillus sp.* lipase to remove BTEX from contaminated water. 54th CENTRAL Canadian Symposium on Water Quality Research, February 27th, 2019, York University, Toronto, Ontario, Canada.

LIST OF PUBLICATIONS OUT OF THIS THESIS

- **Patent and invention disclosure**

1. Davoodi, S. M., **Miri S.**, Brar SK. Enzyme Booster Technology (EnBooT) for advanced decontamination of petroleum hydrocarbons, Provisional filed. Invention disclosure submitted to York innovation office.

- **Peer-reviewed scientific articles**

1. Davoodi, S. M., **Miri, S**., Taheran, M., Brar, S. K., Galvez-Cloutier, R., & Martel, R. (2020). Bioremediation of Unconventional Oil Contaminated Ecosystems under Natural and Assisted Conditions: A Review. **Environmental Science & Technology**, *54*(4), 2054-2067.

2. **Miri, S.,** Saini, R., Davoodi, S. M., Pulicharla, R., Brar, S. K., & Magdouli, S. (2021). Biodegradation of microplastics: Better late than never. **Chemosphere,** 131670.

3. Akhtarian, S., **Miri, S.**, Doostmohammadi, A., Brar, S. K., & Rezai, P. (2021). Nanopore Sensors for Viral Particle Quantification: Current Progress and Future Prospects. **Bioengineered**, 12(2), 9189-9215.

4. Kadri, T., **Miri S.**$^{\Psi}$, Robert T., Brar SK., Rouissi T., Pachapur V.L., Lauzon J. M. (2022). Pilot-scale Production and In-situ Application of Petroleum-Degrading Enzyme cocktail From *Alcanivorax borkumensis* ($^{\Psi}$Equal first authors), **Chemosphere**, 133840.

5. Davoodi, S. M., **Miri, S**., Brar, S. K., Knystautas E., & Martel, R. Simulation of jellyfish type of process for bioremediation application following the marine oil spill. Submitted in Journal of Hazardous Materials.

6. Davoodi, S. M., **Miri, S**., Brar, S. K., Knystautas E., & Martel, R. Application of Arctic inhabitant bacteria to biodegrade PAHs. Ready to submit.

- **Book chapters**

1. **Miri S.**, Ghanei J., Brar S.K., (2021). Characteristic of wastewater and drinking water treatment, Chapter 2 in Modular approach for drinking water and wastewater treatment. (Eds. Satinder Kaur Brar, Pratik Kumar, Agnieszka cuprys). Elsevier.

2. **Miri S**., Rasooli A., Rouissi T., Brar S.K, Martel R., (2020) Potential of Biotechnology for Uranium Extraction. Chapter 5 in Resource Recovery: Zero waste Biomining. Elsevier.

3. **Miri S**., Jain R., Pachapur V.L., Brar S.K., (2019). Advances in antibody-based biosensors in environmental monitoring. Chapter 14 In: Tools, Techniques and Protocols for Monitoring Environmental Contaminants (Eds. Satinder Kaur Brar, Krishnamoorthy Hegde Vinayak Pachapur). Elsevier. (pp. 285-305). Elsevier.

4. **Miri S.**, Rasooli A., Rouissi T., Brar SK., Martel R. Potential of Biotechnology for Uranium Extraction (submitted), Springer.

CHAPTER ONE: INTRODUCTION & RESEARCH OBJECTIVES

PART 1- INTRODUCTION

p-xylene is one of the toxic and volatile organic compounds in petroleum products and is mainly used as a solvent for the manufacturing of chemicals. p-xylene causes health effects from both chronic (>365 days) and acute (<14 days) exposure. The severity and type of health effects depend on the amount of the chemical and the length of time that you are exposed to. Individuals also react differently to different levels of exposure [1]. *p*-xylene is frequently found in groundwater and soil due to leaks, leaching from landfills, and improper waste disposal [2], [3]. To date, many petroleum-contaminated sites have been identified in cold regions that require efficient site management and active remediation [4]. For instance, according to the report of federal contaminated sites inventory (by the Government of Canada), over 23,000 contaminated or suspected contaminated sites were identified across Canada that are contaminated with petroleum products. Major Canadian oil-contaminated sites (more than 70%) are located in the sub-arctic and Arctic climate regions [5]. Likewise, 920 sites in Alaska, close to 200 sites in Antarctica, and more than 100 sites in Russia, Iceland, Greenland, Sweden, Norway, and Finland were identified that are considered as cold climate regions [6].

There are many methods to treat p-xylene including chemical (e.g. flocculation), physical (e.g. adsorption and filtration [7], and biological methods that are based on biodegradation. Mechanical contaminant removal as a physical method on cold climate soils is very expensive. Also, the application of chemical methods can be quite dangerous and challenging when considering the risk of additional environmental impacts due to the addition of chemicals [5]. On a large scale, some disadvantages of the thermal treatment methods may be highlighted such as cost, energy consumption, and some intermediates which may be produced during the thermal process. The thermal method can also influence the quality parameters of soil, such as microorganisms' activity [8]. Biological treatment processes offer potential advantages such as being cost-effective,

environmentally friendly with lesser undue damage to the cold climate environment in comparison to physical, chemical, and thermal approaches [5].

Research so far has focused on BTEX (benzene, toluene, ethylbenzene, xylene isomers) biodegradation; however, especially for *p*-xylene compared to other compounds, the lower degradation rate for xylene isomers has been reported as a result [3].

PART 2- PROBLEM STATEMENT

Based on the literature review, certain problems have been defined for the current research work that needs to be addressed before formulating the hypotheses and objectives. Over the past decade, various technologies such as chemical methods, thermal treatments, and bioremediation have been applied by remediation companies to clean up groundwater, soils, and sediments. The conventional methods can be quite dangerous and challenging when considering the risk of additional environmental impacts due to some intermediates which may be produced during the process as well as high cost and energy consumption. Bioremediation has been considered to be more effective and economical with lesser undue damages to the environment compared to conventional methods. The biodegradation of petroleum hydrocarbons especially BTEX (benzene, toluene, ethylbenzene, and xylene) was well established in the literature. However, most studies reported a low biodegradation rate for p-xylene.

Petroleum-contaminated sites, associated with the legacy and contemporary effects of human activities, remain a serious environmental problem mainly in cold regions. A cold climate site is one at where the average annual air temperature is 10ºC (typically in the range of 4–15 ºC). Also, low temperatures pose an additional challenge for bioremediation that require more time (ranging from 1 to 10 years) to meet cleanup standards. As the harsh condition of the cold ecosystems, they may be more sensitive to the same levels of contamination than the other ecosystems and the

treatment method should be mild and has less impact on the environment. However, there is no agreement for efficient remediation techniques for these types of ecosystems. The enzymatic method has a shorter treatment period than the microbial process because the enzymes transform the substrate in a minute timescale. However, inherent instability and high production cost are the major challenges in the practical and commercial application of enzymatic biodegradation. These discussions provided some technological bottlenecks and suggested further research inputs for making the overall treatment process more sustainable, economical, effective, and toxic-free in nature.

PART 3- CHALLENGES IN APPLICATION OF ENZYMATIC BIODEGRADATION

Some of the relevant problems associated with the contaminant and intermediate concentration analysis and selecting bacterial strains that need timely attention are as follows.

Concentration analysis of volatile compounds

To produce quantitative data, the concentration of contaminants should be analyzed properly. p-xylene is a volatile solvent, so it evaporates easily. Although much literature reported the biodegradation rate of their test based on comparison with their negative control, the efficiency of their biodegradation method did not determine in terms of concentration. Thus, running a negative control is not a feasible method to determine the effectiveness of the biodegradation method. Some of the key points are as follows:

A) Most of the biodegradation tests were set up in serum bottles with at least ¾ of headspace (optimum for biological activities) and during the incubation time, only about 50-60 % of the initial concentration can be detected in the liquid phase. Thus, this design for the biodegradation test will result in measurement bias from aqueous activity. In this case, the initial concentration in the system (liquid and gas phase) was measured and evaporated

concentration was added to obtain the remaining 50, 100, and 200 ppm of contaminants in the liquid phase.

B) Sub-sampling has a negative effect on the reproducibility of data. Sub-samples cannot be stored for analysis since p-xylene crystallizes at temperatures below 13°C and remains on top of the water after melting, causing bias in the determined concentration. The triplicate analysis showed a high variation in the concentration of xylene in the same sup-sample. Also, the vortex of the samples cannot be effective because xylene can stay above water after a few minutes.

C) The water solubility of xylene is 198ppm in water (25°C), therefore the stock of xylene should be prepared in methanol (for example 20000 ppm), and directly added for 200,100 and 50 ppm xylene in the system. This method applies to the standard curve as well.

D) Volatile compound partitioning into the headspace is most strongly affected by this source of measurement bias. The parameter of the instrument (GC head-space) should be optimized based on the matrix of samples. In this study, samples were prepared directly into a headspace vial without sub-sampling as follows: 5000 ml of ultrapure water + 25 µl internal standard + 50 µl sample (the sampling was done with a gas-tight syringe). Then the vials were crimped well. The instrument parameters were optimized as presented in Table 1.1.

E) All technical and biological tests were performed in triplicate for error analysis. Biological replicates were parallel measurements of independent biodegradation tests that capture random biological variation. In technical replications, the same sample is measured repeatedly in order to obtain independent measurements of the random noise associated with protocols or analytical equipment. The results are reported as the mean of triplicate determinations and the error bars represent SE, calculated from the triplicates. Statistical analysis was done by one-

way analysis of variance (ANOVA) followed by Tukey posthoc procedure to determine the differences among three or more numeric variables at a significance level set at $p < 0.05$.

F) EPA method 8260 was used for determining the lowest detection limit [9]. Briefly, standard solutions were prepared in water at concentrations from 0.5 to 200 ppb with a 25 ppb internal standard. The analysis was performed using the static headspce method. The lowest detection limit was determined 10 ppb for this method and equipment. In this research, the standard criteria for p-xylene in soil and groundwater is around 60 ppm and our contaminated samples have around 200 ppm in groundwater and around 10,000 ppm is soil. For our analysis, the calibration curve was prepared raging 10ppb to 2 ppm. The subsamples from each test were diluted more than 100 times for groundwater samples and more than 5000 times for soil samples.

Table 1.1. Instrument parameter for p-xylene concentration analysis using GC-MS with a headspace sampler

Temperature	**Timing**	**Option (PII)**	**Injection mode**
Needle: 90°C **Transfer: 120°C** **Oven: 80°C** **Carrier: 30 psi**	Inject: 0,05 min Pressurize: 0,2 min Withdraw: 0,1 min Thermo: 10,0 min GC cycle: 20,0 min	Shaker on Operating mode: Constant	Inject: 30 psi Column: 30

Toxic intermediates and detection

Although most of the bioremediation treatment methods were found effective in removing petroleum hydrocarbons, some of these methods resulted in the biotransformation of targeted contaminants to intermediate products. Some of these intermediate products are more toxic than the initial parent compounds, so biotransformation is not always a preferred strategy in pollutant management and remediation. Based on this information, biodegradation should focus on the

mineralization of the target contaminate into innocuous products. There are 2 key points in the detection of intermediate products:

A) The intermediate products can be volatile, semi-volatile, or non-volatile compounds, so the detection method can be different from the initial parent compounds. In this case, more than 2 chromatography methods are needed. Firstly, full scan mass detection can be used to determine all the products formed during the reaction. Then each compound can be detected based on the nature of the compound and proper protocol.

B) The time course and condition for the formation of intermediates varied in different samples, hence the sampling should be carried out at different time intervals and different conditions (e.g. without/with shaking). The formation of intermediates is a crucial step in the pathway study of newly isolated bacteria.

Low p-xylene degradation rate

Most of the research has been focused on BTEX (benzene, toluene, ethylbenzene, xylene) biodegradation. However, especially for p-xylene compared to other compounds, a lower degradation rate for xylene isomers has been reported. Alvarez and Vogel (1991) demonstrated that when p-xylene was present alone in basal mineral media, no degradation was observed in the first three weeks [2]. Meanwhile, You et al. (2018) recently reported the lower degradation of *p*-xylene by *Rhodococcus* sp. ZJUT312 compared to other compounds of BTE and also *m* and *o*-xylene [3]. Furthermore, several studies showed that some species of bacteria can only degrade selected compounds of BTEX rather than all of them. One example is that *Cladophialophora* sp. T1 cannot degrade benzene and xylene isomers, and *Acinetobacter baumannii* DD1 and *Magnetospirillum* sp. 15-1 degraded *m* and *p*-xylene with a very low efficiency [10], [11].

Cold temperature inhibition

In the case of cold climate environments, low temperatures (e.g., below 10 °C) pose an additional challenge for biological treatments. Whole microbial cells may require more time (ranging from 1 to 10 years) to meet cleanup standards. Microorganisms inhabiting cold environments cope with several challenges such as limited enzyme activity, slow chemical reaction rates, increased water viscosity and limited water availability as the main solvent for biochemical reactions, denaturation of proteins, and decreased cell membrane fluidity [12]. Commonly, the best (optimized) scheme of biodegradation cannot be easily achieved since the biodegradation efficiency of contaminants is strongly influenced by the temperature, physicochemical characteristics of the pollutant, the contaminated matrices, and microbial growth conditions [13].

High cost of enzymatic treatment

Contaminant removal using enzymatic treatment seems a costly process, however, three points of view can be considered in affordably remediating a contaminated site using enzymes: 1- high biodegradation rate of enzymes in cold environments (less time for remediating), 2- low-cost substrates and enzyme inducers for the production process, and 3- cost-effective methods for downstream processing. All these reasons are discussed below.

1- As bioremediation (using whole microbial cells) is a cost-effective and environment-friendly technology and is powered by enzymes, enzyme production needs to be optimized cost-effectively. Using enzymes has several advantages over whole microbial cells, including the ability to degrade contaminants in a shorter treatment period in harsh environments, high specificity for the pollutant, and no environmental risk. For example, bacterial whole cells need nutrition and air to maintain optimum growth. Considering that some environmental matrices such as groundwater lack nutritional factors for microbial growth, using enzymes could be more feasible from this perspective than the use of whole cells. Also, in cold climate

environments, low temperatures (e.g., below 10 °C) pose an additional challenge for biological treatments. Whole microbial cells may require more time (ranging from 1 to 10 years) to meet cleanup standards [6].

2- The raw materials needed for enzyme production for bioremediation applications are crucial since the high production cost of enzymes has restricted their widespread use of them for remediation purposes [14]. The use of industrial wastes that contain the needed nutrients can be a promising method. Moreover, BTEX is an important industrial chemical that has many applications so, the use of fewer and less expensive substrates such as certain wastes such as used motor oil that contain these chemicals can make enzyme production more cost-effective in environmental applications.

3- The production cost of advanced biotechnological techniques such as enzymes has restricted their industrial use for bioremediation purposes. Downstream processing is a major cost in the production of proteins and enzymes (biological macromolecules). The cost of unit operations and chemicals for downstream processing often determines the economic feasibility of the process [15]. Cost-effective processing such as centrifugation for harvesting the cells and ultrasonication for enzyme extraction and using crude enzyme or ammonium sulfate saturation for partial purification of enzymes can be considered for lowering the cost of treatment. More than 50% of downstream processing cost is involved mainly in the purification process, depending on the application the final enzyme purity can be somewhat low. Thus, the cost of final enzymes can be decreased significantly as well. For medical and related research, high purity is an important factor to run their assays or diseases that can be diagnosed or treated with pure enzymes. Thus, multiple expensive chromatographic steps involve obtaining such

highly pure enzymes [15]. However, for environmental applications, using crude enzymes or low purity enzyme cocktails are feasible solutions for reducing the cost of treatment.

Inherent instability of oxidoreductases

One of the major challenges in the practical and commercial application of monooxygenase enzymes is their inherent instability [16]. Two key points that should be considered for the stability of produced enzymes:

A) Most of the oxidoreductases are membrane-associated enzymes, so they have some hydrophobic peptides, and extraction of them from the cell can affect their activity. Various attempts can be made to mimic the membrane condition to increase their activity after extraction.

B) Oxidoreductases catalyze the exchange of electrons or redox equivalents between donor and acceptor molecules. To accomplish their physiological function, oxidoreductases employ various redox-active centers that can be dependent on co-factors. Common redox centers include amino acid residues (e.g., tyrosine or cysteine), metal ions or complexes (e.g., Cu, Fe, Mo, Fe-S cluster, or heme), and coenzymes (e.g., FMN; FAD; pterin; or pyrroloquinoline quinone, or PPQ). The enzyme formulation should be designed according to the signature catalysis of target enzymes and/or coenzyme dependency.

PART 4- HYPOTHESES

The organic nature of petroleum hydrocarbons makes these contaminants suited to biodegradation where indigenous microorganisms can degrade them [17]. Considering the challenges in biodegradation of p-xylene in cold regions, biotechnological improvements, such as biostimulation, bioaugmentation, use of biosurfactant, enzymes and immobilization methods seem promising methods for an increase of bioremediation effectiveness [6]. To meet the need for

effective decontamination of p-xylene in a cold-climate site, it is necessary to prove the following hypotheses:

Hypothesis I: As mentioned in problems, low degradation rates were reported for p-xylene using well-known BTEX-degrading microorganisms. *Indigenous bacteria isolated from the p-xylene contaminated site could metabolize p-xylene effectively under low temperatures*. Since psychrophilic bacteria have adaptive abilities including the modification of the cell membrane structure that is important in the electron transport chain, the expression of anti-freeze proteins and cold-active enzymes, or production of compatible solutes or altered metabolism [18]. Therefore, cold-adapted indigenous microorganisms can increase bioremediation efficiency of our target contaminated under cold temperatures.

Hypothesis II: In cold temperatures, biological treatments take longer to meet cleanup standards (as described in problem 1.3.4). Biotechnological improvements, such as cold-active enzymes and immobilization methods, may allow a greater efficacy of bioremediation while decreasing remediation time. *Indegionious p-xylene degrading bacteria would produce cold-active oxidative enzymes under aerobic conditions and be applied to contaminated soil and groundwater*. Since the enzymatic method has a shorter treatment period than the microbial process and enzymes transform the substrate in a minute timescale. Moreover, the enzymatic treatment agent can be designed for specific pollutant removal without producing any toxic by-products

Hypothesis III: The major challenges in the practical and commercial application of oxygenases are high production costs and their inherent instability. Immobilization improves enzymes' resistance to a variety of storage and operating conditions. *The use of immobilized enzymes in biotechnological processes is preferred over their free counterpart because of the prolonged availability of enzymes and their re-usability.* However, enzymes are not widely used for

remediation purposes due to their high production costs. The cost of enzyme production should be decreased by the use of fewer and less expensive substrates or cost-effective downstream processing. The enzyme mixture could be produced using industrial wastes such as food and fisheri wasterd and then formulated with high storage and operational stability. A useful tool for reducing costs is the immobilization of enzymes as it enables efficient recovery, reuse, and recycling, as well as increased stability under harsh operational conditions such as high/low pH and temperature.

Hypothesis IV: Large-scale production of enzymes using optimized conditions at the bench scale can determine and influence the scaling-up process. Furthermore, enzymatic biodegradation in soil involves key factors that should be verified in batch tests, soil columns, and 3D-tank tests. To mimic in situ application of enzyme mixture, soil column and tank tests can be used to model the essential characteristics of the environment to predict the consequences of bioremediation. Therefore, *the formulated enzyme mixture could be effectively produced on different scales (bench to large scale) and applied to soil and groundwater (laboratory, to pilot scales).* The scale-up tests would ensure a proper interpretation of the laboratory results and determine the efficiency of enzymatic bioremediation.

PART 5- OBJECTIVES

To prove the above-listed hypotheses, the following objectives were studied for the effective bioremediation of p-xylene.

Objective 1: Investigate metabolic and co-metabolic biodegradation of p-xylene by well-known BTEX-degrading microorganisms (such as *Pseudomonas putida*) using the Group Method of Data Handling (GMDH) and experimental data

Objective 2: Study the pathway of p-xylene biodegradation and compare cold-active strains

Objective 3: Investigate involved enzymes in p-xylene biodegradation and potential application for contaminated groundwater in the cold climate

Objective 4: Evaluate enzymatic biodegradation of highly p-xylene contaminated soil using cold-active enzymes

Objective 5: Explore the co-immobilization of cold-active enzymes for higher stability and reusability

Objective 6: Optimize the operational stability and reusability of cold-active enzymes using magnetic particles

Objective 7: Analyze the scale-up parameters for the enzyme production process from bench scale to industrial-scale bioreactors

Objective 8: Evaluate enzymatic biodegradation efficiency in soil test, laboratory, bench, and pilot tests

PART 6- ORIGINALITY

Soil and groundwater remediation after p-xylene spills can be extremely expensive and time-consuming, therefore the cost and time-efficient biodegradation will be first considered. As p-xylene cannot be used efficiently as a growth substrate by microorganisms, the main aim of this project is to find a mixture for biodegradation of p-xylene in highly contaminated sites (e.g. Quebec, Montreal). The core part of this study is the use of cold-active enzymes for the first time as an efficient p-xylene removal in a cold contaminated site. The present study comprises the following original concepts in methodology:

1) In the past, the bacteria showed a low biodegradation rate of p-xylene or co-metabolism of p-xylene in presence of other compounds (BTE) even at mesophilic temperature. However, this is the first time that isolated bacteria showed metabolic of p-xylene at cold temperatures.

2) This novel study evaluated the characteristics of cold-adapted enzymes using different assays such as spectrophotometric methods and tandem LC-MS/MS.
3) Few studies were carried out in detail on non-growth substrates such as p-xylene, this is the first study on gene expression aspects of biodegradation for p-xylene.
4) This study suggested for the first time the partial purification of the targeted enzymes that can be a feasible solution to the high cost of enzyme production that is leading to the limited application of enzymes for environmental purposes.
5) The formulation of targeted enzymes for the first time suggested the feasibility use of cold-active enzymes for commercial purposes.
6) The use of various support materials such as biochar, zeolite, clay, or additives has been explored for other enzymes. However, this is the first time, they were used for cold-active enzymes to enhance bioactivity and hence p-xylene biodegradation.
7) Scale-up of enzyme production and enzymatic biodegradation tests were performed for the first time in this study, to the best of our knowledge.

Overall, the originality of this research is, "**Development of an advanced biodegradation method using cold-active enzymes, drawn from natural sources for petroleum monoaromatics in cold climate sites".**

PART 7- THESIS LAYOUT

This dissertation consists of SEVEN chapters, FOUR hypotheses and EIGHT objectives as described below.

Chapters	Title for a major goal	Hypotheses	Objectives
1	Introduction and research objectives	-	-

2	Literature Review	-	-
3	Investigation of metabolic biodegradation of p-xylene	Hypothesis I	Objective 1and 2
4	Detection of involved cold-active enzymes	Hypothesis I	Objective 3
4	Application of cold-active enzymes for contaminated soil and groundwater	Hypothesis II	Objective 3, 4
5	Formulation of enzymes for high storage and operational stability	Hypothesis III	Objective 5, 6
6	Scale-up of the enzyme production and biodegradation	Hypothesis IV	Objective 7, 8
7	Conclusions and Recommendations	-	-

CHAPTER TWO: LITERATURE REVIEW

Abstract

In recent years, there have been advances in bioremediation of pollutants with the goal of effective clean-up of environments in an eco-friendly and cost-effective approach. For contamination removal at cold climate sites, bioremediation approaches are appealing due to their potential to be more cost-effective and efficient than alternative, more energy intensive approaches. Recent studies showed both aerobic and anaerobic biodegradation processes are important at cold climate sites. Most of these works are focused on biostimulation and bioaugmentation involved in adding nutrients and hydrocarbon degraders at cold climate sites, but studies on other methods such as the use of biosurfactant, genetically engineered bacteria, cold-adapted enzymes and immobilization method are still limited. This review selectively provides information on bioremediation under aerobic and anaerobic conditions and recent biotechnological advances in bioremediation at cold climate sites. However, the limitations and challenges for petroleum hydrocarbons bioremediation in cold climate remain at large. Further research and field demonstrations are required to determine which method is more effective for biodegradation of petroleum contaminates under such conditions.

2.1. Introduction

The recent economic growth has been paralleled by a rapid increase in global petroleum oil consumption [19] and the widespread use of petroleum products in cold climate regions (e.g., Alaska USA, Canada, Russia) has led to contamination of soil and groundwater at many sites. Petroleum-contaminated sites in cold regions have received significant attention because of their susceptible natural environment to human impacts. As harsh condition of the cold ecosystems, they may be more sensitive to the same levels of contamination than the other ecosystems [20].

To date, many sites with petroleum contamination identified in cold regions that require efficient site management and active remediation [4]. For example, petroleum hydrocarbon soil contamination is relatively localized to approximately 920 sites in Alaska, 377 sites in the Canadian Arctic, closed to 200 sites in Antarctica and more than 100 sites in Russia, Iceland, Greenland, Sweden, Norway, and Finland [21].

Petroleum oil is containing thousands of complex different compounds which are basically separated into cyclic and linear alkanes, aromatic hydrocarbons, resins and asphaltenes, and poorly characterized compounds. The consumption of these compounds has negative health effects on humans include irritation of organs, liver lesions, drowsiness, dizziness and cancer [22]. For this reason, U.S. Environmental Protection Agency classified them as priority pollutants [23]. Therefore, there has been an increasing concern about the human health and environmental risk of petroleum industry activities led to efforts for developed soil and groundwater treatments in cold regions [24].

Over the past decade, various technologies such as chemical treatments, physical treatments, and bioremediation have been applied to remediate groundwater, soils and sediments [25]. Bioremediation is one of the most cost-effective strategies due to its lower equipment, labor, and

energy requirements, compared with classical physicochemical techniques. Also, Bioremediation is one of the best environmental friendly methods to remove petroleum pollutions [26].

In cold regions, low temperatures pose an additional challenge for remediation [20]. A cold climate site is one at which the average annual air temperature is ≤8°C (typically in the range 4–8°C), and where groundwater temperatures are typically 10°C or lower. In these environments, biological treatments require more time to meet cleanup standards [21]. Biotechnological improvements such as biostimulation, bioaugmentation, use of biosurfactant, enzymes and immobilization methods seem promising method for an increase of bioremediation effectiveness.

Most of the previous reviews focused on the biodegradation of petroleum hydrocarbons with the general point of view about affecting factor on bioremediation but a few reviews addressed cold climate sites specifically [20] and no review has yet focused on recent biotechnological advances in this regions. Despite recent growth in bioremediation application in cold regions, the agreement is still limited as to which biotechnological improvement is the most effective for bioremediation under such conditions.

The aim of this review is to address the science gap by summarizing available information to provide an overview about 1) information regarding bioremediation under aerobic and anaerobic condition 2) recent biotechnological expansion of bioremediation technology at cold climate sites 3) consideration of problems and challenges of bioremediation at such sites.

2.2. Bioremediation

The success in the cleanup of the Exxon Valdez oil spill (1989) in Prince William Sound, Alaska created a great interest in the potential of bioremediation technology especially biodegradation [27]. Bioremediation is a process that relies on biological mechanisms (degrade, mineralize, detoxify and transform) to reduce the concentration of pollutants to a harmless state [28].

Bioremediation technologies offer the potential for significant cost savings and practical approaches compared to conventional remediation technologies, such as excavation and thermal treatment, excavation, and disposal in landfills, and pump and treat. Especially at remote sites in the north, conventional technologies are often not practical or feasible, for example requiring electricity provision, transport of chemicals, and their storage, among others [20].

Many microorganisms can degrade pollutants under aerobic (in the presence of oxygen) and anaerobic (in the absence of oxygen) conditions (Fig. 2.1). Microorganisms can generate energy from the oxidation of organic compounds as a source of carbon to CO_2 and assimilate part of this carbon into their new cell material. Aerobic microorganisms use oxygen (O_2) as the final electron acceptor, while anaerobic microorganisms use substances, such as sulfate, nitrate, manganese, iron, and organic intermediates as electron acceptors [29][30].

In aerobic degradation, many pollutants can serve as a source of carbon and energy for microorganisms that are capable of producing degrading enzymes. Monooxygenases and dioxygenases are the most common enzymes that catalyze reactions by incorporating O_2 into the structures (Fig. 2.1). Under anaerobic conditions, microorganisms can carry out the oxidation of substrates by electron transfer to a suitable acceptor. Extensive oxidation can be performed in different respiratory pathways as shown in Fig. 2.1. Based on the literature reported, aerobic bioremediation is the currently practiced approach for the removal of petroleum hydrocarbons in cold regions, and anaerobic bioremediation is a new frontier of learning and needs significant advances for the application stage [5], [6].

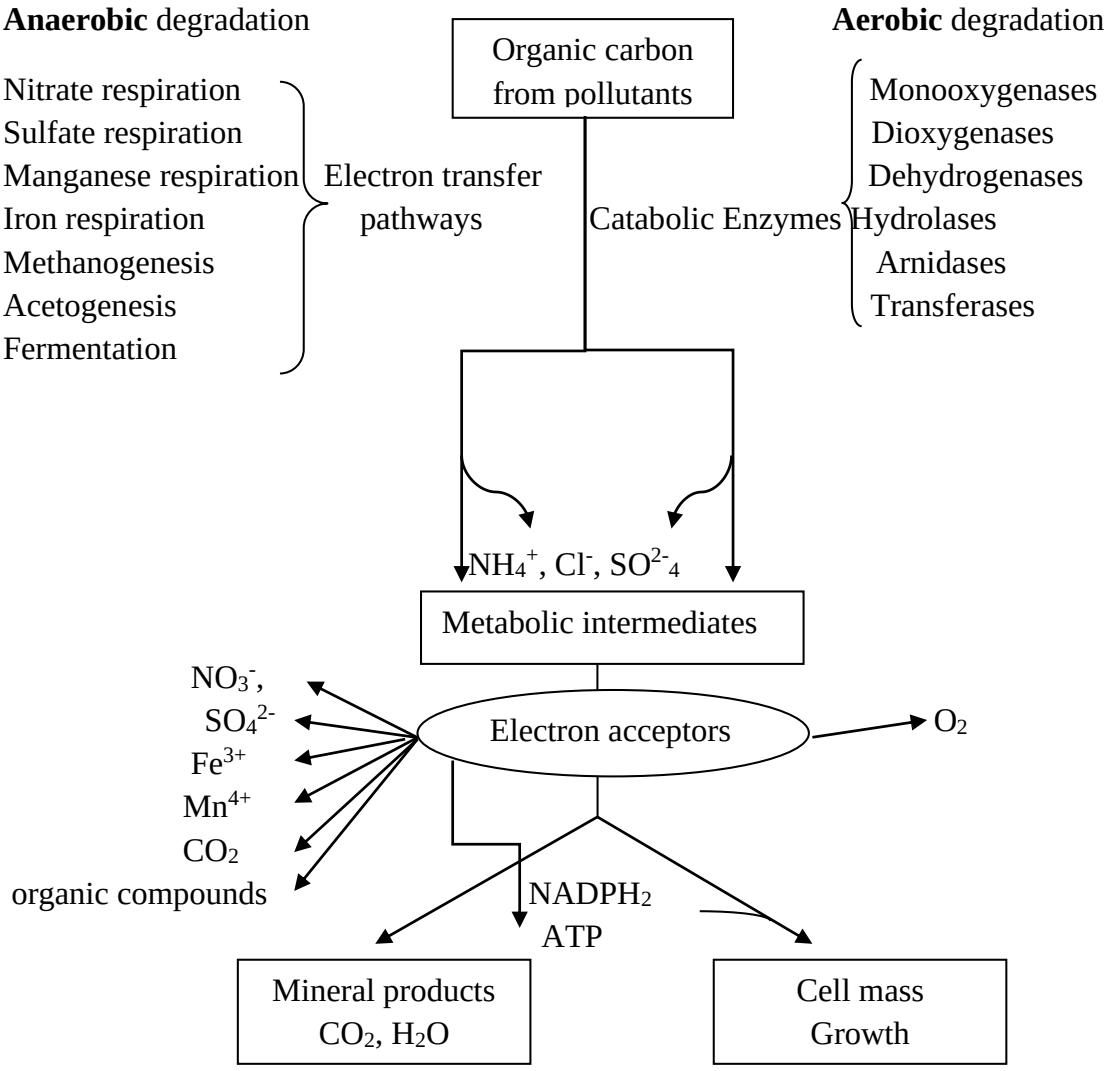

Fig. 2.1. Aerobic and anaerobic biodegradation of pollutants.

2.3. Recent Biotechnological advances

In cold climate regions, increasing temperature generally increases the biodegradation rates of hydrocarbons, but this method is not energy- and cost-effective. The microbial degradation of petroleum hydrocarbons in cold environments has been investigated as a cost and labor-effective technology that generates no harmful end products. Bioremediation in aquatic environments is limited primarily by nutrients, such as phosphorus (P) and nitrogen (N); salinity in the estuarine,

and pressure in the deep sea. Furthermore, nutrient concentrations, oxygen, moisture, and pH-value are determining factors in the biodegradation rates of soil [31], [32].

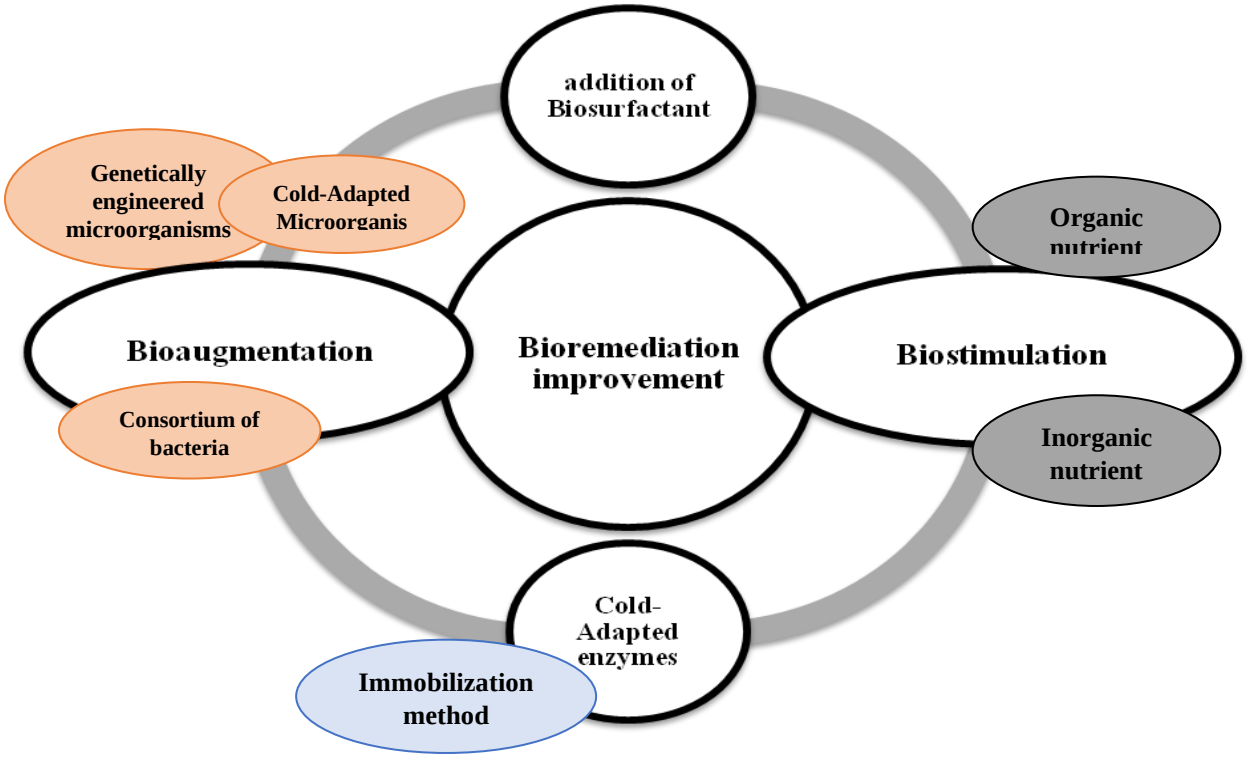

Fig. 2.2. Improvement of bioremediation at cold climate sites. The classification of each technique is hypothetical; some methods could be classified into more than one category. For example, the enzyme and bio-augmented microorganisms can be used as an immobilized form.

Biostimulation and bioaugmentation are active bioremediation approaches that can be applied in cold climate environments for enhancing bioremediation efficiency. Biostimulation is mainly done by adding nutrients, such as nitrogen and phosphorus to stimulate the oil biodegradation by the indigenous bacteria. Bioaugmentation involves the addition of hydrocarbon degraders (indigenous or exogenous inoculum) to the contaminated site [33]. Fig. 2.2 depicts the potential improvement approaches in the bioremediation of petroleum hydrocarbons.

2.4. Biostimulation

In cold climate regions, chemical analysis of soil showed low levels of N and P. Also, it was possible to optimize C-N-P relationships with nutrient addition [34]. Nutrient additives can be added to stimulate bioremediation. They may be natural or synthetic as well as organic or inorganic compounds [35], [36]. Improvement in bioremediation can be attributed to the positive effects of additional N supplements on the synthesis of nucleic acids and amino acids for the rapid cell growth in the medium [36], [37]. Urea is a common source of nitrogen, but C-N ratio optimization with urea led to undesired effects such as induction of rapid nitrification [38], a significant rise in pH, a drop in bacterial viability. Methylene urea is also used with minor effects on the level of soil pH and increases the growth of heterotrophic microbes. This source is more desirable probably because of slow nitrogen release [34]. Nutrients in the form of fertilizer solutions are generally added in three different types (hydrophilic, oleophilic, and slow-release). This report summarizes the results from various recent studies that have indicated the effect of biostimulation with different nutrient additions in cold climate sites (Table 2.1).

Table 2.1. Effect of the different nutrient types for biostimulation on bioremediation of hydrocarbon-contaminated sites in cold regions

Nutrient addition	Effect on bioremediation	Removal efficiency	Nature of pollutant	Reference
0.67 mM NH_4Cl and 1.47 mM KH_2PO_4	Enhancing *n*-alkane and PAH degradation following low-concentration (0.1% [vol/vol]) diesel and crude oil amendments	17-43%	Diesel and crude oil	[39]
NPK fertilizer	It promoted naphthenic oil degradation in Arctic seawater and enhanced microbial community	12%	Naphthenic oil	[40]

Nutrient addition	**Effect on bioremediation**	**Removal efficiency**	**Nature of pollutant**	**Reference**
Potassium nitrate (KNO_3) and sodium triphosphate pentabasic ($Na_5P_3O_{10}$)	Enhancing the microbial community and oil biodegradation	33%	Alkanes and Polycyclic Aromatic Hydrocarbons	[41]
Slow-release granular fertilizer (Nitrofoska®) and a commercial bioremediation product (OSEII®)	The soil indigenous microbiota reduced the concentration of hydrocarbons by up to 50% in 50 days and 87% in 365 days depending on the biostimulation agent used	71-87%	Total petroleum hydrocarbons	[42]
Humate and 20:20:20 fertilizer	Hydrocarbon degradation was notably enhanced in the treated bio-pile during seasonal freezing and early thawing.	57–58%	total petroleum hydrocarbons	[43]
Ammonium nitrate (N source) Monosodium phosphate (P source)	Hydrocarbon removal efficiency increased within 50 days with both N and P sources at Carlini Station (Antarctica).	75.79%	petroleum hydrocarbons (2180 mg kg^{-1})	[44]
BH media B+NP medium 20-20-20 fertilizer	*Dietzia maris* strain NWWC4 with stimulated medium showed the occurrence of significant biodegradation activity of crude oil in both the saline and non-saline slurries of sub-Arctic sites after 18 days.	Non-saline: 37% Saline: 21%	petroleum hydrocarbons	[45]
N and P	The addition of 0.0179 g P/kg and 0.183 g N/kg leads to the highest hydrocarbon removal efficiency during a 45-day field assay in Antarctica.	54.91%	1042 ±73 mg kg^{-1} of fuel hydrocarbons	[46]

Nutrient addition	**Effect on bioremediation**	**Removal efficiency**	**Nature of pollutant**	**Reference**
3 principal phosphate phases (adsorbed phosphate, brushite ($CaHPO_4 \times 2H_2O$), newberyite ($MgHPO_4 \times 3H_2O$))	Adsorbed phosphate and brushite limited the ability of the microbial community to degrade hydrocarbons. In contrast, newberyite had little effect on microbial community composition.	ND	gasoline and diesel hydrocarbons	[47]
Organic compost	The combination of microbial consortia and mature compost as a biostimulant was an appropriate bioremediation approach for reaching values below provincial standard regulations in just 40 days after construction.	48-52%	heating oil (C14–C20)	[48]
Commercial fertilizer (PlantProd) (20% N/20% P2O5/20% K2O, Plant-Prod) and 2000 mg $CaCO3\ kg^{-1}$	Nutrient amendment decreased in total petroleum hydrocarbons concentrations at a sub-Arctic site (Canada) with temperatures between 4.7 and 10°C	55%	total petroleum hydrocarbons	[49]
cod bone meal (diammonium phosphate (DAP))	Degradation in diesel fuel contaminated soil was greatly increased by the addition of cod bone meal compare to unfertilized soil after 6 weeks.	89% - 92%	Diesel hydrocarbon (20,000 mg diesel/kg soil)	[50]
Inipol EAP-22 fertilizer	The rate of degradation was improved because of an increase in the number and variability of heterotrophic	ND	diesel fuel or Arabian light crude oil (500 mL/plot)	[51]

Nutrient addition	Effect on bioremediation	Removal efficiency	Nature of pollutant	Reference
	and hydrocarbon-degrading microorganisms.			
fish compost	The addition of fish compost had a toxic effect on microbial abundance, particularly on hydrocarbon-degrading bacteria	ND	diesel and crude oil hydrocarbon	[52]
Agricultural N-P-K fertilizer	Oil biodegradation was enhanced in fertilized Alpine subsoils at 10 °C.	27-53%	diesel hydrocarbon (5000 mg/kg soil)	[53]

ND: Not determined

Besides, the indigenous microbial activity can be enhanced and stimulated by optimizing the environmental conditions, such as oxygen accessibility, nutrient content, temperature, pH, redox conditions, or electron acceptor accessibility for anaerobic conditions [6]. Utilization of bio-venting (injection of air into the subsurface at low flow rates) successfully enhanced the biodegradation to a peak concentration of 7000 mg/kg of total petroleum hydrocarbons in the sub-Antarctic [50]. Sanscartier, Reimer, Zeeb, and Koch (2011) showed that high airflow resulted in biodegradation 50% greater than under low aeration at 7 °C in soils from the Canadian High Arctic. King et al. (2014) found that bio-venting (275 cm^3/min) was most effective (82.0–92.5% hydrocarbon removal) at 10°C. Chang et al. (2010) bio-stimulated contaminated soil from a sub-Arctic site with nutrient and pH buffer amendments. To obtain a soil pH between 6.5 and 7.0. (neutral pH), 2000 mg/kg of $CaCO_3$ was used in land farm tanks. The results showed that biostimulation with nitrogen and phosphorus nutrient amendments and maintaining neutral pH reduced total petroleum hydrocarbon concentrations by up to 64% over 60 days [54]. However,

relatively little data and studies are available for the effectiveness of the optimization of environmental factors in cold regions.

2.5. Bioaugmentation

The commonly used methods for bioaugmentation are (1) addition of a pure oil-degrading strain; (2) addition of a consortium of microorganisms; (3) addition of genetically engineered microorganisms; and (4) introduction of biodegradation genes that are packaged in a vector to be transferred by conjugation into indigenous and native microorganisms [55]. The following sub-sections will focus on bioaugmentation methods in cold climate regions as a bioremediation tool.

2.5.1. Cold-adapted, oil-degrading microorganisms

Hydrocarbons in the contaminated environment are biodegraded primarily by bacteria, yeast, and fungi. In several studies, it is noted that bioremediation could only be carried out by psychrophilic or psychrotolerant microorganisms in cold climate regions. These kinds of bacteria can grow at temperatures below 20 °C [56]. During the past few decades, most of the cold-adapted microorganisms in petroleum bioremediation were identified as bacterial genera, and a limited number of fungi and yeast were identified in the degradation of petroleum in cold climate regions (Table 2.2). It seems that hydrocarbonoclastic bacteria are significant players in hydrocarbon degradation in cold environments [57]. These bacteria when exposed to low temperature may produce cold-acclimation, cold-shock, anti-freeze proteins, and cold-active enzymes that have higher catalytic activity under cold conditions [58].

In these regions, large seasonal temperature variations reduce the effectiveness of microorganisms for biodegradation, and the use of indigenous microorganisms can solve most of the challenges associated with the bioremediation of polluting substances [59].

The introduced bacteria can be inhibited by indigenous microorganisms or co-pollutants [60]. Common microorganisms which are recognized for their ability to metabolize oil hydrocarbon compounds in cold regions are presented in Table 2.2.

Table 2.2. Microorganisms involved in the degradation of hydrocarbon pollutants in cold climate sites

Microorganism	Growth temperature	Isolation location	Removal efficiency	Nature of pollutant	Reference
Bacillus, [a] *Arthrobacter* [a] *Rhodococcus* [a] *Pseudomonas* [a]	25 °C	Pushkin, Russia	38–43%	oil	[61]
Dietzia maris [a]	10 °C	Sub-Arctic, Canada	37%	Petroleum hydrocarbons	[45]
Chryseobacterium spp. [a] *Bacillus* [a] *Pseudomonas* [a]	10 °C	Oily sludge from a cold environment, China	62.3% 61.6% 60.9%	Crude oil hydrocarbons	[62]
Sphingopyxis flavimaris [a] *Pseudoalteromonas* [a] *Marinobacter antarcticus* [a] *Oleispira antarctica* [a] *Rhodococcus sp. ice-oil-488s* [a] *Sulfitobacter sp* [a] *Hyphomonas rosenbergii* [a]	4°C	Kongsfjorden, Svalbard Islands, Arctic region	17.25% - 81.98 %	Arabian light crude oil (0.05 %) and polycyclic aromatic hydrocarbons (PAH)	[63]
Cycloclasticus [a] *Pseudomonas* [a]	4°C	Contaminated sediments, Makarov Basin, Arctic	ND	Polycyclic aromatic hydrocarbons (PAHs)	[64]
Penicillium commune [b] *Aspergillus fumigates* [b] *Penicillium rugulosum* [b]	5°C	Antarctic soil	ND	Phenol (0.3 g/l)	[65]
Alternaria maritima [b] *Penicillium rugulosum* [b]	23°C	Livingston Island, Antarctica	ND	Polycyclic aromatic hydrocarbons (PAHs)	[66]

Microorganism	Growth temperature	Isolation location	Removal efficiency	Nature of pollutant	Reference
Penicillium waksmanii [b] *Aspergillus fumigatus* [b] *Penicillium chrysogenum* [b] *Mucor sp.* [b]					
Rhodococcus erythropolis [a] *Rhodococcus cercidiphyllus* [a] *Arthrobacter sulfurous* [a] *Pimelobacter simplex* [a]	1-30°C	contaminated alpine soi1, South Tyrol, Italy	95-100% (for n-alkanes)	petroleum hydrocarbon (13,300 mg/kg dry soil)	[67]
Arthroderma sp. [b] *Exophiala* sp. [b] *Hypocrea* sp. [b] *Leptodontidium* sp.[b]	15°C	diesel-contaminated soil of sub-Antarctic Macquarie Island, Australia	ND	Special Antarctic Blend (SAB) diesel fuel	[68]
Pseudomonas borealis [a] *Pseudomonas fluorescens* [a]	4◦C	oil-contaminated soil from Signy Island, Antarctica	ND	polycyclic aromatic hydrocarbon (PAH)	[69]
Rhodotorula creatinivora [c]	10◦C	alpine oil-shale mine soil, Austria	ND	oil hydrocarbons	[70]
Arthrobacter sp. [a]	10◦C	Alpine ice cave in Salzburg, Austria	ND	Phenol (10 mM)	[71]
Oleispira Antarctica [a]	4◦C	hydrocarbon contaminated sea-water from the inlet Rod Bay (Ross Sea), Antarctic coastal marine	ND	crude oil (Arabian light; 0.1%, v/v)	[72]
Sphingomonas spp. [a]	1 °C	Fuel-contaminated soil, Ross Island, Antarctica	ND	Aromatic hydrocarbons heterocycles, aromatic acids, and alcohols	[73]

Microorganism	Growth temperature	Isolation location	Removal efficiency	Nature of pollutant	Reference
Pseudomonas sp p. [a]	4◦C	Fuel contaminated soil, Wright Valley, Antarctica	ND	JP8 jet fuel	[74]
Rhodococcus spp. [a]	-2 °C	oil-contaminated soil from Antarctica, Arctic	ND	oil hydrocarbons	[75]
Pseudomonas spp. B17 & B18 [a]	5 °C	petroleum-contaminated Arctic soils, Baffin Island, Canada	ND	aliphatic compounds and PAHs	[76]

[a] bacterium, [b] Fungi, [C] yeast- ND: Not determined

2.5.2. Consortium of different bacteria

Analysis of 16S rRNA gene sequences shows that the addition of crude oil to the seawater and soil sample induced a rapid shift in the composition of the bacterial community and appearance of aromatic compound-degrading bacteria including genera such as *Georgfuchsia*, *Azoarcus*, *Sulfuritalea*, *Rhodoferax* (all Betaproteobacteria), *Pelotomaculum* (Firmicutes) and *Arthrobacter (*Actinobacteria) [77], [78]. Many bacteria can remove petroleum hydrocarbons from the contaminated environment by degradation under aerobic conditions, such as *Acinetobacter, Pseudomonas, Comamonas, Serratia, Bacillus, Coccobacillus, Burkholderia, Sphingomonas, Terrimonas, Fulvimonas,* and *Chryseobacterium.* It has been shown that the use of bacterial consortium is more efficient than the single strains, probably because of a wider catabolic potential and the enzymatic ability for the degradation of oil compounds [79]. Different microbial species have different preferences for the degradation of hydrocarbons. For instance, some microorganisms prefer mono- or polynuclear aromatics, and others jointly degrade both aromatics and alkanes as well as linear, branched, or cyclic alkanes [35]. Roslee et al., (2021) reported that cold-adapted microbial consortium degraded diesel almost completely at moderately low temperature [80].

The application of different bacterial consortia in cold climate regions requires the determination of the activity and survival of the added microorganisms as well as their genetic materials. For example, sequence analysis of the 16S rRNA gene in the former Colomac Mine, Canadian shield (mean annual air temperature of −5 °C) showed that a wide range of bacteria genera, such as *Geobacter*, *Thiobacillus*, and *Pseudomonas* are involved with the anaerobic degradation of petroleum hydrocarbons [81]. Another study addresses three phenol-degrading isolates from King George Island, Antarctica. Based on 16S rRNA sequences, they were identified as one *Rhodococcus* sp. and two *Arthrobacter* spp. that are capable of completely degrading phenol at the optimum temperature between 10 and 15 °C under aerobic conditions [43]. A mixed cold-adapted bacteria flora including *Rhodococcus* sp., *Pseudomonas* sp., *Stenotrophomonas* sp., and *Sphingobacterium* sp. degraded 53.68% of total petroleum hydrocarbons (TPH) under 10 °C after 30 days [82].

Analysis of stable carbon isotope fractionation is another method to assess bacterial biodegradation by aerobic and anaerobic bacteria in contaminated sites [83]. For example, using C^{14} demonstrated respiration in freezing temperatures such as -16 °C [84], -4 °C [85], -2 °C [86], -18 °C [87], -39°C (controversial) [88], and in Antarctic soils up to -5 °C [14]. Radiolabeled analysis and stable isotope probing have established the presence of active microorganisms with DNA replication in permafrost soils under frozen conditions [89]. These methods have the advantage of labeling the DNA of actively dividing microbes. Tuorto et al. (2014) used C^{13}-acetate to demonstrate microbial DNA replication in permafrost soils [90]. The active community members were part of *Acidobacteria*, *Actinobacteria*, *Chloroflexi*, *Gemmatimonadetes*, and *Proteobacteria phyla*, but Firmicutes were not detected with genome replication and were metabolically active, suggesting

that spore-forming members of this phylum thrive at temperatures ranging from 0 °C to -20 °C [90].

2.5.3 Genetically engineered microorganisms

Artificial consortia or genetically engineered microorganisms (GEMs) with bioremediation potential can be developed with the aid of modern molecular biology techniques [17], [91]. GEMs can be prepared in laboratory conditions by transfer of plasmids containing necessary genetic material from exogenous to indigenous microorganisms [92]. In this method, desirable biodegradation pathways or enzymes can be brought together from different microorganisms to perform specific reactions. This exogenous genetic material can include regulation and construction of novel pathways, improvement of substrate utilization without producing harmful metabolites, catabolic enzymes with more affinity and specificity, increase in bioavailability of pollutants, and improvement of genetic stability [93].

The first step to making this method successful is in selecting suitable genes. Next, recombinant DNA fragments are inserted into suitable vectors and introduced into host cells [35]. Thus, information about psychrophilic enzymes and involved genes in petroleum degradation is needed for the improvement of biodegradation in cold climates [18], [94]. Table 2.3 provides a list of some genes involved in bioremediation in hydrocarbon degradation that can be used in cold-adapted microorganisms with desired degradation properties.

Some studies showed that the presence of some genes in cold-adapted populations was more prevalent than in mesophilic populations. For instance, Whyte et al. (2002) revealed that the *alkB1* gene was more abundant in cold-adapted bacteria (5°C) in the contaminated soils from the Arctic and Antarctica. The results of Luz et al. (2004) also revealed that aromatic dioxygenase genes such as biphenyl dioxygenase (*bphA*) and toluene dioxygenase (*todC1*) were the most frequent in

Antarctica. A better understanding of these genes and their role in the biodegradation of environmental containment is needed before they will be used for GEMs.

Monoaromatic compounds such as toluene are degraded successively to benzyl alcohol, benzoic acid, and catechol which are further transformed to the tricarboxylic acid (TCA) cycle intermediates. Catechol is either oxidized by the intradiol o-cleavage, or the extradiol m-cleavage, due to two different attack locations, consequently, final products might be either (acetyl-CoA + succinate) or (acetaldehyde + pyruvate). All of these ring cleavage reactions are catalyzed by specific dioxygenases. The details of these two ring cleavage pathways can be addressed [32]. As for PAHs, bacteria generally proceed via the action of multicomponent dioxygenases to form cis-dihydrodiols. These primary metabolic are subsequently dehydrogenated to form dihydroxy-PAHs (such as catechol), which can be substrates for ring-fission enzymes that step-by-step depolymerize the compounds until their metabolite can enter other pathways. The study of enzymes is necessary to further understand the pathway in the real biodegradation reaction. So far, degradative genes have been identified and evaluated in terms of different treatment or test conditions (as shown in Table 2.3).

Table 2.3. Microbial genes involved in hydrocarbon degradation

Genes	Microorganism	Catalytic activity	Reference
BphA and *bphE*	*Pseudomonas sp.* Cam-10	Biphenyl dioxygenase	[95]
alkB	*Pseudomonas putida*	Alkane 1-monooxygenase	[96]
alkB1	*Alcanivorax borkumensis* *Rhodococcus erythropolis*	Alkane 1-monooxygenase 1	[97]

Genes	Microorganism	Catalytic activity	Reference
alkB2	*Pseudomonas citronellolis* *Pseudomonas aeruginosa*	Alkane 1-monooxygenase 2	[98]
alkM	*Acinetobacter calcoaceticus*	Alkane-1 monooxygenase	[99]
todC1 *todD*	*Pseudomonas putida*	Benzene 1,2-dioxygenase Cis-toluene dihydrodiol dehydrogenase	[100]
xylE	*Pseudomonas putida*	Catechol 2,3-dioxygenase	[101]
xylX	*Pseudomonas putida*	Toluate 1,2-dioxygenase	[102]
cat23	*Pseudomonas putida*	Catechol 2,3-dioxygenase	[103]
bphA1 *bphA2* *bphB* *bphC* *bphD*	*Pseudomonas putida*	Biphenyl dioxygenase	[104]
xylMA	*Pseudomonas putida*	xylene monooxygenase	[105]
ndoB	*Pseudomonas putida*	naphthalene 1,2-dioxygenase	[106]
nidA1	*Novosphingobium naphthalenivorans*	Naphthalene dioxygenase	[107]
phnAc *nahAc*	*Burkholderia phenazinium* *Burkholderia glathei*	naphthalene dioxygenase	[108]
benA	*Acinetobacter baylyi*	Benzoate 1,2-dioxygenase	[109]

Genes	Microorganism	Catalytic activity	Reference
cbdA	*Burkholderia cepacia (Pseudomonas cepacia)*	2-halobenzoate 1,2-dioxygenase	[110]
Anta	*Acinetobacter baylyi*	Anthranilate 1,2-dioxygenase	[109]
tftA	*Burkholderia cepacia*	2,4,5-trichlorophenoxyacetate monoxygenase	[111]

Furthermore, genetic engineering has been used successfully for the bioremediation of aromatic hydrocarbons [112]. In these reviews, recent advances in engineered biological systems by biomolecular tools were described as the exciting potential for remediating most hazardous compounds [113].

The first report of the construction of psychrophiles with specific degradative ability has been reported in 1988, and it was based on the transfer of the TOL plasmid from the mesophilic *Pseudomonas putida* to a psychrophile of the same species by conjugation; the modified bacteria could degrade toluene at temperatures as low as 0°C [114]. In another study, *tou* cluster, coding for Toluene *o*-Xylene Monooxygenase (ToMO) involved in the degradation of aromatic hydrocarbons from the mesophile *Pseudomonas stutzeri* was cloned and expressed in the Antarctic *Pseudoalteromonas haloplanktis.* They used the psychrophilic expression vector pPM4 under the control of the constitutive psychrophilic promoter P4. The results of the study showed that recombinant cells display maximal activity at the lower temperature tested (4 ◦C) [115]. In the following study by Siani et al. 2006, a research study improved the metabolic capability of recombinant Antarctic *Pseudoalteromonas haloplanktis* by combining the action of recombinant ToMO enzyme. They showed that the new recombinant cells had acquired the capability to grow on all the tested substrates such as copper and several aromatic compounds,

while the previous recombinant bacteria of Siani et al., 2006 could not grow on some of the tested substrates [116]. So far, the expression of multiple genes such as degradative genes, metal-resistant have been identified and evaluated in terms of their application for genetic engineering (Fig. 2.3) It is noticeable that biosafety and environmental risks i.e. release of GEMs in the environment needs to be considered [93]. For example, bioaugmentation with GEMs or non-indigenous microorganisms is banned in Norway, Sweden, Iceland, and Antarctica [31]. It may be due to little information about the potential impacts of modified organisms on ecology and the vulnerability of ecosystems to potentially invasive microorganisms [117].

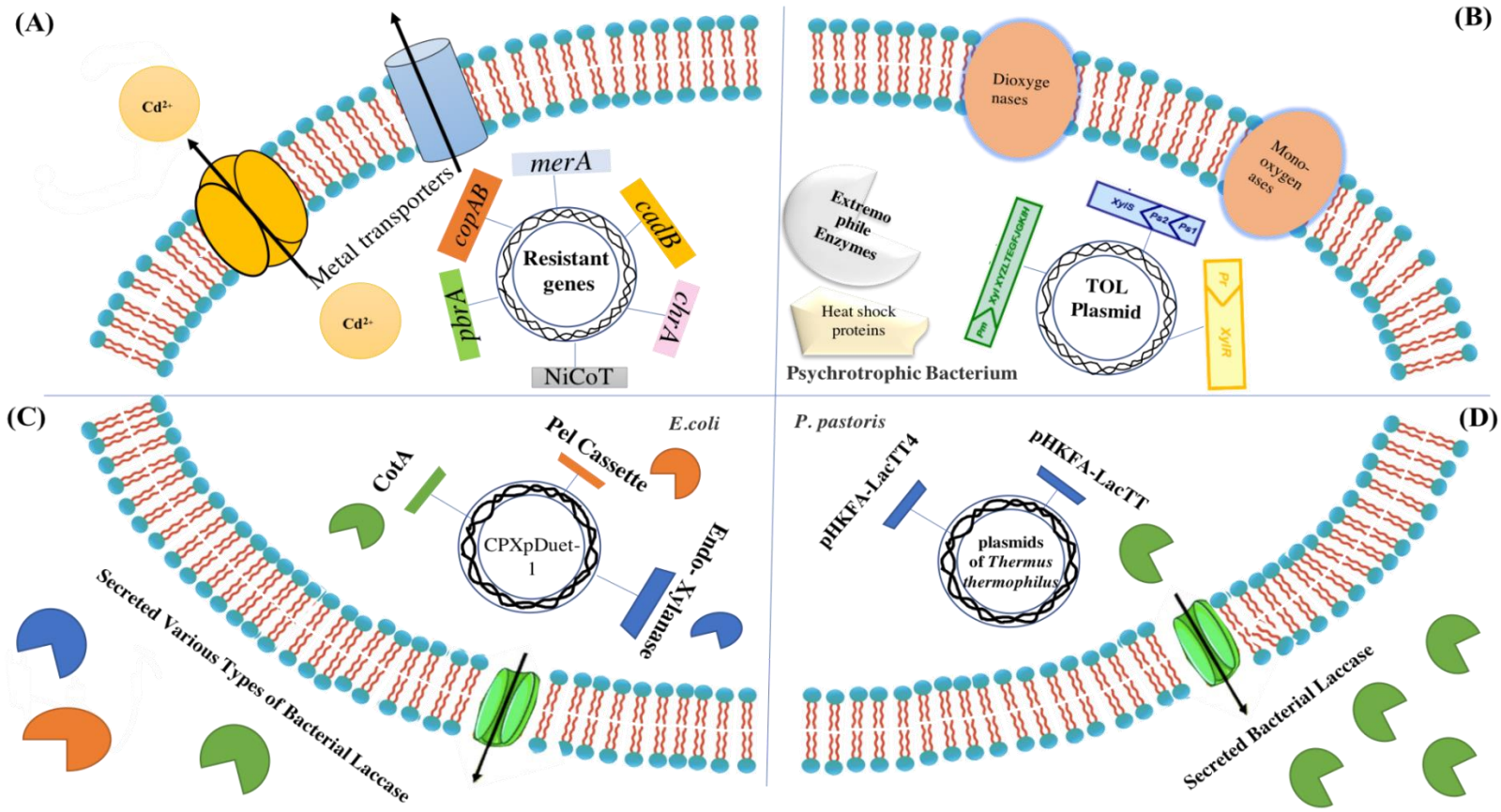

Fig. 2.3. Genetically Engineered Microorganisms (GEMs) demonstrating: (A): genetic engineering might enhance detoxification of toxic metal including nickel, mercury, lead, copper, cadmium, and chromium using construction of plasmids with a combination of different metal-resistant genes such as NiCoT , merA, pbrA, copAB, chrA and cadB. (B): biodegradative genes from a mesophilic microorganism such as *Pseudomonas putida* Q5 might be transformed by conjugation to the naturally isolated psychrophilic bacterium. (C): expression of multiple genes such bacterial laccase (CotA), endoxylanase (Xyl) and pectate lyase (Pel) in a single host and (D): overexpression of laccase from *Thermus thermophilus* might yield high laccase activity

2.6. Addition of Biosurfactants

Biosurfactants are made up of hydrophobic and hydrophilic parts and this structure can increase the bioavailability of hydrocarbons [118]. Microorganisms such as bacteria, yeasts, and fungi can produce biosurfactants, and their secretion can be induced by environmental stresses [119]. For instance, in Polar Regions, bacteria have been isolated that produce biosurfactants and can degrade hydrocarbons [120]. Biosurfactants have been reported to enhance the uptake and metabolization of petroleum hydrocarbons and their use of them is an effective method that can improve the bioremediation of hydrocarbon-contaminated environments [121]. The results of Mohanty and Mukherji (2008) demonstrated that even low-level release of biosurfactant might facilitate the development of cell surface hydrophobicity and also, lowering in surface tension in the cultures grown on diesel and n-hexadecane was over the range 0.004-0.005 mN/m. In addition, it has been reported that the addition of biosurfactants can enhance hydrocarbon biodegradation by emulsification or solubilization and mobilization [122]. Nievas et al. (2008) tested biodegradation of bilge wastes -a fuel oil-type complex residue by a microbial consortium which was emulsifier-producing bacteria. Their results showed a reduction of n-alkanes, solvent mixture, and solvent hydrocarbons around 85%, 58%, and 75% respectively [123].

To date, only a few cold-adapted biosurfactant producers have been characterized [124], [125]. Cai et al. (2014) reported fifty-five biosurfactant producers to belong to genera of *Rhodococcus*, *Alcanivorax*, *Exiguobacterium*, *Bacillus*, *Halomonas*, *Pseudomonas*, *Acinetobacter*, and *Streptomyces* from petroleum hydrocarbon contaminated sources in North Atlantic Canada. Guo et al., (2022) showed that *Planococcus* sp. XW-1 can produce biosurfactant with petroleum as sole source of carbon at low temperature (4 °C). This bacterium was also effective in degrading crude oil, after 21 days of growth at 4 °C in medium with 1% crude oil and 1% (*v*/*v*) bacteria broth, 54% of crude oil was degraded [126].

Malavenda et al. (2015) isolated Biosurfactant-producing bacteria from Arctic and Antarctic shoreline sediments. The isolates were mainly affiliated to the genera *Rhodococcus* (14 isolates), *Pseudomonas* (two isolates), *Idiomarina* (one isolate), and *Pseudoalteromonas* (one isolate) with potential applications in the remediation of hydrocarbon-contaminated cold environments. These 18 isolates were selected for their ability to grow in the presence of crude oil and produce biosurfactants, as they are characterized by the production of high emulsification index values (≥C50 %) and reduction in the surface tension (under 30 mN/m)[120].

2.7. Cold-active enzymes

In the last few years, separated enzymes from microbial sources have been used for bioremediation to overcome the limitations of the slow rate of bioremediation by the whole-cell of microorganisms [127]. Enzymatic bioremediation is improved with molecular tools and can be especially suitable for conditions where rapid remediation is needed [128]. In some studies, enzymes have been added to stimulate the degradation processes, either naturally occurring enzymes or synthetic enzymes [35]. Cold-adapted enzymes have ten-fold greater activity at low temperatures (below 20-30ºC) compared to their mesophilic counterparts [129]. It is reported that no hydrocarbon-degradative enzymes are known to have cold-adapted characteristics. For instance, biphenyl dioxygenase from an arctic isolate demonstrated activity at 4°C but did not have cold-adapted enzyme structures. Psychrophilic and psychrotolerant microbes utilize cold-adapted proteins to bind nucleic acids to compensate for the limitations of temperature-imposed [130]. The involved enzymes in the biodegradation of petroleum products are listed in Table 2.4 however no cold-active enzymes have been reported so far.

Table 2.4. Enzymes involved and their function in the biodegradation of petroleum hydrocarbons

Category of Enzyme	Name	Target contaminant	Function	Microorganism	Reference
Mono-oxygenase	Methane-monooxygenase	Methane-butane, short-chain-length alkanes; C2-C4	oxidizing the C-H bond in methane as well as other alkanes	*Methylococcus Methylosinus Methylocystis Methylomonas*	[131]
	xylene mono-oxygenases	BTEX	Oxidizing the aromatic ring	*Rhodococcus Pseudomonas*	[132]
	P450 oxygenase system	C_5–C_{16} alkanes, cycloalkanes	C_5–C_{16} alkanes, cycloalkanes	*Acinetobacter Caulobacter Mycobacterium*	[133]
	Alkane 1-monooxygenase	Oil contaminants, Aliphatics	oxidizing the C-H bonds	*Pseudomonas*	[98]
Di-oxygenase	Benzene 1,2-dioxygenase	BTEX	Oxidizing the aromatic ring	*Pseudomonas putida*	[134]
	Naphthalene 1,2-dioxygenase	Naphthalene	Catalyze both atoms of molecular oxygen into naphthalene to form cis-(1R,2S)-dihydroxy-1,2-dihydronaphthalene.	*Pseudomonas putida*	[135]

	Catechol 2,3-dioxygenase	Catecholic intermediates	Oxidizing the aromatic ring	*Pseudomonas putida*	[136]
	Catechol 1,2-dioxygenase	Catecholic intermediates	Oxidizing the aromatic ring	*Mycobacterium fortuitum*	[137]
	Toluate 1,2-dioxygenase	p-Toluate m-Toluate o-Toluate 3-Chlorobenzoate	Oxidizing substrate-ringe	*Pseudomonas putida*	[138]
	Biphenyl dioxygenase	polychlorinated biphenyls (PCB)	Catalyze the initial oxygenation of biphenyl	*Pseudomonas putida*	[138]
	2-halobenzoate 1,2 dioxygenase	2-chlorobenzoate (2CB) and benzoate (BA)	Catalyze the oxygenation BA	*Pseudomonas putida*	[104]
	2,4,5-trichlorophenoxyacetate monoxygenase	Chlorinated aromatic compound	Catalyze the oxygenation of aromatic ring	*Acinetobacter baylyi*	[109]
Hydroxylase	Alkane Hydroxylases	C_5–C_{16} alkanes, fatty acids, alkyl benzenes, cycloalkanes	hydroxylate alkanes to alcohols, which are further oxidized to fatty acids and catabolized via the bacterial β-oxidation pathway	*Pseudomonas* *Burkholderia* *Rhodococcus* *Mycobacterium*	[139]

Bioremediation in aquatic environments is limited primarily by nutrients, such as phosphorus (P) and nitrogen (N); salinity in estuarine and pressure in deep-sea. Furthermore, nutrient concentrations, oxygen, moisture, and pH-value are determining factors in the biodegradation rates of soil [21]. Hence, using enzymes rather than whole-cell degrading microorganisms has recently received increasing attention since the enzymatic method can specifically catalyze a series of reactions for pollutant removal without nutrient factors [140]. A further advantage of the enzymatic method is a shorter treatment period than the microbial process because the enzymes transform the substrate in a minute timescale. Moreover, enzymes demonstrate high specificity for their substrate. Thus, the enzymatic treatment agent can be designated for specific pollutant removal [141]. This technique can be applied to contaminants that are catalytically decomposed in stepwise oxidation reactions by various oxidoreductases. For example, Kwean *et.al* applied a combination of oxidative enzymes such as chlorophenol monooxygenases, phenol 4-monooxygenase, putative flavin reductase, and dioxygenase, for the enzymatic degradation of 4-Chlorophenol [13]. Gulloto et. al studied the combined action of toluene o-xylene monooxygenase

to convert mono- and di-polyaromatic hydrocarbons into hydroxylated derivatives and fungal laccase to oxidize their hydroxylated derivatives for complete detoxification [142].

Concerning the challenges in bioremediation of cold-climate groundwater and soil, injection of cold-active enzymes (psychrozymes) directly into the contaminated environment can be promising new methods for increasing the bioremediation rate and decreasing the environmental risks of introducing bacteria and their potential impacts on the ecological system of cold climate regions. To the best of our knowledge, this study is the first report on psychrozymes for petroleum hydrocarbon degradation [6].

However, the high production cost of enzymes has restricted their widespread use of them for remediation purposes [14].

2.7.1. Immobilization

The immobilization method can be used either for enzymes or whole cells. Immobilization is defined imprisonment of cells or enzymes in distinct support or matrix. For example, Su et al., (2021) co-immobilized cold-adaptive fungal-bacterial consortium including *Pseudomonas* sp. SDR4 and *Mortierella alpina* JDR7 for application in remediating PAHs contaminated freeze-thawed soil [143]. To large extent commercialization of these bio-derived catalysts, and their reusability factor becomes mandatory, failing which they would no longer be economic. The use of immobilized enzymes for degradation of the contamination may prove economical because of their stability and reused multiple times [144]. Dodor et al. (2004) demonstrated that immobilized laccase from *Trametes versicolor* can catalyze the oxidation of PAHs. A system with immobilized laccase oxidized more than 80% of PAHs present (initial concentration of 70 μM) during 24 h of incubation. They also showed that the broadened temperature stabilities for immobilized laccase-after one hour of preincubation at 20–50 ◦C, the immobilized enzyme retained 100% of its initial activity, whereas the free laccase had between 60–35% of its activity under the same condition [145]. Moreover, immobilized enzymes show activity in a wide range of pH, thus the stability of enzymes can be enhanced by immobilization [146]. There is no report about immobilized enzymes in bioremediation of cold climate regions, there appears to be a research gap regarding this topic.

The biodegradation rate depends on the physical factors of the environment and the physiological state of the microorganisms. It is proven that the immobilization method can improve microorganisms' resistance to unfavorable, negative, and toxic environmental impacts [147]. For example, Xin et al. (2013) used bioaugmentation with *Mycobacterium* sp. and *Pseudomonas* sp.

immobilized beads in bioremediation of BTEX-contaminated groundwater. Their results showed the maximum biodegradation rates were achieved in the system of the immobilized beads; 97.8% for benzene, 94.2% for toluene, 84.7% for ethylbenzene, and 87.4% for p-xylene. While Daghio et al. (2015) showed the addition of selected immobilized microorganisms did not lead to an increase in hydrocarbon removal. The author proposed that this different behavior could be due to the immobilization of the microbial inoculum on the different support materials [148].

There are different materials available for immobilization, but every material is not suitable. A suitable carrier should be non-toxic for both microbial cells and the environment, insoluble, stable, inexpensive, easily accessible, and suitable for regeneration. Carriers are mostly classified as organic and inorganic. Organic carriers can be also divided into natural and synthetic polymers [149]. The choice of support materials is a determining factor in removal efficiency and could enhance the degradative activity and promote the persistence of external inocula [150]. Some support materials for use in biodegradation compounds are given in Fig. 2.4.

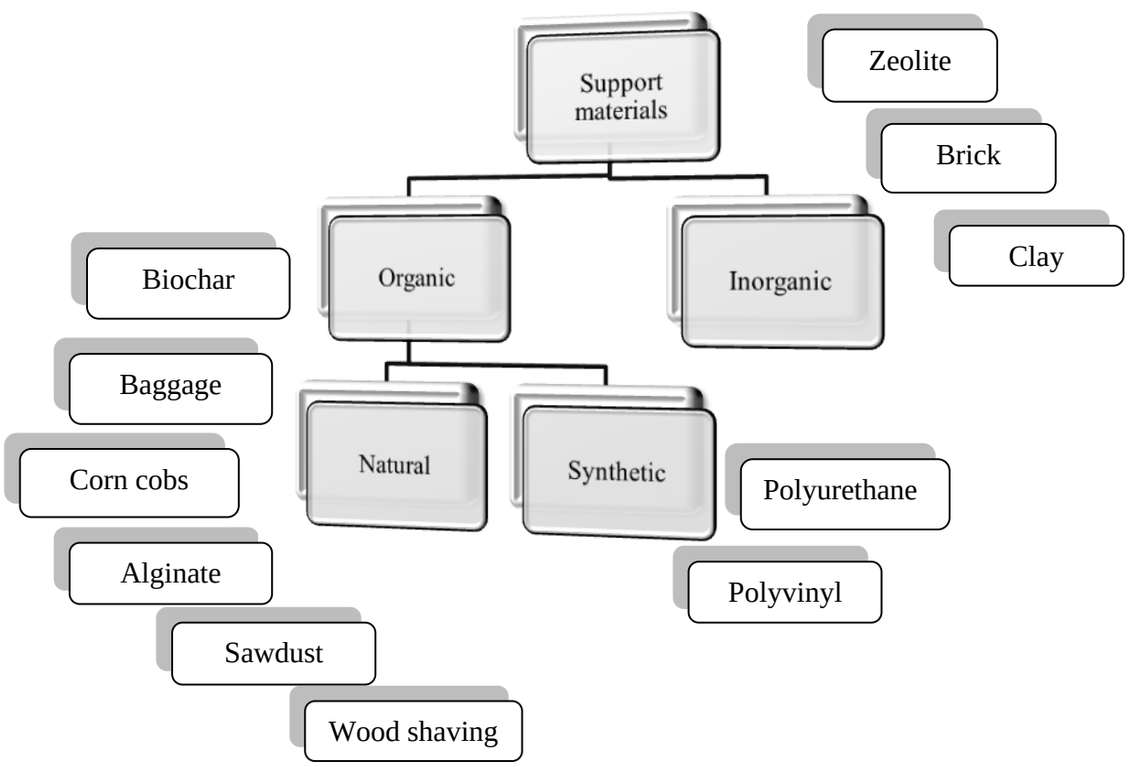

Fig. 2.4. Classification of support materials as carriers for biodegradation

Podorozhko et al. (2008) demonstrated that sawdust is a suitable carrier for the efficient immobilization of *Rhodococcus ruber* as a cold-adapted and hydrocarbon-oxidizing bacterium. Their result showed that highly hydrophobized sawdust was able to accumulate over 70% of n-hexadecane from water medium due to physical adsorption of the carrier, while the same values

for other carriers varied from 10% to 30% depending on the hydrophobicity degree of material [151].

Synthetic organic carriers include polyvinyl, polypropylene, polystyrene, chloride, polyurethane foam, polyvinyl alcohol, and polyacrylonitrile. This class of carriers can be easily formed into various shapes and sizes. Krallish et al. (2006) showed that immobilization on a solid carrier with 2-4 mm in diameter improved phenol degradation by psychrophilic yeast strains of *Rhodotorula creatinivora* and *Cryptococcus terreus*. Phenol degradation by yeast strains attached to solid carriers of zeolite or filter sand was tested at 10°C. The results showed phenol degradation by immobilized yeast strains was always higher on zeolite compared with filter sand [152].

To date, most of the studies for immobilization on bioremediation have generally focused on the performance of immobilized bacteria at moderate temperatures. Dzionek et al. (2016) reviewed the information of recent research on immobilization and found the potential to utilize immobilized single species or consortium of bacteria as a technology to clean up petroleum-contaminated sites. Furthermore, Bayat et al. (2015) focused on the immobilization of microbial cells for the biodegradation of petroleum hydrocarbons in their review. In the mini-review, degradation of oil pollution with immobilized cells was compared to free-living bacterial cells. It was shown that immobilized microbial cells have better and faster performance [149].

On the other hand, the immobilization method affects other factors involved in bioremediation. For example, Hazaimeh et al. (2014) reported that immobilization can significantly increase the production of biosurfactants by a consortium of bacteria which increased the solubility and bioavailability of pollutant hydrophobic hydrocarbons [153].

2.8 Future perspective and conclusion

Recently, several studies have shown that the coldest regions of the earth are heavily exposed to oil-based contaminants [68]. Petroleum-oil products are carcinogenic, mutagenic, potent immune-toxicants, and detrimental to the ecosystem [2]. In the last few years, oil pollution has created serious environmental problems and alarming threats in northern Russia, Canada, Alaska, and the Qinghai Tibet Plateau [78]. Therefore, it is of the utmost importance to implement appropriate clean-up strategies in these low-temperature environments.

p-xylene is a volatile solvent, it can enter surface water, soil, or air in large amounts as a result of an accidental spill during storage and burial at waste sites. Since p-xylene evaporates easily, it is

rarely found in high concentrations in surface water or topsoil, but any p-xylene that does not evaporate from topsoil can travel downward and enter groundwater [6]. There are physical, chemical, thermal, and biological techniques available for removing petroleum hydrocarbons [6]. Physical methods include soil excavation, soil washing, vitrification, and air sparging [28]. Techniques such as solvent extraction, chemical oxidation and reduction, stabilization, and electrochemical process are chemical methods [135]. The thermal technique implements steam injection, temperature elevating, and conductive heating. The biological method includes biostimulation, bioaugmentation, and using biosurfactants and enzymes [28]. All of these techniques possess some limitations and barriers to proper implementation. The cost and feasibility of the techniques, the nature of the contaminants, and the release of intermediate products after remediation should be considered when selecting a remediation method. In low-temperature regions, petroleum hydrocarbons remain in the soil longer than they do in warmer regions [62]. Low bioavailability and harsh climatic conditions contribute to the prolonged stay of oil hydrocarbons in polar soils [138]. In cold regions, it is convenient to implement a biological-based remediation process during the warm season. Among the available treatment methods, one decontaminating technique that is effective at low temperatures is bioremediation which utilizes psychrophiles in oil-polluted sites.

In cold regions, it is convenient to implement a biological-based remediation process during the warm season. Among the available treatment methods, one decontaminating technique that is effective in low temperatures is bioremediation which utilizes cold-active bacteria in oil-polluted sites. Bioremediation is an eco-friendly way to accelerate natural degradation rates by optimizing limiting factors [35]. Unfortunately, microbial activities are usually hindered at low temperatures, which slow the bioremediation process [154]. The rate of degradation retards as the temperature decreases [53].

Several bioremediation strategies for enhancing microbial activity during the degradation of oil-contaminated soil at low temperatures have been employed. However, studies on these methods such as the use of biosurfactants, cold-adapted enzymes, and immobilization methods are still limited.

Using enzymes as an advanced biological method rather than whole-cell degrading microorganisms has recently received increasing attention since the enzymatic method can specifically catalyze a series of reactions for pollutant removal without nutrient factors [140]. One

of the main advantages of the enzymatic method is a shorter treatment period than the microbial process because the enzymes transform the substrate in a minute timescale. Moreover, enzymes demonstrate high specificity for their substrate. Thus, the enzymatic treatment agent can be designated for specific pollutant removal [141]. But, adequate information regarding this field is still underdeveloped compared to studies of bioremediation in tropical and temperate regions. This study will help identify limitations in our current understanding of using enzymes as a biotechnological process that prevent them from being incorporated into applications.

CHAPTER THREE: METABOLIC and CO-METABOLIC BIODEGRADATION of p-XYLENE

PART 1

3.1 Precision Modelling of Co-metabolic Biodegradation of Recalcitrant Aromatic Hydrocarbons in conjunction with experimental data

Saba Miri[1,2], Seyyed Mohammadreza Davoodi[1,2], Mohammad Hossein Karimi Darvanjooghi[1], Satinder Kaur Brar[1, 2*], Tarek Rouissi[2], Richard Martel[2]

1. Department of Civil Engineering, Lassonde School of Engineering, York University, North York, Toronto, Ontario M3J 1P3, Canada
2. Institut national de la recherche scientifique, Centre-Eau, Terre et Environnement, 490, Rue de la Couronne, Québec G1K 9A9, Canada

(*Corresponding author, E-mail E-mail: satinder.brar@lassonde.yorku.ca; satinder.brar@ete.inrs.ca)

Process Biochemistry, 105, 113-127; DOI: 10.1016/j.procbio.2021.03.026

Abstract

The co-metabolic biodegradation of p-xylene (as a non-growth substrate model) by *Pseudomonas putida* (well-known aromatic compounds degrading microorganism) in the presence of Benzene (B), Toluene (T), and Ethylbenzene (E) was studied. Michaelis-Menten/Monod kinetics coupled with co-metabolic degradation expression can be applied for systems containing one growth and one non-growth substrate; thus, the GMDH Group Method of Data Handling (GMDH) was proposed in this study to predict the co-metabolic transformation of non-growth substrates in the presence of more than one growth substrate. Thus, the GMDH Group Method of Data Handling (GMDH) was proposed for the first time to quantify p-xylene degradation (with < 10 % deviation) for the co-metabolic system. GMDH could predict the biomass and *p*-xylene concentration changes in the co-metabolic system without the need for kinetic and interaction parameter determination, while the determination of these parameters is needed for Michaelis-Menten/Monod model. Furthermore, mass balance and enzyme study confirmed the co-metabolic biodegradation of p-xylene in the presence of growth-substrates. This study proved the potential use of the GMDH model for the prediction of co-metabolic degradation; however, further study is needed for other non-growth contaminants to generalize this model.

Keywords: co-metabolism, biodegradation, *Pseudomonas putida*, modelling, GMDH.

Graphical Abstract

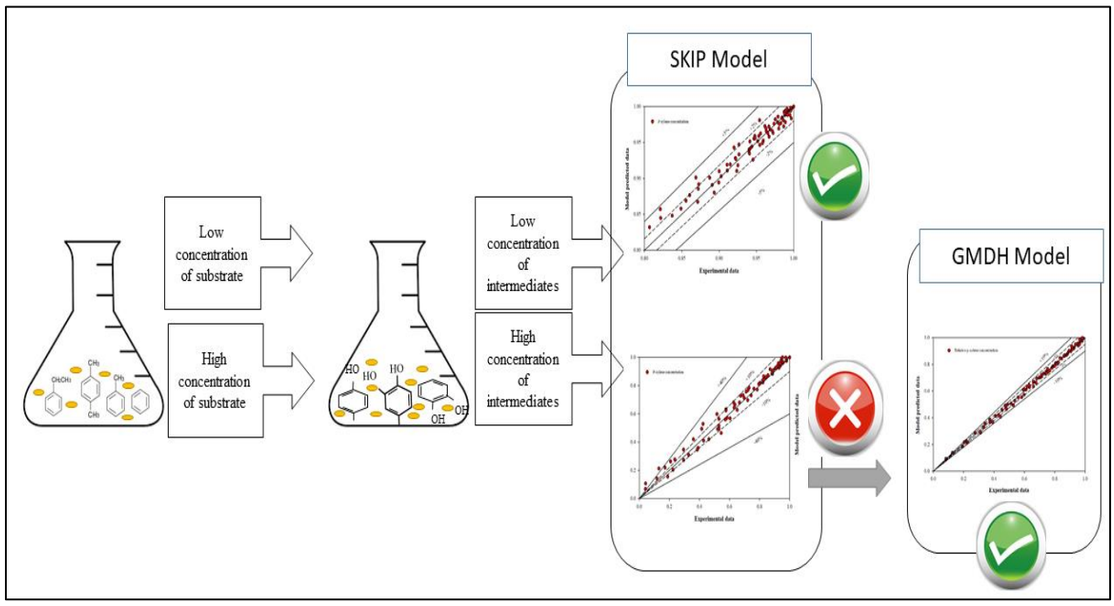

Nomenclature

$\mu_{\max i}$	Maximum specific growth rate of substrate i (h^{-1})
K_I	Inhibition constant (mg/L)
K_{s_i}	Half saturation constant for growth substrate (mg/L)
I_{ji}	Interaction parameter for the effect of substrate j on substrate i
Y_{X/S_i}	Biomass yield (mg cells/mg growth substrate)
${T_g}^C$	Growth substrate transformation yield (mg of co-metabolic substrate/mg of growth substrate)
K_{Ic}	Inhibition constant (mg/L)
K_{sc}	Half saturation constant for non-growth substrate (mg/L)
${T_c}^b$	Biomass capacity
k_c	Maximum specific rate of co-metabolic substrate degradation (mg cells)$^{-1}$ d^{-1}
Y_{X/S_g}	Apparent diffusion coefficient (cm^2/s)
b	First-order endogenous decay coefficient (s^{-1})
p_b	Partial vapor pressure (bar)
P_b	Saturate vapor pressure (bar)
γ_b	Activity coefficient

3.1.1. Introduction

p-xylene is one of the toxic and volatile organic compounds in petroleum products and is mainly used as a solvent for the manufacturing of chemicals. *p*-xylene is frequently found in groundwater and soil due to leaks, leaching from landfills, and improper waste disposal. Research so far has focused on the BTEX (benzene, toluene, ethylbenzene, xylene isomers) biodegradation; however, especially for *p*-xylene compared to other compounds, the lower degradation rate for xylene isomers has been reported as a result [2], [155]. Several studies showed low or no degradation of p-xylene in BTEX-degrading strains, such *Pseudomonas* B1 and X1 [156], *Pseudomonas stutzeri* OX1 [157], *Pseudomonas sp.* BTEX-30 [158], *Pseudomonas putida* AQ8 [159]. However, literature that studied the substrate interaction during aerobic biodegradation of BTEX compounds in saturated hydrodynamic groundwater system reported a lower concentration of p-xylene near the source of BTEX contaminant plume whereas the higher concentration was detected farther downgradient of the source. This observed beneficial effect of BTEX compounds on p-xylene biodegradation was also detectable in batch systems and was attributed to cometabolism of p-xylene while growing on BTE compounds [160].

Co-metabolism has recently emerged as a powerful method for the biodegradation of compounds where microorganisms cannot grow on them as a sole carbon source [161], [162]. During the growth phase in the co-metabolic system., the microorganisms consume growth associated substrates and produce enzymes that can fortuitously transform the non-growth substrate. Some studies reported co-metabolism of p-xylene in presence of other BTE compounds. For example, Chang et al. reported the co-metabolic degradation pattern for p-xylene in presence of toluene by *Pseudomonas* strain B1. Attaway & Schmidt showed that *Pseudomonas* strain BTE1co-metabolized p-xylene in presence of toluene as growth substrate [162].

To understand the behavior of co-metabolic degradation and the fate of non-growth substrates in the environment, inhibition and substrates interaction studies are important. To evaluate the relationship between xylene degradation rate and the biomass concentration on growth substrates, mathematic models was studied using different kinetic models such as the co-metabolic process-based model [163]. For instance, Chan *et.al* proposed a model to describe the kinetic of co-metabolism in the biodegradation of p-xylene in the presence of toluene (TX) or benzene (BX). They mentioned that this model should be applied with care due to the complex enzymatic interactions. However, some literature applied Michaelis-Menten/Monod kinetics coupled with

co-metabolic degradation expression to predict the concentration of p-xylene in presence of more than one growth substrate that might not be theoretically correct [163], [164].

Nowadays, artificial intelligence approaches have been utilized for modeling biological processes, as these models can be generated more accurate outcomes for mixed-substrate utilization than unstructured growth kinetic models. For example, the Group Method of Data Handling (GMDH) neural network is a sub-model of artificial neural network which has been used for the design and optimization of other bioprocesses such as the fed-batch biodegradation. This method can be applied to estimate growth substrate utilization and co-metabolic substrate transformation [165]. By replacing Monod kinetics, Tsipa *et.al* studied the application of a novel experimental-modeling gene regulatory network-growth kinetic (GRN-GK) hybrid framework and showed that the GRN-GK model predicted the biomass yield extremely close to the experimentally observed yield while the traditional models failed to predict the biomass yield accurately [166].

Horvath *et.al* reported the importance of enzyme study, substrate disappearance, and accumulation of end products (transformed non-growth substrate) for interpretation of co-metabolic experimental results [167]. For example, analogue enrichment might fail to stimulate p-xylene degradation or non-analogue enrichment might increase the degradation of pollutants [168]. Other studies also reported increased endogenous respiration of the test organism in the presence of certain hydrocarbons without being oxidized [167]. Such observations indicate that co-metabolism requires considerable care [167]. Herein, this study provided clear-cut evidence on intermediates, carbon mass balance, and involved enzymes in the co-metabolic system to explain the main reason for the observed deviations obtained using the GMDH network from experimental values. In this research paper, the inhibition modified SKIP model as well as Group Method of Data Handling (GMDH) were used to predict the co-metabolic transformation of p-xylene (as a resistant pollutant for biodegradation). As reported in the literature, application of Michaelis-Menten/Monod kinetics coupled with co-metabolic degradation expression to predict the concentration of p-xylene in presence of more than one growth substrate might be theoretically incorrect [156]; thus, GMDH models were applied for the first time for co-metabolic transformation quantification of mixed-substrate systems (i.e., BTEX, BTE,). Moreover, the deviation of predicted results from experimental values was explained by the carbon mass balance study. The activity of involved enzymes and the accumulation of intermediates were evaluated to explain co-metabolism phenomena in detail.

3.1.2. Materials & Methods

Chemicals

Tryptic soy broth (TSB), dibasic potassium hydrogen phosphate (K_2HPO_4), glucose, and agar were purchased from Fisher Scientific (Ontario, Canada). Benzene, toluene, ethylbenzene, *p*-xylene (99.9%), methanol (chromatographic grade) and the standard substances were purchased from Sigma-Aldrich (Mississauga, Ontario, Canada). All chemicals were obtained in analytical grade as commercially available and without further purification. Millipore system (Milford, MA, USA) Milli-Q/Milli-RO was used for HPLC grade water preparation.

Biodegradation and Kinetic experiments

Minimal Salt Media (MSM) was prepared by dissolving 1.8 g/L K_2HPO_4, 4.0 g/L NH_4 CI, 0.2 g/L $MgSO_4.7H_2O$, 0.1 g/L NaCl, 0.01 g/L $FeSO_4$. $7H_2O$ in distilled water [169]. Kinetic degradation of total concentrations (50 and 200 ppm) of *p*-xylene, toluene, and benzene, ethylbenzene were studied in 25 mL of MSM in a 150 mL serum bottle sealed with Teflon rubber septa. In total, 8 batch degradation tests were done for kinetic experiments: 4 single component batch biodegradation for each of toluene, benzene, ethylbenzene and p-xylene, 3 dual substrate batch degradation of benzene and p-xylene, toluene and p-xylene and ethylbenzene and p-xylene, one batch degradation with all BTEX components present. Other literature reported incomplete BTEX biodegradation at high initial concentration due to oxygen depletion in the culture media; thus, the headspace required to supply for growth of bacteria has been calculated (Supplementary material Appendix 1, S.1). The mixture was then incubated at 30ºC on a rotary shaker at 150 rpm. These conditions were selected based on optimum growth and aerobic BTEX biodegradation using *P. putida* [26], [159], [170], [171]. The compounds for each experimental run were added in amounts to obtain an approximate total of 50 and 200 mg/L in the liquid phase.

After the growth in a batch reactor in MSM containing 50 ppm of growth substrates and after around 20, 40 and 60 h that growth substrates (toluene, benzene and ethylbenzene) were degraded, the reactor was stopped. Then, the suspended cultures were transferred to the tubes, centrifuged and washed with mineral medium and centrifuged again. The resting cell transformation experiments were performed at a constant cell concentration of 1500 ppm for the initial p-xylene concentration (50 and 200 ppm). To model the process of co-metabolic transformation of *p*-xylene, it is necessary to perform three series of experiments: 1) the study of benzene, toluene, and

ethylbenzene degradation by the tested strain to obtain the values of $\mu_{max\,i}$(maximum specific growth rate of growth substrate i (h^{-1})) , K_I (inhibition constant (mg/L)) ,K_{s_i}(half saturation constant for growth substrate (mg/L)), Y_{X/S_i}(biomass yield (mg cells/mg growth substrate)) and I_{ji} (interaction parameter for the effect of substrate j on substrate i); 2) the study of *p*-xylene co-metabolic transformation in the presence of benzene, toluene, and ethylbenzene to determine the value of $T_g{}^C$ (Growth substrate transformation yield (mg of cometabolic substrate/mg of growth substrate)) 3) the study of *p*-xylene transformation by substrate-induced *P. putida* in the resting phase to determine the values of K_{Ic}(inhibition constant (mg/L)), K_{sc} (half saturation constant for non-growth substrate (mg/L)), b (first order endogenous decay coefficient (s^{-1})), $T_c{}^b$ (biomass capacity) and K_c (maximum specific rate of co-metabolic substrate degradation (mg cells)$^{-1}$ d^{-1}) [164]. As BTEXs are considered highly volatile compounds; only about 50-60 % of the initial concentration can be detected in the liquid phase. Thus, the needed concentration in the system was measured and added to obtain the remaining 50 and 200 ppm of contaminants in the liquid phase.

Analytical methods

Static headspace gas chromatography was used to measure BTEX concentrations directly in the gas phase, and liquid phase concentrations were calculated using Henry's Law (Supplementary material Appendix 1, S.2) [172]. Chang *et al*. reported that transferring inoculum to the bottle leaving at least 150 ml of headspace, shaken on a rotary shaker at more than 100 rpm resulted in a higher rate of mass transfer of BTEX between the gas and aqueous phases than the maximum biodegradation rate ensuring rapid equilibrium with the liquid phase [156]. Thus, mass transfer phenomena cannot slow down the kinetics of biodegradation under these conditions and aqueous concentration can be measured indirectly by the determination of gas-phase concentrations. However, liquid phase concentration of compounds in different systems were directly measured using gas chromatography coupled with a headspace sampler.

Samples (50 µL) were collected from sealed bottles using a gas-tight sampling syringe directly into the 40 mL headspace bottle containing 5 mL of ultrapure water, 10 µL of fluorobenzene-D5 (100 mg/L diluted in methanol) as internal standard and it was then sealed immediately. The concentration of *p*-xylene was analyzed based on EPA 8021B method and extracted by a Perkin Elmer Turbomatrix HS-40 trap automatic headspace sampler. The gas-phase of samples were quantitatively analyzed using 7890A Gas Chromatograph (DB-1701 column 30m×0.25 mm

i.d.×0.25µm film thickness). Column and detector were maintained at 45 ºC and 300 ºC, respectively. The bacterial growth was monitored by measuring the OD (optical density) at 600 nm with a spectrophotometer. To correlate OD600 values with cell dry weight (DCM), the slope of the plot of OD600 versus DCM was applied. The initial cell concentration was considered around 2 for the inoculation of samples. The OD value was then converted to dry cell mass (DCM) using the equation: DCM (mg/L) = 303.9 × OD600.

Quantification of p-xylene co-metabolic transformation in the presence of one growth substrate

The growth phase (single and dual substrate systems)

For batch degradation, biomass growth can be described by Eq. (1) [163], which can describe biomass growth due to a single or dual growth associated substrates.

$$\frac{1}{X}\frac{dX}{dt} = \mu \qquad (1)$$

The consumption of growth associated substrates in a batch degradation present alone, in a mixture and co-metabolic systems during the growth phase can be described using Eq. (2) [163].

$$-\frac{1}{X}\frac{ds_g}{dt} = \frac{\mu_{xg}}{Y_{X/S_g}} \qquad (2)$$

Transformation of Eq.1 describing the kinetics of microbial growth into the equation representing the rate of substrate biodegradation (Eq. (2)) requires a knowledge of the biomass yield coefficient, Y_{X/S_g}. The value of Y_{X/S_g}, the biomass yield coefficient, was determined for each growth substrate by monitoring the changes in the concentration of substrates and biomass over time for different initial concentrations. The integral average of the experimentally determined biomass yield coefficients was applied as discussed elsewhere [173].

There are several models to describe the specific growth rate for use in Eqs. (1) and (2). Monod and Andrew models are the most common ones used for the biodegradation of a single growth substrate shown as follows [163].

$$\mu_{x_g} = \frac{\mu_{max_g}\, s_g}{K_{sg}+s_g} \qquad (3)$$

$$\mu_{x_g} = \frac{\mu_{max_g} S_g}{K_{sg} + S_g + \frac{S_g^2}{K_{Ig}}} \quad (4)$$

where μ_{max} is the maximum specific growth rate (h^{-1}), K_{s_g} is the saturation coefficient (mg/L), K_{Ig} inhibition coefficient (mg/L) and S_g is the substrate concentration (mg/L). Due to the possibility of substrate inhibition especially in the case of ethylbenzene, a modified Monod model, the Andrew model, shown as Eq. (4) [163] could provide a better fit to experimental data obtained from single substrate experiments. Initial estimation of the value of each kinetic parameter (μ_{max}, K_{s_i}, and K_I) was determined through pure culture experiments by fitting the Andrew and Monod models to single substrate experimental data using Swarm Optimization (PSO) global search method (Supplementary material Appendix 1, S.3). These parameters can be applied for co-metabolic transformation in the presence of toluene, benzene or ethylbenzene provided that total concentration is the same for a single or double system. Fig. A1 shows the schematic diagram of the proposed protocol for the calibration of the models. Following single substrate biodegradation experiments, bi-component mixtures were examined to characterize growth substrate and nongrowth substrate interactions in the co-metabolic systems. Different models have been applied such as sum kinetics with interaction parameters (SKIP model), to describe the specific growth rate during the degradation of multiple interacting substrates as given by Eq.(5) [163]

$$\mu_{x_g} = \frac{\mu_{max_g} S_g}{K_{sg} + S_g + I_g S_I} \quad (5)$$

Where S_I (mg/L), and I_g are the concentrations of non-growth substrate and interaction parameter, respectively. This model accounts for substrate interactions without directly specifying the type of interaction. The parameters for the SKIP model can be estimated by fitting Eq. (5) to experimentally obtained specific growth rates using the PSO method. When substrate "I" does not have any impact on the degradation of substrate "g", the interaction term (I_g) for the latter substrate is simply set to zero. The interaction parameter less than zero also demonstrates that the degradation of the substrate "I" is enhanced in the presence of substrate "g".

Finally, co-metabolic substrate transformation due to the degradation of growth substrate can be expressed as follow [163]

$$-\frac{1}{X}\frac{ds_N}{dt} = (T_g{}^C\ (-\frac{1}{X}\frac{ds_g}{dt}) + K_c\ )\ (\frac{S_N}{S_N + K_{Sc}}) \quad (6)$$

Where $T_g{}^C$ is defined as the growth substrate transformation yield (mg of co-metabolic substrate/ mg of growth substrates), K_c is the maximum specific rate of co-metabolic substrate degradation (mg substrate (mg cells)$^{-1}$ d^{-1}), K_{Sc} is the half-saturation constant for the co-metabolic substrate (mg L^{-1}), S_g is the liquid substrate concentration (mg/L), X is the active microbial concentration (mg/L), and Y_{X/S_g} is the yield coefficient (mg cells/ mg growth substrate). In this model, the rate of co-metabolic transformation is proportional to the concentration of the non-growth substrate (e.g., $\frac{S_N}{S_N+K_{Sc}}$), the half-saturation constant (K_c) and the rate of growth-substrates oxidation.

For the case of co-metabolism, Chang et.al (1993) introduced an expression that incorporated reducing energy consideration into a modification of the saturation kinetic model [156] as given in Eq.(6) ($T_g{}^C$ ($-\frac{1}{X}\frac{ds_g}{dt}$)).

The value of $T_g{}^C$ depends on the initial ratio of growth substrates and co-metabolic concentration that can be determined by drawing a graph of changes in the non-growth substrate versus the concentration of growth substrates in one single culture. The slope of the straight line approximating the experimental data determines the value of $T_g{}^C$. The comprehensive co-metabolic model includes substrate toxicity and other inhibition terms for the growth substrate rate ($\frac{ds_i}{dt}$), as stated in Eq. (6). However, the combination of SKIP and co-metabolic models for a mixture system of more than two components are not theoretically correct. Moreover, the confidential interval of fitting parameters was determined using the partial derivatives using an Excel solver.

The resting cell phase

For quantifying co-metabolism, the *p*-xylene transformation should be studied to determine K_{Ic}, K_{Sc} and K_c in the presence of growth-substrate induced cells (e.g., $\frac{ds_i}{dt}=0$) [164]. The equations describing the experimental profiles of changes in biomass concentration and the specific transformation rate of *p*-xylene by resting cells of *P. putida* take the form of Eqs. (7) and (8) [164]:

$$-\frac{1}{X}\frac{ds_N}{dt}=\frac{S_N K_c}{K_{sc}+S_N+\frac{{S_N}^2}{K_{Ic}}} \quad (7)$$

$$\frac{1}{X}\frac{dX}{dt}=-\frac{q_c}{T_c{}^{b*}}-\mathrm{b} \quad (8)$$

Where b is the first-order endogenous decay coefficient (s^{-1}) and $T_c{}^{b*}$ is true biomass transformation capacity. Hao *et.al* (2002) reported that non-growth substrates might act as a self-

inhibitor and the Andrew model was applied to describe the specific transformation rate by resting cells of *Acinetobacter* sp [156], [174] (Eq.7). In Eq. (8), the first and second expressions incorporated terms for the loss of microbial biomass caused co-metabolism ($\frac{q_c}{T_c{}^{b*}}$) and autoxidation (b, endogenous decay), respectively. In the absence of the growth substrate, the true biomass transformation capacity, $T_c{}^{b*}$, is defined as the mass of p-xylene that would be transformed by the unit mass of pure culture when b = 0. In this study, the value b= 0 was assumed in the calculations that is consistent with other literature [175]. Thus, T^b was the only parameter determined by fitting the experimental profiles of changes in p-xylene and biomass concentration (the slope of the straight line). Then K_c, K_{sc} and K_{IC} were determined by solving the system of Eqs. (7) and (8).

Quantification of p-xylene co-metabolic transformation in the presence of more than one growth substrate

Some literature applied previously mentioned kinetic models (i.e., a combination of SKIP and co-metabolic models) for BTEX components; however, these models are theoretically proposed for dual substrate experiments containing p-xylene and one growth substrate [163]. In this study, the GMDH model was used to evaluate the relation between the input variables (i.e., initial concentration of growth/nongrowth substrates) and output variable (i.e., p-xylene concentration during the time) in the presence of both growth substrates and growth-substrate-induced cells in the resting phase [174].

GMDH-based Neural Network model

The GMDH Shell (GMDH Shell DS 3.8.1) software was used for forecasting the relation between p-xylene concentration and biomas over the time using Group Method of Data Handling (GMDH) algorithm. GMDH Shell also uses the learning algorithm of GMDH, which is based on the knowledge discovery approach of Ivakhnenko [176]. GMDH Shell is used as a tool for real-world data sets and targets different topics like knowledge discovery, predictive analytics, and forecasting software of time series, classification, regression, data-mining tools, and prediction [177]**.** The GMDH algorithm that included a set of data with several inputs and one output to model complex systems was first used by Ivakhnenko [178], [179]. The GMDH network applied a second-degree transfer function to construct a function in a feed-forward network. The effective input variables and the optimal model structure as well as the number of neurons within the hidden layers are automatically determined in the GMDH algorithm [180]. A nonlinear function called the Volterra series, in the form of Eq. (9) [178], [179], is used through a GMDH neural network

to map between the input and output variables. The Volterra series as a two-variable second-degree polynomial is analyzed using Equation Eqs. (9) and (10) [166].

$$\hat{y} = a + \sum_{i=1}^{n} a_i x_i + \sum_{i=1}^{n} \sum_{j=1}^{n} a_{ij} x_i x_j + \sum_{i=1}^{n} \sum_{j=1}^{n} \sum_{k=1}^{n} a_{ijk} x_i x_j x_k + \cdots \quad (9)$$

$$G(x_i, x_j) = a_0 + a_1 x_i + a_2 x_j + a_3 x_i^2 + a_4 x_j^2 + a_5 x_i x_j \quad (10)$$

The purpose of the GMDH algorithm is to determine the $a_i the$ unknown coefficient in the Volterra series. The a_i coefficients are fund for each pair of x_i and x_j input variables using regression [181]. On this basis, the error function was obtained as follow taking into consideration the principle of least squares error [178]:

$$E = \sqrt{\frac{\sum_{i=1}^{n} (y_i - G_i)^2}{n^2}} \quad (11)$$

$$y_i = f(x_1, x_2, x_3, \dots, x_i, \dots, x_j, \dots, x_n) \quad (12)$$

The genetic algorithm, one of the most common evolutionary algorithms, is used to solve optimization problems that are based on natural selection. The new method, i.e. GMDH-Neural Network method is used here to develop an accurate model for simulating p-xylene degradation by using different substrates of toluene, benzene, ethylbenzene [182]. One reason for using the GMDH model is its ability to minimize the number of model neurons and find the smallest model possible with the least complexity. Akaike's Information Criterion (AIC) [180] is used in this study to compare the results. AIC is defined as follows:

$$AIC = n.log(MSE) + 2(N + 1) + C \quad (13)$$

where n is the number of test or train samples, N is the number of model neurons, C is a constant, and the Mean Squared Error (MSE) is defined as follows:

$$MSE = \sqrt{\frac{\sum_{i=1}^{n} (y_{i,Actual} - y_{i,Model})^2}{n^2}} \quad (14)$$

80 % of the experimental data was applied for training (n: the number of train samples = 160) and 20 % of data was applied for validation. The flowchart of the GMDH-based Neural Network method for the biomass concentration and p-xylene concentration is presented in Fig. A2. This model can predict the value of p-xylene and biomass concentration that can be calculated by considering three effective parameters including time (θ in hr), the initial total concentration of substrates and p-xylene (C_T in ppm), and α value in both growth substrates and growth-substrate-induced cells (Fig. A2). The following fitting parameters were developed in this study and used in

the GMDH model in order to predict the experimental data by using the obtained correlation, as given in Eq. (15):

$$\alpha = \frac{\sum ß_i C_i}{C_{Total}} \qquad i = Toluene,\ \ Benzene,\ \ Ethylbenzene \tag{15}$$

Where C_i is the initial concentration of substrates and C_{Total} is the total initial concentration of all substrates in the samples. Furthermore, the value of the proposed parameter ($ß_i$) can be calculated by using the following Eq. (16)

$$ß_i = \exp(-\frac{Mwt_{C,i}}{Mwt_i}) \tag{16}$$

Where Mwt_i is the molecular weight of substrate, which is equal to 92.14, 78.11, 106.17 g/mol for toluene, benzene, and ethylbenzene and $Mwt_{C,i}$ is chain structure molecular weight in the aforementioned components which is equal to 15.0, 0.0, and 29.0 g/mol. According to Eq. (16) for non-chained substrate, the value of $ß_i$ is 1.0 and with the increase in chain molecular weight, the value of this parameter approaches zero (ß = 0.83 and 0.704 for toluene and ethylbenzene). These fitting parameters might change for different test conditions or other types of growth substrates. Following developing the fitting parameters, sensitivity analysis should be done to indicate how different values of these parameters affect the output result. The following Eqs (17) and (18) show the sensitivity of concentration obtained by considering ± 30% in two different initial concentrations of *p*-xylene [183].

$$\text{Sen}_1\,(\%) = \left|\frac{P\text{-}xylene\ Concentration\ (\alpha \pm 30\%,\ \theta,\ C_T) - P\text{-}xylene\ Concentration\ (\alpha \pm 30\%,\ \theta,\ C_T)}{P\text{-}xylene\ Concentration\ (\alpha \pm 30\%,\ \theta,\ C_T)}\right| \tag{17}$$

$$\text{Sen}_2\,(\%) = \left|\frac{Biomass\ Concentration\ (\alpha \pm 30\%,\ \theta,\ C_T) - P\text{-}xylene\ Concentration\ (\alpha \pm 30\%,\ \theta,\ C_T)}{P\text{-}xylene\ Concentration\ (\alpha \pm 30\%,\ \theta,\ C_T)}\right| \tag{18}$$

For co-metabolic degradation during the growth phase, the sensitivity of biomass and *p*-xylene concentrations vs. α, degradation time, and the total concentration of substrates were studied by considering the changes in the value of the aforementioned parameters from ±2 to ±30 %.

Carbon mass balance study

As mentioned previously, the growth of biomass was monitored by measuring the substrate consumption using static headspace gas chromatography and carbon dioxide production. recovered C-CO_2 and the carbon recovered as biomass was determined after substrate exhaustion and the values were corrected using control flasks incubated with no carbon source [184]. The pH measurements for liquid media were made at the end of incubation for adjustment of the water/air

partition of carbon dioxide. Finally, the biomass was collected using 0.45-µm-pore-diameter filtration, placed in the oven, and the dry content was determined. The carbon recovered as biomass was calculated by assuming that 26 g of dry weight contains approximately 1 mol of carbon [185]. Carbon mass balance tests were conducted in triplicate for both cultures and controls.

Identification of intermediates

The bacteria with an optical density (OD600) value of 2.0 were grown in a 150 ml serum bottle contained 25 ml media as mentioned above. To accumulate the possible p-xylene degradation intermediates, the cultures were incubated without/with shaking at 30°C. The time course for the formation of intermediates varied in different samples, hence the sampling was carried out at different time intervals. Intermediates formed during the metabolism and co-metabolism degradation were analyzed using two types of gas chromatography/mass spectrometer; GC-MS with a capillary column, GC-MS with headspace sampler (for possible volatile intermediates, as mentioned above). For the non-volatile intermediates, the results were obtained from GC-MS equipped with a CP-Wax 57 CB column (25 m×0.25 mm×0.20µm, Agilent Technologies, Netherlands). The temperature of the GC oven was programmed from 40°C (held 1 min) to 200°C at 5°C/min (held 10 min). The injector temperature was set at 180°C and the MS interface temperature was set at 250°C and 280°C for the ionization source. All metabolites were identified with a GC/MS by matching the retention times and ion spectra with authentic standards and NIST library data.

Enzymes determination

Bacterial cells were harvested by centrifugation at 5000 × g, washed twice with 20 mM phosphate buffer (pH 7.0), and re-suspended in the same buffer. The cells were disrupted using two frequencies of ultrasounds (22 kHz and 30 kHz) for 6 min. The cellular lysates were centrifuged at 13,000 × g for 20 min, and the supernatant was used for enzyme assays. Possible involved enzymes were analyzed as described below.

-Initial oxidative enzymes

P. putida uses xylene monooxygenase or dioxygenase to initiate degradation of p-xylene via two pathways, the *tod*,or the *tol* pathways:

Xylene monooxygenase (XMO) activity was determined by a colorimetric assay slightly modified from Arenghi [186]. NADPH (final concentration, 0.5 mM) and 35 µl of *p*-xylene in N,N-

dimethylformamide (4% vol/vol) were added to the cellular lysates. At 3-min intervals after incubation at 30°C, 1-ml samples were collected and mixed with 100 µl of 1 M NH_4OH and 100 µl of 2% 4-aminoantipyrine. After the addition of 100 µl of 8% $K_3Fe(CN)_6$, the samples were briefly centrifuged (14,000 x g), then the A500 of the supernatant was measured. Phenolic compound concentrations were calculated by reference to a standard curve for p-cresol (in the range of 0-50 µg/mL). Specific activities were reported as micromoles of compounds produced per minute per milligram of cell protein. Total cell protein concentration was determined by the Bradford method [187].

Xylene dioxygenase activity was spectrophotometrically assayed by the formation of indigo [188]. The enzyme reaction was initiated by the addition of 5 µl of indole 100 mM in N, N-dimethlylformamide to the cellular lysates. The absorbance of the mixture at 400 nm was measured against a blank containing all ingredients except indole. The enzyme activity was defined as the increase in indigo absorbance as a function of time that normalized to the protein content of the sample.

-Ring cleavage enzymes

Catechol 1, 2-dioxygenase (C1,2D), Catechol 2,3-dioxygenase (C2,3D) are key ring cleavage enzymes for degradation by *P. putida*. The reaction mixture (3.0 mL) contained 2.0 mL phosphate buffer, 0.6 mL 1 mM catechol, 0.2 mL deionized water and 0.2 mL cellular lysates. The reaction was kept at 30 °C and the sub-samples were taken every 2 minutes. Catechol 1,2-dioxygenase and catechol 2,3-dioxygenase activities were determined by measuring the production of muconic acid at 260 nm and 2-hydroxymuconic semialdehyde at 375 nm, respectively. One unit of enzyme activity was defined as the amount of enzyme that formed 1 µmol of cis, cis- muconic acid, and 2-hydroxymuconic semialdehyde per minute [175].

Statistical Analyses

Statistical analysis related to the analyzed parameters, such as student t-test, the p-value of all the data sets were performed in ORIGIN software (version 8.5; Origin Lab) [189]. All experiments were performed in triplicates per experiment. Data are presented as mean ± SD.

3.1.3. Results and discussion

Microbial growth kinetic models

Single Substrate Test

Single substrate experiments were carried out at the same initial biomass concentration equal to ($\sim 30\ mg/L$) for the initial concentration of benzene, toluene and ethylbenzene equal to ~50 mg/L ($C_g{}^o$ = 50 ppm) to investigate the biodegradation rates and kinetic parameters. As for Michaelis-Menten/Monod kinetics, the initial concentration of contaminants has been selected below 100 ppm for each substrate in a single solution or 100 ppm of total concentration; otherwise we needed to consider the substrate inhibition and which means more kinetic parameters added to the model. Other literature also did not study initial concentrations more than 100 ppm for modeling the kinetic of degradation. Our experiments also showed that at higher initial concentrations (>100ppm), the kinetic parameters determined from single component degradation processes cannot be used in a specific growth rate model in which more than one growth substrate is present. In other words, the kinetic parameters for a single substrate experiment are the same for a dual mixture with the same total initial concentration experiment as long as the initial concentration is not more than about 100 ppm. The proposed equations obtained for GMDH-model for resting cell phase applied to two initial concentrations of 50 and 200 ppm (p-xylene solubility at ambient temperature = 198 ppm) but for the co-metabolic system, total mixture concentrations of 20, 30, 40, 50,75 and 100 ppm were studied. Due to the presence of a lag period during single substrate experiments and the toxic nature of BTEX, microbial pre-adaption was applied to enhance the activity of the tested strain and overcome substrate inhibition. The cells pre-adapted to 50-200 ppm of benzene, toluene and ethylbenzene were applied to study the performance of the kinetic models. Low concentration of toluene and benzene (30-60 mg/L) required only one pre-adaptation while for concentrations of 100-200 mg/L three consecutive stepwise pre-adaptations were applied to obtain fast degradation of growth substrate at high concentrations. To facilitate the PSO search for the global optimum, a reasonable choice of initial ranges of kinetic parameters and search-space boundaries were determined based on the real microbiological meaning reported in the literature [163]. Fig. 3.1.1 shows the experimental profiles of changes in single substrate and biomass concentrations as well as the solution to the substrate degradation and biomass growth equations using the estimated kinetic parameters. According to the obtained results, in the experiment of a single growth substrate, toluene was degraded fastest, followed by benzene and ethylbenzene.

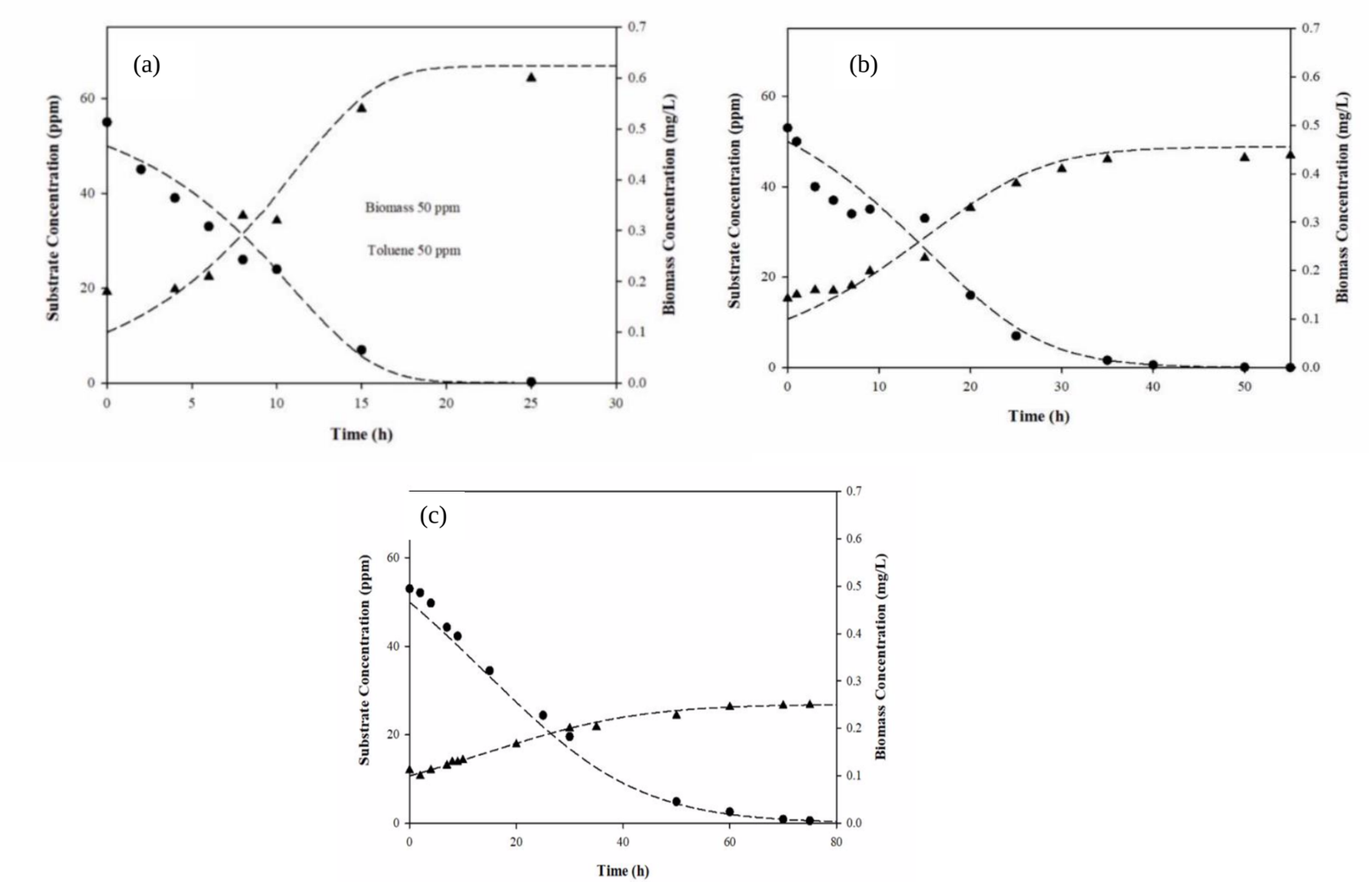

Fig. 3.1.1. (a) Toluene and biomass concentrations; (b) Benzene and biomass and; (c) Ethylbenzene and biomass concentrations, in the aqueous phase for a single substrate experiment and Monod model fit.

Table 3.1.1 shows a summary of the Monod and Andrew kinetic parameter estimates for single substrate biodegradation experiments. The results for substrate inhibition showed a high level of inhibition for ethylbenzene by inducing a lag period; thus, Andrew model fitted ethylbenzene degradation over time [190]. The inability of the Monod and Andrew models to accurately predict the biomass concentration for the results observed from benzene and ethylbenzene degradation results (Fig. 3.1.1) were reported by others in the literature [163]. Moreover, the yield coefficients, Y_{X/S_i}, for toluene, benzene and ethylbenzene were determined by following the changes in the concentration of biomass and substrate over time shown in Table 3.1.1.

Resting cell phase

In order to apply the co-metabolism model to predict p-xylene transformation, K_{Ic}, K_{Sc} and K_c should be determined. For this purpose, the p-xylene co-metabolically utilization (Eq. (7)) term analogous to enzyme kinetics is required to determine the kinetic of p-xylene transformation. First of all, the maximum specific p-xylene transformation rate was determined by extrapolating the linear line (the specific initial reformation rate vs the initial cell concentration, not shown). Then, Eq. (7) was simplified as

$$-\frac{1}{\frac{ds_N}{dt}} = \frac{1}{X_O\, K_c} + \frac{s_N}{X_O K_{Ic}\, K_c} \tag{19}$$

Thus, plotting the inverse of the initial p-xylene transformation rate versus initial p-xylene concentration yields a straight line with a slope of 2×10^{-4}h/(ppm p-xylene)^2 for toluene-assimilated cells. Table. 3.1.1. shows the obtained parameters for each system. After having determined the kinetic parameters, biomass transformation capacity,$T_c{}^b$, was determined by fitting the experimental profiles of changes in biomass and p-xylene concentrations with those obtained as a result of solving the coupled equations for *p*-xylene co-metabolically transformation and the overall growth rates during the resting phase (Fig. 3.1.2) [163]. As mentioned previously, the biomass transformation capacity,$T_c{}^b$, reflects the amount of available reducing power and this parameter depends on the growth history of cell culture. As can be seen in Table. 3.1.1., toluene assimilating cell exhibits higher transformation rate of p-xylene (K_c = 0.0016 mg p-xylene/mg cell h). The information about the co-metabolic transformation either by pre-cultured cell or in the presence of growth substrate would be necessary to study the kinetics of p-xylene degradation.

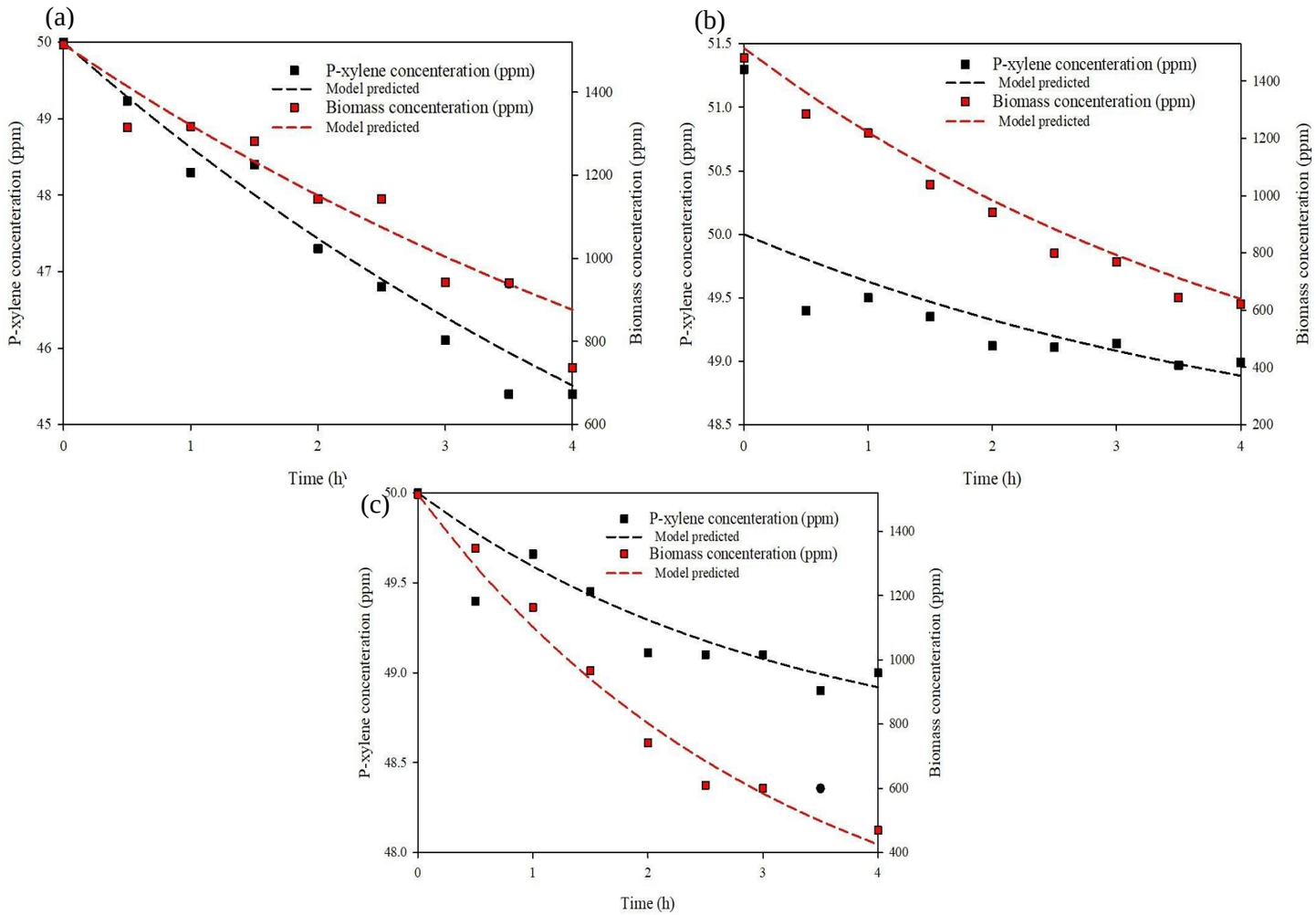

Fig. 3.1.2. Experimental and predicted profiles of changes in the p-xylene and biomass concentrations (ppm) for: a) Toluene-assimilating resting cells $C_g{}^o$ = 50 mg/L.; b) Benzene-assimilating resting cells; c) Ethylbenzene-assimilating resting cells $C_g{}^o$ = 50 mg/L

Table 3.1.1. Kinetic and interactive parameters estimated in this work by PSO method for complex processes involving multiple substrates by P. putida and prediction of the kinetic equation parameters describing the p-xylene transformation by resting cells using the least square method.

C^{o}_{g} = 50 mg/L												
The growth phase (Growth substrates)						Resting cell phase (non-growth substrate)						
Compound	μ_{max} (h^{-1})	K_s(mg/L)	K_I	$Y_{x/s}$ (mg/mg)	$Y_{x/s}$ - R^2	Resting cell	K_c	K_{sc}	K_{Ic}	T^b	p-xylene degradation (%)	R^2
Toluene	0.23±0.09	19.1±1.1	-	2.5±0.7	0.981	Toluene assimilating resting cell	0.0016	20.1	57	8.1±0.7	4.3±0.7	0.986
Benzene	0.16±0.05	47.5±2.5	-	2.1±0.2	0.982	Benzene assimilating resting cell	0.00027	25.4	63	7.2±1.9	1.4±0.1	0.97
Ethylbenzene	0.08±0.01	5.3±0.9	2.4±0.5	0.9±0.2	0.919	Ethylbenzene assimilating resting cell	0.00022	31.7	42	5.4±1.1	1.0±0.4	0.971

For a single substrate test, kinetic parameters (specific growth rate and half-saturation constants) are similar in this study to other reports; yet the rate of p-xylene co-metabolized in the presence of toluene assimilating resting cell (Kc) was slightly higher in the current study. It can be contribute to the difference in type of bacterial population between studies [163], [164], [179].

Co-Metabolic Systems

After quantifying the kinetic parameters for growth substrates utilization during the rapid growth rate and p-xylene co-metabolically transformation in the resting cell phase, co-metabolism models were studied to describe the degradation of *p*-xylenes for the constant initial concentration equal to ~50 mg/l in the presence of growth substrate. To test the bi- component systems containing p-xylene, experiments were carried out at the same initial biomass concentration equal to ~30 mg/L and the total initial concentration was 50 mg/L for components, The specific growth rate models that account for the unspecific type of interactions among dual substrates were determined and substituted into biomass growth and substrate uptake rate equations.

For the binary mixture, Fig. 3.1.3 shows the effect of p-xylene on growth substrate degradation. The most accurate fit was obtained using interaction parameters (i.e., $I_{X,T}$, $I_{X,B}$, $I_{X,E}$) equal to 1.9, 1.4 and 1.3, respectively. These parameters revealed that p-xylene has an inhibitory effect on growth substrates degradation. Kinetic results will be evaluated in the enzyme study section. Comparison of Fig. (3.1.2) and (3.1.3) also can show a slight decrease in toluene, benzene and ethylbenzene degradation (%) (e.g., from 80, 56 and 36 to 72, 48 and 35 %) in the presence of p-xylene.

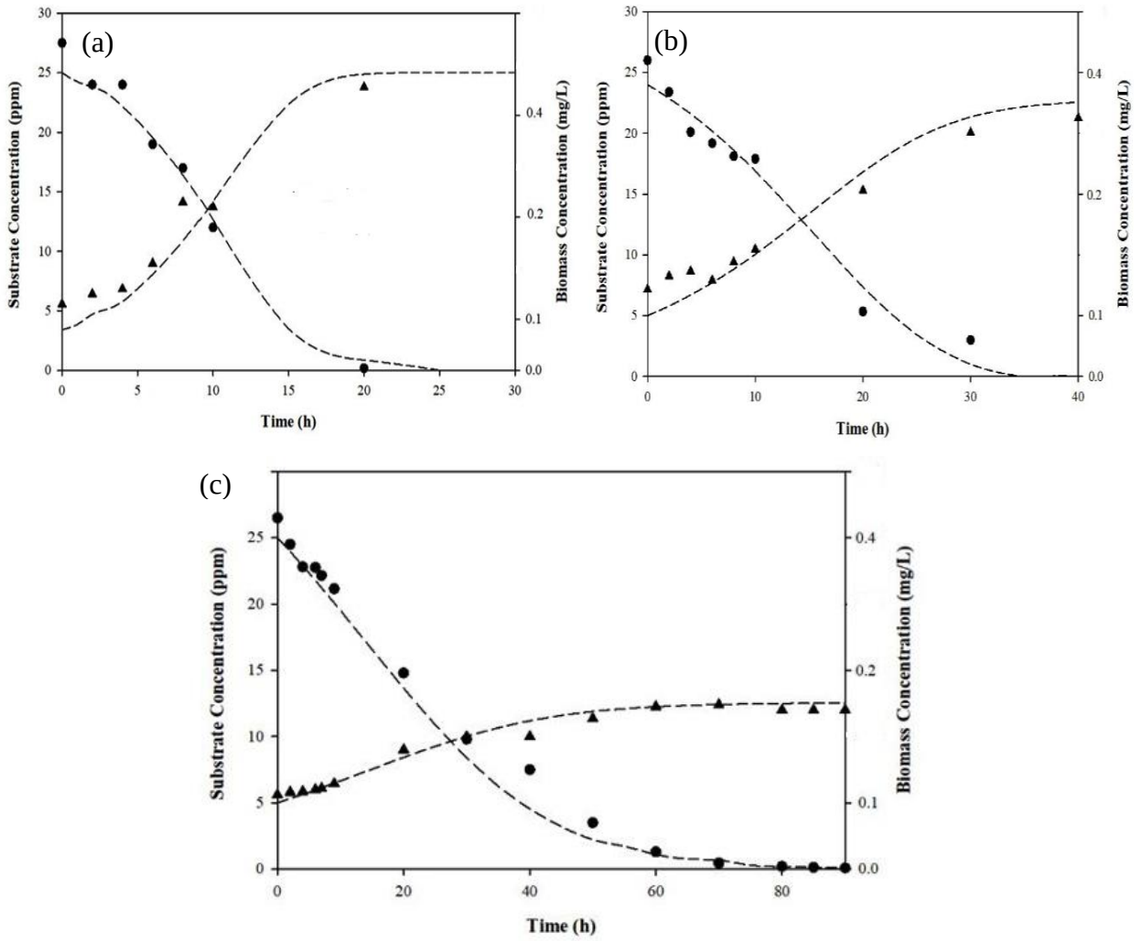

Fig. 3.1.3. (a) Toluene and biomass concentrations; (b) Benzene and biomass and; (c) Ethylbenzene and biomass concentrations, in the aqueous phase in the presence of p-xylene experiment and SKIP model fit.

As can be seen in Fig. 3.1.4, the co-metabolic degradation of p-xylene was enhanced in the presence of either toluene or benzene. As mentioned previously, the study of *p*-xylene transformation by growth substrates induced cells of *P. putida* also showed that toluene assimilating resting cell degraded *p*-xylene more effectively than other substrates (the half-saturation constant of the equation describing *p*-xylene degradation rate by the means of toluene, benzene, and ethylbenzene -assimilating resting cells were: 0.0016, 0.00027, 0.00022 g $_{p\text{-xylene}}$ /h g $_{substrate}$). From student's t-test analysis which was carried out for all mixtures including TX (toluene, xylene,) BX (benzene, xylene), and EX systems to compare the *p*-xylene degradation to the case without any growth substrate; it was found that there was a difference (t-value greater than p-value) between "X" and "TX" (averaging p-value 0.0005 as compared to a t-value of 3.768 for samples) and "X" and "EX" (average p-value 0.005 as compared to a t-value of 2.807 for samples). As discussed in the literature, one advantage of Michaelis-Menten/Monod kinetics is the fact that the incorporation of substrate inhibition and any interactions between two substrates can be modeled by adding an interaction term to the Monod expression and co-metabolic

transformation of the nongrowth substrate (p-xylene) by specific strain can be quantified by coupling xylene transformation to the consumption of growth substrate (toluene, benzene or ethylbenzene) during growth. However, the co-metabolic transformation of xylene in the presence of two or more growth substrates cannot be modeled [156]. Thus, the GMDH-based Neural Network model has been applied in Sec. 3.2 to evaluate the relation between the input variables such as the structure of monoaromatic substrates and p-xylene co-metabolic transformation at a low initial concentration of p-xylene.

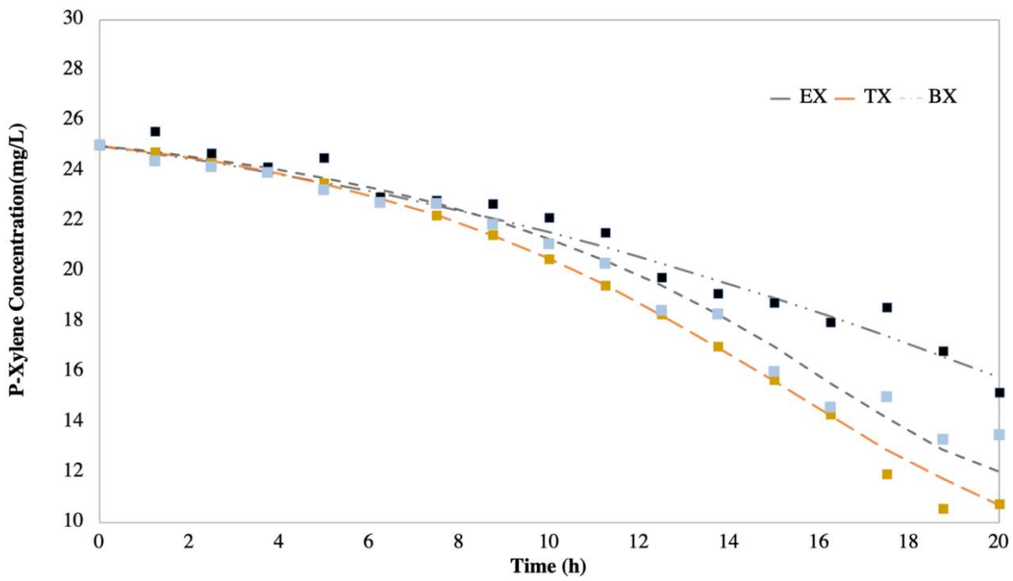

Fig. 3.1.4. *p*-xylene (X) concentrations in the aqueous phase in the presence of experiments (shapes), SKIP (dashes) C^o = 25 mg/L of each component.

GDMH-based Neural Network Model

Resting cell phase

In this section, a mathematic model of *p*-xylene utilization and the overall growth rates during the resting phase (the resting cell transformation) was studied to predict the concentration of *p*- xylene and biomass. For this purpose, sub-functions together with input parameters including degradation time (θ), α value (fitting parameter), and the initial total concentration of *p*-xylene, toluene, benzene, ethylbenzene (C_T) were used in a hybrid group method of data handling (GMDH)-type neural network. This resulted in finding the correlation that estimates *p*-xylene with significantly high precision (R^2 = 0.99), and biomass concentration (R^2 = 0.98); based on the above-mentioned parameters by using GMDH Shell DS software. Using the quadratic sub-functions in the form of equations, the concentrations of *p*-xylene can be calculated by the following correlation (which were obtained by using the GMDH method) in Eq. (20):

$$P - xylene\ concenteration\ (ppm) = SF_{R,6} \quad (20)$$

Eqs. (S4)- (S9) shows the quadratic sub-functions in the form of equations that were used to obtain sub-function $SF_{R,6}$. The concentrations of biomass can be calculated by the following neural network design in Eq. (21) where the values of $BF_{R,1}$, $BF_{R,2}$, $BF_{R,3}$, $BF_{R,4}$, $BF_{R,5}$, $BF_{R,6}$, and $SF_{R,7}$ can be calculated by using the correlations in Eqs. (S10-S16)

$$Biomass\ concenteration\ (ppm) = 303 \times BF_{R,7} \quad (21)$$

So Eqs. (S10) -(S16) shows the quadratic sub-functions in the form of equations that were used to obtain sub-function $BF_{R,7}$.The manner in which the independent parameters correlated is illustrated in Fig (A3) and (A4). The unknown parameters (A_i, B_i, C, D_i, E_i, F_i, G_i, H_i, I_i, J_i, K_i, L_i, M_i and $i = 1 \dots 6$) presented in these equations are shown in Table A1. As mentioned previously, the GMDH method applied input variables and created some subfunctions and subsequently applied this information as input variables and predict the output results. The actual and anticipated data were compared in Fig. 3.1.5. As can be seen, Eq. 20 can estimate the concentration of *p*-xylene with a low deviation from experimental values that is mostly less than 5 and 2.5 % for the initial concentration of 50 and 200 ppm. However, the suggested equation can estimate the values of biomass concentration for an initial concentration of 50, and 200 ppm with a maximum error of about 25 for toluene, benzene and ethylbenzene assimilating cells (Fig. 3.1.5).

To determine the effect of parameters (C_T, α, and θ), a sensitivity analysis was carried out on the correlation obtained for the p-xylene and biomass concentration. As can be seen in Fig. 3.1.6 a and c, by decreasing the value of α toward zero (with increase the chain length) and increasing the degradation time, considerable changes can be observed in the value of p-xylene and biomass concentration. Moreover, the value of biomass concentration does not change significantly by increasing the value of α Fig. 3.1.6 (c) and (d).

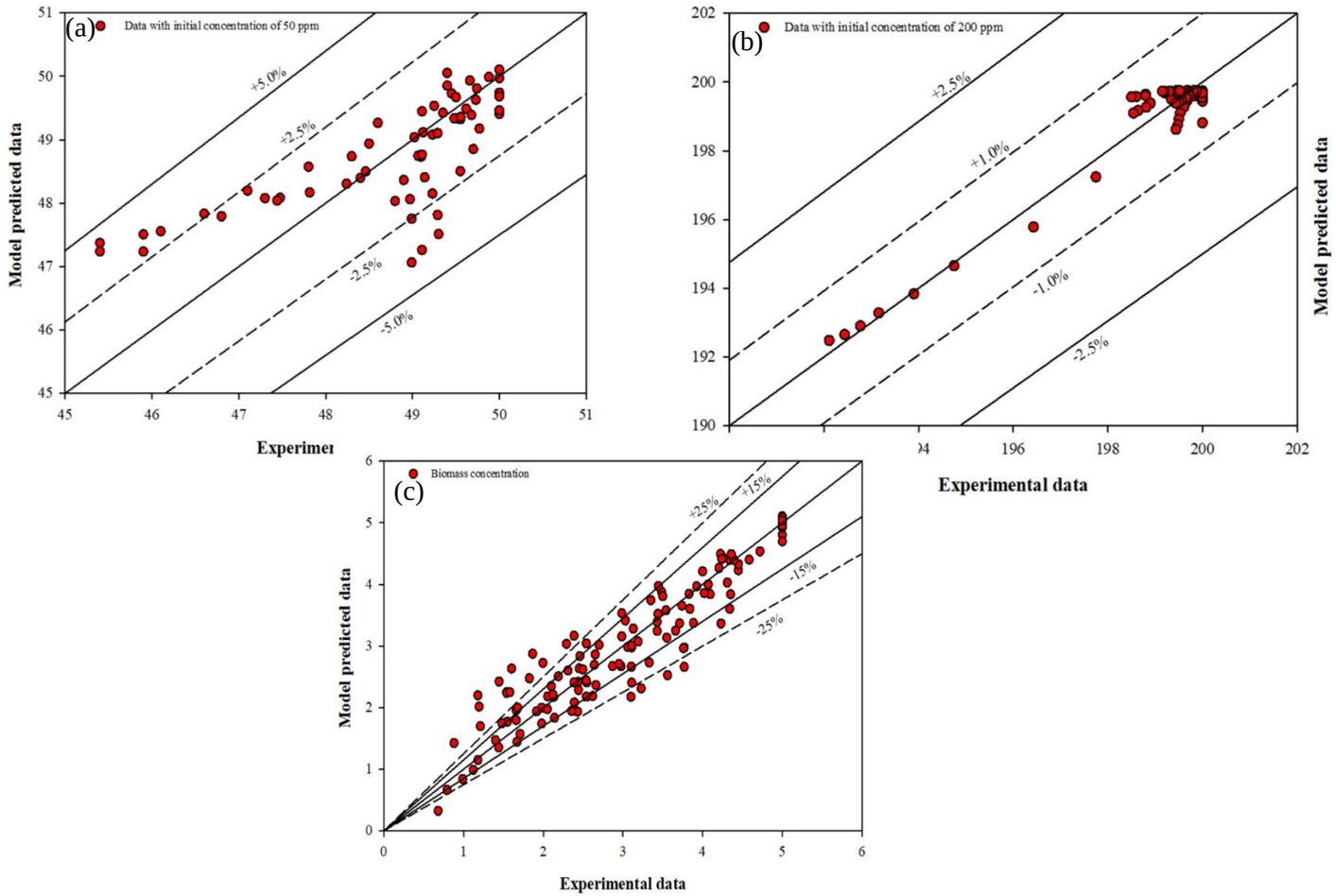

Fig. 3.1**.5. The deviation of calculated data from those obtained experimentally. (a) p-xylene degradation with initial p-xylene concentration of 50 ppm, and (b) 200 ppm. (c) biomass concentration**.

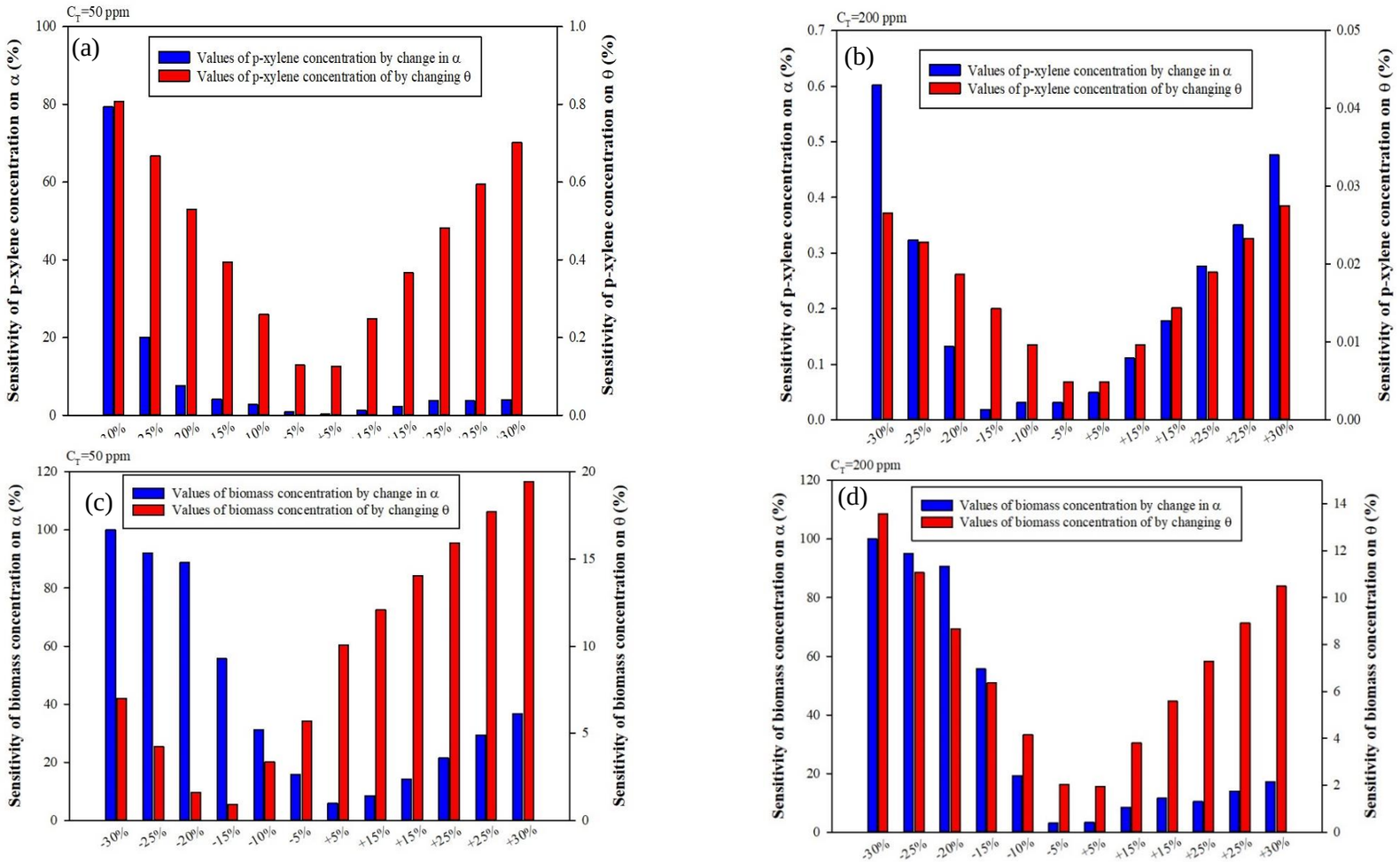

Fig. 3.1.6. Change in (a) p-xylene degradation 50 ppm, (b) p-xylene degradation 200 ppm (c) Biomass 50 ppm (d) Biomass 200 pp

Co-metabolic Systems

In this part of the research, the GMDH-type neural network approach was also utilized to forecast the concentration of *p*-xylene and biomass over time in the presence of a variable concentration of growth substrates (i.e., Toluene, Benzene, Ethylbenzene) with total mixture concentrations of 20, 30, 40, 50,75 and 100 ppm. Important factors including degradation time (θ), the total concentration of substrates (C_T), and α value has been designated as the inputs, and concentration of biomass has been considered as the output of the network. Eq. (22) as well as Eqs. (S17) -(S27) were obtained to calculate the biomass concentration using GMDH shell DS software where the maximum initial concentration of each substrate alone or p-xylene did not exceed 50 ppm:

$$C_{Biomass}\,(\theta, \alpha, C_T) = CF_{11} \tag{22}$$

Eq. (S17) -(S27) shows the quadratic sub-functions in the form of equations that were used to obtain sub-function CF_{11}. The unknown parameters (‘A, ’B,’C, ’D, ’E, ’F, ’G, ’H,’I, ’J, ’K, and ’M) presented in these equations are shown in Table A2. The manner of independent parameters connecting is illustrated in Fig (A5). Since both substrates and p-xylene are contacting at the same time, the metabolic activity of substrates can be assumed as a function of total biomass concentration. Therefore, the degradation time (θ) as well as biomass concentration $C_{Biomass}\,(\theta, \alpha, C_T)$ has been designated as the input variables for the p-xylene concentration prediction using Eqs (23) and (24):

$$p - xylene\ concenteration\,(\theta, C_{Biomass}) = SF_{12} \tag{23}$$

$$SF_{12} = M_1 + M_2.C_T.\theta + M_3.\theta + M_4.\theta.C_{Biomass}\,(0, \alpha, C_T) \tag{24}$$

Fig. 3.1.7 shows the deviations for data obtained for the *p*-xylene and biomass concentration from the actual values. These results reveal that the proposed correlations can predict the values of *p*-xylene or biomass concentrations at the total initial substrate concentration up to 50 ppm with a maximum deviation of near to 5%.

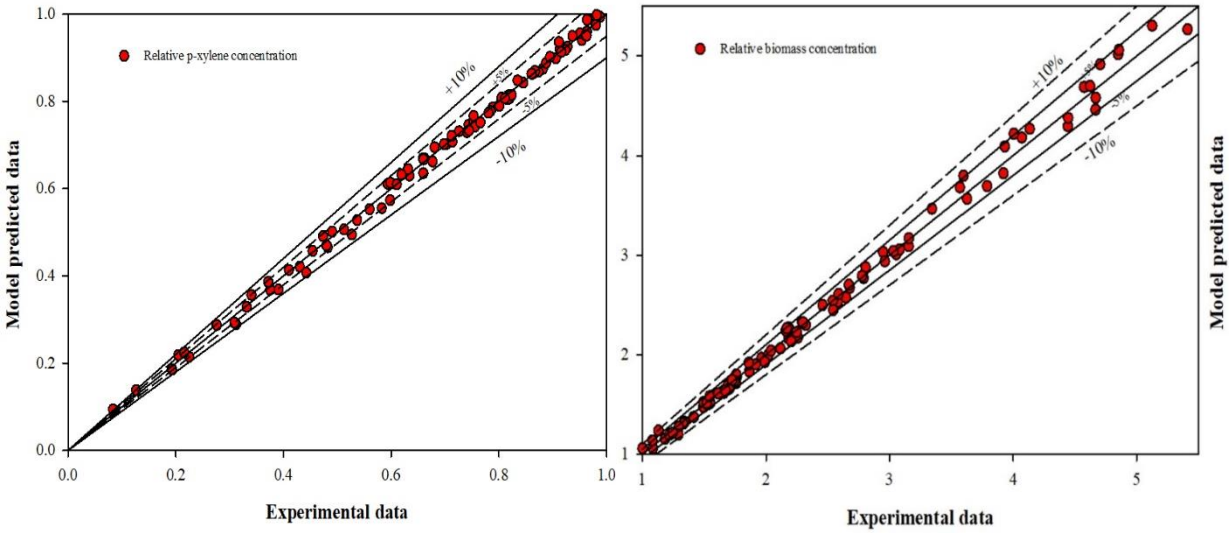

Fig. 3.1.7. The deviation of calculated data from those obtained experimentally for co-metabolic system.

In this part of the research, the sensitivity analysis was used to declare which parameters(θ, α value, and C_T) have the most significant impact on biomass and *p*-xylene concentrations during the growth phase in the co-metabolic system. Fig. 3.1.8 shows that the biomass concentration is more sensitive to the total concentration of substrates in comparison to *p*-xylene concentration and as C_T decreases biomass changes more significantly. However, Li *et al.* showed that the concentration of substrates might significantly affect the co-metabolic degradation of non-growth substrates, unlike our study that varying substrate concentration did not affect *p*-xylene

concentration [175]. It might be due to low T_g^C for *P. putida*. Based on Eq. (6) that expresses the co-metabolic substrate transformation due to the degradation of growth substrate, the first term includes the growth substrate transformation yield parameter and by changing this parameter, the magnitude of the growth substrate concentration effect on non-growth substrate concentration can be decreased or increased. Therefore, for microorganisms with low T_g^C, non-growth concentration can be independent of growth substrate during the growth period.

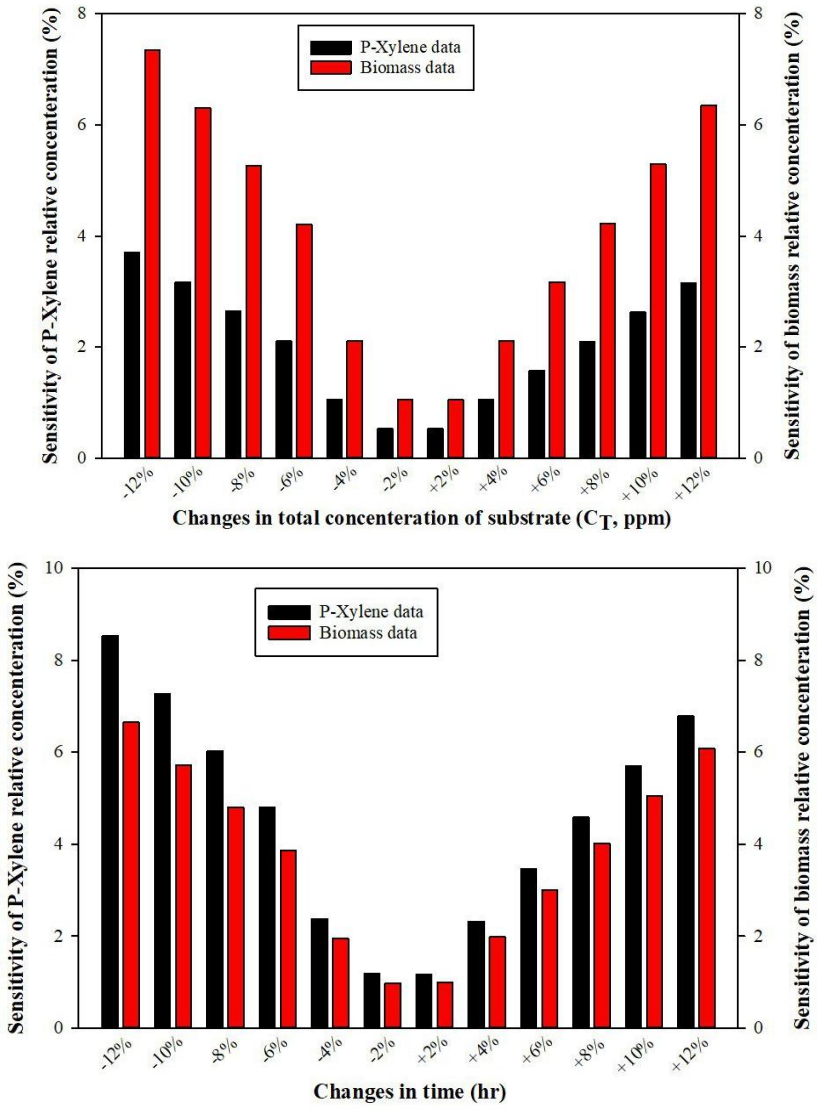

Fig. 3.1.8. Sensitivity analysis on p-xylene and biomass concentration in the co-metabolic system.

Fig. 3.1.9 shows the change of *p*-xylene and biomass concentration vs. α value. As can be seen, the α value equals 0.95 resulted in the optimum *p*-xylene degradation that is closer to the amount of *p*-xylene degradation in the presence of toluene.

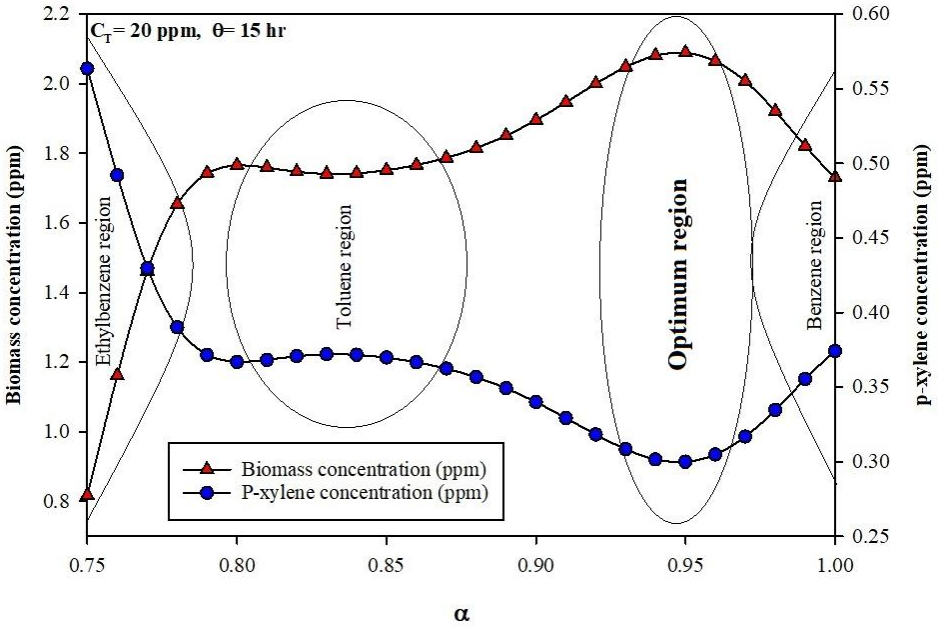

Fig. 3.1.9. Effect of α value on *p*-xylene and biomass concentration in the co-metabolic system

Furthermore, for validation of the correlation proposed for p-xylene concentration over time, an experimental data set was prepared from the results of other scholars and represented in Table. 3.1.2. The results were gathered from those that p-xylene co-metabolically degraded in the presence of benzene, toluene, and ethylbenzene at the same condition (*Pseudomonas* genus of bacteria). This finding shows that the correlation can estimate the experimental results of other studies at the initial biomass concentration range of 30- 50 mg/l and temperature up to 40 $°C$ with deviations ranged from -29.4 to 21.8 %. As mentioned previously, Eq. (23) obtained through the GMDH model can be applied for a very short range of conditions (only *pseudomonas* and only growth substrates benzene, toluene and ethylbenzene). For other conditions, different fitting

parameters can be developed and after sensitivity and regression analysis a new correlation can be used to predict the output results. For instance, more complex systems with more than one non-growth substrate can be simulated by GMDH model after determining suitable parameters that take into account other important factors that might affect the biodegradation process.

Table 3.1.2. The comparison between data obtained by other articles and values obtained by Eq. (23)

System	T($°C$)	Time (h)	Initial biomass (ppm)	$C_{xylene,\ exp}$ (ppm)	$X_{ylene,\ cal}$ (ppm)	Error = $\left(\frac{C_{xylene,exp}-C_{xylene,cal}}{C_{xylene,exp}}\right) \times 100$	Ref
TX	24	15	30	5.8	7.2	-24	[3]
BTEX	ND	15	18	15.1	11.8	21.8	[10]
EBX	25	20	25	1.7	2.2	-29.4	[37]
BX	25	2	20	2.1	2.7	-28	[38]

Identification of intermediates

The results showed that catechol was the central intermediate in the co-metabolic degradation of p-xylene in presence of BTE by *P. putida* (Fig. A6). Tsai *et al.,* reported that catechol is formed during aerobic biodegradation of a variety of aromatic compounds [191]. Arenghi *et al.,* also reported that most of the monoaromatic catabolic pathways give rise to (methyl) catechol further processed through meta cleavage pathways [187]. The reaction products can be easily converted to tricarboxylic acid cycle (TCA cycle) intermediates, which are further broken down into CO_2 and water which provided energy for biomass production [183]. However, when *P. putida* has been cultured on p-xylene as the sole carbon source, p-cresol was the central intermediate. In *P. putida,* p-cresol was derived from the XMO-catalyzed hydroxylation of p-xylene and were not

used for growth, due to lack of ring cleavage enzymes and could be accumulated as a toxic intermediate (Fig. A6).

As can be seen in Fig. (A6), p-xylene firstly converted to 4-methyl benzoic acid then to p-cresol that accumulated at the media in the absence of growth substrate, while p-cresol was not detected in the presence of growth substrates (e.g., BTE). This may be due to the induction of fission enzymes by growth substrates (catechol dioxygenases) and their conversion to CO_2. It also indicated the fortuitously transform the non-growth substrate (p-xylene) and oxidation of p-cresol then ring cleavage during the co-metabolism.

Enzymes detection

The metabolism of a substrate involves multiple enzymatic steps. Generally, the aerobic biodegradation of aromatic hydrocarbon has been divided into the upper pathway, which started from the original compound (hydrocarbon compound without any modification) to central intermediates (modified hydrocarbons), and lower pathways, which transitions from the ring cleavage of intermediates down to the needed molecules for biomass. In this study, a putative pathway for p-xylene co-metabolism by *P. putida* was proposed based on the GC/MS spectra and enzyme assays as well as other literature (diversity of microbial toluene degradation pathways). Degradation of p-xylene via two pathways, the tod, and the *tol* pathways, has been extensively studied in *P. putida* [183]. In the tod pathway, *P. putida* used xylene dioxygenase as a primary enzyme for p-xylene degradation. In this study, the xylene dioxygenase showed no activity in the presence of p-xylene and BTE in MSM, hence *P. putida* did not use the tod pathway in this case. The *tol* pathways begin with mono oxidation and finish with the formation of central intermediates which can be catechol or non-catecholic compounds. The dearomatization of central intermediates undergoes ortho-, meta- or para-cleavage by catechol dioxygenases [168]. The results from XMO

and C1,2D assays showed that *p. putida* degraded BTEX compounds via the *tol* pathway and also the results from XMO and C1,2 D activity validated the use of this pathway (Fig. 3.1.10, 3.1.11)). Based on previous studies and our results, the side chain methyl group can be oxidized in a monooxygenase catalyzed reaction and resulted in (toluic acid) production (Fig. (A6)). As xylenes have two methyl sidechain on their aromatic nucleus, it resulted in the inability of xylenes as a growth substrate and p-cresol accumulated in the culture medium so that their toxicity inhibited the growth of microorganisms (Fig. 3.1.11). This can be attributed to a decrease in the efficiency of catechol dioxygenases that will catalyze the fission of aromatic nucleus [183].

In addition, C1,2D activity showed that (4-methyl) catechol can be cleaved in the ortho position because no activity was detected for C2,3D for the meta-cleavage enzyme (lower pathway). Arenghi *et al.* showed that *Pseudomonas stutzeri* OX1 was able to transform toluene and o-xylene by toluene-o-xylene monooxygenase (ToMO), but ToMO-encoding operon did not contain gene involved ring-cleavage enzymes. Therefore, these genes may be clustered in one or more operons which were independently, but coordinately regulated [179]. Fig. 3.1.10. also shows the same decreasing trend for enzymes activities of both enzymes in the presence of p-xylene. This finding can explain the enhancement of co-metabolic degradation of p-xylene in the presence of either toluene or benzene (Fig. 3.1.4) and inhibitory effect of p-xylene on degradation of growth substrates (Fig. 3.1.3. and 3.1.2).

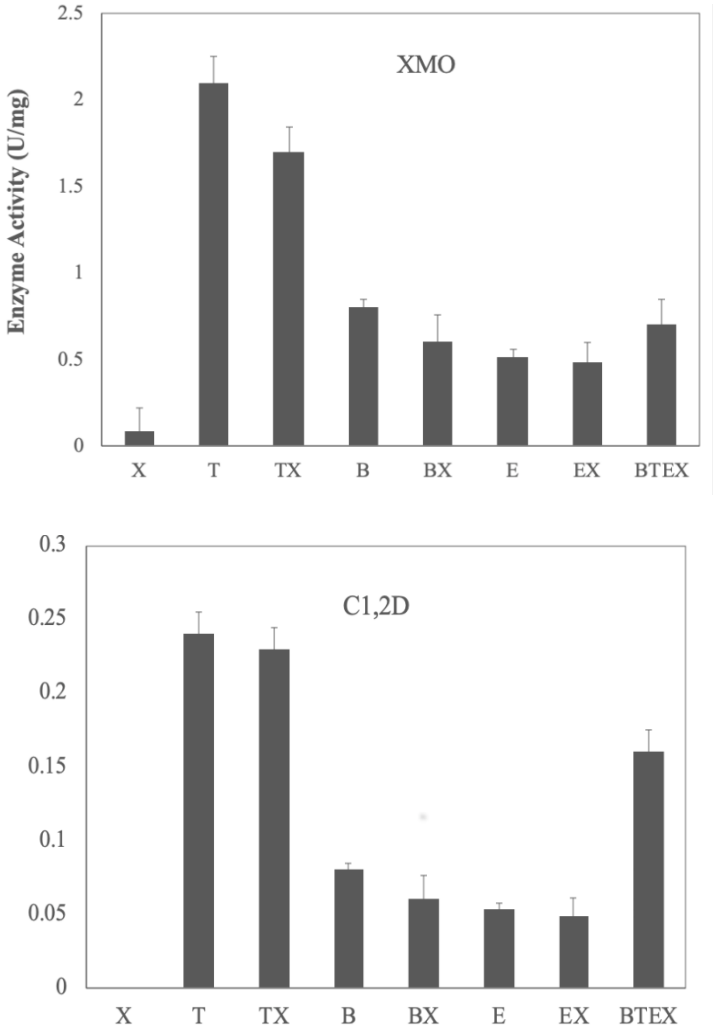

Fig. 3.1.10. XMO and catechol 1,2 dioxygenase activity the bacteria grown in MSM media supplemented with p-xylene and BTE compounds.

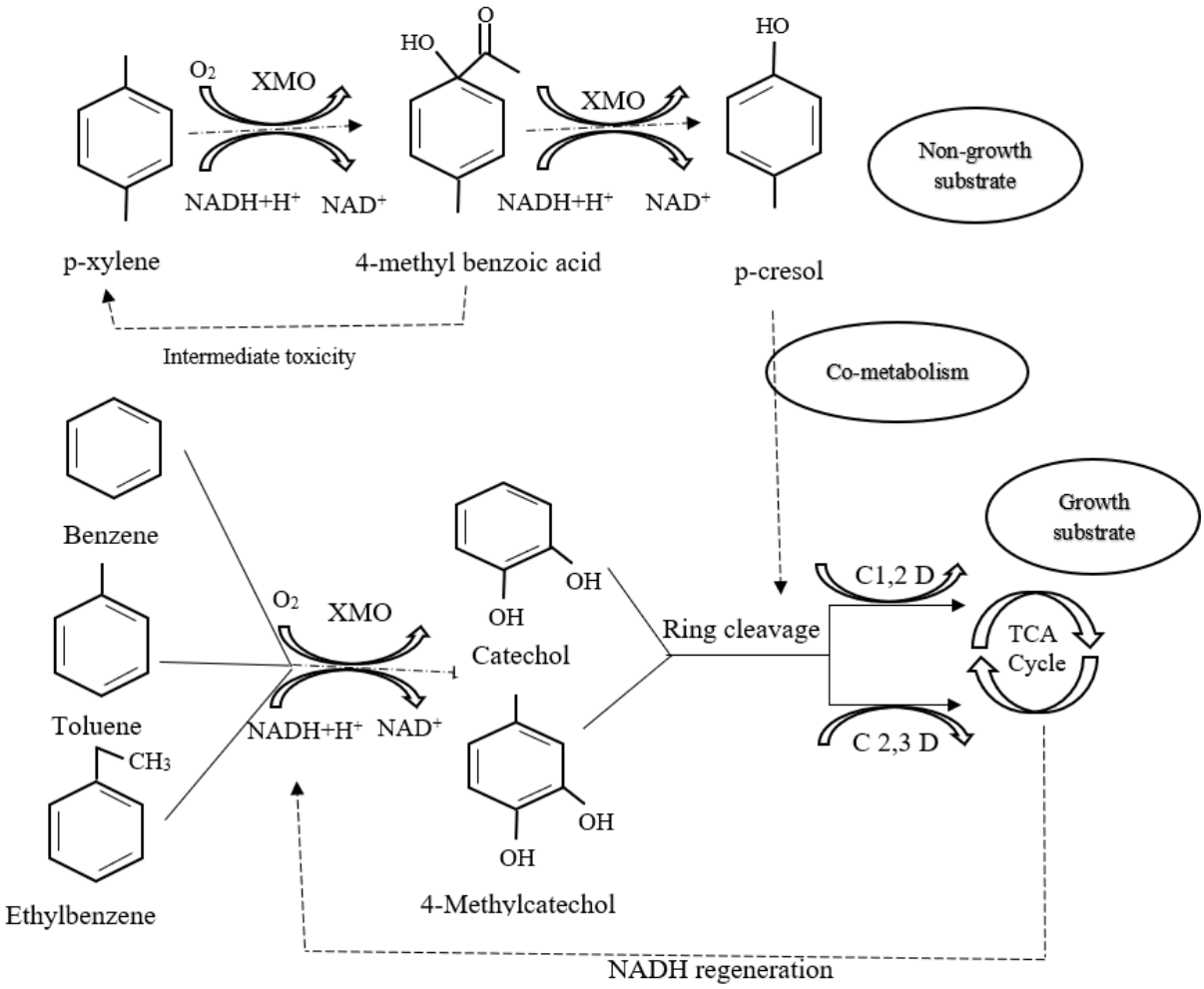

Fig. 3.1.11. Schematic representation of metabolic and co-metabolic pathways of p-xylene as non-growth substrate and BTE as growth substrate by *P. putida* under aerobic condition. In the presence of non-growth/growth substrates, the initial reaction is the formation of central intermediates by xylene monooxygenase (XMO), then the catholic intermediates (catechol and 4-methyl catechol) undergo ring cleavage by catechol 1,2 dioxygenases (C 1,2 D) or catechol 2,3 dioxygenases (C 2,3 D).

Carbon mass balance

Carbon balances were determined by measuring the amounts of consumed C substrate (BTEX) that were recovered as C-biomass and C-CO_2. Initially, carbon balances in the co-metabolic system were constructed including only the amounts of C-biomass and C-CO_2, the carbon recovery was

only about 70% to 85% (Table 3.1.3). To check this incomplete carbon recovery was due to the production of intermediates, the concentration of intermediates was determined. As shown in Table 3.1.3, when the concentration of p-cresol as a central intermediate and other intermediate were taken into account carbon recoveries increased from 96% to 98% (in terms of stoichiometry). Toluene and benzene were used as a growth substrate, and carbon recovery values of about 99% were obtained in the co-metabolism system. The result of carbon recovery was consistent with degradation and biomass results that showed the inhibitory effect of ethylbenzene, it may be due to more accumulation of toxic intermediates (4-Methylcatechol and p-cresol). The carbon recovery values in batches containing ethylbenzene (EX, BTEX) were lower (96%) than in those obtained without ethylbenzene (about 99% in TX and BX). Similarly, Prenafeta-Boldú *et al*. reported a higher carbon recovery value together with the lack of accumulation of intermediates points to mineralization for p-xylene biodegradation in *Cladophialophora* sp. strain T1. While the components that were partially oxidized to dead-end products showed lower carbon recovery value [168].

Table 3.1.3. Carbon balance after the growth of P. putida in the co-metabolic system at total initial concentration was 50 mg/L for components

Substrate(s), initial concentration (µmol))	Concentration of growth substrate(s) (µmol)	Concentration of p-xylene (µmol)	C-Biomass (µmol)	C-CO_2 (µmol)	Concentration of intermediate(s) (µmol)				C recovery (%)	
					4-methyl benzoic acid	p-cresol	Catechol	4-Methylcatechol	Biomass, CO_2	Biomass, intermediate, CO_2
T (297 µmol) +X (260 µmol)	ND	<0.1	145±5	326±3	-	69.5±0.5	-	-	85	98
B (347 µmol) + X (260 µmol)	ND	<0.1	169±2	348±4	-	86.9±0.8	-	-	85	99
E (260 µmol) +X (260 µmol)	ND	<0.1	158±2	227±1	0.2	98.8±0.3	-	12.8±0.5	74	96
B (173 µmol) +T (148 µmol) +E (130 µmol) +X (130 µmol)	ND	<0.1	160±1	338±2	-	64.7±0.4	-	-	85	96

ND: No data; B: Benzene; T: Toluene; E: Ethylbenzene; X: Xylene

3.1.4. Conclusion

The study of *p*-xylene transformation by growth substrates induced cells of *P. putida* showed that toluene assimilating resting cell degraded *p*-xylene more effectively than other substrates. Michaelis-Menten/Monod kinetics coupled with co-metabolic degradation expression can be applied for systems containing one growth and one non-growth substrate; thus, the GMDH Group Method of Data Handling (GMDH) was proposed in this study to predict the co-metabolic transformation of non-growth substrates in the presence of more than one growth substrate. In this study, the observed deviations from experimental values is still lower than 25 % and 5 % in the resting phase for biomass concentration and p-xylene concentration, respectively. However, the proposed equations obtained through the GMDH neural network can be applied for a short range of conditions (e.g., initial substrate and biomass concentration, temperature and genus of bacteria) and co-metabolic degradation of p-xylene in the presence of benzene, toluene and ethylbenzene. Further study can be carried out to predict the p-xylene removal in the presence of other C sources and genus of bacteria. To confirm the co-metabolic degradation of p-xylene, in addition, to measure the degradation of p-xylene over time, mass balance and enzyme study were done. The enzyme study showed a decreasing trend for XMO and C1,2D enzymes that degraded BTEX compounds via the *tol* pathway in the presence of p-xylene. Mass balance study also showed the accumulation of the intermediate due to the absence of growth substrates and subsequently some involved enzymes that are needed for ring cleavage. The central intermediate produced and accumulated in *p*-xylene biodegradation was *p*-cresol. *p*-cresol is considered a carcinogenic and teratogenic compound, so it needs to be removed from the contaminated environment. In comparation with p-xylene as a parent compound, xylene are not classifiable and there is no evidence for its human carcinogenicity. It is reported that intermediate products from biochemical

reactions may be more toxic than their parent compounds, thus the modification of the initial parent compound is not always an effective method in remediation and pollutant management.

BRIDGE-1

Pseudomonas putida as a well-known aromatic compound degrading microorganism degraded p-xylene in the presence of Benzene (B), Toluene (T), and Ethylbenzene (E). This bacteria could not use p-xylene as a sole source of carbon (only it could degrade in the co-metabolic system). The next step was to isolate p-xylene degrading bacteria from the target contaminated site. The purpose of the isolation of indigenous bacteria was to degrade p-xylene as the sole source of carbon under cold temperatures (annual temperature of target site). The gene expression study indicated that encoding genes and their activators explained the differences in the p-xylene metabolism by different bacteria. The involved enzymes were determined for potential application in *p*-xylene biodegradation.

From here on, "Bridge" means: Link between the previous study and the next study.

PART 2

3.2 Biodegradation of p-xylene – A comparison of three psychrophilic *Pseudomonas* strains through the lens of gene expression

Saba Miri[1,2], Azadeh Rasooli[1], Satinder Kaur Brar[1, 2*], Tarek Rouissi[2], Richard Martel[2]

1. Department of Civil Engineering, Lassonde School of Engineering, York University, North York, Toronto, Ontario M3J 1P3, Canada

2. INRS-ETE, Université du Québec, 490, Rue de la Couronne, Québec G1K 9A9, Canada

[*] Corresponding author, Email address: satinder.brar@lassonde.yorku.ca, P: 416-736-5228; 416 736 5228; 416-736-2100 ext. 55228 · F: 416-736-5360

Environmental Science and Pollution Research, 29, 21465–21479; DOI: 10.1007/s11356-021-17387-5

Abstract

p-Xylene is considered a recalcitrant compound despite showing a similar aromatic structure to other BTEXs (benzene, toluene, ethylbenzene, xylene isomers). This study evaluated the p-xylene biodegradation potential of three psychrophilic *Pseudomona*s strains (*Pseudomonas putida* S2TR-01*, Pseudomonas synxantha* S2TR-20, and *Pseudomonas azotoformans* S2TR-09). The p-xylene metabolism-related catabolic genes (*xylM*, *xylA* and *xylE*) and the corresponding regulatory genes (*xylR* and *xylS*) of the selected strains were investigated. The biodegradation results showed that the *P. azotoformans* S2TR-09 strain was the only strain that was able to degrade 200 mg/L p-xylene after 60 h at 15 °C. The gene expression study indicated that the *xylE* (encoding catechol 2,3-dioxygenase) gene represents the bottleneck in *p*-xylene biodegradation. A lack of *xylE* expression leads to the accumulation of intermediates and the inhibition of biomass production and complete carbon recovery. The activity of xylene monooxygenase and catechol 2,3 dioxygenase was significantly increased in *P. azotoformans* S2TR-09 (0.5 and 0.08 U/mg, respectively) in the presence of p-xylene. The expression of the ring cleavage enzyme and its encoding gene (*xylE)* and activator (*xylS*) explained the differences in the p-xylene metabolism of the isolated bacteria and can be used as a novel biomarker of efficient p-xylene biodegradation at contaminated sites.

Keywords: Gene expression; p-xylene; Catechol 2,3-dioxygenase; *xylE*

Graphical Abstract

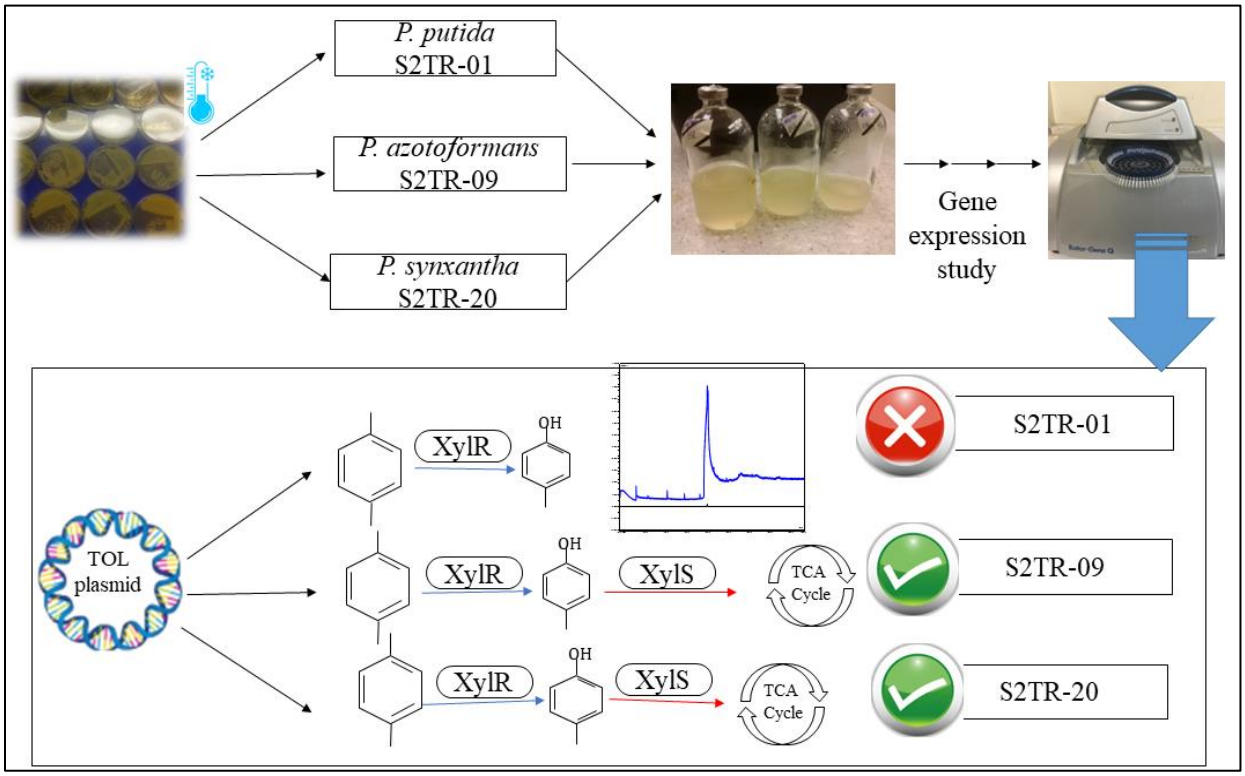

3.2.1. Introduction

The International Tanker Owners Pollution Federation (ITOPF) has identified p-xylene as one of the top 20 chemicals posing a high risk among hazardous and noxious substances (HNS) (Duan et al., 2020). p-Xylene is widely used as an industrial solvent and is highly mobile in the environment in gaseous, liquid, or solid phases [192], [193]. Contaminated sites in cold-climate regions have received significant attention due to their vulnerable natural environment. In recent decades, bioremediation techniques have been considered more effective an to cause less undue damage in cold-climate environments than other remediation techniques, such as physical, chemical, and thermal approaches [194].

Bioremediation is mainly divided into bioaugmentation (introducing competent bacteria) and biostimulation (adding exogenous oxygen and nutrients), and agreement is still limited regarding which method is the most effective for *in situ* bioremediation. It has been reported that the biostimulation method can effectively remediate low concentrations of BTEXs (benzene, toluene, ethylbenzene, xylene isomers) in contaminated groundwater (no more than 5 mg/L for each pollutant); however, it shows low degradation performance at high BTEX concentrations (more than 15 mg/L for each pollutant) in meeting the standards required for potable water [195], [196]. Hence, at highly contaminated sites, the bioaugmentation process might achieve higher bioremediation efficiency. Some field studies conducted in marine environments have suggested that bioaugmentation using indigenous oil-degrading bacteria can be effective if these bacteria are not limited by the prevailing environmental conditions [197].

Microorganisms inhabiting cold environments must cope with a number of challenges, such as limited enzyme activity, slow chemical reaction rates, increased viscosity and limited availability of water (the main solvent for biochemical reactions), protein denaturation and decreased cell

membrane fluidity [198]. To date, many microorganisms participating in petroleum hydrocarbon biodegradation in cold regions that belong to the genera *Pseudomonas*, *Rhodococcus, Alcanivorax, Arthrobacter,* and *Sphingomonas* have been recognized [199]. Psychrophilic bacteria have adaptive abilities, including the ability to modify the cell membrane structure, which is important in the electron transport chain; the expression of antifreeze proteins and cold-active enzymes; the production of compatible solutes; and the alteration of metabolism [200]. Thus, bioaugmentation using cold-adapted indigenous microorganisms can be applied in cold environments to increase bioremediation efficiency. Additionally, it may solve most of the challenges related to large seasonal/daily temperature variations.

To make bioremediation successful, the establishment and maintenance of physical, chemical and biological conditions in the environment is necessary. Introducing competent microorganisms with high potential for enzyme production can be an effective approach for the bioremediation of polluted sites [201], [202]. However, the mode of action and growth of microorganisms in polluted sites need to be further studied to achieve a better understanding [203], owing to the limited success of their application in contaminated environments. Indigenous microorganisms are better adapted to cold environments than any nonindigenous population. The isolation and enrichment of indigenous microbes with biodegradative potential are key steps in bioremediation [204]. However, further research and field demonstrations are required to confirm the applicability of bioaugmentation under environmental conditions. The introduced microorganisms may be inhibited by the indigenous microbial community and protozoan grazers. Therefore, implementation and monitoring steps are necessary after introducing the cultured bacteria to evaluate population susceptibility as well as intrinsic bioremediation.

In addition, the biodegradation of p-xylene is not easy relative to that of other BTEX compounds, and p-xylene is classified as a persistent pollutant and non-growth substrate. The biodegradation of BTEX compounds is generally initiated by mono- or dioxygenase enzymes, which might find it difficult to attack the two methyl groups present in p-xylene [205]. The successful activation of targeted metabolic genes in specific pathways relies mainly on the catabolic enzymes involved and the transcriptional regulation of the pathways [206] to direct the appropriate enzymatic cascades in response to the specific pollutant as a substrate [207].

Several studies have shown low or no degradation of p-xylene by *Pseudomonas* strains, such *Pseudomonas* B1 and X1 [208], *Pseudomonas stutzeri* OX1 [209], *Pseudomonas sp.* BTEX-30 [210], *Pseudomonas putida* AQ8 [211], and *Pseudomonas putida* [212], even at favorable temperatures (20-30 °C). There have been few studies specifically addressing the bioremediation of p-xylene. For example, Rotaro et al. (2010) identified microorganisms in enrichment cultures obtained from a wastewater treatment plant for *p*-xylene degradation. They reported that the dominant bacterial strain was related to *Denitratisoma oestradiolicum* in enriched cultures [213]. Kermanshahi pour et al. (2006) studied the biodegradation kinetics of p-xylene in a new type of biofilm reactor (immobilized soil bioreactor). The most predominant microbial communities in the bioreactor were populations of *Pseudomonas acidovorans* and *Chryseobacterium indologenes* [212]. The TOL plasmid contains the genes encoding the enzymes necessary to aerobically degrade BTEXs and has been extensively studied in *Pseudomonas putida*. However, a few studies have been conducted on TOL plasmid expression in the presence of p-xylene in *Pseudomonas* strains [214]. Moreover, *Pseudomonas* species have been extensively identified in petroleum hydrocarbon-contaminated soil and water in cold regions [199]. However, the potential of

psychrophilic strains for the bioremediation of p-xylene as well as gene expression aspects of biodegradation in cold climates are still unknown.

Therefore, this study was performed with two main objectives: (1) to evaluate the ability of three psychrophilic isolates to biodegrade p-xylene at 15 °C and (2) to investigate the reason for the differences in p-xylene metabolism through a gene expression analysis of the enzymes involved. This study combined biodegradation experiments, gene expression analysis, and enzyme activity tests to identify the mechanism underlying the complete and effective biodegradation of p-xylene by psychrophilic strains. The p-xylene degradation potential of three BTEX-degrading *Pseudomonas* strains was confirmed based on carbon mass balances through the determination of the intermediates produced.

3.2.2. Materials and Methods

Chemicals and culture medium

All the chemicals and culture media used in this work were of analytical and microbial grade and were obtained from Fisher Scientific, Ontario, Canada. Benzene, toluene, ethylbenzene, p-xylene (99.9%), methanol (chromatographic grade), tryptic soy broth (TSB), and tryptic soy agar (TSA) were purchased from Sigma–Aldrich (Mississauga, Ontario, Canada). Carbon-free mineral salt media (MSM) (1.8 g/L K_2HPO_4, 4.0 g/L NH_4Cl, 0.2 g/L $MgSO_4.7H_2O$, 0.1 g/L NaCl, and 0.01 g/L $FeSO_4.7H_2O$) were used for biodegradation tests [215].

Isolation of bacterial strains from soil samples

The bacterial strain used in the present study was isolated from a confidential petroleum-contaminated site in Montreal, Canada, with a typical aquifer temperature of 8 °C to 15 °C. The samples were collected from soil at depths ranging from 5 to 7 m where the p-xylene concentration

was 10,000 mg/kg. The enrichment and adaptation steps were carried out using MSM supplemented with 50-200 mg/L BTEXs. Briefly, the samples were enriched with a 50 ppm BTEX mixture (1:1:1:1) and incubated at 15 ±1 °C at 150 rpm for one month. Then, the mixture (soil and MSM) was transferred to fresh MSM supplemented with a higher concentration (100 or 200 ppm) of BTEXs. After one month, the culture was cultivated in TSA (Sigma–Aldrich, Canada) at 15 °C for 3 days. Isolation and biodegradation tests were carried out between 8 °C and 15 °C (the typical aquifer temperature range at the contaminated site). Single colonies with different morphologies were selected and transferred to TSB and incubated at 15 ±1 °C for 3 days. The strains were characterized by the amplification and sequencing of a 16S rRNA fragment (27F: 5'-AGAGTTTGATCCTGGCTCAG-3', 1492R: 5'-GGTTACCTTGTTACGACTT-3'). The sequences were compared with available sequences in the National Center for Biotechnology Information (NCBI) database. Phylogenetic analysis was performed using the neighbor-joining algorithm of MEGA 7.0 software with 1000 bootstrap replicates [216].

Biodegradation tests

Experiments testing growth ability and the biodegradation of p-xylene were carried out in 150 mL sealed serum bottles containing 200 mg/L p-xylene. The 200 mg/L concentration of p-xylene was selected because this compound is partially insoluble in water, with a solubility of 198 mg/L at 25 °C [217]. This value was considered to provide sufficient bioavailability of this compound to promote the biodegradation efficiency of xylene-utilizing microorganisms. Our previous work also showed that 200 mg/L p-xylene can induce the production of degrading enzymes as well as the expression of genes encoding enzymes relative to 50 and 100 mg/L p-xylene (low and intermediate concentrations) [218]. The medium (at pH 7.0 ± 0.2) was placed in a 150-mL serum bottle sealed with a Teflon-coated rubber stopper, with a 9:1 airspace/liquid ratio. The inoculum was added after

24 h of equilibrium of the p-xylene concentration between the liquid and headspace under the experimental conditions. Inoculation (1% v/v, OD600=2) was carried out using a gas-tight syringe. The inoculated cultures (Od600=2, corresponding to 6×10^7 cells/mL) were incubated at 15 °C in a rotary shaking incubator (150 rpm).

The concentration of p-xylene in the collected liquid phase was detected using GC/MS. As p-xylene is considered a highly volatile compound, only approximately 50 to 60% of the concentration added can be detected in the liquid phase. The concentrations in the liquid and gas phases were measured, and the necessary concentration was compensated to correct the results. Growth experiments indicated that *P. putida* S2TR-01 could not grow on p-xylene as the sole source of energy and carbon. To assess the effect of p-xylene, the cells were grown on TSB medium, harvested via centrifugation at 12,000 × *g* and 4 °C for 5 min, and then inoculated in MSM supplemented with 200 mg/l p-xylene. At selected time intervals, the cells were harvested for further analyses.

Two types of control groups were designed for the tests: 1) abiotic controls inoculated with autoclaved bacteria (121 °C for 20 min) were run in parallel to monitor abiotic processes such as volatilization and bacterial sorption in the biodegradation experiments; and 2) controls consisting of isolates grown in the presence of glucose (2.5 g/L) as the sole source of carbon [219] instead of p-xylene were used for intermediate, gene expression and enzyme analyses.

p-xylene analysis

In each batch study, subsamples (500 µL) were removed from the liquid phase of bottles using a gas-tight syringe for the OD600 and substrate concentration measurements every 6 h. A subsample of 50 µL was prepared in a 40 mL standard headspace bottle containing 5 mL of ultrapure water and 10 µL of fluorobenzene-D5 (100 mg/L diluted in methanol) as an internal standard, and the

bottle was then sealed immediately. The concentrations of p-xylene were analyzed based on the EPA 8021B method, and p-xylene was extracted using a Perkin Elmer Turbomatrix HS-40 trap automatic headspace sampler. The gas phase of the samples was quantitatively analyzed using a 7890A gas chromatograph (DB-1701 column 30 m×0.25 mm i.d. × 0.25 μm film thickness), at temperatures of 45 °C and 300 °C for the column and detector, respectively. The concentration of intermediates was analyzed using a CP-Wax 57 CB column (25 m × 0.25 mm × 0.20 μm, Agilent Technologies, Netherlands) connected to a Varian 2200 gas chromatograph coupled to a Saturn mass detector. Intermediates (p-cresol and p-toluic acid) were not determined by headspace GC/MS because they are semivolatile compounds.

Gene expression analysis

Based on biodegradation and biomass kinetics (results presented in Section 3.2), the timepoints of 10, 20, and 50 h were selected for gene expression analysis to represent the early phase of incubation (lag period of biodegradation), exponential phase of biomass production (mid-period of biodegradation), and stationary phase of biomass (last stage of substrate biodegradation), respectively. Growing cultures were harvested by centrifugation to obtain ~10^{10} cells, and the pellets were then used for RNA extraction and cDNA synthesis as indicated in the supplementary material (Section A1 and Fig. A1).

The *xyl* gene sequence of *Pseudomonas putida* TOL plasmid pDK1 (GenBank accession no. AF019635.1) was used as the complete CDS (Coding Sequence) for primer design. The 16S rRNA sequence of *Pseudomonas putida* (GenBank accession no. MN625925.1) was also used as a template for primer design. Primers for PCR and real-time PCR were designed using Primer3 program version 0.4.0 (http://bioinfo.ut.ee/primer3-0.4.0/) to target the *xylM*, *xylA*, *xylE*, *xylS xylR* and 16S rRNA genes of isolated *Pseudomonas* (Table 3.1.1). Primer-BLAST (Basic Local

Alignment Search Tool) was used to check the specificity of the primers in a wide range of *Pseudomonase* strains. This online primer design platform combines BLAST with a global alignment algorithm to ensure that primers are sensitive enough to detect targets without a number of mismatches to primers [220]. The potential formation of primer dimers and other secondary structures was checked in Gene Runner software Version 6.5.52 Beta. Additionally, plasmid DNA was amplified using the above primers, and the PCR products were checked for their estimated size to ensure that the primers targeted the appropriate genes in the isolated strains. The relative expression of selected genes was analyzed with a real-time PCR System (Rotor-Gene Q-QIAGEN) and a SYBR Green real-time PCR Master Mix kit (QIAGEN, Germany). The reaction components were Taq polymerase, dNTP, $MgCl_2$, SYBR green I dye (20 µL Master Mix), 0.2 µL primers, 0.5 µL cDNA, and 10 µL H_2O. The thermocycling conditions for real-time PCR are shown in Table A2. All experiments were repeated in triplicate in both biological and analytical experiments. Each mRNA expression value was normalized against the threshold cycle of 16S rRNA expression as a housekeeping gene. Our preliminary results showed that 16S rRNA was constitutively expressed during p-xylene biodegradation by the tested *isolates* (CT=14.0±0.7), indicating that it could be used as a reference or housekeeping gene. Mean normalized gene expression ± standard deviation (SD) values were calculated from triplicate analyses. The fold changes of target genes were calculated as $RQ= 2^{-\Delta\Delta ct}$ values using Equations 1 to 3:

$$\Delta C_t = (C_t \text{ of targeted gene}) - (C_t \text{ of housekeeping gene}) \quad (1)$$

$$\Delta\Delta C_t = (\Delta C_t \text{ of experimental test}) - (\Delta C_t \text{ of control test}) \quad (2)$$

$$RQ = 2^{-\Delta\Delta Ct} \quad (3)$$

Our target genes were *xylM, xylA, xylR, xylE,* and *xylS*. Our housekeeping gene was the 16S RNA gene.

One advantage of the relative quantification method is that it does not require the use of standard curves, which makes it faster and easier than other approaches [221]. The melting curve of the real-time PCR products was checked by raising the temperature in increments of 0.3 °C to ensure that only the targeted products were formed. This study applied qPCR to achieve more accurate and quantitative results than are obtained with other analytical methods (such as protein and biochemical analyses) for the TOL plasmid study.

Table 3.2.1. Primer sequences used for PCR and real-time PCR in this study.

Target Gene	Product	Orientation	Primer Sequence (5'-3')	Tm (°C)	Amplicon size (bp)
XylM	Xylene monooxygenase hydroxylase subunit	F R	AATGTCTCGGTTCGGATCAC AGTGGTGTGCCAACTCTTCC	60	114
xylA	Xylene monooxygenase	F R	GCAGCGCTTCTATTTCGTC GAGAGCAATGCGACAATGG	58	166
xylE	Catechol 2,3-dioxygenase	F R	CTTCAAGGTGACCGACGATG GGTGTACTCCTTCTCGGCATAG	60	172
xylS	Transcriptional activator	F R	ACCACAGAATCTTCGGATGC GGCGAAAAATAGTGCTCCTG	60	157
xylR	Transcriptional activator	F R	ACCCGCTCTAGCTCTCCTTC ATCGAGTCGGAACTGTTTGG	60	179
16S rRNA	Ribosomal RNA	F R	CGGAATTACTGGGCGTAAAG TCTACGCATTTCACCGCTAC	59	149

Enzyme and protein assays

Bacterial cells were harvested after 50 h of incubation because the maximum enzyme activity can be assayed when the bacteria are in the stationary phase of growth [222]. The extraction of intracellular products is dependent on the growth phase [223], and it is well documented that the

cell lysis effect can be negligible when bacterial cells reach the stationary growth phase [224]. Our preliminary results also confirmed that 50 h of incubation was the best time for the extraction of intracellular enzymes. These preliminary results were obtained based on the xylene monooxygenase assay in cell suspensions according to Arenghi et al. [225] and in cell lysates after ultrasonication. Briefly, the cells were washed twice by centrifugation at 5000 × *g* with 20 mM phosphate buffer (pH approximately 7.0) and were resuspended in the same buffer. The cells were disrupted by applying two frequencies of ultrasound (22 kHz and 30 kHz) for 6 min The cellular lysates were centrifuged at 13,000 × *g* for 20 min, and the supernatant was used for enzyme assays. Two key enzymes encoded by the *xyl* operon were selected (xylene monooxygenase and catechol 2, 3 dioxygenase), and their activities were measured [218]. Based on enzyme activity tests in psychrophilic isolates, 15 °C was determined to be the optimal temperature for enzymes obtained from the isolates, so all of the enzymes assays were carried out at this optimal temperature. To determine specific activity (units per mg of proteins), the total protein concentration was determined by the Bradford method [226]. Briefly, an acidic solution of Coomassie dye was added to the protein solution, and the absorbance was then measured at 595 nm. The total protein concentration in the samples was determined using a standard curve with known concentrations of bovine serum albumin (BSA).

Xylene monooxygenase activity

Xylene monooxygenase activity was determined by monitoring the increase in the phenolic compound concentration in the medium using a colorimetric assay slightly modified from Arenghi et al. [225]. Briefly, 0.5 mM NADPH (final concentration) and 35 µL of 4% (vol/vol) *p*-xylene in N,N-dimethylformamide were added to the cellular lysates. After incubation at 15 °C, 1-mL samples were collected at 3-min intervals and mixed with 100 µL of 1 M NH_4OH and 100 µL of

2% 4-amino antipyrine. After the addition of 100 µL of 8% $K_3Fe(CN)_6$, the samples were briefly centrifuged (14,000 × *g*), and the A500 of the supernatant was then measured. Phenolic compound concentrations were calculated by reference to a standard curve for p-cresol (in the range of 0-50 µg/mL). Specific activity was defined as micromoles of phenolic compounds produced per minute per milligram of cell protein.

Catechol dioxygenase assay

The reaction mixture (3.0 mL) contained 2.0 mL phosphate buffer, 0.6 mL of 1 mM catechol, 0.2 mL deionized water and 0.2 mL cellular lysates. The reaction was allowed to proceed at 15 °C, and subsamples were taken every 2 minutes. Catechol 2,3-dioxygenase activities were determined by measuring the production of 2-hydroxymuconic semialdehyde at 375 nm. One unit of enzyme activity was defined as the amount of enzyme that formed 1 µmol of muconic acid per minute per milligram of cell protein [205].

Carbon mass balance

The carbon mass balance of each isolate was determined by measuring substrate consumption using GC-head space (as mentioned previously), intermediate, biomass growth, and carbon dioxide production measurements.

Intermediates formed during p-xylene biodegradation were analyzed using two types of gas chromatography/mass spectrometry systems: 1) a GC-MS system equipped with a wax capillary column (for the detection of nonvolatile intermediates) and 2) a GC-MS system equipped with a headspace sampler (for the detection of possible volatile intermediates, as indicated for p-xylene concentration analysis).

The GC-MS system was equipped with a CP-Wax 57 CB column of 25 m × 0.25 mm × 0.20 µm (Agilent Technologies, Netherlands). The temperature of the GC oven was programmed to

increase from 40 °C (held for 1 min) at 5 °C/min to 200 °C (held for 10 min). The injector temperature was set at 180 °C, and the MS interface temperature was set at 250 °C and 280 °C for the ionization source. All metabolites were identified via GC/MS by matching the retention times and ion spectra with authentic standards and NIST library data. Then, the concentrations were determined using the calibration curves of the corresponding standards.

The amounts of carbon recovered as C-CO_2 and the carbon recovered as biomass were determined after substrate exhaustion, and the values were corrected using control flasks incubated with no carbon source. Carbon dioxide was measured chromatographically via GC-MS (7820A GC system Agilent Technologies, Netherlands) [227]. Biomass was collected via 0.45-µm-pore-diameter filtration and placed in an oven, and the dry biomass content was determined. A linear relationship was observed between the OD600 and the cell dry weight of the isolates (cell dry weight (mg/L) =308× OD600, R^2=0.95). The amount of carbon recovered as biomass was calculated by assuming that 26 g dry weight contains approximately 1 mole of carbon [228]. Tijhuis et al., (1993) mentioned that one C-mole of biomass is the amount of biomass which contains 12 g C, which is about 26 g dry weight [228]. Carbon mass balance tests were conducted in triplicate for isolates and control samples.

Statistical analysis

Statistical analysis was performed via one-way analysis of variance (ANOVA) followed by Tukey's post hoc procedure. A probability of less than 0.05 was considered statistically significant. All analytical and biological tests were performed in triplicate. Error bars indicate SD; $n = 3$. The p-xylene removal and target gene expression correlations were analyzed using the two-tailed Pearson correlation test.

3.2.3. Results and Discussion

Identification of psychrophilic isolates

Among all obtained isolates, three psychrophilic bacteria were selected based on their ability to grow on BTEXs and the differences in their behavior regarding p-xylene degradation as the sole source of carbon. The three BTEX-degrading bacteria were named S2TR-01, S2TR-09, and ST2TR-20. The 16S rRNA gene sequences indicated that S2TR-01 was most closely related to the type of strain of *Pseudomonas putida* ATCC 12633^{T}, with 99% sequence similarity. S2TR-09 and ST2TR-20 showed more than 98% similarity to *Pseudomonas azotoformans* DSM 18862^{T} and *Pseudomonas synxantha* ATCC 9890^{T}, respectively. The 16S rRNA gene sequences of each isolate were deposited in the NCBI GenBank database and assigned the accession numbers shown in Fig. A2. Phylogenetic analysis also showed that S2TR-01, S2TR-09, and ST2TR-20 formed a phylogenetic lineage with members of the mentioned strains. *Pseudomonas* spp. is an excellent microorganism for use in bioremediation because of the plasticity and flexibility of its metabolic pathways and its ability to live under diverse environmental conditions (Palleroni and Moore, 2010). Kabelitz et al. (2009) reported that *Pseudomonas* species are the dominant microbial community in ecosystems that are highly contaminated with kerosene and BTEXs. Their results showed that *Pseudomonas* not only survives under harsh conditions, such as low oxygen levels, high loads of aromatic carbon pollutants and high solvent concentrations, but also replicates under these conditions, which is an important indicator of efficient bioremediation [229].

The BTEX degradation abilities of the three isolated bacterial strains were analyzed at 5-30 °C, and all of them showed obvious BTEX degradation at cold temperatures (5-15 °C). The optimum temperature for bacterial growth and biodegradation was 15 °C, and no growth was observed at 30 °C in the presence of BTEXs (Table B1). These strains showed interesting results such as a

high rate of BTEX degradation at a low temperature (15 °C). However, they exhibited different degradation and growth abilities in the presence of p-xylene as the sole source of carbon (Table. B1). Many mesophilic *Pseudomonas* strains have been identified as BTEX degraders, such as *Pseudomonas* B1 and X1 [208], *Pseudomonas stutzeri* OX1 [230], *Pseudomonas sp.* BTEX-30 [210], *and Pseudomonas putida* AQ8 [211]. These strains have also shown low xylene degradation rates even at favorable temperatures (20-30 °C). A study on the effect of the chemical structure of BTEXs on four chemolithotrophic bacteria showed that increases in the number of alkyl groups in a benzene ring and the size of the compounds can increase the toxicity of these compounds [231]. Similarly, the isolated bacteria showed different p-xylene degradation rates (as described in the following section), which could be due to the additional methyl group in p-xylene and its toxic effect relative to other BTE compounds. However, a more detailed toxicity assay is needed to confirm that p-xylene and ethylbenzene, with additional methyl and ethyl groups relative to benzene and toluene, respectively, are more toxic than the latter pair of compounds.

Biodegradation of p-xylene

The p-xylene biodegradation experiments were carried out at an initial p-xylene concentration equal to ~200 mg/L at 15 °C. The changes in biomass and the p-xylene concentration versus time are shown in Fig. 3.2.1. The results indicated that *P. azotoformans* S2TR-09 degraded p-xylene faster than the other isolates after 60 h ($p<0.05$). The biodegradation of p-xylene by *P. synxantha* S2TR-20 was complete after 5 days (120 h). However, *P. putida* S2TR-01 showed no p-xylene degradation even after 10 days of incubation (Fig. 3.2.1). The biomass results confirmed that *P. putida* S2TR-01 could not use p-xylene as the sole source of carbon. Although a small decrease in the p-xylene concentration (~30 mg/L) was observed in the presence of *P. putida* S2TR-01, this change was not attributed to biomass production (Fig. 3.2.1). This was due to the accumulation of

intermediates, as mentioned in the following section on carbon mass balance. As shown in Fig. 3.2.1, the concentration of *P. azotoformans* S2TR-09 biomass increased with time in the presence of p-xylene in the following order: S2TR-09> S2TR-20> S2TR-01 ($p<0.05$). Based on the reported literature, the degradation of p-xylene can be expected to vary among *Pseudomonas* strains. For instance, You et al. (2013) reported that 54% p-xylene degradation was achieved by *P. putida* YNS1 after 96 h of incubation at 30 °C [232]. Jeong et al. (2006) reported 90% removal of p-xylene (5.1 mg) using *Pseudomonas* sp. NBM21 in a biofilter at 30 °C after 4 h [233]. Worsery et al. (1975) showed that *P. putida* mt-2 could degrade p-xylene as a carbon source for growth [214]. These results indicated that each strain has a different degradation ability. The results of this study also showed that the examined psychrophilic isolates present different biodegradative abilities in the presence of p-xylene.

Several researchers have reported that when microbial strains are grown in basal mineral media or media containing p-xylene alone at ambient temperature (20-30 °C), toluene is degraded more readily, and the slowest biodegradation rate is observed for p-xylene (sometimes no biodegradation is reported) [234], [235]. You et al. (2018) reported lower p-xylene biodegradation by *Rhodococcus* sp. ZJUT312 relative to its degradation of other BTE compounds [236]. Wang et al. (2015) reported that *Pandoraea* sp. strain WL1 could degrade 16.6 ~ 99.4 mg/L p-xylene as the sole source of carbon in the liquid phase within 6 to 18 h at 30 °C [161]. In the case of cold-climate environments, low temperatures (e.g., below 10 °C) pose an additional challenge to biological treatments, and it may require more time (ranging from 1 to 10 years) to meet cleanup standards in such areas [199], [237]. The results of this study showed that more time is needed for the complete degradation of p-xylene compared to the times indicated by previous studies. However,

the concentration of contaminants should be considered an important factor because of their toxicity and inhibitory effects.

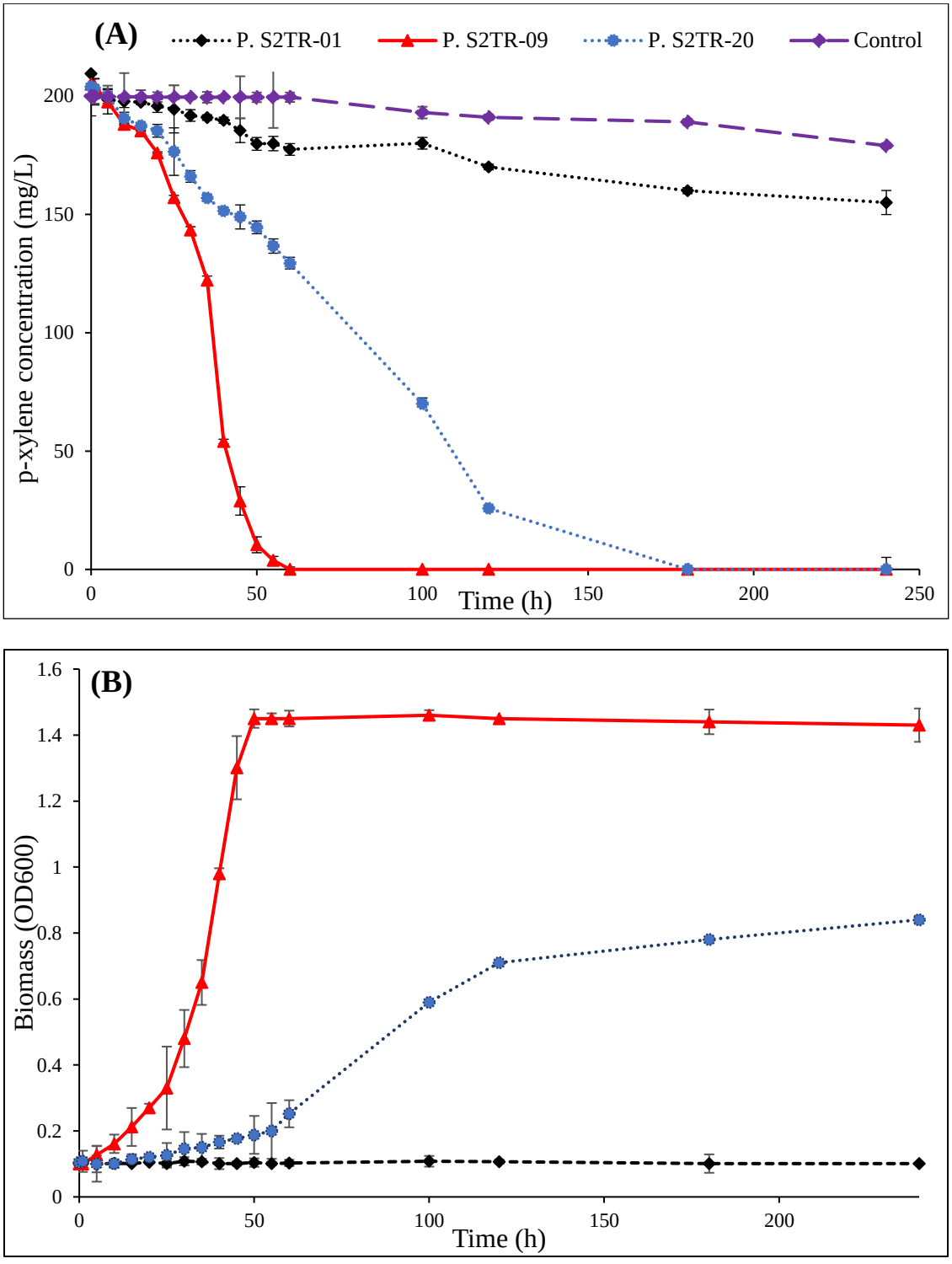

Fig.3.2.1. p-xylene biodegradation (A) and biomass production (B) by *P. putida* S2TR-01, *P. azotoformans* S2TR-09, and *P. synxantha* S2TR-20 with an initial concentration of 200 mg/L. Error bars indicate Standard Deviation (SD); *n* = 3.

Effect of p-xylene on catabolic gene expression

The TOL plasmid is the best-studied catabolic plasmid as a broad-host-range plasmid [238], [239]. Generally, BTEX biodegradation occurs via two pathways (*tod* and *tol)* in *Pseudomonas* strains [240]. In the *tod* pathway, bacteria use xylene dioxygenase as a primary enzyme for p-xylene degradation. Based on our preliminary results and a previous study [218], xylene dioxygenase shows no activity in the presence of p-xylene in the exponential growth phase (data not shown); hence, the isolates did not use the *tod* pathway in this case. As bacteria use one of these pathways, we conclude that these strains contain a TOL-like pathway. We thus followed the expression of TOL-type genes in the presence of p-xylene (Fig. 3.2.2). The genetic organization of the catabolic genes in the TOL plasmid reflects the biochemical pathways, so the catabolic genes can be organized into two operons: *upper* and *meta*-cleavage operons (Fig. 3.2.3). Notably, the proposed genetic map of the TOL plasmid in isolates (Fig. 3.2.3) was described based on isolates with the same catabolic phenotype, and the archetypal TOL plasmid pWWO originated in *P. putida* mt-2. Many other TOL plasmids have been identified that have the same prototype but show different sizes because of gene duplications encompassing entire catabolic operons or parts of catabolic operons (Williams et al., 2004). The comparative sequencing of the TOL plasmids of isolates could be carried out to provide a wealth of information about the role of TOL plasmids and the history of bacterial evolution.

The *upper* operon comprises 5 genes (*xylCMABN*) that encode the enzymes responsible for the monooxidation of aromatic hydrocarbons to their corresponding carboxylic acids. *xylM* and *xylA* encode two subunits of xylene monooxygenase, which is the first and most important enzyme in

the biodegradation pathway of BTEXs [241]. The *meta*-cleavage operon (containing *xylXYZLTEGFJQKIH*) encodes the enzymes responsible for the degradation of benzoate to Krebs cycle intermediates. These 13 genes are conserved as one of the largest operons found in prokaryotes, at over 11 kb [242]. The *xylE* gene encodes a key enzyme, catechol 2,3-dioxygenase, involved in the ring cleavage of aromatic hydrocarbons. The *xylR* and *xylS* genes encode specific transcriptional regulators that activate the expression of two pathway genes, *xylR* and *xylS*, located downstream of the *meta*-cleavage operon (Fig. 3.2.3; [243]. In pWW0, the genes encoding XylS and XylR are located at the 3' end of the *meta*-cleavage operon, which controls the expression of the genes in this pathway (Fig. 3.2.3).

The results presented in Fig. 3.2.2 show that *xylM* and *xylA* were upregulated in all isolates in the presence of p-xylene because xylene monooxygenase is needed to initiate the degradation pathway. The results obtained for *xylM* and *xylA* were consistent with the *xylR* expression profile, showing upregulation in the presence of p-xylene. Although there was no significant difference in the gene expression of *xylM* and *xylA* between the isolates, *xylR* showed a decreasing trend after 10 h of incubation (active time of biodegradation). This may correspond to a decrease in the p-xylene concentration and the negative autoregulation of *xylR*, as reported by de Las Heras et al., [244].

However, Bertoni et al. (1998) and Marqués (1194) reported that *xylR* expression in pWW0 was immediately downregulated after the addition of p-xylene to cells growing on mineral salt media. Our results showed the upregulation of *xylR* in the presence of p-xylene and growth phase-dependent *xylR* expression. Xylene can induce the expression of *xylR* and its encoded protein (XylR), and this protein can bind aromatic compounds and regulate the expression of the genes

encoded by the *upper* operon in the TOL plasmid [242], [243]. Further investigation of the expression of this gene in different strains would provide a wealth of information on this gene.

Pearson's correlation indicated a statistically significant relationship between the expression of target genes and the p-xylene removal rate in *P. azotoformans* S2TR-09 (Table 3.2.2). The p-xylene degradation rate was calculated as the change in the p-xylene concentration divided by the change in time, with 10, 20 and 50 h representing the *lag* period of biodegradation, mid-period of biodegradation, and last stage of biodegradation, respectively. The expression of *xylE* and p-xylene removal were significantly correlated in all isolates ($p < 0.05$), which was consistent with p-xylene degradation in the order of *P.* S2TR-09 > *P.* S2TR-20 > *P.* S2TR-01 ($p<0.05$). The growth of bacterial strains on p-xylene requires the expression of a *meta*-cleavage operon because this pathway funnels the intermediate benzoate derivative into the Krebs cycle, which provides the main source of cellular energy for aerobic microorganisms [245]. Transcriptional stimulation of the *meta*-cleavage operon is activated by the *xylS* regulator, with the interaction of benzoate and methyl benzoate as effectors [242]. As shown in Fig. 3.2.2, gene expression levels differed depending on the degradation ability of the strain and the time of degradation. Our results showed that *xylS* was induced only in the isolates (*P. azotoformans* S2TR-09 and *P. synxantha* S2TR-20) that could grow in the presence of p-xylene, whereas in *P. putida* S2TR-01, *xylS* and the *meta*-cleavage operon were not induced (Fig. 3.2.2).

Table 3.2.2. Correlations between fold change of target gene and p-xylene removal rate

		p-xylene Removal	*xylM*	*xylA*	*xylR*	*xylE*	*xylS*
P. putida S2TR-01	10h	-1.16922	1.12	0.314	0.006	0.019*	0.00017
	20h	-0.1956	0.95	0.32	0.005	0.026*	0.00015
	50h	-0.2	0.78	0.31	0.0015	0.021*	0.00016
P. azotoformans S2TR-09	10h	-1.7	1.29**	0.315**	0.009**	0.345*	0.0019*
	20h	-1.2	1.2**	0.31**	0.0079**	0.39*	0.0026*
	50h	-3.52	1.01**	0.280**	0.005**	0.33*	0.0021*
	10h	-1.35	1.17	0.3	0.0085**	0.12*	0.0012

P. synxantha S2TR-20	20h	-1.87	1.04	0.3	0.0062**	0.15*	0.00118
	50h	-1.98	1.05	0.311	0.0067**	0.18*	0.00125

* Symbolize the significant difference between p-xylene concentration and each targeted gene at $P < 0.05$.
** Symbolize the significant difference between p-xylene concentration and each targeted gene at $P < 0.01$.

Velazquez et al. (2005) showed that upper *xyl* operon gene expression was quickly and strongly induced upon exposure to *m*-xylene, while a certain delay in the induction of the *meta*-cleavage operon genes was observed. They showed that the expression of the *xylE* gene remained upregulated in all growth phases until the end of the experiment. They also mentioned that the most evident change after 3 h of contact of *P. putida* mt-2 with *m*-xylene was the expression of the entire complement of *lower* operon *xyl* genes [246]. Our results showed an upregulation of *xylE* in S2TR-09 during the *lag* period of biodegradation, when metabolites had been accumulated. Even higher relative expression of the gene was observed in the exponential phase of biomass production (Fig. 3.2.2. D).

Generally, the expression of the *meta*-cleavage operon is controlled in two ways: 1) the XylS protein activates the promotors of the operon, which is positively regulated by intermediates such as benzoate derivatives; and 2) the toluene/xylene-activated XylR protein in combination with a sigma factor stimulates transcription from the xylS gene promoter via a cascade regulatory system [247]. Our correlation analysis between the gene expression of *xyl* genes and the p-xylene removal rate showed that a small increase in *xylS* in *P. azotoformans* S2TR-09 had a significant effect on p-xylene removal ($p<0.05$). Previous studies showed that the expression of the *xylR* gene is constitutively high in *Pseudomonas putida* [248], while the *xylS* gene appears to generally be expressed at a low basal level. *xylS* expression seems to be required to activate the *meta*-cleavage operon via its promotor (*Pm*) [247]. Our results showed that *xylS* was NOT induced in S2TR-01, and this result emphasizes that S2TR-01 cannot degrade p-xylene to use it as a sole carbon source.

The differences in the expression of the genes of the *meta*-cleavage operon and its regulatory gene (*xylS*) can explain the differences in p-xylene degradation among the isolates.

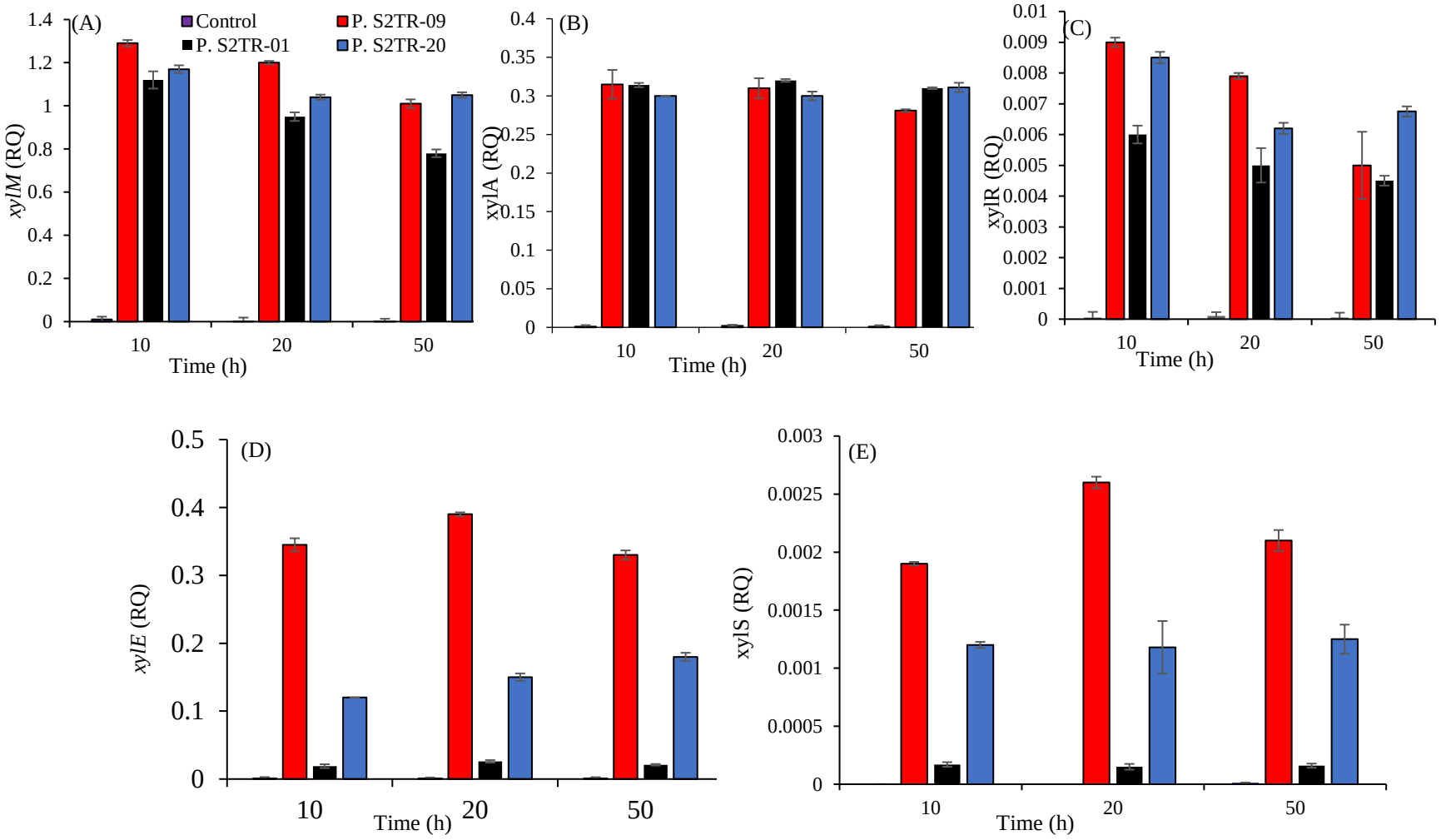

Fig. 3.2.2. Gene expression of *upper* and *meta* operons and their transcriptional regulatory genes in different isolated bacteria (*P. putida* S2TR-01, *P. azotoformans* S2TR-09, and *P. synxantha* S2TR-20) grown on p-xylene, RQ, Relative quantification; Control, the sample form the bacteria grow on media without p-xylene (The presented data results from S2TR-09 due to similar data from other isolates). Error bars indicate Standard Deviation (SD); *n* = 3.

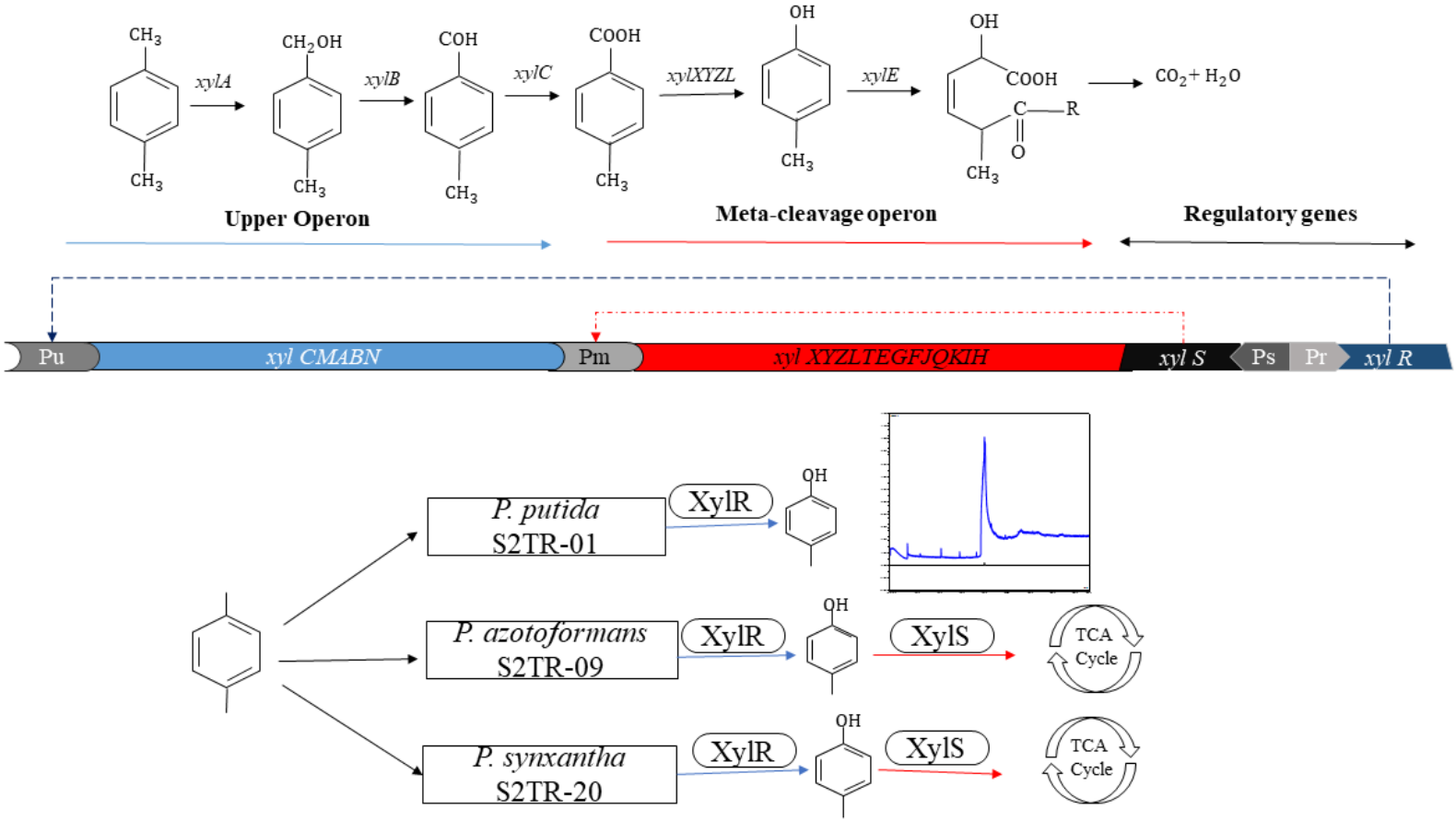

Fig. 3.2.3. Genetic map of the TOL pathway in biodegradation of p-xylene. Biodegradation of p-xylene requires the induction of *xylS* that regulates the meta-cleavage enzymes in isolated strains. The enzymes encoded upper operon transform p-xylene to p-cresols. Then, p-cresol is transformed into TCA cycle intermediates by encoded meta-cleavage enzymes. The structural genes, *xylCMABN,* and *xylXYZLTEGFJOKIH*; regulatory gene, *xyls,* and *xylR;* and promoters, Pu, Pm, Ps, and Pr.

Enzyme activity detection

In aerobic systems, oxygenases are key enzymes in microbial degradation. The key enzymes in the metabolism of p-xylene are xylene monooxygenase and catechol 2,3 dioxygenase [218]. Previous research showed that the oxidation of xylene may be initiated by the direct oxidation of the aromatic ring or the oxidation of one or two methyl groups of the aromatic nucleus by xylene monooxygenase. This enzyme can catalyze multistep oxidation and produce catecholic or noncatecholic derivatives [249]. Then, in the ring dearomatization of central intermediates, *ortho*-, *meta*- or *para*-cleavage by catechol dioxygenases occurs as the crucial step in detoxification [209], [250]. Catechol 2,3-dioxygenase is an iron-containing enzyme that is able to cleave the rings of oxidized derivatives from p-xylene to achieve the complete detoxification of this contaminant [16]. Mass spectra results showed that p-xylene is initially oxidized to central intermediates such as p-toluic acid and p-cresol by xylene monooxygenase (Fig. A3), and in the second step of biodegradation, the dominant intermediate p-cresol is finally decomposed into inert intermediates by catechol 2,3-dioxygenase.

Based on our preliminary time-course experiments, the best time for enzyme activity detection was the stationary phase of bacterial growth, when the cell lysis effect was minimal. Nagy et al. (2001) also reported that when growth reached the stationary phase, the activity of intracellular enzymes approached the maximum, and the cell lysis effect could be negligible at this time [224]. Xylene monooxygenase and catechol 2,3 dioxygenase activities are shown in Fig. 3.2.4. The results showed that xylene monooxygenase was produced in all isolates, which may support the results of the expression analysis of *xylA* and *xylM* as well as intermediate production in the following section. Fig. 3.2.4 shows that the activity of xylene monooxygenase and catechol 2,3 dioxygenase was significantly increased in *P. azotoformans* S2TR-09 (0.5 and 0.08 U/mg,

respectively) in the presence of p-xylene ($p<0.05$). Catechol 2,3 dioxygenase showed low or no activity in *P. putida* S2TR-01 and *P. synxantha* S2TR-20, which was consistent with the observed p-xylene degradation rate. This result indicated that the ring cleavage enzyme is necessary for the biodegradation of p-xylene in the isolates. Arenghi et al. (1999) showed that in *Pseudomonas stutzeri* OX1, toluene and o-xylene could be transformed by toluene-*o*-xylene monooxygenase (ToMO), but the ToMO-encoding operon did not contain genes related to ring-cleavage enzymes. Therefore, these genes may be clustered in one or more operons that are independently but coordinately regulated [225]. Our results also showed that all isolates produced xylene monooxygenase in the presence of p-xylene, but catechol 2,3 dioxygenase was only produced in the S2TR-09 isolate, which was consistent with the gene expression and biodegradation results.

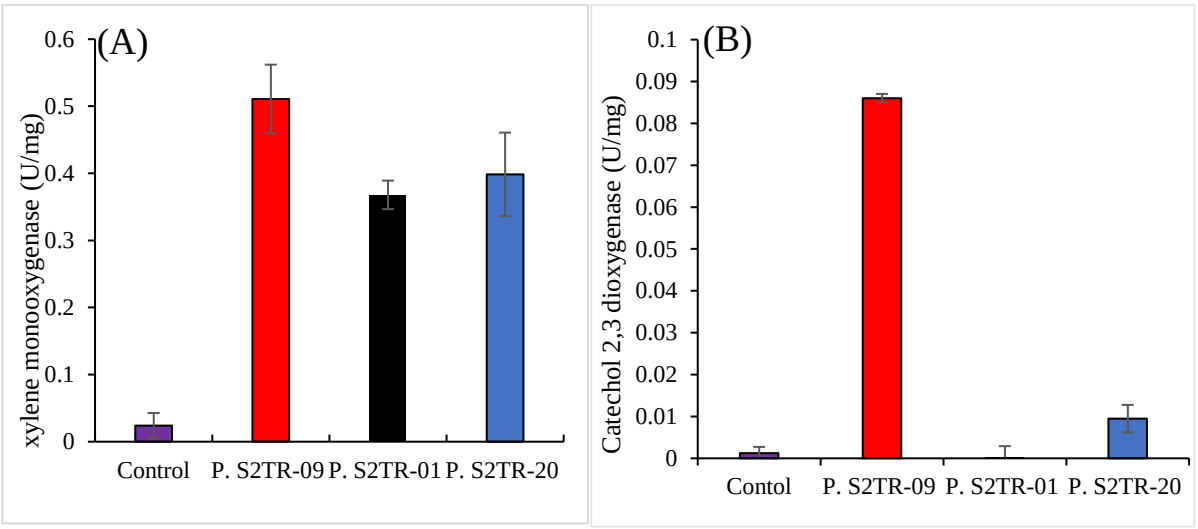

Fig. 3.2.4. Xylene monooxygenase and catechol 2,3 dioxygenase activity in different isolated bacteria (*P. putida* S2TR-01, *P. azotoformans* S2TR-09, and *P. synxantha* S2TR-20) grown on p-xylene. Control, the sample from the bacteria grow on media without p-xylene (the presented data results from S2TR-09 due to similar data from other isolates). Error bars indicate Standard Deviation (SD); $n = 3$.

Carbon mass balance

The carbon mass balances in each isolate were determined by measuring the amounts of consumed C (p-xylene) that were recovered as C-CO_2 and biomass. Initially, the carbon balances were determined based only on the amounts of C-CO_2 and C-biomass after 60 h of incubation (the late stage of p-xylene biodegradation). The carbon recovery rates were 91%, 97%, and 85% in *P. putida* S2TR-01, *P. azotoformans* S2TR-09, and *P. synxantha* S2TR-20, respectively (Table 3.2.3). To investigate the reason for this incomplete carbon recovery, the intermediates were detected at 60 h (based on the p-xylene biodegradation results), and their concentrations were then measured. The GC/MS results showed that p-xylene was converted first to p-toluic acid and then to p-cresol, which accumulated in the media of *P. putida* S2TR-01 and *P. synxantha* S2TR-20, while no intermediates were detected in the presence of *P. azotoformans* S2TR-09 (Fig. A3). The examination of p-cresol biodegradation also confirmed that *P. azotoformans* S2TR-09 and *P. synxantha* S2TR-20 could degrade 200 mg/l p-cresol within 10 h and 45 h, respectively, while *P. putida* S2TR-01 showed no p-cresol degradation after 60 h (Fig. A4). The formation of toluic acid and p-cresol in the presence of *P. putida* S2TR-01 indicated a small decrease in p-xylene concentration (Fig. 3.2.1). This was attributed to p-xylene transformation and NOT to degradation and biomass production. As shown in Table 3.2.3, when the concentrations of p-cresol, as the central intermediate, and other intermediates (p-toluic acid) were taken into account, the carbon recovery rates increased from 91% to 94% for *P. putida* S2TR-01, 97% to 99% for *P. azotoformans* S2TR-09 and 85% to 96% for *P. synxantha* S2TR-20. The results were consistent with the growth ability and production of ring cleavage enzymes of strains in the presence of p-xylene. The significantly high percentages of p-xylene conversion to biomass (~33%) and CO_2 (~66%) indicated the predominant fate of p-xylene in the presence of S2TR-09 was incorporation into cell materials and mineralization. The carbon recovery rates in isolates with a low p-xylene degradation

rate (S2TR-01 and 20) were lower (94 and 96%) than that in *P. azotoformans* S2TR-09 (99%). Similarly, Prenafeta-Boldú et al. (2002) reported a higher carbon recovery rate together with a lack of accumulation of intermediates, pointing to mineralization for BTE biodegradation in *Cladophialophora* sp. strain T1, while o- and m-xylene isomers were partially oxidized to dead-end products and showed lower carbon recovery values. These authors showed that toluene and ethylbenzene were both used for growth; approximately 67% of the carbon source was converted to CO_2, and 21% was recovered as biomass [251]. Moreover, Zhange et al. (2013) reported that *Mycobacterium cosmeticum* byf-4 converted o-xylene to CO_2 (65%) and biomass (27%), which resulted in 92% carbon recovery, while the removal efficiency was 99.99% [252]. These results highlight the importance of the carbon mass balance assay in the evaluation of microorganisms for the biodegradation of contaminants.

The metabolism of a substrate involves multiple enzymatic steps. As mentioned previously, the aerobic biodegradation of aromatic hydrocarbons has been divided into the *upper* pathway, which starts with the original compounds (hydrocarbon compounds without any modification) and produces central intermediates (modified hydrocarbons), and the lower pathway, beginning with the ring cleavage of intermediates and producing the molecules needed for biomass production [243].

Tsai et al. reported that catechols are formed during the aerobic biodegradation of a variety of aromatic compounds [250]. Arenghi et al. also reported that most of monoaromatic catabolic pathways give rise to (methyl) catechols, which are further processed through *meta* cleavage pathways [209]. The reaction products can be easily converted to tricarboxylic acid cycle (TCA cycle) intermediates, which are further broken down into CO_2 and water, providing energy for biomass production [240]. However, the results of this study showed that p-cresol was the central

intermediate and correlated well with the observations regarding gene expression (*xylE* and *xylS* in the presence of p-xylene). The results suggest that the ability to grow on p-xylene is correlated with the expression of ring cleavage enzymes and that a lack of ring cleavage enzymes or low concentrations of these enzymes may lead to the accumulation of toxic intermediates.

Table 3.2.3. Carbon balance in three isolated bacteria after 60h of incubation at 15°C

Isolate	Initial concentration of p-xylene (µmol)	C- of p-xylene (µmol)	C-Biomass (µmol)	C-CO_2 (µmol)	Concentration intermediates (µmol)		C-recovery (%)	
					p-toluic acid	p-cresol	Substrate, Biomass, CO_2	Substrate, Biomass, intermediates, CO_2
P. putida S2TR-01	2,080±65	1,870±50	6±0.4	10±2	25±0.8	50±2	91	94
P. azotoformans S2TR-09	2,120±87	<0.1	689±21	1,388±76	ND	15±0.5	97	99
P. synxantha S2TR-20	2,090±63	1467±31	85±12	227±18	31±0.8	198±5	85	96

3.2.4. Conclusion

p-Xylene, which belongs to the high-risk hazardous and noxious substances, is a persistent pollutant in terms of its recalcitrance to biodegradation. The preferential utilization of a substrate depends on genetic regulation in bacteria rather than a simple adaptation. In this study, three psychrophilic bacterial strains, *P. putida* S2TR-01, *P. azotoformans* S2TR-09, and *P. synxantha* S2TR-20, were evaluated for their p-xylene degradation abilities. *P. azotoformans* S2TR-09 catabolized p-xylene after 60 h, while the two other strains showed lower p-xylene degradation at 15 °C. The biomass results also followed the order S2TR-09> S2TR-20> S2TR-01. The gene expression study showed that no significant differences in the expression of the *xylM* and *xylA* genes among all isolates, while *xylE* and *xylS* genes were induced only in isolates *P. azotoformans*

S2TR-09 and *P. synxantha* S2TR-20, which could grow in the presence of p-xylene. Therefore, the expression of *xylE* (encoding a ring cleavage enzyme) and its activator (*xylS*) was correlated with the p-xylene removal rate. Enzyme activity tests also confirmed that all isolates produced xylene monooxygenase in the presence of p-xylene, while a ring-cleavage enzyme (catechol 2,3 dioxygenase) was produced only in the isolate that could grow on p-xylene as the sole source of carbon. The expression of *xylE* and *xylS* or the production of catechol 2,3 dioxygenase can be considered a biomarker of complete, efficient biodegradation of p-xylene. The analysis of intermediates confirmed the formation of p-toluic acid and p-cresol as dead-end products in isolates with lower p-xylene degradation rates (S2TR-01 and S2TR-20), which was consistent with the lack of ring cleavage enzymes. *P. azotoformans* S2TR-09 may be useful for the bioremediation of p-xylene at contaminated sites, and the expression of *xylE* and *xylS* may be considered a biomarker of the efficient biodegradation of p-xylene in isolated bacteria. Monitoring the expression of these genes can also provide persons responsible for site management with immediate feedback on the complete degradation of p-xylene after bioaugmentation. However, further studies and field demonstrations are required to confirm the applicability of the bioaugmentation method using *P. azotoformans* S2TR-09 at cold-climate sites.

CHAPTER FOUR: COLD ACTIVE ENZYME BOOSTER TECHNOLOGY for POTENTIAL APPLICATION in GROUNDWATER and SOIL

PART 1

3.1 Psychrozymes as novel tools to biodegrade p-xylene and potential use for contaminated groundwater in the cold climate

Saba Miri[1,2], Seyyed Mohammadreza Davoodi[1,2], Satinder Kaur Brar[1, 2*], Tarek Rouissi[2], Yi Sheng[3], Richard Martel[2]

1. Department of Civil Engineering, Lassonde School of Engineering, York University, North York, Toronto, Ontario M3J 1P3, Canada

2. INRS-ETE, Université du Québec, 490, Rue de la Couronne, Québec G1K 9A9, Canada

3. Department of Biology, life science, York University, North York, Toronto, Ontario Canada

(*Corresponding author, E-mail: satinder.brar@lassonde.yorku.ca; satinder.brar@ete.inrs.ca)

Bioresource Technology, 321, 124464; DOI: 10.1016/j.biortech.2020.124464

Abstract

Sites contaminated by petroleum hydrocarbons in cold-climate regions have recently received significant attention due to their sensitive ecosystem and human health impacts. Two cold-adapted *pseudomonas* strains were isolated from contaminated groundwater and soil. As xylene monooxygenase from *Pseudomonas synxantha* S2TR-26 and catechol 2,3-dioxygenase from *Pseudomonas mandelii* S2TR-08, have a matching end product, they acted in symphony to degrade p-xylene. Their unique thermodynamic and kinetic behavior permits them to achieve rapid degradation of p-xylene at low temperatures (<15°C). The results showed that the sequential action led to the conversion of 200 mg/l of p-xylene within 72h and complete degradation after 120h. The cocktail of these enzymes with a ratio of 1:1.5 (xylene monooxygenase: catechol 2, 3-dioxygenase) confirmed the complete degradation of p-xylene within 48h at 15°C. This approach will allow efficient biodegradation of p-xylene to minimize the bioremediation duration in cold-climate regions.

Keywords: biodegradation, cold-climate, p-xylene, monooxygenase, dioxygenase

Graphical Abstract

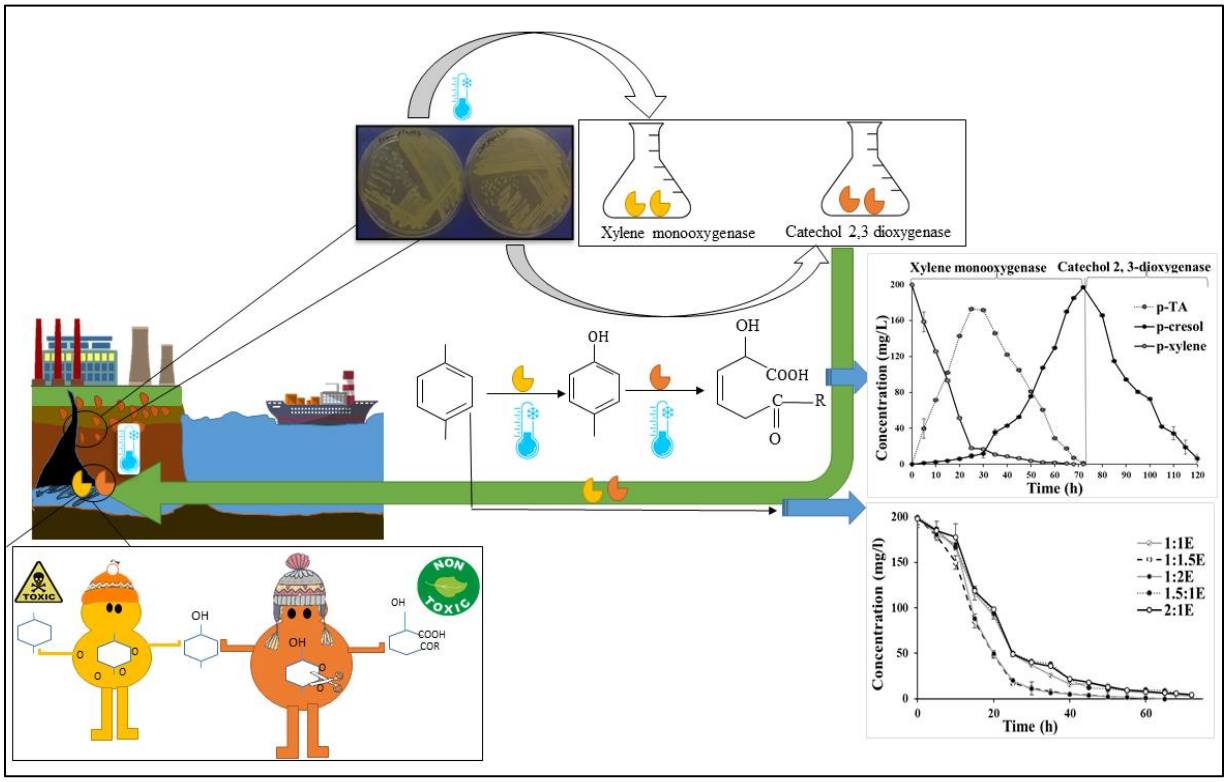

4.1.1. Introduction

p-xylene is widely used as a solvent and can be distributed as a pollutant in the environment sourced from various industries, such as leather, paint, rubber and printing, gasoline, airplane fuel. As p-xylene is a liquid, it can enter surface water, soil or air in large amounts as a result of an accidental spill during storage and burial at waste sites. Since p-xylene evaporates easily, it is rarely found in high concentrations in surface water or topsoil, but any p-xylene that does not evaporate from topsoil can travel downward and enter groundwater [253]. Remediation techniques based on the addition of chemicals and mechanical processes can be problematic due to the risk of additional environmental impacts [254]. Even though all petroleum aromatic hydrocarbons show relative resistance to degradation because of the stability of the pi-electron cloud resulting in the large negative resonance energy, bioremediation of m- and p-xylene is of great interest [255]. Xylene-degrading microorganisms, from the genera *Rhodococcus* and *Pseudomonas* have been isolated with different xylene degradation pathways (Miri et al., 2019). Commonly, the best (optimized) scheme of biodegradation cannot be easily achieved since the biodegradation efficiency of contaminants is strongly influenced by the physicochemical characteristics of the pollutant, the contaminated matrices, and microbial growth conditions [13].

Hence, the biochemical remediation method based on using enzymes, rather than whole-cell degrading microorganisms, has recently received increasing attention since the enzymatic method can specifically catalyze a series of reactions for pollutant removal [13], [256]. As bioremediation (using whole microbial cells) is a cost-effective and environment-friendly technology and it is powered by enzymes, the enzyme production needs to be optimized cost-effectively. Using enzymes have several advantages over whole microbial cells, for example, enzymatic method has a shorter treatment period than the microbial process because the enzymes transform the substrate

in a minute timescale. In the case of cold climate environments, low temperatures (e.g., below 10 °C) pose an additional challenge for biological treatments, whole microbial cell may require more time (ranging from 1 to 10 years) to meet cleanup standards [199]. Moreover, enzymes demonstrate high specificity for their substrate. Thus, the enzymatic treatment agent can be designated for specific pollutant removal without producing any toxic by-products [256]. This technique can be applied for contaminants that are catalytically decomposed in stepwise oxidation reactions by various oxidoreductases. For example, Kwean *et.al* applied the combination of oxidative enzymes such as chlorophenol monooxygenases, phenol 4-monooxygenase, putative flavin reductase, and dioxygenase, for enzymatic degradation of 4-Chlorophenol [13]. Gulloto et.al studied the combined action of toluene o-xylene monooxygenase to convert mono- and di-polyaromatic hydrocarbons into hydroxylated derivatives and fungal laccase to oxidize their hydroxylated derivatives for complete detoxification [257].

Concerning the challenges in bioremediation of cold-climate groundwater, injection of psychrozymes directly to the contaminated environment can be promising new methods for increasing the bioremediation rate and decreasing the environmental risks compared to conventional bioremediation (using whole microbial cells). The use of enzymes for human consumption dates back to more than 2000 years ago and numerous food products contain enzymes. To the best of our knowledge, there is no report on the ill effect of enzymes on humans, animal species, and plants. Although enzymes are considered as a biocatalyst, it does not categorize as biological hazards (Government of Canada & U.S. Food and Drug Administration). In addition, introducing bacteria and their potential negative impacts on the ecological system of cold climate regions led to the superiority of using enzymes over whole microbial cells and all previous remediation approaches. After enzymatic remediation, the enzymes as cellular proteins

break down into peptides and eventually into amino acids. There is no report on environmental hazards and negative effects of peptides and free amino acids. To the best of the authors' knowledge, this study is the first report on psychrozymes for petroleum hydrocarbon degradation [199]. Thermodynamic parameters, such as Gibbs free energy, activation energy, enthalpy and entropy should be also studied to understand the adaptive strategy of cold-active enzymes. This study aims to develop an alternative and novel enzymatic approach to effectively degrade p-xylene in cold and contaminated groundwater sites. The action of xylene monooxygenase and catechol 2, 3-dioxygenase was sequentially and simultaneously tested in the groundwater sample. Cost-effective enzyme purification processes and improvement in stability were proposed to show that using enzymes can be economically competitive with using whole microbial cells.

4.1.2. Materials and Methods

Chemicals and culture media

All chemicals used were obtained in an analytical and microbiological grade that is commercially available from Sigma-Aldrich (Mississauga, Ontario, Canada) and Fisher Scientific (Ontario, Canada). Mineral salt media (MSM) was used for p-xylene degradation experiments to provide inorganic nutrients and their composition modified from Rahul [215]. The pH was adjusted to around 7.0 ± 0.2 using HCl and NaOH, before each experiment.

Characteristics of groundwater and soil sample

The groundwater and soil samples used in the present study were provided by the industrial collaborator in this work from a confidential petroleum site in Montreal, Canada. This site was selected because of its intense p-xylene contamination since 2003 at depths ranging from 5 to 7 m and an approximately 10 m reach of a river. The initial characterizations of the site showed that

the concentration of p-xylene in the soil exceeds 10,000 mg/kg, groundwater is also affected by the free phase p-xylene and with a concentration of 200 mg/L dissolved p-xylene.

Isolation of p-xylene degrading bacteria from the soil sample

The isolation was carried out by enrichment and adaption techniques using MSM supplemented with 50, 100 and 200 mg/l of p-xylene (low, intermediate and high concentration). About 0.5 g of soil or 1 ml of groundwater sample was mixed with 25ml MSM supplemented with 50 mg/l of p-xylene. All tests were performed in 150 mL- sealed serum bottles with a Teflon-coated butyl rubber septum and aluminum cap. Isolation and biodegradation tests were carried out between 8 to 15°C, which is the typical aquifer temperature in the contaminated site. Thereafter, 10 mL of the enriched culture was added to a fresh MSM supplemented with 100 mg/l of p-xylene and incubated at 8 ±1°C, 150 rpm for one month. The procedure was repeated for the media supplemented with 200 mg/l of p-xylene for the microbial adaptation (ranging from 50 to 200 mg/L). The enriched culture was inoculated onto tryptic soy agar (TSA) plate. After incubation at 8 ±1°C for 3–5 days, single colonies with different morphology were selected and each of them was inoculated to the fresh MSM with 200 mg/l of p-xylene as the standalone carbon and energy source and incubated at a range of 4±1 to 35±1°C for testing its p-xylene degrading ability, under different temperatures. The biodegradation efficiency was calculated by the following Eq. (1).

$$degradation\ (\%) = \frac{C_n - C_0}{C_0} \times 100 \qquad \textit{Eq. (1)}$$

Where, C_n and C_0 are the concentration of test and abiotic control, respectively.

As the isolated strains could keep growing at 4°C, the strains were kept in -20 and -80°C in tryptic soy broth (TSB) media with 20% glycerol (v/v) for short- and long-term storage respectively.

Strain identification and characterization

The strains were identified with 16S ribosomal RNA gene, the gene fragment was amplified using the following universal primers for PCR: 27F (5′- AGAGTTTGATCCTGGCTCAG-3′), 1492R (5′-GGTTACCTTGTTACGACTT-3′). The amplified products were sequenced and then the 16S rRNA fragment sequences were compared with the reference sequences using the BLASTn program [258] in the National Center for Biotechnology Information (NCBI) database. Thereafter, the phylogenetic analysis was developed using the neighbor-joining algorithm of MEGA 7.0 software with 1000 bootstraps [259]. Biochemical characteristics of the selected strains were investigated and compared with *Pseudomonas putida* (ATCC 33015) as a reference strain. This strain was purchased from NRRL (Northern Regional Research Laboratory).

Growth in presence of p-xylene and enzyme production

Among a total of 27 isolates obtained two isolates, S2TR-08 and S2TR-09 were selected based on their ability to grow on p-xylene at 8 ±1°C.

Bacterial growth was measured using optical density (OD) with a spectrophotometer at A600 nm. To achieve enough biomass, the isolates were initially grown on Tryptic soy agar (TSA), then a fresh colony was transferred to 100 ml TSB for 24 h at 8ºC,150 rpm until reaching an OD_{600nm}~1-1.2 that corresponded to 1.1×10^9 cells/ml. About 2×10^9 cell/ml of fresh culture was inoculated in 25 mL of MSM supplemented with 50, 100 and 200 mg/L of p-xylene in a 150-mL sealed serum bottle and incubated at 8 ±1°C for 15 days on an incubator shaker at 150 rpm.

Enzyme determination

Cells were harvested from the media by centrifugation (5000 × g at 4 ±1°C), and the pellet was washed twice with phosphate buffer (pH 7.2) and then re-suspended in the same amount of media. The cell disruption was carried out on ice using an Ultrasonifier (Branson Ultrasonics Corporation,

Danbury, CT, USA) at 22 kHz and 30 kHz frequencies of ultrasounds for 10 min. The cell lysates were used as crude enzymes for further analysis.

To determine protein concentration, the Bradford assay was performed using Pierce™ BCA Protein Assay Kit (Thermo Fisher Scientific, Canada) and bovine serum albumin (BSA) standard curve [226]. Based on enzyme activity tests in different temperatures (mentioned in the results section), 15°C was determined as an optimal temperature for psychrozymes obtained from isolates, so all the enzyme assays were carried out at their optimal temperature.

Xylene monooxygenase activity assay

Xylene monooxygenase activity was measured with p-xylene as a substrate and monitoring the production of phenolic compounds by using a colorimetric assay modified from Arenghi et al., [225]. NADPH (final concentration, 0.5 mM) was added to the cell lysate, then 35 µl of p-xylene (4% v/v) in N,N-dimethylformamide was added to the reaction mixture. After incubation at 15 ±1°C, every 5-min interval, 1ml sub-samples were collected and mixed with 100 µl of NH_4OH (1 M) and 100 µl of 4-amino antipyrine (2% w/v). After the addition of 100 µl of 8% Potassium ferricyanide, the samples were centrifuged (14000 × g), the A500 of the supernatant was measured and then calculated by reference to the p-cresol of 0-50 µg/mL standard curve. One unit of specific activity was defined as the amount of catalyst that produced 1 µmol of p-cresol per minute per milligram of cell protein.

Xylene dioxygenase activity assay

Xylene dioxygenase activity was assayed based on the formation of indigo. The enzyme reaction was carried out using 5 µL of indole 100 mM as a substrate in N, N-dimethylformamide to the cellular lysates. The absorbance of the reaction mixture at 500 nm was recorded against a blank

containing all ingredients except the substrate. The enzyme activity was defined as the increase in indigo absorbance per time unit normalized to the protein content of the sample [260].

Catechol dioxygenases activity assays

Catechol 2, 3-dioxygenase and catechol 1, 2-dioxygenase activities were assayed by monitoring the production of 2-hydroxymuconic semialdehyde and muconic acid at 375 nm and 260 nm, respectively. About 3-mL of the mixture contained 0.6 mL catechol (1 mM), 2.0 mL phosphate buffer (pH=7.0), 0.2 mL cellular lysates and 0.2 mL deionized water. The reaction mixture was allowed to proceed at 15 °C and the sub-samples were taken every 2 min. One unit of enzyme activity was defined as the amount of enzyme that produced 1 µmol of cis, cis- muconic acid and 2-hydroxymuconic semialdehyde per time unit [261].

Kinetic analysis of enzymes

As mentioned in the results, p-xylene is initially oxidized to the central intermediates, such as p-toluic acid and p-cresol, by monooxygenase, and then in the second step of biodegradation, p-cresol is finally decomposed into inert intermediates by the ring-fission enzyme (dioxygenase). For the kinetic study, each step was assumed as a one-substrate enzyme-catalyzed reaction with two or more intermediates. Daniel *et.al* proposed that the initial rate equation for enzyme mechanisms with more than one intermediate would be in a form very similar to the Michaelis-Menten equation $\{v = v_m / \{1+k_m/[S]\}$. So initial-rate measurements were carried out at constant enzyme concentration and the Michaelis constant K_m and maximal velocity were evaluated from the plot of *v versus* [S] using GraphPad Prism version 8. Moreover, the plot of reaction velocity for each enzyme was prepared to study the rate behavior of enzymes. This plot also indicated that free substrate is present in great excess over the total enzyme concentration.

Thermodynamic parameters

Gibbs free energy, activation energy, enthalpy and entropy were studied to understand the adaptive strategy of cold-active enzymes. The enzymatic activities were recorded over a wide range of temperatures (4 -70°C). The rate of a reaction can be described by two models: the Arrhenius model and the more sophisticated Eyring-Polanyi model. The former model (Arrhenius model) used the activation energy, as the energy required to reach the activated transition state; which includes the chemical potential and kinetic energy. However, the Eyring model applied the Gibbs energy for the transition state activation that includes entropy and an enthalpy term (Huang et al., 2011). Transition states can be modeled by the Eyring-Polanyi Eq. (2):

$$Kcat = \frac{K\, k_B\, T}{h}\, exp\,(- \frac{\Delta G^{\#}}{RT}) \qquad Eq(2)$$

Where K_{cat} is the reaction rate, K the transmission coefficient may be approximated 1, K_B Boltzmann constant (1.38×10^{-23} J K^{-1}), T the temperature, h and R are the Planck (6.63×10^{-34} J s) and gas (8.31 J K^{-1} mol^{-1}) constant respectively.

Using the isothermal Gibbs equation $\Delta G^{\#} = \Delta H^{\#} - T\Delta S^{\#}$, and assuming the transmission factor =1,

$$Kcat = \frac{K\, k_B\, T}{h}\, exp\,(- \frac{\Delta H^{\#}}{RT} + \frac{\Delta S^{\#}}{R}) \qquad Eq.(3)$$

Upon rearranging, we get a linear form of Eq. (4):

$$ln\,(Kcat) = - \frac{\Delta H^{\#}}{R}\frac{1}{T} + \frac{\Delta S^{\#}}{R} + ln\,(\frac{k_B\, T}{h}) \qquad Eq.(4)$$

Analysis of gene coding enzymes

Gene expression levels of *xylM* and *xylE* in isolated bacteria were analyzed using qRT-PCR. To determine whether the p-xylene concentration is reflected in the transcription of the TOL plasmid for enzyme production in different p-xylene concentrations (50, 100 and 200 mg/l). As mentioned above (the growth condition), the harvested cells were used for total RNA extraction by the

BioBasic total RNA kit (BS584, Canada). To eliminate the genomic DNA, the extracted RNA mixture was treated by using DNase I (Qiagen, Germany). To synthesize cDNA, a reverse transcription reaction (RT-PCR) was performed using the same concentration of RNA in each reaction by cDNA Synthesis Kit (Takara Shuzo, Japan). The obtained cDNA was used for PCR and real-time PCR. Gene expression level was determined using a real-time PCR Rotor-Gene Q system (Qiagen, Germany) using the SYBR Green master mix (Rotor-Gene Q).

Partial Purification of Enzymes

The target enzymes were partially purified by ammonium sulfate (Burgess, 2009). Briefly, the crude enzyme mixture was subjected to 20%, 30%, 40%, 50%, and 60% ammonium sulphate saturation with rapid stirring on ice (0 ±1°C). The pellets obtained from each ammonium sulfate cut were completely dissolved in phosphate buffer (pH=7.0) and stored at 4 ±1°C. Protein concentration was quantified by Pierce™ BCA Protein Assay Kit and sodium dodecyl sulfate-polyacrylamide gel electrophoresis (SDS-PAGE). SDS-PAGE was performed on 10% polyacrylamide separation and 4% stacking gels. After electrophoresis, the loaded samples were visualized using Coomassie Staining Solution.

Bioconversion and biodegradation test

All tests with enzymes were performed in Minimal Salt Media (MSM) supplemented with the substrates p-xylenes at 8± 1°C, 150 rpm. The conversion test of p-xylene was characterized in a sealed bottle containing water and 50, 100 and 200 mg/l of p-xylene. The concentration in tests was selected based on the water solubility of p-xylene at 25ºC (~200 mg/l) [262]. Usually, 10 U/mg of xylene monooxygenase and 10 U/mg of catechol 1,2-dioxygenase (1:1) were added to the conversion and degradation media. For kinetic and thermodynamic analysis, the sequential action of enzymes was studied in the ratio of 1:1. In the sequential action, the catechol 1, 2-

dioxygenase was added to the xylene monooxygenase converted media after xylene isomers transformation whereas in the simultaneous action tests both xylene monooxygenase and catechol 1,2-dioxygenase were added simultaneously to the reaction mixtures. The tests were also carried out in 150 ml with a 9:1 airspace: liquid ratio sealed with a Teflon rubber stopper containing 25 ml of reaction volume. The concentration of p-xylene was detected with GC/MS (as mentioned in the following section) in the aquatic phase. As p-xylene is considered a highly volatile compound; only about 50 to 60% of the concentration added can be detected in the liquid phase. The concentration in the liquid phase was measured and the needed concentration was compensated to correct the detection results. The biodegradation test was also evaluated for groundwater samples from the contaminated site, similarly, as mentioned for sequential and simultaneous tests. First and second-order reaction rate equations were used to compare the biodegradation kinetics at higher and lower concentrations of p-xylene at sequential and simultaneous action of enzymes.

Analytical procedures

The concentration of p-xylene was determined using a 7890A Gas Chromatograph (DB-1701 column 0.25 mm i.d. × 30 m× 0.25µm film thickness) equipped with a Perkin Elmer Turbomatrix HS-40 trap automatic headspace sampler. The temperature was set at 45 ºC for the column and 300 ºC for the detector. 50 µl of samples were injected directly into the 40 mL headspace bottle containing10 µl of fluorobenzene-D5 (100 mg/l diluted in methanol) as an internal standard and 5 ml of ultrapure water.

Full scan mass detection is used to determine the products formed by the action of enzymes. The concentration of products at different time intervals during kinetic trials was analyzed from the areas of the substrates and compounds peaks. p-, o- and m-cresol were not determined by GC/MS equipped headspace, therefore their concentration was determined by a CP-Wax 57 CB column

(25m×0.25mm×0.20µm, Agilent Technologies, Netherlands) connected to a Varian 2200 Gas-chromatograph coupled to a Saturn Mass Detector. The products appearing during the bioconversion were initially identified using NIST library data, then the concentration was determined using the calibration curves of their standards. All analytical and biological tests were performed in triplicates.

Statistical analysis

Statistical analysis was done by one-way analysis of variance (ANOVA) followed by Tukey posthoc procedure to determine the differences among three or more numeric variables at a significance level set at $p<0.05$.

4.1.3. Results and discussion

Identification of isolates

Among all the isolates obtained, S2TR-08 from groundwater sample and S2TR-26 from soil samples were selected based on their ability to grow on p-xylene as a sole carbon and energy source. When two isolates were grown on TSA at 8ºC for 3 days, the following colony morphologies from each were observed; smooth, white and raised with a circular shape colony. They could grow at between 4 ±1ºC and 25±1ºC, but not well at 37±1ºC as previously reported for *P. mandelii* strain [263]. This characteristic showed that these two strains have no potential pathogenicity toward humans and animals. The partial 16S rRNA sequencing showed that S2TR-08 was close to the type strain of *Pseudomonas mandelii* strain CIP 105273^T with 99% identity. The sequence identity of S2TR-26 was 99% with a type of strain of *Pseudomonas synxantha* ATCC 9890^T. The sequences for S2TR-08 and S2TR-26 have been deposited in the NCBI Genbank database and were assigned the accession of MN197757 and MN197891,

respectively. Phylogenetic analysis also grouped S2TR-08 and S2TR-26 with the type of *Pseudomonas mandelii* (*P. mandelii*) and *Pseudomonas synxantha* with 98% bootstrap support.

Pseudomonas mandelii (*P. mandelii*) was first isolated by Verhille [264] from a mineral water sample in France and later on isolated from mineral water in South Korea, and agricultural soil samples in Canada, the United States and China [265], [266]. Li et al. (2013) reported the isolation of psychrotrophic *P. mandelii* strain from the soil in Changbai Mountain, China that could grow at 4-37°C and produce a high amount of poly-β-hydroxybutyrate [266].

Liu et al. (2013) isolated a cold-tolerant consortium from contaminated soil, which can degrade nitrobenzene and aniline nitro-aromatic and aromatic amino compounds at 10°C. In this consortium, *P. mandelii* was detected as a dominant species (37.7%) although the percentage of *P. synxantha* was quite low (<0.1%) it has degradation ability at 10°C [267]. Since *P. mandelii* and *P. synxantha* have no prior record of pathogenicity and ability to degrade p-xylene as a sole source of carbon, they are therefore a good and novel candidate for bioremediation application in contaminated sites. However, the main aim of this study is to use enzymatic biodegradation that avoids the release of microorganisms into the contaminated environment. The biochemical characteristics of isolate S2TR-08 and S2TR-26 were compared with the biochemical characteristics of *Pseudomonas putida* (ATCC 33015). The results from biochemical tests confirmed that isolated bacteria and *Pseudomonas putida* are within one species, but different strains.

Effect of temperature on p-xylene biodegradation

In cold regions, low temperature poses the main challenge for bioremediation that requires more time to meet cleanup standards [199]. In the contaminated site, the temperature of groundwater was regularly monitored, and it was reported to range from 8ºC to 15 ºC. To bioremediate this

contaminated groundwater, the selected isolates have to survive and produce degrading enzymes under this temperature. A series of p-xylene biodegradation tests were conducted at different temperatures (4, 8, 15, 25 and 35 ±1ºC) using MSM supplemented with 200 mg/l of p-xylene (as the sole carbon source) to investigate the effect of different temperatures on degradation by selected bacteria strains. The results showed a low biodegradation efficiency at a duration range from 5 to 15 days at all tested temperatures. Although many researchers reported that *Pseudomonas* strains could not degrade p-xylene efficiently even at favorable temperatures for bacterial growth [268], *P. mandelii* S2TR-08 and *P. synxantha* S2TR-26 appear to be unique in their ability to grow with p-xylene as a sole carbon source at low temperature (4<T<15±1 ºC).

As shown in Fig. 4.1.1, p-xylene can be degraded by selected isolates at all tested temperatures after one month of incubation. Thereafter, after incubation for 30 days, most of p-xylene was degraded at 4 ºC (*P. mandelii*: 82.59 ± 3.75%, *P. synxantha*: 99.96 ± 0.04%), 15 ºC (*P. mandelii*: 99.95± 0.03%, *P. synxantha*: 99.99± 0.01%) and 25 ºC (*P. mandelii*: 89.45 ± 0.71%, *P. synxantha*: 92.34 ± 6.09%). By contrast, the selected isolates exhibited a low degradation at 35 ºC (*P. mandelii*: 57.12 ± 1.90%, *P. synxantha*: 68.71± 3.09%). The results indicated that the two selected isolates are psychrophilic bacteria, and the optimum degradation temperature is 4 to 15 ºC. Based on this result and preliminary results, the enzymes from assimilating resting cells could be an effective approach to minimize the time of biodegradation in cold climate regions. Since bacterial whole cells need nutrition and air to maintain the optimum growth, considering that groundwater lacks nutritional factors for microbial growth, using enzymes could be more feasible from this perspective than the use of whole cells [269].

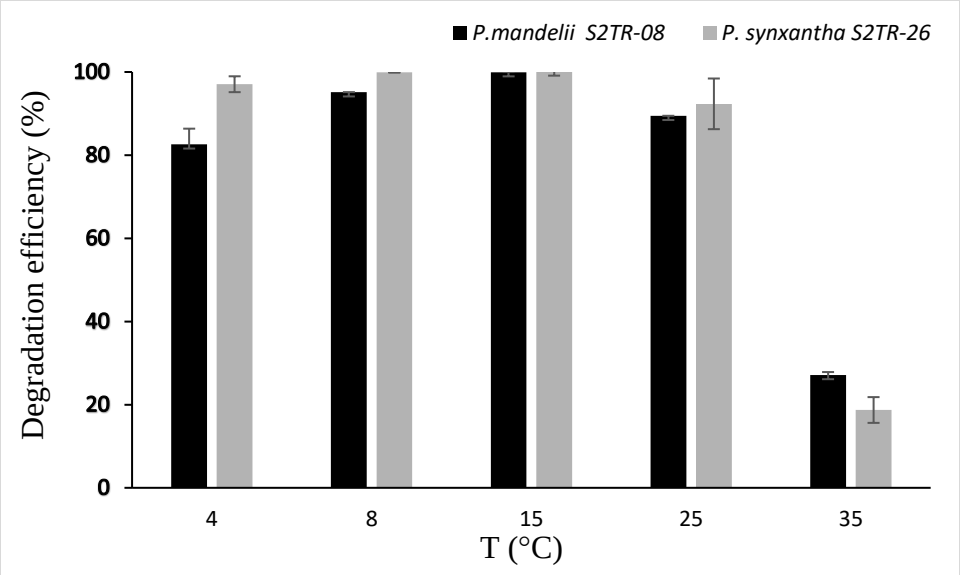

Fig. 4.1.1. p-xylene degradation efficiency by *P. mandelii* S2TR-08 and *P. synxantha* S2TR-26 at different temperatures after one-month incubation.

Enzyme determination

One of the determining factors in enzyme expression is the concentration of the substrate. The cultured bacteria in MSM supplemented 50, 100 and 200 mg/l of p-xylene at 8 ºC and after 30 days of incubation were used for enzyme determination. The time-course experiments also demonstrated that 30 days of incubation was the best time when the growth reaches its stationary phase and the production of the enzyme is near to maximum (data not shown). Nagy at al., (2001) showed that enzyme activity was near to maximum when the growth reached the stationary phase and the cell lysis effect could be negligible in enzyme activity [224].

As p-xylene is considered partially insoluble in water and range of 162-198 mg/l can dissolve in water at 25 °C. The value of 200 mg/l and lower than this value (50 and 100 mg/l) are consistent with a sufficient bioavailability for these compounds to favorable biodegradation efficiency by xylene-utilizing microorganisms. Table 4.1.1 shows the results from xylene monooxygenase, xylene dioxygenase, catechol 1, 2-dioxygenase and catechol 2, 3-dioxygenase activity. The cell

lysate from cultured bacteria in presence of 50, 100 and 200 mg/l of substrate showed a significant difference in enzyme activity in order of 200>100>50 ($p<0.05$), and for enzyme production, 200 mg/l of p-xylene seemed to be optimal substrate concentration ($p<0.05$). The present study corroborates with previous studies showing that p-xylene degradation depends on the mono oxidation of the methyl side-chain of the aromatic nucleus and its fission [13]. The cell lysate from *P. mandelii* S2TR-08 showed high catechol 2, 3-dioxygenase activity (11.28 ± 0.45 U/mg), while the cell lysate from *P. synxantha* S2TR-26 showed high xylene monooxygenase activity (9.85 ± 0.70 U/mg). Based on previous studies, biodegradation pathways begin with mono oxidation and finish with the formation of catechol or non-catecholic compounds as intermediates [270]. By comparison, the degradation efficiency of p-xylene at 8 ºC, using two psychrophilic enzymes could be more effective; xylene monooxygenase from *P. synxantha* S2TR-26 for the oxidation of p-xylene to the phenolic product, followed by the ring fission using catechol 2, 3-dioxygenase from *P. mandelii* S2TR-08. It has been reported a strong effect of temperature on cell membrane permeability of *Pseudomonas sp.* to phenolic compounds [271], so a decrease of cell membrane permeability at low temperature could result in different xylene monooxygenase and catechol 2,3-dioxygenase production in two isolates.

Table 4.1.1. Enzymes determination in *P. mandelii* S2TR-08 and *P. synxantha* S2TR-26. ND, non-detected; Data (means ± errors, n=5) were analyzed by one-way ANOVA; different letters within each column indicates significance among the enzyme produced in the presence of different concentration of p-xylene (for instance, $^{ab}P<0.05$, a, between 50 and 100; b: between 10 and 200); * is considered significance among enzyme activity in different strain.

	p-xylene concentration (mg/L)	*P. mandelii* S2TR-08	*P. synxantha* S2TR-26
xylene monooxygenase (U/mg)	50	0.81 ± 0.02	3.16 ± 0.41*
	100	1.04 ± 0.10^{a}	5.21 ± 0.16^{c}*
	200	1.76 ± 0.05^{ab}	9.85 ± 0.70^{cd}*

xylene dioxygenase (U/mg)	50	ND	ND
	100	ND	ND
	200	ND	ND
catechol 2,3-dioxygenase (U/mg)	50	4.07± 0.85	ND
	100	9.30 ± 0.12^{e}	ND
	200	11.28 ± 0.45^{ef}	ND
catechol 1,2-dioxygenase (U/mg)	50	ND	0.02 ± 0.01
	100	ND	0.08 ± 0.01ns
	200	ND	0.12 ± 0.02ns

Enzyme characterization and thermodynamic parameter detection

Xylene monooxygenase was precipitated at 60-70% cut of ammonium sulphate however catechol 2,3-dioxygenase was precipitated at 30-40% cut of ammonium sulphate. The SDS-PAGE analysis confirmed the presence of xylene monooxygenase at approximately 80 kDa and catechol 2,3-dioxygenase at approximately 35 kDa and a decrease in protein content. The partial purification of enzymes showed that the specific activity increased around 5 times more than the crude enzyme mixture.

The high production cost of enzymes has restricted their industrial use for environmental purposes and downstream processing is a major *cost* in the *production* of enzymes and proteins. Enzyme purification is the most important process in downstream processing to remove interfering compounds and other cellular proteins and enzymes. The objective behind deciding the strategy for purification is to obtain the desired purity level for the target application. In environmental applications, there is a need for a quick, controllable, and simple to remove other cell components and interfering substances. Ammonium sulfate has been used over the last hundred years and remained the most widely used in industries because it is cheap, very soluble in water, and relatively no toxic substance to living organisms [272]. The partial purification of enzymes using

ammonium sulfate is a feasible solution to the high cost of enzyme production which is leading to the limited application of enzymes for environmental purposes.

The results from enzyme activity in different temperatures showed that xylene monooxygenase and catechol 2, 3-dioxygenase from *P. synxantha* S2TR-26 and *P. mandelii* S2TR-08 were most active at 15°C. To compare their mesophilic counterpart enzymes, the mesophilic homologue (mesozymes) of xylene monooxygenase and catechol 2, 3-dioxygenase were produced from *P. putida*. The specific activity of xylene monooxygenase and catechol 2, 3-dioxygenase from isolated bacteria were 10 and 11 U/mg respectively, however, at the same temperature (15°C), their mesophilic counterparts were 2 and 3 U/mg, respectively. Fig. 4.1.2 illustrates that the enzymes from isolated bacteria are psychrophilic and *P. putida* produced mesophilic enzymes (most active at 50°C). The present results corroborate with previous studies regarding features of cold adaptation processes. The main fact of physiological adaptation is the production of enzymes having around tenfold higher specific activity in low temperatures to compensate for the slow reaction rates in this temperature range [53]. The observations suggest that xylene monooxygenase and catechol 2, 3-dioxygenase have been adapted, in terms of temperature dependency (4 - 25°C), to the growing range of its host.

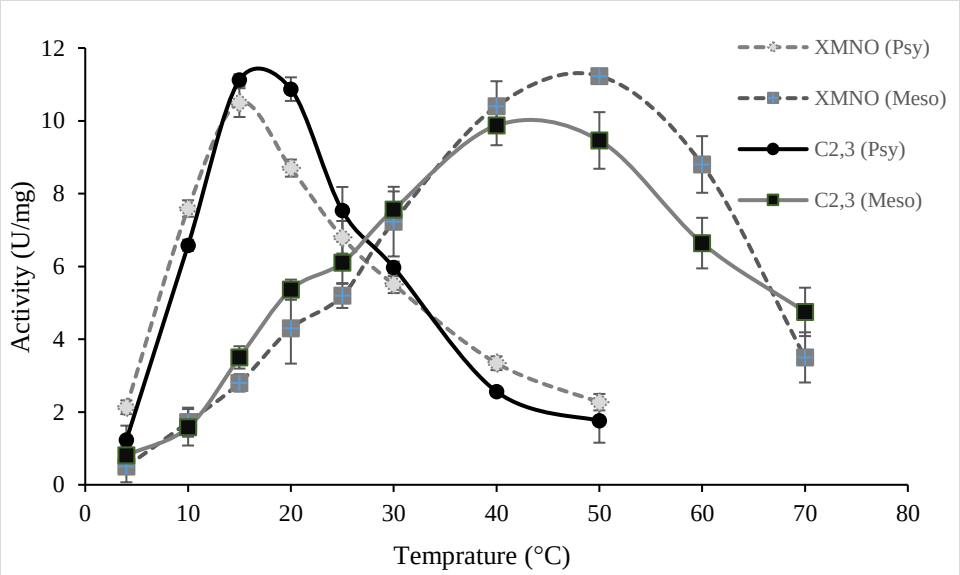

Fig. 4.1.2. Temperature dependency of selected enzyme activity. XMNO, xylene monooxygenase; C2,3, catechol 2,3-dioxygenase; Psy, Psychrozymes; Meso, Mesozymes.

Turnover number (K_{cat}) represent the maximum number of substrates transformed to product per enzyme active site per time. Table 4.1.2 shows the high turnover number of psychrozymes at 15°C and mesozymes at 50°C. The height of the energy level between the ground state of enzyme-substrate and the transition state enzyme-substrate can be calculated by the relation between the temperature dependency and K_{cat}. The values of activation energy ($\Delta G^{\#}$) correspond to the energy level (barrier) required for reactions to occur, the lower this barrier level, the higher activity occurred. High activity of psychrozymes in low temperatures corresponds to a decrease of $\Delta G^{\#}$ (the free energy of activation). As illustrated in Table 4.1.2, the psychrophilic xylene monooxygenase and catechol 2, 3-dioxygenase showed a decrease of $\Delta G^{\#}$ (14.7 and 14.2 Kcal mol^{-1}) compare to their mesophilic counterparts (16.3 and 14.7 Kcal mol^{-1}) at 15°C. The enthalpy of activation ($\Delta H^{\#}$) is related to the ease of bond breaking and making (binding energy) in the generation of the transition-state complex from the ground state. The lower $\Delta H^{\#}$ value of psychrozymes at low temperature corresponds to the faster the rate. Accordingly, the reduced

enthalpy in the psychrozymes reaction could explain the main adaptive mechanism to low temperatures (Feller, 2013). Moreover, psychrophilic enzymes possess lower $\Delta H^{\#}$ values reducing the adverse effect of low temperatures on enzymatic reaction rate. The entropic contribution $T\Delta S^{\#}$ for the psychrozymes is lower than mesozymes at low temperatures. Table 4.1.2 shows the variations of the thermodynamic parameters (namely $\Delta(\Delta G^{\#})_{P-M}$, $\Delta(\Delta H^{\#})_{P-M}$ and $\Delta(\Delta S^{\#})_{P-M}$). This comparison provides some information to the understanding of how psychrophilic enzymes can deal with low temperatures. The $\Delta(\Delta G^{\#})_{P-M}$ shows the difference of K_{cat}, due to the relation between $\Delta G^{\#}$ and K_{cat} according to Eq. (2). The negative value of $\Delta(\Delta G^{\#})_{P-M}$ confirms that psychrozymes are more active than mesozymes at low temperatures (Georlette et al., 2004). Numerous analyses carried out on psychrozymes proved that the $\Delta(\Delta H^{\#})_{P-M}$ and $\Delta(\Delta S^{\#})_{P-M}$ has always negative value whatever the sign of the activation enthalpy and entropy (positive/negative) at low temperature. As expected, the value of $\Delta(\Delta G^{\#})_{P-M}$, $\Delta(\Delta H^{\#})_{P-M}$ and $\Delta(\Delta S^{\#})_{P-M}$ were negative at 15°C (Table 4.1.2).

It is well documented that all studied psychrophilic enzymes possess lower $\Delta H^{\#}$ values and resulted in reducing K_{cat} dependence on the temperature and consequently the effect of low temperatures on enzymatic reaction rates [273]. Overall, reducing the enthalpy can be the main cold-adaptive parameter for psychrozymes indicating greater flexibility and lower stability at or near the active site of psychrozymes. Based on the central concept in the cold adaptation that flexibility should increase at the active site that is responsible for the high catalytic activity of enzymes [274], in contrast, other residues of the enzyme are not involved in catalysis may not show low stability. It can be interpreted that high stability in some residues of the enzyme structure could contribute to a decrease in $T\Delta S^{\#}$, the unfavorable entropic contribution [275].

Table 4.1.2. Turnover number and thermodynamic parameters for selected enzymes at relevant temperatures (most active temperature).

Enzymes	At 15°C (288K)							At 50°C (323K)						
	K_{cat} (S^{-1})	$\Delta G^{\#}$ (Kcal mol^{-1})	$\Delta H^{\#}$ (Kcal mol^{-1})	$T\Delta S^{\#}$ (Kcal mol^{-1})	$\Delta(\Delta G^{\#})$ (Kcal mol^{-1})	$\Delta(\Delta H^{\#})_E$ (Kcal mol^{-1})	$T\Delta(\Delta S^{\#})$ (Kcal mol^{-1})	K_{cat} (S^{-1})	$\Delta G^{\#}$ (Kcal mol^{-1})	$\Delta H^{\#}$ (Kcal mol^{-1})	$T\Delta S^{\#}$ (Kcal mol^{-1})	$\Delta(\Delta G^{\#})$ (Kcal mol^{-1})	$\Delta(\Delta H^{\#})_E$ (Kcal mol^{-1})	$T\Delta(\Delta S^{\#})$ (Kcal mol^{-1})
XMNO (Psy)	36.5 ±3.2	14.774	14.772	-0.00217	-1.538	-1.543	-0.00558	7.87±0.07	16.240	16.292	0.05263	0.578	0.608	0.03056
XMNO (Meso)	0.6±0.05	16.312	16.315	0.00341				65.1±1.3	15.662	15.684	0.02207			
C2,3 (Psy)	104±1	14.234	14.232	-0.00282	-0.52	-1.433	-0.00138	0.028	18.580	18.677	0.09724	3.267	3.331	0.0727
C2,3 (Meso)	38.8	14.754	14.753	-0.00144				100.6±4.2	15.322	15.346	0.02452			

Gene expression analysis

To confirm the results of enzyme activity assays, the expression level of the encoding genes for involved enzymes (*xylM* and *xylE*) was investigated when enzyme activity reached the highest amount in isolated strains. The TOL plasmid encodes the key enzymes for the oxidative catabolism of xylenes in *Pseudomonas* sp. Xylene and toluene can be degraded by the progressive oxidation of a methyl side chain to carboxylic acid such as toluic acid for p-xylene, followed by oxygenated cleavage of the aromatic ring [276]. Xylene monooxygenase is the first enzyme and is responsible for the oxidation of the methyl side chain of xylene. *xylM* gene encodes the xylene monooxygenase subunit, this subunit is an important component of the hydroxylation reaction of the carbon side chain [276]. Catechol 2,3-dioxygenase in the fission enzyme responsible for ring cleavage and *xylE* encodes this enzyme under the regulation of TOL plasmid [277].

Fig. 4.1.3 shows the gene expression of two important genes (*xylE* and *xylM*) in isolated strains in the presence of different p-xylene concentrations (50, 100 and 200 mg/l). The result of gene expression analysis indicated that isolated bacteria responded to the high concentration of p-xylene with an increase in the expression level of *xylM* and *xylE* in *P. synxantha* S2TR-26 and *P. mandelii* S2TR-08 respectively. The results from *xylM* showed that this gene was highly expressed in *P. synxantha* S2TR-26 exposed to p-xylene at 200 mg/l (RQ=1.02). *xylM* gene expression in *P. mandelii* S2TR-08 was significantly lower than *P. synxantha* S2TR-26 ($p<0.05$). *xylE* gene expression was induced only in *P. mandelii* and also unregulated in the high concentration of p-xylene (200 mg/l). All the results of gene expression analysis were consistent with enzyme activity results (Table 4.1.1). The findings of this study were also in agreement with the studies that showed that some microorganisms can produce enzymes to degrade the majority of the hydrocarbons whereas others may be specific to substrates [278]. Gescher et al. (2006) showed that some

contaminants could not be completely mineralized by a single bacterium strain. As xylene monooxygenase and catechol 2,3-dioxygenase have a matching end product, they can synchronize together to degrade p-xylene completely.

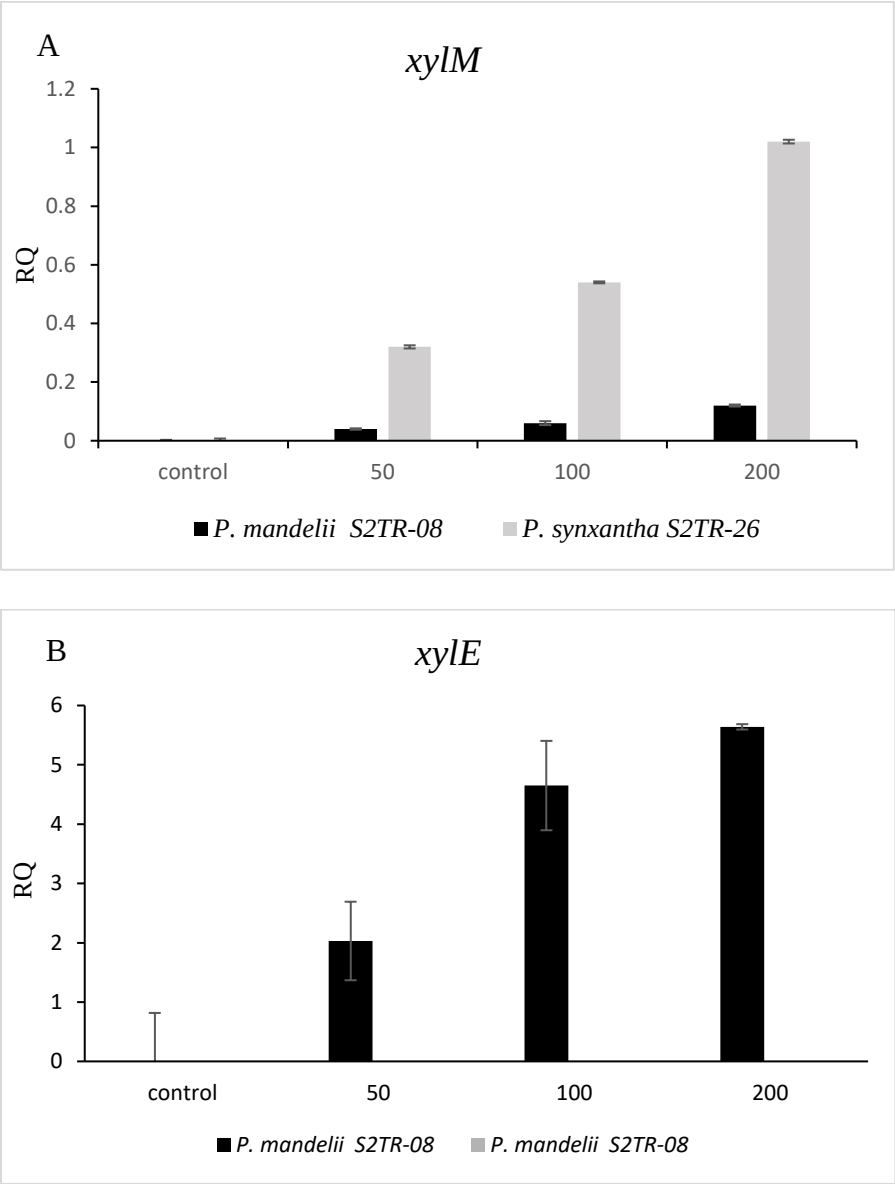

Fig. 4.1.3. Gene expression of *xylM* (A) and *xylE* (B) gene at different concentrations of p-xylene (50, 100 and 200 mg/l, RQ, Relative quantification; Control, the sample from the bacteria grow on media without p-xylene.

The action of xylene monooxygenase on p-xylene

Full scan mass detection is used to determine the products formed by the action of xylene monooxygenase. Then, the transformation time courses were investigated quantitatively for detected intermediates.

Xylene monooxygenase can hydroxylate xylene isomers in the ortho, meta, and para positions [279], the oxidation may be initiated by direct oxidation or oxidation of one or two methyl groups of the aromatic nucleus [280]. The results showed that p-xylene was firstly converted to p-toluic acid and then converted to p-cresol. The further conversions of cresol to catecholic derivatives (methylcatechols) were previously observed with xylene isomers [281], while they were not detected in the present results and the accumulation of p-cresol was detected during the incubation time. A possible reason could be that xylene monooxygenase has a higher affinity for xylene isomers than for p-cresols [282]. Some literature used xylene monooxygenase to oxidize the methyl group of aromatic hydrocarbons that should follow ring 2, 3 or 1,2-dioxidation [283].

For partially purified enzyme, lack of ring-cleavage enzyme was the main reason for p-cresol accumulation however, a similar result was observed using the crude enzymes mixture. This could be due to the low catechol 1, 2-dioxygenase activity for ring cleavage in *P. mandelii* S2TR-08. In Fig. 4.1.4, the time courses of p-xylene transformation were reported, and a maximal concentration of p-toluic acid was observed within 20-30h. The transformation of p-toluic acid to p-cresol reaches completion within 72h (Fig. 4.1.4). Gullotto et al. (2008) reported that toluene o-xylene monooxygenase from *Pseudomonas* sp. OX1 could transform toluene to p-cresol and methylcatechol within 24 h at 30 °C [257]. The results showed that p-cresol is the last product of multi-step oxidation of xylene monooxygenase enzyme even at a longer time if the other substrates (p-toluic acid and p-xylene) were not present. Although bacterial multicomponent

monooxygenases are highly homologous, they have different affinity and substrate specificities [284].

The oxidation rates of p-xylene were tested using pure and crude enzymes with equal specific xylene monooxygenase activity (10-11 U/mg of xylene monooxygenase activity). The oxidation rate of p-xylene using crude xylene monooxygenase was 7±2% less than pure enzyme. All further tests were carried out using partially purified enzymes. Although the industrial utilization of purified enzymes for environmental purposes is not economically justified, the ammonium sulphate precipitation method is relatively inexpensive and stabilizes the protein structure [285]. The stability test of these enzymes showed that partially purified catechol 2, 3-dioxygenase and xylene monooxygenase was quite stable (remaining ~ 99% of their activity) at storage condition (4 ºC ± 1) after 10 days, while crude enzymes lost ~ 50% of their activity in that given time. The high degradation rate and improved stability of enzymes should be considered for deciding on the application of crude enzymes or partially purified enzymes. Since the reduced reaction rates and lower stability in the crude enzyme cocktail can potentially negate the economic gain enabled by the removal of the enzyme purification process. Besides, the higher stability and reaction rate of partially purified enzymes for complete mineralization of p-xylene in the cold climate region can confirm the economical superiority of enzymes over whole microbial cells.

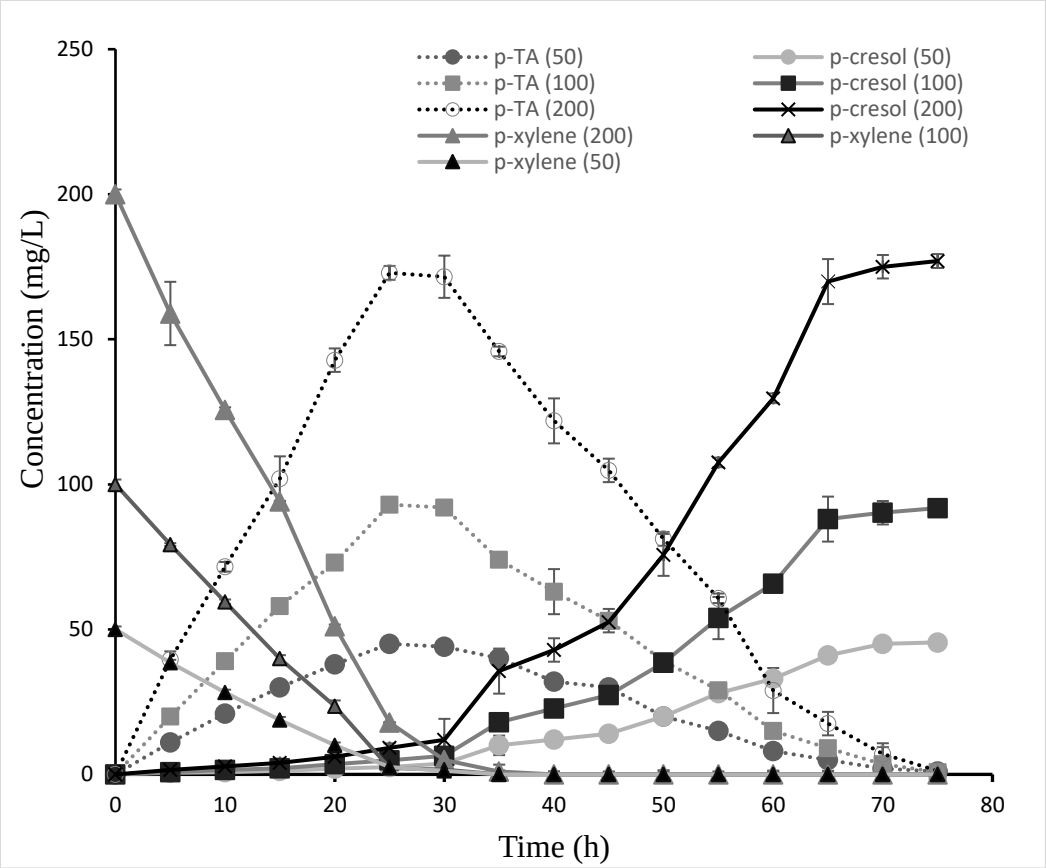

Fig. 4.1.4. Xylene monooxygenase action on p-xylene in time course. The standard deviation values of three replicates are also shown. p-TA (50), p-toluic acid in concentration of 50 mg/l; (100) and (200) in concentration of 100 and 200 mg/l.

Action of catechol 2, 3-dioxygenase on bioconversion products

As the results showed the last products of xylene monooxygenase conversion were p-cresol, and the oxidation rates of p-cresol were tested using partial pure and crude catechol 2, 3-dioxygenase with equal specific activity (10-12 U/mg). The oxidation rate of p-cresol using crude catechol 2, 3-dioxygenase was 26±5% less than the partially pure enzyme. P-cresol as the final product of xylene monooxygenase conversion in the concentration range of 50-200 mg/l was transformed leading to its complete disappearance within 40-50h (Fig. 4.1.5).

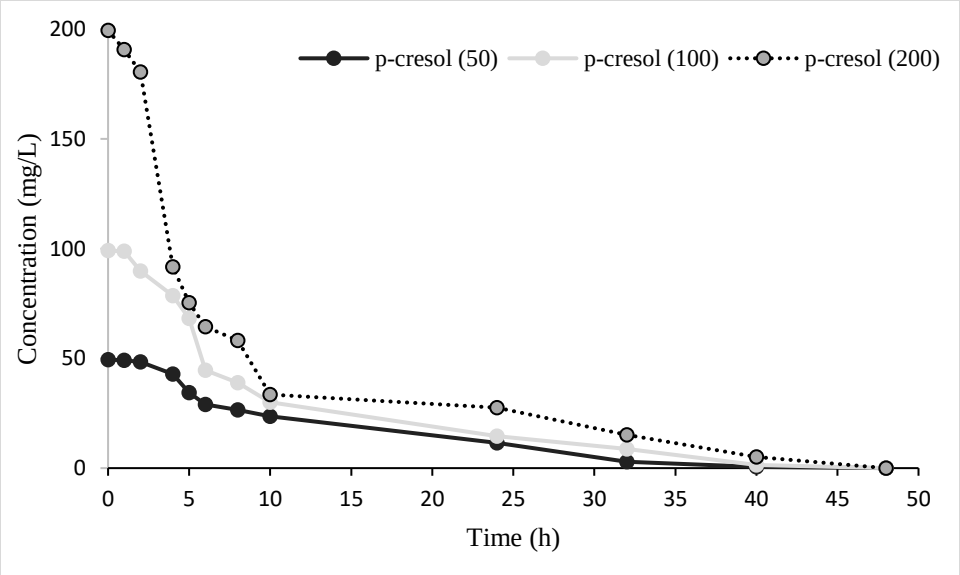

Fig. 4.1.5. The dynamics of p-cresol oxidation by catechol 2, 3-dioxygenase at 15 ºC. (50) initial concentration of 50 mg/L, (100) initial concentration of 100 mg/L and (200) initial concentration of 200 mg/L.

Full scan mass detection was carried out to determine the final products formed by the action of catechol 2, 3-dioxygenase. As a result, no specific product was formed after the complete action of this enzyme that confirmed the complete degradation of p-cresol (as central intermediate) to inert products. Cresol is considered a carcinogenic and teratogenic compound [286], therefore, they need to be removed from the contaminated environment. It is reported that intermediate products from biochemical reactions may be more toxic than their parent compounds, thus the modification of the initial parent compound is not always an effective method in remediation and pollutant management. Therefore, biodegradation techniques should be designed for the mineralization of the compound to completion from an environmental point of view. However, several literature proposed biodegradation and biochemical techniques with misunderstandings in the sequences of biochemical steps [287]. In this context, enzymes are proteins produced by all living organisms; they act as a catalyst for a specific reaction to avoid the production of toxic by-products. Xylene monooxygenase specifically catalyzed the multi-step oxidation of the aromatic

nucleus of p-xylene and produce p-cresol as the last product. Catechol 2, 3-dioxygenase showed a high affinity to p-cresol to degrade it to inert products. These results showed the complete mineralization of p-xylene without any toxic by-products.

Catechol dioxygenase can also play a key role in the degradation and finally detoxification of such compounds. Merimaa et al. (2006) showed that *p*-cresol-degrading *pseudomonas* used catechol 2,3-dioxygenase to initiate the *meta* pathway leading to the formation of acetaldehyde and pyruvate for their metabolic cycles [288]. Choi et al. (2013) showed that in the xylene pathway, abundances of key metabolic intermediates were governed by their differing affinities to the various involved xylene metabolic enzymes [280]. The current results also showed the high affinity of p-xylene and p-toluic acid to xylene monooxygenase and the high affinity of p-cresol to catechol 2,3 dioxygenase.

Moreover, the p-xylene degradation rate was used to determine the parameters of the Michaelis-Menton model. The kinetics of p-xylene conversion to p-cresol and p-cresol conversion to inert intermediates was determined (Table. 4.1.3). The catalytic efficiency (ratio of K_{cat}/K_m) was used for the evaluation of overall kinetic efficiency. The enzyme-specific constant has been reported to decrease for the second step of degradation.

Table 4.1.3. The Michaelis-Menten parameters for monooxygenase and dioxygenase

	V_{max} (mM/min)	K_m(mM)	Catalytic Efficiency (K_{cat}/K_m, min^{-1} mM^{-1})
P-xylene (xylene monooxygenase)	0.48	1.51	0.402
p-Cresol (Catechol 2,3 dioxygenase)	20.77	3.92	0.44

Simultaneous action of enzymes

The mixture of xylene monooxygenase and catechol 2, 3-dioxygenase was applied for degradation of 200 mg/L of p-xylene in the groundwater sample. As mentioned previously, xylene monooxygenase from *P. synxantha* S2TR-26 and catechol 2, 3-dioxygenase from *P. mandelii* S2TR-08 were used for the formulation of the enzyme cocktail. The enzymes were mixed in different ratios, and the initial activity of each enzyme was around 10 U/mg.

To determine the synergistic action, the activity of the enzyme was compared between individual enzymes and the mixture of them. If the enzyme activity in the mixture is greater than individual enzyme activity, they have a synergistic effect otherwise it is known as the addition effect [289]. The results showed that enzyme activities were the same in the mixture and individual enzymes. This proves that xylene monooxygenase and catechol 2, 3-dioxygenase work in an additive manner. The results showed that 10 U/mg of xylene monooxygenase is sufficient to achieve 90% of p-xylene degradation after 30h (Fig. 4.1.6). The highest biodegradation of p-xylene was found in enzymes with mixed ratios of 1:1.5 and 1:2 (xylene monooxygenase: catechol 2, 3-dioxygenase). As shown in Fig. 4.1.6, p-xylene degradation remained the same with the addition of catechol 2, 3-dioxygenase, so considering the commercial cost, an enzyme mixture with a ratio of 1:1.5 can be considered an effective enzyme cocktail. Thus, the ratio of 1:1.5 was needed to obtain the complete degradation of p-xylene within 48h. Gullotto et al. (2008) also reported that extra addition of 0.1 U/ml laccases was needed for the simultaneous action of toluene o-xylene monooxygenase and laccase to complete the degradation of toluene [257].

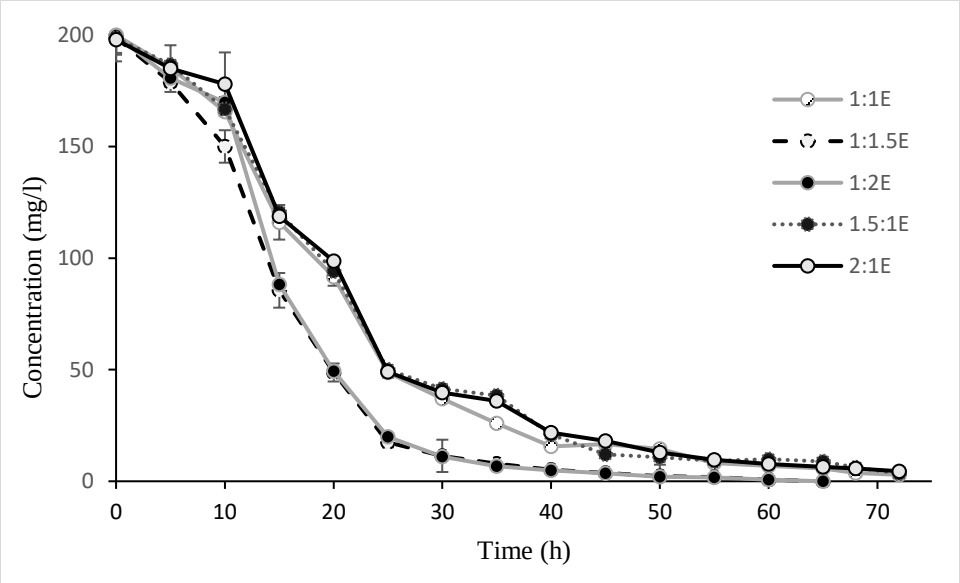

Fig. 4.1.6. The degradation of p-xylene by in the enzymatic cocktails within the different ratios

The requirement of further addition of catechol 2, 3-dioxygenase in enzyme cocktail has probably to be ascribed to inactivation through oxidation mechanisms and loss of its active site iron atom because of some poor substrate such as cresols and chloro- or methylcatechols [290].

As mentioned previously, the main concern in biodegradation is the final toxic products, full scan mass detection was hence carried out to determine the final product. As a result, no specific product was produced after the complete action of the enzyme cocktail (1:1.5) that confirmed the complete degradation of p-xylene within 48h.

To quantitatively compare the sequential and simultaneous method, average degradation rates (ADR) and specific degradation rates (SDR) were calculated for both methods. The ADR was calculated as the slope of the plot of the p-xylene concentration/time including the lag period, whereas SDR is the slope of the plot without a lag phase [210]. The result of p-xylene concentration in enzymes mixed ratio of 1:1 was considered for the calculation of SDR and ADR for considering the same enzyme activity in two methods. The end time for SDR was 25h, while for ADR was

60h. The SDR for sequential (7.22 mg L^{-1} h^{-1}) was slightly higher than for simultaneous (6.21 mg L^{-1} h^{-1}). The ADR value for sequential was the same as for simultaneous (3.1 mg L^{-1} h^{-1}). Considering the enzyme activity of 10U/mg of each enzyme, the SDR of the sequential method was 0.7 mg L^{-1} h^{-1} for each unit of enzyme and 0.6 mg L^{-1} h^{-1} in the simultaneous method. The results from the lab-scale tests demonstrated that the biodegradation rate was higher in the sequential method in terms of enzyme activity, however considering the operational limitations for field tests in cold-climate regions and the need for the sequential injection of enzymes in a given time makes the concomitant method more feasible method for biodegradation of p-xylene in cold contaminated sites. Also, an extra addition of catechol 2, 3-dioxygenase can increase the SDR of a simultaneous method to 7.7 mg L^{-1} h^{-1}.

Both the sequential and simultaneous methods, there was a perfect fit for biodegradation of p-xylene at high and low concentrations of substrate with the classic Michaelis–Menten kinetic model. According to this model, the degradation rate of p-xylene will be zero-order at high substrate concentrations however at low substrate concentrations, the degradation rate will be first order. R^2 value observed was 0.99 for zero-order at a concentration of 200-25 ppm, 0.97 for the first order at a concentration of less than 5ppm in the sequential method and the same agreement with the simultaneous method (R^2=0.97 and 0.96 for zero and first order at mentioned concentrations). The kinetic data showed no inhibition during the biodegradation at a high concentration of p-xylene as the catalytic process which followed both zero and first order.

Although, remediation using enzymatic treatment can be a costly process. Three points of view can show the significance of the current study in affordably remediating contaminated groundwater using enzymes: 1- high biodegradation rate of crude/partial purified enzymes in cold

environments (less time for remediating), 2- cost-effective method for partial purification; and 3- less or no environmental risk of enzymatic remediation compared to other approaches.

4.1.4. Conclusion

The combination of enzymes from *Pseudomonas* sp can be a promising method for conditions that which rapid remediation is needed. The result of this study showed that xylene monooxygenase from S2TR-26 and catechol 2, 3-dioxygenase from S2TR-08 are cold-adapted and degradative enzymes. Feasible protocols for sequential and simultaneous action of enzymes were proposed for p-xylene biodegradation in cold-climate regions. The sequential action of the enzymes is preferred to their simultaneous action because in the latter the addition of catechol 2, 3-dioxygenase is required. However, the simultaneous method can also be a feasible method for cold sites where the multi-step operation is limited. In both these approaches, the enzymes as a degradable biocatalyst will break down into their monomers (amino acids) after enzymatic remediation. The free amino acids can be used by the indigenous bacterial community in groundwater with a lesser impact on the environment compared to all previous remediation approaches. The biological processes using enzymes are far more sustainable. They can catalysis a specific reaction without a high amount of activation energy, auxiliary materials, or solvents. The present study proposed a cold-active enzyme mixture for mineralization of p-xylene and no produced intermediates with the goal of complete detoxification at low temperatures.

BRIDGE-2

Batch test experiments showed that the cocktail of selected enzymes (xylene monooxygenase: catechol 2, 3-dioxygenase) with a ratio of 1:1.5 could completely degrade 200 mg/l of p-xylene in groundwater samples within 48h. The unique thermodynamic and kinetic behavior of the selected cold-active enzymes permit them to achieve rapid degradation of p-xylene at low temperatures (<15°C). *The next step was to test p-xylene degradation using the enzyme cocktail for soil samples under low temperatures to confirm the potential application of the enzyme cocktail in the contaminated site.* After batch tests, bioremediation of p-xylene contaminated soil was carried out in soil column tests with the injection of different concentrations of enzyme cocktails at 15±1ºC.

PART 2

4.2 Enzymatic biodegradation of highly p-xylene contaminated soil using cold-active enzymes: A soil column study

Saba Miri[1,2], Seyyed Mohammadreza Davoodi[1,2], Thomas Robert[2], Satinder Kaur Brar[1, 2*], Richard Martel[2], Tarek Rouissi[2]

1. Department of Civil Engineering, Lassonde School of Engineering, York University, North York, Toronto, Ontario M3J 1P3, Canada
2. INRS-ETE, Université du Québec, 490, Rue de la Couronne, Québec G1K 9A9, Canada

(*Corresponding author, E-mail E-mail: satinder.brar@lassonde.yorku.ca; satinder.brar@ete.inrs.ca)

Journal of Hazardous Materials, 423, 127099; DOI: 10.1016/j.jhazmat.2021.127099

Abstract

Enzymatic bioremediation is a sustainable and environment-friendly method for the clean-up of contaminated soil and water. In the present study, enzymatic bioremediation was designed using cold-active enzymes (psychrozymes) which catalyze oxidation steps of p-xylene biodegradation in highly contaminated soil (initial concentration of 13,000 mg/kg). The enzymes were obtained via co-culture of two psychrophilic *Pseudomonas* strains and characterized by kinetic studies and tandem LC-MS/MS. To mimic *in situ* application of enzyme mixture, bioremediation of p-xylene contaminated soil was carried out in soil column (140 mL) tests with the injection (3 pore volume) of different concentrations of enzyme cocktails (X, X/5, and X/10). Enzyme cocktail in X concentration contained about 10 U/mL of xylene monooxygenase (XMO) and 20 U/mL of catechol 2, 3 dioxygenases (C2,3D). X/5 and X/10 correspond to 5x and 10x dilution of enzyme cocktail respectively. The results showed that around 92-94% p-xylene removal was achieved in the treated soil column with enzyme concentration X, X/5 after second enzyme injection. While the p-xylene removal rate obtained by X/10 concentration of enzyme was less than 30% and near to untreated soil column (22.2%). The analysis of microbial diversity and biotoxicity assay (root elongation and seed germination) confirmed the advantage of using enzymes as a green and environmentally friendly approach for decontamination of pollutants with minimal or even positive effects on microbial community and also enrichment of soil after treatment.

Keywords: p-xylene; Enzymatic bioremediation; Cold-active enzymes; Biodiversity; Soil column

Graphical Abstract

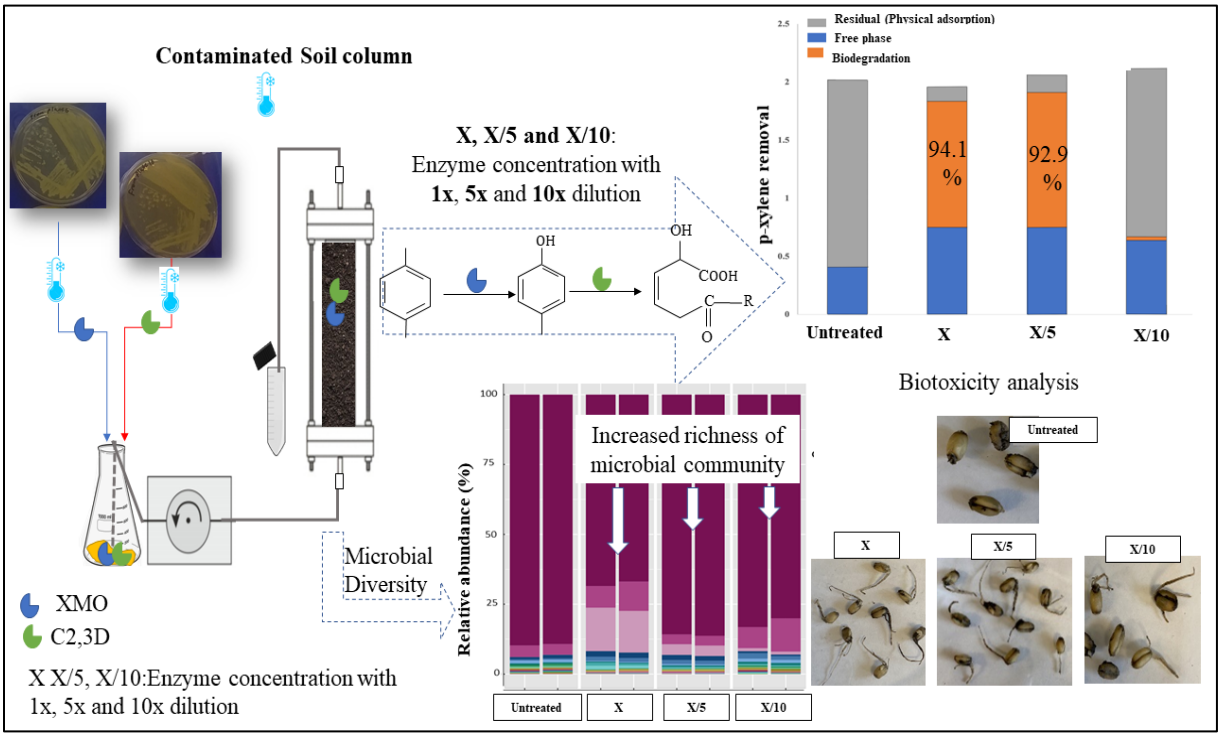

Nomenclature

Acronyms

XMO	Xylene Monooxygenase
C2,3D	Catechol 2, 3 Dioxygenases
BTEX	Benzene, Toluene, Ethylbenzene, Xylene
LC-MS/MS	Liquid Chromatography-tandem Mass Spectrometry
TSB	Tryptic Soy Broth
OD600	Optical Density at 600 nm
CFU	Colony-Forming Units
OUT	Operational Taxonomic Units

Symbols

X X/5, X/10	Enzyme concentration with 1x, 5x and 10x dilution
a	Competitive adsorption coefficient
R^2	Correlation coefficient
C_t	Concentration of p-xylene at any time (g l^{-1})
Co	Initial oil concentration (ppm) (g l^{-1})
D_L	Axial dispersion coefficient (cm)
C_O	Initial p-xylene concentration (ppm)
Ce	P-xylene equilibrium concentration in the liquid phase (mg l^{-1})
k_F	Freundlich adsorption isotherm constant (mg g^{-1} ($l\ g^{-1}$) $^{1/n}$))
k_m	Michaelis constant (cm min^{-1})
k_{cat}	Reaction rate ($l\ g^{-1}$)
m	Mass of dry soil (kg)
m_1	Saturated soil column mass (g)
m_2	Mass of water in both ends reservoir (g)
m_3	Mass of the dry column (g)
M_{total}	P-xylene total mass (mg)
M_{free}	The mass of the p-xylene in the free phase (mg)
M_{air}	The mass of p-xylene absorbed in the air (g)
M_{water}	The mass of pollutant in the liquid phase
M_{soil}	The mass of p-xylene absorbed on soil particles (g)
N	Total number of components
n	Isotherm constant
K	hydraulic conductivity (cm/s)
K_m	Adsorbent mass (g)
K_{cat}	Intra-particle transfer rate constant (mg g^{-1} $min^{-1/2}$)
k_{obs}	Constant rate (1 min^{-1})
$\bar{q}_{e,calc}$	Average of calculated adsorption capacity at equilibrium (mg gv)
$q_{e,meas}$	Experimental adsorption capacity (mg g^{-1})

R_{enzyme}	Retardation factor
V_{max}	Flow rate (mg l^{-1})
V_{enzyme}	Breakthrough volume (ml)
v	Pore water velocity
χ	*Chi-square*
θ	Porosity of column

4.2.1. Introduction

In the last several decades, soil and groundwater pollution from petroleum hydrocarbons has been paralleled by a rapid increase in demand for petroleum oil, leakage from pipelines and tanks, unsafe waste disposal, and transportation (Mosmeri et al., 2019). p-xylene is one of the most widely used aromatic petroleum hydrocarbons as a solvent in various industries such as rubber, leather, printing, paint, gasoline, and airplane fuel production. Since p-xylene is considered a volatile hydrocarbon, it evaporates from topsoil, but any remaining p-xylene can infiltrate through the soil profile and contaminate groundwater [253].

In cold climate regions, the widespread use of petroleum products has led to contamination of terrestrial and aquatic systems at many sites [237]. The management of contaminated sites in these regions is often confounded by the environmental, logistical, financial, and legislative challenges associated with operating in the harsh condition of the cold regions [291]. A cold climate site is one at which the average annual air temperature is less than 15ºC (typically in the range of 4–15 ºC). In the cold ecosystems, they may be more sensitive to the same levels of contamination than the other ecosystems and treatment methods should be mild and with a lower impact on the environment [254].

Over the past decade, various technologies such as chemical methods, physical treatments, thermal treatments, and bioremediation have been applied groundwater, soils, and sediments clean-up. In cold sites, some disadvantages of these methods may be highlighted such as cost, energy consumption, and production of toxic intermediates. Contaminated soil excavation as the physical methods on cold climate soils (such as Remote and northern sites) is very expensive because of high mobilization and on-site monitoring costs, limited equipment availability, and short seasonal work windows [292]. The chemical and thermal methods can be quite hazardous and challenging

when considering the risk of additional environmental impacts due to some intermediates which may be produced during the process as well as high cost and energy consumption [293]. Bioremediation has been considered to be more effective and economical with lesser undue damages to cold climate environments compared to the other methods. However, the highest biodegradation efficiency cannot be easily achieved since the biodegradation of pollutants is strongly influenced by the physicochemical characteristics of the contaminants, the polluted matrices (soil, water, and air), and microbial growth conditions (temperature, oxygen, and nutrition) [13].

Hence, using degrading enzymes rather than whole-cell degrading microorganisms has recently received increasing attention [13]. Enzymatic bioremediation has several potential advantages over whole-cell bioremediation such as 1) shorter treatment period; the enzymes transform the substrate in a minute timescale; 2) safe technology to humans and other living organisms; enzymes have no ill effect on humans, animals, and plants; 3) no toxic by-products; the enzymatic reagents can be designed for complete pollutant degradation; 4) highly specific; enzymes can specifically catalyze a series of reactions for pollutant removal; 5) no environmental risk; the enzymes as cellular proteins break down into their building blocks (amino acids) after remediation without any further harmful effects. Despite such advantages, the high production cost and stability of enzymes restrict their application for environmental purposes [269]. In this study, the use of less expensive substrates(such as crustacean waste) was proposed for enzyme production, and the production of cold-active enzymes was improved by the co-culture of two psychrophilic bacteria.

Monooxygenases and dioxygenases are key enzymes in the degradation and detoxification of petroleum aromatic hydrocarbons through oxidation, hydroxylation, and ring cleavage [212]. In the case of p-xylene, the oxidation can be initiated by the oxidation of one or two methyl side

chains by xylene monooxygenases (XMO). Then, the complete dearomatization of the produced intermediates (catecholic or non-catecholic compounds) proceeds by catechol dioxygenases (C2,3D as a ring-fission enzyme) [16]. Enzymatic bioremediation can be suitable for conditions that rapid remediation is needed (such as cold sites) and also stimulate the degradation processes in the contaminated site [35]. Cold-active enzymes have almost ten-fold greater activity at low temperatures (below 20–30 C) compared to their mesophilic counterparts [275]. Several studies reported enzymes involved in the bioremediation of petroleum hydrocarbon using cold-adapted microorganisms (Table 4.2.1). However, a few studies have been conducted in the application of cold-active enzymes for petroleum contaminant degradation. For example, our previous study showed that cold-active xylene monooxygenase and catechol 2,3-dioxygenase can be used for enzymatic biodegradation of p-xylene in groundwater at 15 °C [218]. The aim of the present study is the use of psychrophilic enzymes for the first time for p-xylene bioremediation in the soil at a low temperature. p-xylene was studied as a model of mono-aromatic hydrocarbon and recalcitrate contaminant. Since p-xylene is the most potent inhibitor compare to other compounds of BTEX (Benzene, Toluene, Ethylbenzene, Xylene). Limited studies are available on bioremediation of p-xylene alone and no enzymatic bioremediation report for p-xylene clean-up except our previous studies [218].

Table 4.2.1. Cold-active enzymes involved in biodegradation of petroleum hydrocarbons.

Enzymes	Target pollutant	Microorganism	Temperature	Ref.
Alkane-1 monooxygenase	Tetradecane (n-C_{14})	*Oleispira antarctica* RB-8	16°C and 4°C	[294]
Catechol 2,3-dioxygenase Catechol 1,2-dioxygenase	Phenol	*Candida subhashii* (strain A01$_1$) *Candida oregonenis* (strain B02$_1$)	18 °C	[295]

		Schizoblastosporion starkeyi-henricii (strain $L01_2$)		
Alkane 1-monooxygenase	*n*-alkanes ranging from C_{12} to C_{36}	*Nocardia soli* Y48 *Rhodococcus erythropolis* YF28-1	20 ºC	[78]
Alkane 1-monooxygenase 2 Phenol 2-monooxygenase Phenylacetone monooxygenase Biphenyl 2, 3-dioxygenase Naphthalene 1,2-dioxygenase	C5-C20 alkanes Phenol Ketone Benzene Naphthalene	*Colwellia* *Cycloclasticus*, *Porticoccaceae* and *Spongiiabcteraceae*	5 °C	[296]
Anthranilate 1,2-dioxygenase Catechol 1,2-dioxygenase	Anthranilate	*Pseudomonas* sp. strain PAMC 25931	10–25°C	[43]
Catechol and chlorocatechol 1,2-dioxygenase	2-, 3-, and 4-chlorobenzoate	*Rhodococcus erythropolis*	10–30°C	[297]
Biphenyl dioxygenase	Biphenyl	*Hydrogenophaga* sp. IA3-A	5°C	[298]
Alkane 1-monooxygenase 1 & 2	Total petroleum hydrocarbons (TPH)	*Pseudomonas putida* GPo1 *Rhodococcus* sp. strain Q15 *Acinetobacter* sp. strain ADP-1	5°C	[299]

However, enzymatic biodegradation in soil involves key factors that should be verified in batch tests and soil columns. To mimic *in situ* application of enzyme mixture, soil column tests can be used to model the essential characteristics of the environment to predict the consequences of bioremediation. To the best of our knowledge, there is no study available on the characterization and application of soil column systems for enzymatic biodegradation of petroleum hydrocarbons.

To ensure correct interpretation of the results obtained, soil samples and columns were characterized and then used for enzymatic biodegradation. The effect of enzymatic bioremediation on the intrinsic microorganisms of soil was studied using next-generation sequencing before and after treatment. Then, the biotoxicity assays were conducted to confirm which concentration of enzyme cocktail should be applied for complete detoxification. Since intermediate products from biochemical reactions may be more toxic than their parent compounds, thus the modification of the initial parent compound is not always an effective method for remediation of pollutants. Several works of literature proposed biodegradation and biochemical techniques with misunderstandings of detoxification of targeted contaminants [287]. Therefore, biotoxicity assays need to be conducted to ensure the correct interpretation of the efficiency of the remediation agent and complete detoxification was achieved after treatment. This study aims to investigate (1) the production and characterization of psychrophilic enzymes, (2) the application of enzymes for remediation of highly p-xylene contaminated soil in columns, (3) the impact of enzymatic bioremediation on the intrinsic microorganisms using next-generation sequencing of the16s RNA and (4) biological toxicity of treated soil using seed germination of winter wheat. These results may form a basis for the development of a biochemical remediation method using oxygenases for *in situ* enzymatic bioremediation not only for p-xylene but also for other petroleum aromatic hydrocarbons.

4.2.2. Materials and methods

Chemicals and bacterial strains

The chemicals were purchased from Fisher Scientific (Ontario, Canada) and Sigma-Aldrich (Mississauga, Ontario, Canada) in analytical/microbial grade and were not further purified. The Bradford assay kit was purchased from Sigma-Aldrich (Ontario, Canada).

Isolation and characterization of *Pseudomonas synxantha* S2TR-26 and *Pseudomonas mandelii* S2TR-08 were described in our recent previous study [218]. Briefly, the strains were cultured and incubated in Minimal Salt Medium (MSM) containing 0.8 g K_2HPO_4, 4.0 g/L NH_4CI, 0.1 g/L NaCl, 0.2 g/L $MgSO_4.7H_2O$, 0.01 g/L $FeSO_4.\ 7H_2O$ (Rahul & Chandrajit, 2011) supplemented with 50-200 mg/L of p-xylene at 15±1°C on a rotary shaker (150 rpm). 15±1°C was considered for all tests as an average annual temperature of the contaminated site and optimum temperature for these cold-active enzymes.

Enzymes production and characterization

Target enzymes were produced based on the co-culture of *Pseudomonas synxantha* S2TR-26 and *Pseudomonas mandelii* S2TR-08. The enzyme production was carried out in 250 mL serum bottles containing 50 mL of MSM supplemented with 18 g/Lcrustacean waste, 2 g of soy peptone, and 200 mg/L of p-xylene. The enzyme production was described in detail in the supplementary information (section S1).

Determination of peptide sequences

The cell hydrolysate was partially purified using 20-60% ammonium sulphate saturation with rapid stirring on ice and the resulted pellets were dissolved in 50 mM Tris-HCl buffer (pH 6.8) [285]. Dialysis was performed against the same buffer overnight. The protein concentration was determined using a Bradford assay kit using bovine serum albumin as a standard [226]. To provide a reference data set for peptide spectrum match (PSM) analysis for target enzymes, the partially purified enzymes were prepared using the suspension trapping (S-Trap) method as described in detail in the supplementary information (section S3). Resulted peptides were subjected to mass determination analysis using a mass spectrometer coupled to an EASY-nLC 1000 system (Thermo Fisher Scientific, USA) and mass spectrometry (MS)-MS sequence analysis using Orbitrap Elite

mass spectrometer (Thermo Fisher Scientific, USA) as described in the supplementary information. All raw data were processed using the software Proteome Discoverer (version 2.2, Thermo Fisher Scientific, USA), then aligned with the protein database of Universal Protein Resource, UniProt (www.uniprot.org) and BLASTP (https://blast.ncbi.nlm.nih.gov) [300].

Enzyme activity assays and kinetic analysis

XMO and C2,3D activity was assayed according to our previous work [15]. Total cell protein was measure by the Bradford assay kit as mentioned above [226].

The optimum temperature of enzymes, catalytic efficiency (K_{cat}/K_m) was determined in different temperatures in the range 5-50±1 ℃. Enzyme kinetics of XMO and C2,3D were studied by using p-xylene and catechol (as mentioned above) as enzyme substrates. Substrate ranges (0.1-10 mM) and enzyme amounts were adjusted throughout the temperature range to optimize accuracy. Michaelis-Menten constants (K_m),V_{max} and catalytic efficiency (K_{cat}/K_m) were calculated using the plot of velocity versus substrate using GraphPad Prism version 8. All enzyme activity tests were replicated three times and the reaction velocity for each enzyme was evaluated to show the presence of free substrate in great excess over the total enzyme concentration [301].

Determination of p-xylene

About 0.05 g of soil was placed in 10 mL headspace vials filled with 5 mL of methanol as the extracting solvent and then vortexed for 5 minutes. The sub-samples (50µL) were removed from the liquid phase using a gas-tight syringe and prepared in a 40 mL standard GC-headspace bottle. The sub-samples were added to 5 mL of ultrapure water, 10 µL of fluorobenzene-D5 (100 mg/L diluted in methanol) as internal standard then sealed immediately. Each sub-sample was analyzed in triplicate. The p-xylene concentration was determined using a Perkin Elmer Turbomatrix HS-40 trap automatic headspace sampler and then the gas phase was analyzed using 7890A Gas

Chromatograph (DB-1701 column 30 m × 0.25 mm i.d. × 0.25 µm film thickness) equipped with a Saturn Mass Detector (GC/MS). The column and vial pressures were 15 and 35 psi, respectively. The quantification was carried out using a standard curve constructed using by extraction of p-xylene spiked soil samples [302] as mentioned above. The standard calibration graphs were linear with correlation coefficients (R^2) being greater than 0.995.

Soil characteristics

The soil samples used for column test experiments were provided by TechnoRem (our industrial collaborator in this work) and have been collected from a contaminated site in Quebec, Canada. This site was selected because of its intense p-xylene contamination since 2003 at depths ranging from 5 to 7m and an approximately 10 m reach of a river. This site is considered as a cold climate site in which the average annual air temperature is 8◦C (typically in the range 4–8 ◦C), and where groundwater temperatures are typically 15◦C or lower. Biodegradation tests were carried out at 15±1◦C, which is the typical aquifer temperature in the contaminated site. The soil samples were originally contaminated with p-xylene and have been artificially contaminated until an initial concentration of 13,000 mg/kg was obtained (average concentration in site). Sieving analysis was carried out according to the American Society for Testing and Materials (ASTM) D422-63 procedure [303]. Grain size distribution and characteristics of the soil are summarized in Supplementary material (Section S1).

Soil column set-up and characterization

The soil columns used were made from a stainless steel cylinder (wall thickness of 2 mm, 3.5 cm in diameter, and 14.5 cm in length (140 mL)). Soil column set-up was described in detail in the supplementary information (section S2). Each set had two replicates. For laminar flow through the porous column bed, the hydraulic conductivity K of each column was calculated using Darcy's

law (Eq. (1)) following a permeability test which was conducted in duplicates. Three hydraulic gradients were imposed for each column at 5, 10, and 15 cm/cm (Fig. A6). This range of hydraulic gradients might be appropriate for the packed column because it did not alter soil fabric, structure, and the rearrangement of the soil particles and it did not result in channelization in the cracks in the soil samples [304].

$$K = \frac{Q}{A \times \frac{(H2-H1)}{L}} \quad (1)$$

Where K is hydraulic conductivity (cm/s), Q is the flux (cm^3/s), A is cross-sectional area (cm^2), H_2 and H_1 are the hydraulic heads and L is the length of column (cm). Hydraulic conductivity, indicating permeability of porous media, measurement is necessary to study the ability of fluid (enzyme mixture in aqueous solution) to flow through the porous media and evaluate the enzyme accessibility to contaminated soils. The pore volume of each column was measured according to Eq. (2):

$$PV = m_1 - m_2 - m_3 \quad (2)$$

Where, m_1, m_2 and m_3 are the saturated soil column mass, the mass of water in both ends reservoir (including the attached tubing sections at the time of water injection), and the mass of the dry column respectively. The conversion of the mass of water into volume was assumed at room temperature to calculate the pore volume. The pore volume and the porosity (the media's own internal porosity (pore volume/total volume of the soil column) of each packed column were evaluated [237], [305].

The dynamic behavior of water flowing into the packed soil columns was described by measuring the axial dispersion coefficient to evaluate the assumption of dispersed plug flow. The axial dispersion coefficient (D_L) in the packed column was measured by injecting a conservative tracer

(Br^-). This ion is not initially present in soil and in enzyme solution, is not affected by soil adsorption, and has no effect on enzymes activity. The concentration of Br^- collected in the effluent samples over time was measured using an ion-selective electrode detector. Dispersity by using the one-dimensional Ogata-Banks (1-D) dispersion according to Eq. (3):

$$\frac{C}{C_0} = \frac{1}{2}\left[erfc\left(\frac{x-vt}{\sqrt{4\,D_L t}}\right)\right] \quad (3)$$

Where C is the concentration in column outflow, C_0 is the initial Br^- concentration (1000 µg/L in this study), $erfc$ is the complementary error function, x is the depth (position in the column), v is the pore water velocity, and t is the time. Dispersion coefficient measurement is needed to evaluate if the column is packed properly and if a diffusion-dominated flow may exist. The volume of Br^- solution injected at C/C_0 = 0.5 gives the transport pore volume of the column. The ratio of the volume of enzyme solution injected at C/C_0 = 0.5 to the one of Br^- gives the retardation factor (R_{enzyme}) or the adsorption coefficient (K_D) of the enzyme in the soil according to equations (4) and (5). This is very important information to calculate how much enzyme solution is needed to flood completely the porous media while achieving an enzyme activity that is equivalent to the solution being injected. Fetter et al., (1999) showed that the Freundlich sorption isotherm coefficient (K_f) can be calculated using the retardation factor as follow:

$$K_f = \frac{(R_{enzyme}-1)\theta}{n\,C^{n-1}\rho_b} \quad (4)$$

$$R_{enzyme} = V_{enzyme} / V_{Br^-} \quad (5)$$

Where R is the retardation factor, θ the porosity, ρ_b the bulk density and n Freundlich isotherm constant.

Mass distribution of p-xylene in soil

The concentration of p-xylene is one of the important factors that impacts its biodegradation. Thus, the distribution of p-xylene on the solid, liquid, and gas phases have been studied to investigate pollutant availability for biodegrading and the effect of enzymatic bioremediation on the fate of p-xylene. A mass balance Eq. (6) can be applied to calculate the mass distribution of p-xylene in soil, air, soil, water, and a free phase of contaminant mixture. The mass balance equation is as follows:

$$M_{total} = M_{free} + M_{air} + M_{water} + M_{soil} \quad (6)$$

Where M_{total} is the p-xylene total mass (mg), in four phases; M_{air} is mass of p-xylene in the air and can be calculated from ideal gas law and Henry's law, M_{free} is the mass of the p-xylene in the free phase (mg); M_{soil} is the mass of p-xylene absorbed on soil particles (g); and M_{water} is the mass of pollutant in the liquid phase. Although some microorganisms can use sorbed p-xylene (M_{soil}), the majority of microbial species can metabolize only those p-xylene molecules in the aqueous solution ($M_{water} = V_{water}\ S_{water}$). That V_{water} and S_{water} are volumes of water and water solubility. Thus, a great deal of effort has been made to apply the enzyme solutions to enhance pollutant removal from soil media by gathering contaminants and degraders in a common location. Then, processes that lower the substrate bioavailability, such as adsorption, cannot reduce the p-xylene's biodegradation rate anymore.

To explain the fixation of p-xylene from a solution onto the surface of soil particles, equilibrium isotherm equations have been developed. The Freundlich isotherm is an isotherm successfully used to express the adsorption of aromatic compounds onto soil particles. According to this isotherm, the adsorption at equilibrium is expressed by :

$$M_{soil} = m\,K_f C_e^{\,1/n} \quad (7)$$

Where m, K_f, C_e are the mass of dry soil (kg), sorption equilibrium constant, and concentration of p-xylene at equilibrium after sorption (mg/L), respectively. The constants defined in Eq. (7) are defined by regressing the log of mass of sorbed on the soil particles (M_{soil}) and the log of the p-xylene equilibrium concentration in the liquid phase (C_e). The adsorption experiments were conducted at room temperature (20 - 22 ℃) by weighing out an appropriate amount of soil (5 g) and placing it in glass containers with Teflon liners in the caps. Various aqueous solution concentrations were added to the soil to achieve 1 g H_2O/ 3.2 g dry Soil. These concentrations were obtained by diluting the p-xylene stock solution. The volume of solution added to the medium was adjusted to maintain the minimum headspace. To measure volatilization losses, the aqueous solutions with no medium and the concentration to those used in the adsorption study were shaken. We assumed that the concentration of p-xylene in the liquid phase was equal to its solubility and the gas and liquid phases were at equilibrium. Moreover, 24h was considered for the equilibrium time to confirm that adsorption equilibrium was reached in soils [306]. To study the effect of the presence of the enzymes in the solution on adsorption of p-xylene and subsequently the mass distribution of p-xylene in soil, the Freundlich isotherm model was used for multi-component adsorption systems (Eq. (8))

$$q_i = K_{fi}\, C_{ei} \left(\sum_{j=1}^{N} a_{ij}\, C_{ej}\right)^{\frac{1}{n_j}-1} \qquad (8)$$

Where K_{fi}, q_i, n, N are the Freundlich constant for component i (mg kg^{-1}) (mg $^{-1})^{-1/n}$, the equilibrium adsorption capacity (g of p-xylene/ g of soil), constant indicative of sorption intensity, and the total number of components in the system. The subscripts i and j are the indices that represent each component in the system. For each component, the model parameters K_{fi}, n and a_{ij} were determined to describe the simultaneous adsorption behavior of enzyme and p-xylene present

in an aqueous solution. Non-linear regression method was applied to minimize the error distribution between the predicted isotherm and experimental data based on the definition of the error function (standard deviation of relative errors (Eq.(9)):

$$r^2 = \frac{\sum(q_{exp}-\bar{q}_{calc})^2}{\sum(q_{exp}-\bar{q}_{calc})^2+\sum(q_{exp}-q_{calc})^2} \quad (9)$$

Where n is the number of observations in the experimental data, $q_{e,meas}$ (mg/g), $q_{e,calc}$ (mg/g) and $\bar{q}_{e,calc}$ (mg/g) are experimental adsorption capacity, theoretically calculated adsorption capacity at equilibrium, and the average of $q_{e,calc}$. Finally, the experimental data were analyzed statistically by hypothesis testing applying the *Chi-square* (χ) test to study the effect of the enzyme content on p-xylene adsorption.

$$\chi^2 = \sum_{i=1}^{n} \frac{\sum(q_{exp}-q_{calc})^2}{q_{exp}} \quad (10)$$

Null hypothesis Ho: p-xylene adsorption is higher with higher enzyme content. Alternate hypothesis Ha: p-xylene adsorption decrease in the presence of enzymes [307].

Batch adsorption experiments were studied by a conventional method [237]. Briefly, the soil samples were placed in a 15 mL tube containing 10 mL of enzyme solution. At a low initial concentration of enzyme, the tubes were shaken at room temperature to reach equilibrium. At the end of the adsorption period, the samples were centrifuged, and the solution was filtered to avoid any sorbents in the aqueous phase. Then the remaining enzyme activity in the supernatant was measured.

Degradation kinetics of p-xylene in the soil column

Many chemical and biological degradation processes follow first-order kinetics, which is characterized using a single exponential rate constant. After determining the mass distribution of

p-xylene in the column, and p-xylene removal by means of different mechanisms, the biodegradation kinetics study can be carried out to compare the p-xylene degradation rate in terms of half-life time ($t = \frac{0.693}{k_{obs}}$), using the fitting curve of $C_t = C_0 \cdot e^{-k_{obs}t}$. Where C_0 ,and C_t are the p-xylene concentration at the initial and t time,and k_{obs} represents the rate constant with the unit of reciprocal time. The soil samples were divided into three parts: top, middle, and bottom soil layers and marked as Top, Mid, and Bot for the untreated and treated columns.

Enzyme stability in soil batch tests

A batch test was performed separately of the columns in 150 mL-serum bottles sealed with an aluminum cap and a rubber septum with the same condition of soil column (static incubation at 15±1˚C). 2g of dried soil (contaminated with p-xylene) was mixed with an enzyme mixture. Two control groups were designed: (1) enzyme mixture without soil, and (2) soil sample without any enzymic treatment. Sub-samples were taken each 2 days to determine residual activities for XMO and C2,3D over 4 weeks.

Enzymatic biodegradation of p-xylene in soil columns

The packed soil columns include six treatments are shown in Table 4.2.2. The enzyme mixture contained 10 U/mg of XMO and 20 U/mg of C2,3D and was injected into the soil column as influents until saturation. The effluents were collected for each 5 mL at regular intervals to determine the enzyme activity and Br^- concentration (Fig. C4).

As mentioned in Table 4.2.2, the soil column tests were carried out over 8 weeks at 15±1°C (average annual temperature of the targeted site). The enzyme injections were repeated after 4 weeks for the columns that were planned to open after 8 weeks. The time intervals for injection were selected based on the enzyme stability results in batch tests.

To determine the p-xylene concentration in soil samples, about 0.1 g of soil were taken from the head, middle and bottom part of the soil column (depth of 2, 7, and 12 cm) in triplicate for each part. To extract the contaminant, the soil samples were mixed with 10 mL of methanol and vortexed for a few seconds (10-15 sec). Then, 50µL of the sub-samples were used for p-xylene concentration analysis using headspace gas chromatography as mentioned in section 2.4.

Table 4.2.2. Soil column treatment and experimental conditions.

Soil column No.	Experimental properties	Treatment duration	Description
1 2	Autoclaved soil column	4 weeks 8 weeks	As a sterile control for determination of natural biodegradation rate
3 4 5	Untreated soil column	Time 0 4 weeks 8 weeks	As a control for determination of the initial concentration of contaminant and natural biodegradation rate
6 7	Treated soil column with enzyme concentration X	4 weeks 8 weeks (with an enzyme injection after 4 weeks)	X corresponds to a concentration of 10 U/mL XMO and about 20 U/mL C2,3D.
8 9	Treated soil column with enzyme concentration X/5	4 weeks 8 weeks (with an enzyme injection after 4 weeks)	X/5 corresponds to 5 times dilution of the enzyme mixture
10 11	Treated soil column with enzyme concentration X/10	4 weeks 8 weeks (with an enzyme injection after 4 weeks)	X/10 corresponds to 10 times dilution of an enzyme mixture

Microbial community determination

Next-generation sequencing was carried out to investigate the effect of enzymatic biodegradation on the microbial community. Total microbial DNA was extracted from soil samples using MoBio PowerMag Soil DNA Isolation Kit according to manufacturer protocol. The concentration and

quality of extracted DNA were measured using NanoDrop 2000 (Thermo Scientific, USA). The V4 region of the 16S rRNA gene was amplified using 515F- GTGYCAGCMGCCGCGGTAA and GGACTACNVGGGTWTCTAAT, then the amplified sequences were analyzed by the Illumina Miseq platform (Metagenomics Facility at McMaster University, Canada). The process of demultiplexing was carried out for sequence runs using Illumina's Casava software. Then, the cutadapt tool was applied for the removal of primers from the sequencing data. The filtered and trimmed forward and reverse paired-end reads at the opposing primers were proceed in DADA2. The chimeric sequences were removed and the output sequences were clustered to operational taxonomic units (OUT) at a threshold of 97% using Abundant OTU +. The output sequences were identified taxonomically using the SILVA 132 database (version 4). The phylogenetic diversity values, maximum likelihood total branch length, were calculated using the p-distance method in MEGA7 [259]. Alpha diversity statistics and beta diversity analysis were performed using the web-based platform of MicrobiomeAnalyst-comprehensive statistical, visual, and meta-analysis of microbiome data [308].

Biotoxicity assay

Soil samples from soil column tests were used for seed germination of winter wheat (eastern Canadian wheat). Winter wheat is very important in Canadian agriculture with a seeded area of 636 thousand hectares in 2019-2020. Besides that, wheat (*Triticum aestivum)* is one of the sensitive species to petroleum contaminations and recommended by environmental regulatory organizations (e.g., International Organisation for Standardisation (ISO), Organisation for Economic Cooperation and Development (OECD), and the US EPA) for analysis the chronic effects of soil contaminants [309]. Tests were performed according to Vaajasaari [310] with some modification and 3 replicates of each soil sample. Briefly, a test unit consisted of 75 mm covered glass Petri

dishes with 50 g wet weight of soil samples. About 10 seeds were added to each dish and were incubated for 7 days in a sealed chamber to minimize p-xylene loss during experiments. At the end of the test, the number of the germinated seeds and root elongation were calculated and compared to the control groups (clean and contaminated soil sample).

Statistical analysis

As mentioned above, data in this study are summarized as the mean ± standard deviation (SD). Statistical analysis was performed using one-way ANOVA analysis followed by Tukey posthoc procedure to determine the differences among test groups at a significance level of $p<0.05$.

4.2.3. Results and Discussion

Production of enzymes mixture

Pseudomonas synxantha S2TR-26 (*P.* S2TR-26) and *Pseudomonas mandelii* S2TR-08 (*P.* S2TR-08) as cold-adapted bacteria were used for the production of cold-active enzymes cocktail. *P.* S2TR-26 and *P.* S2TR-08 were selected based on the ability to degrade mono-aromatic hydrocarbons at <15°C. Aerobic biodegradation of p-xylene is usually initiated by mono-oxidation of the alkyl side chain (by XMO) to the formation of central intermediates which was p-toluic acid and mainly p-cresol. Then, the dearomatization of central intermediates undergoes *meta*-cleavage by catechol 2, 3 dioxygenases (C2,3D) as the crucial step of detoxification [218]. It was therefore hypothesized that by incorporating both strains, benefits from enzymes produced in each strain with the elimination of toxic intermediates produced during incomplete removal of p-xylene. It was observed that p-xylene was degraded faster in the co-culture of bacteria than the monoculture of each strain that resulted in higher biomass and enzyme production. The results in monoculture showed that *P.* S2TR-26 can produce 10.41 ± 0.5 U/mg of XMO and *P.* S2TR-08 produced 15.59 ± 0.64 U/mg of C2,3D after 24h (Fig. 4.2.1). Fig. 4.2.1 shows that the enzyme production was

increased in the co-culture of *P.* S2TR-26 and *P.* S2TR-08 (15.38 ± 0.83 U/mg of XMO and 20.62 ± 0.53 of C2,3D).

Bordenave et al., [311] reported that the complete biodegradation of hydrocarbons requires a mixture of different bacterial groups. A similar result was also observed during BTEX biodegradation by two bacterial strains, *Pseudomonas putida* F1 and *Pseudomonas stutzeri* OX1 [312], and a co-culture of *Pseudomonas putida* and *P. fluorescens* in a fibrous-bed bioreactor for BTEX removal [313].

The result of this study also showed that the co-culture of *Pseudomonas synxantha* S2TR-26 and its enzymes could degrade p-xylene to the inert final product (Fig. C5). It can be due to the presence of both enzymes are required for oxidation of the alkyl side chain and the dearomatization of intermediates (XMO and C2,3D).

Some studies proposed using genetically engineered microorganisms (GEMs) for having desirable biodegradation pathways or enzymes in a single strain. Since, these enzymes can be brought together from different microorganisms to perform specific reactions in a single strain with the ability to produce more enzymes [199]. However, biosafety and environmental risks of potential release of GEMs in the environment need to be considered [256]. For example, using GEMs or nonindigenous microorganisms is banned in Norway, Sweden, Iceland, Canada, and Antarctica [31]. It may be due to little information about the potential impacts of modified organisms on ecology and vulnerability of ecosystems to the potentially invasive microorganism [53]. The main aim of the present study is to propose a green, safe, and environmentally friendly remediation method for *in-situ* applications. Therefore, using the co-culture of indigenous bacteria (*Pseudomonas synxantha* S2TR-26 and *Pseudomonas mandelii* S2TR-08) was preferable compared to GEMs for the enzyme production.

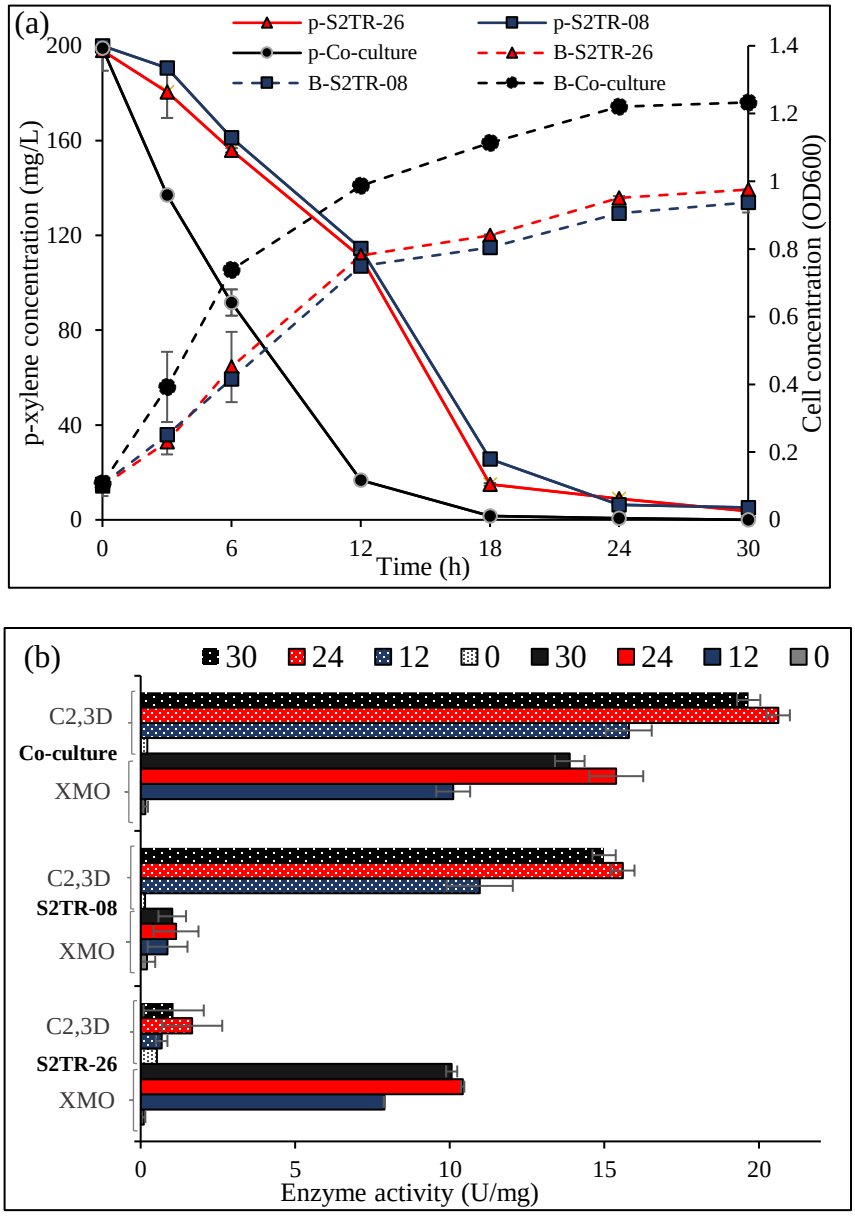

Fig. 4.2.1. p-xylene degradation, biomass and enzyme production by *Pseudomonas mandelii* S2TR-08 and *Pseudomonas synxantha* S2TR-26 in monoculture (S2TR-08 and S2TR-26) and co-culture mode: (a) biodegradation of p-xylene and biomass production (b) enzyme activity during the time. p-: p-xylene concentration; B-: biomass concentration, XMO: Xylene Monooxygenase, (C2,3D) Catechol 2,3-dioxygenase.

Identification of enzymes by LC-MS/MS

The partial purification of enzymes showed that XMO and C2,3D were precipitated at 60–70% and 30–40% cut of ammonium sulphate respectively. SDS-PAGE confirmed the presence of XMO

and C2,3D at approximately 80 and 35 kDa respectively. Each protein cut that contained the target enzyme activity, was subjected to trypsin digestion and then liquid chromatography-Tandem mass spectrometry (LC-MS/MS) identification. According to Jardine et al., (2018), LC-MS/MS can provide substantially more information on the detection of enzymes compared with conventional assays [300].

The identified proteins with ≥1% false discovery rate (FDR) are listed in Table 4.2.3, where FDR indicates the reliability of identified differentially expressed proteins. The sequences of two partial purified enzyme mixtures showed the presence of other proteins (as shown in Table 4.2.3), however, they did not show strict identity to the sequences of any proteins of known oxidoreductase function in the mixture. This can show that XMO and C2,3D are key enzymes responsible for the biodegradation of p-xylene. All protein identified originated from *Pseudomonas synxantha* (ATCC 9890, CFBP 5591, CIP 59.22, DSM 18928) and *Pseudomonas mandelii* (ATCC 700871, CCUG 42058, CFML 95-303, CIP 105273, DSM 17967). Previous research showed that oxidation of xylene can be initiated by direct oxidation of one or two methyl groups of the aromatic ring by xylene monooxygenase. This enzyme can catalyze multi-step oxidation and produce catecholic or non-catecholic derivatives [280]. Then, the ring de-aromatization of central intermediates undergo *ortho*-, *meta*- or *para*-cleavage by catechol dioxygenases as the crucial step of detoxification [250]. Catechol 2,3-dioxygenase is an iron-containing enzyme able to *meta*-cleave the ring of the produced intermediate for complete detoxification of p-xylene [16].

It is reported that catechol 2,3-dioxygenase and xylene monooxygenase subunits were identified in different *Pseudomonas* strains, it may be due to the location of these genes on the plasmid. *Pseudomonas* species play a major role in the degradation of BTEX and represent about 86.9% of

bacterial species found in oil-contaminated sites [198]. TOL plasmids encode the key enzymes in the metabolic pathways for the degradation of xylenes, and their catecholic or non-catecholic derivatives [281]. Horizontal gene transfer (by plasmids) is one of the main mechanisms for adaptation to environmental changes such as pollution to acquire new metabolic traits [314]. This strongly indicates the fact that the sequence of the catalytic center of cold-active enzymes is identical to that of mesophilic homologs [275]. Accordingly, structural adaptations such as molecular plasticity or flexibility are thought to modify the catalytic activity and thermodynamic properties that lead to cold activity [218].

Table 4.2.3. Identification of partially purified enzymes by LC-MS/MS analysis and assignment to the corresponding UniProtKB entry

Sample description	Molecular function	Protein/ Enzyme	Mass[a] (kDa)	Mass[b] (kDa)	Gene	UniProt ID	Coverage (%)
Partially purified enzyme mixture 1 (30–40% cut)	Extradiol ring-cleavage dioxygenase	Catechol dioxygenase	35.1	35.2	*xylE*	P06622	65
	Iron storage	Bacterioferritin	18	18.4	*bfr*	A0A255WUV7	16
	Ribonucleoprotein	50S ribosomal protein L3	22.5	22	*rplC*	A0A059KZB9	6
	Produces ATP from ADP in the presence of a proton gradient across the membrane	ATP synthase subunit beta	49.5	50	*atpD*	A0A024ED61	4
	Plays a role in cell protection against oxidative stress by detoxifying peroxides	Alkyl hydroperoxide reductase C	20.4	20.8	*OU5_0185*	A0A024E2Y4	5
	Prevents misfolding and promotes the re-folding and proper assembly of unfolded polypeptides produced under stress conditions	60 kDa chaperonin	56.2	57	*groL*	A0A024E424	3
Partially purified enzyme mixture 2	Oxidoreductase	xylene monooxygenase	82.4	82.1	*xylA*	A0A5M9J2D1	48
	Monooxygenase activity	Xylene monooxygenase subunit 1	41.5	41.3	*xylM*	P21395	23

(60–70% cut)	GTPase activity	Elongation factor Tu	43.5	43.2	*tuf*	A0A0R2YBZ6	14
	Electron transfer activity	Cytochrome c oxidase (Cbb3-type) subunit CcoO	22.4	24.1	*ccoO*	A0A0R2Z3T7	11
	glutamate-ammonia ligase activity	Glutamine synthetase	51.6	51.6	*glnA*	A0A5D3GGF0	1

[a] Molecular mass was calculated from the respective UniprotKB entry (Theoretical Mass).

[b] Molecular mass was obtained from LC-MS/MS (Experimental Mass).

Kinetic study and characterization of enzymes

Apparent catalytic parameters of XMO and C2,3D on p-xylene and catechol were determined at 10-50 °C. The results showed that the K_m value rose more rapidly compare to V_{max} as the temperature approached 50°C and the enzyme approached the denaturation point. Nevertheless, the value of V_{max} and K_m increases substantially with temperature, catalytic efficiency (K_{cat}/K_m) was decreased in higher temperatures (Fig. 4.2.2). A consequence of the fact that the value of V_{max}/K_m decreased as the temperature increased is that the time is taken for enzyme activity assay, and also denaturation effect begins to be significant at the higher temperature. The result of this study highlighted the central concept of lower stability and flexibility at or near the active site of cold-active enzymes. Based on this concept, the flexibility of enzyme structure should be increased at the active site for high catalytic activity and cold adaptation at low temperatures (Fields & Somero, 1998). The optimum temperature for XMO and C2,3D as determined by the value of V_{max}/K_m is in the range of 10-20°C (average of 15°C). The present results corroborate with previous studies regarding psychrophilic enzymes that reducing K_{cat} dependence on the temperature resulted in higher enzymatic reaction rates at low temperatures and consequently the growing range of its host [273]. In addition, Santiago et al., (2016) mentioned that the cold-adapted enzymes generally exhibit an increase of K_{cat} (catalytic rate) allowed by a decrease in enthalpy

(ΔH) due to a reduced number of protein-ligand interactions and an increase in entropy (ΔS) due to changes in their stability and flexibility (central concept) [315].

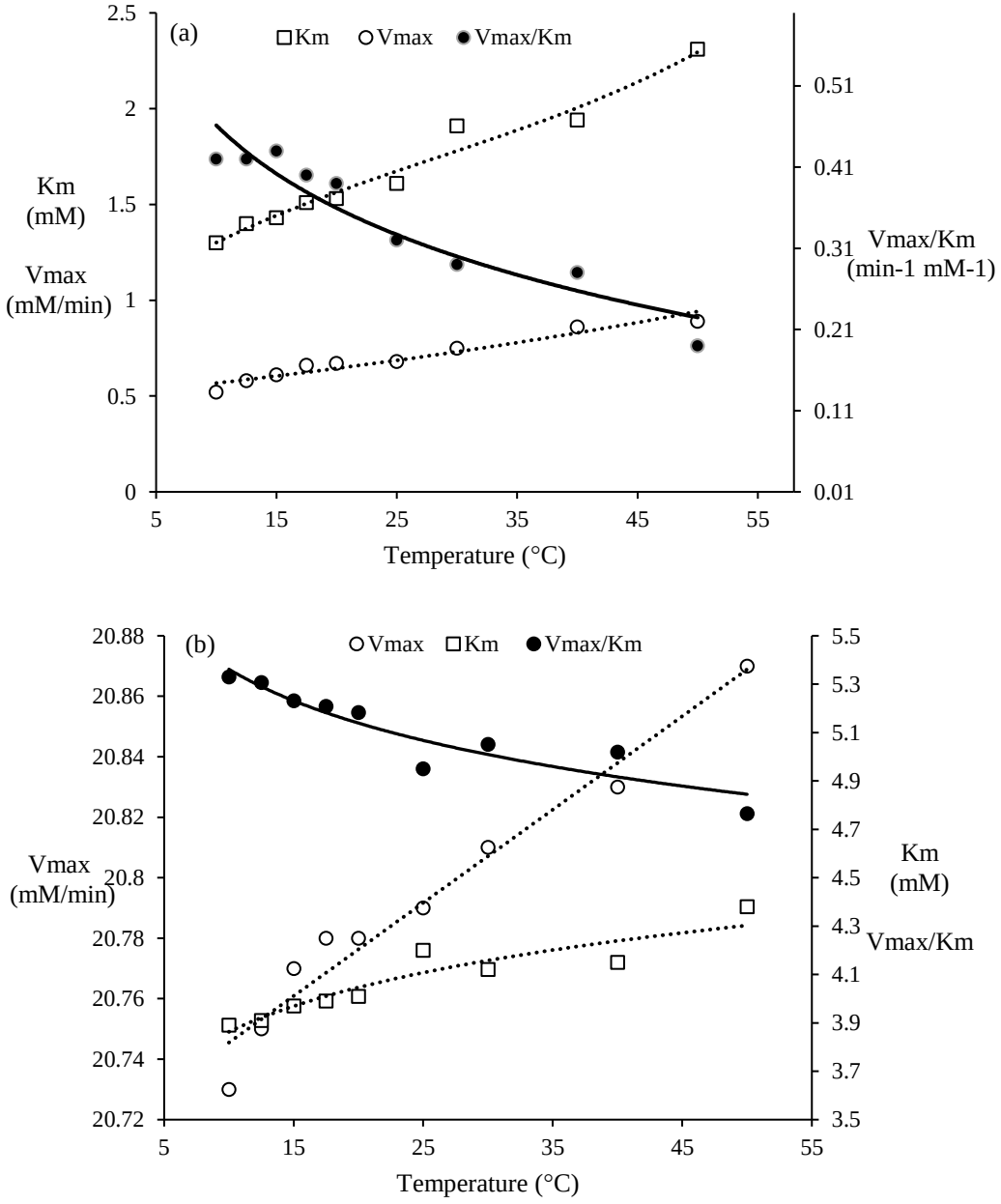

Fig. 4.2.2. Plots of K_m,V_{max} and V_{max}/K_m against temperature for: (a) Xylene Monooxygenase (XMO) and (b) Catechol 1,2-dioxygenase (C2,3D).

Enzyme stability in soil

Stability tests in batch for XMO and C2,3D were conducted to determine the operational stability of enzymes in soil context and the necessary period required to re-inject a fresh enzyme solution in the column tests to maximize the degradation efficiency. Fig. 4.2.3 shows the profile of the relative activity of XMO and C2,3D to the activity of the first day which is the highest. The enzyme activities were determined at 15 ±1°C in the presence of contaminated soil for 4 weeks in 2 days intervals to evaluate their stability during the soil column test. The results demonstrated that both XMO and C2,3D enzymes showed the presence of activity until 26 days in presence of soil with a half-life of 8.66 days and 9.33 days, respectively. During the first 14 days of the experiment, XMO and C2,3D lost 50 and 40% of their activity in presence of the soil. XMO and C2,3D maintained 1% and 6% of their catalytic activity within 30 days, that is the necessary period required to re-inject a fresh enzyme solution in the column test.

In recent years, various oxidoreductases especially tyrosinases, laccases, dioxygenases, and peroxidases have found many applications in technological processes, but they are characterized by low operational stability. For example, crude catechol 2,3 dioxygenase from *Stenotrophomonas maltophilia* KB2 showed no activity after 24h incubation at 4 °C [316]. Pure laccase from *Trametes versicolor* lost about 90% of its initial activity after 10 days at room temperature [317].

A few studies reported enzyme adsorption on soil surfaces and the stabilized enzymes into the soil. However, many studies have been done separately on enzymatic activity in soil context and adsorption of enzymes on different solid surfaces [318]. The adsorption of enzymes/proteins on the soil solid phase is known as a quasi-reversible phenomenon with great significance. Adsorption can stabilize enzymes by increasing their resistance toward denaturation. Since unique three-

dimensional structures of enzymes are essential for their activities. Enzymes gradually lose their activity during the time due to the conformational and structural changes (denaturation of proteins) or their cofactors. Adsorption of enzymes on solid supports can decrease this effect by increasing the structural rigidity of the protein [319]. However, the information on the mechanism of the enzyme interaction with the soil surface is scarce at present [320].

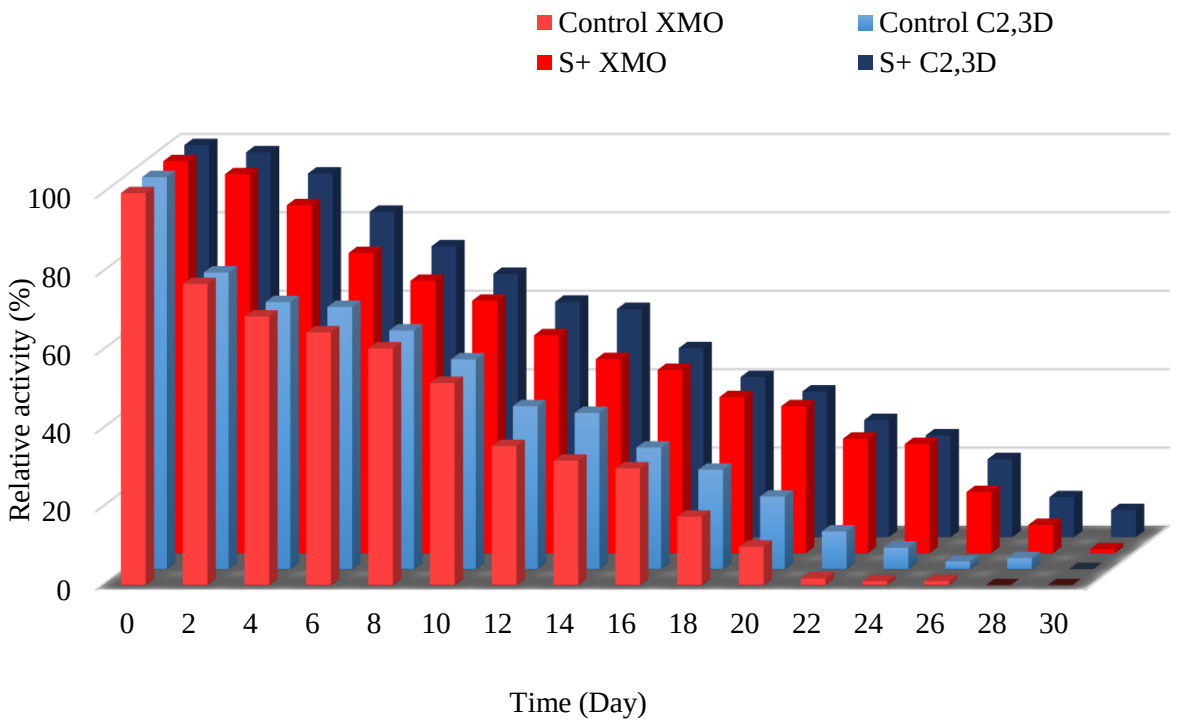

Fig. 4.2.3. Stability of Xylene Monooxygenase (XMO) and Catechol 2,3-dioxygenase (C2,3D) enzymes in the batch test. S: enzyme mixture (XMO and C2,3D) in presence of contaminated Soil, Control: the enzyme mixture without soil.

Soil and Column Characterization

The variation of the zeta potential with the pH of the soil sample is presented (Fig. C2). As can be seen in Fig.C2., the zeta potential of soil suspended in water remained negative across the pH range studied with the isoelectric point at pH < 3 due to the presence of oxygen-containing function

groups on the surface of the soil sample. Thus, the electrostatic attraction between soil particles and p-xylene molecules (weakly positively charged) increases the adsorption capacity.

Fourier-transform infrared spectrum of soil particles is presented in Fig. C3. The spectra give information on the abundance of the presence of oxygen-containing function groups on the surface of the soil sample. For example, C=O stretching peaks appeared between 1,600 and 1,900 cm^{-1} depicts the presence of carbonyl components. Absorption peaks around 640 cm^{-1} might characterize the bending vibration of Si—O—Si (siloxane) functional group in the asymmetric and symmetric vibration region representing the presence of silica as chief components in the soil sample. The infrared spectrum of the clean soil sample depicts an adsorption peak around 850 cm^{-1} indicating the symmetric and asymmetric stretch vibration for Si—O—Si, respectively. The peak at 953 cm^{-1} was assigned to the bending vibration of Si-OH groups. The absorption band around 2,920 cm^{-1} is shown in Fig.C3 that depicts the C—H symmetric vibration of the saturated hydrocarbons and the O—H band due to stretching vibration at 3,435 cm^{-1}. Unlike the siloxane groups that are inert toward deprotonation, the presence of hydroxyl group that is protonated at low pH explained the positive charge of oil surface at acidic conditions [321]. Finally, C-N stretching absorption is found at 1200 to 1350 cm^{-1}.

Table C2 presents the characteristic of the packed soil columns used for treatment experiments. Different soil samples are mixed to prepare a uniform soil type for the experiments, soil type was a mixture of coarse, medium, and fine particles (with grain size 0.25-2.0 mm) that refers to site stratigraphy description presented in Fig. C1. To predict the exact distribution of enzymes and get a more accurate indication of saturation time, the dispersion was measured using total protein concentration in the effluent samples by the Bradford method. Fig. C4 shows the relative

concentrations of the conservative tracer and total protein in effluent samples during enzyme injection.

Bromide as a conservative tracer was used to measure the dispersion and get a more accurate indication of the arrival time. The EXCEL solver was applied to minimize the sum of the square of the errors and adjusting the value of the axial dispersion coefficient. Fig. C4 shows that for the packed soil columns, the low value of the axial dispersion coefficient (D_{ax} = 0.301 cm^2/min) might be assumed the characteristic of normal well-packed beds which can be neglected for liquid phase systems (Q = 5 mL/min). This value was selected based on hydraulic conductivity results that the range of flow rates used during these experiments did not produce any pressure drop through the column bottom and top caps [212]. According to the results of velocity (0.000096 m/s = 8.2944 m/day) and diffusion coefficient of bromide in water at 20^oC (1.6 x$10^{-4}m^2$/day), findings showed that for the Pe = (Length of the column x velocity of water) /diffusion coefficient) greater than 1 (74647.6) and convection was the dominant transport mechanism.

Mass distribution of p-xylene in the column

The column study showed retardation of enzymes solution (R=3.4 and K_f = 0.38 $((mg/g)(L/mg)))^{1.01}$) and the breakthrough curve following the plug flow pulse arrival of enzyme solution. Thus, the adsorption isotherm data for enzyme solution onto contaminated soil particles was studied in a batch system in order to obtain a good initial guess of soil adsorption capacity and soil/pollutant/enzyme interaction during the bioremediation. The results from the Freundlich and multicomponent Freundlich adsorption model for the three sets of experimental data obtained for p-xylene are presented in Fig. 4.2.4. Parameters K_{fi}, n_i, and aij for multicomponent adsorption isotherm for each component are given in Table C3. The obtained coefficient of determination (R^2) showed that the multicomponent adsorption Freundlich isotherm model fits the data well. The

competitive adsorption coefficients (interaction parameter) obtained for the components in the system less than zero demonstrated the lower p-xylene adsorption in the presence of enzyme solutions (Table.C3). Hypothesis testing to infer that the higher content of enzyme in the solution helps in higher adsorption of p-xylene is also rejected. From Eq.(12), the calculated value of χ^2 is $\chi 2_{observed}$=4.79 wheres $\chi 2_{tabulated}$ =3.84 at 5 % level of significance for 1 degree of freedom for χ^2 distribution (Abdehagh et al., 2016). To validate the multicomponent adsorption Freundlich isotherm model, the equilibrium concentrations of p-xylene were predicted at the high level of enzyme concentration R^2=0.95.

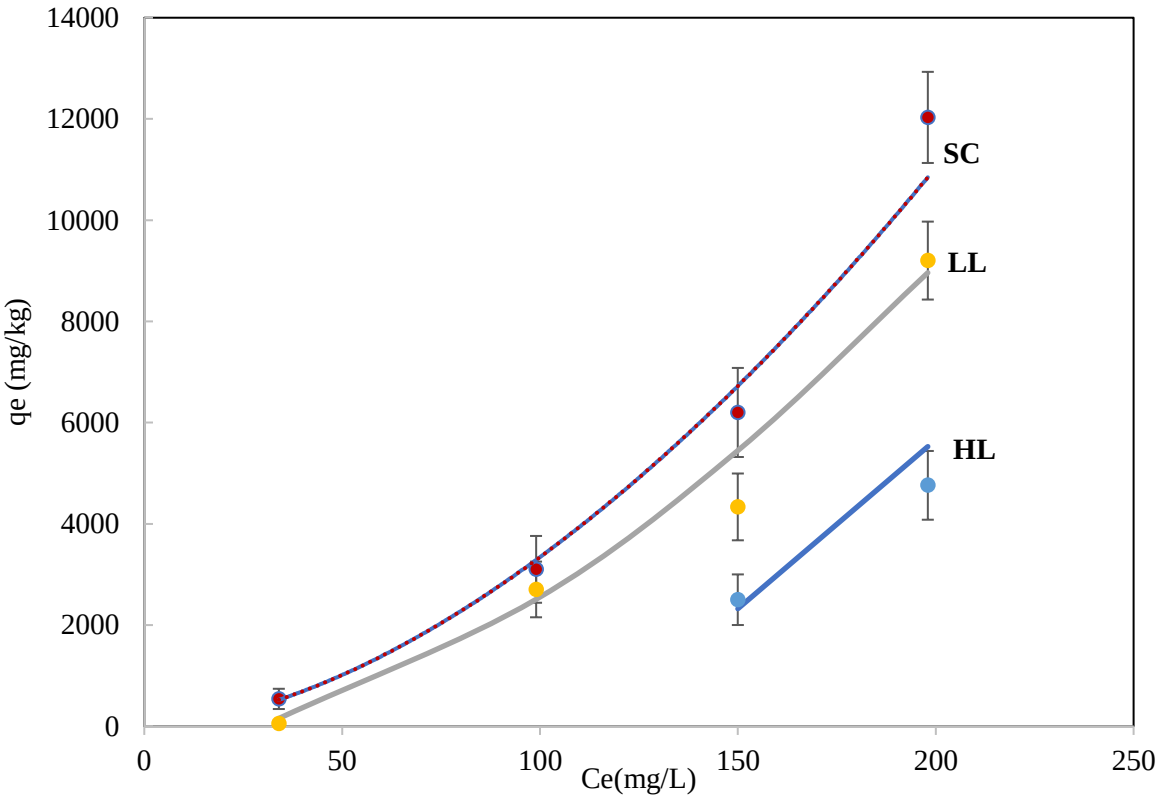

Fig. 4.2.4. Plots of experimental (*symbols*) and predicted (*curves*) multicomponent Freundlich isotherm fits for p-xylene for single compound (SC), the low-level concentration of enzyme (LL= X/5) and high-level concentrations of the enzyme (HL=X) at 15°C

As mentioned previously, processes that lower the bioavailability of the substrate such as adsorption, can reduce the p-xylene's biodegradation rate. The adverse effect of p-xylene adsorption might decrease since the p-xylene coefficient in soil and the total mass of p-xylene in solid-phase decreased in the presence of enzyme solution. As mentioned previously, the presence of carbonyl and hydroxyl functional groups on soil particles resulted in a negative surface charge whereas p-xylene molecules are weakly positively charged across the pH range 3-12. Thus, it is plausible that the $\pi - \pi$ electron-donor-acceptor mechanism involving the carbonyl oxygen-atom of soil particle surface as the electron-donor and the aromatic ring of p-xylene as the electron-acceptor was responsible for the uptake of pollutant [322].

However, the presence of the amine functional group might also enhance the adsorption of the enzyme. Thus, the decreased mass of adsorbed p-xylene in the presence of unfolding enzyme solution can be attributed to the displacement of pollutants from solid adsorbents due to the adsorption of a fraction of the protein. Table 4.2.4 shows the mass distribution of p-xylene in different phases for soil samples at the soil water content of 1 g H_2O/3.24 g Dry Soil.

Table 4.2.4. Measurement and calculation of p-xylene mass balance in different phases for soil samples at the soil water content of 1 g H_2O/3.24 g Dry Soil.

	Total p-xylene [a]			
	Control		X/5 Enzyme concentration	
	Calculated (g)	Measured	Calculated (g)	Measured
Adsorption M_{soil}	0.161 [a]	12.03 g/kg soil [g]	0.137	7.8 g/kg soil
Volatilization M_{air}	0.009 [b]	NA	0.0009	NA
Soil Solution M_{water}	0.001 [c]	198 ppm [h]	0.001	198

Free phase M_{free}	0.041 [d]	NA	0.064	NA

[a] *Total p-xylene added 0.211 g* to 16.2 g soil

[b] $M_{soil} = m\ K_f\ C_e^{\ 1/n}$

[c] $M_{air} = H\ S_{water}$ *where H is p-xylene's Henry's constant,* 1.4×10^{-3} *atm* m^3*/mol and ideal gas law,* $n = PV_{air}/RT$*, where* V_{air} *= 5 ml and T= 15*℃

[d] $M_{water} = S_{water}\ V_{water}$ *where* V_{water} *=5 mL*

[e] M_{free} *calculated using Eq. (6) where* M_{total} *= 0.211 g*

[f] *Not available*

[g] *mg/kg soil*

p-xylene removal

Fig. 4.2.5 shows the bar chart graph representing (a) the residual p-xylene after injection 1 and 2 for different enzyme concentrations and (b) p-xylene removal due to biodegradation and water flushing (free phase). The average mean p-xylene removal was 22.2, 94.1, 92.9, and 31.4 % for untreated soil column, treated soil column with enzyme concentration X, X/5, and X/10, respectively. The poor removal efficiency of p-xylene in the untreated soil column can be attributed to the removal of p-xylene in the free phase and liquid phase by washing (water flooding). As can be seen in Fig. 4.2.5 (b), the enzymatic treatment resulted in the removal of adsorbed pollutants and at the same time increase the free phase that can enhance p-xylene removal from soil media. Considering the fact that the residual p-xylene following the enzymatic treatment using X/10 concentration of enzyme was low and residual p-xylene in the presence of enzyme concentrations X/5 and X after 8 weeks were almost the same ($P>0.25$), we can conclude that the X/5 can be appropriate concentration for soil enzymatic bioremediation system.

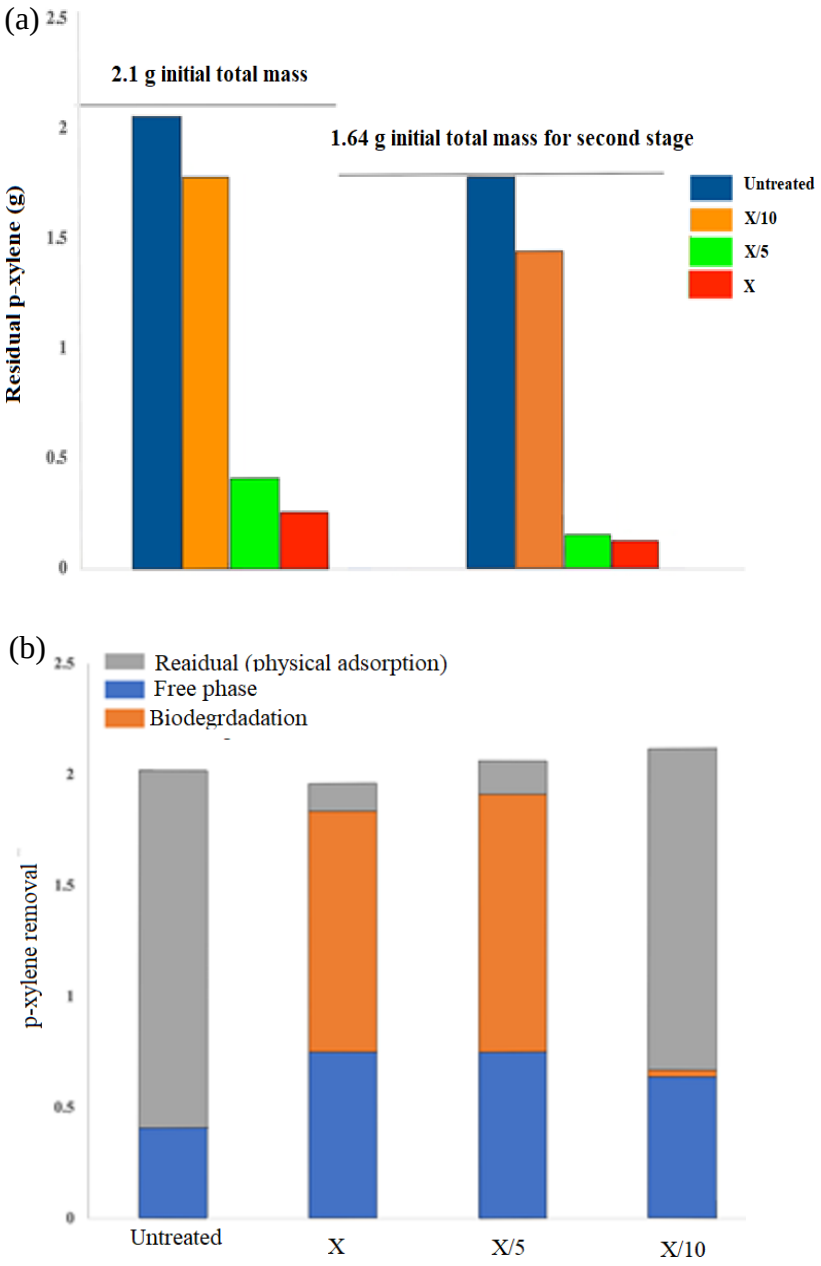

Fig. 4.2.5. a) residual p-xylene after injection 1 and 2 for different enzyme concentrations b) p-xylene removal

Degradation kinetics of p-xylene in the column soil

Our results showed that p-xylene concentration in soil samples in time 8 weeks of incubation increased for some layers that might be due to the mass distribution of p-xylene between different phases. Thus, $C_t = C_0 \cdot e^{-k_{obs}t}$ and its linear form could not provide a good fit to experimental data obtained from some layered soils (data not shown here). In this study, the average mean residual

p-xylene has been applied to determine the degradation rate constant due to the fact that the p-xylene degradation dynamics were fitted as $C_t = C_0 \cdot e^{-k_{obs}t}$. The obtained kinetic parameters of degradation are listed in Table 4.2.5. Kinetic parameters clearly showed that degradation was the fastest in treated soil columns with enzyme concentration X (t ½=1.82 week) followed by in treated soil columns with enzyme concentration X/5 (t ½=2.05 week) and X/10 (t ½=18.23 week).

Moreover, the degradation rate constant (k_{obs}) of p-xylene increased significantly in treated soil columns with enzyme concentrations X and X/5 compared to the untreated column.

Table 4.2.5. Estimated parameters of pseudo-first-order kinetic model at different concentration of enzyme

Kinetic Model	Parameters	Untreated				x				x/5				x/10			
		Top	Mid	Bot	Average	Top	Mid	Bot	Average	Top	Mid	Bot	Average	Top	Mid	Bot	Average
$C_t = C_0 \cdot e^{-k_{obs}t}$	R^2	0.92*	0.91*	-	0.94*	0.99*	0.97*	0.64*	0.98*	0.99*	0.98*	0.93*	0.99*	0.94*	0.99*	0.98*	0.99*
	Half-life time (week)	77±2	99±3	-	533.08 ±1.18	1.89 ±0.42	1.83 ±0.19	1.33 ±0.13	1.82 ±0.15	2.33±0.204	1.92 ±0.109	1.82 ±0.14	2.05 ±0.22	21.04 ±1.14	40.76 ±3.14	10.3 ±2.1	18.23 ±1.18
	Degradation constant (1/week) †	0.009 ±0.002	0.007 ±0.003	0	0.0013 ±.0058	0.374 ±0.011	0.382 ±0.102	0.521 ±0.201	0.381 ±0.109	0.297 ±0.029	0.361 ±0.184	0.38 ±0.13	0.337 ±0.019	0.033 ±0.012	0.017 ±0.004	0.07 ±0.01	0.038 ±0.019

* Significant at 0.05 probability level

† Least Significant Difference (LSD) test ($P \leq 0.05$) showed that the reaction rate constant (k_{obs}, $Week^{-1}$) and half-life ($t_{1/2}$, week) values for degradation of p-xylene in the soils under treatment are significantly different.

Fig. 4.2.6 shows the degradation kinetics of p-xylene in the soil enzymatic bioremediation system based on the average of layered soils column. At different concentrations of the enzyme (X and X/5), the content of p-xylene was decreased to a range of 0.2-.25 at 4 weeks and subsequently, the decreasing trend became slowly for the next enzyme injection. This result was in agreement with p-xylene degradation in Fig. 4.2.5 in which in the initial 4 weeks, the p-xylene removal rate sharply increased while after the second injection, the increasing trend has become slow. Moreover, from the fact that the p-xylene removal rate obtained by X/10 concentration of enzyme was low and average values of p-xylene removal in the presence of enzyme concentrations X/5 and X after 8 weeks were almost the same, we can conclude that the X/5 can be appropriate concentration for soil enzymatic bioremediation system. Our previous work [323] studied the simultaneous and sequential action of enzymes, applied for degradation of 200 ppm of p-xylene in the groundwater. The time-course experiments indicated above 90 % removal of p-xylene in 60 h; however, the current study showed that less than 80 % of p-xylene was removed from the column in the presence of enzyme solutions X and X/5 in 28 days that can be attributed to the different initial concentration of p-xylene and simultaneous adsorption of p-xylene in soil particles.

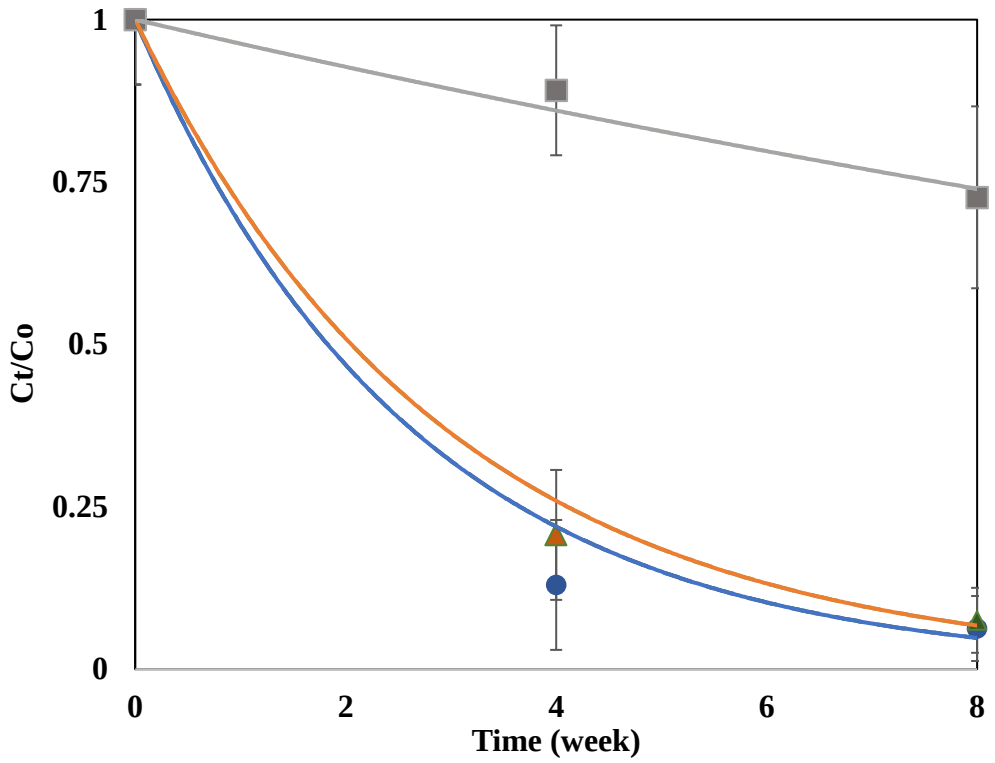

Fig. 4.2.6. The degradation kinetics of p-xylene in the soil bioremediation system: (a) fitting of p-xylene degradation by the pseudo-first-order kinetic model (linear form) (b) fitting of p-xylene degradation by the pseudo-first-order kinetic model (non-linear form)

Microbial community analysis

To understand how the process of biodegradation affects the composition of the microbial community, it is necessary to analyze the microbial response to the treatment agent. The fate of enzymatic treatment and its effect on the microbial community were performed using the next-generationsequencing of 16s rRNA after 8 weeks of treatment. The genus-level microbial community composition in soil column samples is shown in Fig. 4.2.7. The results showed important shifts in the microbial community after enzymatic treatment. The genus *Pseudomonas* was dominant with more than 50% relative abundance in all soil samples. Meanwhile, they observed in lower abundance in treated soil samples compared to untreated soil. This decrease in *Pseudomonas* abundance after enzymatic treatment was probably due to the detoxifying and

regeneration of microbial community resulted in improving soil health with higher species diversity. It is clearly stated that petroleum hydrocarbons can decrease species diversity and reduced biomass (negative effect on soil microbial activity and composition) [324]. The low nutrient status of contaminated soil often hinders microbial growth resulted in the dissipation of contaminants [97]. The enzymes are proteins that is arranged as a chain of amino acids as the fundamental building blocks. After enzymatic remediation, the enzymes as degradable biocatalysts break down into amino acids and serve as growth-promoting for the indigenous bacterial community [325].

In comparison to untreated soil (control), the abundance of *Stenotrophomonas* and *Pseudoxanthomonas* was significantly increased in treated soil with enzymes. The concentration of enzymes used for the treatment indicated a significant difference in increasing the abundance of these genera (X>X/5>X/10) which was probably due to differences in p-xylene concentration, intermediates formation, and protein content as a nutrient for indigenous microorganisms. As per the results of p-xylene and p-cresol concentration, using an enzyme with the concentration of X resulted in a more intermediate concentration (p-cresol), compared to treated soil with enzyme X/5. Meanwhile, p-xylene concentration is decreased in all treated soil samples. Li et al., (2002) show that *Stenotrophomonas maltophilia* T3-c could not grow in the MSM media supplemented xylene as a growth substrate and can co-metabolize it in presence of toluene [326]. Recently, Elufisan et al., (2020) also showed that *Stenotrophomonas sp*. Persol isolated from a crude oil-contaminated soil, could not use xylene as the sole source of carbon in Bushnell Hass medium [327]. However, Bera et al., (2019) reported that *Stenotrophomonas* sp. (MF004205) strain DBK3 utilized p-cresol with a maximum growth rate of 0.1160 h^{-1} [328]. Therefore, p-xylene was transformed to p-cresol in presence of an enzyme with a concentration of X and p-cresol affected

the abundance of *Stenotrophomonas* as a genus with the ability to degrade p-cresol. To visualize the relative patterns of high abundance at the genus level, the heat map was presented in Fig. 4.2.7b. The heat map clearly shows the microbial community shift in a treated soil sample with enzyme X and X/5 but the soil sample with concentration X/10 shows a similar community with the control group.

At the class level, the abundance of *Gammaproteobacteria* was increased in soil samples treated with enzyme X and X/5 (>60000) compare to the control sample (~25000) and soil treated with enzyme X/10 (~20000) (Fig. D8). It is clearly stated that *proteobacteria* are dominant members of the enrichments with monoaromatic hydrocarbons (BTEX) and play a key role in the biodegradation of such contaminants [329]. Moreover, a significant increase in the abundance of *Bacilli* and *Alphaproteobacteria* was observed in soil samples treated with enzyme X in comparison to the control group. These two classes of bacteria consist of several groups of aerobic to facultatively anaerobic bacteria [330]. It may be because of oxygen consumption during enzymatic reaction that shifts in community composition toward metabolic diversity.

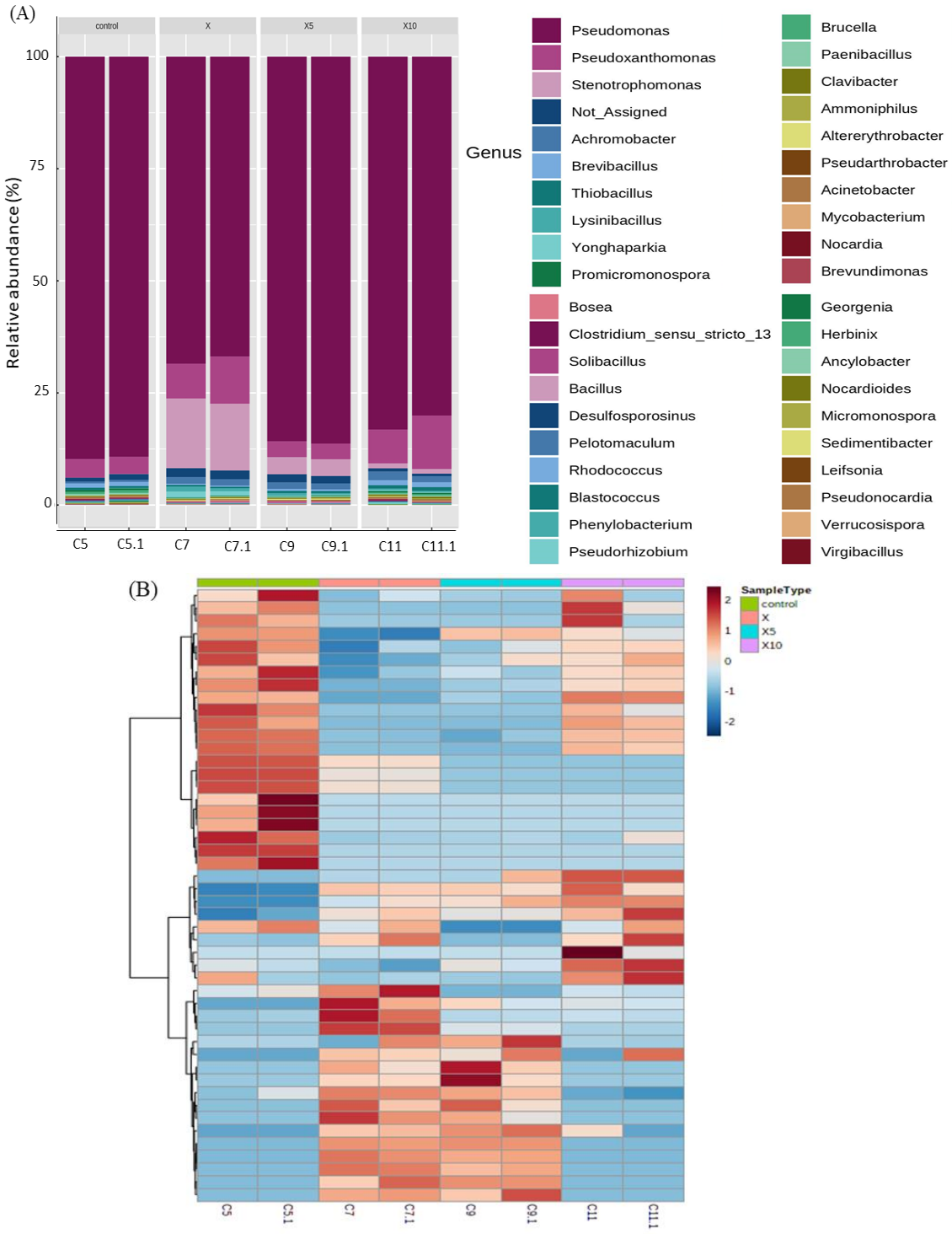

Fig. 4.2.7. Genus-level comparison of the microbial community (A): Area plot for direct quantitative comparison of abundance in each sample, (B): Heatmap for comparison of abundance patterns between different samples, C5 and C5-1 (control group and its replicate), C7 and C7-1 (treated soil with enzyme X and its replicate), C9 and C9-1 (treated

soil with enzyme X/5 and it's replicate) C11, C11-1 (treated soil with enzyme X/10 and its replicate).

Alpha diversity of the microbial community

Knowledge of microbial diversity can be helpful for the selection of a green and environmentally friendly approach for the remediation of contaminants. Microbial community diversity and composition within each sample were assessed by using Chao, Shannon indexes, and phylogenetic diversity (Table 4.2.6). The results showed important shifts in the microbial community diversity after enzymatic treatment. The soil sample from the column treated with enzyme X showed the highest richness. According to observed species and all indices, the enzymatic treatment can increase the richness and positive impact on of microbial community. In accordance with the present results, previous studies showed that the presence of contaminants decreased the richness of species [234]. Moreover, chemical oxidation treatments such as using oxygen releasing compounds (CaO_2) and Fenton or modified Fenton reagent ($CaO_2/H_2O_2 + FeSO_4$) adversely affect microbial diversity and richness [331]. These results prove the advantage of using enzymes as a green and environmentally friendly approach for decontamination of pollutants with minimal or even positive effects on microbial community and also enrichment of soil after treatment.

The increasing richness and phylogenetic diversity (Fig. D9) were consistent with the enzyme concentration used for treatment X>X/5>X10, it can be due to efficient decontamination during the time and enrichment of soil after degradation of the enzyme structure. Since the enzymes as degradable protein structures break down into amino acids and served as a growth-promoting for indigenous bacteria. Although all richness estimator (observes species from the operational taxonomic unit (OUT), Shannon) was consistent with phylogenetic diversity trend in all soil samples, Chao-1 showed the same average value in control and soil sample treated with enzyme concentration X/10. The main reason is that some species richness estimators such as Chao mainly

depended on the number of rare species and then significantly affected by the experimental procedure [332]. Thus, using different indexes is recommended for the analysis of the result from OTU. The refraction curve was analyzed to determine the number of observed OTUs and the sequencing depth of each sample. Fig. D10 shows that all samples reached the sequencing plateau that confirmed the acceptable sequence depth for all samples used for the analysis. The refraction curve also showed that species richness and sequence sample size were slightly higher in treated soil with enzyme X/10 than in control.

Table 5.2.6. Diversity indices for microbial communities of the soil column samples.

Sample	Description	Observed species (97%)	Phylogenetic diversity (PD)	Chao-1 (97%)	Shannon (97%)
Control	Untreated soil column	30620	2.979	55.5	0.823
X	Treated soil column with enzyme concentration X	43557	3.613	76.5	2.086
X/5	Treated soil column with enzyme concentration X/5	39800	3.157	74	1.79
X/10	Treated soil column with enzyme concentration X/10	35215	3.00	55.5	1.168

Beta diversity of the microbial community

The differences and significance of microbial communities between different soil samples were visualized using PCoA (Principal Coordinate Analysis). Fig. 4.2.8 showed the Bray-Curtis and Jaccard indexes from beta diversity analysis at the genus level. Beta diversity is a key concept to describe the distribution of diversity in different soil samples. The results showed that untreated soil samples (control) were separated from the treated soil with enzyme ($p<0.012$). While the soil

samples treated with enzymes were grouped to the upside of the plot (Fig. 3.2.8A), the control samples were grouped separately which shows the distance of control and treated samples. Moreover, the Jaccard method grouped soil samples treated with enzyme X and X/5 to the right side and control and soil treated with enzyme X/10 on the left side of the plot (Fig. 4.2.8B). Both matrices confirmed that enzymatic treatment of soil with concentrations X and X/5 can change the microbial community and dilution of enzymes 10 times was not effective compared to undiluted and 5 times dilution which is consistent with the results from alpha diversity and p-xylene concentration. According to the results, injection of the enzyme with concentrations X and X/5 is suggested for p-xylene contaminated soil treatment which had higher removal and enriches the soil microbial community. Sutton et al., (2013) reported that a highly significant reduction was observed in microbial diversity in soil contaminated with petroleum hydrocarbons. They mentioned that reduced diversity may result from the selective ecological pressure of contaminants, including (1) the presence of a toxic concentration of contaminant and natural biodegradation products, (2) the dominance of a less diverse pool of microbes that can degrade the petroleum hydrocarbons and contaminate-originating hydrocarbons, (3) imbalance C:N:P ratios in soil due to the presence of carbon-rich petroleum, leading changing the nutrition composition and reduced nutrition availability for the microbial community, and (4) electron acceptor limitation for indigenous bacteria may have resulted in form microbial mineralization of contaminant [333]. Following the present results, effective contaminant removal can help to regenerate the microbial community to normal conditions.

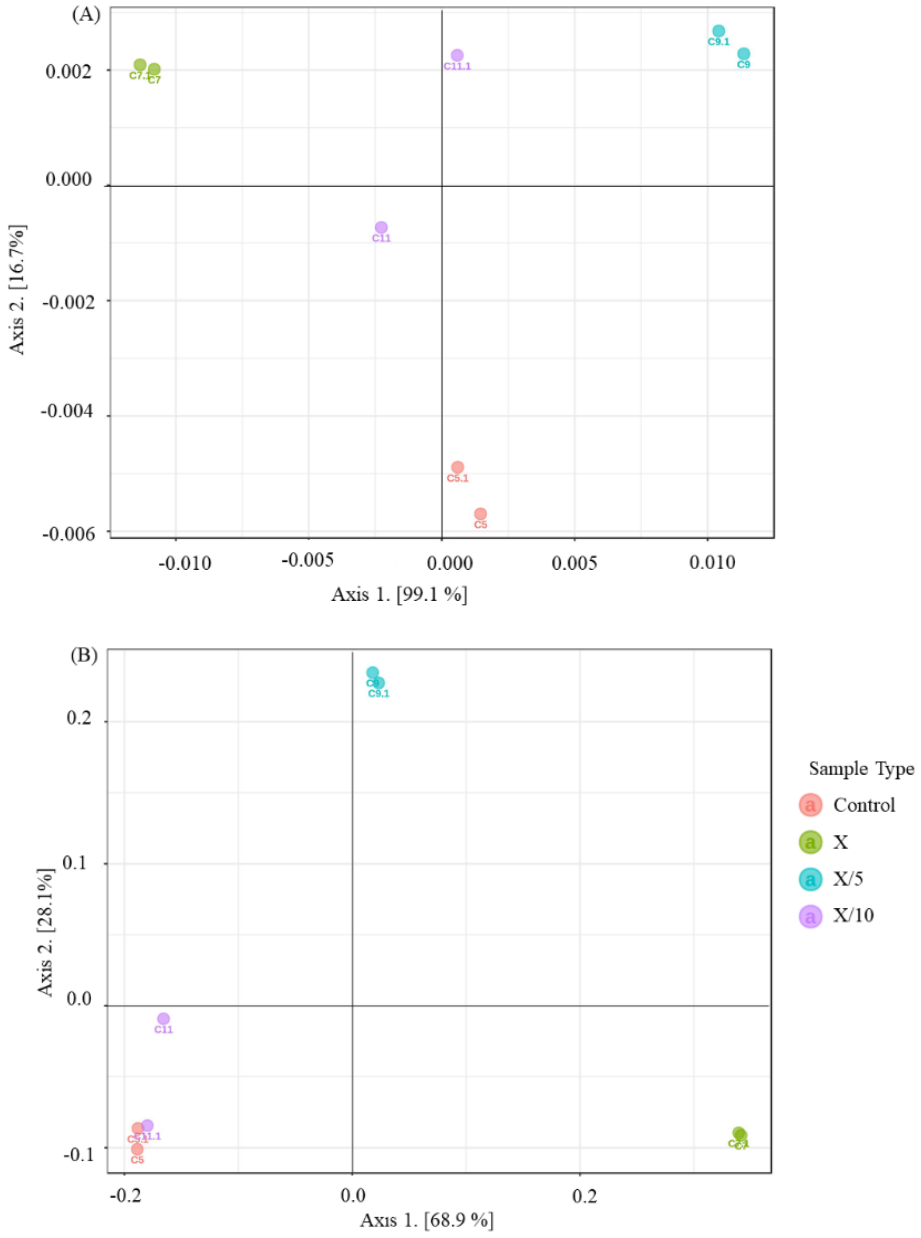

Fig. 4.2.8. Principal coordinates analysis (PCoA) derived Bray-Curtis index and Jaccard distances from beta diversity analysis

Biotoxicity assay

The results of the biotoxicity tests were depicted in Fig. 4.2.9. In general, seed germination tests showed that the presence of p-xylene inhibits seed germination as well as root elongation. However, the control group (test with clean soil) showed the highest number of germinated seed

and root elongation, enzymatic treatment increased seed germination and root length compared to the untreated soil (contaminated soil). The number of germinated seeds in treated soil by an enzyme with concentration X and X/5 were 18 and 15 out of 20 seeds, while in untreated soil and treated soil by an enzyme with concentration X/10 was 3 and 6 respectively. The results from root elongation also were consistent with seed germination and showed the order of clean soil > treated soil with enzyme X > treated soil with enzyme X/5 > treated soil with enzyme X/10 > untreated soil. The result showed that soil treated with X was more effective than X/5 and X/10, which indicated that p-xylene and its toxic intermediates were degraded more completely by the enzyme with concentration X. Environmentally acceptable endpoints for the soil remediation include the chemical concentration of target contaminant and biological responses [334]. It is reported that the hydrophobic properties of petroleum hydrocarbons limit the ability of plants to absorb nutrients and water from the soil. Additionally, low molecular weight hydrocarbons such as p-xylene are rather more toxic than higher molecular weight hydrocarbons due to their high bioavailability to plants [309]. Some studies recommended evaluating the root elongation test as a more sensitive indicator than seed germination tests for petroleum hydrocarbons [335]. However, the result of the present study showed high sensitivity of these two biotoxicity tests for p-xylene bioremediation that was consistent with the results from p-xylene concentration and microbial community. Also, winter wheat species can be used as a model bioindicator in assays to evaluate the toxicity of soil after bioremediation that was consistent with the report of Bank &Schultz (2005). They showed that selection of wheat as a bioindicator has several advantages over other plants such as the ability to grow in a wide range of soil types, high germination efficiency, and worldwide availability [336].

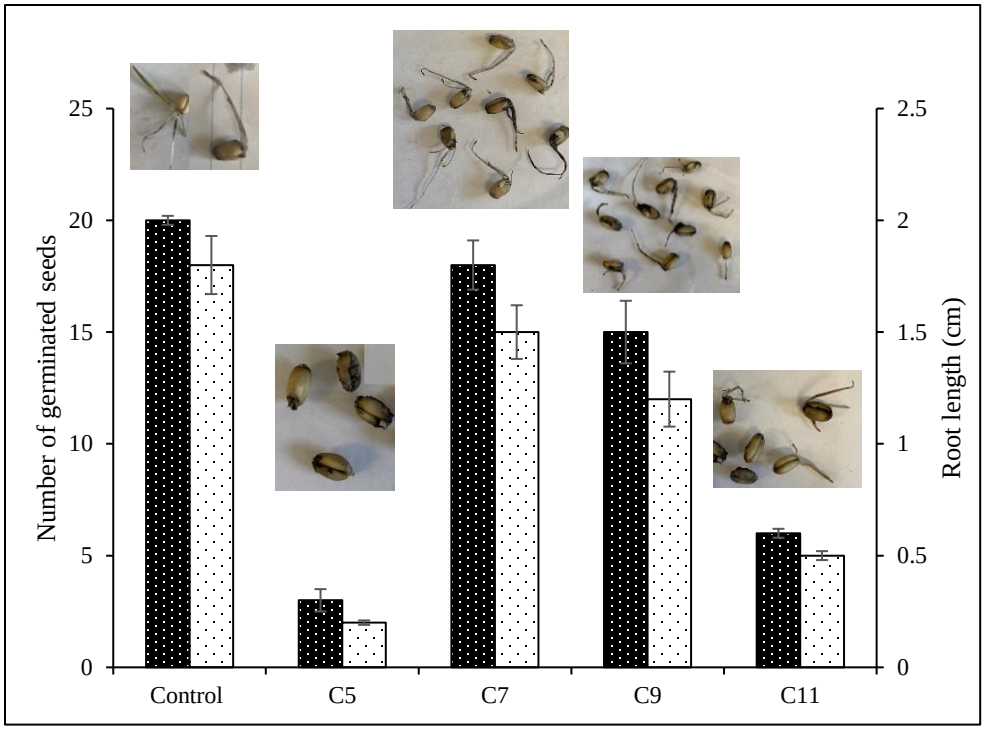

Fig. 4.2.9. Biotoxicity analysis of uncontaminated soil (control) untreated soil (C5) and enzymatically treated soils with different concentrations of enzyme mixture, treated soil with enzyme X (C7), treated soil with enzyme X/5 (C9), and treated soil with enzyme X/10 (C11).

4.3.4. Conclusion

The present work demonstrates that enzymatic bioremediation is a promising tool for p-xylene removal from highly contaminated soil. The enzyme stability test determined the necessary period required to re-inject a fresh enzyme in the soil column tests. Soil column test was suitable for the study of enzymatic bioremediation in cold climate sites. The enzymatic treatment resulted in the removal of adsorbed pollutants and at the same time increased the free phase recovery that enhanced p-xylene removal from soil media. Moreover, the average values of p-xylene removal after 8 weeks indicated that the 5x of enzyme cocktail can be an appropriate concentration for soil enzymatic bioremediation in the soil column system. Dilution of the enzyme cocktail can reduce the cost of treatment. Meanwhile, the increasing microbial richness and phylogenetic diversity

were consistent with the enzyme concentration used for treatment, it can be due to efficient decontamination during the time and enrichment of soil after degradation of the enzyme structure. The results from next-generation sequencing and seed germination tests proved the advantage of using enzymes for bioremediation with a positive effect on microbial community and also detoxification of pollutants after treatment. Further studies (e.g. pilot-scale test using soil tank and production of enzymes on larger scales) are under investigation to evaluate the application of this method in contaminated sites. More studies on other petroleum hydrocarbons, mixed contamination, other soil types and climatic conditions such as different pH and temperatures need to be studied to understand the advantages and limitations of this remediation method.

CHAPTER FIVE: STABILITY ENHANCEMENT of COLD ACTIVE ENZYME BOOSTER TECHNOLOGY

PART 1

5.1. Sustainable Production and co-immobilization of cold-active enzymes from *Pseudomonas* sp. for BTEX biodegradation

Saba Miri[1,2], Jose Alberto Espejel Perez[3], Satinder Kaur Brar[1, 2*], Tarek Rouissi[2], Richard Martel[2]

1. Department of Civil Engineering, Lassonde School of Engineering, York University, North York, Toronto, Ontario M3J 1P3, Canada
2. Institut national de la recherche scientifique, Centre-Eau, Terre et Environnement, 490, Rue de la Couronne, Québec G1K 9A9, Canada
3. Department of Chemical Sciences, University La Salle Mexico, 45 Benjamin Franklin Cuauthmoc, Mexico City ZP 06140, Mexico

(*Corresponding author, E-mail E-mail: satinder.brar@lassonde.yorku.ca; satinder.brar@ete.inrs.ca)

Environmental Pollution, 285, 117678; DOI: 10.1016/j.envpol.2021.117678

Abstract

Toluene/*o*-Xylene Monooxygenase (ToMO) is equipped with a broad spectrum of aromatic substrate specificity (such as BTEX; benzene, toluene, ethylbenzene, and isomers of xylenes). TOMO has can hydroxylate more than a single position of aromatic rings in two consecutive monooxygenation reactions. Catechol 1,2-dioxygenase (C1,2D) is an iron-containing enzyme able to cleave the ring of catechol (the converted product from ToMO) for complete detoxification of BTEX. In this study, cold-active ToMO and C1,2D were produced using newly isolated psychrophilic *Pseudomonas* S2TR-14 in the minimal salt medium supplemented with crustacean waste and different concentrations of used motor oil (0.2- 2% (v/v)). Crude ToMO and C1,2D were immobilized into micro/nano biochar-chitosan matrices and used for BTEX biodegradation. The results showed that the highest enzyme production (12 U/mg for ToMO and 22 U/mg for C1,2D) was achieved at the presence of 0.5% v/v used motor oil compared to the control group without motor oil (0.07 and 0.06 U/mg). High immobilization yield was achieved due to covalent bonding of ToMO (92.26% for micro matrix and 77.20% for nano matrix) and C1,2D (87.57% for micro matrix and 74.79% for nano matrix) with matrices. FTIR spectra confirmed the immobilization of enzymes on the surface of microbiochar and nanobiochar-chitosan matrices as proper support. The immobilization increased the storage stability of the enzymes with more than 50% residual activity after 30 days at 4±1 ºC, while the free form of enzymes had less than 10% of its activity. Immobilized enzymes degraded more than 80% of BTEX (~200 mg/L in groundwater and ~10,000 mg/kg in soil) at 10 ±1°C in groundwater and soil. Therefore, integrated use of microbiochar and nanobiochar with chitosan for co-immobilization of ToMO and C1,2D can be a potential way to remove petroleum hydrocarbons with higher efficiency from contaminated groundwater and soil.

Keywords: Toluene/o-Xylene Monooxygenase; *Pseudomonas*; catechol 1,2-dioxygenase; micro and nano-biochar; chitosan; BTEX

Graphical Abstract

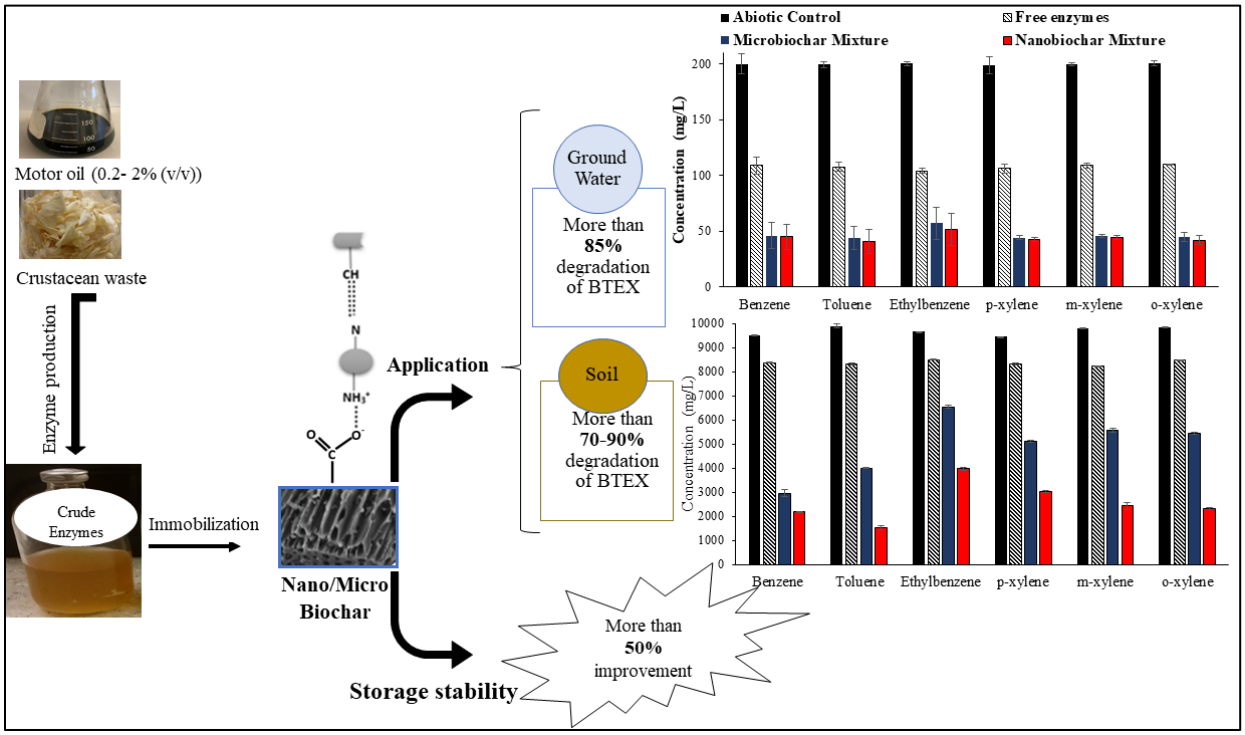

5.1.1. Introduction

Benzene, toluene, ethylbenzene, and a mixture of xylene isomers are abundant compounds in most of the crude petroleum–oils. These compounds are considered an important class of environmental contaminants due to their toxic and carcinogenic properties [337]. BTEX-contaminated sites in cold regions have received significant attention because of their susceptible environment to human impacts. The cold ecosystems may be more sensitive to the same levels of contamination than the other ecosystems [338]. Although different physical and chemical methods for the removal of these contaminants are known; bioremediation is preferred over these methods due to its cost-effectiveness, efficiency and the benefit of its eco-friendly manner [339].

In cold regions, the temperature is the limiting factor in the rate and degree of microbial hydrocarbon biodegradation and affects volatilisation and viscosity of hydrocarbon. Commonly, the optimized scheme of biodegradation cannot be easily achieved since the biodegradation efficiency of contaminants is strongly influenced by the contaminated matrices, the physicochemical characteristics of the pollutant, and microbial growth conditions [13]. Biotechnological improvements such as using cold-active enzymes and immobilization methods seem promising methods for increasing the efficiency of bioremediation at such climates [52]. The enzymatic treatment agent can be designated for pollutant removal, considering the advantage of the shorter treatment period and higher specificity of enzymes than the microbial process [13], [340].

Aerobic BTEX biodegradation is typically initiated by mono-oxidation of the alkyl side chains to form central intermediates which can be catecholic or non-catecholic compounds. Then, the ring de-aromatization of central intermediates undergoes *ortho*-, *meta*- or *para*-cleavage by catechol dioxygenases as the crucial step of detoxification [340]. Monooxygenases and dioxygenases are

key enzymes involved in the attack of the aromatic hydrocarbon ring and reported in most of the biodegradation pathways of the individual BTEX compounds [341]. For example, Choi et al., (2013) reported that *Pseudomonas* sp. BCNU 106 can degrade BTEX via toluene dioxygenase and xylene monooxygenase [280]. Cafaro et al. (2004) suggested that toluene o-xylene monooxygenase (ToMO) as a multi-component protein from *Pseudomonas stutzeri* OX1 can oxidize the individual BTEX compounds [342].

One of the major challenges in the practical and commercial application of oxygenases is their inherent instability [343]. It is proven that immobilization method improve the enzymes' resistance to various storage and operational conditions. The use of immobilized enzymes in biotechnological processes is preferred over their free counterpart because of the prolonged availability of enzymes and their re-usability [318]. Different types of minerals and natural polymers such as chitosan and biochar can be used for immobilizing enzymes for improvement of their storage and operational stability. Biochar is the carbon-rich by-product of heating biomassabove 250°C in an air-limited environment [344]. Chitosan (known as poly-β(1 → 4)-2-amino-2-deoxy-d-glucose) is derived from the deacetylation of chitin, the amino polysaccharide in the exoskeleton of crustacean sand, that shows improved solubility in dilute acids in comparison with the chitin. Since chitosan is an inexpensive, hydrophilic, inert, biocompatible support material, it has attracted great attention for enzyme immobilization. Also, the presence of some amino groups can facilitate the covalent binding of enzymes in chitosan [345] and can be used as a cross-linker for enzyme and carrier support.

Micro/nanoscale immobilization technology can provide an opportunity for co-immobilization of multienzymes in terms of high surface area [346]. According to previous studies, (micro/nano)biochar was suitable support for enzyme immobilization (laccase) to remove the

micropollutants from water and soil. They reported the specific characteristics of biochar, such as high surface area, porous structure, low cost, thermal/microbial resistance and functional groups [347]. To the best of our knowledge, this is the first report on the co-immobilization of oxidoreductase enzymes on micro and nano biochar for the biodegradation of petroleum hydrocarbons. Although cold-active bacteria and their enzymes have been suggested for many applications, the immobilization of cold-active oxygenases on biochar has not been reported yet. Herein, this study investigated the co-immobilization of cold-active oxygenases in the micro- and nanobiochar-chitosan matrices for BTEX biodegradation at low temperature (10°C). The application of the immobilized cold-active enzymes was tested in highly BTEX contaminated groundwater and in soil. For sustainable enzyme production, crustacean waste and used motor oil were used for the production media of cold-active ToMO and C1,2D by isolated *Pseudomonas* S2TR-14. Finally, the stability, half-life, reusability of immobilized enzymes, and diffusion effects in the porous matrix were studied. Our studies suggest that cold-active enzymes can offer greater value upon sustainable immobilization and production, and maybe preferable due to higher catalytic efficiency compare to their mesophilic counterparts for BTEX biodegradation in cold sites.

5.1.2. Materials and Methods

Materials

The following analytical/microbilogical grade chemicals were all purchased from Fisher Scientific (Ontario, Canada): Tryptic soy broth/agar (TSB, TSA), glucose, NaOH, and HCl, yeast extract. Chitosan (100,000-300,000 g/mol molecular weight) was purchased from Fisher Scientific, Australia. Glutaraldehyde solution (aqueous solution, 25% (w/w), tripolyphosphate pentosodium TPP (≥ 99%), ethanol (≥ 99%) were obtained from Sigma-Aldrich (Mississauga, Ontario, Canada).

Minimal Salt Medium (MSM) was prepared by dissolving 1.8 g K_2HPO_4, 4.0 g NH_4Cl, 0.01 g $FeSO_4$. $7H_2O$, 0.1 g NaCl, 0.2 g $MgSO_4.7H_2O$ in 1-liter of distilled water (Miri et al., 2021b). Pinewood biochar was supplied by Pyrovac Inc. (Quebec, Canada). The nano and micro-sized pinewood biochar were kindly provided by Dr. Mitra Naghdi. Briefly, nano-biochar with a specific surface area of 47.3 m^2/g and an average size of 60 ±20 nm, micro-biochar with uniform particle size lower than 75 μm was prepared using a planetary ball mill [348].

Isolation and identification of BTEX-degrading bacteria

The soil samples were collected from a contaminated petroleum site, nearby Montreal, Quebec, Canada. The soil was originally contaminated with petroleum monoaromatic hydrocarbons (~10,000 mg/kg) having an average annual minimum of 5±1°C, average annual maximum of 15± 1°C (average temperature of 10°C considered for tests). The soil samples were collected in summer under open-field conditions from depths ranging from 5 to 7 below surface. Isolation of BTEX-degrading bacteria was carried out immediately after transferring by adding 1 g of the contaminated soil in a crimp sealed serum bottle (150 mL) contained 25 mL of MSM supplemented with 200 mg/L of BTEXs (in a 1:1:1:1:1:1 ratio) as the sole carbon source. This concentration is considered higher with toxic effects on aquifer microbes and bacterial strain with growth ability in this concentration is considered as a BTEX-resistant culture (Varona-Torres et al., 2017). The bottles were incubated at 200 rpm, 10 ± 1°C. After 1 month, the culture was plated onto TSA using the spread plate technique and incubated at 10 ± 1°C for 1 week. Morphologically distinct colonies were selected, and tested for BTEX biodegradation at different temperatures ranging from 4 - 20 ± 1°C.

Genomic DNA of the selected isolate was PCR-amplified using universal 16S rRNA primers (27F, 5′-AGAGTTTGATCCTGGCTCAG-3′ and 1492R, 5′-GGTTACCTTGTTACGACTT-3′) via

colony PCR [349]. The resulting PCR products were sequenced and 16S rRNA gene sequences were compared with available sequences in the National Center for Biotechnology Information (NCBI) GeneBank using a BLASTN algorithm. A phylogenetic tree was developed using the neighbor-joining method of MEGA version 7.0 with 1000 bootstraps [350].

Enzyme production

The crustacean waste from a Canadian seafood processing plant at Gaspesie Peninsula, Quebec was used to produce enzymes from the selected isolate (hereafter named *Pseudomonas* S2TR-14). The oven-dried seafood waste residues (shells of shrimp, crab, prawn, lobster, and krill) were finely powdered in a grinder and stored at 4 °C (Pachapur et al., 2016). The overall composition of the seafood waste is presented in the supplementary material (S1). The enzyme production was performed in a 150-mL serum bottle contained 50 mL of MSM supplemented with 18 g/L crustacean waste, 10 g/L of glucose, 0.1% of yeast extract and different concentrations of motor oil (0.2- 2% (v/v)). The sterile medium (pH 7.0±0.2) was inoculated with 10% (v/v) of bacterial culture and incubated at 10±1°C, 150 rpm for 3 days. Then, the culture was centrifuged at 4000 *x* g. (4 °C) for 20 min. The pellet was washed twice with phosphate buffer (pH 7.0 ± 0.2) and then ultrasonicated (22kHz, 10 min) for cell disruption and extraction of intracellular enzymes (Kadri et al., 2018). The cell lysate was filtered through PTFE filter with pore size of 0.45 µm and the cell free filtrate was stored at 4˚C for further use as a crude enzyme mixture.

Enzyme assays

ToMO activity was quantitatively determined using the spectrophotometric method with toluene as the substrate [340]. 35 µL of N,N-dimethylformamide containing 4% (vol/vol) toluene was mixed with the cellular lysates. At 3-min intervals after incubation at 10 ±1°C, 1-mL samples were mixed with 100 µL of 1 M NH_4OH and 100 µL of 2% 4-amino antipyrine. After the addition of

100 µL of 8% $K_3Fe(CN)_6$, the samples were briefly centrifuged (14,000 × *g*) and absorbance at 500 nm was measured against the enzyme-free control. A reference curve was determined by using 0-50 µg/mL of p-cresol as a product of the reaction.

The activity of catechol 1, 2-dioxygenase was measured according to Li et al., [261] with some modification. Briefly, 0.6 mL of catechol (10 mM) was added to 2.0 mL phosphate buffer, and 0.4 mL cellular lysates. The enzyme activity was assayed by the production of muconic acid at 260 nm.

The total protein was measure by Pierce™ BCA Protein Assay Kit (Thermo Fisher Scientific, Canada) using bovine serum albumin (standard protein) to calculate the specific activity of enzymes.

One enzyme unit was defined as the amount of enzyme that produces 1 micromole of compounds per time unit per mg of total protein.

Immobilization of enzymes on biochar-chitosan matrices

Activation of biochars (nanobiochar and microbiochar) was carried out to increase surface area with NH_2 and COOH groups for better adsorption. 8 g of biochar samples was suspended in 1 L of H_2SO_4: HNO_3 (concentrated solution 3:1 v/v) and sonicated for 3 h using an ultrasonic bath. The suspended biochar was diluted with Milli-Q water and centrifuged to remove the acid and this procedure was repeated several times, until neutrality. The oxidized biochar was lyophilized overnight and kept at room temperature for drying.

About 2 g of each (micro or nanobiochar and chitosan) was mixed in 2% v/v acetic acid under shaking conditions for 24h. Later, 5 mL of crude enzyme solution (crude ToMO and C1,2D) was added under shaking conditions for 2h. About 0.25 mg/mL of tripolyphosphate pentasodium was added in a dropwise manner under similar conditions as mentioned. After 2h incubation, 0.02%

v/v glutaraldehyde was also added dropwise to the solution. This mixture was allowed to stand overnight at 25± 2°C (RT). The pellet of immobilized enzymes was washed by phosphate buffer (pH 7.0 ± 0.2) and centrifuged (16,000 ×g and 4°C for 10 min) for 3 to 4 times before drying and further use. The above process was repeated three times for enzyme immobilization.

Determination of immobilization efficiency and kinetic parameters

Protein loading and immobilization yields were used for the evaluation of immobilization efficiency [351] according to Eq. (1) and (2) as given below:

$$Protein\ loading\ yield\ (\%) = \frac{Amount\ of\ protein\ loaded}{Amount\ of\ protein\ introduced} \times 100 \quad (1)$$

$$Immobilization\ yeild\ (\%) = \frac{Specific\ activity\ of\ immobilized\ target\ enzyme}{Specific\ activity\ of introduced\ \ target\ enzyme} \times 100$$

(2)

Immobilization of ToMO and C1,2D on biochar-chitosan matrix was further confirmed by analyzing enzyme leaching [352]. The leaching test was carried out by 0.1 g of immobilized enzymes in 1 mL of sodium phosphate buffer (pH 7.0) with continuously stirring for 1 h, 6h, 12h, 24 h, and 48 h. The mixture was centrifuged 16,000 ×g at 4°C and then the supernatant was analyzed for enzyme activity. The leaching (%) was calculated according to Eq. (3)

$$Leaching\ (\%) = \frac{Amount\ of\ protein\ in\ supernatant}{Amount\ of\ protein\ immobilized} \times 100 \quad (3)$$

Kinetic parameters were determined by Michaelis-Menten model for free and immobilized enzymes to describe the kinetic behavior [13]. Briefly, the initial rate of substrate removal (toluene for ToMO and catechol for C1,2D) was measured at different substrate concentrations (0.1-1.0 mM). Then, V_{max}, $K_{m,}$ and catalytic efficiency (K_{cat}/K_m) were calculated for free and immobilized enzymes using GraphPad Prism version 8.

When enzymes are immobilized on the internal pore surface of porous particles, substrates (i.e., toluene) diffuses through the porous pathways among pores and reacts with enzyme immobilized on pore surfaces. To evaluate if immobilization of enzyme experiences diffusional limitations or not. Some literature applied the effectiveness factor, as the ratio of the reaction rate with diffusion limitation to the reaction rate without diffusion limitation can be applied. Under diffusion limitation, the rate per unit volume is usually expressed in terms of the effectiveness factor as follows:

$$r = \eta \frac{V_m'[S_1,s]}{k_m + [S_1,s]}$$

Thus, the Thiele modulus for porous spherical reaction systems that follow the Michaelis rate expression was given by Blais et.al as:

$$\emptyset = \frac{r}{3} \sqrt{\frac{V_{max}}{K_m . D_e}} \quad (4)$$

The relationship between effective factor η and the Thiele modulus for low substrate concentration is given by

$$\eta = \frac{1}{\emptyset}\left(\frac{1}{tanh 3\emptyset} - \frac{1}{3\emptyset}\right) \quad (5)$$

The effective diffusivity of the substrate S_1 in porous particles is related to the particle's porosity, the geometrical tortuosity, the substrate diffusivity in bulk solution by

$$D_e = k_p(\lambda) k_r(\lambda)\, \varepsilon\, D_0 / \tau \quad (6)$$

Where τ is tortuosity of the pores and is assumed to be equal to 1 (e.g., uniform cylindrical pores) in this work. $k_r\ (\lambda)$ and. $k_p\ (\lambda)$ are the hydrodynamic drag and the equilibrium partition coefficient both functions of the ratio of the substrate molecule size to pore size, λ. Ferry et.al proposed the following Eq.(9) to calculate $k_p\ (\lambda)$ for spherical molecules in a cylindrical pore with no wall-molecule interactions:

$$k_p\ (\lambda) = \ (1 - \lambda)^2 \tag{7}$$

Brenner et.al also proposed following Eq. for small λ

$$k_r\ (\lambda) = (1 + \frac{9}{8\lambda \ln(\lambda)} - 1.54\lambda)/\ (1 - \lambda)^2 \tag{8}$$

Using Eq.(9-10), k_p and k_r values are calculated for toluene and summarized in Table D1.

The pores were considered as a long cylinder from the center of the sphere to the surface of biochar particles. The diameter and length of each cylinder are assumed 30 nm and 5 μm. Thus, the effective diffusivity of substrate S_1 through 30 nm pore is 4.6×10^{-6} $cm^2.s^{-1}$.

FT-IR spectroscopy

Fourier transform infrared (FT-IR) spectra of micro/nanobiochar-chitosan matrices and enzyme immobilized matrices were recorded by placing a sample on the gripper plate and the diamond crystal to have consistent contact between the sample and the diamond crystal. FT-IR spectrum was recorded for each sample in the wavenumber range of 4000–400 cm^{-1} using a Nicole IS50 spectrometer (USA) equipped with attenuated total reflectance (ATR) accessory (4 cm^{-1} resolution). Each spectrum was repeated with 16 scans per sample, and their average was used for plotting.

Storage stability assessment

The enzyme samples (free and immobilized form) were stored at 4±1ºC and room temperature (RT); 25 ± 2 ºC, which are typical storage temperatures for industrial purposes for 30 days and residual enzyme activity were assayed as mentioned above.

Biodegradation and reusability test

For BTEX-biodegradation tests, the groundwater sample was supplemented with 200 mg/L of BTEX as the sole source of carbon. The characterization of groundwater samples showed the presence of carbonates (hard water) with a pH of 7.2 ± 0.4. About 20 mg of immobilized enzymes (each matrix) were added with 25mL of MSM medium in 150 mL sealed serum bottles. The incubation was carried out at 10 ±1◦C (the typical aquifer temperature in the contaminated site) for 24h under shaking conditions (150 rpm). The sub-samples (50µL) were removed from the liquid phase of bottles using a gas-tight syringe and prepared in a 40 mL standard GC-headspace bottle. The sample bottle was containing 5 mL of ultrapure water, 10 µL of fluorobenzene-D5 (100 mg/L diluted in methanol) as internal standard and then sealed immediately. The extraction of BTEX was carried out using a Perkin Elmer Turbomatrix HS-40 trap automatic headspace sampler and then the gas phase was analyzed using 7890A Gas Chromatograph (DB-1701 column 30 m × 0.25 mm i.d. × 0.25 µm thickness) connected to a Varian 2200 Gaschromatograph coupled to a Saturn Mass Detector. The concentration was quantified from the areas of the substrates and compound's peaks using a standard curve.

Soil BTEX-biodegradation test was performed in 150 mL sealed serum bottles containing 2g of the soil sample, 20 mg of immobilized enzymes and 25 mL of MSM medium at 10 ±1◦C ,150 rpm. The soil is saturated with water for optimal biodegradation conditions [353]. The incubation and sub-sample preparation were carried out as mentioned above. The soil was originally contaminated

with BTEX and has been artificially contaminated with BTEX until an initial concentration of 10,000 mg/kg (the average BTEX concentration in the contaminated site). The liquid phase concentration of compounds in groundwater and soil systems was directly measured using gas chromatography coupled with a headspace sampler. The mineralogy of soils varies in different parts of the site; quartz, feldspar, clay minerals and carbonates were found in soil samples. The soil sample comprised 59% of particles with a size range between 1-5 mm, 38% with a size range of 250-500 µm and 3% of fine particles (< 250 µm in size). The physical characteristics of the soil were determined as follows: moisture content of 24.17± 0.5%, pH 7.1±0.2, total solids: 75.36±0.91%.

For reusing the enzyme, the immobilized enzymes were removed after decantation (at 10,000 ×g for 20 min) and methanol was used for the washing. Then, it was dried in a desiccator and used in a fresh groundwater sample supplemented with 200 mg/L of BTEX for 5 different cycles.

Two control groups were included in biodegradation experiments: 1) sterile controls with autoclaved (121 °C for 30 min) soil and 2) reference controls with original soil samples without any treatment. Abiotic losses of BTEX were monitored in the sterile control sample and the evaporation loss was compensated in the liquid phase before each test. In other words, each compound was added to obtain an approximate specific total of 200 mg/L (groundwater sample) and 10,000 mg/kg (soil sample) in the liquid phase. Chang et al. reported that in a bottle (250ml) with at least 150 ml of headspace, shaken on a rotary shaker at more than 100 rpm can result in a higher rate of mass transfer of BTEX between the gas and aqueous phases than the maximum biodegradation rate ensuring rapid equilibrium with the liquid phase [354]. Thus, mass transfer phenomena may not slow down the kinetics of biodegradation under mentioned conditions.

The contribution of adsorption was performed with micro/nano biochar-chitosan matrices (with inactivate enzymes) in the BTEX reaction the same as mentioned above. As proteins have adsorption, the immobilized enzymes were deactivated by incubation at 75±1ºC for 1h [355]. To determine the amount of BTEX adsorbed on matrices, the mixtures were decanted (at 10,000 ×g for 10 min) and the adsorbed BTEX were extracted using 5 mL of methanol by vortex shaker, then the concentration was measured as mentioned above.

Statistical Analysis

All experiments were performed in triplicate (for analytical and biological tests) and the calculated average of replicates was used along with their standard deviation. SPSS software was used to determine their statistical significance using (ANOVA) followed by Tukey posthoc procedure. A *p*-value of 0.05 was considered the level of significance. Repeated measures ANOVA was used to calculate the difference between the biodegradation ability of immobilized enzymes into micro and nanobiochar-chitosan matrices.

5.1.3. Results & Discussion

Isolation and characterization of strain S2TR-14

An isolated bacterial strain, S2TR-14, was selected based on the ability to degrade BTEX at 10 ±1°C. Psychrophilic bacteria have an optimum temperature at or below 15 °C for growth. The resulted colonies on TSA plate had morphological characteristics of whitish, smooth and raised with a circular shape. Nucleotide fragment sequences of 16S rRNA gene of strain S2TR-14 was deposited in the GenBank database (NCBI accession number: MN197883). According to the analysis of the phylogenetic tree (Fig. E1), the selected strain (S2TR-14) showed a close phylogenetic relationship with the strains of *Pseudomonas* genus. S2TR-14 showed the highest similarity (99%) with *Pseudomonas* strain N-8 and *Pseudomonas* sp. PK8.

Several mesophilic *Pseudomonas* strains have been reported for BTEX biodegradation [356]. It is mentioned that indigenous microorganisms are more adapted to cold environments than any non-indigenous population. Isolation and enrichment of indigenous microbes with biodegradative potential are key steps for the bioremediation [357]. Isolation of psychrotrophic microorganisms was also carried out for biodegradation of aromatic hydrocarbons in low temperatures, but only by few researchers. For example, Chablain et al. isolated two psychrotrophic toluene-degrading *Pseudomonas putida* strains from the soil, but they reported that toluene is the growth-limiting factor for the isolated bacteria at all temperatures [358]. Liu et al. (2013) isolated a cold-tolerant consortium from contaminated soil, which can degrade nitrobenzene and aniline nitro-aromatic and aromatic amino compounds at 10°C [26].

Enzymes production

Biodegradation pathways of mono-aromatic hydrocarbons begin with mono oxidation and finish with the formation of catechol isomers or non-catecholic compounds as intermediates [266]. The metabolism of a substrate involves multiple enzymatic steps. Aerobic biodegradation of aromatic hydrocarbon has been divided into the *upper* pathway, which started from the original compound (hydrocarbon compound without any modification) to central intermediates (modified hydrocarbons). The lower pathway, transitions from the ring cleavage of intermediates down to the needed molecules for biomass [359].

Our preliminary results showed that *Pseudomonas* strain S2TR-14 initiated the oxidation of the methyl side chain of the aromatic nucleus by ToMO then followed the ring fission by C1,2D. Thus, the presence of ToMO and C1,2D are needed for complete detoxification of BTEX.

The chemical nature of inducers has a significant role in the efficacy of enzyme production, and the induction of oxygenases by BTEX was reported using *Pseudomonas* species [280]. BTEXs are

important industrial chemicals that have many applications so, the use of fewer and less expensive substrates can make the use of enzymes more cost-effective in environmental applications. In this study, enzymes were produced using a different concentration of used motor oil ranging from 0.2% to 2% as a source of BTEXs. Also, crustacean waste was used as a cost-effective source of calcium and proteins that can promote bacterial growth [360]. The raw materials needed for enzyme production for bioremediation applications are crucialsince the high production cost of enzymes has restricted the widespread use of them for remediation purposes [361].

Fig. 5.1.1 demonstrates the production of ToMO and C1,2D by S2TR-14 and their activity in the presence of different concentrations of used motor oil at 10 ±1°C. Our initial studies showed that new motor oil could not induce ToMO and C1,2D production (data are not shown), it may be due to the absence of BTEX. Baker et al. reported that used motor oil was a potential source of BTEX with concentrations ranging (from 29 to 2000 mg/L). The concentration of *m* and *p*-xylene was higher, typically 1500-2000 mg/L, compared to those of other BTEX compounds. While BTEX was not detected in any of the five tested new motor oil [361].

As shown in Fig. 5.1.1, the highest enzymes production was obtained (12 U/mg for ToMO and 22 U/mg for C1,2D) at 0.5% v/v after 72h. The enzyme activity is presented as an enzyme unit per total protein content in the enzyme mixture. The bacteria grown with 2% v/v of used motor oil showed low ToMO and C1,2D production (0.07 and 0.08 U/mg respectively), which was similar to the control sample (0.07 and 0.06 U/mg) that was the batch without motor oil. It can be due to the toxic effect of a high concentration of used motor oil on bacterial growth. Most of the petroleum hydrocarbons led to toxic effects on bacterial growth and inhibit their activity mainly because of their chemical structure. Despite the toxicity effect, the obtained data showed that used motor oil

in low concentration (0.5% v/v) can play a potential role as inducers for ToMO and C1,2D production.

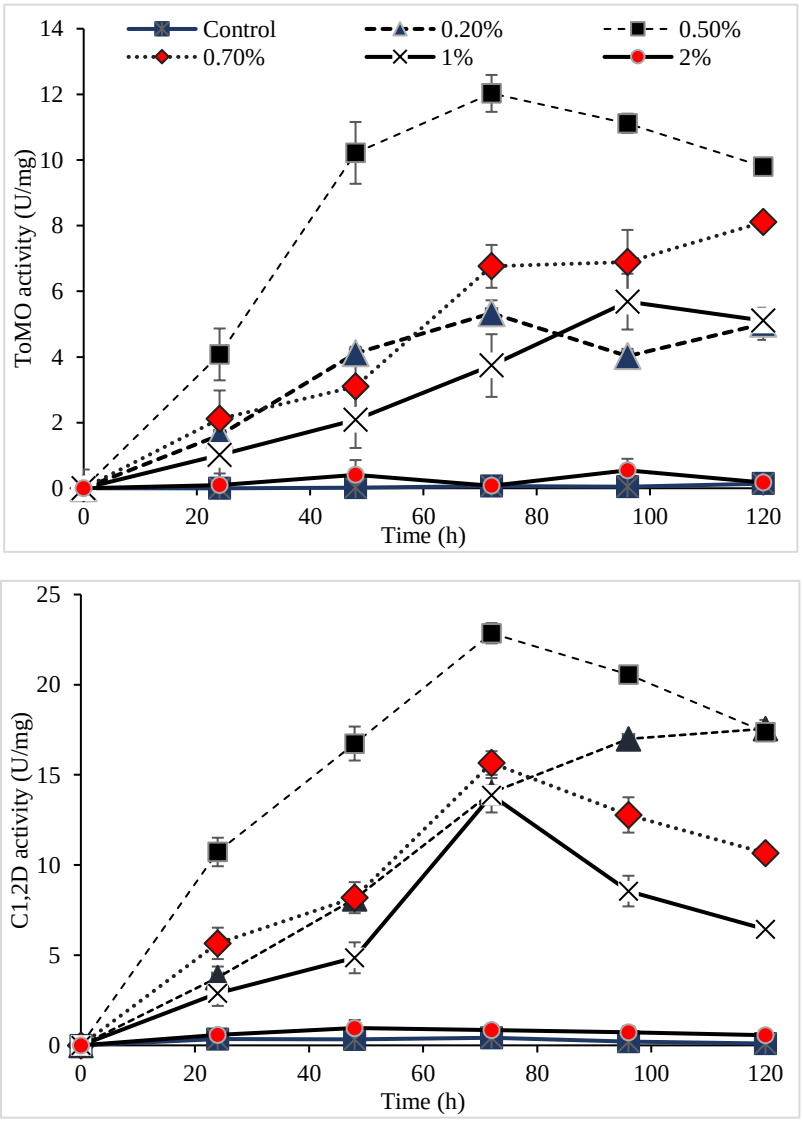

Fig. 5.1.1. Enzymes production at different concentrations of used motor oil (0.2-2%v/v), control samples contained media without any used motor oil.

Immobilization efficiency of biochar mixtures

Biochar was selected as an economical and renewable support material for the development of immobilized and encapsulated value-added bio-products such as enzymes [173]. Mico/nano-sized biochar can provide a larger specific surface area for the co-immobilization of enzymes. Surface activation of biochar, which can serve as an effective binding agent, has been known to facilitate

the crosslinking between amine and carboxylic groups [362]. Chitosan was also selected as a coating polymer since we can modify its surface by complexation-interpenetration (using tripolyphosphate pentosodium) to improve biocompatibility and have controlled porosity in matrices [363].

ToMO and C1,2D were immobilized into the micro and nanobiochar-chitosan matrices. Table 5.1.1 shows total protein loading and its yield, specific activity and its yield on two matrices. As can be seen, biochars-chitosan matrices gave high immobilization yield for ToMO (92.26% for micro matrix and 77.20% for nano matrix) and C1,2D (87.57% for micro matrix and 74.79% for nano matrix). Almeida et al. (2017) used lipase from *Burkholderia cepacia* immobilized on biochar, however, they did not evaluate the immobilization efficiency [364]. Lipase from psychrotolerant *Pseudomonas* sp. ISTPL3 immobilized on biochar gave an immobilization yield of 83.04% [365]. The chitosan-nanobiochar composite was used for laccase immobilization from *Trametes versicolor* with 35% effective binding efficiency [366]. Despite the satisfactory results obtained from the immobilization of enzymes on activated biochar, the immobilization of oxygenases is very limited yet.

Some studies mentioned that the physical properties of support material for enzyme immobilization can increase loading capacity as well as the surface area and then reduce the mass transfer resistance which improves the efficiency of immobilization. The result of this study showed a similar efficiency of immobilization on the micro and nano biochar-chitosan matrices and the size of the particle in microbiochar and nanobiochar did not affect the immobilization efficiency (160.5 and 145.5 µg/mL of protein loading). This may be due to the reactive functional group of chitosan [367] which gave the same efficiency for microbiochar and nanobichar in the immobilization of enzymes. The results showed that the leaching of protein from the micro and

nanobiochar-chitosan matrices was less than 10% for each matrix after 48h of incubation (Fig. E2) which augurs well for subsequent reusability of the immobilized enzymes in an aquatic medium. Another study reported immobilized lipase on biochar with 21.4% leaching after 1 h incubation at 25 °C, while it had good reusability for 3 cycles of biodiesel production [365]. Referencing the result of this study, chitosan can decrease the leaching of proteins from solid support (such as activated biochar). For example, Woo et al., (2015) showed that crosslinked chitosan coating onto mesoporous material can effectively prevent the leaching of carbonic anhydrase under shaking conditions [368].

Immobilization efficiency of biochar mixtures

Biochar was selected as economical and renewable support material for the development of immobilized and encapsulated value-added bio-products such as enzymes [173]. Mico/nano-sized biochar can provide a larger specific surface area for the co-immobilization of enzymes. Surface activation of biochar, which can serve as an effective binding agent, has been known to facilitate the crosslinking between amine and carboxylic groups [362]. Chitosan was also selected as a coating polymer since we can modify its surface by complexation-interpenetration (using tripolyphosphate pentosodium) to improve biocompatibility and have controlled porosity in matrices [363].

ToMO and C1,2D were immobilized into the micro and nanobiochar-chitosan matrices. Table 5.1.1 shows total protein loading and its yield, specific activity and its yield on two matrices. As can be seen, biochars-chitosan matrices gave high immobilization yield for ToMO (92.26% for micro matrix and 77.20% for nano matrix) and C1,2D (87.57% for micro matrix and 74.79% for nano matrix). Almeida et al. (2017) used lipase from *Burkholderia cepacia* immobilized on biochar, however, they did not evaluate the immobilization efficiency [364]. Lipase from

psychrotolerant *Pseudomonas* sp. ISTPL3 immobilized on biochar gave an immobilization yield of 83.04% [365]. The chitosan-nanobiochar composite was used for laccase immobilization from *Trametes versicolor* with 35% effective binding efficiency [369]. Despite the satisfactory results obtained from the immobilization of enzymes on activated biochar, the immobilization of oxygenases is very limited yet.

Some studies mentioned that the physical properties of support material for enzyme immobilization can increase loading capacity as well as the surface area and then reduce the mass transfer resistance which improves the efficiency of immobilization. The result of this study showed the similar efficiency of immobilization on the micro and nano biochar-chitosan matrices and the size of the particle in microbiochar and nanobiochar did not affect the immobilization efficiency (160.5 and 145.5 µg/mL of protein loading). This may be due to the reactive functional group of chitosan [367] which gave the same efficiency for microbiochar and nanobichar in the immobilization of enzymes. The results showed that the leaching of protein from the micro and nanobiochar-chitosan matrices was less than 10% for each matrix after 48h of incubation (Fig. E2) which agrees well for subsequent reusability of the immobilized enzymes in an aquatic medium. Another study reported immobilized lipase on biochar with 21.4% leaching after 1 h incubation at 25 °C, while it had good reusability for 3 cycles of biodiesel production [365]. Referencing the result of this study, chitosan can decrease the leaching of proteins from solid support (such as activated biochar). For example, Woo et al., (2015) showed that crosslinked chitosan coating onto mesoporous material can effectively prevent the leaching of carbonic anhydrase under shaking conditions [368].

Table 5.1.1. Immobilization of ToMO and C1,2D on microbiochar and nanobiochar mixture

Material used for immobilization	Total protein loaded (µg/mL)	Total protein loading yield (%)	ToMO specific activity (U/mg.protein)	ToMO immobilization yield (%)	C1,2D specific activity (U/mg.protein)	C1,2D immobilization yield (%)	Leached ToMO (%)	Leached C1,2D (%)
Micro-biochar + chitosan	160.5± 0.87	12.96	11.9± 0.1	92.26	20.01± 0.5	87.57	2.1	2.4
Nano-biochar + chitosan	145.5± 1.03	16.59	9.28± 0.02	77.20	17.09± 0.32	74.79	1.5	2.2

Kinetics

As mentioned in the method section, toluene and catechol degradation rate from free and immobilized ToMO and C1,2D was used respectively for the detection of Michaelis-Menten model parameters (Table 5.1.2). It was reported that ToMO exhibits specificity to toluene as substrate and catalyzed toluene oxidation to catechol as its metabolite [370]. In addition, Kalogeris et al., (2006) reported that C1,2D showed high specificity for catechol and subsequently cleave the aromatic rings. They also mentioned that both free and immobilized forms of the enzyme showed identical substrate specificity patterns toward catechol as their substrate [371]. In the case of the free enzyme and particle-immobilized enzyme system's kinetic constants, the Lineweaver-Burk (LB) graphical method was applied from data obtained at two different substrate concentrations of 0.1 and 0.5 mM. As can be seen in Table 5.1.2., since the K_m for free and immobilized enzymes are the same, there is no diffusion limitation for nanoparticles. Using Eq.(6) the Thiele modulus can be calculated for the nanoporous glass with a 30 nm pore diameter. The obtained modulus value was approximate 5.7×10^{-6}corresponding to an effective factor of $>$ 0.99. This value suggests according to the effectiveness factor versus the Thiele modulus showing that the system was reaction limited. The V_{max} was slightly decreased after immobilization on both matrices (0.46 and 0.45). The K_m of immobilized enzymes were 1.43 and 1.42 which was slightly lower than the value of free enzyme (1.51) indicating the enhanced affinity of ToMO for toluene. These results

showed that the loss/enhancement of enzyme activity was almost negligible after immobilization. This phenomenon is attributed to the denaturation and/or the strong association of enzymes with its support [13]. It is noticeable that the V_{max} for Toluene was approximately 20 times more than the V_{max} for catechol. It could be explained the phenomenon that the initial oxidation steps required greater activation energy compare to the later steps of biodegradation since the stability of the substrate decreases as the biodegradation proceed [13]. The overall kinetics efficiency (known as the enzyme-specific constants) was evaluated using the catalytic efficiency of ToMO and C1,2D (k_{cat}/K_m). Table 5.1.2 showed that the catalytic efficiency for immobilized enzymes on both matrices was almost similar to free enzymes. These results indicated that the loss of enzyme activity was negligible during immobilization.

Table 5.1.2. The Michaelis-Menten parameters for ToMo and C1,2D.

		V_{max} (mM/min)	K_m(mM)	K_{cat} (min^{-1})	∅	Catalytic Efficiency (K_{cat}/K_m, min^{-1} mM^{-1})
Toluene (ToMO)	**Free enzyme**	0.48	1.51	0.608	-	0.40
	Micro-biochar Matrix	0.46	1.43	0.61	7.1×10^{-3}	0.42
	Nano-biochar Matrix	0.45	1.42	0.59	5.7×10^{-6}	0.41
Catechol (C1,2 D)	**Free enzyme**	20.77	3.92	1.73		0.44
	Micro-biochar Matrix	20.65	3.91	1.71	-	0.43
	Nano-biochar Matrix	20.43	3.89	1.74	-	0.44

Characterization of biochar mixtures with enzymes

FTIR measures the quantity of infrared radiation absorbed versus frequency by atoms at a different frequency. When a sample is subjected to infrared radiation (IR), the difference of charge between carbon atoms in the sample induces the formation of an electric dipole and the appearance of these

electric dipoles generates detectable signals [372]. In this study, biochar-chitosan matrices with enzymes and without enzymes were subjected to FTIR spectra to compare them and evaluate the characteristics of the immobilized enzymes.

Fig. 5.1.2 presents the FTIR spectra of immobilized enzymes on micro and nano biochar-chitosan matrices. Three main peaks were detected in the spectra of the immobilized enzymes including: 1) a strong band at 3264 cm^{-1} was assigned to NH_2 and OH vibrations; 2) a peak at 1635 cm^{-1} corresponding to CONH linkage, and 3) a band at 700-900cm^{-1} was attributed to C–H bending vibration.

The bands at 3264 cm^{-1} were corresponding to the vibration of N-H groups from the chitosan [373]. The vibration peak at 1647-1636 cm^{-1}, was increased with the C=N group formation as a result of the glutaraldehyde cross-linking reaction [348]. Glutaraldehyde as a bi-functional cross-linker is capable of crosslinking the support and enzyme. After the reaction of biochar mixture with enzymes, all three bands and peaks showed higher intensity which confirmed the immobilization of enzymes on the surface of biochar matrices. Protein-derived bands at around 3000 and 3400 cm^{-1} could be seen. The microbiochar and nanobiochar matrices had similar spectra and they had a single spectrum in Fig. 5.1.2.

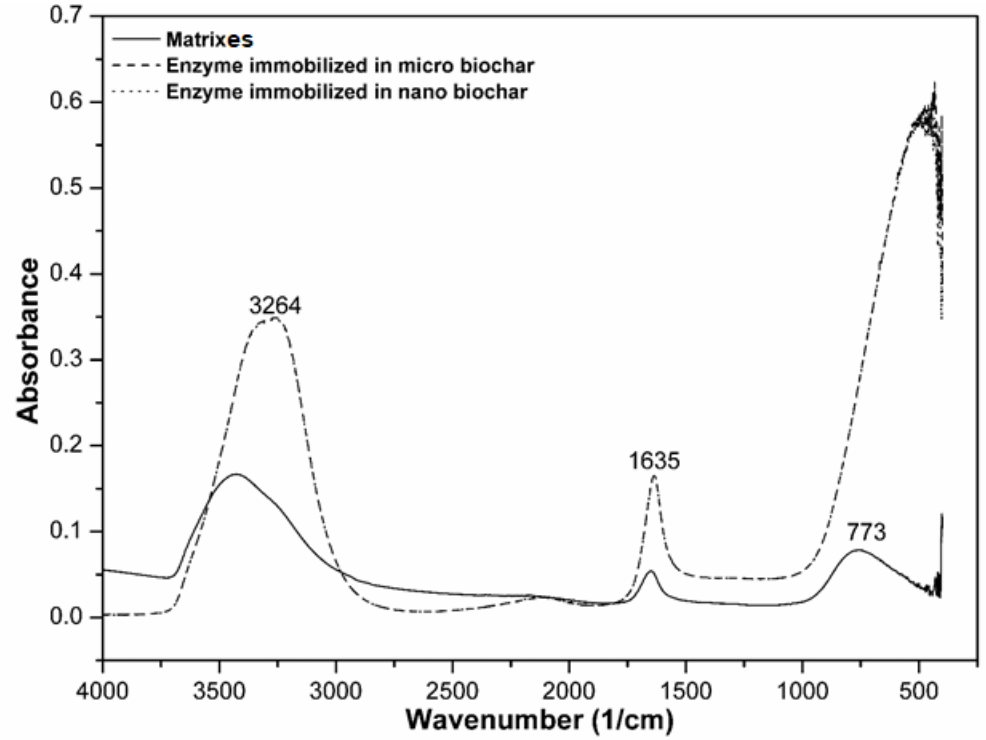

Fig. 5.1.2. FTIR spectra of biochar-chitosan matrices. four spectra can be observed; two matrices: Microbiochar-chitosan matrix and nanobiochar-chitosan matrix, two spectra from immobilized enzyme into two different matrices. Since the matrices have similar spectra they can be observed as a single spectrum and also after immobilization of enzyme, they had similar spectra

Based on this result and the previous studies [362], a schematic structure of the immobilized enzyme on the biochar-chitosan matrix was proposed in Fig. 5.1.3. The enzymes were immobilized on activated biochar through physical adsorption and covalent bonding because of the acid treatment of biochar. Carboxylic groups on the surface of biochar can react with amino groups of the enzymes and aldehyde groups on chitosan react with amino groups in ToMO and C1,2D then formed imino group (CH=N). Chitosan has a linear structure of glucosamine and N-acetylglucosamine linked in a β-1,4 manner. Free amine groups are chemically active groups in the chitosan structure located in the C2 position of the glucose residue in the polysaccharide chain

and the hydroxyl groups. These active groups can be involved in hydrogen or electrostatic bonding [374].

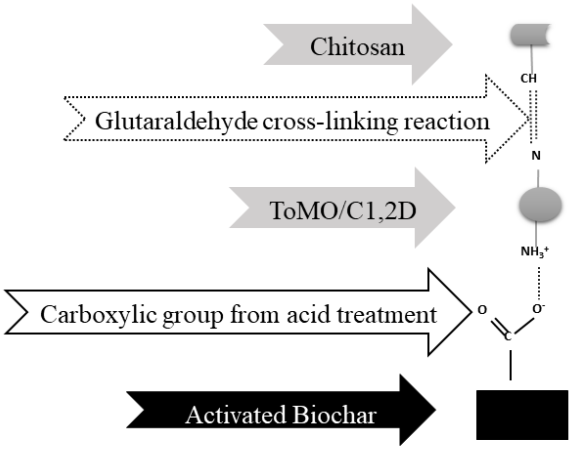

Fig. 5.1.3. Schematic of immobilized enzymes in the biochar-chitosan matrix. ToMO, Toluene/o-Xylene Monooxygenase; C1,2D, Catechol 1,2-dioxygenase.

Storage stability

Oxygenases catalyze the initial reactions of aerobic catabolic pathways for aromatic compounds by incorporating either a single oxygen atom (monooxygenases) or two atoms of molecular oxygen (dioxygenases). For monooxygenases that require the NAD(P)H cofactor (nicotinamide adenine dinucleotide cofactors), the reaction is separated into two steps: (1) the oxidation of NAD(P)H to generate two reducing equivalents and; (2) the hydroxylation of substrates. Some monooxygenases are flavoprotein enzymes and the two reactions carry out in a single polypeptide chain. However, multicomponent monooxygenases catalyze NAD(P)H oxidation and the hydroxylation reaction by separate polypeptides [375]. Generally, the major challenge in the practical and commercial application of enzymes are lack of stability under storage conditions such as ambient temperature (293–298 K) or at refrigerator temperature (276-278 K)

[343], [376]. Unique three-dimensional structures of enzymes are essential for their activities. Enzymes gradually lose their activity over the time due to the conformational and structural changes (denaturation of proteins) or their cofactors. Immobilization of enzymes on solid supports such as biochars can decrease this effect by increasing the structural rigidity of the protein [343].

On the other hand, ToMO consists of two polypeptide subunits; one of these subunits is a hydroxylase and membrane-bound component, and its activity depends on ferrous ions and phospholipids [377]. Suzuki et al., (1991) determined the primary structure (amino acids sequence) of xylene monooxygenase from *Pseudomonas putida* that consists of two different subunits encoded by the TOL plasmid [378]. Multimeric enzymes have limited stability outside the cell, probably due to the dissociation of subunits resulting in the loss of activity [351].

Also, C1,2D is a non-heme iron oxidative enzyme that catalyzes aromatic ring cleavage with the incorporation of ferrous ions in its active site and molecular oxygen. Tsai & Li (2007) purified C1,2D from a phenol degrading *Candida albicans* TL3 and analyzed the amino acid sequence and metal content of this enzyme. They reported that C1,2D is a homodimer and each subunit contained one iron ion [379]. The ferrous ion at the active site of ToMO and C1,2D makes these enzymes more sensitive to autooxidation and oxidation than other enzymes and, consequently, to deactivation [343].

Moreover, the active sites of psychrophilic enzymes are less stable than that of the mesophilic enzymes to have less activation energy at low temperatures. The lower enthalpy of cold-active enzymes at low temperature corresponds to the faster the rate. Our previous study showed that the reduced enthalpy in the cold-active can explain the main adaptive mechanism to low temperatures [212]. Therefore, the inactivation rate of psychrophilic enzymes is faster than their mesophilic or thermophilic homologs [380].

The kind of solid support used for immobilization is a determining factor for the protective effect of the immobilization method. To the best of the authors' knowledge, there is no report on the protective effect of biochar for immobilization of cold-active ToMO and C1,2D.

The stability of ToMO and C1,2 D are shown in Fig. 5.1.4 at room temperature (20 ± 2 ºC) and 4 ± 1ºC for 30 days, which are typical storage temperatures. Fig. 5.1.4 (A and C) showed that immobilized enzymes onto biochar-chitosan matrices have maintained more than 50% of their residual activity at 4 ± 1 ºC while free enzymes had less than 10% of their activity after 30 days. The results from low-temperature storage are similar to the results observed with the room temperature storage effect. However, the residual activity at room temperature was generally less than 4 ºC, which may be due to more changes in the structure and conformation of enzymes at higher temperatures. The improved stability of immobilized enzymes can be attributed to the increased resistance of enzymes to the conformational changes as well as lower structural flexibility of the ToMO and C1,2D in the immobilized form [381]. However, the immobilization of enzymes by multipoint attachments provided a solution for the low stability of enzymes, the multipoint attachment between two complex structures is very complicated and may result in the de-activation of enzymes after immobilization. It is necessary to obtain a very intensive and non-distortive binding in the area of contact between the enzymes and the support. This critical point was found to be the correct choice of the immobilization system [382]. Notomista et al., (2009) showed that the binding energy between the enzyme and substrate indicates the stability of Toluene/*o*-xylene Monooxygenase from *Pseudomonas* sp. strain OX1. Destabilization of xylene monooxygenase depends on the loss of weak forces such as van der Waals interactions between the C-H groups at its active site [383]. Also, the results obtained from micro biochar-chitosan matrix were similar to nano biochar-chitosan matrix because the nature of the support material and

mechanism of enzyme binding was the same. Lonappan et al. compared pig manure, pinewood, and almond shell micro-biochars for immobilization of laccase using covalent binding, their results showed that different biochars showed various laccase residual activity and pinewood showed better storage stability compared to other biochars [319]. In this study, pinewood biochar was used for the first time as carriers of ToMO and C1,2 D. Wojcieszyńska et al. immobilized catechol 2,3-dioxygenase on alginate hydrogel for improving functional stability (50.63% of initial activity after 35 days). The improvement was contributed to increasing the structural rigidity of the enzyme [384]. The lower stability reported in this study might be the fact of more flexibility of cold-active enzyme structures. One of the main challenges with cold-active enzymes is their inherent instability, due to greater flexibility and lower stability at or near the active site compared to their mesophilic counterparts [385].

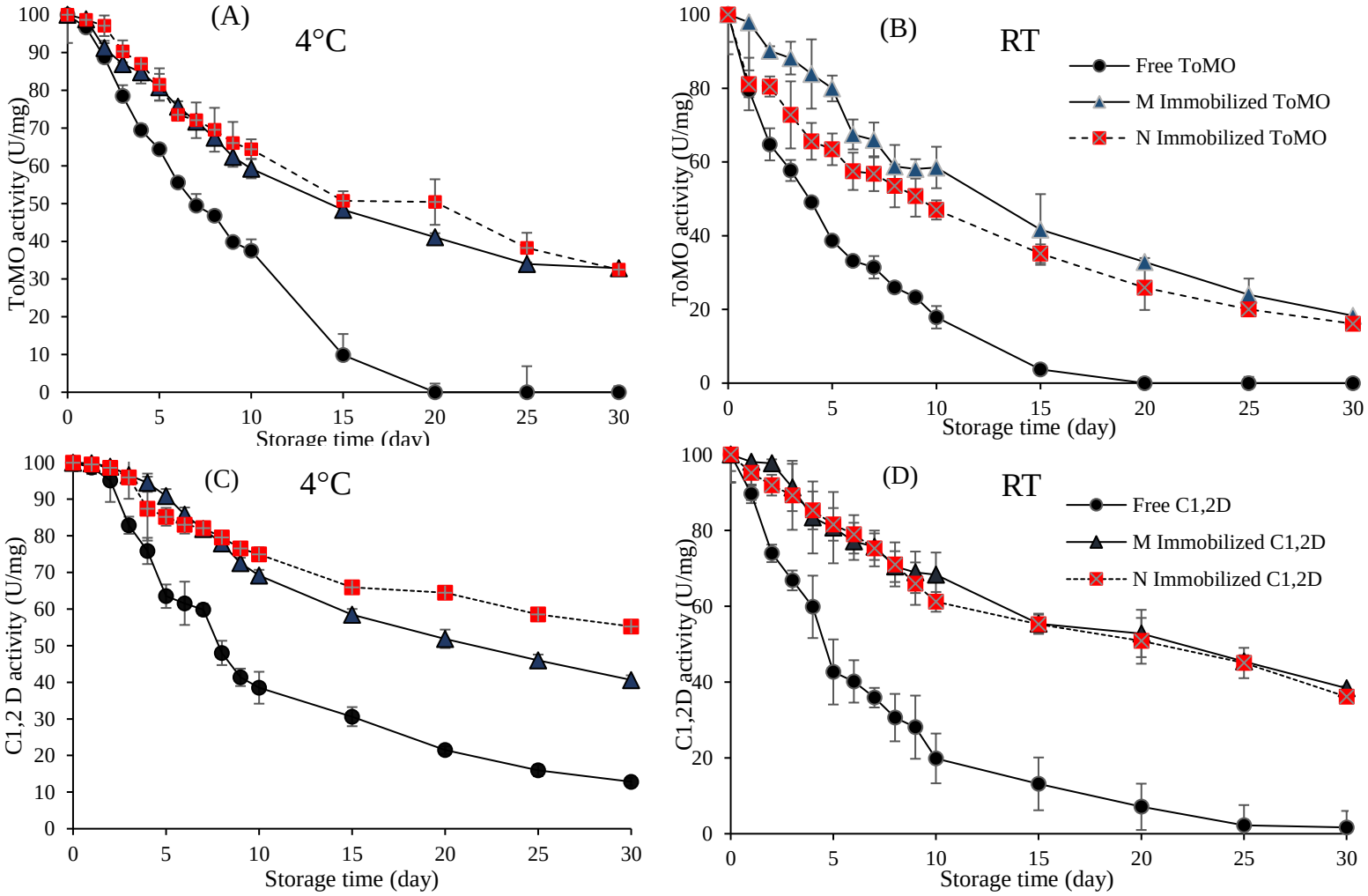

Fig. 5.1.4. Storage effects on A) the activity of ToMO at 4 ºC ± 1, B) the activity of ToMO at room temperature (RT) 20 ºC ± 2, C) the activity of C1,2D at 4 ºC ± 1 and D) the activity of C1,2D at room temperature (RT) 20 ºC ± 2. M immobilized, enzyme immobilized on microbiochar matrix; N immobilized, enzyme immobilized on nanobiochar matrix.

Application of immobilized enzymes for BTEX biodegradation test

Contaminated groundwater sample

Fig. 5.1.5 shows the concentration of BTEX after 24h of incubation with free and immobilized enzymes in contaminated groundwater samples (with 200 mg/L of each BTEX compound) at 10 ±1°C. The degradation tests clearly showed that immobilized enzymes had biodegradation ability for all BTEX compounds (more than 85% of degradation for all the compounds) (Fig. 5.1.5) while the free enzyme had less than 50% BTEX degradation. Reference controls with original groundwater were almost similar to abiotic control (referred to as autoclaved) due to low microbial density in groundwater samples and the results of abiotic controls were presented in Fig. 5.1.5. With immobilized enzymes, near 100% biodegradation was achieved after 48h (Fig. E3) while with the free enzyme, about 20% of BTEX compounds were detected in the media. Xin et al. (2013) reported the biodegradation of high concentration BTEX-contaminated groundwater (the total concentration of BTEX was about 100 mg/L; 25 mg/l for each compound) at 25˚C using immobilized *Pseudomonas* sp. YATO411 and *Mycobacterium* sp. CHXY119 beads. In batch tests, they reported 100% biodegradation ethylbenzene, *p*-xylene, and toluene after 120, 210, and 400h respectively. However, only 5% of benzene was degraded after 400h [386].

The observed different biodegradation efficiencies using whole microbial cells can be due to two key processes: 1) adaptation and; 2) toxicity of by-products. In general, petroleum hydrocarbon-degrading bacteria show a lag growth phase in contact with the contaminants. During this lag phase, the involved enzymes in the degradation pathway are produced to convert and transport the contaminant through the cell membrane. The lag phase differs greatly based on adaptation mechanisms of bacterial cells and toxicity of by-products during biodegradation. According to the chemical structure of petroleum aromatic hydrocarbons, all of them are relatively resistant to

degradation due to the stability of large negative resonance energy resulting from the stability of the pi-electron cloud. However, using enzymes rather than the whole microbial cells can address these two challenges, because there is no lag phase and degradation starts as soon as the pollutants came in contact with the enzymes. In addition, the enzymes transform the substrate on a minute timescale and can specifically catalyze a reaction without producing any toxic by-products [13].

The substrate interaction can result in a difference in biodegradation of each contaminant by whole bacterial cells. For example, p-xylene can be co-metabolized in presence of other BTE compounds. During the growth phase in the co-metabolic system., the microorganisms consume growth-associated substrates and produce enzymes (the same pathway of biodegradation) that can fortuitously transform the non-growth substrate. Toluene/*o*-Xylene Monooxygenase (ToMO) has a broad substrate range such as BTEX, and catechol 1,2-dioxygenase (C1,2D) can cleave the ring of catechol as a product from ToMO. However, the enzymes responsible for the degradation of BTEX can have specificity and affinity to each substrate that can allow the study of biodegradation in quaternary mixtures. The efficiency of a substrate is determined by its Km value, the lower this value the better the substrate. Our primary result for Km difference for the BTEXs compound was not significant. These results were consistent with substrate concentration using GC/MS equipped headspace sampler. Usually, the most efficient substrate may be taken in activity assays, in this case, toluene was considered an efficient substrate for ToMO and catechol for C1,2D.

Although nano-biochar can provide a greater surface area than micro-biochar, the biodegradation results from nano biochar-chitosan were similar micro biochar-chitosan. The particle size of the support establishes the total surface area and affects the capacity for binding of enzymes [346]. However, as mentioned earlier, the difference in immobilization efficiency for micro and nano-sized matrices was not significant which resulted in the equivalent degradation efficiency.

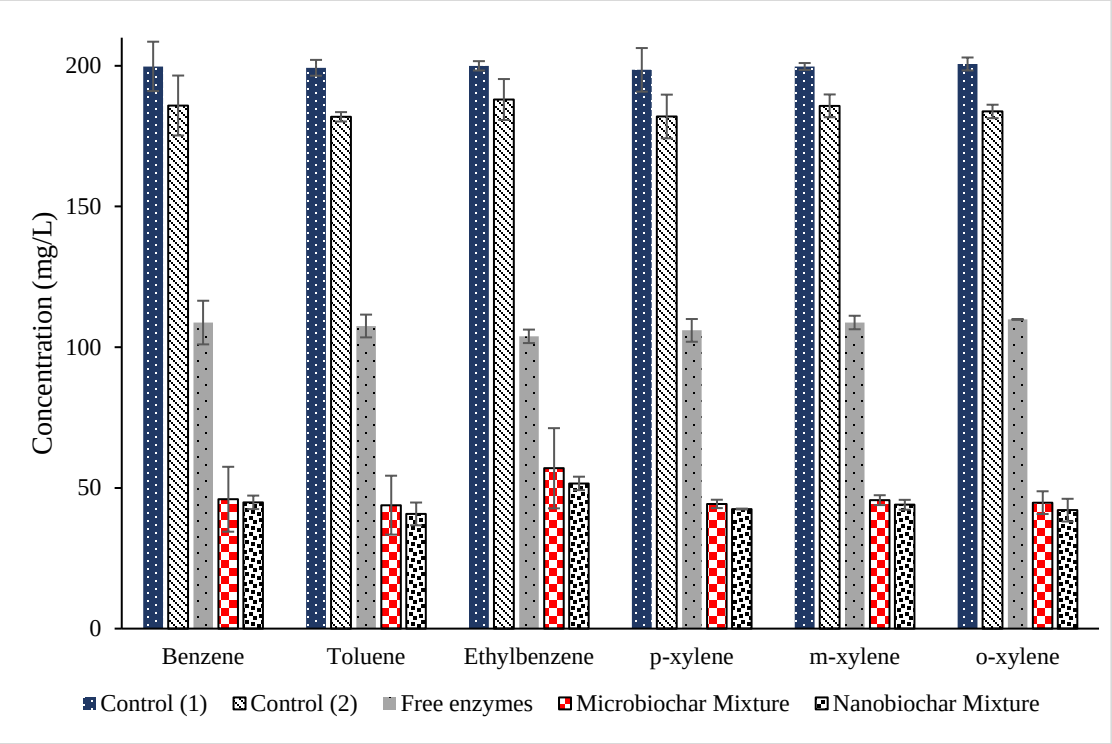

Fig. 5.1.5. Biodegradation of BTEX by free and immobilized enzymes on micro and nano biochar-chitosan matrices, control (1) samples contained groundwater and BTEX without the addition of any enzymes and matrices, the control (2) samples contained groundwater and BTEX with deactivated enzymes immobilized on biochar-chitosan matrices. Capital letters (A-F) indicated the significant difference between the control samples and test samples. Small letters (a-f) indicated the significant difference between the free enzyme sample and immobilized enzymes. The difference between control samples (1 and 2) was not significant and the control (2) sample was used as a control group for comparison with test groups in statistical tests. For Microbiochar and Nanobiochar that were not statistically significant, the letters were not shown. The significance level was 0.05.

Contaminated soil sample

Considering the fact of soil heterogeneity, four sets of experiments and five repetitions were performed for soil tests. Fig. 5.1.6 illustrates the concentration of BTEX in contaminated soil after 2 and 4 weeks of incubation at 10 ±1°C.

In the experiment set with the free enzymes, the decrease of degradation rate between 2 weeks and 4 weeks may be explained by less activity of free enzymes as a result of their less stability in comparison with immobilized form. Practically, the first weeks of enzymatic/non-enzymatic

treatments are important because can determine the efficiency of the method, efforts to enhance the enzyme activity (stability) should be directed to this period [387].

Results presented in Fig. 5.1.6 have shown that the best degradation percentages for all compounds were detected in immobilized enzymes on the nano biochar-chitosan matrix treatment. The reason for the more efficiency of the nano-sized matrix can be a better distribution of nanoparticles than microparticles and more contact between immobilized enzymes and their substrates (BTEX). The biodegradation of BTEX in sterile and non-sterile soil showed less than 2% (Fig. 5.1.6). It is reported that abiotic conditions lead to reduced bioavailability of petroleum hydrocarbons as a limiting factor for biodegradation during the period of treatment [387].

The lower performance of enzymes in the soil as compared to water samples can be attributed to the presence of organic and inorganic soil constituents as enzyme inhibitors. As shown in Fig. 5.1.6, a more inhibitory effect on the activity of free enzymes was observed. Probably, macro/nano biochar-chitosan matrices surrounding the immobilized enzyme protected it against organic and inorganic soil constituents. Generally, the immobilization of enzymes on support material may cause changes in the structural conformation of proteins. These conformational structure changes may partially cover the hydrophobic channels of the enzyme by which the substrate penetrates the active site. These changes result in the decrease of the local concentration of the enzyme inhibitors (organic or inorganic soil constituents). Consequently, immobilization increases the resistance of the enzyme to the inhibitory and toxicity effect of compounds [343].

It was hypothesized that some amount of BTEX was adsorbed to the nano/micro biochar matrices and protein structure of enzymes that may not have undergone enzymatic biodegradation. Our results showed that in both samples (groundwater and soil), the adsorption was less than 20% and

15% after 24h and 4 weeks of incubation for water and soil systems, respectively. However, the contribution of biodegradation was more than 70-90% in both matrices.

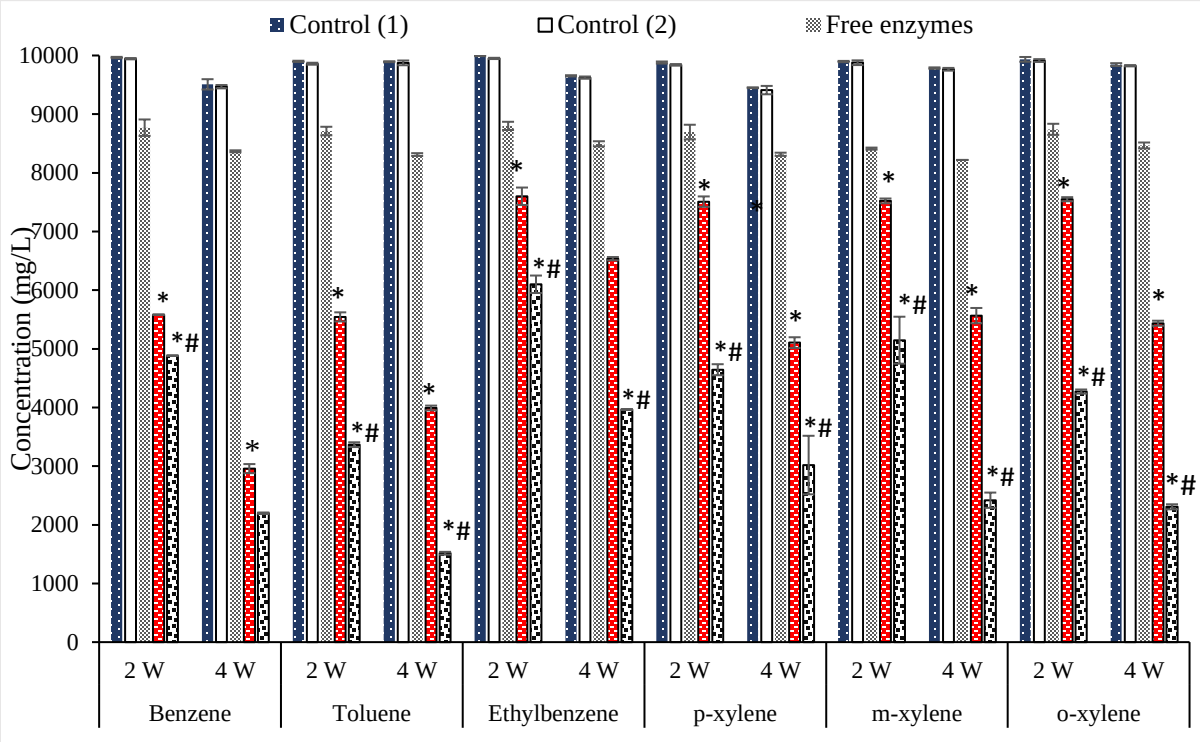

Fig. 5.1.6. Biodegradation of BTEX by immobilized enzymes on micro and nano-biochar matrices in contaminated soil incubated for 2 weeks (2W) and 4 weeks (4W). Control 1, abiotic control (sterile soil) was used to determine abiotic losses. Control 2, non-sterile control contained soil and deactivated enzymes immobilized on biochar-chitosan matrices. *, indicated the significant difference between free enzyme samples and immobilized enzyme samples. #, indicated the significant difference between microbiochar enzyme sample and nanobiochar enzymes. For those there was no statistically significant difference between samples, the symbols were not shown. The significance level was 0.05.

Operational stability (reusability) of immobilized ToMO and C1,2 D

The operational reusability of immobilized enzymes was investigated for 5 cycles in groundwater samples, due to the solid nature of soil with different particle sizes, separation of immobilized enzymes by available methods (such as centrifugation, filtration, etc.) was not possible for soil context. Besides that, the sedimentation of nano-biochar matrix was not effective by centrifugation

(at 16000×g for 10min) due to the small size of the matrix, and complete separation of suspended nanoparticles from aqueous medium may not practical [388]. Hence, the operational reusability of immobilized enzymes was carried out only for micro biochar-chitosan matrix in the groundwater sample. As shown in Fig. 5.1.7, ToMO immobilized on micro biochar-chitosan matrix retained 53% and 15% activity and C1,2D also retained 65% and 22% activity after 3 and 5 cycles of reusability respectively. Although free ToMO is very well described (Bertoni et al., 1998; Sazinsky et al., 2004) there is rather little information about the immobilized ToMO. However, several studies mentioned higher reusability for immobilized catechol 1,2-dioxygenase. For instance, immobilized C1,2D from *Pseudomonas putida* on alginate beads was mentioned to retain more than 70% of its catalytic activity over 5 cycles [389]. One reason for the lower reusability of C1,2D in this study is the fact of greater flexibility at or near the active site of psychrophilic enzymes that makes them more unstable compared to their mesophilic counterparts [385].

In addition, ToMO and C1,2D have been identified as one the most complex and multicomponent monooxygenase for hydroxylation of aromatic compounds such as BTEX, phenols, etc [390]. Immobilization of co-factors such as NAD, NADH can also increase the stability of such enzymes. For example, lactate dehydrogenase was stabilized by its cofactor NAD, NADH against thermal inactivation conditions [391]. However, such co-factors (NADPH/NADH) are expensive and the high cost of enzymes has restricted their industrial use for environmental purposes. NADH/NADPH regeneration systems may enhance the stability of petroleum-degrading enzyme cocktails more cost-effectively. Ji et al. proposed formate dehydrogenase from *Candida boidinii* for NADH regeneration system. They reported a higher degradation rate of oil in high concentration and enhanced operational stability of the enzyme cocktail [392]. However, Bes et al., (1995) concluded that immobilization of cofactor regenerating enzymes, Ferredoxin-$NADP^+$

reductase, does not appear to be strictly necessary for improving operational stabilization for NADP-dependent redox enzymes [382]. Thus, more studies are needed for the co-immobilization of nicotinamide adenine dinucleotide co-factors or NADH/NADPH regeneration systems that may retain the activity after repeated use [393].

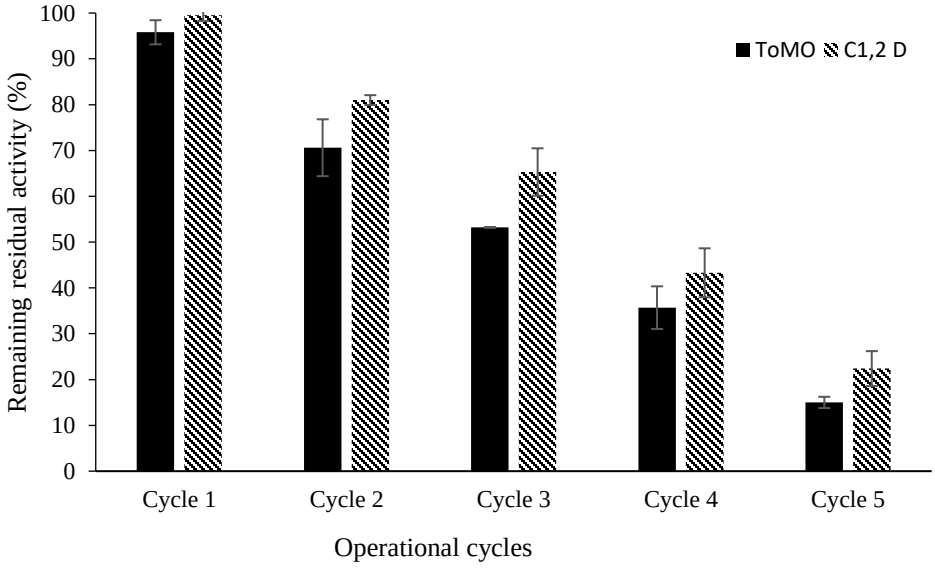

Fig. 5.1.7. Operational stability of Toluene/o-xylene Monooxygenase (ToMO) and catechol 1, 2-dioxygenase (C1,2D) enzymes immobilized micro biochar-chitosan matrix.

Comparison micro and nano biochar matrices

To compare the immobilized enzyme from the application point of view, the obtained results from this study showed that enzymes immobilized on nano biochar-chitosan matrix can effectively be used in contaminated soil with more than 80% BTEX biodegradation. While nanobiochar cannot be effective for usability in the soil system and groundwater system, a study reported that the immobilized catechol dioxygenase onto nanosponges showed high reusability for the production of muconic acid in the small-scale bioreactor even after 50 cycles without enzyme detachment from the carrier [394]. Although the nano-sized matrix could provide more surface area, the obtained results in this study showed the same storage stability as micro-sized matrix. Also, the biodegradation efficiency was the same in the groundwater sample. Considering the high cost of

production of nano-size particles, their limited reusability in some contexts and less convenient usage of the enzyme-support complex in the reaction, the nano biochar matrix could be selected in specific conditions or bioreactors. The results of this study showed that micro biochar-chitosan matrix could be applied as a desirable carrier in terms of reusability and its successful application for co-immobilization of multienzymes for biodegradation of BTEX in low temperatures.

5.1.4. Conclusions

Psychrophilic *Pseudomonas* S2TR-14 was isolated from a contaminated cold-climate site. *Pseudomonas* S2TR-14 produced a high amount of cold-active enzymes (12 U/mg of ToMO and 22 U/mg of C1,2D) in the medium composed of crustacean waste and 0.5% v/v of used motor oil. Both nano and micro biochars-chitosan matrices gave high binding capacity for co-immobilization of ToMO (92.26 and 77.20%) and C1,2D (87.57 and 74.79%). The leaching of protein from the micro and nanobiochar-chitosan matrices was negligible (less than 10% after 48h of incubation). More than 85% and 70% of biodegradation of BTEX were observed using the immobilized enzymes in groundwater and soil samples, respectively. Immobilization of cold-active ToMO and C1,2D enhanced their storage stability, more than 50% of its residual activity at 4 ± 1 ºC, and operational stability after 3 and 5 cycles of reusability.

BRIDGE-3

Selected enzymes (xylene monooxygenase: catechol dioxygenase) were immobilized into micro/nano biochar-chitosan matrices and used for BTEX biodegradation. Both nano and micro biochars-chitosan matrices gave high binding capacity for co-immobilization of selected cold-active enzymes. However, separation and reuse of immobilized enzymes were not possible for soil context due to the solid nature of soil with different particle sizes. Also, the storage stability of the enzymes could be improved for these enzymes. *The next step was to evaluate the immobilization of selected enzymes onto magnetic carriers for the simple magnetic separation of immobilized enzymes from soil matrix.* Then, pH tolerance, temperature stability, storage stability, and more importantly, reusability were tested using free form and immobilized enzymes.

PART 2

5.2. Immobilized Cold-Active Enzymes onto Magnetic Chitosan Microparticles as a Highly Stable and Reusable Carrier for p-xylene Biodegradation in Soil

Saba Miri[1,2], Anupriya Ravula[3], Shiva Akhtarian[4], Satinder Kaur Brar[1, 2*], Richard Martel[2], Tarek Rouissi[2]

1. Department of Civil Engineering, Lassonde School of Engineering, York University, North York, Toronto, Ontario M3J 1P3, Canada
2. INRS-ETE, Université du Québec, 490, Rue de la Couronne, Québec G1K 9A9, Canada
3. Department of Biology, Life Science, York University, North York, Toronto, Ontario Canada
4. Department of Mechanical Engineering, Lassonde School of Engineering, York University, North York, Toronto, Ontario M3J 1P3, Canada

(*Corresponding author, E-mail E-mail: satinder.brar@lassonde.yorku.ca; satinder.brar@ete.inrs.ca)

Submitted to Process Biochemistry

Abstract

Stability and reusability properties are the two most important factors that determine an enzyme's application in industry. To this end, cold-active xylene monooxygenase (XMO) and catechol 1,2-dioxygenase (C1,2D) from a psychrophile were immobilized on magnetic chitosan microparticles using glutaraldehyde as a linker agent. The immobilization process was optimized based on four variables, such as magnetic particle, chitosan, glutaraldehyde, and enzyme concentrations. The immobilized enzymes were characterized by Fourier Transform Infrared Spectroscopy (FTIR) and Scanning Electron Microscope (SEM). The immobilized enzymes showed improved pH tolerance ranging from 4.0 to 9.0, better temperature stability ranging from 5 to 50, higher storage stability (∼70% activity after 30 days of storage), and more importantly, reusability (∼40% activity after 10 repetitive cycles of usage) compared to their free form. Also, the immobilization of enzymes increased the effectiveness of the enzymatic treatment of p-xylene in soil (initial concentration of 10,000 mg/kg). As a result of the superior catalytic properties of immobilized XMO and C1,2D, they offer great potential for in situ or ex situ bioremediation of pollutants in soil or water.

Keywords: Cold active, Immobilization, Magnetic, chitosan, Composite

Graphical Abstract

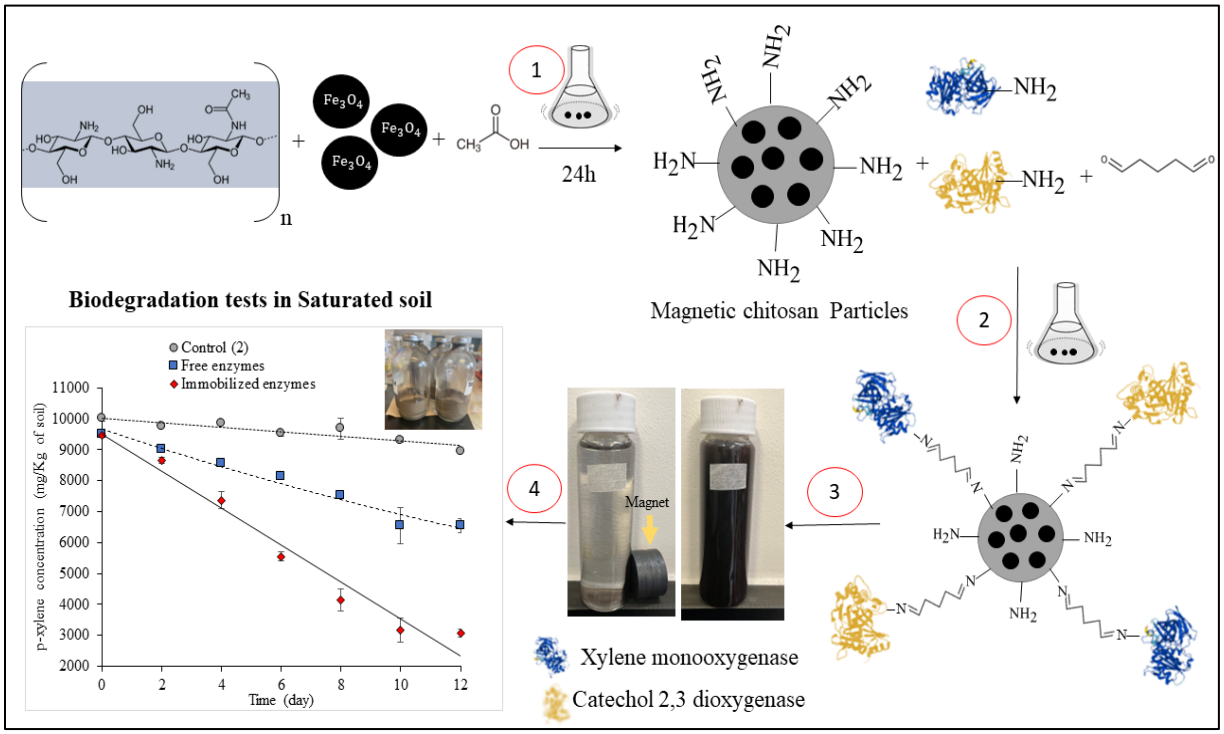

5.2.1. Introduction

Living systems rely upon enzymes to catalyze a variety of chemical reactions. Due to enzymes' specific properties, such as their chemo-, stereo-, and regioselectivity, they are generally preferred over chemicals as catalysts. Hence, using enzymes has recently received increasing attention for pollutant removal as an environment-friendly technology. However, enzymes are not widely used for remediation purposes due to their high production costs. A useful tool for reducing costs is the immobilization of enzymes as it enables efficient recovery, reuse, and recycling, as well as increased stability under harsh operational conditions such as high/low pH and temperature. An important challenge of using immobilized enzymes is the identification of new matrix materials with appropriate structural characteristics, such as morphology and surface functionalities, and compositions, as well as the understanding of enzyme–matrix interactions for the improvement of catalysis [395], [396].

Many different carriers can be used to immobilize enzymes [397]. Among all of them, chitosan (known as poly-β (1 → 4)-2-amino-2-deoxy-d-glucose) is a linear polysaccharide that has been often used for the immobilization of enzymes [398]. The chitosan polymer has many interesting properties, including biocompatibility, availability of reactive functional groups for chemical modifications, hydrophilicity, mechanical stability, renewability, and ease of preparation in multiple geometrical configurations suitable for various biodegradation processes. A further benefit of chitosan is its low cost, allowing it to be used to prepare low-cost carriers for large-scale applications. Enzymes can be immobilized by cross-linking chitosan and activation by glutaraldehyde [399]. In addition, magnetic carriers can be used for the simple magnetic separation of immobilized enzymes. Magnetic chitosan carriers have already been prepared and used for immobilizing several enzymes as depicted in Table 5.2.1. In many cases, magnetic chitosan

particles are used for immobilization of mesophilic enzymes for various applications (Table 5.2.1.), but are not used for cold-active enzymes and biodegradation of petroleum hydrocarbons.

Table 5.2.1. Magnetic chitosan-based carriers for enzyme immobilization, their applications and reusability

Enzyme	Carrier	Application	Reusability	Ref.
Lipase	Magnetic chitosan beads	Synthesis of flavor esters	5 cycles with more than 70% of its initial activity	[400]
Glucose oxidase and catalase	Magnetic chitosan microspheres	Production of Sodium gluconate from glucose	10 with more than 60% of their remaining activity	[401]
Lipase	*β*-cyclodextrin grafted and aminopropyl-functionalized chitosan/Fe_3O_4 magnetic nanocomposites	Synthesis of fruity flavor esters	15 cycles with a slight decrease (15%) in the relative activity	[402]
Laccase	Magnetic chitosan nanoparticles modified with amino-functionalized ionic liquid containing ABTS	Removal of 2,4-dichlorophenol, bisphenol A, indole and anthracene	6 cycles with a removal efficiency of 93.2 % for 2,4-dichlorophenol.	[403]
Lactase (β-d-galactosidase)	Magnetic chitosan microsphere	Biomedical applications	10 recycles with more than 65 % of its initial activity	[404]
α-amylase	Chitosan-magnetite composite	Food, fermentation, detergent applications, textile and paper industry	10 cycles with 45–55% of its initial activity	[405]
Porcine pancreatic lipase	Magnetic chitosan nanoparticles modified with imidazole-based functional ionic liquid	ND	10 recycles with more than 84.6% of its initial activity	[406]
Laccase	Chitosan beads magnetized with Fe_3O_4 NPs	Removal of Evans blue, Direct blue 15, Reactive black 5 and Acid red 37 azo dyes	10 cycles with 47% of remaining activity	[407]
Xylanase	Magnetic chitosan	Production of xylooligosaccharides with food and pharmaceutical applications	3 cycles retaining 50% of its initial activity	[408]
Cellulase	Magnetic Chitosan Nanoparticles	Glucose production	10 cycles with more than 80% of its initial activity	[409]
Glucoamylase	Magnetic chitosan microspheres	Production of glucose from starch	10 cycles with 45–68.4% of its initial activity	[410]
Lipase and β-galactosidase	Magnetic chitosan microparticles	ND	8 cycles with more than 90% of its initial activity	[399]
Pullulanase	Magnetic chitosan beads	Improves the saccharification of starch to produce glucose	10 cycles retaining 64.8% residual activity	[411]

Xylene monooxygenase (XMO) and catechol 1,2-dioxygenase (C1,2D) are key enzymes involved in the oxidation of aromatic hydrocarbon rings and reported in most of the biodegradation pathways of mono-aromatic hydrocarbons. For instance, Wang et al., (2021) reported that *Pseudomonas stutzeri* can degrade toluene and benzene by expressing toluene/*o*-xylene monooxygenase [412]. Wongbunmak et al., (2020) suggested that XMO played important roles in toluene and *m*-xylene biodegradation by *Bacillus amyloliquefaciens* subsp. *plantarum* strain W1 [413]. Moreover, XMO from *P. putida* mt-2, could catalyze only m-xylene and p-xylene [414]. Our previous research also showed that cold-active *Pseudomonas* strains produced cold-active xylene monooxygenase and catechol 2,3 dioxygenase that can degrade p-xylene under low temperatures (<15ºC). Cold-active enzymes have the potential to provide greater value in terms of sustainable immobilization and production and may be preferred as a result of their higher catalytic activity in comparison to their mesophilic counterparts for biodegradation of contaminants in cold environments. Our previous finding also showed that the inherent instability of these enzymes is one of the major challenges in the practical and commercial application of these enzymes [16], [415].

The current study hence focused on evaluating the stability and reusability of immobilized XMO and C1,2D for biodegradation of p-xylene in highly contaminated soil. Immobilization of cold-active enzymes was optimized for maximum immobilization yield. Later, the kinetic parameters of enzymes were determined before and after immobilization. To the best of our knowledge, no reports have systematically evaluated the use of magnetic chitosan carriers for immobilization of cold-active XMO and C1,2D and how these immobilized enzymes can be applied to the degradation of petroleum hydrocarbons in soil.

5.2.2. Materials and Methods

Bacterial strains and enzyme preparation

Isolation and characterization of psychrophilic *Pseudomonas* S2TR-14 were described in our previous study (Miri et al., 2021). Briefly, the selected strain was cultured in tryptic soy broth (TSB) at 15±1°C and 150 rpm. A correlation was obtained between optical density at 600 nm (OD600) and the number of viable bacteria by counting colony-forming units (CFU). Each OD600 value corresponds to 1.2×10^8 of viable *Pseudomonas* S2TR-14. Enzyme production was carried out according to our previous study [415] with some modifications. 18 g/L of crustacean waste, 2 g/L of yeast extract, and 200 mg/L of p-xylene were used as the source of calcium, proteins, and carbon respectively. After 24h of incubation, the culture was centrifuged at 3810 *x* g for 20 min. Then, the pellet was collected and washed twice with phosphate buffer (pH 7.2) and then re-suspended in the same buffer then ultrasonicated at 22-30 kHz frequencies for 10 min on ice (Branson Ultrasonics Corporation, Danbury, CT, USA). It is noticeable that 15 ± 1 °C was considered the optimum temperature for these cold-active enzymes and all tests were carried out at this temperature.

Magnetic particle preparation

There are several methods for the synthesis of Fe_3O_4 depending on the particle size to be obtained. In this study, magnetic microparticles were synthesized by the method of (Singh et al., 2016). Briefly, the magnetic microparticles (MPs) were obtained by reduction of $FeCl_2.7H_2O$ and $FeCl_3.6H_2O$ chlorides in an aqueous ammonia solution under vigorous stirring. 5.4 g of $FeCl_3.6H_2O$ followed by 2.0 g of $FeCl_2.4H_2O$ was dissolved in 25 mL of 0.4 M HCl solution. The solution was added dropwise to 250 mL of a 1.5 M NaOH solution with vigorous stirring. A black precipitate was formed immediately. The synthesized magnetic microparticles were washed

several times using deoxygenated water and separated using a simple permanent magnet and dried using a vacuum until further use.

Optimization of the immobilization parameters by RSM

Immobilization of enzymes onto magnetic chitosan microparticles was carried out according to Kumari et al. with modification [396]. The optimum levels of parameters of enzyme immobilization on magnetic particles for the maximum immobilization yield were determined statistically using the Box-Behnken design of experiment (BBD) in the Response Surface Methodology (RSM). Table E1 shows the defined factors including magnetic particle, chitosan, glutaraldehyde, and enzyme concentrations, along with their related levels. Levels for the factors were selected based on preliminary experiments. Experimental design, model calculation, graph drawing, and statistical analyses were performed using Minitab® software (Version 8.0.6, Stat-Ease Inc., Minneapolis, USA). The response model was assessed using ANOVA to evaluate its adequacy and significance. Based on the best results of the one-at-a-time approach, a selected concentration of the magnetic microparticles (stock solution 3 mg/mL) was taken in a microcentrifuge tube. A magnetic bar was used to settle the microparticle. Each gram of magnetic microparticles and chitosan was mixed in 2% v/v acetic acid under shaking conditions for 24 h. These magnetic particles were washed extensively with water and activated using glutaraldehyde through overnight incubation at room temperature. Later, crude enzyme solution was added under shaking conditions for 2 h. To remove excess glutaraldehyde and free enzymes, these particles were washed five times with 50 mM phosphate buffer (pH=7.2). This mixture was allowed to stand overnight at 4ºC under the vacuum condition for drying.

According to Eq. (1), immobilization yields were calculated and used to evaluate the response of independent variables (Box et al., 1978).

$$Immobilization\ yield\ (\%) = \frac{Specific\ activity\ of\ immobilized\ target\ enzyme}{Specific\ activity\ of introduced\ \ target\ enzyme} \times 100$$

(1)

Enzymes kinetic parameter analysis

To describe the kinetic behavior, v_{max}, K_m, and catalytic efficiency (K_{cat}/K_m) were determined by the Michaelis-Menten model as described by [140]with some modifications. The Michaelis-Menten model, as given in Eq 2. was used to describe the kinetic behavior of enzymes.

$$v = \frac{v_{max} C_s}{K_m + C_s} \quad (2)$$

Where v and v_{max} correspond to the rate of substrate utilization and its maximum rate, C_S corresponds to the initial substrate concentration and K_m corresponds to the half-substrate constant (for enzyme-substrate affinity indication). The initial rate of production of compounds (p-cresol for xylene monooxygenase and catechol 1, 2-dioxygenase for muconic acid) was measured at different substrate concentrations (0.1–1.0 mM). Then, the parameters were calculated using GraphPad Prism version 9.3.1.

Enzyme leaching test

The leaching test was carried out by 0.1 g of immobilized enzymes in 1 mL of sodium phosphate buffer (pH 7.0) with continuously stirring for 1 h, 6h, 12h, 24 h, and 48 h. The mixture was centrifuged 16,000 ×g at 4°C and then the supernatant was analyzed for enzyme activity. The leaching (%) was calculated according to Eq. (3):

$$Leaching\ (\%) = \frac{Amount\ of\ protein\ in\ supernatant}{Amount\ of\ protein\ immobilized} \times 100 \quad (3)$$

Effect of pH and temperature

For pH stability, aliquots of 500 μL of free enzymes (40 U/mg C1,2D and 20 U/mg XMO) and 0.1 mg of immobilized enzymes (initial activity 400 U/g of C1,2D per gram of support and 200 U/g

of XMO per gram of support) were added to test tubes containing 2 mL of buffers (pH range of 2 to 10). The residual activity of free and immobilized samples was measured. The thermal stability was assessed by incubating free and immobilized enzymes at different temperatures (5-50 °C) for 8 h and measuring the residual activity in the same way that was explained for pH stability.

Biodegradation and reusability tests

Bioremediation experiments were carried out in 150 mL sealed serum bottles containing 25 mL of contaminated groundwater or 5 g of soil sample and 0.2 g of immobilized enzyme. The groundwater sample was characterized as hard water due to the presence of carbonates. The soil and groundwater were originally contaminated with p-xylene and have been artificially contaminated until an initial concentration at the contaminated site (10,000 mg/Kg in soil and 200 mg/L in groundwater). Before the beginning of incubation, soil moisture was adjusted to 70% of water holding capacity using groundwater. Three sets of controls were designed: 1) control treatment using sterilized soil/groundwater by autoclave (121 °C, 30 min) that simulated abiotic losses; 2) reference controls without any treatment that simulated natural attenuation; 3) control treated with magnetic chitosan microparticles without enzymes that determined the adsorption of p-xylene to the carrier. To study the reusability of the immobilized XMO and C1,2D, the immobilized enzymes were removed using a magnet and washed with methanol after the first cycle of enzymatic reaction. It was later suspended in a fresh reaction mixture to evaluate the enzyme activity. The initial activity of the enzymes was considered as 100% and activity in the cycle was reported as a relative percentage of the initial activity.

Analytical methods

Gas Chromatography/Mass Spectrometry (GC/MS)

For sample preparation, approximately 0.05 g of soil was placed in 10 mL headspace vials containing 5 mL of methanol as the extracting solvent. Then, samples were vortexed for 5 minutes and 50 µL of sub-sample was removed. A gas-tight syringe was used to remove the sub-samples (50 µL) from the liquid phase of bottles and prepare them in 40 mL standard GC-headspace vials. Each vial was containing 5 mL of ultrapure water, and 10 µL of fluorobenzene-D5 (100 mg/L) as an internal standard. p-xylene concentration was measured using a 7890A Gas Chromatograph coupled to a Saturn Mass Detector (GC/MS) equipped with a 40-trap automated headspace sampler as described in detail in our previous study [415]. The concentration of the substrates and compounds was determined by measuring the areas of their peaks and a calibration curve.

Fourier transform infrared (FT-IR) spectroscopy

FTIR spectra of each sample were measured using an FTIR spectrophotometer (Nicole IS50) equipped with an attenuated total reflectance (ATR). Each spectrum was repeated with 16 scans per sample in the spectral range from 500 to 4000 cm^{-1} at room temperature. The average of spectra for each sample was used for plotting.

Scanning electron microscope (SEM)

The morphological changes of MPs before and after coating with chitosan and enzyme immobilization were evaluated by a scanning electron microscope (Thermofisher Quanta 3D). The acceleration voltage and working distance for each image were 30 kV and 1–5 mm, respectively. Before observation, the samples were coated with a gold-conductive layer.

Liquid Chromatography with tandem mass spectrometry (LC-MS/MS)

For the identification of proteins, the enzyme mixture was prepared using the S-Trap mini spin column (Protifi, USA) according to the manufacturer's instructions. The peptides were analyzed using a mass spectrometer coupled to an EASY-nLC 1000 system (Thermo Fisher Scientific,

USA) and using Orbitrap Elite mass spectrometer (Thermo Fisher Scientific, USA) to determine their mass. Proteome Discoverer (version 2.2, Thermo Fisher Scientific, USA) was used to process the raw data. The identification of a protein was established with greater than 99.0% probability and contained at least two distinct peptides. The Protein Prophet algorithm assigned probabilities to proteins. Then the data was aligned with the protein database of the Universal Protein Resource at UniProt (www.uniprot.org) and BLASTP (https://blast.ncbi.nlm.nih.gov).

Enzyme activity and protein concentration assays

Xylene monooxygenase activity was assayed using the spectrophotometric method as described by [416] with some modifications. Briefly, 4% xylene was prepared in N, N-dimethylformamide as the substrate. 35 µL of 4% p-xylene was added to the cell lysates and incubated at 15 ± 1 °C. The sub-samples (1 mL) were collected at 3 minutes intervals and mixed with 100 µL of ammonium hydroxide (1 M), 100 µL of 4-amino antipyrine (2%), and 100 µL of 8% potassium ferricyanide. The mixture was briefly centrifuged (14,000 × *g*) and the production of p-cresol (product of the enzymatic reaction) was determined at 500 nm.

Catechol 1, 2-dioxygenase activity was determined by the measurement of muconic acid production using a spectrophotometric method [417]. 600 µL of 10 mM catechol (as the substrate) was added to 2.0 mL phosphate buffer (pH 7.0 ± 0.2), and 400 µL of cell lysate. The absorbance of the mixture was measured at 500 nm every 3 minutes.

To calculate the specific activity of target enzymes, the total protein of cell lysates was determined by a bicinchoninic acid (BCA) protein assay kit (Pierce™ Protein Assay Kit, Thermo Scientific, US). One unit of enzyme activity was defined as the amount of enzyme that produces 1 µmol of compounds (p-cresol or muconic acid) per minute per mg of total protein.

Statistical analysis

An analysis of variance (ANOVA) was conducted using SPSS software (Version 23) on a completely randomized design. Analytical and biological tests were performed in triplicate, and the calculated means of the replicates were used along with their standard deviations. The level of significance was set at a p-value of 0.05.

5.2.3. Results and Discussion

Enzyme mixture characterization

Pseudomonas S2TR-14 was used to produce the cold-active enzyme mixture. Enzyme activity assays showed that the enzyme mixture contained 20 U/mg for XMO and 41 U/mg for C1,2D. This result corroborated with previous studies that showed the highest enzyme production was obtained in the media supplemented with crustacean waste, yeast extract, and 200 mg/L of p-xylene [16], [415]. Yeast extract and crustacean waste offer effective sources of calcium, nitrogen, and proteins that can facilitate bacterial growth. p-xylene can induce the production of XMO and C1,2D as crucial enzymes in the p-xylene biodegradation pathway. p-xylene is usually degraded by aerobic biodegradation through the mono-oxidation of its alkyl groups (by XMO) resulting in several intermediates such as p-toluic acid, and p-cresol, etc. The next step of de-aromatization is meta-cleavage by catechol 1, 2 dioxygenases (C1,2D) which is crucial for the detoxification process [16], [416].

In addition, results from LC-MS/MS spectra showed that more than 50 different proteins were detected in the enzyme mixture (Table E2). The False discovery rate (FDR) indicates the reliability of identified differentially expressed proteins and for the identified proteins, FDR $\geq$ 1% was considered. Two enzyme sequences were detected in the mixture in the presence of other proteins (Table E2). According to Table E2, XMO and C1,2D showed the highest number of total peptide hits, affirming their identification, and indicating their high abundance in the crude enzyme

mixture. According to previous research, oxidation of xylene can be initiated by direct oxidation of one or two methyl groups of the aromatic ring by xylene monooxygenase. In addition to catalyzing multi-step oxidation, this enzyme can also produce catecholic or non-catecholic derivatives [418].

The main reason for the presence of other proteins is that a crude enzyme mixture was used in this study. The process of enzyme production involves several steps of purification and downstream processing, which must be completed for minimal impurities and high specificity. Each step increases the cost of production, which also limits the application of enzymes [395]. Therefore, using crude enzyme mixtures can significantly reduce the cost of production and result in affordably remediating options for contaminated soil.

Optimization of the immobilization compounds

In the present study, the effect of four parameters, such as magnetic particles, chitosan, glutaraldehyde, and enzyme concentrations on immobilization yield was studied with the help of response surface methodology (RSM) (Table E3). The enzyme activity of C1,2D was considered for the calculation of immobilization yield as this enzyme was the dominant enzyme in the mixture with a higher v_{max} and ease of testing compared to XMO (as described in the following section). The interaction model between immobilization yield (Y) and the four tested variables is given in Eq 4:

$$\begin{aligned} Y = {} & 12.8 - 7.15\,X_1 + 42.3\,X_2 + 6.75\,X_3 + 9.96\,X_4 - 1.432\,X_1X_1 - 41.0\,X_4X_4 \\ & - 1.319\,X_3X_3 - 0.543\,X_4X_4 + 5.76\,X_1X_2 + 2.205\,X_1X_3 + 0.330\,X_1X_4 \\ & - 5.45\,X_2X_3 - 0.03\,X_2X_4 + 0.076\,X_3X_4 \end{aligned} \quad (4)$$

Where, X_1, X_2, X_3, and X_4 represent chitosan, glutaraldehyde, magnetic microparticles, and enzymes respectively.

The accuracy and significance of the factors were accomplished by calculating F and P-values. Statistical significance is defined as $P > 0.05$, whereas nonsignificant means $P > 0.1$. The ANOVA results showed that the amount of chitosan and introduced enzyme had significant linear effects on immobilization yield (Table 5.2.2). In addition, the direct interaction between chitosan and magnetic particles, X_1X_3, (P=0.014) showed a significant influence, while the two-level interaction of other compounds was nonsignificant. The quadratic effects of chitosan (P=0.023), glutaraldehyde (P=0.044), and enzyme (P=0.013) were also significant on immobilization yield.

Table 5.2.2. Regression analysis of four tested variables on immobilization yield from the Box-Behnken experiment.

Source	Coefficient (Coef)	F-value	P-value
Model	95.00	13.15	0.000**
X1-Chitosan	-9.02	6.74	0.017*
X2-Glutaraldehyde	-0.37	0.01	0.906
X3-Magnetic particle	4.75	2.05	0.168
X4-Enzyme	22.78	39.42	0.000**
X1X2	8.64	2.67	0.118
X1X3	16.54	7.31	0.014*
X1X4	5.44	0.71	0.410
X2X3	-6.82	1.44	0.244
X2X4	-0.09	0.00	0.987
X3X4	1.05	0.03	0.868
X1X1	-12.89	6.07	0.023*
X2X2	-10.25	4.62	0.044*
X3X3	-8.24	3.37	0.082
X4X4	-16.43	7.41	0.013*

* Significant (0.01 < P-Value < 0.05). ** Very significant (P-value < 0.001).

Analytical results showed that the optimal ratio for immobilization of enzymes was found to be chitosan 3% (W/V), glutaraldehyde 0.42% (V/V), magnetic microparticles 4.48% (W/V), and enzymes 10.3% (V/V). As expected, the immobilization yield reached up to 98.66%, when the content of chitosan and magnetic particles increased to 3% (w/v) and 4.48% (w/v), the immobilization yield reached the maximum value, and then decreased as the two independent

variables increased (Fig. 5.2.1A and 5.2.1D). Previous studies have demonstrated that chitosan can be used as a cross-linker for enzymes and carrier support. Since chitosan contains amino groups that facilitate the covalent attachment of enzymes [16]. Meanwhile, glutaraldehyde as a powerful crosslinker can prevent enzyme leakage from support and chitosan. Reddy & Lee (2013) also mentioned that composites of magnetic chitosan exhibit good sorption properties towards various toxic pollutants in aqueous solutions. In addition to having a fast adsorption rate and high adsorption efficiency, these magnetic composites are also easy to recover and reuse [419]. Although the cross-linking of enzymes adsorbed on aminated supports is possible by glutaraldehyde [420], the interaction between the amount of glutaraldehyde and other variables on immobilization yield was nonsignificant (Fig. 5.2.1B). The leaching test results confirmed that glutaraldehyde prevented the leaching of enzymes from the chitosan-coated magnetic particles.

As described in Fig. 5.2.1C and 4.2.1D, with increasing dosages of the introduced enzymes (up to 10% V/V), the immobilization yields gradually enhanced and then declined. This downward trend indicated the maximum protein adsorption capacity of the magnetic chitosan carrier. Similarly, Mahdavinia et al., (2018), showed that the adsorption of bovine serum albumin (BSA) by magnetic hydrogel beads continues and then is followed by a decrease in the rate of BSA uptake because of reaching saturation adsorption in the final step [421].

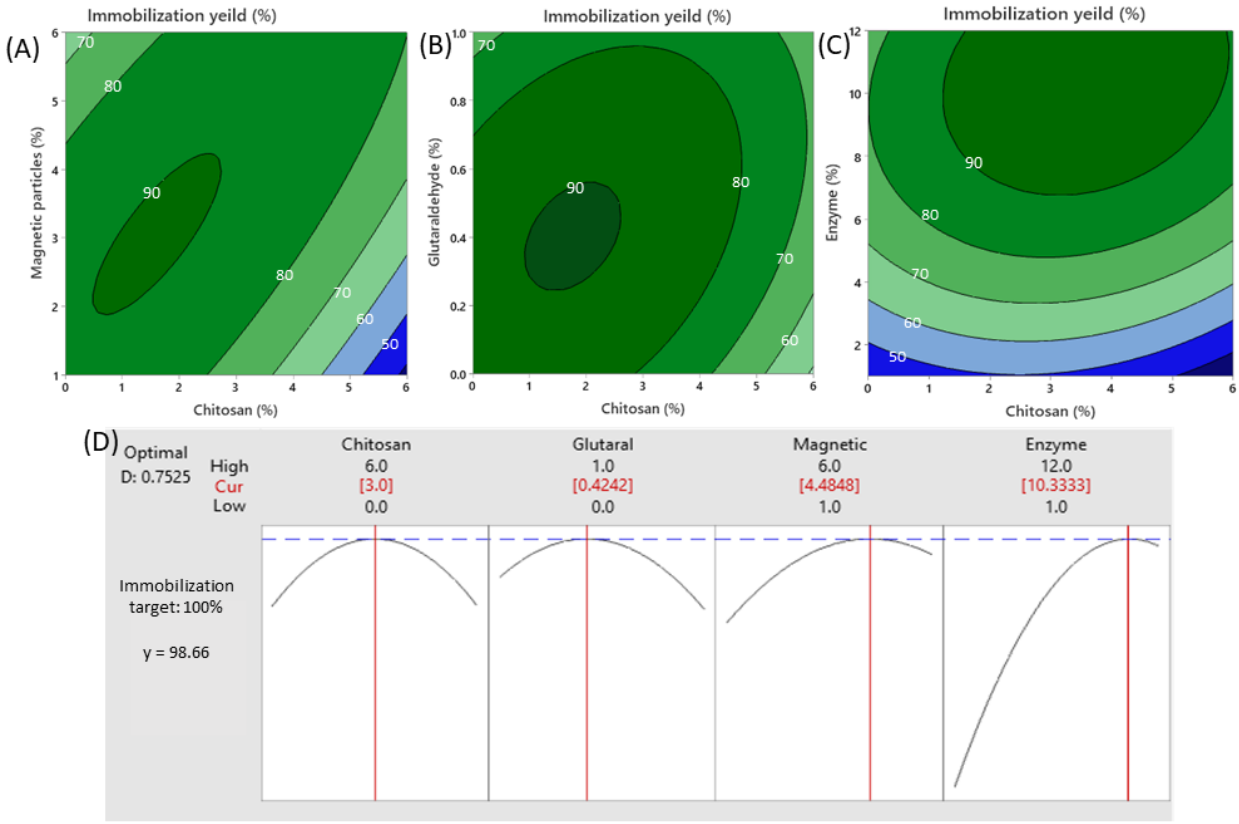

Fig. 5.2.1. Contour Plots (A-C) and response optimization (D) of immobilization yield at different magnetic particles, chitosan, glutaraldehyde, and enzymes content

Immobilized and free enzymes Kinetics

The Michaelis-Menten model parameters were detected by measuring the degradation rates of p-xylene and catechol using free and immobilized XMO and C1,2D respectively (Table 5.2.3). According to Ma et al. (2013), XMO is specific for toluene as a substrate and catalyzes the oxidation of toluene to catechol as its end product [370]. Similarly, it has been reported that C1,2D cleaves aromatic rings by showing high specificity for catechol [371]. The Lineweaver-Burk (LB) graphical method was used to determine the kinetic constants of enzymes in free and immobilized forms using two different substrate concentrations (0.1 and 0.5 mM). Since the K_m for free and immobilized enzymes is the same, there is no diffusion limitation for magnetic chitosan

microparticles, as shown in Table 5.2.3. In addition, it is noteworthy that in contrast to our prior study [16], enzymes are not immobilized on the internal surface of pores in porous particles, thus diffusion limitations of the substrate appear to be negligible in this study because enzymes are immobilized on the surface of the carrier. These results showed that v_{max} for p-xylene (substrate of XMO) was less than for catechol (substrate of C1,2D). This phenomenon may be attributed to the fact that the initial steps in oxidation require higher activation energy than the latter steps in biodegradation, since the stability of the substrate is decreased in each step of biodegradation [15], [140]. Table 5.2.3 shows that almost no enzyme activity and kinetic parameters were increased or decreased following immobilization. K_{cat} / K_m of XMO and C1,2D were used to calculate the overall kinetic efficiency (known as the catalytic efficiency). The catalytic efficiency of immobilized enzymes is similar to that of free enzymes. Hence, the loss of enzyme activity due to denaturation and/or strong attachment of enzymes to their support was negligible during immobilization.

Table 5.2.3. Kinetics parameters for XMO and C1,2D

Enzyme	v_{max} (mM min^{-1})	K_m (mM)	K_{cat} (min^{-1})	Catalytic Efficiency (min^{-1} mM^{-1})
XMO (Free)	0.45 ± 0.03	1.40 ± 0.12	0.8 ± 0.2	0.57 ± 0.12
XMO (Immobilized)	0.48 ± 0.04	1.39 ± 0.23	0.83 ± 0.25	0.59 ± 0.23
C1,2D (Free)	20.13 ± 0.74	3.71 ± 0.33	1.71 ± 0.34	0.46 ± 0.03
C1,2D (Immobilized)	21.06 ± 0.98	3.69 ± 0.45	1.73 ± 0.13	0.46 ± 0.11

Characterization of immobilized enzymes

Scanning electron microscope (SEM)

The surface morphology of the supporting material was analyzed to confirm the immobilization of enzymes on magnetic chitosan microparticles. The surface morphology of native MPs and chitosan (Fig. 5.2.2I A and 5.2.2I B), chitosan-coated MPs (Fig. 5.2.2I C), and glutaraldehyde

treated MPs (Fig. 5.2.2I D), and enzyme immobilized MPs (Fig. 5.2.2I E and 5.2.2I F) was studied using SEM. Fig. 5.2.2E and 5.2.2F show that the enzyme has been successfully immobilized onto MPs, as indicated by the white patches in the circle. Although, there is no major effect seen on the surface features of magnetic chitosan microparticles after immobilization of enzymes, clumping and white patches were observed after enzyme immobilization. This observation can be attributed to the changes in the carrier surface after the addition of crude enzymes. Since the molecular weight of xylene monooxygenase and catechol 1,2-dioxygenase are approximately 80 kDa and 35 kDa [15] which corresponds to a particle size lower than 5 nm [319]. Based on the micrographs, a minimum magnification was achieved of 1 μm and further magnification was not possible due to the limitations of the instrument. Similarly, Agrawal et al., (2020) showed changes in the overall morphology of functionalized graphene quantum dots after the immobilization of β-amylase [395]. Lonappan et al., (2018) also observed clumping after immobilization of crude laccase onto micro-biochars [319].

Fourier transform infrared (FTIR) spectroscopy

To verify the immobilization of enzymes onto MPs, FTIR spectra have been compared for the immobilized enzymes (Fig. 5.2.2II B) with those of native chitosan (Fig. 5.2.2II A), and glutaraldehyde-treated MPs (Fig. 5.2.2II C). FTIR spectra for MPs are also presented in Fig. 5.2.2II D. FTIR analysis can provide general information regarding the functional groups of the samples and changes after each process [422]. A peak obtained at ~1630 cm^{-1} (Fig. 5.2.2II B) revealed the presence of CONH linkage between MPs composite as organic support and enzyme. Bands at 3264 cm^{-1} (Fig. 5.2.2A) and ~570 cm^{-1} (Fig. 5.2.2B and 4.2.2C) correspond to N–H groups from the chitosan and Fe–O groups from MPs [422]. The difference in the stretching band of Fe–O was observed at 570 to 580 cm^{-1} (Fig. 5.2.2B and 4.2.2C) and the N–H stretching vibrational band from

1653 to 1633 cm^{-1}. This phenomenon could be assigned to the fact that iron ions became bound with NH_2 groups of chitosan and enzymes [423]. The bands at 2918 and 1625 cm^{-1} can be attributed to the CH-stretching and the amide-type 1 vibrational modes of chitosan, respectively.

Based on Beauchamp Spectroscopy Tables, the band at 1056 cm^{-1} corresponds to the presence of the C-O group which confirmed the presence of oxygen-containing functional groups on immobilized MPs. Similarly, Agrawal et al., (2020) showed the presence of the C-O group on graphene quantum dots after functionalizing using glutaraldehyde and 3-aminopropyltriethoxysilane [395].

(I)

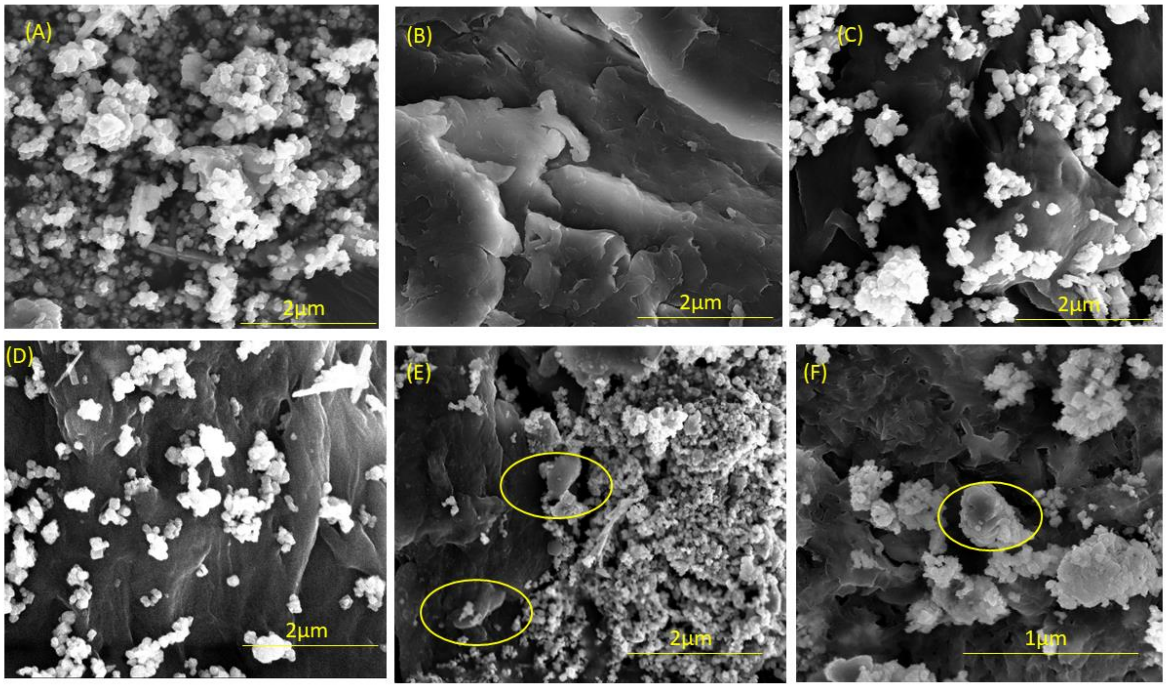

(II)

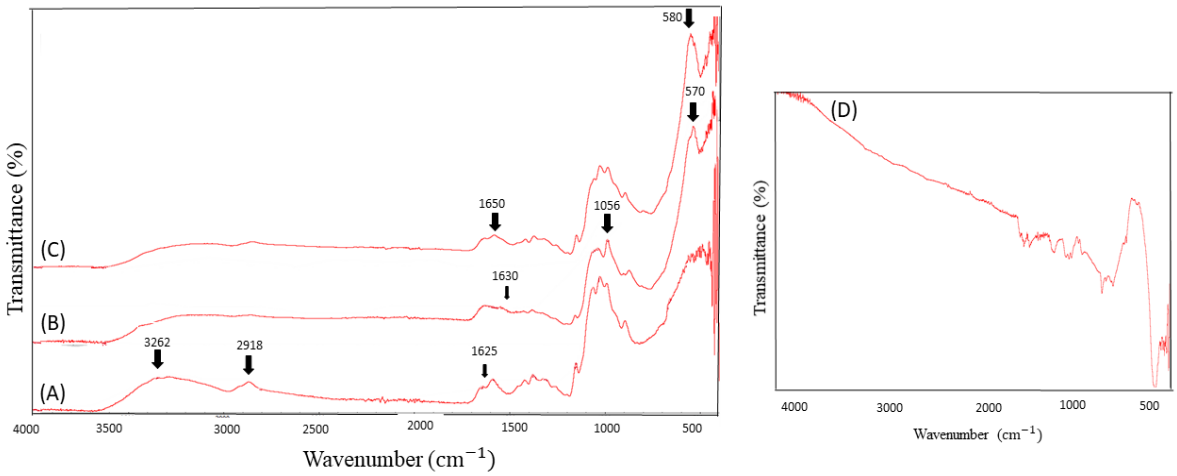

Fig. 5.2.2. I) SEM images of (A) Native MPs at 2 µm (B) Native chitosan at 2 µm (C) Chitosan coated MPs at 2 µm (D) Glutaraldehyde treated MPs at 2 µm (E) Enzymes immobilized MPs at 2 µm and (F) Enzymes immobilized MPs at 1µm magnification. II) spectra displaying marked changes in the range of 500–4000 cm^{-1}, FTIR analysis of (A) Native chitosan (B) Enzyme immobilized MPs (C) Glutaraldehyde treated MPs (D) Native MPs.

Enzymes leaching

The results showed that the leaching of protein from the magnetic chitosan microparticles, and glutaraldehyde was lower than 5% after 48 h of incubation under shaking conditions (Fig. F2). This augurs well for subsequent reusability of the immobilized enzymes treated with both linkers in an aquatic medium. The results confirmed that using one of the linkers led to a higher leaching of proteins (around 13% for glutaraldehyde and 21% for chitosan). A few studies suggested that using both chitosan and glutaraldehyde could decrease the amount of protein that is leached from solid supports. For example, Naghdi et al., (2019) showed that only 2% of laccase leached out from functionalized nano-biochar composite after 120 h of incubation [366]. Ariaeenejad et al., (2021) showed that leaching of cellulase, hemicellulase, and cellulase + hemicellulase cocktails from magnetite-cellulose nanocrystals were around 10% after 5h [424].

Effect of pH and temperature

The effect of pH on both free and immobilized enzymes was determined in this study in the pH range of 2.0 to 10. The maximum activity of free enzymes was present at pH 7, whereas in the case of immobilized enzymes they showed the maximum activity at the pH range of 6.0–9.0. (Fig. 5.2.3A). The immobilized enzymes showed greater pH stability (4.0–9.0), indicating that it becomes less sensitive to changes in pH. In the immobilized form of the enzymes, the pH is influenced by the interaction between the charged residues of the amino acids in the enzymes and the functional groups on the matrix. As a result of physicochemical force perturbations at extreme pH, the conformational state of a free enzyme may be altered, which leads to a reduction in its activity. In contrast, immobilized enzyme stability can be attributed to a multipoint attachment of the enzyme to the matrix, which prevents denaturation [366].

The optimum temperature graph for free and immobilized enzymes revealed that there was no change in optimum temperature at low temperatures after immobilization (Fig. 5.2.3b). However, the immobilized XMO and C1,2D showed higher activity than the free enzymes in the temperature range of 25-50°C. Fernandez–Lafuente et al., (2000) reported that immobilized thermophilic catechol 2,3-dioxygenase (C2,3D) from *Bacillus stearothermophilus* had a much higher optimal temperature (approx. 20°C) than the free enzyme. In that study, C2,3D was immobilized on highly activated glyoxylic agarose beads using multiple covalent links between the enzyme and matrix. It was suggested that covalent links stabilized the quaternary structure of this enzyme and increased the rigidity of the subunit structures [425]. However, to the best of our knowledge, literature showing the effect of immobilization on cold-active C1,2D and XMO is not available. Mukhopadhyay et al., (2015) showed that the activity and stability of cold-active laccase were enhanced after being entrapped in a single-walled nanotube. They also reported that immobilized cold-active laccase exhibited thermostability as well as psychrostability [426].

Similarly, our results showed immobilized cold-active XMO and C2,3D had high stability at both lower and higher temperatures. A major challenge with cold-active enzymes is their inherent instability, as they are more flexible and unstable near the active site than their mesophilic counterparts [15], [369]. Therefore, immobilization of cold-active enzymes seems a promising method for increasing the structural rigidity of cold-active enzymes and addressing this challenge. The significance of these results is that psychrophilic enzymes can be modified to tolerate drastically high temperatures without changing their primary structure.

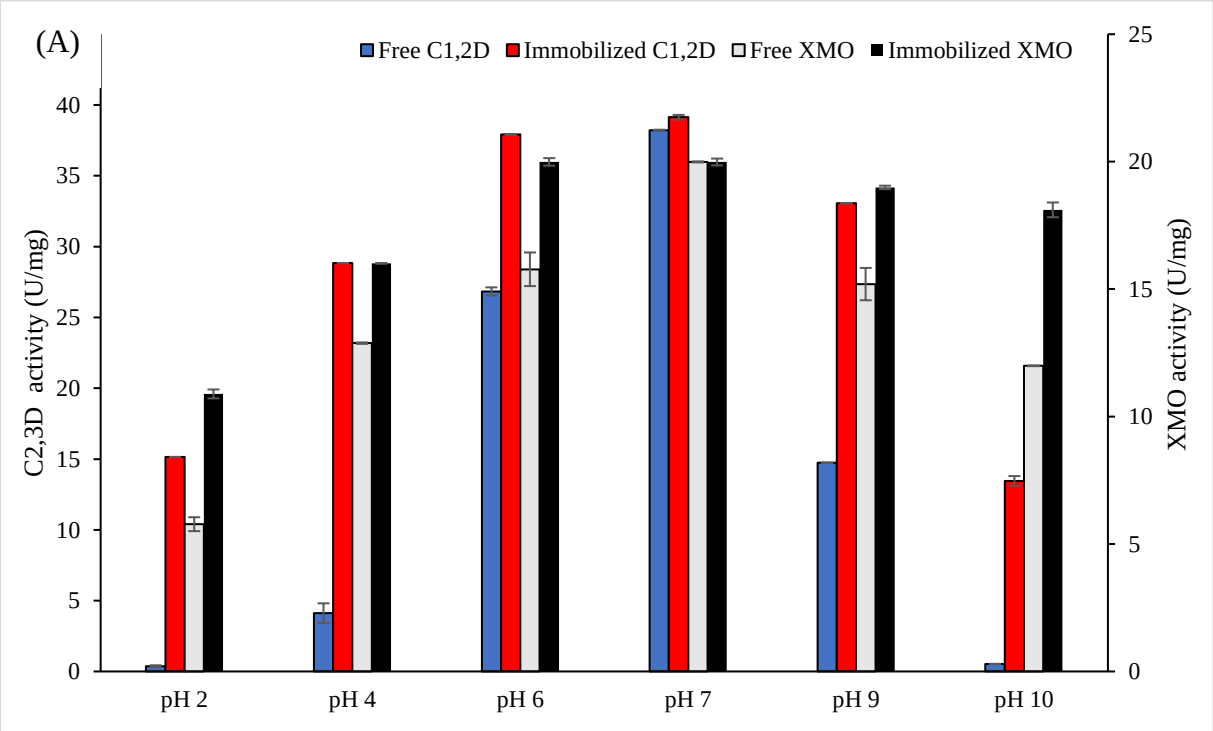

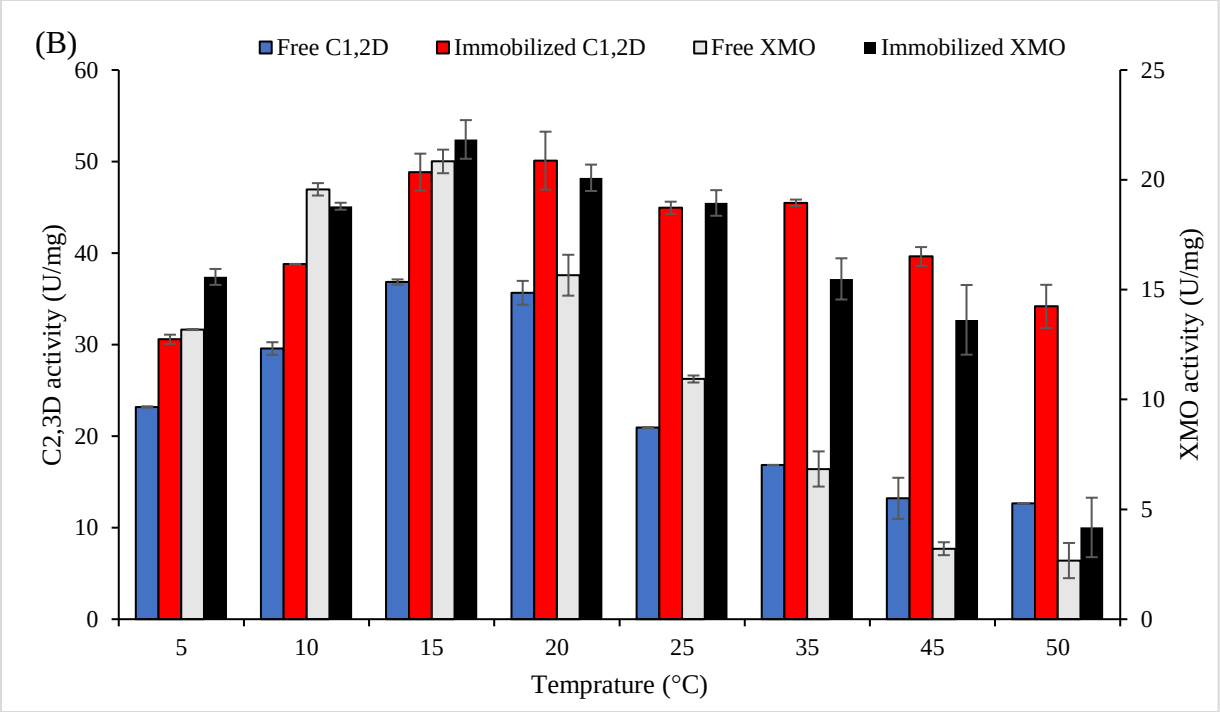

Fig. 5.2.3. Enzyme activity of free and immobilized XMO and C1,2D: (A) Effect of pH and (B) Effect of temperature

Reusability and storage stability

In practical applications, reusability and storage stability are crucial. In industrial and environmental processes, enzyme recyclability has a significant impact on cost reduction. The reusability of the immobilized XMO and C1,2D was conducted in 10 repetitive batch reactions (Fig. 5.2.4a). Immobilized XMO and C1,2D could maintain ~80% of their initial activity after 5 cycles and ~40% activity after 10 cycles (Fig 5.2.4a). These results showed that the immobilized enzyme activity decreased when the recycling number was increased. There are two possible reasons for this observation: 1) enzymes leached out during repeated use and; 2) denaturation and the conformational changes because of repeated use. There is no available literature on the immobilization of cold-active XMO and C1,2D except in our previous study [16]. The result of the current study is a significant improvement in the reusability of these enzymes compared to our

previous study which showed that XMO and C1,2D retained 15% and 22% of their initial activity after 5 cycles of use [16]. One reason for the higher reusability of XMO and C1,2D in this study is the fact of using different immobilization methods and more concentrations of glutaraldehyde and chitosan as enzyme linker agents. In this study, 3% (w/v) chitosan and 0.42% (v/v) glutaraldehyde were used for the preparation of immobilized enzymes. While in our previous study, we used 2% (w/v) chitosan and 0.02% (v/v) glutaraldehyde for the immobilization of these enzymes onto nano- and micro-biochar. These results also highlight the importance of optimizing immobilization compounds to maximize immobilization properties. Using glutaraldehyde and chitosan as enzyme linker agent are widely reported in the literature [420], [427] however, the immobilization compounds should be optimized for each enzyme.

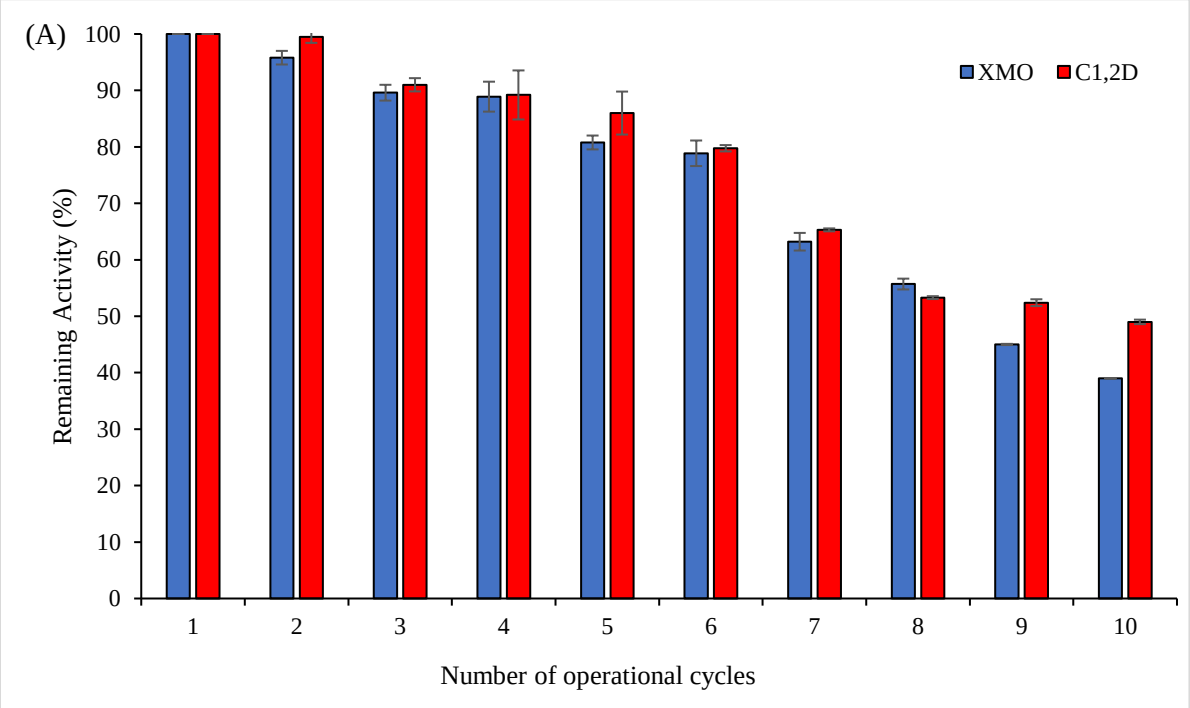

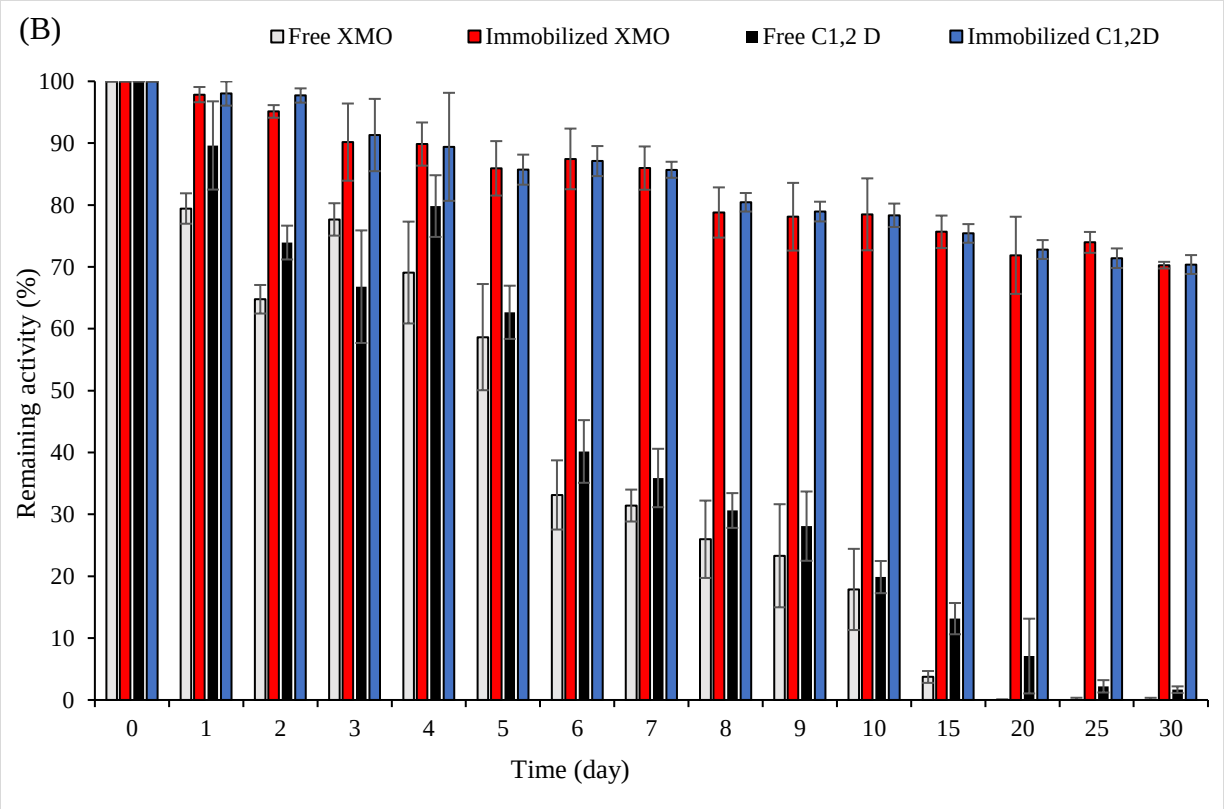

Fig. 5.2.4. Remaining enzymes activity of free and immobilized XMO and C1,2D (A) Effect of repeated use of immobilized enzymes (B) Time of storage on the stability of free and immobilized enzymes.

In enzyme immobilization, one of the most critical parameters is storage stability. The stability of both free XMO and immobilized C1,2D was evaluated by storing them at room temperature (25 ± 2 ◦C) in dried form and measuring enzyme activities at certain time intervals. According to Fig. 5.2.4B, immobilized enzymes showed activity of more than 70% after 30 days of storage at room temperature. The higher conformational stability of covalently immobilized enzymes may be attributable to the multipoint attachment of enzymes to magnetic chitosan microparticles through glutaraldehyde as a cross-linking agent. Very few reports are available on the immobilization of cold-active enzymes as compared to mesophilic and thermophilic enzymes, but most of the literature reported low thermostability of cold-active enzymes at temperatures higher than 20ºC. This low thermostability is due to the molecular flexibility of an active site of cold-active enzymes

[428]. The results of the current study showed a significant improvement in storage stability of immobilized cold-active enzymes compared to our previous study which reported less than 30% of XMO and 50% of C1,2D remaining activity after 30 days at room temperature [16].

Biodegradation of p-xylene

p-xylene has been identified by the International Tanker Owners Pollution Federation (ITOPF) as one of the top 20 chemicals posing a high risk among hazardous and noxious substances (HNS) [429]. There are numerous applications for p-xylene as a solvent in industry and it is highly mobile under a wide range of environmental conditions in either a liquid, gaseous, or solid form [430]. p-xylene is considered one the most persistent pollutant in terms of its recalcitrance to biodegradation. In aerobic systems, the oxidation of xylene may be initiated either by the direct oxidation of the aromatic ring or by the direct oxidation of one or two methyl groups of the aromatic nucleus by XMO. This enzyme is capable of multistep oxidation and can produce catecholic or non-catecholic derivatives (Choi et al. 2013). Then, as the crucial step in detoxification, para-, meta-, or ortho-cleavage by catechol dioxygenases occurs during the ring de-aromatization of central intermediates [416]. In this study, free and immobilized enzymes (XMO and C1,2D) were used for p-xylene biodegradation (Fig 5.2.4). For each test, approximately equal amounts of enzyme mixture in terms of enzyme activity (10 U/mg of XMO and 20 U/mg of C1,2 D) were added either in biodegradation test with free or immobilized form. The changes in the p-xylene concentration versus time are shown in Fig. 5.2.5. The degradation results indicated that immobilized enzymes had better biodegradation ability compared to free enzymes (Fig. 5.2.5). The possible reason was that when enzymes are immobilized onto adsorbents such as magnetic chitosan, the probability of contact between the substrate molecule and the immobilized enzymes was higher compared to free enzymes, resulting in a high reaction rate.

In the experiment set with the free enzymes, the decrease of degradation rate after 2 days may be explained by the lower activity of free enzymes as a result of high concentration of p-xylene and their less stability in comparison with immobilized form. Qiu et al., (2021) showed that too high substrate concentration (2,4-dichlorophenol) could inhibit the enzymatic reaction in the free form of enzymes (laccase). While immobilized laccase onto modified magnetic chitosan nanoparticles showed a good removal performance even at a high concentration of 2,4-dichlorophenol [403].

Few studies have been conducted on the immobilization of cold-adapted enzymes, and most have shown that the immobilization method improves the thermal stability of cold-active enzymes [431]. For example, Rahman et al., (2016) reported that immobilization of cold-active esterase onto Fe_3O_4~cellulose nanocomposite enhanced catalytic properties such as prolonged half-life, better temperature stability, higher storage stability, improved pH tolerance, and reusability [432]. In practice, the first weeks after enzymatic or nonenzymatic treatments of contaminated soils are important, as they determine the effectiveness of the method. During this time, efforts should be made to enhance the stability of enzymes. Similarly, our results showed that about 20% of p-xylene was degraded after 6 days using free enzymes, while immobilized enzymes degraded 44% of p-xylene after 6 days. These results indicated that immobilization increased the effectiveness of enzymatic treatment of p-xylene contaminated soil.

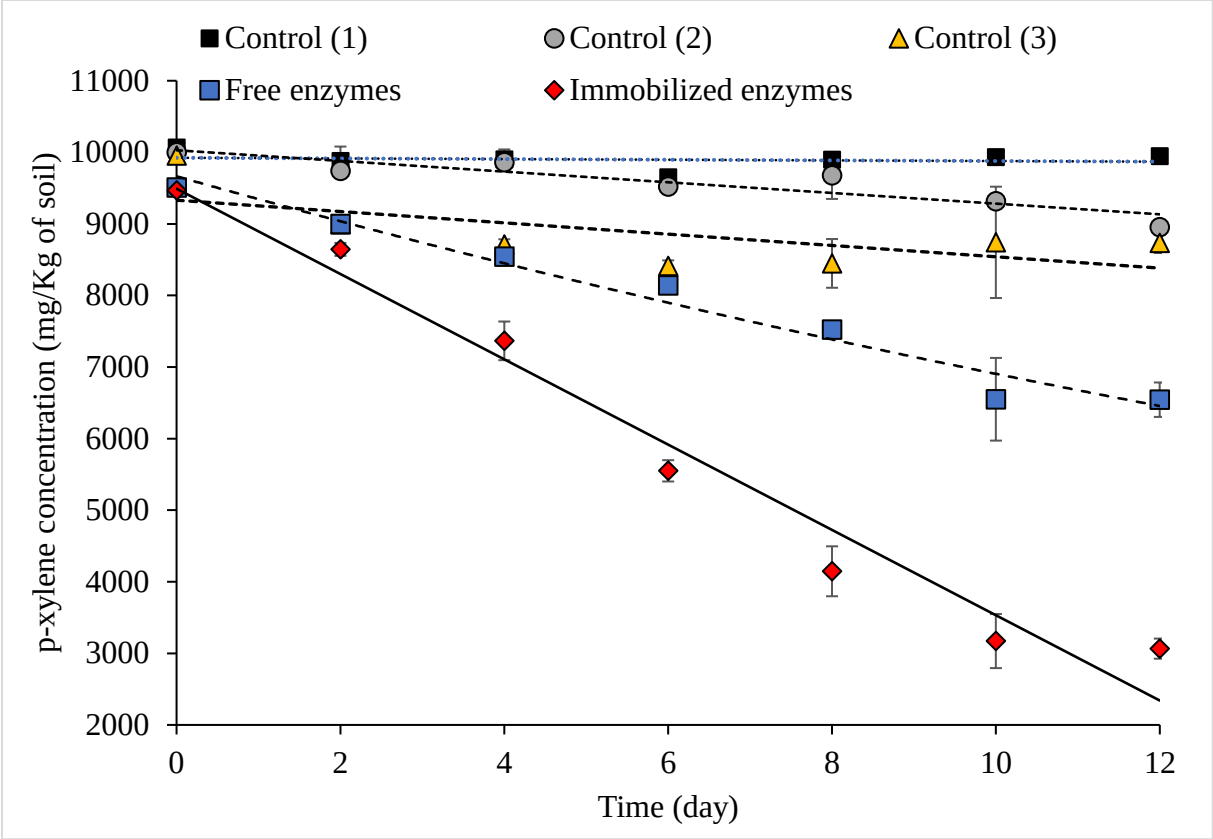

Fig. 5.2.5. p-xylene biodegradation in soil sample by free XMO and C1,2D mixture, immobilized XMO and C1,2D onto magnetic chitosan microparticles, control 1 showed the effect of abiotic losses, control 2 showed the effect of natural biodegradation by indigenous microorganisms, and control 3 showed the effect of adsorption of p-xylene to magnetic chitosan microparticles.

5.2.4. Conclusion

Two cold-active enzymes (XMO and C1,2D) were immobilized on magnetic chitosan microparticles through cross-linking of glutaraldehyde. Optimization of the amount of each compound involved in immobilization (chitosan, glutaraldehyde, magnetic microparticles, and enzymes) showed that the highest immobilization yield could be achieved up to 98%. In addition, immobilization of these enzymes improved their catalytic characteristics in terms of pH tolerance, thermal stability, reusability, and time of storage stability. Also, immobilized enzymes had a 2-fold higher p-xylene degradation rate in soil compared to the free form. The catalytic improvement

makes the immobilized enzymes suitable for the remediation of contaminants such as p-xylene in soil.

CHAPTER SIX: SCALE-UP of COLD ACTIVE ENZYME BOOSTER

6. Feasibility Study and Scale-up of Enzymatic Biodegradation

Saba Miri[1,2], Thomas Robert[2,3], Satinder Kaur Brar[1,2*], Richard Martel[2], Tarek Rouissi[2], Jean-Marc Lauzon[3]

[1]Department of Civil Engineering, Lassonde School of Engineering, York University, North York, Toronto, Ontario M3J 1P3, Canada

[2]INRS-ETE, Université du Québec, 490, Rue de la Couronne, Québec, Canada G1K 9A9.

[3] TechnoRem Inc., 4701, rue Louis-B.-Mayer, Laval, Québec, H7P 6G5, Canada

*Correspondence author: Tel: + 418 654 3116; Fax: + 418 654 2600; E-mail: satinder.brar@lassonde.yorku.ca

Technical report submitted to TechnoRem Inc. (Industrial partner of this project).

Abstract

The biodegradation of petroleum hydrocarbons under cold environments has received increasing attention, whereas the scale-up study of biodegradation is still missing. Herein, we isolated cold-adapted bacteria (S2TR-06), which were affiliated with *Arthrobacter* sp. and could produce cold-active oxidoreductase enzymes involved in p-xylene biodegradation. Based on the intermediate analysis, xylene monooxygenase (XMO) was able to transform p-xylene into a p-cresol intermediate. Catechol 2, 3-dioxygenase (C2,3D) cleaved the ring of the p-cresol. For enzyme production and effective induction, injection of 100 mg/L p-xylene into the production medium was needed every 6 h (multi-pulse addition of inducer). Enzyme production was investigated on 4 different scales (serum bottles, 5-L, 15-L, and 150-L bioreactors). The results showed a shorter fermentation time and the highest enzyme activity and production (107 g/L for biomass, 109 U/mL for XMO, and 203 U/mL for C2,3D after 24h) were achieved in the 150-L bioreactor due to enhanced oxygenation. The stability of enzymes can be increased up to 3-folds by adding $FeSO_4$ at 0.1% (w/v) before extraction of enzymes. Soil tests also showed that biodegradation is scale-dependent, and an understanding of involved factors is needed for the successful implementation of laboratory-scale data in the field. The maximum biodegradation rate decreased from 100% at lab-scale (aqueous phase batch test of 150 mL) to 36% in the 3 300-L sand tank (pilot-scale) tests due to limited access of enzymes to trapped p-xylene in soil pores, low dissolved oxygen in the water-saturated zone, soil heterogeneity, and presence of free NAPL phase. This study could provide key guidance for the enzymatic bioremediation of mono-aromatic pollutants in unsaturated and water-saturated zones under cold conditions.

Keywords: biodegradation; cold temperatures, cold-active enzymes; enzyme production, sand tank

Graphical Abstract

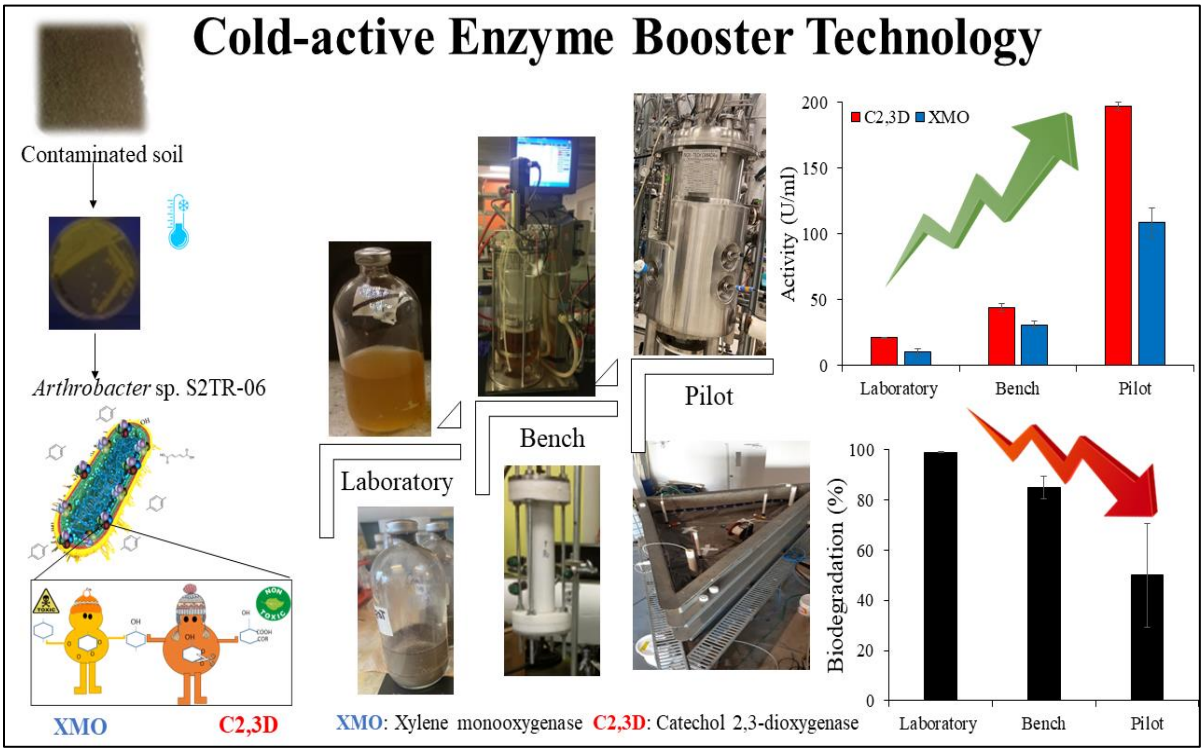

6.1. Introduction

Soil contamination caused by human activities requires remediation to both mitigate environmental risks and facilitate redevelopment. Petroleum contamination in soil is one of the major modern society environmental concern that produces adverse human health consequences. For soil remediation and redevelopment of polluted sites, bioremediation offers a sustainable alternative to physical-chemical processes [433].

Cold region ecosystems are more sensitive to damage by oil spills than warmer climates. Gentle but effective remediation approaches have recently received significant attention [434]. It is desirable to use techniques that minimize further ecological damage caused by a physical disturbance in the remediation of contaminated soils. In this regard, *in-situ* bioremediation is becoming more popular as it is cost-effective and more sustainable than traditional ex-situ or chemical and thermal technologies. However, biological treatment of petroleum contamination may require a year to ten years to meet cleanup standards because low temperatures limit microbial growth and their activity. In addition, petroleum compounds persist for centuries under cold temperatures and may have a half-life in the range of tens to hundreds of years if not remediated [435].

The use of cold-active enzymes that maintain their activity at low temperatures, has a great potential for bioremediation of contaminated sites. This is because enzymes can transform the substrate in a minute timescale under low temperatures, therefore enzymatic treatment has a shorter treatment period than the microbial process in cold region sites [436]. Enzymatic treatment can be designed for stepwise oxidation reactions by different oxidoreductases to completely detoxify the contaminants. For instance, Kwean et al. (2018) used four different oxidative enzymes, including phenol 4 monooxygenase, chlorophenol monooxygenase, putative flavin

reductase, and dioxygenase for the degradation of 4-chlorophenol. In our recent trials, alkane hydroxylase and lipase were applied for the degradation of $C_{10} – C_{50}$ at diesel-contaminated sites [437].

Generally, biodegradation of benzene, toluene, ethylbenzene, and xylene isomers (BTEX) involved *tod* or *tol* pathways [438]. Our previous study showed that p-xylene degraded mainly via *tol* pathway from isolated bacteria that organized into *upper* and *meta* cleavage operons. The *upper* operon contains five genes (*xylCMABN*) encoding enzymes involved in the monooxidation of aromatic hydrocarbons to their carboxylic acids such as xylene monooxygenase. *Meta*-cleavage operon (encoding *xylXYZLTEGFJQKIH*) encodes enzymes responsible for converting benzoate to Krebs cycle intermediates. Catechol 2,3-dioxygenase is one of the key enzymes in the meta operon that is involved in the ring cleavage of aromatic hydrocarbons [415].

Among the main challenges involved in enzymatic bioremediation is the large volume of enzymes necessary to facilitate timely remediation. The successful application of enzymatic remediation depends on the bench to large scale studies with reliable and reproducible results using scale-up bioreactors and biodegradation tests. Understanding scale-dependent phenomena are the most challenging aspect of implementing laboratory data at the field scale. To the best of our knowledge, the production of cold-active enzymes has not been scaled up and the effect of these enzymes on the biodegradation of petroleum hydrocarbons has not been fully investigated. The experiments described here were conducted to describe and measure the relative impacts of the scale-up process on both enzyme production and their overall biodegradation efficiency for treating soil contaminated by p-xylene.

6.2. Materials and methods

Soil samples

Several soil samples were collected by TechnoRem Inc. (our industrial partner in this work) from a p-xylene contaminated site located near Montreal, Quebec, Canada. The average minimum annual temperature at this site is 5 ± 1 ºC, and the average maximum annual temperature is 15 ± 1 ºC (the average temperature of 10 ºC is considered for laboratory testing). Originally, the soil was contaminated with p-xylene at an initial concentration of ~10,000 mg/kg.

Identification of p-xylene-degrading isolate

Isolation of bacteria was performed using Minimal Salt Medium (MSM) supplemented with 50, 100, and 200 mg/L p-xylene (low, intermediate, and high concentration) by enrichment and adaptation techniques as described previously [218]. MSM contained 4.0 g NH_4Cl, 1.8 g/L K_2HPO_4, 0.2 g/L $MgSO_4.7H_2O$, 0.01 g/L $FeSO_4$. $7H_2O$, 0.1 g/L NaCl in distilled water. The selected isolates were identified based on 16S ribosomal RNA gene sequences. The fragments of the gene were amplified using universal primers (27F and 1492R). The 16S rRNA fragment was sequenced and compared against the reference sequences in the National Center for Biotechnology Information (NCBI) database using the BLASTn program. Phylogenetic analysis was conducted using the neighbor-joining algorithm of the MEGA 11.0 software with 1000 bootstraps. Biochemical characteristics of the isolated strain were investigated and compared with *Arthrobacter ramosus* NRRL B-3159^T as a reference strain. This strain was purchased from NRRL (Northern Regional Research Laboratory).

Enzyme production scale-up

Inoculum preparation and batch tests

Since isolated bacteria can grow at 4˚C, the selected strain was stored at -80 ◦C in a TSB media solution containing 20% glycerol (v/v). Our preliminary results showed that this selected strain

could grow at the maximum rate at 30˚C while producing cold-active enzymes. Inoculum for enzyme production was prepared in TSB at 20˚C and 150 rpm. Bacterial biomass was measured using optical density at A600 nm (OD600). OD600nm ~2–2.2 was used for inoculum preparation which corresponded to 2×10^9 cells/mL. In this study, the inoculum size was 10% (v/v) for all enzyme production experiments. All batch tests were performed in 150-mL sealed serum bottles containing 25 mL of TSB and 50, 100, and 200 mg/L of p-xylene. The concentration in tests was selected based on the water solubility of p-xylene at 25 °C (~200 mg/L) [262].

Fermentation in 5, 15, and 150L bioreactors

The fermentation study was conducted in 5-L, 15-L, and 150-L bioreactors (Labfors 5, Infors HT, Switzerland) with stirred baffled vessels and working volumes of 3, 10, and 100 L, equipped with dissolved oxygen (DO), pH probes, and a controller for temperature and airflow. The programmable logic control (PLC) system was run by iFix 3.5 software for automatic control and monitoring of temperature, aeration, DO, pH, foaming, and agitation speed. Buffers at pH 4 and pH 7 (VWR scientific products, Canada) were used to calibrate the pH sensor (Mettler Toledo, Columbus, OH, USA). The oxygen sensor was calibrated using sodium thiosulfate to 0% and air-saturated distilled water to 100%. The probes and sensors were calibrated before sterilization. Sterilization of the bioreactors was performed at 121ºC for 20 minutes. Polypropylene glycol (Sigma, Canada) (0.01% v/v) was sterilized and used as an antifoaming agent.

Downstream processing

After fermentation, the broth was centrifuged by a continuous solids-discharge centrifuge at a rate of 5L/min, which could harvest more than 90% of cells from the broth. Then enzymes were extracted from cells using an industrial ultrasonic processor (2000 watts, 20kHz, Hielscher, USA). The enzyme solution was kept at 4±1°C until further use. Different additives were selected

according to the literature on enzyme formulation and then tested on the concentrated cells to increase the storage stability of enzymes (Table 6.1). Storage stability is required for larger-scale field tests, since these require the enzyme broth to be transported and temporarily stored on-site before mixing and injection into the soils. Storage temperatures during this process cannot be practically controlled in the same fashion as in a lab. As can be seen in Table 5.1, each additive can play a specific role in increasing the stability of enzymes.

According to available literature, zeolite and clay (montmorillonite) were used for physical adsorption [439]. After extraction of enzymes (formulated with iron (II) sulfate based on the results), 10% w/v of zeolite or clay was added and mixed at 4±1 °C. The obtained slurry was dried under vacuum conditions at 4±1°C.

Table 6.1. Additives used in enzyme stability studies

Category	Compound	Amount (v/v or w/v)	Function	References
Ligands	Benzyl acetate	1%	Ligands occupy the active site of enzymes to preserve them from unfolding	[440]
Salts	$Cacl_2$	1%	The bridging function of Ca^{+2} increases molecular rigidity	[276]
	$FeSO_4$	1%	Ionic effect, Cofactor of active site	[440]
Cryoprotectants	Glycerine	20%	Protection from damage during freeze-thawing and temperature effect	[313]
Synthetic polymers	polyethylene glycol	20%	The formation of intra- and intercross links or hydrogen bonds with the protein surface	[356]
Miscellaneous additives	Tween 80	1%	ND	[441]
	Phospholipids	30%	Membrane mimic condition	[440]
Bio/surfactants	Rhamnolipid	10%	Membrane mimic condition	[440]

	Triton X-100	1%	Membrane mimic condition	[440]
Sugars	Molasses	1%	Positive effect on water activity and a decreased possibility of microbial contamination	[241]
Other chemicals	Boric acid	0.5%	Protease inhibition	[390]
	H_2O_2	1%	Providing O_2 for enzymes function	[385]

ND: Not Determined

Biomass measurements and enzyme activity assays

The cell density measurement and enzyme assay methods used were similar to those in our previous work [415]. Briefly, samples were taken during the time course of fermentation, and aliquots of 1 mL were centrifuged at 10,000 rpm at 4ºC for five minutes. The cell pellet was washed three times with phosphate buffer (0.1 M, pH 7.2). The pellet was dried and weighed for determining dry cell mass (DCM). DCM was correlated with OD600 values using the equation: DCM (mg/L) = 303.9 × OD600.

To determine enzyme activity, the cell pellet from the fresh sample was re-suspended in phosphate buffer (0.1 M, pH 7.2), and ultrasonicated at frequencies between 22 and 30 kHz for 10 minutes (30s on and 30s off) on ice. Xylene monooxygenase activity (XMO) was measured with p-xylene as substrate by monitoring the production of p-cresol at 500 nm as described by Arenghi et al., [340]. Catechol 2,3-dioxygenase (C2,3D) activity was determined by measuring the production of 2-hydroxymuconic semialdehyde at 375 nm [261]. One unit of enzyme activity was defined as the amount of enzyme that produced 1 µmol of product per minute. It is noticeable that the enzyme activity of C2,3D was considered for further analysis as this enzyme was the dominant enzyme in the mixture with a higher v_{max} and ease of activity testing compared to XMO.

Biodegradation studies

Batch tests

All batch tests were performed in 150 ml- sealed serum bottles with a Teflon-coated butyl rubber septum and aluminum cap. 10 gr of soil and 5 ml of groundwater samples supplemented with p-xylenes (obtained from ParaChem, QC, Canada) at 15± 1°C, 150 rpm. The tests were also carried out in 150 ml with a 9:1 airspace: liquid ratio sealed with a Teflon rubber stopper containing 25 ml of reaction volume. As p-xylene is considered a highly volatile compound; only about 50 to 60% of the concentration added can be detected in the liquid phase. The concentration in the liquid phase was measured and the needed concentration was compensated to correct the detection results.

Soil column tests

The soil samples used for column test experiments were provided by the company Inc., (our industrial partner). Sieving analysis was carried out according to the ASTM D422-63 procedure [303] for grain size distribution analysis. The size of particles between 250 µm and 2 mm was used for column tests. The soil samples were homogenized and dried at 60°C for 24h to remove the moisture. The soil samples were originally contaminated with p-xylene and have been artificially contaminated with pure p-xylene until an initial concentration of 10,000 mg/kg (average concentration in site).

The soil columns (1.9 cm in diameter and 14.4 cm in length, 163 mL)) with a bulk soil density of 1.8±0.02 g/cm^3 were used and each set had two replicates. Columns were consisting of a stainless-steel cylinder (2 mm thick)**,** clamped between PTFE (Teflon©) endplates retaining a Teflon reservoir for fluid distribution at both ends. To avoid particle losses, one stainless-steel mesh was inserted at both the inlet and outlet ends of the column, and two Vitton© O-rings were used to seal the cylinder with the endplates.

Column packing and water saturation were carried out according to Martel and Gélinas [442]. Briefly, dry packing was carried out using pouring discrete soil portions (with a spoon) into the column and then mechanically pressed with a plunger. The soil portions were deposited in layers of 1 cm and each layer was artificially contaminated with p-xylene using a micropipette of 100 µL to a final concentration of 10,000 mg/kg of soil. To ensure hydraulic connectivity between the layers, lightly scarifying the soil surface (0.5 cm of each layer) was carried out after compaction and before the addition of another layer. This procedure was repeated several times until the top of the soil column was reached. A total of 11 soil columns were prepared to run a total of 6 different experiments, which are shown in Table 6.2. CO_2 was circulated through the columns at a pressure of 4 psi for 30 min to flush entrapped air out of soil pores. Unlike air, CO_2 is a water-soluble gas, and its bubbles can quickly dissolve in water. The columns were saturated overnight with deaerated water (approximately 5 pore volume) flowing from bottom to top using a peristaltic pump (2 ml/min) to eliminate CO_2.

The saturated packed columns were weighed and the volume of pores (PV) in each column was measured according to Eq. (1):

$$PV = m_1 - m_2 - m_3 \qquad \text{Eq.(1)}$$

Where, m_1, m_2 and m_3 are the fully water-saturated soil column mass, the mass of water in both ends of the column (inflow and outflow reservoirs) (at time of water injection), and the mass of the dry soil packed column respectively. The conversion of the mass of water into volume was assumed at ambient temperature to calculate the porosity. The bulk density of the soil after packing was 1.8 ±0.02 g/cm^3.

The experiments described in Table 6.2 involved the injection of the different types of enzyme solution through the initially water-saturated column. The solutions were injected from the bottom

up into the column where they displaced the residents water. Injection was carried out until column effluents reached the same enzyme activity as the inlow solution. A conservatice tracer (Br^-, concentration of 100 mg/L) was also used in the enzyme solutions to monitor the advection/dispersion properties of the enzyme solution during the injection process. To monitor the breakthrough concentration of the column effluents, 5 mL samples of the effluents were collected at regular intervals to determine the enzyme activity and the tracer breakthrough (Br^- concentration). Usually, 10 U/mL of XMO and 15 U/mL of C2,3D (1:1.5) were added to the degradation media.

Table 6.2. Soil column treatment

Soil column No.	Experimental properties	Treatment duration	Description
1	Untreated soil column	0h	As a control for determination of the initial concentration of the contaminant
2	Autoclaved soil column	4 weeks	As a sterile control for the determination of abiotic natural biodegradation rate
3		8 weeks	
4	Untreated soil column	4 weeks	As a control for the determination of natural attenuation rate
5		8 weeks	
6	Treated soil column with enzyme concentration X	4 weeks	X corresponds to a concentration of the enzyme mixture (XMO of about 20 U/mL and a crude C2,3D of about 40 U/mL).
7		8 weeks (with a 2nd enzyme injection after 4 weeks)	
8	Treated soil column with enzyme concentration X/5	4 weeks	X/5 corresponds to 5 times dilution of the enzyme mixture
9		8 weeks (with a 2nd enzyme injection after 4 weeks)	
10	Treated soil column with enzyme concentration X/10	4 weeks	X/10 corresponds to 10 times dilution of the enzyme mixture
11		8 weeks (with a 2nd enzyme injection after 4 weeks)	

The soil column tests were carried out in total either 4 or 8 weeks at 15±1°C (the average annual temperature at the site). For selected experiments, the enzyme injections were repeated after 4 weeks (Table 6.2). The time interval between injections 1 (t = 0 week) and 2 (t = 4 weeks) was established based on the enzyme stability tests.

Soil tank tests

An intermediate-scale experiment was conducted in the laboratory to test the performance of enzyme solutions for the remediation of p-xylene contaminated soil in an environment representative of field-like conditions, but where laboratory control still ensured the ability to conduct proper mass-balance determination. Field-like features provided by the intermediate scale model are the following: large soil volume with heterogeneities in the distribution of the contaminant, soil that did not undergo previous treatment such as drying or sieving, a 3-D environment with 3-D advection/dispersion controlled flow, the presence of a saturated zone, an unsaturated zone as well as a capillary fringe, the initial presence of a layer of free-phase p-xylene, and the ability to mimic the seasonal fluctuations of the groundwater table. Moreover, as illustrated on Fig. 6. 1, the sand tank represents 1/8th of a 5-spot pattern consisting of 1 injection well at the center of the pattern, and 1 extraction well at each corner of the square pattern. In the soil remediation industry, five-spot patterns are one of the patterns typically used for the radial injections of reactive in the soil such as surfactants [442].

The triangular stainless-steel tank with an internal volume of 4 m^3 was filled with uncontaminated humid soil collected from the experimental site provided by TechnoRem (our industrial partner) in a way that was representative of the soil layering encountered at the site, which is characterized by heterogeneous backfilled material (the experimental site consists of a former p-xylene storage facility located in a port along a major river). The soil corresponds to medium sand with silt and

gravel (d_{50} = 1.5 mm; d_{10} = 0.1 mm). The properties of the soil tank are presented in Table 6.3 and schematically depicted in Fig. 6.1. The well layout inside the tank included injection and extraction wells (0.05 m in diameter, IW1, and EW1) and 2 observation wells (0.05 m in diameter: OW1 and OW2). For all wells, standard PVC pipes with #10-slot size screens (0.3 mm) were used and extended from the base of the tank to 0.20 m below the soil surface.

Following the saturation of the model from the bottom up using tap water, a tracer test with bromide used as a conservative tracer was performed to measure the advection/dispersion properties of the 3-D model and characterize the tracer breakthrough curves. The displacement of the tracer solution inside the tank was constantly monitored with an electrical conductivity probe (YSI probe model 556), including at the outlet. A total volume of 400L of tracer solution was injected into the tank.

The soil was then contaminated with p-xylene obtained from Chemco inc. (Quebec, Canada) as described by Robert (2015). Briefly, p-xylene was injected with peristaltic pumps inside all observation and injection/extraction wells, at the top of the water table which was previously set at 0.5 m above the tank base, at a flow rate of 0.5 L/min per well. Then the water table level was increased and decreased periodically between elevations of 0.5 m to 1.0 m above the tank base to ensure that p-xylene went through all the soil layers [443]. This approach mimicked a p-xylene spill flowed by natural fluctuations of the groundwater table. A plastic cover was anchored in place on top of the soil and sealed to the inner walls of the tank to prevent p-xylene losses due to evaporation/volatilisation. After 3 cycles of groundwater table fluctuation, excess p-xylene was pumped out of the tank using peristaltic pumps.

Table 6.3. Soil tank characteristics

Soil volume	Soil thickness	Soil mass	Dry soil density	Total soil porosity
3.3 m^3	1.48 m	6541 kg	1978 kg/m^3	0.342

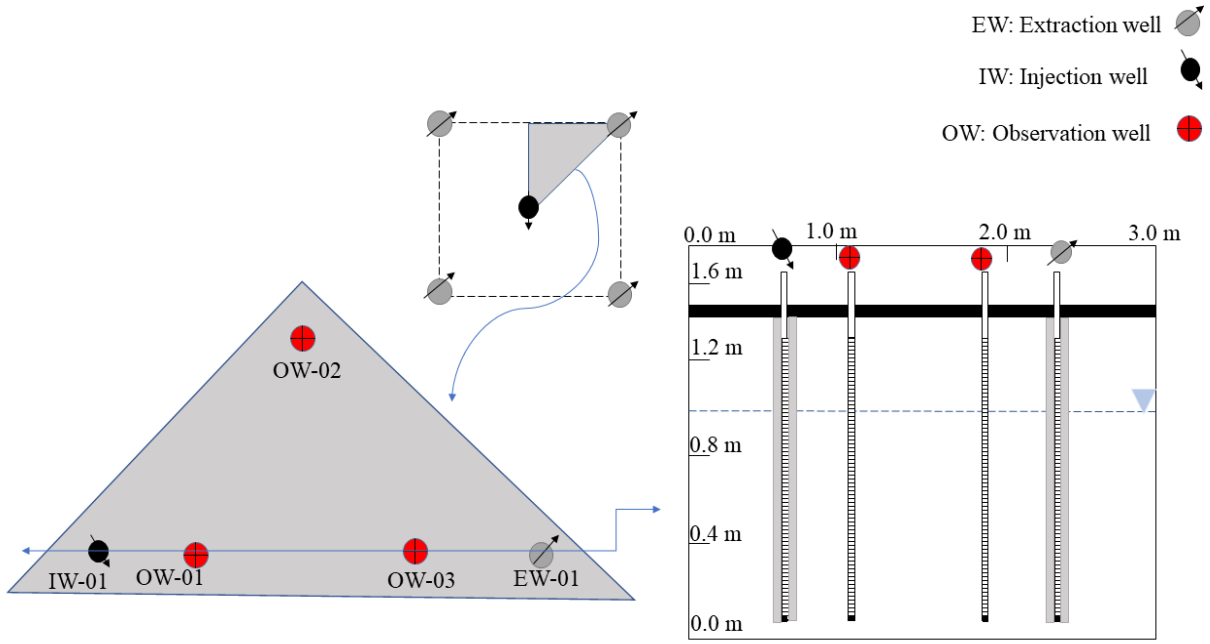

Fig. 6.1. Soil tank plan view and layout, IW: Injection well, EW: Extraction Wells, OW: Observation wells. The cross-section illustrates that injection, extraction and observation wells are screened across the entire thickness of the saturated zone.

Enzyme solution injection

In this pilot-scale study, three different injection scenarios were tested as described in Table 6.4. For each scenario, concentrated enzyme solution was diluted to the desired volume using tap water in a 1000 L HDPE reservoir. Based on our column test studies, the enzyme solution used for scenarios 1 and 2 contained about 10 U/mL of XMO and 20 U/mL of C2,3D could be diluted 5 times (X/5). For scenario 3, the enzyme solution was not diluted. During all injections, the solution in the reservoir was mixed every half hour to ensure uniformity of the enzyme distribution.

For scenarios 1 and 2, the tests were carried out with the top of the water table initially at 1,10 m above the base of the tank (the top of the soil layer is at an elevation of 1.48 m above the base of the tank). For those scenarios, contaminated p-xylene soil was located mostly below the groundwater table. Also, our previous results showed that the injection of around 3 pore volumes

is needed to saturate the packed soil [415]. A total of 1050 L of enzyme solution was injected into the tank via the injection well using a peristaltic pump at an average flow rate of 1 L/min. Another peristaltic pump was used at the extraction well of the tank and was retrieving water/enzyme solution at the same flow rate to ensure steady-state conditions throughout the test (meaning the groundwater table was kept at a constant elevation in the tank).

For scenario 3, the water level in the sand tank was lowered to an average elevation of 26.0 cm above the bottom of the tank before the injection of the enzyme solution. The purpose of this scenario was to test another injection strategy where the contaminated soil manual stainless steel is initially dewatered to reduce the dilution of the enzyme with resident pore water following its injection, promote better contact between the contaminated soil and the enzymes, and to supply some oxygen into the treatment zone before the injection of the enzyme solution. The solution was injected at an average flow rate of 1 L/min simultaneously into the injection/extraction wells.

Table 6.4. Injection strategies for introducing enzyme solution into the soil tank

Experiment	Injection volume (Pore volume)	Dilution factor	Injection method	Additive for enzyme solution
Scenario 1	3PV	X/5	Circulation (Injection through IW and extraction from EW until soil tank saturation)	NO additive
Scenario 2	3PV	X/5	Circulation	Triton X-100 (1% v/v)
Scenario 3	1PV	X	Direct injection (Injection through IW and EW without extraction)	0.1% $FeSO_4$

Sampling and analysis

Soil samples were collected at several locations before, in between and at the end of carrying out the 3 tests (Fig. 6.2). Initial conditions before the injection of the first enzyme solution were obtained with soil samples collected at locations F1, F2 and F3 on the map. Details about which soil core was performed after which injection are reported in the result section. At each location, the soil was collected between depths of 0.0 to 0.4 m, 0.4 to 0.7 m, 0.7 to 1.0 m, and 1.0 to 1.4 m using a 0.05 cm in diameter manual stainless steel coring device between depths 0.0 to 0.4 m, 0.4 to 0.7 m, 0.7 to 1.0 m, and 1.0 to 1.4 m using manual stainless steel cores (Fig. 6.2). The corer was clean between each sampling location and depth using methanol and water. The soil samples from each depth (e.g., 0.0 -0.4m) were mixed and subsamples when analyzed for p-xylene concentrations. In a 40 mL headspace vial containing 10 mL of methanol as the extracting solvent, approximately 0.05 g of soil was placed and vortexed for five minutes. Soil analyses was performed by a commercial government-accredited laboratory (Bureau Veritas, lab method STL SOP-00145, analysis method MA.400-COV 2.0). Groundwater samples collected for the analysis pf bromide and enzyme activity were collected using a peristaltic pump. The intake of the inflow line to the pump (6.4 mm PTFE tubing) was positioned in the center of the screened interval of each sampled well. Approximately 0.2 L of water was purged prior to collecting the sample.

Bromide analysis was done using a previously calibrated Orion bromide-specific electrode**.** Enzyme activity was determined as described above.

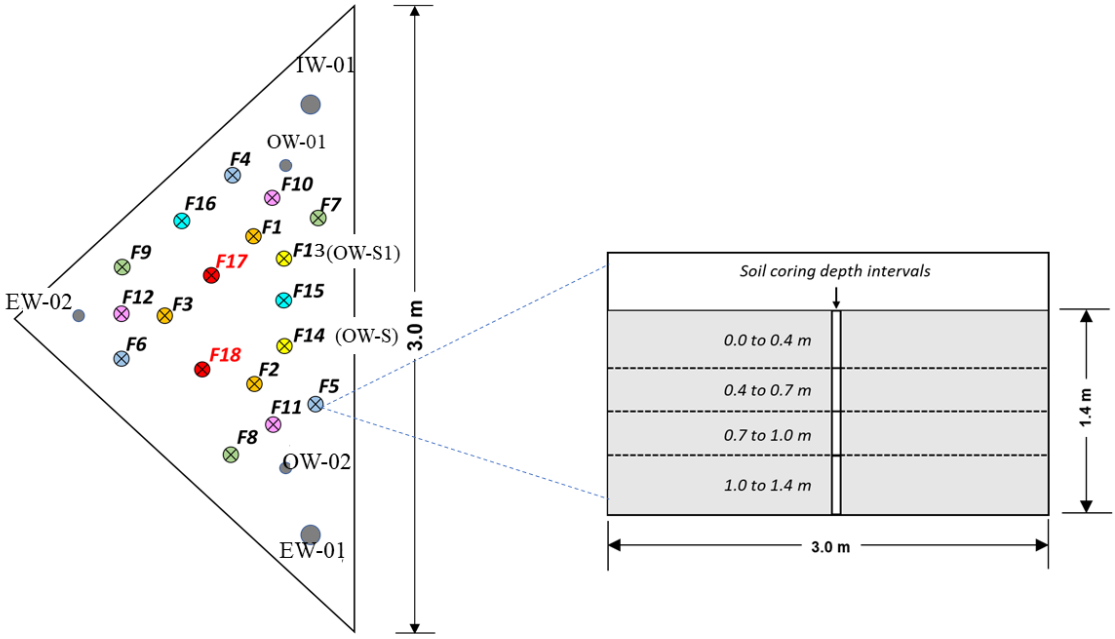

Fig. 6.2. Plan view (left) and cross-sectional view (right) of soil sampling locations in the sand tank studies.

Microbial community analysis

DNA in the mixed soil samples from the soil tank was extracted and purified using MoBio PowerMag Soil DNA Isolation Kit according to manufacturer protocol. A 20 ng of each sample DNA was used for a PCR reaction**.** The V4 region primers 515F- GTGYCAGCMGCCGCGGTAA and GGACTACNVGGGTWTCTAAT were used for amplifying the 16s rRNA genes. Sequencing was then performed using an Illumina Miseq platform according to the manufacturer's instructions, at Metagenomics Facility at McMaster University, Canada. Sequences from pyrosequencing were analyzed primarily with Illumina's Casava software and then the output sequences were clustered to operational taxonomic units (OUT) [444]. Data were screened with the BLAST program (www.ncbi.nlm.nih.gov) and then visualized by MicrobiomeAnalyst-comprehensive statistical (www.microbiomeanalyst.ca).

Statical analysis

Biological tests were performed in triplicates. For the soil analysis, duplicate samples were collected on 10% of the samples, as recommended by the Ministry of the environment for field sampling procedures. Data are presented as a mean ± standard deviation (SD). ANOVA analysis followed by Tukey posthoc procedure was used to determine the differences between test groups at a significance level of $p<0.05$.

6.3. Results and Discussion

Screening of isolated bacteria

The results from p-xylene degradation showed that 4 strains of isolated bacteria can grow on p-xylene as the sole source of carbon at 5 ºC ±0.05 ºC (Fig. 6.3A). These strains (isolates 6, 9, 15, and 16) showed the highest p-xylene degradation ability. At higher temperatures, the results showed that most of the isolated bacteria can degrade p-xylene at 10 and 25 ±0.05 ºC, thus these bacteria are all mesophilic bacteria and four strains (isolates 6, 9, 15, and 16) are cold-adapted strains and can be used for further studies. Santiago et al. (2016) reviewed cold-active enzymes isolated from different microorganisms with an interesting enzymatic activity. Interestingly, they mention that although most cold-active enzymes have been isolated from psychrophiles and psychrotolerant microorganisms, some enzymes with high activity at low temperatures have been obtained from mesophilic and even thermophilic microorganisms [436]. It is surprising to discover cold-active enzymes from mesophilic organisms but there are good examples of cold-active enzymes isolated from mesophilic organisms such as cold-active lipase from *Candida albicans* [445], cold-active β-amylase from *Arabidopsis*, and thermophilic and cold-active β-galactosidase isolated from *Pyrococcus furiosus* [64].

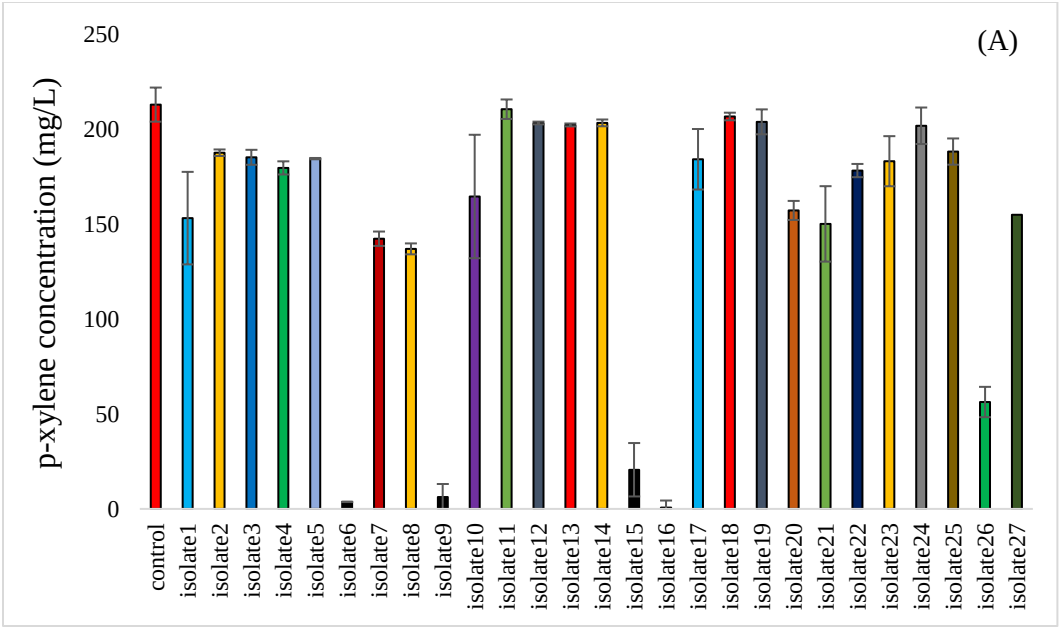
(A)
p-xylene concentration (mg/L)
250
200
150
100
50
0
control
isolate1
isolate2
isolate3
isolate4
isolate5
isolate6
isolate7
isolate8
isolate9
isolate10
isolate11
isolate12
isolate13
isolate14
isolate15
isolate16
isolate17
isolate18
isolate19
isolate20
isolate21
isolate22
isolate23
isolate24
isolate25
isolate26
isolate27

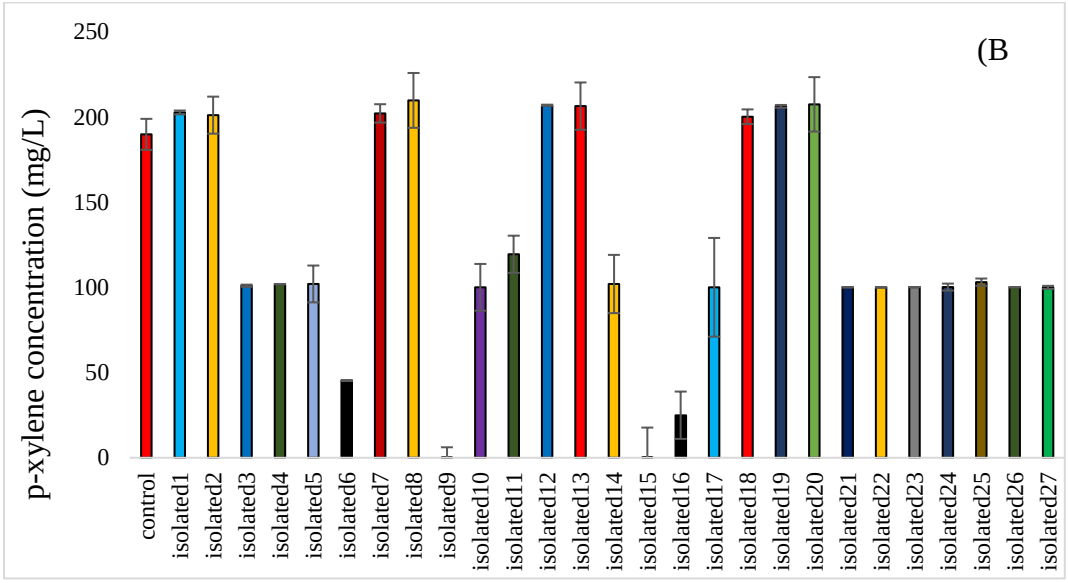
(B
p-xylene concentration (mg/L)
250
200
150
100
50
0
control
isolated1
isolated2
isolated3
isolated4
isolated5
isolated6
isolated7
isolated8
isolated9
isolated10
isolated11
isolated12
isolated13
isolated14
isolated15
isolated16
isolated17
isolated18
isolated19
isolated20
isolated21
isolated22
isolated23
isolated24
isolated25
isolated26
isolated27

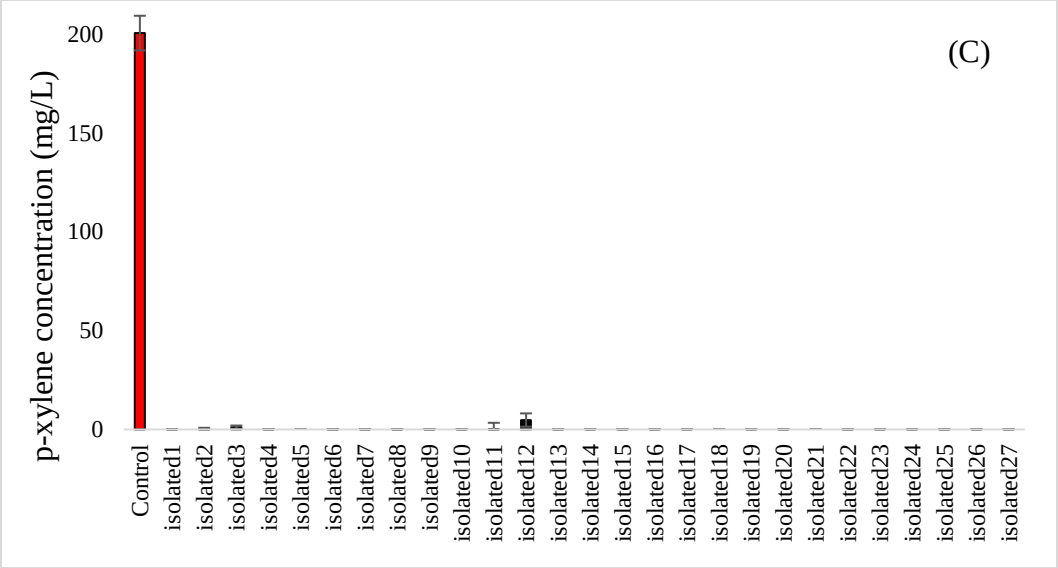

Fig. 6.3. Biodegradation of p-xylene by isolated bacterial strains A) biodegradation test at 5 ºC, B) biodegradation test at 10 ºC, and C) biodegradation test at 25 ºC

Identification of p-xylene degrader

S2TR-06 was selected among all the isolates tested because of its ability to grow rapidly on p-xylene as a sole carbon source at 4 ºC. After growing on TSA for 3 days at 4 ºC, the following colony morphologies were observed: yellow, smooth, and raised with a circular shape. The partial 16S rRNA sequencing showed that S2TR-06 was close to the type strains of *Arthrobacter psychrochitiniphilus* strain GP3^{T} and *Arthrobacter ramosus* NRRL B-3159^{T}, with 97.62% and 96.68 % identity respectively. Phylogenetic analysis showed that strain S2TR-06 was grouped with members of the genus *Arthrobacter* and formed a distinct cluster with the strains of *A. psychrochitiniphilus* CB2015-323-DE-0554 (96 % 16S rRNA gene sequence similarity) and *A. alpinus* strain UICS2-7-1 (96.46 %) in the neighbor-joining tree (Fig. 6.4). Levels of 16S rRNA gene sequence similarity between strain S2TR-06 and the known strains recognized *Arthrobacter* species were also <98.0 %. Biochemical characterization also differentiated strain S2TR-06 from the type strains of *Arthrobacter ramosus* NRRL B-3159^{T} (Fig. 6.4B). For example, growth of S2TR-06 is absent at 37 °C, with the fastest growth at 15–25 °C, while *Arthrobacter ramosus*

NRRL B-3159^T showed different growth abilities at those temperatures. Based on the phylogenetic and phenotypic evidence presented in Fig.6.4, strain S2TR-06 is considered to represent a novel species of the genus *Arthrobacter*, for which we propose the name *Arthrobacter* sp. S2TR-06. The sequence of the 16S ribosomal RNA gene for S2TR-06 has been deposited in the NCBI Genbank database and was assigned the accession of MN203655.1.

A variety of strains of the genus *Arthrobacter* have been isolated from a variety of sources; several of these strains are psychrophilic, which allows them to survive at low temperatures. It has been reported that *Arthrobacter psychrophenolicus* and *Arthrobacter chlorophenolicus* are useful for bioremediation in cold climates, due to their ability to degrade phenolic compounds at low temperatures [446]. *Arthrobacter alpinus* sp. nov. was first isolated by Zhang et al., (2010) from alpine soil that showed psychrophilic characterization and different phenotypic characteristics with *Arthrobacter* species strains [252].

(A)

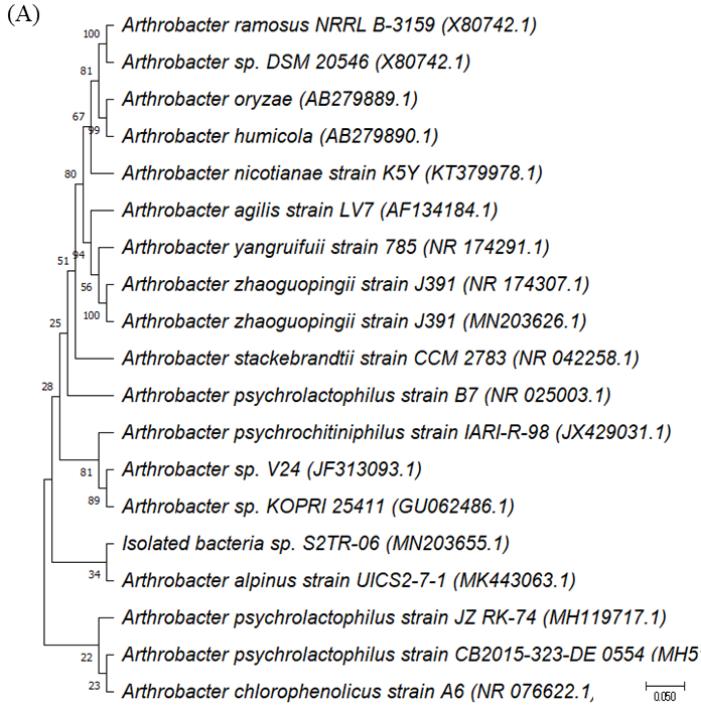

(B)

Biochemical characteristics	S2TR-06	*Arthrobacter ramosus* (NRRL B-3159^T)
Color of colony	Y	Y
Motility	-	-
Growth at 37 °C	-	+
Growth at <10 °C	+	-
Catalase	+	+
H_2S production	-	-
Urease	-	-
Indole test	-	-
Gelatinase	-	-
Citrate	-	-
Nitrate reduction	+	-
α-Glucosidase	+	+
β-Galactosidase	+	+
β-Glucuronidase	+	+

Fig. 6.4. Phylogenetic position of the isolated strain in comparison with related *Arthrobacter* species based on neighbor-joining analysis of 16S rRNA gene sequences (A), Biochemical characteristics of S2TR-06 and *Arthrobacter ramosus* NRRL B-3159^T (B), Y: Yellow, +: positive, -: negative

Identification of the pathway

Based on degradation results, *Arthrobacter* sp. strain S2TR-16 (isolated bacteria) can use p-xylene as a sole carbon source thus this bacterium was selected for further studies. To determine the pathway for degradation of p-xylene by *Arthrobacter* sp. strain S2TR-06, possible involved enzymes (such as esterase, lipase, xylene monooxygenase, xylene dioxygenase, catechol 1,2-dioxygenase, and catechol 2,3-dioxygenase) were analyzed. The intermediates produced in the presence of selected bacteria were determined (Fig. 6.5). The results showed that xylene monooxygenase was able to transform p-xylene into a p-cresol intermediate. Catechol 2, 3-dioxygenase are needed for ring cleavage of p-cresol. This study indicated that catechol 2, 3-dioxygenase represents the bottleneck for *p*-xylene co-metabolism, and the lack of its expression leads to the accumulation of intermediates and inhibits its complete mineralization in p-xylene metabolism. Our previous study showed that the p-xylene metabolism depends on catabolic genes and the different p-xylene metabolism of various isolated bacteria can be explained by the expression of the ring cleavage enzyme and its encoded gene (*xylE*) and activator (*xylS*) [323].

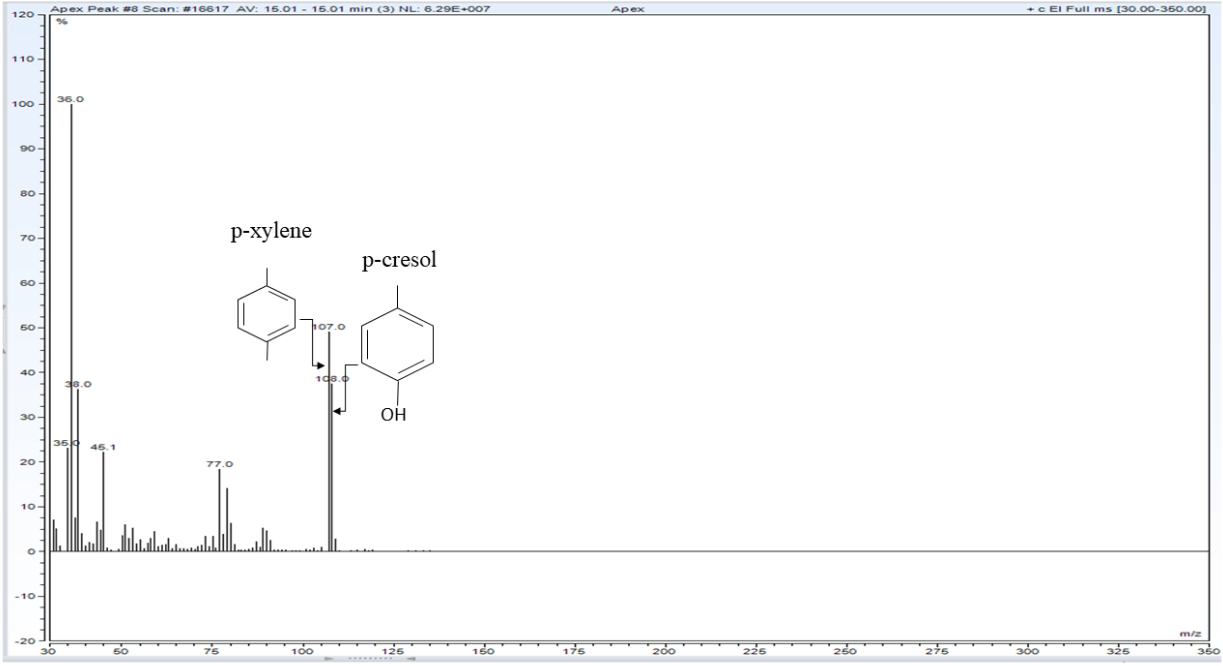

Fig. 6.5. Mass spectrum for central intermediates in presence of p-xylene

Effect of different inducers on XMO and C2,3D production

The chemical composition of inducers has a significant impact on enzyme production and BTEX compounds induce oxygenase production in degrading bacteria. Despite a similar aromatic structure of BTEX compounds, they have different effects on the expression of the involved enzymes and their encoding genes [323]. Consequently, differences in oxygenase production in response to different inducers are expected. In addition, catechol as an important intermediate in aerobic biodegradation of a variety of aromatic compounds also was selected for the study of its effect on enzyme production [447]. The biomass, XMO, and C2,3D activities produced with the different inducers are shown in Fig. 6.6. Significant differences were observed in biomass production after 18h of incubation using different inducers. The biomass results showed that the presence of p-xylene did not inhibit the growth of bacteria compared to the control test containing standard media without any inducer (Fig. 6.6a). XMO activity was lower than 5 U/mL when using benzene, toluene, and catechol as an inducer. XMO and C2,3D activities were 6 U/ml and 15 U/mL

in the presence of p-xylene after 6 h of incubation (Fig. 6.6b and 6.6c). Although catechol could induce C2,3D up to 18 U/ml, XMO activity was less than 2U/mL in the presence of catechol. The presence of both enzymes in the mixture is needed for complete detoxification of p-xylene at the contaminated site. This result demonstrated that p-xylene can induce the production of XMO and C2,3D without any inhibition effect on bacterial growth. Aravind et al., (2020) reported that *Paracoccus* sp. MKU1 exhibits a constitutive expression of gene clusters that correspond to interradial (catechol 1,2 dioxygenase) and extra radial cleavage (catechol 2,3 dioxygenase) and their expression is significantly increased in the presence of catechol in a concentration-dependent manner. According to their results, mRNA levels of catechol 2,3 dioxygenase were ~1.9-fold higher in glucose-containing cultures than catechol 1,2 dioxygenase, and ~2.1-fold higher in catechol-induced cultures of *Paracoccus* sp. MKU1 [448].

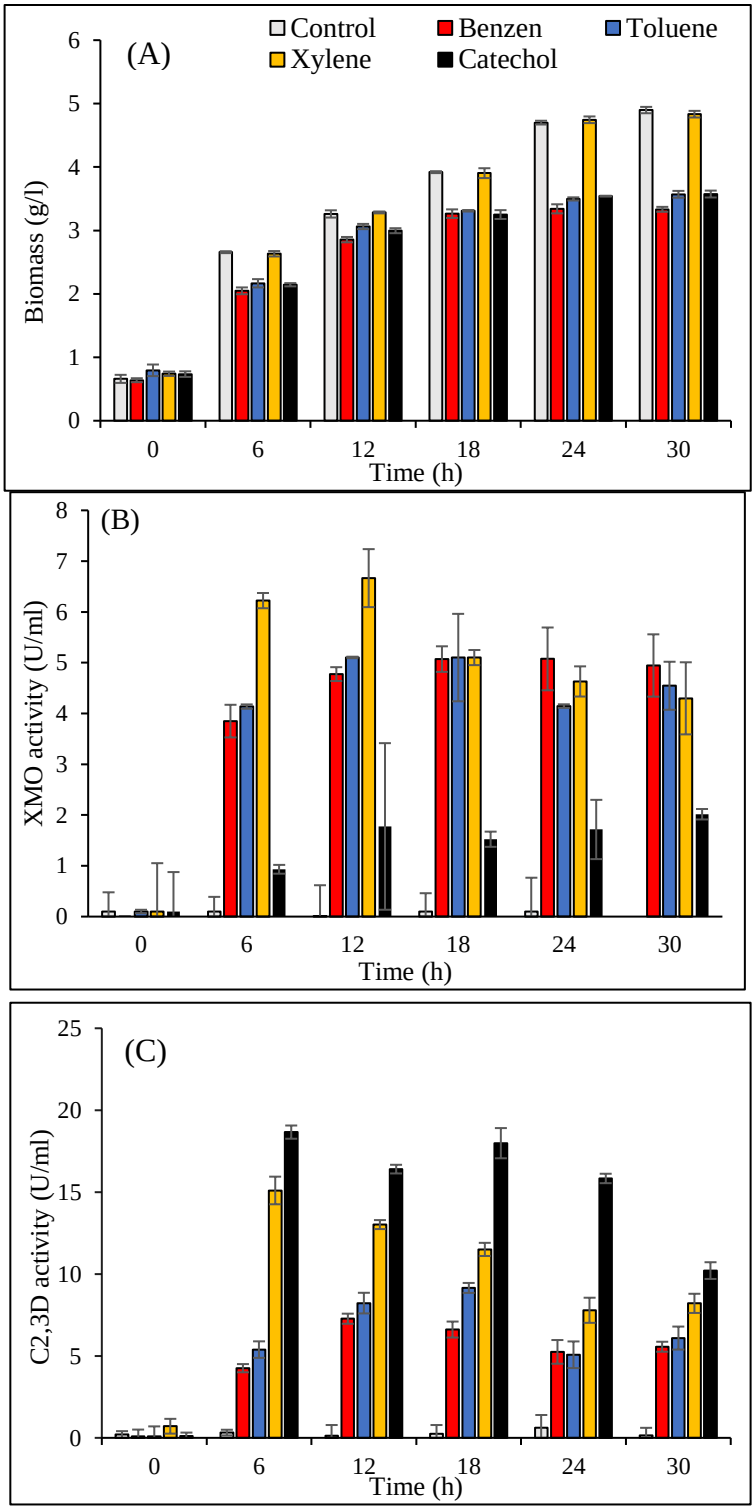

Fig. 6.6. Effects of different inducers on the production of: biomass (A), XMO (B) and C2,3D (C) in batch experiments.

Effect of different concentrations of the inducer

The effects of different concentrations of p-xylene (50, 100, and 200 mg/L) on enzyme production were determined using standard media. Fig. 6.7. shows the effects of p-xylene concentration on biomass and XMO and C2,3 D activities. As Fig. 6.7. shown, XMO and C2,3D activities (7± 1 U/ml and 17± 2 U/ml) at a p-xylene concentration of 100 mg/L after 6h of incubation were significantly greater than those of 50 and 200 mg/L. As expected, a high concentration of p-xylene (200 mg/L) can inhibit growth and enzyme production. Generally, petroleum hydrocarbons have caused toxic effects on bacterial growth and inhibited their activity due to their chemical composition. Bühler et al., (2002) showed that there is a close relationship between the toxicities of substrates (e.g., xylene) and products (e.g., alcohols and aldehydes) that can be indicative of a possible application of XMO in recombinant *E. coli*. They also showed that unoxidized substrates inhibit the second and third oxygenation steps of XMO as a multistep biocatalyst [440].

The results of time-course experiments showed that biomass increased over time however enzyme activities decreased over time. This was due to p-xylene depletion over the time of fermentation. Based on this, 6h was selected for continuous or multi-pulse addition of p-xylene. Similarly, Aravind et al. (2020) showed that the mRNA expression levels of catechol 1,2 dioxygenase were increased by 1.5 and 1.7 folds with the addition of catechol at the concentrations of 50 and 100 mg/L, respectively, while catechol at a concentration of 200 mg/L strongly inhibited catechol 1,2 dioxygenase expression[448].

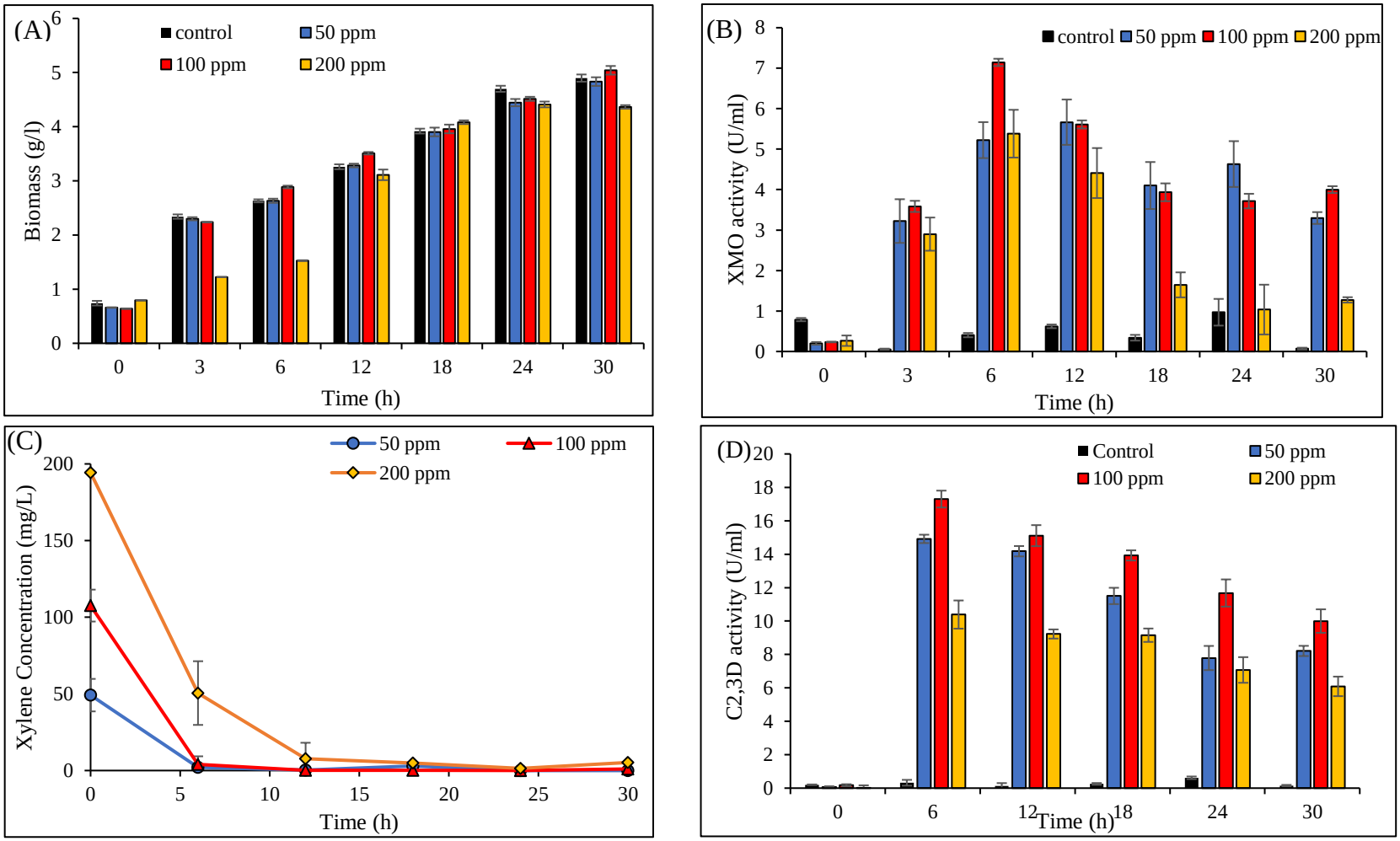

Fig. 6. 7. The effect of different concentrations of p-xylene (50, 100 and 200 mg/L) on production of biomass (A), XMO (B), C2,3D (D), and xylene concentration during batch experiments (C).

Enzyme production in bioreactors

5-L Bioreactor

The production of xylene monooxygenase and catechol 2,3-dioxygenase was carried out in batch and feed-batch mode by inducing p-xylene each 6h of fermentation (multi-pulse injection of inducer). Injection of 100 mg/L p-xylene into the production medium (each 6h) increased the activities to around 20 U/mg of xylene monooxygenase and 30U/mg of catechol 2,3-dioxygenase in 24h of fermentation time (Fig. 6.8). The results confirmed that the fed-batch fermentation mode can increase enzyme production by around 3-fold compared to batch mode. The time course profiles of the enzyme activities, cell growth, dissolved oxygen, and p-xylene concentration are shown in Fig. 6.8. The pH value did not show any changes during the fermentation (the value range was between 7.1 and 7.3). The agitation speed and aeration level were monitored during fermentation depending on the dissolved (DO). The results showed that DO decreased significantly in 3 h after each injection which was consistent with a high p-xylene degradation rate. The productivities of enzyme production and p-xylene degradation increased at 24h when the biomass growth reached to stationary phase. To the best of our knowledge, no study is available on the fermentation study of these enzymes. Although some studies reported the expression and production of these enzymes in genetically engineered bacteria or using these enzymes as whole-cell biocatalysts, there is no research on the production of XMO and C2,3D from native microorganisms in bioreactors. For instance, Luo & Lee, (2017) designed and cloned metabolic genes including XMO into *Escherichia coli* for converting p-xylene to terephthalic acid. According to their results from the two-phase fermentation process, terephthalic acid production can be improved by increasing the OD600 value before induction and p-xylene feeding [449].

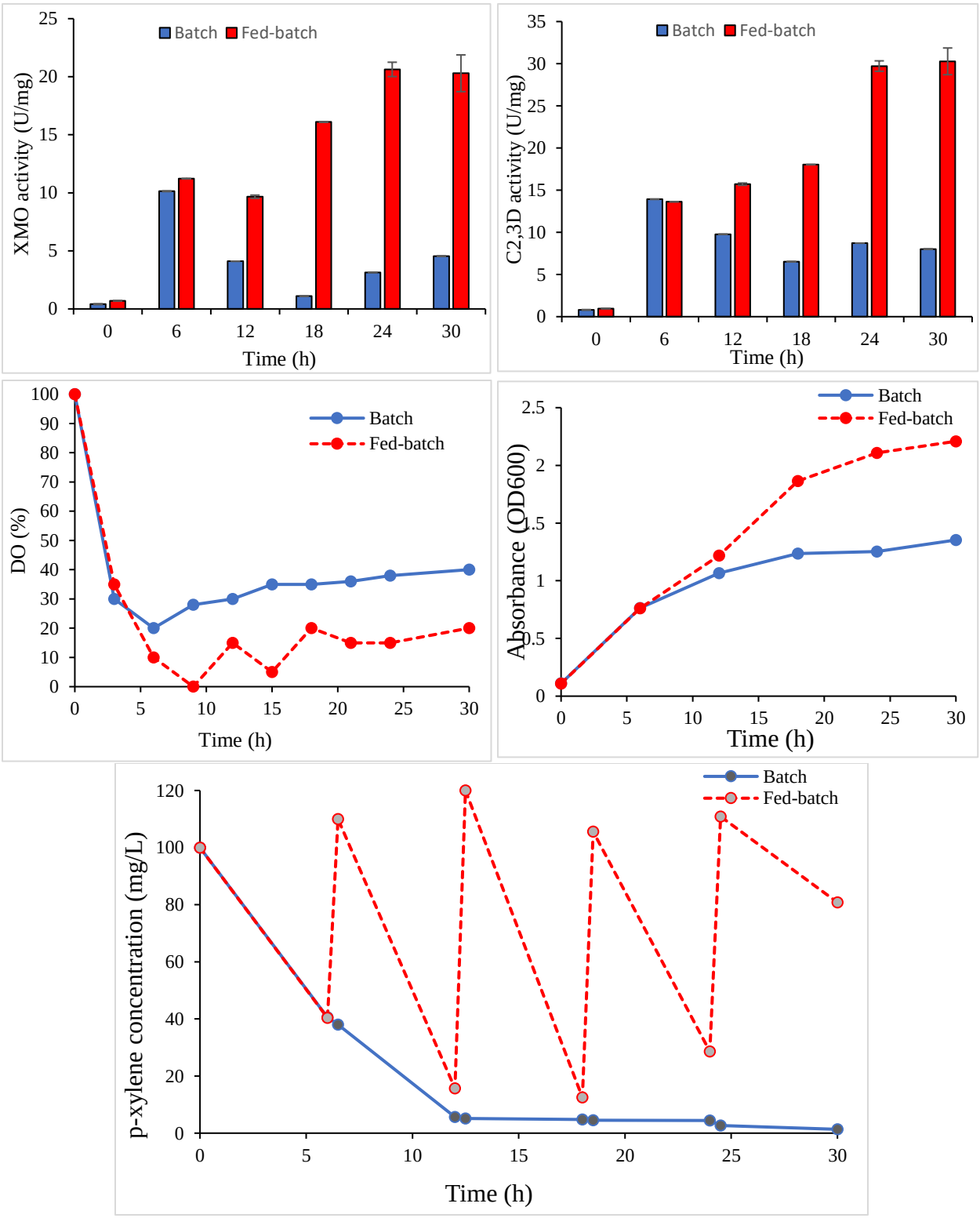

Fig. 6.8. Xylene monooxygenase (XMO) and catechol 2,3-dioxygenase (C2,3D) activity profile, cell growth, dissolved oxygen, and p-xylene concentration in 5-L bioreactor

15-L Bioreactor

Based on our results from 5-L bioreactor studies, 100 mg/L of p-xylene and 6h were selected for induction of enzyme production at each time interval. The scale-up of enzyme production was conducted from a 5-L stirred-tank bioreactor to 15-L bioreactor with a working volume of 10L to investigate the performance of enzyme production in bioreactors. The results showed that multi-pulse induction at 6h intervals could be a better option to further enhance the production of XMO and C2,3D, because of the relatively lower concentrations of p-xylene at each 6h compared to continuous induction and the inhibition of high concentrations of p-xylene in continuous induction mode. Although no report on the production of these target enzymes (XMO and C2,3D) in bioreactors is available, some studies showed that multi-pulse addition of medium can improve the enzyme production using microorganisms. For instance, Liu et al. (2021) reported that multi-pulse fed-batch enhanced the production of lignin peroxidase using a recombinant *Aspergillus nidulans* strain in a 1.5 L stirred-tank bioreactor. They reported that maximum lignin peroxidase activity (1,645 mU/L) was obtained using multi-pulse fed-batch fermentation [308].

Results showed a significant decrease in the DO values during the first stage of fermentation (time 0–24 h) (Fig. 6.9). DO was regulated at 25 %, the minimum required for bacterial cells, by cascade mode of the airflow rate and agitation speed. After the addition of the inducer (p-xylene), a maximum aeration rate up to 95.5% (190 L/min) and agitation reaching 95% (190 rpm) was needed to maintain DO of more than 20%. However, the DO was not able to be maintained above 25% in some stages of the fermentation. After 24 hours, DO was increased by more than 30 %, which indicated that DO can be a signal for substrate depletion and the end of the fermentation time. This high oxygen requirement was due to oxidation and degradation of p-xylene along with biomass production. Nielsen et al., (2006) estimated the oxygen requirements for biomass production

of *Achromobacter xylosoxidans* during the degradation of both benzene and ethylbenzene. They measured the specific rate of oxygen consumption in presence of benzene (0.041 ± 0.008 mgO_2 mg a cell dry $weight^{-1}$ h^{-1}) and ethylbenzene (0.053 ± 0.022 mgO_2 mg a cell dry $weight^{-1}$ h^{-1}) as sole substrates in a bioscrubber (Nielsen et al., 2006). It is noticeable that the determination of the volumetric mass transfer coefficient (k_La) was not feasible using the dynamic volumetric gassing-out method due to the low DO value during fermentation and when the airflow valve was closed, DO was near 0 in less than 3s. Similarly, Nielsen et al., (2006) suggested using bioscrubber for measurement of microbial O_2 requirements associated with volatile organic compounds degradation instead of a bioreactor [450].

Our results showed that XMO and C2,3D activities increased up to 31 and 44 U/mL after 24h respectively (Fig. 6.9). The production was increased around 4- and 2.5-fold for XMO and C2,3D, when compared to shake flask tests. It has been demonstrated that stirred-tank bioreactors can provide increased mass and heat transfer and aeration compared to shake flasks [451].

Gummadi & Kumar (2008) showed that combined feeding of inducer and carbon source at 12 h enhanced production of pectin lyase and pectate lyase by *Debaryomyces nepalensis* in a 2.4-L bioreactor. They showed that this feeding strategy can increase the productivity of pectin lyase and pectate lyase by 1.2- and 1.4-fold compared to the batch culture [452].

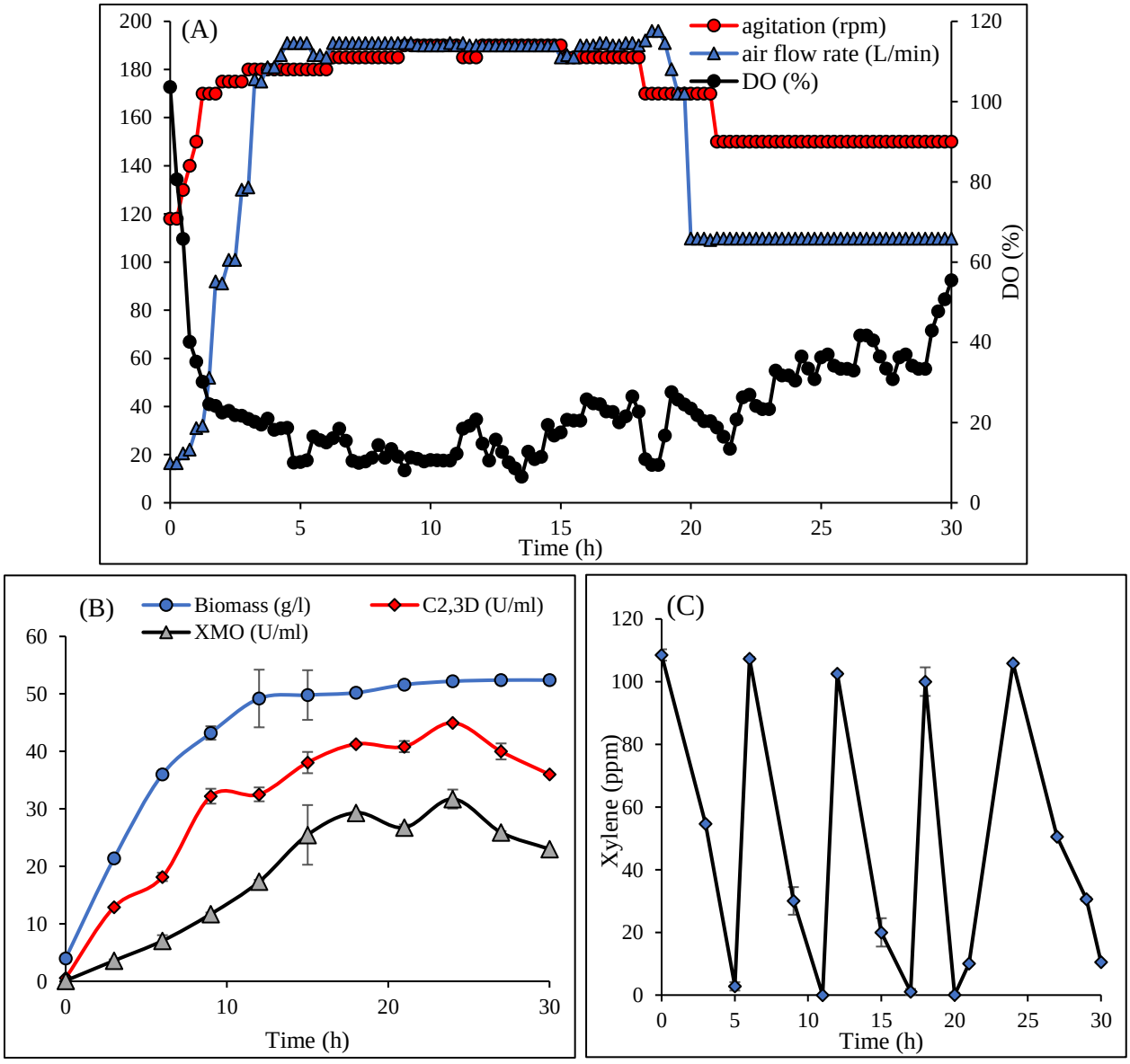

Fig. 6.9. Profile of different fermentation parameters (agitation, air flow rate, and DO) (A), production of XMO, C2,3D, and biomass(B), xylene concentration (C) in 15-L bioreactor

150-L Bioreactor

Pilot-scale is usually considered to be between 50 and 300 liters [453]. In this study, 150-L bioreactors were considered as pilot-scale bioreactors for the production of XMO and C2,3D, where operational conditions, hydrodynamic parameters, and agitation are similar to those in the large-scale production. As mentioned previously, multi-pulse feeding of the inducer (100 mg/L of

p-xylene) at 6h was the best strategy for enhanced production XMO and C2,3D by *A. psychrolactophilus* S2TR-06 in the 15-L bioreactor. Thus, a larger scale of 150-L bioreactor was investigated with the previously selected operational mode. Profiles of fermentation parameters such as aeration, DO, agitation, and production of XMO, C2,3D, and biomass are presented in Fig. 6.10.

As expected, DO values showed a decrease in the first 2h of fermentation, and maximum aeration and agitation were applied to maintain the DO value greater than 25%. In addition to applying maximum aeration and agitation, air pressure was increased in the bioreactor after 3 h of fermentation (Fig. F2). Our results showed that adding pressure inside the jar of the bioreactor increased DO concentration up to 35% during fermentation (Fig. 6.10a). This strategy can be applied to certain aerobic microbial fermentation where the bioreactor tank can tolerate the high air pressure. In this study, a stainless-steel bioreactor was used that can tolerate higher air pressure compared to 15-L glass bioreactors. A study performed by Liu et al. (2016) also found that increasing the total air pressure in the cultivation system increased the oxygen solubility of the liquid medium. They reported that the pure oxygen supplement can be omitted from high-cell-density fermentation of *Pichia pastoris* if the air pressure is increased. Although mixing pure oxygen into the inlet airflow is effective in small-scale fermentation, it is highly expensive and dangerous in large-scale fermentation [26].

According to Fig. 6.11b, *Arthrobacter* sp. S2TR-06 growth started immediately after inoculation and reached its maximum (107 g/l) value at 15h and then followed by a stationary phase. Moreover, maximum XMO and C2,3D activity (109 and 203 U/mL, respectively) was obtained at 21 h of fermentation. Despite similar operating conditions in the 15-L and 150-L bioreactors (similar nutrients, substrate, and inducer concentration), the production of biomass, XMO and

C2,3D were higher in the 150-L bioreactor than in the 15-L bioreactor with maximum values of 52 g/L for biomass, 31 U/mL for XMO and 44 U/mL for C2,3D after 24h. These results demonstrated that a shorter fermentation time and the highest enzyme activities and productions were achieved in a 150-L bioreactor. This could be related to better oxygenation of the 150-L bioreactor and the sensitivity of *A. psychrolactophilus* S2TR-06 towards oxygen limitation, as the minimum DO was higher during fermentation compared to the 15-L bioreactor. However, better aeration, agitation, impeller size, and the ratio height/diameter can influence oxygen transfer in larger scale bioreactors [454]. These results were comparable which found Kadri et al., (2022) who demonstrated the effect of scaling-up on the number of cells, alkane hydroxylase, and lipase produced by *Alcanivorax borkumensis.* They reported that the 150-L fermenter showed a better oxygen transfer rate compared with the bench-scale bioreactors which affected the cell growth that doubled the cell number and enzyme production. Moreover, Ndao et al. (2017) compared the cell count of *Bacillus thuringiensis* in three different bioreactors (15 liters, 150 liters, and 2000 liters). The study concluded that when there is more oxygen supply and transfer, there is more bacterial growth and better performance, which was significant in the 2000-L fermenter [455].

(A

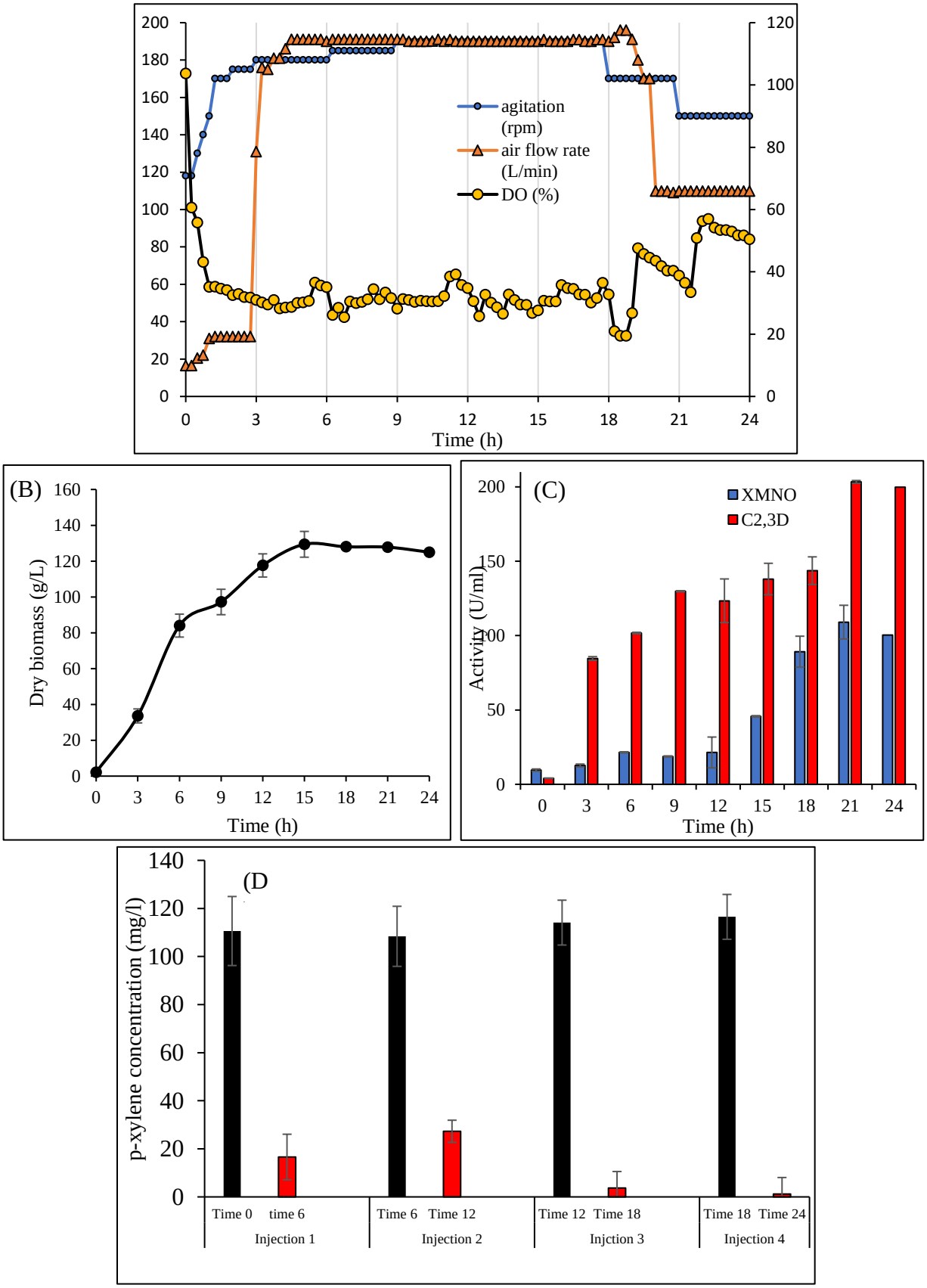

Fig. 6. 10. Profile of different fermentation parameters (agitation, air flow rate, and DO) (A), production of biomass (B), production of XMO, C2,3D (C) in 150 L bioreactor

Enzyme stability

XMO and C2,3D are membrane-bound enzymes and are considered Fe^{2+}-dependent enzymes [456]**.** Since these enzymes require metals as cofactors, predominantly iron (Fe^{3+}, Fe^{2+}) for their catalytic function. In the present study, C2,3D activity showed that the presence of Fe^{2+} increased up to 50% compared to the enzyme activity without any $FeSO_4$ (Table 6.5). The impacts of phospholipids and rhamnolipid were positive on the enzyme activity of C2,3D. These compounds could play a key role as membrane compounds because some hydrophobic interactions between fragments of the polypeptide chain are known to be responsible for maintaining the native structure and catalytic activity of the membrane-bound enzymes [457].

As Fe^{2+} showed significantly higher activity of C2,3D, more experiments were conducted by adding $FeSO_4$ at different concentrations (0.1, 0.5, and 1% v/v) before and after the extraction of enzymes. Our results showed that adding $FeSO_4$ at 0.1% before extraction of enzymes can enhance the activity of both enzymes (XMO and C2,3D) up to 3-folds compared to the control group. Time-course experiments also indicated that more than 60% of activity remained after 90 days. Similarly, Adewale et al., (2021) showed that Fe^{2+} led to a 22-fold increase of catechol 2,3-dioxygenases from a lignin-degrading (*Bacillus ligniniphilus*) [458]. One reason for the lower effect of Fe^{2+} in our study is that a crude enzyme was used in this study while Adewale et al., (2021) purified the enzyme. As purified C2,3D contained very little metal due to the Method reporting limit. It is also possible to explain this observation by the presence of ferredoxin in crude enzyme solution which can bring the iron atom back to the reduced state and activate C2,3D [458]. In addition, our crude enzyme solution contained cold-active proteases which have negative effects on enzyme activity during storage. In this study, the proteolytic activity of the crude enzyme mixture was determined by Kunitz method (1947). Our results showed the presence of 270U/ml

of proteases (proteolytic activity) in the crude enzyme solution. It was documented that autolysis (proteases) promoted changes in the spatial configuration and led to enzyme inactivation [441].

Table 6.5. Effect of chemical additives on C2,3D activity under the storage conditions

Compound	C2,3D Activity		
	As % of control	As % of original activity (after 2 days)	As % of original activity (after 7 days)
Benzyl acetate	54%	32%	14%
$CaCl_2$	101%	83%	75%
$FeSO_4$	150%	100%	100%
Glycerine	101%	97%	22%
Polyethylene glycol	84%	56%	33%
Tween 80	81%	94%	77%
Phospholipids	136%	95%	72%
Rhamnolipid	120%	94%	89%
Triton X-100	100%	98%	85%
Molasses	100%	72%	34%
Boric acid	85%	50%	21%
H_2O_2	36%	11%	0%

Preparation of enzyme powder

Enzyme purification is a costly process and is considered a major cost in the production of enzymes. The high production cost of enzymes has restricted their industrial use for environmental purposes.

As mentioned in the previous section, high proteolytic activity was detected in the enzyme solution under storage conditions and purification of each needed enzyme is not economical for environmental purposes. Therefore, dried and concentrated preparation approaches can be used to lower costs and improve the storage stability of enzymes [459]. For this purpose, montmorillonite and zeolite were used for the physical adsorption of enzymes. The results showed that enzyme adsorption to clay was higher than the zeolite (Table 6.6). The remaining activity of the enzyme (activities relative to the activity at day 0) showed that montmorillonite maintained around 90% of the enzyme activity after 90 days of storage at 4ºC. Similarly, Olagoke et al., (2020) showed that pure montmorillonite adsorbed amylase and supported the high activity of this enzyme at the end of the incubation (100 days). They also mentioned that fewer and weaker bonds between enzymes (amylase and cellulase) and soil minerals result in a smaller impact on the active sites of the enzyme [439].

Table 6.6. Enzyme activity of C2,3D adsorbed to zeolite and clay

Adsorbent	Initial Activity	Storage at RT (Remaining activity, %)			Storage at 4˚C (remaining activity %)		
		30 days	60 days	90 days	30 days	60 days	90 days
Zeolite	3062.6 U/g	2552.3U/g (83%)	1504.5 U/g (49%)	1023.3 U/g (33%)	3052.9 U/g (99%)	2901.6 U/g (95%)	2802.7 U/g (91%)
Clay	3622.3 U/g	3029.9 U/g (83%)	2694.4 U/g (74%)	2054.5 U/g (57%)	3508.2 U/g (96%)	3451.9 U/g (95%)	3289.6 U/g (91%)

Due to the solid nature of soil with different particle sizes, the application of enzyme solution in liquid form for in-situ remediation can be more favorable from an industrial perspective at cold climate sites. Thus, experiments on the release of the adsorbed enzyme to clay were done and the results are presented in Fig. 6.11. The results showed that more than 80% of enzymes can be recovered by water under shaking conditions. As shown in Fig. 6.11, the release of the enzyme

from clay in the presence of buffer is less than in water. Clay-enzyme complexes were more stable in the presence of buffer due to the presence of ions and salts. Haskå (1974) reported that about one gram of montmorillonite (clay) per liter of cell-free culture solution is sufficient to adsorb 97% of the bacteriolytic enzymes (alanyl-e-N-lysine endopeptidase). They also reported that only 40% of enzymes can be eluted using a solution with high ionic strength or high pH [460].

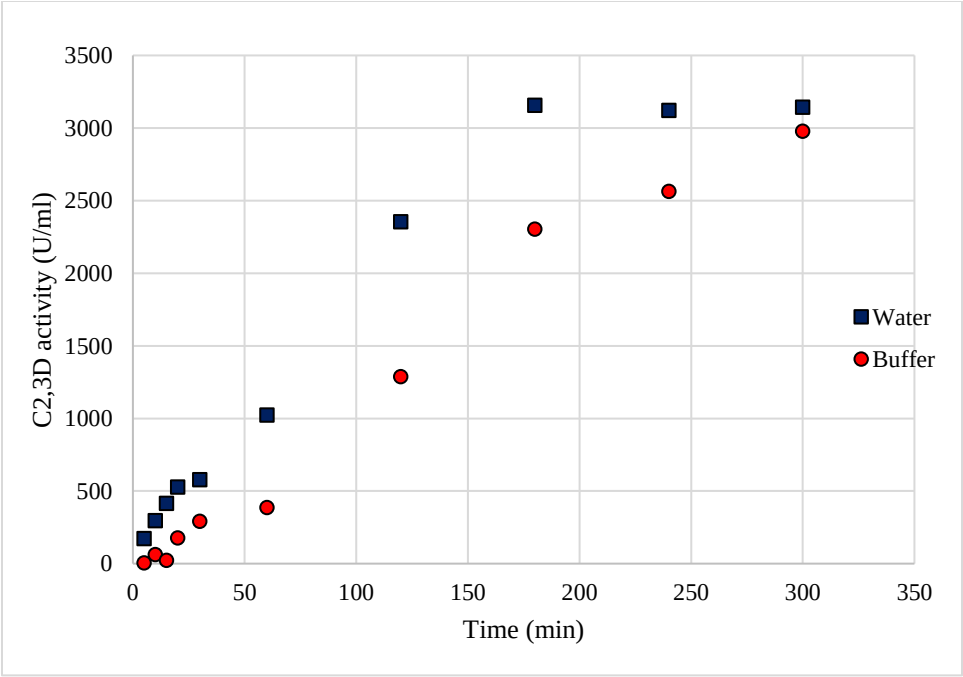

Fig. 6.11. Enzyme recovery from clay in the presence of water and buffer under shaking conditions

Biodegradation scale-up

Soil batch tests

The feasibility of enzymatic biodegradation of p-xylene was first evaluated in batch tests using soil and water samples from the contaminated site. All tests were done in triplicates, in a serum bottle, and water-saturated soil. The sub-samples were analyzed for p-xylene concentration after 7 days. Results showed that p-xylene degradation was completed after 7 days using the enzyme mixture from *Arthrobacter* sp. S2TR-06 (Fig. 6.12). Time-course experiments were carried out and described in our previous studies [16].

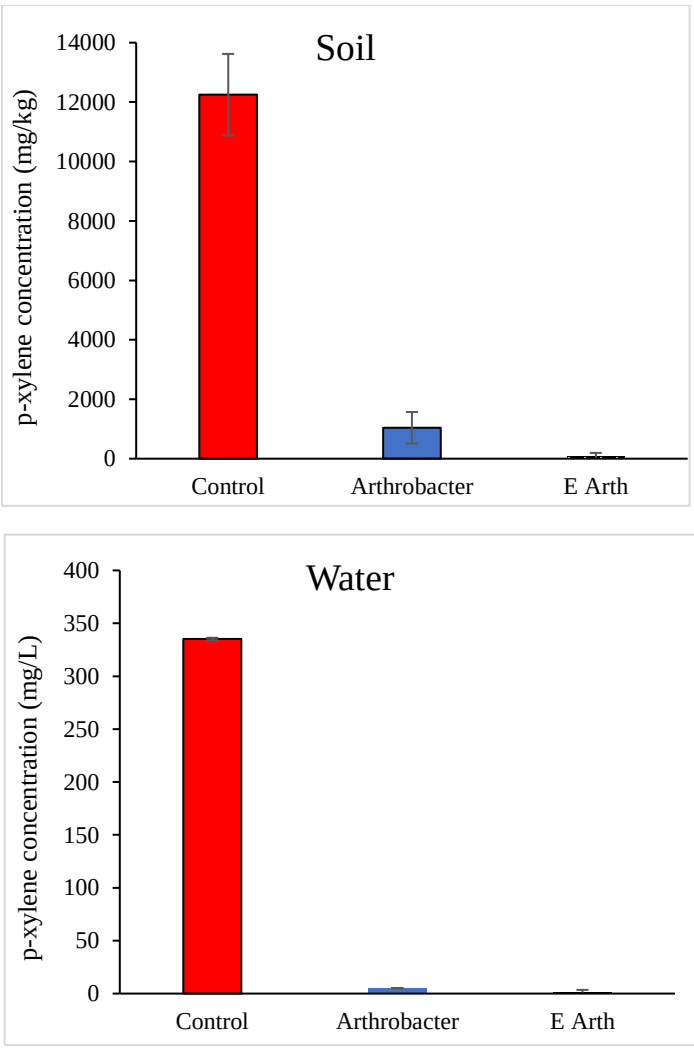

Fig. 6.12. p-xylene degradation in soil and water samples using whole-cell bacteria (Arthrobacter sp. strain S2TR-16) and its enzyme mixture.

Column tests

Soil texture

The characteristics of the 140 mL packed soil columns used for treatment experiments are presented in Table 6.7. The mineralogy of soils varies in different parts of the site since it is mostly backfilling material, and, in addition to quartz and feldspar, clay minerals and carbonates are present.The results of groundwater characterization also confirmed the presence of carbonates (hard water) with a pH of 7.2±0.4 (Biogénie, 2009). The soil sample comprised 59% of particles between 1-5 mm, 38% within 250 µm-500 µm, and 3% with <250 µm in size (very fine particles).

The physical characteristics of the soil were determined as follows: moisture content of 24.17± 0.5%, pH 7.1±0.2, and total solids: 75.36±0.91%.

Table 6.7. Characterization and initial condition of the soil column experiment

Soil column No.	column volume (cm^3)	Soil density in column(1) (g/cm^3)	Soil intrinsic permeability (m^2)	Pore volume (cm^3)	Hydraulic conductivity (cm/s)
1	140.39	1.88	$7.5\text{-}9.2\times10^{-13}$	50±0.5	1.3×10^{-6}
2	139.37	1.79		49±0.5	1.4×10^{-6}
3	141.41	1.71		50±0.5	2.4×10^{-6}
4	140.39	1.72		50±0.5	2.2×10^{-6}
5	139.36	1.82		49±0.5	1.5×10^{-6}
6	140.39	1.78		50±0.5	2.3×10^{-6}
7	139.36	1.9		49±0.5	2.4×10^{-6}
8	139.36	1.84		50±0.5	2.5×10^{-6}
9	139.36	1.9		50±0.5	1.6×10^{-6}
10	139.36	1.81		49±0.5	2.9×10^{-6}
11	140.39	1.7		50±0.5	1.7×10^{-6}

(1) Soil density was selected based on site soil density ranging from 1.7-1.9 g/cm^3.

Different soil samples from field boreholes were mixed to prepare a homogeneous soil type for the experiments. The soil texture corresponds to a poorly sorted mix of coarse, intermediate, and fine-grained material, and the grain size distribution curve is presented in Fig. 6.13. As mentioned earlier, only the grain size fractions between 0.25 and 2.0 mm were kept for the column tests.

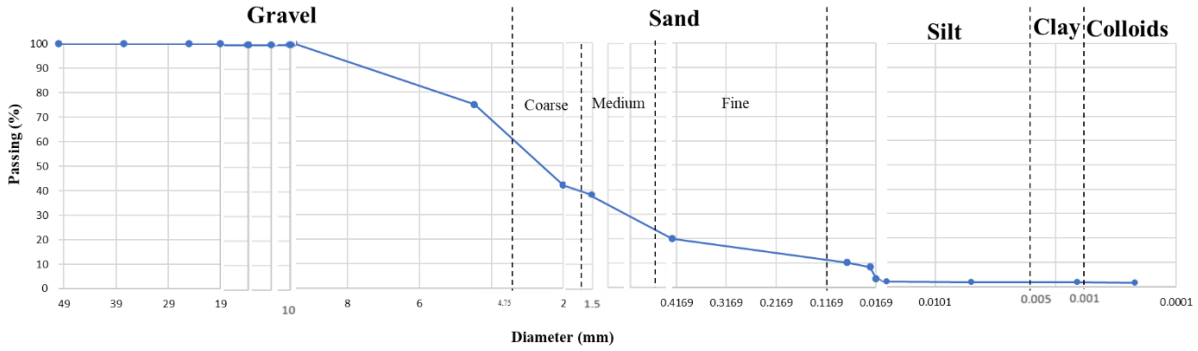

Fig. 6.13. Particle-size analysis of soil

The Breakthrough curves

The breakthrough curves obtained at the column outlet representing normalized concentrations of the conservative tracer (Br-) and C2,3D (as a major enzyme in the mixture) in the column effluent following enzyme injection are presented in Fig. 6.14. The results show a delay in breakthrough between the enzyme and the conservative tracer. This retardation is from enzyme adsorption to soil particles during flow through the porous media. Fig. 6.14 shows that about 3 PV of the enzyme (~120mL) should be injected to compensate for the enzyme losses to adsorption and have the same enzyme activity throughout the soil as in the stock solution.

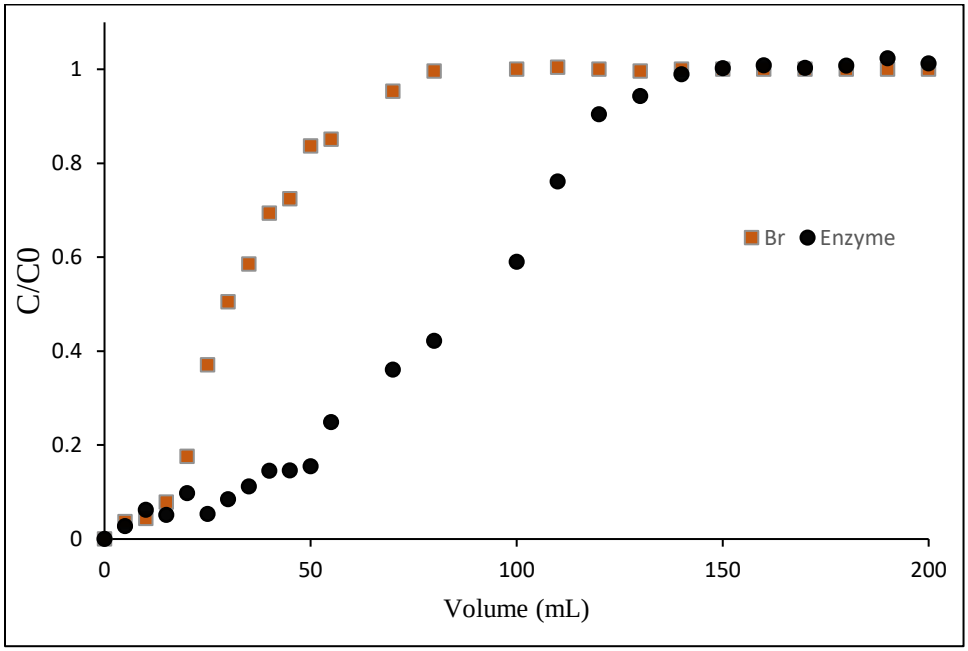

Fig. 6.14. Breakthrough curve for tracer (Br-) and enzyme in the column effluent

Enzyme mixture from *Arthrobacter* sp. strain S2TR-16 can degrade 90.21% and 88.53% of p-xylene in soil with concentrations X and X/5 after 8 weeks (Table 6.8). These similar degradation rates obtained with different enzyme concentrations indicate that a dilution factor of 5 of the stock solution can be used for future tests. This dilution factor plays a significant role in reducing the cost of treatment associated with this technology (Table 6.8).

Table 6.8. p-xylene degradation in soil column using enzyme mixture

Time	Sample	p-xylene concentration in soil (mg/kg)	Average	Relative degradation rate (%)
time 0	Initial concentration 1	12,500	11,667	-
time 0	Initial concentration 2	12,000		
time 0	Initial concentration 3	10,500		
4 weeks	Control	16,500	15,333	-
4 weeks	Control	12,000		
4 weeks	Control	17,500		
4 weeks	Concentration X1	3,050	1,589	89.63
4 weeks	Concentration X2	1,650		
4 weeks	Concentration X3	68		
4 weeks	Concentration X/5 (1)	2,900	2,550	83.36
4 weeks	Concentration X/5 (2)	3,550		
4 weeks	Concentration X/5 (3)	1,200		
8 weeks	Control	9,000	8,000	-
8 weeks	Control	8,000		
8 weeks	Control	7,000		
8 weeks	Concentration X1	650	783	90.21
8 weeks	Concentration X2	800		
8 weeks	Concentration X3	900		
8 weeks	Concentration X/5 (1)	1,250	917	88.53
8 weeks	Concentration X/5 (2)	650		
8 weeks	Concentration X/5 (3)	850		

Intermediate scale test (sand tank)

Initial soil characterization

Prior to the enzyme injection, the physical properties of water inside the soil tank were determined. The results showed a pH of 6.62, the temperature of 23.76 (^{o}C), the electrical conductivity of 4795 µS/cm, dissolved oxygen (DO) of 3.80 mg/L, and redox potential of -108.1 mV. Before enzyme injection, results of soil sampling showed that p-xylene concentrations in soil well exceeded the reference criteria of 50 mg/kg in almost all the sampled locations. The highest concentrations ranging from 5 700 mg/kg to 7 500 mg/kg were measured in the depth interval of 0.7 to 1.0 m, which corresponds to an elevation interval of 0.4 to 0.7 m above the bottom of the tank.

First injection scenario

Fig. 6.15 illustrates the tracer concentration (Br^-) and the enzyme activity monitored at the extraction well (EW-02) as a function of the cumulative volume injected. EW-02 is located in the corner of the tank which is opposite the injection-extraction axis. Between all monitoring wells installed, it is at that location that the tracer breakthrough occurred at the latest. As shown in Fig. 6.15a, the concentration of Br- at EW-02 reached 91% of the total concentration of Br^- injected into the soil tank after the overall injection of 1050 L of solution in the tank. However, at the same location, the enzyme breakthrough curve showed marked fluctuations and the maximum enzyme activity measured at EW-02 is less than 80% of the enzyme activity of the solution injected at the end of the injection. There are potential explanations for this type of behavior: preferential flow inside the tank, uneven adsorption of the enzyme onto the soil particles and dilution with pore water trapped within the heterogeneous soil layers. These explanations are all linked with the heterogeneous nature of the soil obtained at the experimental site (backfill material) and the proportion of fine-grained soil present within the backfill material. It is however expected that these conditions are representative of the true field-scale environment.

These conditions also led to variations in p-xylene concentrations and biodegradation results as well (Fig. 6.15b). Results showed reductions in p-xylene concentrations ranging from 30 % to 55 % for the first injection of enzyme solution. This reduction was observed only for the contaminated soils located in the saturated zone, which was the target of the injection

These results and their comparison with the better degradation rates that were obtained with previous column tests (where the contact between the injected enzyme and the contaminants trapped within soil pores was facilitated by the 1D-design) highlight the main technical challenges for in-situ remediation at a larger field-like scale. These challenges are: (1) achieving a uniform

distribution of the enzyme solution throughout the soil to remediate, and (2) limited access of remediation agents to the residual contaminant trapped as droplets by capillary forces in the capillary fringe inside the vadose zone, as well as in the saturated zone [443]. Another potential limiting factor is the presence of dissolved oxygen in the targeted zone. Such breakthrough curves suggested that monitoring of enzyme activity through all observation and extraction wells is needed to confirm the limited distribution of enzymes in all locations of the soil tank. Following the first injection, since p-xylene remained in the tank at concentrations above the targeted xylene regulatory limit of 50 mg/kg, a second injection was planned.

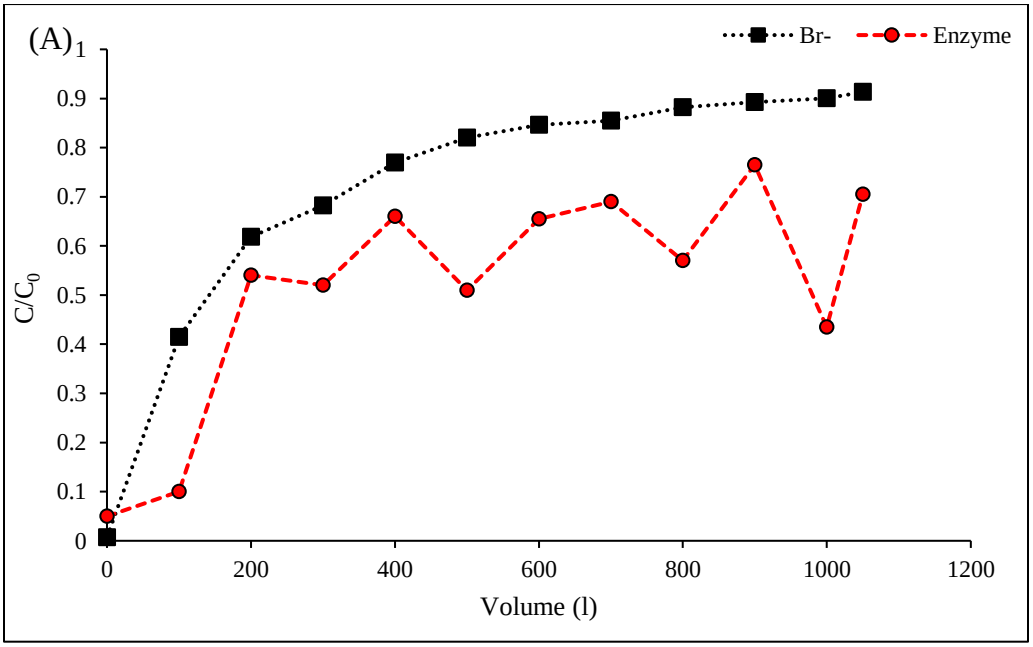

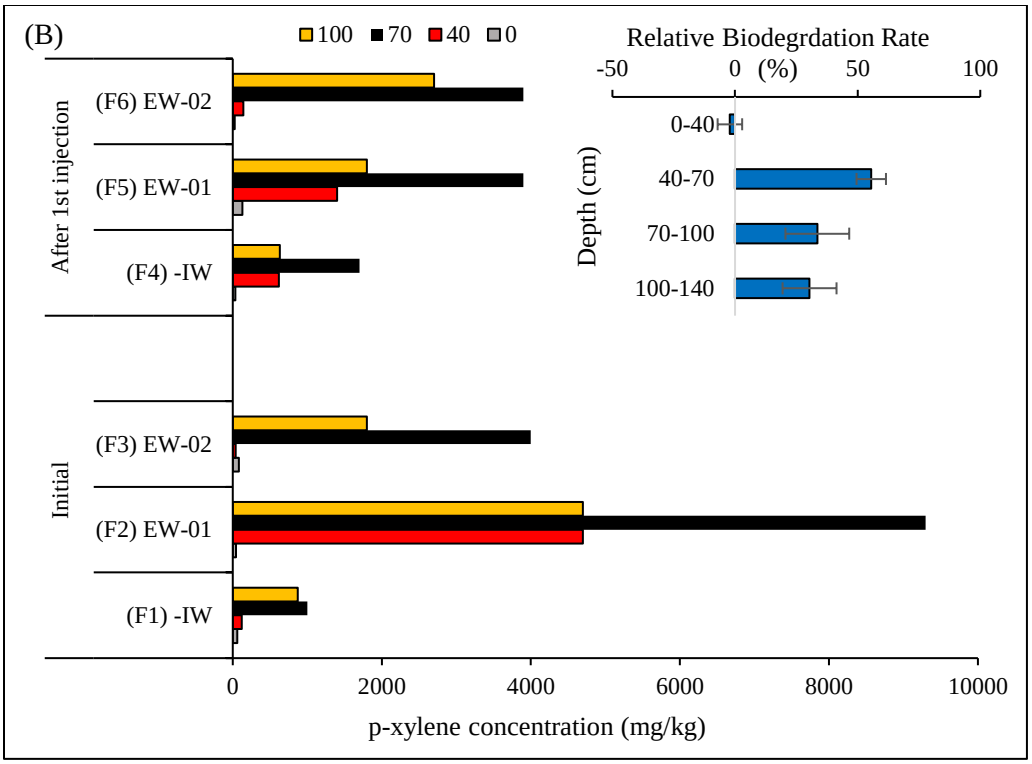

Fig. 6.15. Breakthrough curves of tracer and enzyme at EW-02 during the enzyme injection in the sand tank (A); p-xylene concentration in the soil before and after enzymatic treatment (B) Relative degradation rate of p-xylene after 1st injection of enzyme solution at depth intervals parented in right side.

Second injection scenario

As the second injection tested the addition of Triton X-100 surfactant along with the enzyme to increase the availability of the organic-phase contaminant (p-xylene) to the enzyme in the aqueous phase. Mohanty & Mukherji (2013) reported that Triton X-100 aided bioavailability by emulsification of non-aqueous phase liquid into the aqueous phase and enhanced the direct uptake of contaminant by *Burkholderia multivorans* (naphthalene degrader). While rhamnolipid (biosurfactant) did not affect the emulsification and bioavailability of non-aqueous phase liquid [461]. p-xylene degradation using enzyme solution with Triton X-100 (1% v/v) was investigated (Fig. 6.16a). This concentration was selected since it is reported that such high concentrations of Triton X-100 (> 1 000 mg/L) rapidly increased the biodegradation of petroleum hydrocarbons due

to the presence of surfactant micelles [461]. As shown in Fig. 6.16a, the second injection did not yield satisfactory results through the contaminated soil intervals, with no effect on depths below 70 cm. Moreover, concentrations in the non-saturated zone increase, probably as a result of mobilized p-xylene which may have been favored by the surfactant, since it has the effect of lowering both interfacial tensions between the p-xylene and the water and surface tension between p-xylene and air. Such mobilization was already observed by Zoller and Reznik (2006) when they tested an enhanced bioremediation methodology combining surfactants and surfactant-nutrient mixtures (SSNM) for the in-situ remediation of fuel-contaminated aquifers. A major result of SSNM addition was the enhanced mobilization of bulky nonaqueous phase liquids (NAPL) and the enhanced desorption, solubilization, and dispersion of the NAPLs that were entrapped, which however facilitated their enhanced biodegradation [462].

The potential impact of residual remediating agents on microbial communities is also a question of concern when analyzing the poor results obtained in the saturated zone. For these reasons, it is critical to evaluate the potential impact of enzymatic treatment on the microbial community for soil wherein the following step can be in conjunction with natural attenuation. Based on microbial community analysis before and after the enzymatic treatment, there were significant changes in the microbial community following enzymatic treatment (Fig. 6.16b). In all soil samples, *Pseudomonas* was the dominant genus with more than 50% relative abundance. Interestingly, we observed a decrease in abundance in treated soil samples when compared to untreated soil samples. The abundance of *Thermicanus* was significantly increased in enzymatically treated soil in comparison to untreated soil (control). This genus is characterized as a fermentative microaerophile and uses H_2 under anoxic conditions [463]. This result can be an indication that using enzymes resulted in a decrease in dissolved oxygen in the soil and water. The

possible explanation is that XMO and C2,3D are oxidoreductase enzymes and use molecular oxygen for the oxidation of their substrate (p-xylene). Moreover, *Hydrogenophaga* was also detected after enzymatic treatment of the soil. Most of the strains of this genus are classified as denitrifying microorganisms which are facultative anaerobic microorganisms [464]. Thus, the initial assumption that enough oxygen would be present in the tank to support the enzymatic processes is most likely false, and a third injection scenario was prepared with the objective of ensuring an initial supply of oxygen through the porous media.

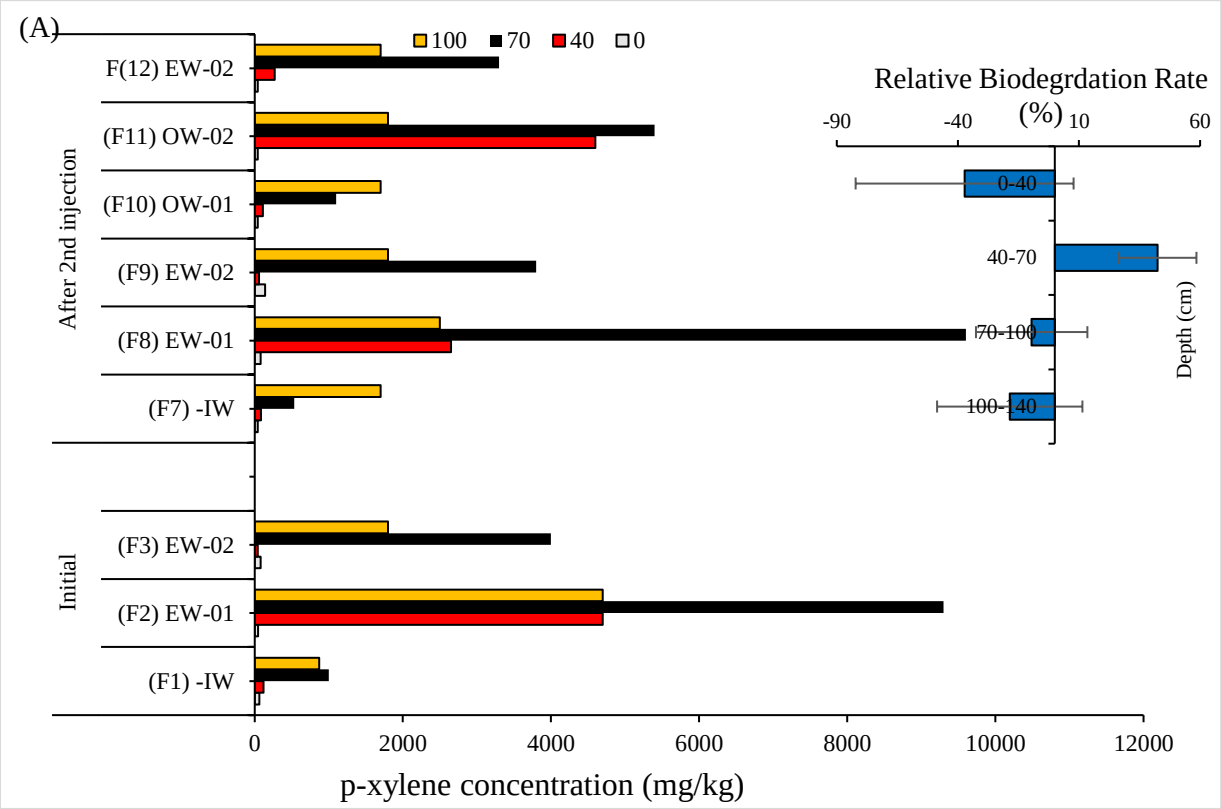

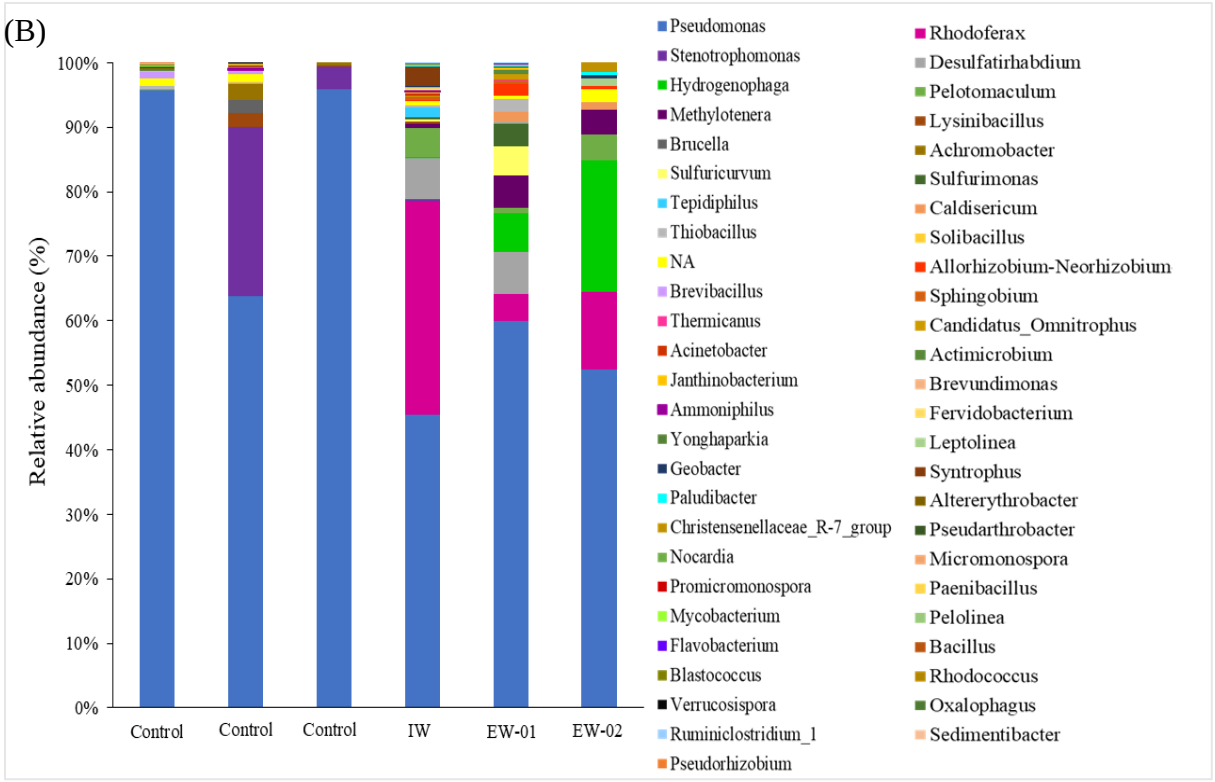

Fig. 6.16. p-xylene concentration in soil samples before and after 2nd injection of enzyme mixture, degradation rate after 2nd enzymatic treatment at depth intervals parented in right side (A) Genus-level comparison of the microbial community (B), control: contaminated soil before treatment. IW: soil samples collected near Injection well, EW-01 and EW-02: soil samples collected near extraction wells 01 and 02, OW-01 and OW-02: soil samples collected near observation wells 01 and 02.

Third injection scenario

The third scenario adopted a different injection strategy to ensure the presence of oxygen in the targeted treatment zone. To that effect, the water table was initially lowered below the 70-100 cm depth interval. This ensured that air invaded the porous media over that depth, even if water remained as soil humidity and into the capillary fringe. The soil surface is located at an elevation of 140.6 cm above the bottom of the tank. The water inside the tank was characterized using a Hanna multiparameter field probe as followed: pH 6.62, temperature 23.76 ºC, electrical conductivity 4795 µS/cm, dissolved oxygen 0.80 mg/L, redox potential -108.1 mV. As expected, dissolved oxygen was near zero. The enzyme solution was also characterized as follows: pH 6.05,

temperature 22.40 ^{o}C, electrical conductivity 2588 µS/cm, dissolved oxygen 0.15 mg/L, redox potential -74.5 mV.

In this scenario, 0.1% of $FeSO_4$ was added to the enzyme mixture and direct injection was used to increase the contact of enzymes with trapped p-xylene into the soil matrix. The enzymatic solution contained around 100 U/mL of XMO and 200 U/mL of C2,3D activity and 0.1% of $FeSO_4$. The solution was slowly injected into the tank to make the water level increase as uniformly as possible into the tank (flooding). There was no extraction performed for that scenario. The injection was performed until the water level reached the top of the sand. The injection was followed by a 2-month waiting period to allow the enzyme degradation mechanisms to occur. The enzyme activity in groundwater sampled in the wells at the end of the injection along with the remaining p-xylene concentration at the end of the 2-month waiting period without water flow in to the tank is presented in Fig. 6.17. The study showed that the enzyme mixture containing 0.1% of $FeSO_4$ could decrease the p-xylene concentration in all the locations of the soil tank (Fig. 6.17a) but at varying levels.

Monitoring of the dissolved oxygen during and after the injection provided surprising results. It appears that the formulation created a reductive environment, and the dissolved oxygen supplied by the tap water used for the preparation of the enzyme solution was depleted before the start of the injection. However, based on the injection strategy, oxygen was still present inside the soil pores prior to the injection.

There are two possible explanations for this observation: 1) Fe plays a role in the regeneration of enzymes for a longer period that is consistent with the results from stability tests 2) sulfate (SO_2^{-4}) acts as an electron acceptor in absence of oxygen. The first X-ray structure of a catechol dioxygenase from *P. putida*, showed that the nonheme iron(III) cofactor is ligated by four amino

acid side chains (His-460, His-462, yr-408, and Tyr-447). Anderson & Lovley (2000) showed that benzene oxidation was dependent upon sulfate reduction. They showed that sulfate reduction was the predominant terminal electron-accepting process and stimulate anaerobic benzene degradation in the treatment zone [465].

In addition, direct injection of the enzyme without extraction could help the interaction of enzymes with trapped p-xylene in soil particles. The sample from OW-01 showed the highest activity compared to OW-02 and OW-03. The order of the results was as follows: Injection solution >OW-01>OW-02>OW-03 (Fig 6.8b). It is noticeable that OW-01 is located close to the injection well. These results indicated the combined effects of adsorption on soil particles and dilution of the injected solution by pore water (i.e. the residual water still present within soil pores at the time of the injection). Since the soil inside the tank is heterogeneous with a significant fine-grained fraction, the presence of an important capillary fringe is expected, and trapped water within this capillary fringe has the effect of diluting the solution as it progresses into the soil. Although the detected enzyme activity in all observation wells was less than injection stock, more than 1 U/ml of enzyme activity (> 30% of the injected solution) was observed in all locations of the soil tank (Fig 5.17b). Fig. 6.17a shows that the degradation rates obtained were at best in the range of those obtained for the first injection scenario.

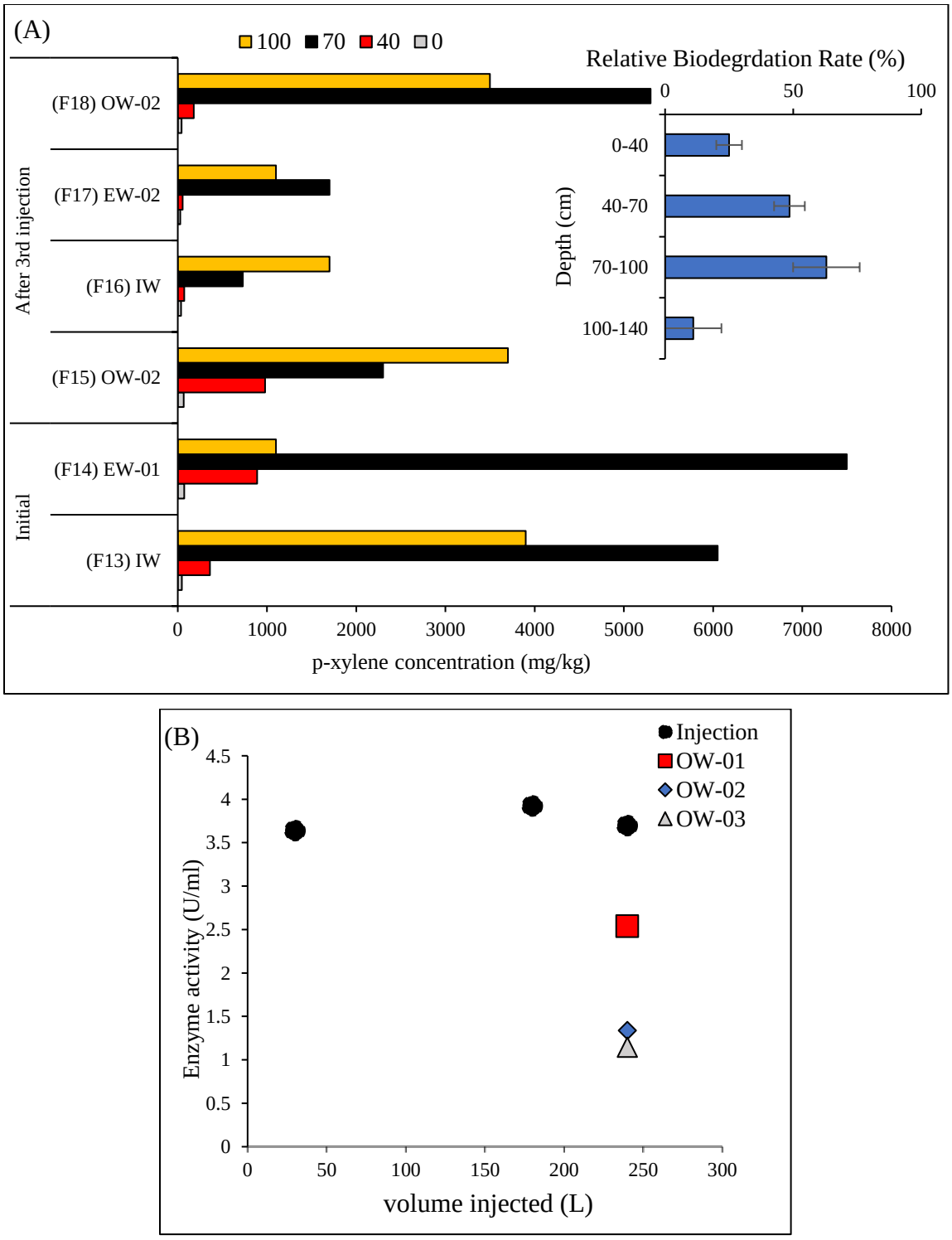

Fig. 6.17. p-xylene concentration in soil samples before and after 3rd injection of enzyme mixture, relative degradation rate at depth intervals presented on the right side (A), enzyme activity in observation wells after injection (B)

Comparison of results at different experimental scales

Even though biodegradation of petroleum hydrocarbon contamination is a commonly used technology to remediate soils and groundwater, due to the difficulties associated with field-scale studies, estimations of biodegradation rates are usually conducted at the bench-scale in laboratory studies. The measured biodegradation rate appears to decrease as the experimental scale is increased. Our results also confirmed that the biodegradation rate decreased as the experimental scale increased (Table 6.9). Understanding the scale-dependent phenomena is the main challenge faced by the use of bioremediation techniques for the successful implementation of laboratory-scale data in the field scenario.

It is noticeable that enzymatic treatment is not the only technology for remediation of petroleum hydrocarbons and many sites are now being remediated using multiple technologies. In the presence of a free-phase of petroleum hydrocarbons, it is necessary to apply other technologies like vacuum extraction to remove the recoverable free-phase liquids. It is believed that implementing an aggressive multiphase extraction step prior to the enzyme injections would have most likely improved the results.

Table 6.9. The scale-up effect on enzymatic biodegradation of p-xylene in soil

Enzyme production scale	Maximum enzyme activity	Biodegradation test scale (Test system)	Maximum Biodegradation rate (%)	Biodegradation Time	Influencing factors
150 ml serum bottles	7 ± 1 U/ml of XMO 17± 2 U/ml of C2,3D	Laboratory-scale (150-mL sealed serum bottles)	~100	7 days	• Initial concentration of the contaminant
5-L Bioreactor	20 ± 1 U/ml of XMO 30 ± 1 U/ml of C2,3D	Bench-scale (Soil column	90.21	8 weeks	• Treatment time • Enzyme concentration

150-L Bioreactor	109 ± 1U/ml for XMO 203± 1 U/ml for C2,3D	Pilot test (soil tank test)	68	12 weeks	• Injection pattern • Dissolved oxygen • Soil heterogeneity • Free phase of contaminant

Expanding applications

To further study the degradation ability of enzyme solution, batch tests (150 mL) were conducted for BTEX compounds in the water matrix (Table 6.10). The initial concentration of each compound was selected based on its solubility in water. The results showed that among the six substrates, XMO and C2,3D have a higher affinity for toluene. XMO and C2,3D showed affinity to substrates as follows: Toluene>p-xylene>benzene>ethylbenzene> m-xylene> o-xylene. This observation confirmed that this enzyme solution could remove BTEX relatively easily, which was consistent with our previous literature [212]. The degradation rate for each compound was more than 90% after 7 days under batch conditions. Although, batch tests are a good indication of the potential application of this enzyme solution for BTEX remediation, further analyses, and scale-up studies are needed to confirm successful in situ bioremediation of BTEX. Moreover, more applications are expected for this enzyme solution since XMO and C2,3D are bacterial multicomponent monooxygenase and dioxygenase that can hydroxylate a wide array of aromatic compounds. For example, Donadio et al., (2015) used XMO for the biotransformation of phthalan, 2-phenoxyethanol, and 2-indanol to produce antioxidant compounds (monocyclic phenols and catechols). Pieper (2005) mentioned that C2,3D was involved in the aerobic biodegradation of chlorocatechols as an important intermediate of 4-chlorobiphenyl [466]. The possible explanation is that *P. putida* strain CE2010 mineralized biphenyl by a similar *tod* (toluene) and *cmt* (cumate) pathways in the absence of an authentic biphenyl pathway [467].

Table 6.10. Degradation in batch experiment (150 mL) of different substrates in water by XMO and C2,3D

Substrate	Initial concentration (mg/L)	Concentration after 7 days (mg/L)	Relative biodegradation rate (%)
Benzene	909.62 ± 20.34	5.56 ± 0.51	99.38
Toluene	520.17 ± 12.41	0.87 ± 0.31	99.83
Ethylbenzene	151± 0.71	2.13 ± 0.01	98.58
p-xylene	198.1 ± 0.54	0.01 ± 0.031	99.94
m-xylene	145 ± 0.21	10.56 ± 0.2	92.71
o-xylene	169.5 ± 0.52	15.69 ± 0.13	90.74

6.4. Conclusion

Our work established scale-up tests related to enzymatic biodegradation of p-xylene in soil under cold temperatures. The enzyme solution containing XMO and C2,3D was produced from a novel cold-adapted strain, *Arthrobacter* sp. strain S2TR-06. This enzyme solution could biodegrade p-xylene at the fastest rate ranging from 68-100% in highly contaminated soil. The scale-up studies showed that enzyme production improved (~7 to 109 U/mL for XMO, and 17 to 203 U/mL for C2,3D) as the bioreactor size increased (150 mL to 150 L). The biodegradation rate decreased from 100% to 36% in serum bottles and the soil tank due to limited access of enzymes to trapped p-xylene in soil pores, low dissolved oxygen, soil heterogeneity, and the presence of free phase. Biodegradation tests with other substrates (BTEXs) showed that this enzyme solution can be used for bioremediation of the tested contaminants in water. However, further studies and field demonstrations are required to confirm the applicability of this enzyme for BTEX-contaminated soil.

CHAPTER SEVEN: CONCLUSIONS, AND RECOMMENDATIONS

7.1. CONCLUSIONS

From the obtained results, the following conclusions can be drawn:

1. p-xylene is considered a non-growth substrate for well-known aromatic degrading microorganisms such as *Pseudomonas putida*. these bacteria can use Benzene (B), Toluene (T), and Ethylbenzene (E) as a sole source of carbon and can degrade p-xylene only in the presence of these compounds (co-metabolic biodegradation). The Group Method of Data Handling (GMDH) neural network can be used to design and optimize bioprocesses such as fed-batch biodegradation. The enzyme study showed that xylene monooxygenase (XMO) and catechol 1, 2 dioxygenases (C1,2D) enzymes are involved in the co-metabolism of p-xylene. The accumulation of an intermediate due to the lack of growth substrates has been determined by the mass balance study.
2. The p-xylene metabolism depends on catabolic genes (*xylM*, *xylA* and *xylE*), and the corresponding regulatory genes (*xylR* and *xylS*). Our gene expression study using three psychrophilic *Pseudomona*s strains (*Pseudomonas putida* S2TR-01, *Pseudomonas synxantha* S2TR-20, and *Pseudomonas azotoformans* S2TR-09) showed the main reason for the differences in BTEX and p-xylene degrading strains. This study showed no significant differences in the expression of the *xylM* and *xylA* genes among all isolates, while *xylE* and *xylS* genes were induced only in isolates *P. azotoformans* S2TR-09 and *P. synxantha* S2TR-20, which could grow in the presence of p-xylene. A lack of *xylE* expression (encoding catechol 2,3 dioxygenase) leads to the accumulation of dead-end products such as p-toluic acid and p-cresol and the inhibition of biomass production and complete carbon recovery.
3. Cold-active XMO and C2,3D have a matching end product. They acted in symphony to degrade p-xylene. Their unique thermodynamic and kinetic behavior permits them to achieve

rapid degradation of p-xylene at low temperatures (<15°C). No specific product was produced after the complete action of the enzyme cocktail (1:1.5) that confirmed the complete degradation of p-xylene within 48h in groundwater samples at 15°C.

4. To mimic *in situ* application of enzyme mixture, bioremediation of p-xylene contaminated soil was carried out in soil column (140 mL) tests. Enzyme cocktail in X concentration contained about 10 U/mL of XMO and 20 U/mL of C2,3D. X/5 and X/10 correspond to 5x and 10x dilution of enzyme cocktail respectively. The average values of p-xylene removal after 8 weeks indicated that the 5x dilution of the enzyme cocktail can be an appropriate concentration for soil enzymatic bioremediation in the soil column system (92-94% p-xylene degradation). Dilution of the enzyme mixture can reduce the cost of treatment.
5. One of the major challenges in the practical and commercial application of oxygenases is their inherent instability. Based on our studies, micro/nano biochar-chitosan composites were suitable to support enzyme immobilization (xylene monooxygenase and catechol dioxygenase). The degradation tests clearly showed that immobilized enzymes had biodegradation ability for all BTEX compounds (more than 85% of degradation for all the compounds) in groundwater samples. Our results confirmed that immobilization of cold-active degrading enzymes enhanced their storage stability, more than 50% of its residual activity at 4 ± 1 ºC for 30 days.
6. Magnetic carriers can be used for the simple magnetic separation of immobilized enzymes. To this end, cold-active XMO and C1,2D from a psychrophile were immobilized on magnetic chitosan microparticles using glutaraldehyde as a linker agent. Our results showed that the immobilized enzymes had improved pH tolerance ranging from 4.0 to 9.0, better temperature stability ranging from 5 to 50 °C, higher storage stability (~70% activity after 30 days of

storage), and more importantly, reusability (~40% activity after 10 repetitive cycles of usage) compared to their free form. In addition, the immobilization of enzymes increased the effectiveness of the enzymatic treatment of p-xylene in soil (initial concentration of 10,000 mg/kg).

7. A novel cold-adapted strain, *Arthrobacter* sp. strain S2TR-06 showed the highest performance in the production of these involved enzymes. Therefore, this strain was used for scale-up production of enzymes. The obtained enzyme mixture could biodegrade p-xylene at the fastest rate ranging from 68-100% in highly contaminated soil from batch tests to pilot-scale tests. The scale-up studies showed that enzyme production improved (~7 to 109 U/ml for XMO, and 17 to 203 U/ml for C2,3D) as the bioreactor scale increased (150 ml to 150 L). From the obtained results, it can be concluded that the biodegradation rate is a scale-dependent phenomenon and scale-up studies are needed. The current research showed that there are several promising opportunities for the future application of enzymes (Enzyme Booster Technology) for the clean-up of contaminated soil and groundwater.

7.2. REMARKS

Hypothesis No.	HYPOTHESIS	REMARKS
1	Indigenous bacteria isolated from the p-xylene contaminated site could metabolize p-xylene effectively under low temperatures (<15ºC).	Well-known aromatic degrading microorganisms such as *Pseudomonas putida* could not degrade p-xylene as a sole source of carbon, while *Pseudomonas azotoformans* S2TR-09, *Pseudomonas synxantha* S2TR-26, *Pseudomonas mandelii* S2TR-08, *Pseudomonas* S2TR-14, and *Arthrobacter* sp. S2TR-06 isolated from the contaminated site degraded p-xylene. Some of these isolated bacteria are psychophilic and some of them are mesophilic and cold-adapeted.
2	Indegionious p-xylene degrading bacteria would produce cold-active oxidative enzymes under aerobic conditions and be applied to contaminated soil and groundwater.	Xylene monooxygenase catalyzes the multi-step oxidation of the aromatic nucleus of p-xylene and produces p-cresol as the last product. Catechol 2, 3-dioxygenase showed a high affinity for p-cresol to degrade it to inert products. Based on thermodynamic analysis, the reduced enthalpy in the cold-active enzymes' reaction could explain the

		main adaptive mechanism to low temperatures. According to the results presented in chapter 3, part 1 and 2, the mixture of these enzymes can completely mineralize p-xylene within 48h in groundwater and 7 days in soil without producing any toxic byproducts.
3	Immobilization improves enzymes' resistance to a variety of storage and operating conditions. The use of immobilized enzymes in biotechnological processes is preferred over their free counterpart because of the prolonged availability of enzymes and their re-usability.	Co-immobilization of cold-active xylene monooxygenase and catechol dioxygenase onto nano/micro biochars-chitosan matrices improved their p-xylene biodegradation in soil (70-90% after 4 weeks). Also, immobilization enhanced their storage stability at 4 ± 1 ºC for 30 days as discussed in chapter 4, part 1.
		Improved pH tolerance ranging from 4.0 to 9.0, better temperature stability ranging from 5 to 50 ºC, higher storage stability (~70% activity after 30 days of storage) was observed for immobilized enzymes onto magnetic chitosan carriers (chapter 4, part 2). More importantly, immobilized enzymes can easily be separated from water and soil

		matrices for reuse. Approximately 40% activity of these enzymes was restored after 10 repetitive cycles of usage.
4	Large-scale production of enzymes using optimized conditions at the bench scale can determine and influence the scaling-up process. The formulated enzyme mixture could be effectively produced on different scales (bench to large scale) and applied to soil and groundwater (laboratory, to pilot scales).	Enzyme production was improved in pilot-scale bioreactors but biodegradation rate decreased in soil tank test. Maximum rate of biodegradation can be achieved by understanding influencing factors in the scaling-up process (achieving higher biodegradation rate in different injection scenarios in chaper 5).

7.3. FUTURE RECOMMENDATIONS

Though the project objectives were successfully performed and disseminated in form of published articles, still limitations persist and hence future recommendations.

A. Global Objective 1: As listed in the objective section, global objective 1 states "Investigate metabolic and co-metabolic biodegradation of p-xylene using modeling and experimental data". A major limitation of this objective lies in expanding the use of the GMDH model for the prediction of co-metabolic degradation of other non-growth contaminants to generalize this model. The proposed GMDH model can be applied to a very short range of conditions (only *pseudomonas*, selected initial substrate and biomass concentration, temperature and only growth substrates benzene, toluene and ethylbenzene. *Additional studies can be carried out to predict the removal of p-xylene in the presence of other C sources and by other genus of bacteria.*

B. Global Objective 2: As listed in the objective section, global objective 2 states "Study the pathway of p-xylene biodegradation and compare cold-active strains". One major limitation lies in the differences in isolated bacteria when it comes to other adaptation pathways than p-xylene biodegradation. *The comparative genomic analysis will be needed to understand other adaptation mechanisms such as toxicity tolerance, antifreeze proteins, phage integrases, etc.* Since genomic architecture may have been altered through horizontal gene transfers in degrading stains. To better analyze the difference between isolates, a whole-genome analysis of each degrading isolate can provide more information about the adaptation mechanism. As in this study, *it would be preferable to conduct a complete genome analysis of Arthrobacter sp. S2TR-06 as a novel cold-adapted strain.*

C. Global Objective 3 and 4: Global objective 3 and 4 are related to “Investigate involved enzymes in p-xylene biodegradation and potential application for contaminated groundwater and soil in the cold climate”. Through these objectives, two major enzymes were investigated for p-xylene biodegradation. However, another "possible" limitation that surrounds this objective is the presence of other involved proteins or enzymes that may indirectly contribute to p-xylene biodegradation. For instance, ferrodoxins are iron–sulfur proteins that mediate electron transfer in a range of metabolic reactions. Although LC-MS-MS was used for determining proteins in the enzyme mixture, *more precise approaches such as next-generation sequencing technologies can be used for the determination of every single protein in the mixture*. For instance, transcriptomics studies based on genomics can provide information about the response of selected isolates in the presence of different substrates. This analysis will help to understand the composition of the enzyme mixture precisely.

D. Global Objective 5 and 6: As listed in the objective section, global objectives 5 and 6 are related to “The immobilization of enzymes for higher storage, operational stability and reusability”. The major limitation of this objective lies in the use of immobilized enzymes for *in situ* application to the soil matrix. Technically, the injection of micro-sized solids can clog injection wells. Further studies will be needed for the *injection of immobilized enzyme into the soil matrix based on the type and depth of the fluid injected.*

E. Global Objective 7 and 8: As listed in the objective section, global objectives 7 and 8 are related to “Scale-up of the enzyme production and biodegradation tests”. Although pilot-scale tests were conducted using soil tank tests that can represent the saturated zone in the contaminated site, still experiments were carried out under control conditions such as temperature, water level, pH and etc. Therefore, *field tests will be needed to evaluate the performance of this technology under*

field conditions. For commercializing this technology, different field tests are needed as each site has its geological characteristics. Furthermore, reselecting media components for high-volume enzyme production at a cost-effective basis. In this study, standard media was used in the production of enzymes in bioreactors. *Less expensive substrates should be used for scale-up studies*. Also, a feasibility study of enzyme production under unsterile conditions can be done to reduce the cost of the production and potential on-site production. Moreover, results from the soil tank test showed the limitation of oxygen after enzymatic treatment. Therefore, *biodegradation tests can be done under anaerobic conditions to comprehend the role of additives in the enzyme mixture*.

BIBLIOGRAPHY

[1] R. Kandyala et al., "Xylene: An overview of its health hazards and preventive measures," *Journal of oral and maxillofacial pathology: JOMFP*, vol. 14, no. 1, p. 1, 2010.

[2] P. J. Alvarez and T. M. Vogel, "Substrate interactions of benzene, toluene, and para-xylene during microbial degradation by pure cultures and mixed culture aquifer slurries," *Applied and Environmental Microbiology*, vol. 57, no. 10, pp. 2981–2985, 1991.

[3] J. You et al., "BTEX degradation by a newly isolated bacterium: Performance, kinetics, and mechanism," *International Biodeterioration & Biodegradation*, vol. 129, pp. 202–208, 2018.

[4] S. H. Ferguson et al., "Effect of temperature on the microbial ecology of a hydrocarbon-contaminated Antarctic soil: Implications for high temperature remediation," *Cold Reg Sci Technol*, vol. 53, no. 1, pp. 115–129, 2008.

[5] S. Habib et al., "Bioremediation of petroleum hydrocarbon in Antarctica by microbial species: an overview.," *Pertanika Journal of Science & Technology*, vol. 26, no. 1, 2018.

[6] S. Miri et al., "Recent biotechnological advances in petroleum hydrocarbons degradation under cold climate conditions: A review," *Critical Reviews in Environmental Science and Technology*, vol. 49, no. 7, pp. 553–586, 2019.

[7] M. Radwan et al., "Application of electro-Fenton process for treatment of water contaminated with benzene, toluene, and p-xylene (BTX) using affordable electrodes," *Journal of Water Process Engineering*, vol. 31, p. 100837, 2019.

[8] E. Soleimani, "Synthesis, spectroscopic and thermal studies of biologically active complexes containing a macrocycle derived from piperazine and pyridine-2, 6-dicarboxylic acid," *Journal of Thermal Analysis and Calorimetry*, vol. 115, no. 3, pp. 2191–2201, 2014.

[9] R. Bardsley, "Detection limits of EPA method 8260 with static and dynamic headspace GC--MS analysis," *LC-GC North America*, vol. 27, no. 9, pp. S27–S27, 2009.

[10] I. Meyer-Cifuentes et al., "Isolation and characterization of Magnetospirillum sp. strain 15-1 as a representative anaerobic toluene-degrader from a constructed wetland model," *PLoS One*, vol. 12, no. 4, p. e0174750, 2017.

[11] Y. Zhou et al., "Multi-substrate biodegradation interaction of 1, 4-dioxane and BTEX mixtures by Acinetobacter baumannii DD1," *Biodegradation*, vol. 27, no. 1, pp. 37–46, 2016.

[12] N. Hassan et al., "Temperature driven membrane lipid adaptation in glacial psychrophilic bacteria," *Frontiers in Microbiology*, vol. 11, p. 824, 2020.

[13] O. S. Kwean et al., "4-Chlorophenol biodegradation facilitator composed of recombinant multi-biocatalysts immobilized onto montmorillonite," *Bioresour Technol*, vol. 259, pp. 268–275, 2018.

[14] C. Bakermans et al., “Molecular characterization of bacteria from permafrost of the Taylor Valley, Antarctica,” *FEMS Microbiol Ecol*, vol. 89, no. 2, pp. 331–346, 2014.

[15] S. Miri et al., “Psychrozymes as novel tools to biodegrade p-xylene and potential use for contaminated groundwater in the cold climate,” *Bioresource Technology*, vol. 321, Feb. 2021 [Online]. Available: 10.1016/j.biortech.2020.124464.

[16] S. Miri et al., “Sustainable production and co-immobilization of cold-active enzymes from Pseudomonas sp. for BTEX biodegradation,” *Environmental Pollution*, vol. 285, p. 117678, 2021.

[17] R. S. Peixoto et al., “Petroleum-degrading enzymes: bioremediation and new prospects,” *Enzyme Res*, vol. 2011, 2011.

[18] R. Helland et al., “The 1.4 Å crystal structure of the large and cold-active Vibrio sp. alkaline phosphatase,” *Biochimica et Biophysica Acta (BBA)-Proteins and Proteomics*, vol. 1794, no. 2, pp. 297–308, 2009.

[19] S. J. Varjani and V. N. Upasani, “Core flood study for enhanced oil recovery through ex-situ bioaugmentation with thermo-and halo-tolerant rhamnolipid produced by Pseudomonas aeruginosa NCIM 5514,” *Bioresour Technol*, vol. 220, pp. 175–182, 2016.

[20] D. van Stempvoort and K. Biggar, “Potential for bioremediation of petroleum hydrocarbons in groundwater under cold climate conditions: A review,” *Cold Regions Science and Technology*, vol. 53, no. 1, pp. 16–41, 2008.

[21] D. M. Filler et al., *Bioremediation of petroleum hydrocarbons in cold regions*. Cambridge University Press, 2008.

[22] T. Tunsaringkarn et al., “Occupational exposure of gasoline station workers to BTEX compounds in Bangkok, Thailand.,” *Int J Occup Environ Med*, vol. 3, no. 3, pp. 117–125, 2012.

[23] B. Jiang et al., “Biodegradation of benzene, toluene, ethylbenzene, and o-, m-, and p-xylenes by the newly isolated bacterium Comamonas sp. JB,” *Appl Biochem Biotechnol*, vol. 176, no. 6, pp. 1700–1708, 2015.

[24] S. J. Varjani and V. N. Upasani, “Comparative studies on bacterial consortia for hydrocarbon degradation,” *Screening*, vol. 2, no. 10, pp. 5377–5383, 2013.

[25] E. Ferrarese et al., “Remediation of PAH-contaminated sediments by chemical oxidation,” *Journal of Hazardous Materials*, vol. 152, no. 1, pp. 128–139, 2008.

[26] Z. Liu, *Benzene and toluene biodegradation with different dissolved oxygen concentrations*. Arizona State University, 2015.

[27] R. M. Atlas, *Microbial ecology: fundamentals and applications*. Pearson Education India, 1998.

[28] C. C. Azubuike et al., “Bioremediation techniques–classification based on site of application: principles, advantages, limitations and prospects,” *World Journal of Microbiology and Biotechnology*, vol. 32, no. 11, pp. 1–18, 2016.

[29] M. H. van Agteren et al., *Handbook on biodegradation and biological treatment of hazardous organic compounds*, vol. 2. Springer Science & Business Media, 1998.

[30] R. Boopathy, “Anaerobic degradation of petroleum hydrocarbons in sediments,” in *Current developments in biotechnology and bioengineering*, Elsevier, 2017, pp. 475–490.

[31] D. M. Filler et al., “Remediation of frozen ground contaminated with petroleum hydrocarbons: feasibility and limits,” in *Permafrost soils*, Springer, 2009, pp. 279–301.

[32] A. A. Olajire and J. P. Essien, “Aerobic degradation of petroleum components by microbial consortia,” *Journal of Petroleum & Environmental Biotechnology*, vol. 5, no. 5, p. 1, 2014.

[33] D. M. Filler et al., “Remediation of frozen ground contaminated with petroleum hydrocarbons: feasibility and limits,” in *Permafrost soils*, Springer, 2009, pp. 279–301.

[34] R. Peltola et al., “Nitrification in polluted soil fertilized with fast-and slow-releasing nitrogen: a case study at a refinery landfarming site,” *Environmental pollution*, vol. 143, no. 2, pp. 247–253, 2006.

[35] G. O. Adams et al., “Bioremediation, biostimulation and bioaugmention: a review,” *International Journal of Environmental Bioremediation & Biodegradation*, vol. 3, no. 1, pp. 28–39, 2015.

[36] K. Shirai et al., “Heavy-oil-degrading bacteria isolated by long-term enrichment in alumina columns containing heavy oil C,” *Biosci Biotechnol Biochem*, vol. 59, no. 11, pp. 2159–2161, 1995.

[37] L. A. Nwaogu et al., “Degradation of diesel oil in a polluted soil using Bacillus subtilis,” *African Journal of Biotechnology*, vol. 7, no. 12, p. 1939, 2008.

[38] J. Kurola et al., “Activity, diversity and population size of ammonia-oxidising bacteria in oil-contaminated landfarming soil,” *FEMS Microbiol Lett*, vol. 250, no. 1, pp. 33–38, 2005.

[39] S. M. C. Murphy et al., “Diesel and crude oil biodegradation by cold-adapted microbial communities in the Labrador Sea,” *Appl Environ Microbiol*, vol. 87, no. 20, pp. e00800-21, 2021.

[40] H. Nõlvak et al., “Microbial community dynamics during biodegradation of crude oil and its response to biostimulation in Svalbard seawater at low temperature,” *Microorganisms*, vol. 9, no. 12, p. 2425, 2021.

[41] H. Z. Hamdan and D. A. Salam, “Microbial community evolution during the aerobic biodegradation of petroleum hydrocarbons in marine sediment microcosms: Effect of biostimulation and seasonal variations,” *Environmental Pollution*, vol. 265, p. 114858, 2020.

[42] J. Villalba Primitz et al., “Bioremediation of hydrocarbon-contaminated soil from Carlini Station, Antarctica: effectiveness of different nutrient sources as biostimulation agents,” *Polar Biology*, vol. 44, no. 2, pp. 289–303, 2021.

[43] J. Kim et al., “Enhanced bioremediation of nutrient-amended, petroleum hydrocarbon-contaminated soils over a cold-climate winter: The rate and extent of hydrocarbon biodegradation and microbial response in a pilot-scale biopile subjected to natural seasonal freeze-thaw temperatures,” *Science of the Total Environment*, vol. 612, pp. 903–913, 2018.

[44] L. M. M. Álvarez et al., “Bioremediation of hydrocarbon-contaminated soils in cold regions: Development of a pre-optimized biostimulation biopile-scale field assay in Antarctica,” *Science of the Total Environment*, vol. 590, pp. 194–203, 2017.

[45] W. Chang et al., “Selective biostimulation of cold-and salt-tolerant hydrocarbon-degrading Dietzia maris in petroleum-contaminated sub-Arctic soils with high salinity,” *Journal of Chemical Technology & Biotechnology*, vol. 93, no. 1, pp. 294–304, 2018.

[46] L. M. M. Álvarez et al., “Bioremediation of a petroleum hydrocarbon-contaminated Antarctic soil: optimization of a biostimulation strategy using response-surface methodology (RSM),” *Cold Regions Science and Technology*, vol. 119, pp. 61–67, 2015.

[47] S. D. Siciliano et al., “Total phosphate influences the rate of hydrocarbon degradation but phosphate mineralogy shapes microbial community composition in cold-region calcareous soils,” *Environmental Science & Technology*, vol. 50, no. 10, pp. 5197–5206, 2016.

[48] F. Gomez and M. Sartaj, “Field scale ex-situ bioremediation of petroleum contaminated soil under cold climate conditions,” *International Biodeterioration & Biodegradation*, vol. 85, pp. 375–382, 2013.

[49] W. Chang et al., “Comparison of the effects of variable site temperatures and constant incubation temperatures on the biodegradation of petroleum hydrocarbons in pilot-scale experiments with field-aged contaminated soils from a cold regions site,” *Chemosphere*, vol. 82, no. 6, pp. 872–878, 2011.

[50] J. L. Walworth et al., “Nutrient amendments for contaminated peri-glacial soils: use of cod bone meal as a controlled release nutrient source,” *Cold Reg Sci Technol*, vol. 37, no. 2, pp. 81–88, 2003.

[51] D. Delille et al., “Biostimulation of natural microbial assemblages in oil-amended vegetated and desert sub-Antarctic soils,” *Microb Ecol*, vol. 47, no. 4, pp. 407–415, 2004.

[52] D. Delille et al., “Effect of nutrient enrichments on the bacterial assemblage of Antarctic soils contaminated by diesel or crude oil,” *Polar Record*, vol. 39, no. 4, pp. 309–318, 2003.

[53] R. Margesin, “Potential of cold-adapted microorganisms for bioremediation of oil-polluted Alpine soils,” *Int Biodeterior Biodegradation*, vol. 46, no. 1, pp. 3–10, 2000.

[54] W. Chang et al., “Comparison of the effects of variable site temperatures and constant incubation temperatures on the biodegradation of petroleum hydrocarbons in pilot-scale

experiments with field-aged contaminated soils from a cold regions site," *Chemosphere*, vol. 82, no. 6, pp. 872–878, 2011.

[55] S. el Fantroussi and S. N. Agathos, "Is bioaugmentation a feasible strategy for pollutant removal and site remediation?," *Curr Opin Microbiol*, vol. 8, no. 3, pp. 268–275, 2005.

[56] L. J. Wardell, "Potential for bioremediation of fuel-contaminated soil in Antarctica," *Soil and Sediment Contamination*, vol. 4, no. 2, pp. 111–121, 1995.

[57] O. G. Brakstad et al., "Biodegradation of petroleum oil in cold marine environments," in *Psychrophiles: From biodiversity to biotechnology*, Springer, 2017, pp. 613–644.

[58] F. Berger et al., "Cold shock and cold acclimation proteins in the psychrotrophic bacterium Arthrobacter globiformis SI55," *Journal of Bacteriology*, vol. 178, no. 11, pp. 2999–3007, 1996.

[59] J. P. Verma and D. K. Jaiswal, "Book review: advances in biodegradation and bioremediation of industrial waste." Frontiers Media SA, 2016.

[60] R. Margesin and F. Schinner, "Biological decontamination of oil spills in cold environments," *Journal of Chemical Technology & Biotechnology*, vol. 74, no. 5, pp. 381–389, 1999.

[61] L. G. Bakina et al., "Bioaugmentation: possible scenarios due to application of bacterial preparations for remediation of oil-contaminated soil," *Environmental Geochemistry and Health*, vol. 43, no. 6, pp. 2347–2356, 2021.

[62] J. Wang et al., "Cold-adapted bacteria for bioremediation of crude oil-contaminated soil," *Journal of Chemical Technology & Biotechnology*, vol. 91, no. 8, pp. 2286–2297, 2016.

[63] F. Crisafi et al., "Isolation and degradation potential of a cold-adapted oil/PAH-degrading marine bacterial consortium from Kongsfjorden (Arctic region)," *Rendiconti Lincei*, vol. 27, no. 1, pp. 261–270, 2016.

[64] C. Dong et al., "Distribution of PAHs and the PAH-degrading bacteria in the deep-sea sediments of the high-latitude Arctic Ocean," *Biogeosciences*, vol. 12, no. 7, pp. 2163–2177, 2015.

[65] K. Litova et al., "Growth of Antarctic fungal strains on phenol at low temperatures.," *Journal of BioScience & Biotechnology*, 2014.

[66] M. G. Gerginova et al., "Biodegradation ability of fungal strains isolated from Antarctic towards pah," in *Proceedings of the 13th international conference of environmental science and technology Athens, Greece*, 2013, pp. 5–7.

[67] R. Margesin et al., "Low-temperature biodegradation of petroleum hydrocarbons (n-alkanes, phenol, anthracene, pyrene) by four actinobacterial strains," *International Biodeterioration & Biodegradation*, vol. 84, pp. 185–191, 2013.

[68] B. C. Ferrari et al., “Recovering greater fungal diversity from pristine and diesel fuel contaminated sub-Antarctic soil through cultivation using both a high and a low nutrient media approach,” *Front Microbiol*, vol. 2, p. 217, 2011.

[69] Y. Ma et al., “Pseudomonas, the dominant polycyclic aromatic hydrocarbon-degrading bacteria isolated from Antarctic soils and the role of large plasmids in horizontal gene transfer,” *Environmental Microbiology*, vol. 8, no. 3, pp. 455–465, 2006.

[70] P. Bergauer et al., “Biodegradation of phenol and phenol-related compounds by psychrophilic and cold-tolerant alpine yeasts,” *Chemosphere*, vol. 59, no. 7, pp. 909–918, 2005.

[71] R. Margesin et al., “Degradation of phenol and toxicity of phenolic compounds: a comparison of cold-tolerant Arthrobacter sp. and mesophilic Pseudomonas putida,” *Extremophiles*, vol. 8, no. 3, pp. 201–207, 2004.

[72] M. M. Yakimov et al., “Oleispira antarctica gen. nov., sp. nov., a novel hydrocarbonoclastic marine bacterium isolated from Antarctic coastal sea water,” *Int J Syst Evol Microbiol*, vol. 53, no. 3, pp. 779–785, 2003.

[73] C. A. Baraniecki et al., “Characterization of Sphingomonas sp. Ant 17, an aromatic hydrocarbon-degrading bacterium isolated from Antarctic soil,” *Microbial Ecology*, pp. 44–54, 2002.

[74] G. Panicker et al., “Cold tolerance of Pseudomonas sp. 30-3 isolated from oil-contaminated soil, Antarctica,” *Polar Biol*, vol. 25, no. 1, pp. 5–11, 2002.

[75] A. K. Bej et al., “Cold-tolerant alkane-degrading Rhodococcus species from Antarctica,” *Polar Biology*, vol. 23, no. 2, pp. 100–105, 2000.

[76] L. G. Whyte et al., “Biodegradation of petroleum hydrocarbons by psychrotrophic Pseudomonas strains possessing both alkane (alk) and naphthalene (nah) catabolic pathways,” *Applied and environmental Microbiology*, vol. 63, no. 9, pp. 3719–3723, 1997.

[77] M. Sperfeld et al., “Microbial community of a gasworks aquifer and identification of nitrate-reducing Azoarcus and Georgfuchsia as key players in BTEX degradation,” *Water Res*, vol. 132, pp. 146–157, 2018.

[78] S. Yang et al., “Crude oil treatment leads to shift of bacterial communities in soils from the deep active layer and upper permafrost along the China-Russia crude oil pipeline route,” *PLoS One*, vol. 9, no. 5, p. e96552, 2014.

[79] A. K. Mukherjee and N. K. Bordoloi, “Biodegradation of benzene, toluene, and xylene (BTX) in liquid culture and in soil by Bacillus subtilis and Pseudomonas aeruginosa strains and a formulated bacterial consortium,” *Environmental Science and Pollution Research*, vol. 19, no. 8, pp. 3380–3388, 2012.

[80] A. F. A. Roslee et al., “Growth optimisation and kinetic profiling of diesel biodegradation by a cold-adapted microbial consortium isolated from Trinity Peninsula, Antarctica,” *Biology (Basel)*, vol. 10, no. 6, p. 493, 2021.

[81] C. W. Yeung et al., “Bacterial community evidence for anaerobic degradation of petroleum hydrocarbons in cold climate groundwater,” *Cold Reg Sci Technol*, vol. 86, pp. 55–68, 2013.

[82] T. Teng et al., “Biodegradation of crude oil under low temperature by mixed culture isolated from alpine meadow soil,” *Water, Air, & Soil Pollution*, vol. 232, no. 3, pp. 1–12, 2021.

[83] R. U. Meckenstock et al., “Assessment of bacterial degradation of aromatic hydrocarbons in the environment by analysis of stable carbon isotope fractionation,” *Water, Air and Soil Pollution: Focus*, vol. 2, no. 3, pp. 141–152, 2002.

[84] N. S. Panikov and S. N. Dedysh, “Cold season CH4 and CO2 emission from boreal peat bogs (West Siberia): Winter fluxes and thaw activation dynamics,” *Global Biogeochemical Cycles*, vol. 14, no. 4, pp. 1071–1080, 2000.

[85] K. S. Larsen et al., “Repeated freeze–thaw cycles and their effects on biological processes in two arctic ecosystem types,” *Applied Soil Ecology*, vol. 21, no. 3, pp. 187–195, 2002.

[86] G. J. Michaelson and C. L. Ping, “Soil organic carbon and CO2 respiration at subzero temperature in soils of Arctic Alaska,” *Journal of Geophysical Research: Atmospheres*, vol. 108, no. D2, p. ALT-5, 2003.

[87] B. Elberling and K. K. Brandt, “Uncoupling of microbial CO2 production and release in frozen soil and its implications for field studies of arctic C cycling,” *Soil Biology and Biochemistry*, vol. 35, no. 2, pp. 263–272, 2003.

[88] N. S. Panikov et al., “Microbial activity in soils frozen to below− 39 C,” *Soil Biology and Biochemistry*, vol. 38, no. 4, pp. 785–794, 2006.

[89] I. Altshuler et al., “Microbial life in permafrost,” in *Psychrophiles: from biodiversity to biotechnology*, Springer, 2017, pp. 153–179.

[90] S. J. Tuorto et al., “Bacterial genome replication at subzero temperatures in permafrost,” *ISME J*, vol. 8, no. 1, pp. 139–149, 2014.

[91] D. H. Pieper and W. Reineke, “Engineering bacteria for bioremediation,” *Curr Opin Biotechnol*, vol. 11, no. 3, pp. 262–270, 2000.

[92] J. D. van Elsas et al., “Microbiological and molecular biological methods for monitoring microbial inoculants and their effects in the soil environment,” *Journal of Microbiological Methods*, vol. 32, no. 2, pp. 133–154, 1998.

[93] M. Urgun-Demirtas et al., “Use of genetically engineered microorganisms (GEMs) for the bioremediation of contaminants,” *Crit Rev Biotechnol*, vol. 26, no. 3, pp. 145–164, 2006.

[94] N. Y. Yusof et al., “Structure prediction of Fe (II) 2-oxoglutarate dioxygenase from a psychrophilic yeast Glaciozyma antarctica PI12,” in *AIP Conference Proceedings*, 2015, vol. 1678, no. 1, p. 030014.

[95] M. Abdulrasheed et al., “Response surface methodology optimization and kinetics of diesel degradation by a cold-adapted Antarctic bacterium, Arthrobacter sp. strain AQ5-05,” *Sustainability*, vol. 12, no. 17, p. 6966, 2020.

[96] J. B. van Beilen et al., “Analysis of Pseudomonas putida alkane-degradation gene clusters and flanking insertion sequences: evolution and regulation of the alk genesThe EMBL accession numbers for the sequences reported in this paper are AJ245436 [P. putida (oleovorans) GPo1 alk gene clusters and flanking DNA], AJ233397 (P. putida P1 alk gene clusters and flanking DNA), AJ249793 (P. putida P1 nahKJ genes), AJ249825 [P. putida (oleovorans) GPo1 16S RNA gene] and AJ271219 (P. putida P1 16S RNA gene).,” *Microbiology (N Y)*, vol. 147, no. 6, pp. 1621–1630, 2001.

[97] S. Schneiker et al., “Genome sequence of the ubiquitous hydrocarbon-degrading marine bacterium Alcanivorax borkumensis,” *Nat Biotechnol*, vol. 24, no. 8, pp. 997–1004, 2006.

[98] M. N. P. Remus-Emsermann et al., “Complete genome sequence of Pseudomonas citronellolis P3B5, a candidate for microbial phyllo-remediation of hydrocarbon-contaminated sites,” *Stand Genomic Sci*, vol. 11, no. 1, pp. 1–12, 2016.

[99] L. G. Whyte et al., “Prevalence of alkane monooxygenase genes in Arctic and Antarctic hydrocarbon-contaminated and pristine soils,” *FEMS Microbiology Ecology*, vol. 41, no. 2, pp. 141–150, 2002.

[100] T. Skvortsov et al., “Draft genome sequences of Pseudomonas putida UV4 and UV4/95, toluene dioxygenase-expressing producers of cis-1, 2-dihydrodiols,” *Genome Announc*, vol. 6, no. 1, pp. e01419-17, 2018.

[101] A. Greated et al., “Complete sequence of the IncP-9 TOL plasmid pWW0 from Pseudomonas putida,” *Environmental Microbiology*, vol. 4, no. 12, pp. 856–871, 2002.

[102] A. K. Bej et al., *Polar microbiology: the ecology, biodiversity and bioremediation potential of microorganisms in extremely cold environments*. CRC Press, 2009.

[103] A. P. Luz et al., “A survey of indigenous microbial hydrocarbon degradation genes in soils from Antarctica and Brazil,” *Can J Microbiol*, vol. 50, no. 5, pp. 323–333, 2004.

[104] K. Furukawa et al., “Biphenyl dioxygenases: functional versatilities and directed evolution,” *J Bacteriol*, vol. 186, no. 16, pp. 5189–5196, 2004.

[105] R. N. Austin et al., “Xylene monooxygenase, a membrane-spanning non-heme diiron enzyme that hydroxylates hydrocarbons via a substrate radical intermediate,” *JBIC Journal of Biological Inorganic Chemistry*, vol. 8, no. 7, pp. 733–740, 2003.

[106] C. G. Flocco et al., “Occurrence and diversity of naphthalene dioxygenase genes in soil microbial communities from the Maritime Antarctic,” *Environ Microbiol*, vol. 11, no. 3, pp. 700–714, 2009.

[107] S. Kaiya et al., “Isolation and functional gene analyses of aromatic-hydrocarbon-degrading bacteria from a polychlorinated-dioxin-dechlorinating process,” *Microbes Environ*, p. 1112010337, 2009.

[108] S. Klemm, “Microbial responses to the biostimulation of Subartic hydrocarbon-contaminated soil under seasonal freeze-thaw conditions,” 2010.

[109] V. Barbe et al., “Unique features revealed by the genome sequence of Acinetobacter sp. ADP1, a versatile and naturally transformation competent bacterium,” *Nucleic Acids Res*, vol. 32, no. 19, pp. 5766–5779, 2004.

[110] B. Haak et al., “Cloning, nucleotide sequence, and expression of the plasmid-encoded genes for the two-component 2-halobenzoate 1, 2-dioxygenase from Pseudomonas cepacia 2CBS,” *Journal of Bacteriology*, vol. 177, no. 3, pp. 667–675, 1995.

[111] K. Itoh et al., “Root nodule Bradyrhizobium spp. harbor tfdA α and cadA, homologous with genes encoding 2, 4-dichlorophenoxyacetic acid-degrading proteins,” *Applied and Environmental Microbiology*, vol. 70, no. 4, pp. 2110–2118, 2004.

[112] E. L. Ang et al., “Recent advances in the bioremediation of persistent organic pollutants via biomolecular engineering,” *Enzyme Microb Technol*, vol. 37, no. 5, pp. 487–496, 2005.

[113] T. C. Zhang et al., “Biological treatment of hazardous waste,” in *Current developments in biotechnology and bioengineering*, Elsevier, 2017, pp. 311–340.

[114] R. J. Kolenc et al., “Transfer and expression of mesophilic plasmid-mediated degradative capacity in a psychrotrophic bacterium,” *Appl Environ Microbiol*, vol. 54, no. 3, pp. 638–641, 1988.

[115] L. Siani et al., “Recombinant expression of Toluene o-Xylene Monooxygenase (ToMO) from Pseudomonas stutzeri OX1 in the marine Antarctic bacterium Pseudoalteromonas haloplanktis TAC125,” *J Biotechnol*, vol. 126, no. 3, pp. 334–341, 2006.

[116] E. Parrilli et al., “Engineering of a psychrophilic bacterium for the bioremediation of aromatic compounds,” *Bioeng Bugs*, vol. 1, no. 3, pp. 213–216, 2010.

[117] R. Margesin, *Permafrost soils*, vol. 16. Springer Science & Business Media, 2008.

[118] I. M. Banat et al., “Microbial biosurfactants production, applications and future potential,” *Appl Microbiol Biotechnol*, vol. 87, no. 2, pp. 427–444, 2010.

[119] C. N. Mulligan, “Recent advances in the environmental applications of biosurfactants,” *Current Opinion in Colloid & Interface Science*, vol. 14, no. 5, pp. 372–378, 2009.

[120] R. Malavenda et al., “Biosurfactant production by Arctic and Antarctic bacteria growing on hydrocarbons,” *Polar Biol*, vol. 38, no. 10, pp. 1565–1574, 2015.

[121] G. Mohanty and S. Mukherji, “Biodegradation rate of diesel range n-alkanes by bacterial cultures Exiguobacterium aurantiacum and Burkholderia cepacia,” *International Biodeterioration & Biodegradation*, vol. 61, no. 3, pp. 240–250, 2008.

[122] T. T. Nguyen et al., “Rhamnolipid biosurfactant mixtures for environmental remediation,” *Water Res*, vol. 42, no. 6–7, pp. 1735–1743, 2008.

[123] M. L. Nievas et al., “Biodegradation pattern of hydrocarbons from a fuel oil-type complex residue by an emulsifier-producing microbial consortium,” *J Hazard Mater*, vol. 154, no. 1–3, pp. 96–104, 2008.

[124] M. M. Yakimov et al., “Characterization of antarctic hydrocarbon-degrading bacteria capable of producing bioemulsifiers.,” *New Microbiol*, vol. 22, no. 3, pp. 249–256, 1999.

[125] F. Pini et al., “Molecular and physiological characterisation of psychrotrophic hydrocarbon-degrading bacteria isolated from Terra Nova Bay (Antarctica),” *European Journal of Soil Biology*, vol. 43, no. 5–6, pp. 368–379, 2007.

[126] P. Guo et al., “Isolation and characterization of a biosurfactant producing strain Planococcus sp. XW-1 from the cold marine environment,” *Int J Environ Res Public Health*, vol. 19, no. 2, p. 782, 2022.

[127] H. Thatoi et al., “Bacterial chromate reductase, a potential enzyme for bioremediation of hexavalent chromium: a review,” *Journal of Environmental Management*, vol. 146, pp. 383–399, 2014.

[128] T. D. Sutherland et al., “Enzymatic bioremediation: from enzyme discovery to applications,” *Clinical and experimental pharmacology and physiology*, vol. 31, no. 11, pp. 817–821, 2004.

[129] G. Feller and C. Gerday, “Psychrophilic enzymes: hot topics in cold adaptation,” *Nature reviews microbiology*, vol. 1, no. 3, pp. 200–208, 2003.

[130] E. R. Master et al., “Biphenyl dioxygenase from an arctic isolate is not cold adapted,” *Appl Environ Microbiol*, vol. 74, no. 12, pp. 3908–3911, 2008.

[131] I. R. McDonald et al., “Diversity of soluble methane monooxygenase-containing methanotrophs isolated from polluted environments,” *FEMS Microbiology Letters*, vol. 255, no. 2, pp. 225–232, 2006.

[132] G. Bertoni et al., “Analysis of the gene cluster encoding toluene/o-xylene monooxygenase from Pseudomonas stutzeri OX1,” *Applied and Environmental Microbiology*, vol. 64, no. 10, pp. 3626–3632, 1998.

[133] J. B. van Beilen and E. G. Funhoff, “Expanding the alkane oxygenase toolbox: new enzymes and applications,” *Current Opinion in Biotechnology*, vol. 16, no. 3, pp. 308–314, 2005.

[134] A. P. Luz et al., “A survey of indigenous microbial hydrocarbon degradation genes in soils from Antarctica and Brazil,” *Can J Microbiol*, vol. 50, no. 5, pp. 323–333, 2004.

[135] C. G. Flocco et al., “Occurrence and diversity of naphthalene dioxygenase genes in soil microbial communities from the Maritime Antarctic,” *Environ Microbiol*, vol. 11, no. 3, pp. 700–714, 2009.

[136] M. Luz Paje and I. Couperwhite, “Benzene metabolism via the intradiol cleavage in a Rhodococcus sp.,” *World Journal of Microbiology and Biotechnology*, vol. 12, no. 6, pp. 653–654, 1996.

[137] A. S. da Silva et al., “Properties of catechol 1, 2-dioxygenase in the cell free extract and immobilized extract of Mycobacterium fortuitum,” *Brazilian Journal of Microbiology*, vol. 44, pp. 291–297, 2013.

[138] A. K. Bej et al., *Polar microbiology: the ecology, biodiversity and bioremediation potential of microorganisms in extremely cold environments*. CRC Press, 2009.

[139] Y. Nie et al., “Diverse alkane hydroxylase genes in microorganisms and environments,” *Sci Rep*, vol. 4, no. 1, pp. 1–11, 2014.

[140] O. S. Kwean et al., “4-Chlorophenol biodegradation facilitator composed of recombinant multi-biocatalysts immobilized onto montmorillonite,” *Bioresour Technol*, vol. 259, pp. 268–275, 2018.

[141] M. Alcalde et al., “Environmental biocatalysis: from remediation with enzymes to novel green processes,” *TRENDS in Biotechnology*, vol. 24, no. 6, pp. 281–287, 2006.

[142] A. Gullotto et al., “Combined action of a bacterial monooxygenase and a fungal laccase for the biodegradation of mono-and poly-aromatic hydrocarbons,” *Bioresour Technol*, vol. 99, no. 17, pp. 8353–8359, 2008.

[143] J. Mehta et al., “Recent advances in enzyme immobilization techniques: Metal-organic frameworks as novel substrates,” *Coordination Chemistry Reviews*, vol. 322, pp. 30–40, 2016.

[144] D. E. Dodor et al., “Oxidation of anthracene and benzo [a] pyrene by immobilized laccase from Trametes versicolor,” *Enzyme and Microbial Technology*, vol. 35, no. 2–3, pp. 210–217, 2004.

[145] E. Skoronski et al., “Immobilization of laccase from Aspergillus oryzae on graphene nanosheets,” *Int J Biol Macromol*, vol. 99, pp. 121–127, 2017.

[146] D. Wasilkowski et al., “Changes in enzyme activities and microbial community structure in heavy metal-contaminated soil under in situ aided phytostabilization,” *CLEAN–soil, air, Water*, vol. 42, no. 11, pp. 1618–1625, 2014.

[147] M. Daghio et al., “Hydrocarbon degrading microbial communities in bench scale aerobic biobarriers for gasoline contaminated groundwater treatment,” *Chemosphere*, vol. 130, pp. 34–39, 2015.

[148] Z. Bayat et al., “Immobilization of microbes for bioremediation of crude oil polluted environments: a mini review,” *Open Microbiol J*, vol. 9, p. 48, 2015.

[149] V. Rivelli et al., “Persistence and degrading activity of free and immobilised allochthonous bacteria during bioremediation of hydrocarbon-contaminated soils,” *Biodegradation*, vol. 24, no. 1, pp. 1–11, 2013.

[150] E. A. Podorozhko et al., “Hydrophobised sawdust as a carrier for immobilisation of the hydrocarbon-oxidizing bacterium Rhodococcus ruber,” *Bioresource Technology*, vol. 99, no. 6, pp. 2001–2008, 2008.

[151] I. Krallish et al., “Phenol degradation by immobilized cold-adapted yeast strains of Cryptococcus terreus and Rhodotorula creatinivora,” *Extremophiles*, vol. 10, no. 5, pp. 441–449, 2006.

[152] M. Hazaimeh et al., “Enhanced crude oil hydrocarbon degradation by self-immobilized bacterial consortium culture on sawdust and oil palm empty fruit bunch,” *Ann Microbiol*, vol. 64, no. 4, pp. 1769–1777, 2014.

[153] J. Aislabie et al., “Potential for biodegradation of hydrocarbons in soil from the Ross Dependency, Antarctica,” *Applied Microbiology and Biotechnology*, vol. 49, no. 2, pp. 210–214, 1998.

[154] J. You et al., “BTEX degradation by a newly isolated bacterium: Performance, kinetics, and mechanism,” *International Biodeterioration & Biodegradation*, vol. 129, pp. 202–208, 2018.

[155] M. Chang et al., “Kinetics of competitive inhibition and cometabolism in the biodegradation of benzene, toluene, and p-xylene by two Pseudomonas isolates.,” *Biotechnology and Bioengineering*, vol. 41, no. 11, pp. 1057–1065, 1993.

[156] F. L. G. Arenghi et al., “Organization and regulation of meta cleavage pathway genes for toluene and o-xylene derivative degradation in Pseudomonas stutzeri OX1,” *Appl Environ Microbiol*, vol. 67, no. 7, pp. 3304–3308, 2001.

[157] K. Khodaei et al., “BTEX biodegradation in contaminated groundwater using a novel strain (Pseudomonas sp. BTEX-30),” *International Biodeterioration & Biodegradation*, vol. 116, pp. 234–242, 2017.

[158] I. Chicca et al., “Degradation of BTEX mixture by a new Pseudomonas putida strain: role of the quorum sensing in the modulation of the upper BTEX oxidative pathway,” *Environmental Science and Pollution Research*, vol. 27, no. 29, pp. 36203–36214, 2020.

[159] C. Abegglen and H. Siegrist, “Micropolluants Dans Les Eaux Usées Urbaines. Etape de Traitement Supplémentaire Dans Les Stations d’épuration,” *Swiss Federal Office for the Environment, Connaissance de l’environnement*, vol. 1214, 2012.

[160] Q. Wang et al., “Experimental and kinetic study on the cometabolic biodegradation of phenol and 4-chlorophenol by psychrotrophic Pseudomonas putida LY1,” *Environmental Science and Pollution Research*, vol. 22, no. 1, pp. 565–573, 2015.

[161] M. T. Ashraf et al., “Process of p-xylene production by highly selective methylation of toluene,” *Industrial & Engineering Chemistry Research*, vol. 52, no. 38, pp. 13730–13737, 2013.

[162] J. v Littlejohns and A. J. Daugulis, “Kinetics and interactions of BTEX compounds during degradation by a bacterial consortium,” *Process Biochemistry*, vol. 43, no. 10, pp. 1068–1076, 2008.

[163] A. Gąszczak et al., “Kinetics of cometabolic biodegradation of 4-chlorophenol and phenol by stenotrophomonas maltophilia KB2,” *Chemical and Process Engineering*, vol. 39, no. 4, 2018.

[164] I. Kalavrouziotis et al., “Group method of data handling (GMDH) in modelling of growth dynamics of trees irrigated with wastewater,” *Int J Environ Pollut*, vol. 21, no. 4, pp. 350–364, 2004.

[165] A. Tsipa et al., “Optimal bioprocess design through a gene regulatory network–Growth kinetic hybrid model: Towards replacing Monod kinetics,” *Metab Eng*, vol. 48, pp. 129–137, 2018.

[166] R. S. Horvath, “Microbial co-metabolism and the degradation of organic compounds in nature,” *Bacteriol Rev*, vol. 36, no. 2, pp. 146–155, 1972.

[167] F. X. Prenafeta-Boldú et al., “Substrate interactions during the biodegradation of benzene, toluene, ethylbenzene, and xylene (BTEX) hydrocarbons by the fungus Cladophialophora sp. strain T1,” *Applied and Environmental Microbiology*, vol. 68, no. 6, pp. 2660–2665, 2002.

[168] J. E. Zajic and B. Supplisson, “Emulsification and degradation of ‘Bunker C’ fuel oil by microorganisms,” *Biotechnology and Bioengineering*, vol. 14, no. 3, pp. 331–343, 1972.

[169] J. D. Rasinger et al., “Evaluation of an FIA operated amperometric bacterial biosensor, based on pseudomonas putida F1 for the detection of benzene, toluene, ethylbenzene, and xylenes (BTEX),” *Anal Lett*, vol. 38, no. 10, pp. 1531–1547, 2005.

[170] A. Yavas and B. Icgen, “Aerobic bacterial degraders with their relative pathways for efficient removal of individual BTEX compounds,” *CLEAN–Soil, Air, Water*, vol. 46, no. 11, p. 1800068, 2018.

[171] C.-W. Lin et al., “Multi-substrate biodegradation kinetics of MTBE and BTEX mixtures by Pseudomonas aeruginosa,” *Process biochemistry*, vol. 42, no. 8, pp. 1211–1217, 2007.

[172] M. González-Pleiter et al., “Secondary nanoplastics released from a biodegradable microplastic severely impact freshwater environments,” *Environmental Science: Nano*, vol. 6, no. 5, pp. 1382–1392, 2019.

[173] O. J. Hao et al., “Kinetics of phenol and chlorophenol utilization by Acinetobacter species,” *Chemosphere*, vol. 46, no. 6, pp. 797–807, 2002.

[174] Y. Li et al., “Aerobic degradation of trichloroethylene by co-metabolism using phenol and gasoline as growth substrates,” *International Journal of Molecular Sciences*, vol. 15, no. 5, pp. 9134–9148, 2014.

[175] A. G. Ivakhnenko and G. A. Ivakhnenko, “The review of problems solvable by algorithms of the group method of data handling (GMDH),” *Pattern recognition and image analysis c/c of raspoznavaniye obrazov i analiz izobrazhenii*, vol. 5, pp. 527–535, 1995.

[176] Y. Shinohara et al., “Predictive evaluation for software testing progress via GMDH networks,” *Electronics and Communications in Japan (Part III: Fundamental Electronic Science)*, vol. 82, no. 5, pp. 22–28, 1999.

[177] I. Ebtehaj et al., “GMDH-type neural network approach for modeling the discharge coefficient of rectangular sharp-crested side weirs,” *Engineering Science and Technology, an International Journal*, vol. 18, no. 4, pp. 746–757, 2015.

[178] A. G. Ivakhnenko, “Polynomial theory of complex systems,” *IEEE transactions on Systems, Man, and Cybernetics*, no. 4, pp. 364–378, 1971.

[179] T. Kondo, “Revised gmdh-type neural network algorithm with a feedback loop identifying sigmoid function neural network,” in *Proceedings of the ISCIE International Symposium on Stochastic Systems Theory and its Applications*, 2006, vol. 2006, pp. 137–142.

[180] S. J. Farlow, *Self-organizing methods in modeling: GMDH type algorithms*. CrC Press, 2020.

[181] A. Jamali, “Pareto robust design of controllers with probabilistic uncertainties using multi objective evolutionary algorithms,” Ph. D. Thesis, University of Guilan, 2009.

[182] A. Abdollahi et al., “Experimental study to obtain the viscosity of CuO-loaded nanofluid: effects of nanoparticles’ mass fraction, temperature and basefluid’s types to develop a correlation,” *Meccanica*, vol. 53, no. 15, pp. 3739–3757, 2018.

[183] F. X. Prenafeta-Boldú et al., “Substrate interactions during the biodegradation of benzene, toluene, ethylbenzene, and xylene (BTEX) hydrocarbons by the fungus Cladophialophora sp. strain T1,” *Applied and Environmental Microbiology*, vol. 68, no. 6, pp. 2660–2665, 2002.

[184] L. Tijhuis et al., “A thermodynamically based correlation for maintenance Gibbs energy requirements in aerobic and anaerobic chemotrophic growth,” *Biotechnol Bioeng*, vol. 42, no. 4, pp. 509–519, 1993.

[185] F. L. G. Arenghi et al., “Identification of the Pseudomonas stutzeri OX1 toluene–o-xylene monooxygenase regulatory gene (touR) and of its cognate promoter,” *Appl Environ Microbiol*, vol. 65, no. 9, pp. 4057–4063, 1999.

[186] M. M. Bradford, "A rapid and sensitive method for the quantitation of microgram quantities of protein utilizing the principle of protein-dye binding," *Anal Biochem*, vol. 72, no. 1–2, pp. 248–254, 1976.

[187] M. L. B. da Silva and P. J. J. Alvarez, "Indole-based assay to assess the effect of ethanol on Pseudomonas putida F1 dioxygenase activity," *Biodegradation*, vol. 21, no. 3, pp. 425–430, 2010.

[188] P. Kumar et al., "Agro-industrial residues as a unique support in a sand filter to enhance the bioactivity to remove microcystin-Leucine aRginine and organics," *Science of the total environment*, vol. 670, pp. 971–981, 2019.

[189] K. H. Kwon and S. H. Yeom, "Optimal microbial adaptation routes for the rapid degradation of high concentration of phenol," *Bioprocess Biosyst Eng*, vol. 32, no. 4, pp. 435–442, 2009.

[190] F. L. G. Arenghi et al., "Organization and regulation of meta cleavage pathway genes for toluene and o-xylene derivative degradation in Pseudomonas stutzeri OX1," *Appl Environ Microbiol*, vol. 67, no. 7, pp. 3304–3308, 2001.

[191] M. Boonsaner et al., "Phytoremediation of BTEX contaminated soil by Canna× generalis," *Ecotoxicol Environ Saf*, vol. 74, no. 6, pp. 1700–1707, 2011.

[192] D. E. C. Mazzeo et al., "Application of micronucleus test and comet assay to evaluate BTEX biodegradation," *Chemosphere*, vol. 90, no. 3, pp. 1030–1036, 2013.

[193] S. Habib et al., "Bioremediation of petroleum hydrocarbon in Antarctica by microbial species: an overview.," *Pertanika Journal of Science & Technology*, vol. 26, no. 1, 2018.

[194] Y. K. Kunukcu, "In situ bioremediation of groundwater contaminated with petroleum constituents using oxygen release compounds (ORCs)," *Journal of Environmental Science and Health, Part A*, vol. 42, no. 7, pp. 839–845, 2007.

[195] K.-F. Chen et al., "Control of petroleum-hydrocarbon contaminated groundwater by intrinsic and enhanced bioremediation," *Journal of Environmental Sciences*, vol. 22, no. 6, pp. 864–871, 2010.

[196] M. Nikolopoulou et al., "Evaluation of autochthonous bioaugmentation and biostimulation during microcosm-simulated oil spills," *Mar Pollut Bull*, vol. 72, no. 1, pp. 165–173, 2013.

[197] N. Hassan et al., "Temperature driven membrane lipid adaptation in glacial psychrophilic bacteria," *Frontiers in Microbiology*, vol. 11, p. 824, 2020.

[198] S. Miri et al., "Recent biotechnological advances in petroleum hydrocarbons degradation under cold climate conditions: A review," *Critical Reviews in Environmental Science and Technology*, vol. 49, no. 7, pp. 553–586, 2019.

[199] D. Georlette et al., "Some like it cold: biocatalysis at low temperatures," *FEMS Microbiol Rev*, vol. 28, no. 1, pp. 25–42, 2004.

[200] H. Chandran et al., “Microbial biodiversity and bioremediation assessment through omics approaches,” *Frontiers in Environmental Chemistry*, vol. 1, p. 570326, 2020.

[201] S. Bhandari et al., “Microbial enzymes used in bioremediation,” *Journal of Chemistry*, vol. 2021, 2021.

[202] D. R. Lovley, “Cleaning up with genomics: applying molecular biology to bioremediation,” *Nature Reviews Microbiology*, vol. 1, no. 1, pp. 35–44, 2003.

[203] D. K. Chaudhary and J. Kim, “New insights into bioremediation strategies for oil-contaminated soil in cold environments,” *International Biodeterioration & Biodegradation*, vol. 142, pp. 58–72, 2019.

[204] Y. Li et al., “Aerobic degradation of trichloroethylene by co-metabolism using phenol and gasoline as growth substrates,” *International Journal of Molecular Sciences*, vol. 15, no. 5, pp. 9134–9148, 2014.

[205] V. de Lorenzo and J. Pérez-Martín, “Regulatory noise in prokaryotic promoters: how bacteria learn to respond to novel environmental signals,” *Mol Microbiol*, vol. 19, no. 6, pp. 1177–1184, 1996.

[206] E. Díaz and M. A. Prieto, “Bacterial promoters triggering biodegradation of aromatic pollutants,” *Current Opinion in Biotechnology*, vol. 11, no. 5, pp. 467–475, 2000.

[207] M. Chang et al., “Kinetics of competitive inhibition and cometabolism in the biodegradation of benzene, toluene, and p-xylene by two Pseudomonas isolates.,” *Biotechnology and Bioengineering*, vol. 41, no. 11, pp. 1057–1065, 1993.

[208] F. L. G. Arenghi et al., “Organization and regulation of meta cleavage pathway genes for toluene and o-xylene derivative degradation in Pseudomonas stutzeri OX1,” *Appl Environ Microbiol*, vol. 67, no. 7, pp. 3304–3308, 2001.

[209] K. Khodaei et al., “BTEX biodegradation in contaminated groundwater using a novel strain (Pseudomonas sp. BTEX-30),” *International Biodeterioration & Biodegradation*, vol. 116, pp. 234–242, 2017.

[210] I. Chicca et al., “Degradation of BTEX mixture by a new Pseudomonas putida strain: role of the quorum sensing in the modulation of the upper BTEX oxidative pathway,” *Environmental Science and Pollution Research*, vol. 27, no. 29, pp. 36203–36214, 2020.

[211] S. Miri et al., “Biodegradation of p-xylene—a comparison of three psychrophilic Pseudomonas strains through the lens of gene expression,” *Environmental Science and Pollution Research*, vol. 29, no. 15, pp. 21465–21479, Mar. 2022 [Online]. Available: 10.1007/s11356-021-17387-5.

[212] A.-E. Rotaru et al., “Highly enriched Betaproteobacteria growing anaerobically with p-xylene and nitrate,” *FEMS Microbiol Ecol*, vol. 71, no. 3, pp. 460–468, 2010.

[213] M. J. Worsey and P. A. Williams, “Metabolism of toluene and xylenes by Pseudomonas (putida (arvilla) mt-2: evidence for a new function of the TOL plasmid,” *Journal of Bacteriology*, vol. 124, no. 1, pp. 7–13, 1975.

[214] M. A. K. Rahul and C. Balomajumder, “Biodegradation of waste gas containing mixture of BTEX by B. Sphaericus,” *Research Journal of Chemical Sciences*, vol. 1, no. 5, pp. 52–60, 2011.

[215] K. Tamura et al., “MEGA5: molecular evolutionary genetics analysis using maximum likelihood, evolutionary distance, and maximum parsimony methods,” *Mol Biol Evol*, vol. 28, no. 10, pp. 2731–2739, 2011.

[216] R. L. Bohon and W. F. Claussen, “The solubility of aromatic hydrocarbons in water1,” *J Am Chem Soc*, vol. 73, no. 4, pp. 1571–1578, 1951.

[217] S. Miri et al., “Psychrozymes as novel tools to biodegrade p-xylene and potential use for contaminated groundwater in the cold climate,” *Bioresource Technology*, vol. 321, p. 124464, 2021.

[218] T. del Castillo and J. L. Ramos, “Simultaneous catabolite repression between glucose and toluene metabolism in Pseudomonas putida is channeled through different signaling pathways,” *J Bacteriol*, vol. 189, no. 18, pp. 6602–6610, 2007.

[219] J. Ye et al., “Primer-BLAST: a tool to design target-specific primers for polymerase chain reaction,” *BMC Bioinformatics*, vol. 13, no. 1, pp. 1–11, 2012.

[220] M. W. Pfaffl, “A new mathematical model for relative quantification in real-time RT–PCR,” *Nucleic Acids Res*, vol. 29, no. 9, pp. e45–e45, 2001.

[221] S. le Meur et al., “Production of medium-chain-length polyhydroxyalkanoates by sequential feeding of xylose and octanoic acid in engineered Pseudomonas putida KT2440,” *BMC Biotechnol*, vol. 12, no. 1, pp. 1–12, 2012.

[222] S. T. L. Harrison, “Bacterial cell disruption: a key unit operation in the recovery of intracellular products,” *Biotechnol Adv*, vol. 9, no. 2, pp. 217–240, 1991.

[223] Z. Nagy et al., “β-Galactosidase of Penicillium chrysogenum: production, purification, and characterization of the enzyme,” *Protein Expr Purif*, vol. 21, no. 1, pp. 24–29, 2001.

[224] F. L. G. Arenghi et al., “Identification of the Pseudomonas stutzeri OX1 toluene–o-xylene monooxygenase regulatory gene (touR) and of its cognate promoter,” *Appl Environ Microbiol*, vol. 65, no. 9, pp. 4057–4063, 1999.

[225] M. M. Bradford, “A rapid and sensitive method for the quantitation of microgram quantities of protein utilizing the principle of protein-dye binding,” *Anal Biochem*, vol. 72, no. 1–2, pp. 248–254, 1976.

[226] N. Srivastva et al., “Degradation kinetics and metabolites in continuous biodegradation of isoprene,” *Bioresour Technol*, vol. 206, pp. 275–278, 2016.

[227] L. Tijhuis et al., “A thermodynamically based correlation for maintenance Gibbs energy requirements in aerobic and anaerobic chemotrophic growth,” *Biotechnol Bioeng*, vol. 42, no. 4, pp. 509–519, 1993.

[228] N. Kabelitz et al., “Enhancement of the microbial community biomass and diversity during air sparging bioremediation of a soil highly contaminated with kerosene and BTEX,” *Appl Microbiol Biotechnol*, vol. 82, no. 3, pp. 565–577, 2009.

[229] F. L. G. Arenghi et al., “Identification of the Pseudomonas stutzeri OX1 toluene–o-xylene monooxygenase regulatory gene (touR) and of its cognate promoter,” *Appl Environ Microbiol*, vol. 65, no. 9, pp. 4057–4063, 1999.

[230] L. O. Odokuma and S. I. Oliwe, “Toxicity of substituted benzene derivatives to four chemolithotrophic bacteria isolated from the New Calabar River,” *Global Journal of Environmental Sciences*, vol. 2, no. 2, pp. 72–77, 2003.

[231] Y. You et al., “Biodegradation of BTEX mixture by Pseudomonas putida YNS 1 isolated from oil-contaminated soil,” *Journal of Basic Microbiology*, vol. 53, no. 5, pp. 469–475, 2013.

[232] E. Jeong et al., “Removal of p-xylene with Pseudomonas sp. NBM21 in biofilter,” *J Biosci Bioeng*, vol. 102, no. 4, pp. 281–287, 2006.

[233] I. Meyer-Cifuentes et al., “Isolation and characterization of Magnetospirillum sp. strain 15-1 as a representative anaerobic toluene-degrader from a constructed wetland model,” *PLoS One*, vol. 12, no. 4, p. e0174750, 2017.

[234] P. J. Alvarez and T. M. Vogel, “Substrate interactions of benzene, toluene, and para-xylene during microbial degradation by pure cultures and mixed culture aquifer slurries,” *Applied and Environmental Microbiology*, vol. 57, no. 10, pp. 2981–2985, 1991.

[235] J. You et al., “BTEX degradation by a newly isolated bacterium: Performance, kinetics, and mechanism,” *International Biodeterioration & Biodegradation*, vol. 129, pp. 202–208, 2018.

[236] S. M. Davoodi et al., “Bioremediation of unconventional oil contaminated ecosystems under natural and assisted conditions: a review,” *Environmental Science & Technology*, vol. 54, no. 4, pp. 2054–2067, 2020.

[237] S. Benson and J. Shapiro, “TOL is a broad-host-range plasmid,” *Journal of Bacteriology*, vol. 135, no. 1, pp. 278–280, 1978.

[238] B. F. Smets et al., “Stability and conjugal transfer kinetics of a TOL plasmid in Pseudomonas aeruginosa PAO 1162,” *FEMS Microbiol Ecol*, vol. 15, no. 3–4, pp. 337–349, 1994.

[239] H. Yu et al., “The roles of intermediates in biodegradation of benzene, toluene, and p-xylene by Pseudomonas putida F1,” *Biodegradation*, vol. 12, no. 6, pp. 455–463, 2001.

[240] B. Bühler et al., “Characterization and application of xylene monooxygenase for multistep biocatalysis,” *Appl Environ Microbiol*, vol. 68, no. 2, pp. 560–568, 2002.

[241] S. Marqués and J. L. Ramos, “Transcriptional control of the Pseudomonas putida TOL plasmid catabolic pathways,” *Mol Microbiol*, vol. 9, no. 5, pp. 923–929, 1993.

[242] R. Moreno et al., “The Crc global regulator inhibits the Pseudomonas putida pWW0 toluene/xylene assimilation pathway by repressing the translation of regulatory and structural genes,” *Journal of Biological Chemistry*, vol. 285, no. 32, pp. 24412–24419, 2010.

[243] A. de Las Heras et al., “Increasing signal specificity of the TOL network of Pseudomonas putida mt-2 by rewiring the connectivity of the master regulator XylR,” 2012.

[244] J.-S. Seo et al., “Bacterial degradation of aromatic compounds,” *Int J Environ Res Public Health*, vol. 6, no. 1, pp. 278–309, 2009.

[245] F. Velázquez et al., “Inferring the genetic network of m-xylene metabolism through expression profiling of the xyl genes of Pseudomonas putida mt-2,” *Mol Microbiol*, vol. 57, no. 6, pp. 1557–1569, 2005.

[246] J. L. Ramos et al., “Regulatory circuits controlling transcription of TOL plasmid operon encoding meta-cleavage pathway for degradation of alkylbenzoates by Pseudomonas,” *Mol Microbiol*, vol. 1, no. 1, pp. 293–300, 1987.

[247] S. Inouye et al., “Determination of the transcription initiation site and identification of the protein product of the regulatory gene xylR for xyl operons on the TOL plasmid,” *J Bacteriol*, vol. 163, no. 3, pp. 863–869, 1985.

[248] E. J. Choi et al., “Comparative genomic analysis and benzene, toluene, ethylbenzene, and o-, m-, and p-xylene (BTEX) degradation pathways of Pseudoxanthomonas spadix BD-a59,” *Appl Environ Microbiol*, vol. 79, no. 2, pp. 663–671, 2013.

[249] S.-C. Tsai and Y.-K. Li, “Purification and characterization of a catechol 1, 2-dioxygenase from a phenol degrading Candida albicans TL3,” *Arch Microbiol*, vol. 187, no. 3, pp. 199–206, 2007.

[250] F. X. Prenafeta-Boldú et al., “Substrate interactions during the biodegradation of benzene, toluene, ethylbenzene, and xylene (BTEX) hydrocarbons by the fungus Cladophialophora sp. strain T1,” *Applied and Environmental Microbiology*, vol. 68, no. 6, pp. 2660–2665, 2002.

[251] L. Zhang et al., “Biodegradation of benzene, toluene, ethylbenzene, and o-xylene by the bacterium Mycobacterium cosmeticum byf-4,” *Chemosphere*, vol. 90, no. 4, pp. 1340–1347, 2013.

[252] M. Fay et al., “Toxicological profile for xylene,” 2007.

[253] S. Habib et al., “Bioremediation of petroleum hydrocarbon in Antarctica by microbial species: an overview.,” *Pertanika Journal of Science & Technology*, vol. 26, no. 1, 2018.

[254] S. A. B. Weelink et al., “Degradation of BTEX by anaerobic bacteria: physiology and application,” *Reviews in Environmental Science and Bio/Technology*, vol. 9, no. 4, pp. 359–385, 2010.

[255] M. Alcalde et al., “Environmental biocatalysis: from remediation with enzymes to novel green processes,” *TRENDS in Biotechnology*, vol. 24, no. 6, pp. 281–287, 2006.

[256] A. Gullotto et al., “Combined action of a bacterial monooxygenase and a fungal laccase for the biodegradation of mono-and poly-aromatic hydrocarbons,” *Bioresour Technol*, vol. 99, no. 17, pp. 8353–8359, 2008.

[257] S. F. Altschul et al., “Basic local alignment search tool,” *J Mol Biol*, vol. 215, no. 3, pp. 403–410, 1990.

[258] K. Tamura et al., “MEGA5: molecular evolutionary genetics analysis using maximum likelihood, evolutionary distance, and maximum parsimony methods,” *Mol Biol Evol*, vol. 28, no. 10, pp. 2731–2739, 2011.

[259] M. L. B. da Silva and P. J. J. Alvarez, “Indole-based assay to assess the effect of ethanol on Pseudomonas putida F1 dioxygenase activity,” *Biodegradation*, vol. 21, no. 3, pp. 425–430, 2010.

[260] Y. Li et al., “Aerobic degradation of trichloroethylene by co-metabolism using phenol and gasoline as growth substrates,” *International Journal of Molecular Sciences*, vol. 15, no. 5, pp. 9134–9148, 2014.

[261] R. L. Bohon and W. F. Claussen, “The solubility of aromatic hydrocarbons in water1,” *J Am Chem Soc*, vol. 73, no. 4, pp. 1571–1578, 1951.

[262] S.-H. Jang et al., “Genome sequence of cold-adapted Pseudomonas mandelii strain JR-1.” Am Soc Microbiol, 2012.

[263] S. Verhille et al., “Taxonomic study of bacteria isolated from natural mineral waters: proposal of Pseudomonas jessenii sp. nov. and Pseudomonas mandelii sp. nov.,” *Syst Appl Microbiol*, vol. 22, no. 1, pp. 45–58, 1999.

[264] C. E. Dandie et al., “Analysis of denitrification genes and comparison of nosZ, cnorB and 16S rDNA from culturable denitrifying bacteria in potato cropping systems,” *Syst Appl Microbiol*, vol. 30, no. 2, pp. 128–138, 2007.

[265] R. Li et al., “Psychrotrophic Pseudomonas mandelii CBS-1 produces high levels of poly-β-hydroxybutyrate,” *Springerplus*, vol. 2, no. 1, pp. 1–7, 2013.

[266] N. Liu et al., “Analysis of biodegradation by-products of nitrobenzene and aniline mixture by a cold-tolerant microbial consortium,” *Journal of Hazardous Materials*, vol. 260, pp. 323–329, 2013.

[267] G. Gallastegui et al., “Performance and macrokinetic analysis of biofiltration of toluene and p-xylene mixtures in a conventional biofilter packed with inert material,” *Bioresour Technol*, vol. 102, no. 17, pp. 7657–7665, 2011.

[268] L. Kumar and N. Bharadvaja, “Enzymatic bioremediation: a smart tool to fight environmental pollutants,” in *Smart Bioremediation Technologies*, Elsevier, 2019, pp. 99–118.

[269] F. L. G. Arenghi et al., “Organization and regulation of meta cleavage pathway genes for toluene and o-xylene derivative degradation in Pseudomonas stutzeri OX1,” *Appl Environ Microbiol*, vol. 67, no. 7, pp. 3304–3308, 2001.

[270] J. L. Slabbert, “Improved bacterial growth test for rapid water toxicity screening,” *Bull. Environ. Contam. Toxicol.;(United States)*, vol. 37, no. 4, 1986.

[271] M. Moo-Young, *Comprehensive biotechnology*. Elsevier, 2019.

[272] D. Georlette et al., “Some like it cold: biocatalysis at low temperatures,” *FEMS Microbiol Rev*, vol. 28, no. 1, pp. 25–42, 2004.

[273] P. A. Fields and G. N. Somero, “Hot spots in cold adaptation: localized increases in conformational flexibility in lactate dehydrogenase A4 orthologs of Antarctic notothenioid fishes,” *Proceedings of the National Academy of Sciences*, vol. 95, no. 19, pp. 11476–11481, 1998.

[274] G. Feller and C. Gerday, “Psychrophilic enzymes: hot topics in cold adaptation,” *Nature reviews microbiology*, vol. 1, no. 3, pp. 200–208, 2003.

[275] M. Suzuki et al., “Primary structure of xylene monooxygenase: similarities to and differences from the alkane hydroxylation system,” *J Bacteriol*, vol. 173, no. 5, pp. 1690–1695, 1991.

[276] S. Inouye et al., “Molecular cloning of regulatory gene xylR and operator-promoter regions of the xylABC and xylDEGF operons of the TOL plasmid.,” *J Bacteriol*, vol. 155, no. 3, p. 1192, 1983.

[277] L. Ciric et al., “Hydrocarbon utilization within a diesel-degrading bacterial consortium,” *FEMS Microbiol Lett*, vol. 303, no. 2, pp. 116–122, 2010.

[278] G. Vardar and T. K. Wood, “Protein engineering of toluene-o-xylene monooxygenase from Pseudomonas stutzeri OX1 for enhanced chlorinated ethene degradation and o-xylene oxidation,” *Appl Microbiol Biotechnol*, vol. 68, no. 4, pp. 510–517, 2005.

[279] E. J. Choi et al., “Comparative genomic analysis and benzene, toluene, ethylbenzene, and o-, m-, and p-xylene (BTEX) degradation pathways of Pseudoxanthomonas spadix BD-a59,” *Appl Environ Microbiol*, vol. 79, no. 2, pp. 663–671, 2013.

[280] T. Maruyama et al., “Isolation and characterization of o-xylene oxygenase genes from Rhodococcus opacus TKN14,” *Appl Environ Microbiol*, vol. 71, no. 12, pp. 7705–7715, 2005.

[281] V. Cafaro et al., “Phenol hydroxylase and toluene/o-xylene monooxygenase from Pseudomonas stutzeri OX1: interplay between two enzymes,” *Appl Environ Microbiol*, vol. 70, no. 4, pp. 2211–2219, 2004.

[282] L. P. Wackett et al., “Benzylic monooxygenation catalyzed by toluene dioxygenase from Pseudomonas putida,” *Biochemistry*, vol. 27, no. 4, pp. 1360–1367, 1988.

[283] M. H. Sazinsky et al., “Crystal structure of the toluene/o-xylene monooxygenase hydroxylase from Pseudomonas stutzeri OX1: insight into the substrate specificity, substrate channeling, and active site tuning of multicomponent monooxygenases,” *Journal of Biological Chemistry*, vol. 279, no. 29, pp. 30600–30610, 2004.

[284] R. R. Burgess, “Protein precipitation techniques,” *Methods Enzymol*, vol. 463, pp. 331–342, 2009.

[285] A. Shukla et al., “Pseudomonas Oxygenases: Nature and Function,” in *Pseudomonas: Molecular and Applied Biology*, Springer, Cham, 2016, pp. 193–230.

[286] J.-D. Gu, “Biodegradation testing: so many tests but very little new innovation,” *Applied Environmental Biotechnology (Transferred)*, vol. 1, no. 1, 2016.

[287] M. Merimaa et al., “Grouping of phenol hydroxylase and catechol 2, 3-dioxygenase genes among phenol-and p-cresol-degrading Pseudomonas species and biotypes,” *Arch Microbiol*, vol. 186, no. 4, pp. 287–296, 2006.

[288] R. Agrawal et al., “Synergistic enzyme cocktail to enhance hydrolysis of steam exploded wheat straw at pilot scale,” *Frontiers in Energy Research*, vol. 6, p. 122, 2018.

[289] Y. Jouanneau, “Oxidative inactivation of ring-cleavage extradiol dioxygenases: mechanism and ferredoxin-mediated reactivation.” Springer, 2009.

[290] D. Camenzuli and B. L. Freidman, “On-site and in situ remediation technologies applicable to petroleum hydrocarbon contaminated sites in the Antarctic and Arctic,” *Polar Research*, vol. 34, no. 1, p. 24492, 2015.

[291] D. R. van Stempvoort and P. Grande, *Bioremediation of petroleum hydrocarbons in soil and groundwater under cold climate conditions: a review, implications for applications in Canada*. National Water Research Institute, 2006.

[292] M. Pazos et al., “Decontamination of soils containing PAHs by electroremediation: a review,” *J Hazard Mater*, vol. 177, no. 1–3, pp. 1–11, 2010.

[293] B. H. Gregson et al., “Protein expression in the obligate hydrocarbon-degrading psychrophile Oleispira antarctica RB-8 during alkane degradation and cold tolerance,” *Environ Microbiol*, vol. 22, no. 5, pp. 1870–1883, 2020.

[294] W. Filipowicz et al., “Mechanisms of post-transcriptional regulation by microRNAs: are the answers in sight?,” *Nature reviews genetics*, vol. 9, no. 2, pp. 102–114, 2008.

[295] O. G. Brakstad et al., “Biodegradation of petroleum oil in cold marine environments,” in *Psychrophiles: From biodiversity to biotechnology*, Springer, 2017, pp. 613–644.

[296] M. Luz Paje and I. Couperwhite, “Benzene metabolism via the intradiol cleavage in a Rhodococcus sp.,” *World Journal of Microbiology and Biotechnology*, vol. 12, no. 6, pp. 653–654, 1996.

[297] E. R. Master et al., “Biphenyl dioxygenase from an arctic isolate is not cold adapted,” *Appl Environ Microbiol*, vol. 74, no. 12, pp. 3908–3911, 2008.

[298] L. G. Whyte et al., “Biodegradation of variable-chain-length alkanes at low temperatures by a psychrotrophic Rhodococcus sp,” *Appl Environ Microbiol*, vol. 64, no. 7, pp. 2578–2584, 1998.

[299] J. L. Jardine et al., “Screening of potential bioremediation enzymes from hot spring bacteria using conventional plate assays and liquid chromatography-Tandem mass spectrometry (Lc-Ms/Ms),” *J Environ Manage*, vol. 223, pp. 787–796, 2018.

[300] R. K. Scopes, “The effect of temperature on enzymes used in diagnostics,” *Clinica chimica acta*, vol. 237, no. 1–2, pp. 17–23, 1995.

[301] H.-S. Shin, “Determination of MTBE, TBA and BTEX in soil by headspace gas chromatography-mass spectrometry,” *Bull Korean Chem Soc*, vol. 33, no. 5, pp. 1693–1698, 2012.

[302] D. ASTM, “Standard test method for particle-size analysis of soils,” 2007.

[303] A.-M. O. Mohamed and E. K. Paleologos, *Fundamentals of geoenvironmental engineering: understanding soil, water, and pollutant interaction and transport*. Butterworth-Heinemann, 2017.

[304] R. K. Singh et al., “From protein engineering to immobilization: promising strategies for the upgrade of industrial enzymes,” *Int J Mol Sci*, vol. 14, no. 1, pp. 1232–1277, 2013.

[305] C. T. Test, “OECD GUIDELINE FOR THE TESTING OF CHEMICALS,” 2000.

[306] A. Kaushal and S. K. Singh, “Critical analysis of adsorption data statistically,” *Applied Water Science*, vol. 7, no. 6, pp. 3191–3196, 2017.

[307] J. Chong et al., “Using MicrobiomeAnalyst for comprehensive statistical, functional, and meta-analysis of microbiome data,” *Nat Protoc*, vol. 15, no. 3, pp. 799–821, 2020.

[308] M. A. I. Khan et al., “Toxicity assessment of fresh and weathered petroleum hydrocarbons in contaminated soil-a review,” *Chemosphere*, vol. 212, pp. 755–767, 2018.

[309] K. Vaajasaari et al., “Comparisons of terrestrial and aquatic bioassays for oil-contaminated soil toxicity,” *Journal of Soils and Sediments*, vol. 2, no. 4, pp. 194–202, 2002.

[310] S. Bordenave et al., “Effects of heavy fuel oil on the bacterial community structure of a pristine microbial mat,” *Applied and Environmental Microbiology*, vol. 73, no. 19, pp. 6089–6097, 2007.

[311] K. Nagarajan and K.-C. Loh, “Formulation of microbial cocktails for BTEX biodegradation,” *Biodegradation*, vol. 26, no. 1, pp. 51–63, 2015.

[312] H. Shim et al., “A continuous fibrous-bed bioreactor for BTEX biodegradation by a co-culture of Pseudomonas putida and Pseudomonas fluorescens,” *Advances in Environmental Research*, vol. 7, no. 1, pp. 203–216, 2002.

[313] K. G. Stuart-Keil et al., “Plasmids responsible for horizontal transfer of naphthalene catabolism genes between bacteria at a coal tar-contaminated site are homologous to pDTG1 from Pseudomonas putida NCIB 9816-4,” *Appl Environ Microbiol*, vol. 64, no. 10, pp. 3633–3640, 1998.

[314] M. Santiago et al., “Discovery, molecular mechanisms, and industrial applications of cold-active enzymes,” *Front Microbiol*, vol. 7, p. 1408, 2016.

[315] D. Wojcieszyńska et al., “Properties of catechol 2, 3-dioxygenase from crude extract of Stenotrophomonas maltophilia strain KB2 immobilized in calcium alginate hydrogels,” *Biochemical Engineering Journal*, vol. 66, pp. 1–7, 2012.

[316] R. Xu et al., “Laccase immobilization on chitosan/poly (vinyl alcohol) composite nanofibrous membranes for 2, 4-dichlorophenol removal,” *Chemical engineering journal*, vol. 222, pp. 321–329, 2013.

[317] R. Datta et al., “How enzymes are adsorbed on soil solid phase and factors limiting its activity: A Review,” *Int Agrophys*, vol. 31, no. 2, p. 287, 2017.

[318] L. Lonappan et al., “Covalent immobilization of laccase on citric acid functionalized micro-biochars derived from different feedstock and removal of diclofenac,” *Chemical Engineering Journal*, vol. 351, pp. 985–994, 2018.

[319] W. Norde, “My voyage of discovery to proteins in flatland... and beyond.,” *Colloids Surf B Biointerfaces*, vol. 61, no. 1, pp. 1–9, 2007.

[320] C. Sögaard et al., “Silica sol as grouting material: a physio-chemical analysis,” *Nano Converg*, vol. 5, no. 1, pp. 1–15, 2018.

[321] M. B. Ahmed et al., “Sorption of hydrophobic organic contaminants on functionalized biochar: Protagonist role of π-π electron-donor-acceptor interactions and hydrogen bonds,” *J Hazard Mater*, vol. 360, pp. 270–278, 2018.

[322] S. Miri et al., “Precision modelling of co-metabolic biodegradation of recalcitrant aromatic hydrocarbons in conjunction with experimental data,” *Process Biochemistry*, vol. 105, pp. 113–127, 2021.

[323] S. A. Hoang et al., “Rhizoremediation as a green technology for the remediation of petroleum hydrocarbon-contaminated soils,” *Journal of Hazardous Materials*, vol. 401, p. 123282, 2021.

[324] S. Miri et al., “Precision modelling of co-metabolic biodegradation of recalcitrant aromatic hydrocarbons in conjunction with experimental data,” *Process Biochemistry*, vol. 105, pp. 113–127, Jun. 2021 [Online]. Available: 10.1016/j.procbio.2021.03.026.

[325] F. Li and L. Zhu, “Effect of surfactant-induced cell surface modifications on electron transport system and catechol 1, 2-dioxygenase activities and phenanthrene biodegradation by Citrobacter sp. SA01,” *Bioresour Technol*, vol. 123, pp. 42–48, 2012.

[326] T. O. Elufisan et al., “The Polycyclic Aromatic Hydrocarbon (PAH) degradation activities and genome analysis of a novel strain Stenotrophomonas sp. Pemsol isolated from Mexico,” *PeerJ*, vol. 8, p. e8102, 2020.

[327] S. Bera et al., “Optimization of p-cresol biodegradation using novel bacterial strains isolated from petroleum hydrocarbon fallout,” *Journal of Water Process Engineering*, vol. 31, p. 100842, 2019.

[328] L. Huang et al., “Effect of temperature on microbial growth rate–mathematical analysis: the Arrhenius and Eyring–Polanyi connections,” *J Food Sci*, vol. 76, no. 8, pp. E553–E560, 2011.

[329] J. T. Csotonyi et al., “An alphaproteobacterium capable of both aerobic and anaerobic anoxygenic photosynthesis but incapable of photoautotrophy: Charonomicrobium ambiphototrophicum, gen. nov., sp. nov.,” *Photosynth Res*, vol. 107, no. 3, pp. 257–268, 2011.

[330] H. Mosmeri et al., “Bioremediation of benzene-contaminated groundwater by calcium peroxide (CaO2) nanoparticles: continuous-flow and biodiversity studies,” *J Hazard Mater*, vol. 371, pp. 183–190, 2019.

[331] Y. He et al., “Comparison of microbial diversity determined with the same variable tag sequence extracted from two different PCR amplicons,” *BMC Microbiol*, vol. 13, no. 1, pp. 1–8, 2013.

[332] N. B. Sutton et al., “Impact of long-term diesel contamination on soil microbial community structure,” *Appl Environ Microbiol*, vol. 79, no. 2, pp. 619–630, 2013.

[333] D. C. L. Wong et al., “Prediction of ecotoxicity of hydrocarbon-contaminated soils using physicochemical parameters,” *Environmental Toxicology and Chemistry: An International Journal*, vol. 18, no. 11, pp. 2611–2621, 1999.

[334] J. Tang et al., “Eco-toxicity of petroleum hydrocarbon contaminated soil,” *Journal of Environmental Sciences*, vol. 23, no. 5, pp. 845–851, 2011.

[335] M. K. Banks and K. E. Schultz, “Comparison of plants for germination toxicity tests in petroleum-contaminated soils,” *Water Air Soil Pollut*, vol. 167, no. 1, pp. 211–219, 2005.

[336] S. V. Surendra et al., “Degradation of monoaromatics by Bacillus pumilus MVSV3,” *Brazilian Archives of Biology and Technology*, vol. 60, 2017.

[337] I. Snape et al., “Contaminants in freezing ground and associated ecosystems: key issues at the beginning of the new millennium,” *Polar Record*, vol. 39, no. 4, pp. 291–300, 2003.

[338] C. Elizabeth Rani Juneius, “A Novel Lipopeptide Bacterial Biosurfactant for Bioremediation,” in *Integrated Waste Management in India*, Springer, 2016, pp. 139–154.

[339] F. L. G. Arenghi et al., “Identification of the Pseudomonas stutzeri OX1 toluene–o-xylene monooxygenase regulatory gene (touR) and of its cognate promoter,” *Appl Environ Microbiol*, vol. 65, no. 9, pp. 4057–4063, 1999.

[340] A. Yavas and B. Icgen, “Aerobic bacterial degraders with their relative pathways for efficient removal of individual BTEX compounds,” *CLEAN–Soil, Air, Water*, vol. 46, no. 11, p. 1800068, 2018.

[341] V. Cafaro et al., “Phenol hydroxylase and toluene/o-xylene monooxygenase from Pseudomonas stutzeri OX1: interplay between two enzymes,” *Appl Environ Microbiol*, vol. 70, no. 4, pp. 2211–2219, 2004.

[342] U. Guzik et al., “Immobilization as a strategy for improving enzyme properties-application to oxidoreductases,” *Molecules*, vol. 19, no. 7, pp. 8995–9018, 2014.

[343] E. M. Karppinen et al., “Petroleum hydrocarbon remediation in frozen soil using a meat and bonemeal biochar plus fertilizer,” *Chemosphere*, vol. 173, pp. 330–339, 2017.

[344] L. Racine et al., “Chitosan-based hydrogels: recent design concepts to tailor properties and functions,” *Polymer International*, vol. 66, no. 7, pp. 981–998, 2017.

[345] N. R. Mohamad et al., “An overview of technologies for immobilization of enzymes and surface analysis techniques for immobilized enzymes,” *Biotechnology & Biotechnological Equipment*, vol. 29, no. 2, pp. 205–220, 2015.

[346] L. Lonappan et al., “Covalent immobilization of laccase on citric acid functionalized micro-biochars derived from different feedstock and removal of diclofenac,” *Chemical Engineering Journal*, vol. 351, pp. 985–994, 2018.

[347] M. Naghdi et al., “Fabrication of nanobiocatalyst using encapsulated laccase onto chitosan-nanobiochar composite,” *Int J Biol Macromol*, vol. 124, pp. 530–536, 2019.

[348] H. Packeiser et al., “An extremely simple and effective colony PCR procedure for bacteria, yeasts, and microalgae,” *Appl Biochem Biotechnol*, vol. 169, no. 2, pp. 695–700, 2013.

[349] K. Tamura et al., “MEGA5: molecular evolutionary genetics analysis using maximum likelihood, evolutionary distance, and maximum parsimony methods,” *Mol Biol Evol*, vol. 28, no. 10, pp. 2731–2739, 2011.

[350] R. A. Sheldon and S. van Pelt, “Enzyme immobilisation in biocatalysis: why, what and how,” *Chemical Society Reviews*, vol. 42, no. 15, pp. 6223–6235, 2013.

[351] S. K. S. Patel et al., “Large-scale aerosol-assisted synthesis of biofriendly Fe 2 O 3 yolk–shell particles: a promising support for enzyme immobilization,” *Nanoscale*, vol. 8, no. 12, pp. 6728–6738, 2016.

[352] M. J. Barden, “Wisconsin’s Guidance on Naturally Occurring Biodegradation as a Remedial Action Option,” in *Symposium on Natural Attenuation of Ground Water*, 1994, p. 127.

[353] M. Chang et al., “Kinetics of competitive inhibition and cometabolism in the biodegradation of benzene, toluene, and p-xylene by two Pseudomonas isolates.,” *Biotechnology and Bioengineering*, vol. 41, no. 11, pp. 1057–1065, 1993.

[354] M. Polakovič et al., “Approaches for improved identification of mechanisms of enzyme inactivation,” in *Progress in Biotechnology*, vol. 15, Elsevier, 1998, pp. 77–82.

[355] H. H. Attaway and M. G. Schmidt, “Tandem biodegradation of BTEX components by two Pseudomonas sp.,” *Current Microbiology*, vol. 45, no. 1, pp. 30–36, 2002.

[356] D. K. Chaudhary and J. Kim, “New insights into bioremediation strategies for oil-contaminated soil in cold environments,” *International Biodeterioration & Biodegradation*, vol. 142, pp. 58–72, 2019.

[357] P. A. Chablain et al., “Isolation of a soil psychrotrophic toluene-degrading Pseudomonas strain: influence of temperature on the growth characteristics on different substrates,” *Res Microbiol*, vol. 148, no. 2, pp. 153–161, 1997.

[358] R. Moreno et al., “The Crc global regulator inhibits the Pseudomonas putida pWW0 toluene/xylene assimilation pathway by repressing the translation of regulatory and structural genes,” *Journal of Biological Chemistry*, vol. 285, no. 32, pp. 24412–24419, 2010.

[359] J. Brzeszcz and P. Kaszycki, “Aerobic bacteria degrading both n-alkanes and aromatic hydrocarbons: an undervalued strategy for metabolic diversity and flexibility,” *Biodegradation*, vol. 29, no. 4, pp. 359–407, 2018.

[360] R. J. Baker et al., “Used motor oil as a source of MTBE, TAME, and BTEX to ground water,” *Groundwater Monitoring & Remediation*, vol. 22, no. 4, pp. 46–51, 2002.

[361] M. Naghdi et al., “Immobilized laccase on oxygen functionalized nanobiochars through mineral acids treatment for removal of carbamazepine,” *Science of The Total Environment*, vol. 584, pp. 393–401, 2017.

[362] E. Taqieddin and M. Amiji, “Enzyme immobilization in novel alginate–chitosan core-shell microcapsules,” *Biomaterials*, vol. 25, no. 10, pp. 1937–1945, 2004.

[363] L. C. Almeida et al., “Use of conventional or non-conventional treatments of biochar for lipase immobilization,” *Process Biochemistry*, vol. 61, pp. 124–129, 2017.

[364] K. Khosla et al., “Biodiesel production from lipid of carbon dioxide sequestrating bacterium and lipase of psychrotolerant Pseudomonas sp. ISTPL3 immobilized on biochar,” *Bioresour Technol*, vol. 245, pp. 743–750, 2017.

[365] M. Naghdi et al., “Fabrication of nanobiocatalyst using encapsulated laccase onto chitosan-nanobiochar composite,” *Int J Biol Macromol*, vol. 124, pp. 530–536, 2019.

[366] M. Amid et al., “Microencapsulation of purified Amylase enzyme from Pitaya (Hylocereus polyrhizus) peel in Arabic Gum-Chitosan using freeze drying,” *Molecules*, vol. 19, no. 3, pp. 3731–3743, 2014.

[367] K. M. Woo et al., “Crosslinked chitosan coating on magnetic mesoporous silica with pre-adsorbed carbonic anhydrase for carbon dioxide conversion,” *Chemical Engineering Journal*, vol. 276, pp. 232–239, 2015.

[368] S. Miri et al., “Recent biotechnological advances in petroleum hydrocarbons degradation under cold climate conditions: A review,” *Critical Reviews in Environmental Science and Technology*, vol. 49, no. 7, pp. 553–586, Apr. 2019 [Online]. Available: 10.1080/10643389.2018.1552070.

[369] F. Ma et al., “Biotransformation of benzene and toluene to catechols by phenol hydroxylase from Arthrobacter sp. W1,” *Appl Microbiol Biotechnol*, vol. 97, no. 11, pp. 5097–5103, 2013.

[370] E. Kalogeris et al., “Properties of catechol 1, 2-dioxygenase from Pseudomonas putida immobilized in calcium alginate hydrogels,” *Enzyme and Microbial Technology*, vol. 39, no. 5, pp. 1113–1121, 2006.

[371] A. G. Osorio et al., “H2SO4/HNO3/HCl—Functionalization and its effect on dispersion of carbon nanotubes in aqueous media,” *Applied Surface Science*, vol. 255, no. 5, pp. 2485–2489, 2008.

[372] Y. Pang et al., “Biodegradable and biocompatible high elastic chitosan scaffold is cell-friendly both in vitro and in vivo,” *Oncotarget*, vol. 8, no. 22, p. 35583, 2017.

[373] C. Branca et al., “Role of the OH and NH vibrational groups in polysaccharide-nanocomposite interactions: A FTIR-ATR study on chitosan and chitosan/clay films,” *Polymer (Guildf)*, vol. 99, pp. 614–622, 2016.

[374] S. Harayama et al., “Functional and evolutionary relationships among diverse oxygenases.,” *Annu Rev Microbiol*, vol. 46, pp. 565–601, 1992.

[375] A. A. A. de Queiroz et al., “Alginate–poly (vinyl alcohol) core–shell microspheres for lipase immobilization,” *Journal of Applied Polymer Science*, vol. 102, no. 2, pp. 1553–1560, 2006.

[376] J. P. Shaw and S. Harayama, “Characterization in vitro of the hydroxylase component of xylene monooxygenase, the first enzyme of the TOL-plasmid-encoded pathway for the mineralization of toluene and xylenes,” *Journal of Fermentation and bioengineering*, vol. 79, no. 3, pp. 195–199, 1995.

[377] M. Suzuki et al., “Primary structure of xylene monooxygenase: similarities to and differences from the alkane hydroxylation system,” *J Bacteriol*, vol. 173, no. 5, pp. 1690–1695, 1991.

[378] S.-C. Tsai and Y.-K. Li, “Purification and characterization of a catechol 1, 2-dioxygenase from a phenol degrading Candida albicans TL3,” *Arch Microbiol*, vol. 187, no. 3, pp. 199–206, 2007.

[379] G. Feller and C. Gerday, “Psychrophilic enzymes: hot topics in cold adaptation,” *Nature reviews microbiology*, vol. 1, no. 3, pp. 200–208, 2003.

[380] E. Weber et al., “Immobilization of P450 BM-3 monooxygenase on mesoporous molecular sieves with different pore diameters,” *Journal of Molecular Catalysis B: Enzymatic*, vol. 64, no. 1–2, pp. 29–37, 2010.

[381] M. T. Bes et al., “Selective oxidation: stabilisation by multipoint attachment of ferredoxin NADP+ reductase, an interesting cofactor recycling enzyme,” *Journal of Molecular Catalysis A: Chemical*, vol. 98, no. 3, pp. 161–169, 1995.

[382] E. Notomista et al., “Molecular determinants of the regioselectivity of toluene/o-xylene monooxygenase from Pseudomonas sp. strain OX1,” *Appl Environ Microbiol*, vol. 75, no. 3, pp. 823–836, 2009.

[383] D. Wojcieszyńska et al., “Properties of catechol 2, 3-dioxygenase from crude extract of Stenotrophomonas maltophilia strain KB2 immobilized in calcium alginate hydrogels,” *Biochemical Engineering Journal*, vol. 66, pp. 1–7, 2012.

[384] P. A. Fields and G. N. Somero, “Hot spots in cold adaptation: localized increases in conformational flexibility in lactate dehydrogenase A4 orthologs of Antarctic notothenioid fishes,” *Proceedings of the National Academy of Sciences*, vol. 95, no. 19, pp. 11476–11481, 1998.

[385] B.-P. Xin et al., “Bioaugmented remediation of high concentration BTEX-contaminated groundwater by permeable reactive barrier with immobilized bead,” *J Hazard Mater*, vol. 244, pp. 765–772, 2013.

[386] S. Admon et al., “Biodegradation kinetics of hydrocarbons in soil during land treatment of oily sludge,” *Biorernediation journal*, vol. 5, no. 3, pp. 193–209, 2001.

[387] O. Akbulut et al., “Separation of nanoparticles in aqueous multiphase systems through centrifugation,” *Nano Lett*, vol. 12, no. 8, pp. 4060–4064, 2012.

[388] E. Kalogeris et al., “Properties of catechol 1, 2-dioxygenase from Pseudomonas putida immobilized in calcium alginate hydrogels,” *Enzyme and Microbial Technology*, vol. 39, no. 5, pp. 1113–1121, 2006.

[389] G. Bertoni et al., “Analysis of the gene cluster encoding toluene/o-xylene monooxygenase from Pseudomonas stutzeri OX1,” *Applied and Environmental Microbiology*, vol. 64, no. 10, pp. 3626–3632, 1998.

[390] N. F. Haard, “Specialty enzymes from marine organisms,” *Food technology (Chicago)*, vol. 52, no. 7, pp. 64–67, 1998.

[391] L. Ji et al., “Enzyme cocktail containing NADH regeneration system for efficient bioremediation of oil sludge contamination,” *Chemosphere*, vol. 233, pp. 132–139, 2019.

[392] A. K. Agarwal and R. J. Auchus, “Minireview: cellular redox state regulates hydroxysteroid dehydrogenase activity and intracellular hormone potency,” *Endocrinology*, vol. 146, no. 6, pp. 2531–2538, 2005.

[393] G. di Nardo et al., “Catalytic properties of catechol 1, 2-dioxygenase from Acinetobacter radioresistens S13 immobilized on nanosponges,” *Dalton Transactions*, no. 33, pp. 6507–6512, 2009.

[394] D. C. Agrawal et al., “Immobilization of fenugreek β-amylase onto functionalized graphene quantum dots (GQDs) using Box-Behnken design: Its biochemical, thermodynamic and kinetic studies,” *International Journal of Biological Macromolecules*, vol. 144, pp. 170–182, 2020.

[395] A. Kumari et al., “Multiple thermostable enzyme hydrolases on magnetic nanoparticles: An immobilized enzyme-mediated approach to saccharification through simultaneous xylanase, cellulase and amylolytic glucanotransferase action,” *Int J Biol Macromol*, vol. 120, pp. 1650–1658, 2018.

[396] T. Xie et al., “Recent advance in the support and technology used in enzyme immobilization,” *African Journal of Biotechnology*, vol. 8, no. 19, 2009.

[397] B. Krajewska, “Application of chitin-and chitosan-based materials for enzyme immobilizations: a review,” *Enzyme Microb Technol*, vol. 35, no. 2–3, pp. 126–139, 2004.

[398] K. Pospiskova and I. Safarik, “Low-cost, easy-to-prepare magnetic chitosan microparticles for enzymes immobilization,” *Carbohydr Polym*, vol. 96, no. 2, pp. 545–548, 2013.

[399] G. Bayramoglu et al., “Immobilization of Candida rugosa lipase on magnetic chitosan beads and application in flavor esters synthesis,” *Food Chemistry*, vol. 366, p. 130699, 2022.

[400] Y. Liu et al., “Co-immobilization of glucose oxidase and catalase in porous magnetic chitosan microspheres for production of sodium gluconate,” *International Journal of Chemical Reactor Engineering*, 2022.

[401] J. Zhao et al., “Immobilization of lipase on β-cyclodextrin grafted and aminopropyl-functionalized chitosan/Fe3O4 magnetic nanocomposites: An innovative approach to fruity flavor esters esterification,” *Food Chemistry*, vol. 366, p. 130616, 2022.

[402] X. Qiu et al., “Co-immobilization of laccase and ABTS onto amino-functionalized ionic liquid-modified magnetic chitosan nanoparticles for pollutants removal,” *Journal of Hazardous Materials*, vol. 401, p. 123353, 2021.

[403] P. Ke et al., “Synthesis and characterization of a novel magnetic chitosan microsphere for lactase immobilization,” *Colloids and Surfaces A: Physicochemical and Engineering Aspects*, vol. 606, p. 125522, 2020.

[404] V. U. Bindu and P. v Mohanan, “Thermal deactivation of α-amylase immobilized magnetic chitosan and its modified forms: A kinetic and thermodynamic study,” *Carbohydrate Research*, vol. 498, p. 108185, 2020.

[405] H. Suo et al., “Synthesis of functional ionic liquid modified magnetic chitosan nanoparticles for porcine pancreatic lipase immobilization,” *Materials Science and Engineering: C*, vol. 96, pp. 356–364, 2019.

[406] H. Nadaroglu et al., “Biodegradation of some azo dyes from wastewater with laccase from Weissella viridescens LB37 immobilized on magnetic chitosan nanoparticles,” *Journal of Water Process Engineering*, vol. 31, p. 100866, 2019.

[407] J. Gracida et al., “Improved thermal and reusability properties of xylanase by genipin cross-linking to magnetic chitosan particles,” *Appl Biochem Biotechnol*, vol. 188, no. 2, pp. 395–409, 2019.

[408] L. Zang et al., “Preparation of magnetic chitosan nanoparticles as support for cellulase immobilization,” *Ind Eng Chem Res*, vol. 53, no. 9, pp. 3448–3454, 2014.

[409] J. Wang et al., “Reversible immobilization of glucoamylase onto magnetic chitosan nanocarriers,” *Appl Microbiol Biotechnol*, vol. 97, no. 2, pp. 681–692, 2013.

[410] L. Zhang et al., “Photochemical preparation of magnetic chitosan beads for immobilization of pullulanase,” *Biochemical Engineering Journal*, vol. 46, no. 1, pp. 83–87, 2009.

[411] B. Wang et al., “Optimization, reconstruction and heterologous expression of the gene cluster encoding toluene/o-xylene monooxygenase from Pseudomonas stutzeri in Escherichia coli and its successive hydroxylation of toluene and benzene,” *Biotechnology & Biotechnological Equipment*, vol. 35, no. 1, pp. 1632–1642, 2021.

[412] A. Wongbunmak et al., “BTEX biodegradation by Bacillus amyloliquefaciens subsp. plantarum W1 and its proposed BTEX biodegradation pathways,” *Sci Rep*, vol. 10, no. 1, pp. 1–13, 2020.

[413] S. Panke et al., “An alkane-responsive expression system for the production of fine chemicals,” *Applied and Environmental Microbiology*, vol. 65, no. 6, pp. 2324–2332, 1999.

[414] S. Miri et al., “Enzymatic biodegradation of highly p-xylene contaminated soil using cold-active enzymes: A soil column study,” *Journal of Hazardous Materials*, vol. 423, Feb. 2022 [Online]. Available: 10.1016/j.jhazmat.2021.127099.

[415] F. L. G. Arenghi et al., “Organization and regulation of meta cleavage pathway genes for toluene and o-xylene derivative degradation in Pseudomonas stutzeri OX1,” *Appl Environ Microbiol*, vol. 67, no. 7, pp. 3304–3308, 2001.

[416] Y. Li et al., “Aerobic degradation of trichloroethylene by co-metabolism using phenol and gasoline as growth substrates,” *International Journal of Molecular Sciences*, vol. 15, no. 5, pp. 9134–9148, 2014.

[417] H. J. Choi et al., “Isolation and characterization of BTEX tolerant and degrading Pseudomonas putida BCNU 106,” *Biotechnology and bioprocess engineering*, vol. 18, no. 5, pp. 1000–1007, 2013.

[418] D. H. K. Reddy and S.-M. Lee, “Application of magnetic chitosan composites for the removal of toxic metal and dyes from aqueous solutions,” *Adv Colloid Interface Sci*, vol. 201, pp. 68–93, 2013.

[419] O. Barbosa et al., “Glutaraldehyde in bio-catalysts design: A useful crosslinker and a versatile tool in enzyme immobilization,” *Rsc Advances*, vol. 4, no. 4, pp. 1583–1600, 2014.

[420] G. R. Mahdavinia et al., “Model protein BSA adsorption onto novel magnetic chitosan/PVA/laponite RD hydrogel nanocomposite beads,” *Int J Biol Macromol*, vol. 107, pp. 719–729, 2018.

[421] S. M. Pourmortazavi et al., “Fabrication of Fe3O4 nanoparticles coated by extracted shrimp peels chitosan as sustainable adsorbents for removal of chromium contaminates from wastewater: The design of experiment,” *Composites Part B: Engineering*, vol. 175, p. 107130, 2019.

[422] J. Safari and L. Javadian, “Chitosan decorated Fe 3 O 4 nanoparticles as a magnetic catalyst in the synthesis of phenytoin derivatives,” *RSC Advances*, vol. 4, no. 90, pp. 48973–48979, 2014.

[423] S. Ariaeenejad et al., “Immobilization of enzyme cocktails on dopamine functionalized magnetic cellulose nanocrystals to enhance sugar bioconversion: A biomass reusing loop,” *Carbohydrate Polymers*, vol. 256, p. 117511, 2021.

[424] R. Fernandez–Lafuente et al., “Immobilization of functionally unstable catechol-2, 3-dioxygenase greatly improves operational stability,” *Enzyme Microb Technol*, vol. 26, no. 8, pp. 568–573, 2000.

[425] A. Mukhopadhyay et al., “Enhanced functionality and stabilization of a cold active laccase using nanotechnology based activation-immobilization,” *Bioresource Technology*, vol. 179, pp. 573–584, 2015.

[426] M. L. Verma et al., “Chitin and chitosan-based support materials for enzyme immobilization and biotechnological applications,” *Environmental Chemistry Letters*, vol. 18, no. 2, pp. 315–323, 2020.

[427] N. Mhetras et al., “Cold active lipases: biocatalytic tools for greener technology,” *Applied Biochemistry and Biotechnology*, vol. 193, no. 7, pp. 2245–2266, 2021.

[428] W. Duan et al., “The pathways by which the marine diatom Thalassiosira sp. OUC2 biodegrades p-xylene, combined with a mechanistic analysis at the proteomic level,” *Ecotoxicology and Environmental Safety*, vol. 198, p. 110687, 2020.

[429] D. E. C. Mazzeo et al., “Application of micronucleus test and comet assay to evaluate BTEX biodegradation,” *Chemosphere*, vol. 90, no. 3, pp. 1030–1036, 2013.

[430] J. P. Lee et al., “A cold-active acidophilic endoglucanase of Paenibacillus sp. Y2 isolated from soil in an alpine region,” *Journal of Applied Biological Chemistry*, vol. 60, no. 3, pp. 257–263, 2017.

[431] M. A. Rahman et al., “Immobilization of a novel cold active esterase onto Fe3O4∼ cellulose nano-composite enhances catalytic properties,” *Int J Biol Macromol*, vol. 87, pp. 488–497, 2016.

[432] M. C. Tomei and A. J. Daugulis, “Ex situ bioremediation of contaminated soils: an overview of conventional and innovative technologies,” *Critical Reviews in Environmental Science and Technology*, vol. 43, no. 20, pp. 2107–2139, 2013.

[433] P. Greenslade and P. Convey, “Exotic Collembola on subantarctic islands: pathways, origins and biology,” *Biological Invasions*, vol. 14, no. 2, pp. 405–417, 2012.

[434] I. Errington et al., “Ecosystem effects and the management of petroleum-contaminated soils on subantarctic islands,” *Chemosphere*, vol. 194, pp. 200–210, 2018.

[435] M. Santiago et al., “Discovery, molecular mechanisms, and industrial applications of cold-active enzymes,” *Front Microbiol*, vol. 7, p. 1408, 2016.

[436] T. Kadri et al., “Pilot-scale production and in-situ application of petroleum-degrading enzyme cocktail from Alcanivorax borkumensis,” *Chemosphere*, vol. 295, May 2022 [Online]. Available: 10.1016/j.chemosphere.2022.133840.

[437] H. Yu et al., “The roles of intermediates in biodegradation of benzene, toluene, and p-xylene by Pseudomonas putida F1,” *Biodegradation*, vol. 12, no. 6, pp. 455–463, 2001.

[438] F. K. Olagoke et al., “Persistent activities of extracellular enzymes adsorbed to soil minerals,” *Microorganisms*, vol. 8, no. 11, p. 1796, 2020.

[439] B. Bühler et al., “Characterization and application of xylene monooxygenase for multistep biocatalysis,” *Appl Environ Microbiol*, vol. 68, no. 2, pp. 560–568, 2002.

[440] P. v Iyer and L. Ananthanarayan, “Enzyme stability and stabilization—aqueous and non-aqueous environment,” *Process biochemistry*, vol. 43, no. 10, pp. 1019–1032, 2008.

[441] R. Martel et al., “Aquifer washing by micellar solutions:: 3 Field test at the Thouin Sand Pit (L’Assomption, Quebec, Canada),” *Journal of Contaminant Hydrology*, vol. 30, no. 1–2, pp. 33–48, 1998.

[442] G. A. F. Roberts, “Solubility and solution behaviour of chitin and chitosan,” in *Chitin chemistry*, Springer, 1992, pp. 274–329.

[443] J.-G. Na et al., “Microbial community analysis of anaerobic granules in phenol-degrading UASB by next generation sequencing,” *Biochemical Engineering Journal*, vol. 112, pp. 241–248, 2016.

[444] D.-M. Lan et al., “A novel cold-active lipase from Candida albicans: cloning, expression and characterization of the recombinant enzyme,” *International Journal of Molecular Sciences*, vol. 12, no. 6, pp. 3950–3965, 2011.

[445] A. Backman and J. K. Jansson, “Degradation of 4-chlorophenol at low temperature and during extreme temperature fluctuations by Arthrobacter chlorophenolicus A6,” *Microb Ecol*, vol. 48, no. 2, pp. 246–253, 2004.

[446] S.-C. Tsai and Y.-K. Li, “Purification and characterization of a catechol 1, 2-dioxygenase from a phenol degrading Candida albicans TL3,” *Arch Microbiol*, vol. 187, no. 3, pp. 199–206, 2007.

[447] M. K. Aravind et al., “Bioengineered graphene oxide microcomposites containing metabolically versatile Paracoccus sp. MKU1 for enhanced catechol degradation,” *ACS Omega*, vol. 5, no. 27, pp. 16752–16761, 2020.

[448] Z. W. Luo and S. Y. Lee, “Biotransformation of p-xylene into terephthalic acid by engineered Escherichia coli,” *Nat Commun*, vol. 8, no. 1, pp. 1–8, 2017.

[449] D. R. Nielsen et al., “Direct estimation of the oxygen requirements of Achromobacter xylosoxidans for aerobic degradation of monoaromatic hydrocarbons (BTEX) in a bioscrubber,” *Biotechnol Lett*, vol. 28, no. 16, pp. 1293–1298, 2006.

[450] A. Karimi et al., “Oxygen mass transfer in a stirred tank bioreactor using different impeller configurations for environmental purposes,” *Iranian J Environ Health Sci Eng*, vol. 10, no. 1, pp. 1–9, 2013.

[451] S. N. Gummadi and D. S. Kumar, “Batch and fed batch production of pectin lyase and pectate lyase by novel strain Debaryomyces nepalensis in bioreactor,” *Bioresource Technology*, vol. 99, no. 4, pp. 874–881, 2008.

[452] F. Garcia-Ochoa and E. Gomez, “Bioreactor scale-up and oxygen transfer rate in microbial processes: an overview,” *Biotechnol Adv*, vol. 27, no. 2, pp. 153–176, 2009.

[453] T. Kadri et al., “Ex-situ biodegradation of petroleum hydrocarbons using Alcanivorax borkumensis enzymes,” *Biochemical Engineering Journal*, vol. 132, pp. 279–287, 2018.

[454] A. Ndao et al., “Pilot-scale biopesticide production by Bacillus thuringiensis subsp. kurstaki using starch industry wastewater as raw material,” *Journal of Environmental Science and Health, Part B*, vol. 52, no. 9, pp. 623–630, 2017.

[455] J. P. Shaw and S. Harayama, “Characterization in vitro of the hydroxylase component of xylene monooxygenase, the first enzyme of the TOL-plasmid-encoded pathway for the mineralization of toluene and xylenes,” *Journal of Fermentation and bioengineering*, vol. 79, no. 3, pp. 195–199, 1995.

[456] K. Martinek et al., “The principles of enzymes stabilization: VI. Catalysis by water-soluble enzymes entrapped into reversed micelles of surfactants in organic solvents,” *Biochimica et Biophysica Acta (BBA)-Enzymology*, vol. 657, no. 1, pp. 277–294, 1981.

[457] P. Adewale et al., “A novel Bacillus ligniniphilus catechol 2, 3-dioxygenase shows unique substrate preference and metal requirement,” *Sci Rep*, vol. 11, no. 1, pp. 1–16, 2021.

[458] A. Ghandi et al., “Powders containing microorganisms and enzymes,” *Handbook of Food Powders*, pp. 593–624, 2013.

[459] G. Haskå, “Influence of clay minerals on sorption of bacteriolytic enzymes,” *Microb Ecol*, vol. 1, no. 1, pp. 234–245, 1974.

[460] S. Mohanty and S. Mukherji, “Surfactant aided biodegradation of NAPLs by Burkholderia multivorans: comparison between Triton X-100 and rhamnolipid JBR-515,” *Colloids and Surfaces B: Biointerfaces*, vol. 102, pp. 644–652, 2013.

[461] U. Zoller and H. Rubin, “Feasibility of in situ NAPL-contaminated aquifer bioremediation by biodegradable nutrient–surfactant mix,” *Journal of Environmental Science and Health, Part A*, vol. 36, no. 8, pp. 1451–1471, 2001.

[462] A. S. Gößner et al., “Thermicanus aegyptius gen. nov., sp. nov., isolated from oxic soil, a fermentative microaerophile that grows commensally with the thermophilic acetogen Moorella thermoacetica,” *Appl Environ Microbiol*, vol. 65, no. 11, pp. 5124–5133, 1999.

[463] S. Tang et al., “Microbial coupling mechanisms of nitrogen removal in constructed wetlands: a review,” *Bioresource Technology*, vol. 314, p. 123759, 2020.

[464] R. T. Anderson and D. R. Lovley, “Anaerobic bioremediation of benzene under sulfate-reducing conditions in a petroleum-contaminated aquifer,” *Environ Sci Technol*, vol. 34, no. 11, pp. 2261–2266, 2000.

[465] D. H. Pieper, “Aerobic degradation of polychlorinated biphenyls,” *Appl Microbiol Biotechnol*, vol. 67, no. 2, pp. 170–191, 2005.

[466] Y. Ohta et al., “Pseudomonas putida CE2010 can degrade biphenyl by a mosaic pathway encoded by the tod operon and cmtE, which are identical to those of P. putida F1 except for a single base difference in the operator–promoter region of the cmt operon,” *Microbiology (N Y)*, vol. 147, no. 1, pp. 31–41, 2001.

APPENDICES

APPENDIX A. Supplementary information of section 3.1.

Calculation regarding the oxygen requirements of such growth in MSM media in the presence of Benzene.

Based on stoichiometry, approximately 0.04 mol of oxygen is required for complete mineralization of 0.01 mol of benzene. Hence, in a closed system, 2.56 mM of benzene respired to make energy will require about 10.24 mM of oxygen. The oxygen concentration in media (liquid phase) was noted to be 50 times lower. We can thus conclude as calculated below there will need to be more than 50 replenishment cycles (turnovers) of dissolved oxygen pool in the growth media to supply the need of respiring the benzene. The replenishment is usually achieved by vigorous shaking (150 rpm). The growth media is surrounded by air which has an oxygen fraction of 20 % equivalent to about 10 μmole per liter of air. Thus, a headspace of a few times the culture volume contains enough oxygen for the culture growth.

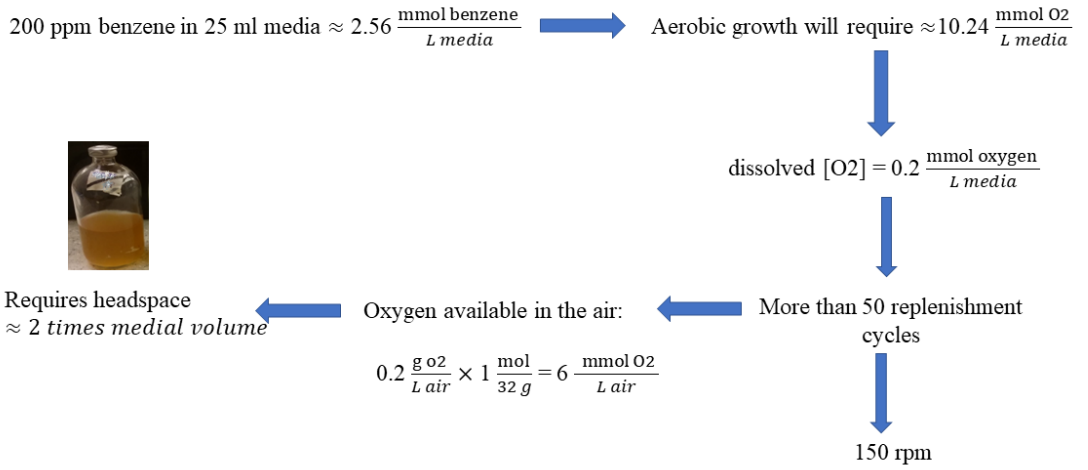

Headspace gas chromatography

The chromatographic peak area, A_b of compound t in the gas phase above the sample is proportional to its partial vapor pressure:

$A_b = C_B\, p_b$

For a given sample size, each compound has a specific value of C_B. According to Henry's Law, the partial pressure of the volatile compounds above the sample depends on the analyte concentration in the liquid phase and the saturated vapor pressure of pure component at a given temperature, P_b:

$$p_b = \gamma_b X_b\, P_b$$

Where γ_b is the activity coefficient and should be determined for each system (e.g., BT, BTEX, etc.). These expressions can be combined to obtain an equation upon which headspace analysis is based:

$$X_b = \frac{Ab}{\gamma_b CB\, P_b};$$

The denominator is a constant calibration factor that has to be determined by measurement and calibrating the headspace sampling system. The calibration must be performed under conditions identical to the sample analysis at 30 ℃.

Calibration and Validation of the SKIP Model

Model parameters for single and multiple substrate systems can be estimated by applying the particle Swarm Optimization (PSO) global search method. PSO is launched with the initialization of a swarm of particles in the n-dimensional search space (n = the number of kinetic parameters for each system). A population of candidate solutions (particles) possesses positions (solution and fitness), velocity and individual best position as well as the swarm that maintains its global best position in the research space. PSO moves these particles toward the best solutions (kinetic model parameters that provide the minimum value of the loss function) according to mathematical

models. The movement of these particles is guided by their own best-known position as well as the entire swarm's best-known position (Trigueros et al., 2010). **Fig.A1** shows a schematic diagram of the curve fitting method using PSO.

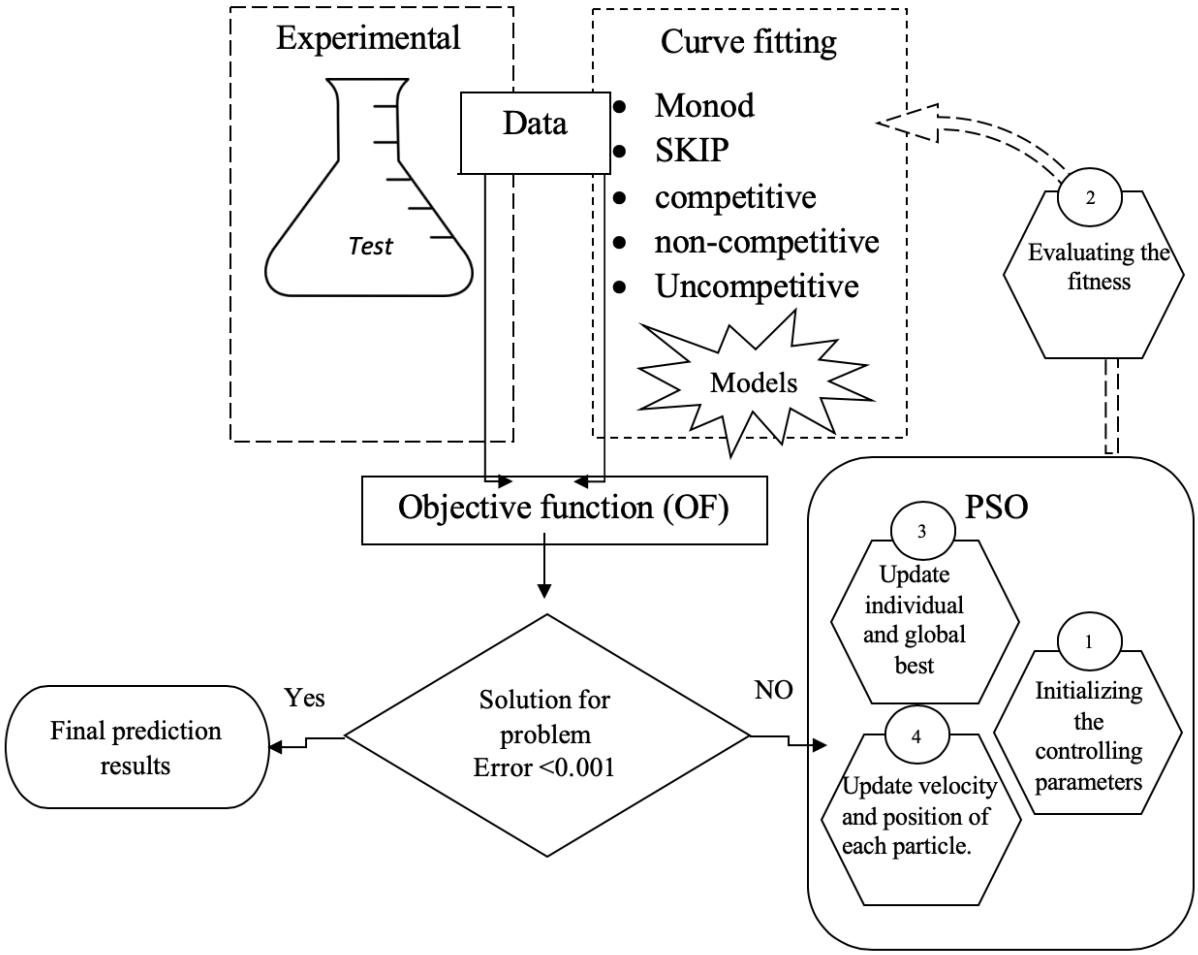

Figure A1. Schematic diagram of the proposed protocol for the calibration of the models for p-xylene co-metabolism in the presence of easily degradable substrates (e.g., benzene, toluene, and ethylbenzene).

The PSO algorithm consists of four steps: 1.) Initializing the controlling parameters and the population of the particles, 2.) Evaluating the fitness of each particle by calculating the objective for each solution, 3.) Update individual and global best and, 4). Update the velocity and position of each particle. These steps are repeated until the stopping condition is met. In other to update the

position of each particle, two vectors are considered including position and velocity vectors. The velocity vector shows the direction and intensity of movement and each particle's velocity and position are updated in each iteration using this equation (Trigueros et al., 2010):

$$\overrightarrow{v_i^{(t+1)}} = w^{(t)}\overrightarrow{v_i^{(t)}} + C_1 r_1 \left(\overrightarrow{X_{ibest}^{(t)}} - \overrightarrow{X_i^{(t)}}\right) + C_2 r_2 \left(\overrightarrow{X_{gbest}^{(t)}} - \overrightarrow{X_i^{(t)}}\right) \quad \text{(S1)}$$

$$\overrightarrow{x_i^{(t+1)}} = \overrightarrow{x_i^{(t)}} + \overrightarrow{v_i^{(t+1)}} \quad \text{(S2)}$$

Where $\overrightarrow{v_i^{(t)}}$ is the particle's velocity at time t, $\overrightarrow{X_i^{(t)}}$ is the particle's position at time t, $\overrightarrow{X_{ibest}^{(t)}}$ is the particle's individual best solution as of time t, and $\overrightarrow{X_{gbest}^{(t)}}$ is the swarm's best solution as of time t. As can be seen in **Eq. S1**, there is no subscript *i* for $\overrightarrow{X_{gbest}^{(t)}}$ Because we have just one best solution in the swarm for all particles. The two last terms in **Eq. S1** are called cognitive and social components. The cognitive component calculates the distance between the current location. In the social component, the particle calculates the distance between its current position and the best position found by the entire swarm. In the first term, the current velocity is multiplied by a variable called inertia ($w^{(t)}$). Inertia maintains the current movement direction and tunes exploration and exploitation. This controlling parameter corresponds to the distance the individual particle travels in each iteration and normally decreased linearly from 0.9 to 0.2 because exploration is increased, and exploitation is decreased proportionally to the number of iterations. However, in this work inertia equals 1. Finally, we have the acceleration constant c_1 and c_2 for the last two components in the velocity vector. These controlling parameters represent the weighting of the stochastic acceleration terms that pull each particle toward individual and group best positions. When c_1

equals zero but c_2 equals one, we have the lowest level of exploration and the highest level of exploitation that means there are no individual components and every particle follows the best solution obtained. However, when c_1 is equal to one but c_2 equals zero that means every particle search for one part of the search landscape and there is no information exchanged between the particles because they do not need to know where the global best is. In the former case, there is no convergence and particles do not convey towards one solution. Based on other literature that applied PSO optimization approaches for solving mathematical problems (Alam et al., 2015), in this work, C_1 and C_2 were equal 1.496 to balance controlling parameters for both exploration and exploitation consideration. During the search for the global optimum of the loss function (objective function), to fit models on the experimentally obtained specific growth rates, the objective of curve fitting (the loss function) is defined by the square of the differences between the observed and predicted values, calculated by the following **Eq. S3**:

$$\text{Objective Function} = \sum_{i=1} \left(\frac{\mu^{exp} - \mu^{pred}}{\mu^{exp}} \right)^2 \quad \textbf{(S3)}$$

As mentioned previously, the observed data set is composed of independent parameters (e.g., overall specific growth rate) as well as the dependent parameter (e.g., the concentration of substrates). The validation of mathematical models for mixtures of more than two substrates is studied in other literature. When the total concentrations of pollutants are constant in the mixture, the kinetic parameters are the same in the single substrate and the multiple substrate mixtures. Thus, the kinetic parameters such as μ_{max}, K_s and K_I, determined from single component degradation might be used in specific growth rate models in which more than one growth-limiting substrate is present. However, there is increased complexity in modeling multiple substrate degradation because of substrate interactions. In this study, the degradation of pure compounds and bi-component mixtures was examined to characterize substrate interactions

during the biodegradation of each BTEX compounds in mixtures by *P. putida (Littlejohns and Daugulis, 2008).*

Co-metabolic system

Quadratic sub-functions in the form of equations are provided as follow

$SF_{R,6} = A_1 + A_2.C_T + A_3.C_T.SF_{R,5} + A_4C_T^2 + A_5SF_{R,5} + A_6SF_{R,5}^2$	(S4)
$SF_{R,5} = B_1 + B_2SF_{R,4} + B_3SF_{R,4}SF_{R,3} + B_4SF_{R,4}^2 + B_5SF_{R,3} + B_6SF_{R,3}^2$	(S5)
$SF_{R,4} = C_1 + C_2SF_{R,1} + C_3SF_{R,1}SF_{R,2} + C_4SF_{R,1}^2 + C_5SF_{R,3} + C_6SF_{R,2}^2$	(S6)
$SF_{R,3} = D_1 + D_2.\alpha + D_3.\alpha.SF_{R,2} + D_4.\alpha^2 + D_5SF_{R,2} + D_6SF_{R,2}^2$	(S7)
$SF_{R,2} = F_1 + F_2.C_T + F_3.\theta.C_T + F_4.{C_T}^2 + F_5.\theta + F_6.\theta^2$	(S8)
$SF_{R,1} = E_1 + E_2.C_T + E_3.\alpha.C_T + E_4.{C_T}^2 + E_5.\alpha + E_6.\alpha^2$	(S9)
$BF_{R,7} = G_1 + G_2.BF_{R,5} + G_3.BF_{R,5}.BF_9 + G_4BF_{R,5}^2 + G_5BF_{R,6}$	(S10)
$BF_{R,6} = K_1 + K_2.\alpha + K_3.\alpha.BF_{R,4} + K_4.\alpha^2 + K_5.BF_{R,4} + K_6.BF_{R,4}^2$	(S11)
$BF_{R,4} = L_1 + L_2.C_T + L_3.BF_{R,2} + L_4.{C_T}^2$	(S12)
$BF_{R,5} = H_1 + H_2.\theta + H_3.\theta.BF_{R,3} + H_4.\theta^2 + H_5.BF_{R,3} + H_6.BF_{R,3}^2$	(S13)
$BF_{R,3} = J_1 + J_2.BF_{R,1}$	(S14)
$BF_{R,2} = M_1 + M_2.\alpha.C_T + M_3.{C_T}^2 + M_4.\alpha + M_5.\alpha^2$	(S15)
$BF_{R,1} = I_1 + I_2.\theta + I_3.\theta^2$	(S16)
$CF_1 = \acute{H}_1 + \acute{H}_2.\theta + \acute{H}_3.\theta^2 + \acute{H}_4.\theta^{0.5}$	(S17)

$CF_2 = \acute{G_1} + \acute{G_2}\,.\,\theta + \acute{G_3}\,.\,\theta.\alpha + \acute{G_4}.\theta^2 + \acute{G_5}.\alpha + \acute{G_6}.\alpha^2$	(S18)
$CF_3 = \acute{I_1} + \acute{I_2}.C_T + \acute{I_3}.C_T.\alpha^{-2} + \acute{I_4}.{C_T}^2 + \acute{I_5}.\alpha^{-2} + \acute{I_6}.\alpha^{-4}$	(S19)
$CF_4 = \acute{J_1} + \acute{J_2}\,.\,{C_T}^{0.2} + \acute{J_3}\,.\,{C_T}^{0.4}$	(S20)
$CF_5 = \acute{K_1} + \acute{K_2}.\alpha + \acute{K_3}.\alpha^{-1} + \acute{K_4}.\alpha^2 + \acute{K_5}.\alpha^{-2} + \acute{K_6}.\alpha^{-4}$	(S21)
$CF_6 = \acute{E_1} + \acute{E_2}\,.\,CF_1 + \acute{E_3}\,.\,CF_1.CF_4 + \acute{E_4}.CF_1^2 + \acute{E_5}.CF_4 + \acute{E_6}.CF_4^2$	(S22)
$CF_7 = \acute{D_1} + \acute{D_2}\,.\,CF_2 + \acute{D_3}\,.\,CF_2.CF_3 + \acute{D_4}.CF_2 + \acute{D_5}.CF_3 + \acute{D_6}.CF_3^2$	(S23)
$CF_8 = \acute{F_1} + \acute{F_2}\,.\,C_T + \acute{F_3}\,.\,C_T.CF_1 + \acute{F_4}.{C_T}^2 + \acute{F_5}.CF_1 + \acute{F_6}.CF_1^2$	(S24)
$CF_9 = \acute{C_1} + \acute{C_2}.CF_7 + \acute{C_3}.CF_6.CF_7 + \acute{C_4}.{CF_7}^2 + \acute{C_5}.CF_6 + \acute{C_6}.CF_6^2$	(S25)
$CF_{10} = \acute{B_1} + \acute{B_2}.CF_5 + \acute{B_3}.CF_5.CF_8 + \acute{B_4}.{CF_5}^2 + \acute{B_5}.CF_8 + \acute{B_6}.CF_8^2$	(S26)
$CF_{11} = \acute{A_1} + \acute{A_2}.CF_{10} + \acute{A_3}.CF_9.CF_{10} + \acute{A_4}CF_{10}^2 + \acute{A_5}CF_9 + \acute{A_6}CF_9^2$	(S27)

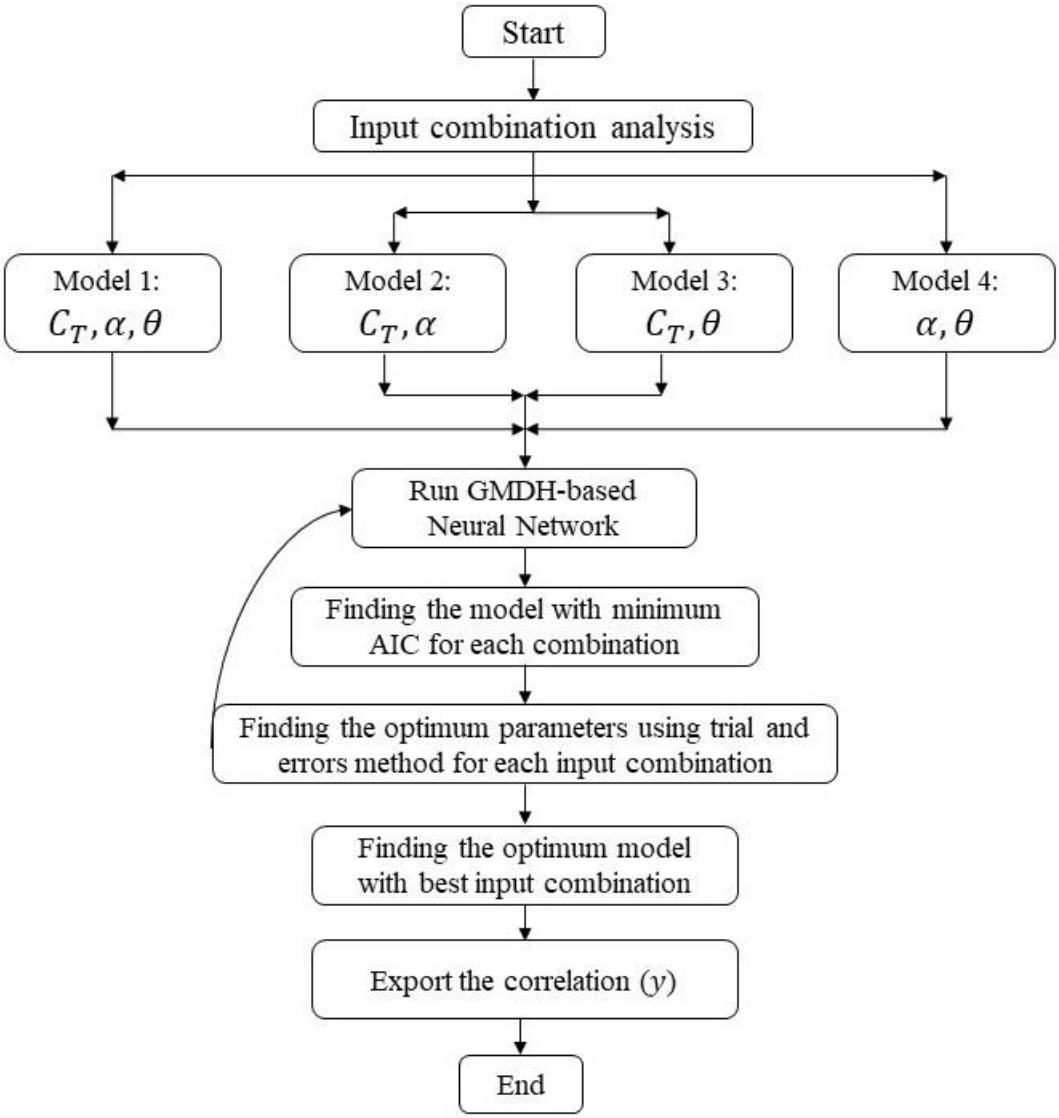

Figure A2. GMDH-based Neural Network modeling flowchart (Ebtehaj et al., 2015)

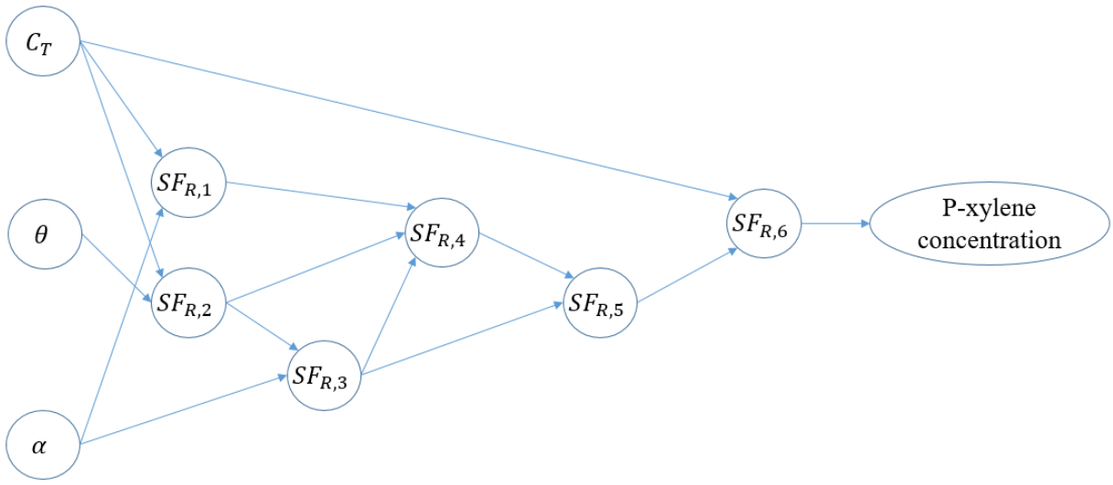

Figure A3. Neural network design of *p*-xylene concentration in resting cells phase system as a function of C_T, α, and θ

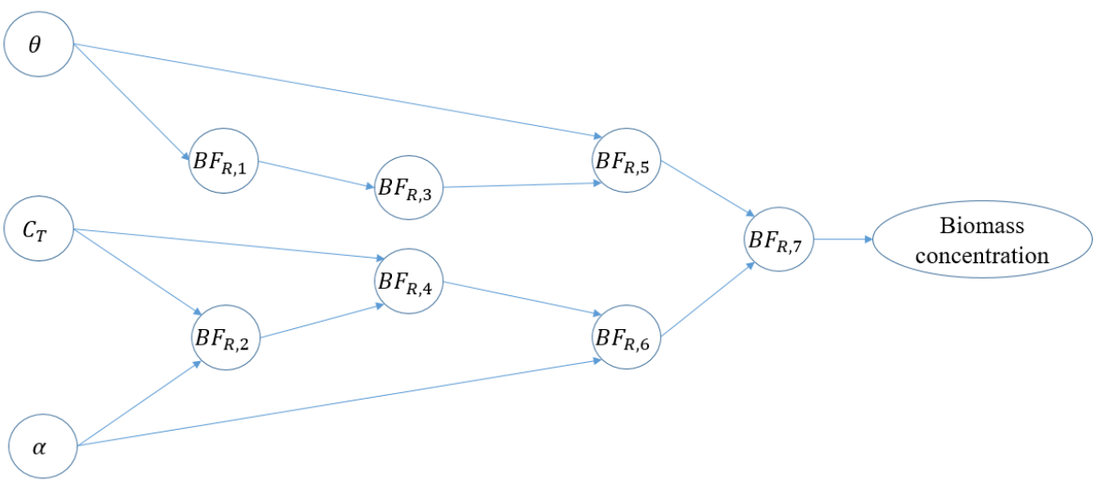

Figure A4. Neural network design of biomass concentration in resting cells phase system as a function of C_T, α, and θ.

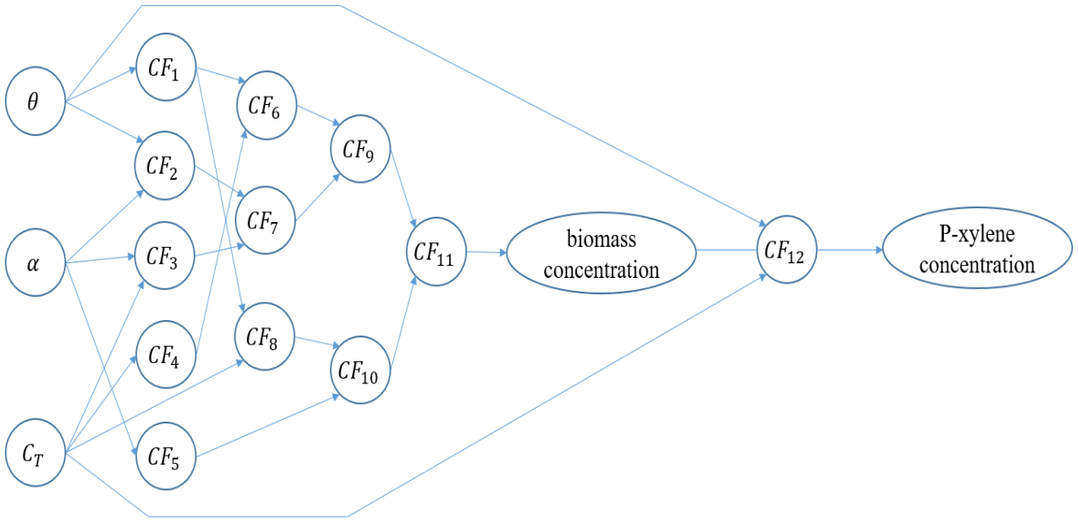

Figure A5. Neural network design of biomass concentration in the co-metabolic system as a function of C_T, α, and θ.

Table A1. The values of parameters obtained by using the GMDH-type Neural Network model for the resting cell phase system.

	A	B	C	D	E	F	G	H	I	J	K	l	M
1	725.604	2.54125	72.6518	-8.21641	15.4344	23.8003	-6.37368	4.31707	4.95065	-2.04×10^{-13}	-339.304	2.5793	-2.5489
2	-17.7841	-0.05815	-1.74018	13.9511	0.417669	0.405073	2.0963	0.031728	-1.3322	1	146.719	-0.003719	-0.0137
3	0.435826	-6.13114	-0.175955	-0.05928	-0.05947	0.000531	-0.35958	-0.78398	0.133408	-	-49.9248	0.005461	4.82×10^{-5}
4	-0.14363	3.06699	0.095518	-4.71643	0.002555	0.002377	-0.00036	0.018542	-	-	4.05739	-5.27×10^{-5}	11.0802
5	0.640629	0.97662	0.884549	1.04131	14.0451	-0.82017	2.09392	2.10717	-	-	174.612	-	-4.6012
6	-0.21962	3.06449	0.087925	5.88E-05	-4.71643	0.065132	-	0.398532	-	-	-20.2814	-	-

Table A2. The values of parameters obtained by using the GMDH-type Neural Network model for the co-metabolic system.

	$\acute{A}$	$\acute{B}$	$\acute{C}$	$\acute{D}$	$\acute{E}$	$\acute{F}$	$\acute{G}$	$\acute{H}$	$\acute{I}$	$\acute{J}$	$\acute{K}$	$\acute{M}$
1	-0.064397 2	0.909837	-0.032324 4	0.96018	2.29003	1.15803	-5.23754	1.24453	-0.0116735	6.74851	-75820	0.951057
2	0.692093	-0.556443	0.988663	-0.147365	-1.02776	-.0216566	0.114487	0.168001	0.0291875	-6.77441	-42118.3	0.00070363 7
3	-2.20656	0.579193	1.65828	0.799761	0.913253	0.0199207	0.0393297	-0.0040712 5	-0.00529862	2.14212	-64008.7	-0.0286163
4	1.14046	0.066655	0.970974	-0.168989	-0.00078527 5	-6.93143×10 $^{-6}$	-0.0020490 8	-0.328604	-6.93143×10 $^{-6}$	-	9026	0.0138204
5	0.359605	-0.295921	0.043888 7	-0.441951	-1.03112	-0.042475	5.29382	0.083006	2.51258	-	-22584.6	-
6	1.05206	0.0014127 8	0.665684	0.093836 1	-	0.00078527 5	-	-	1.2266	-	-	-

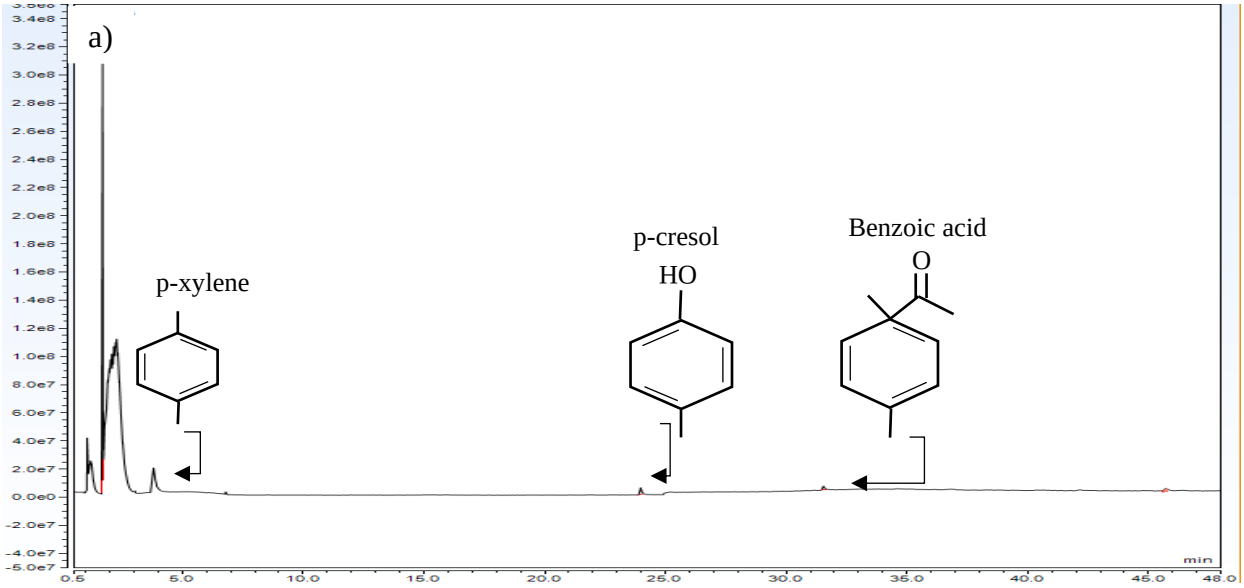
a)
p-xylene
p-cresol
HO
Benzoic acid
O
min

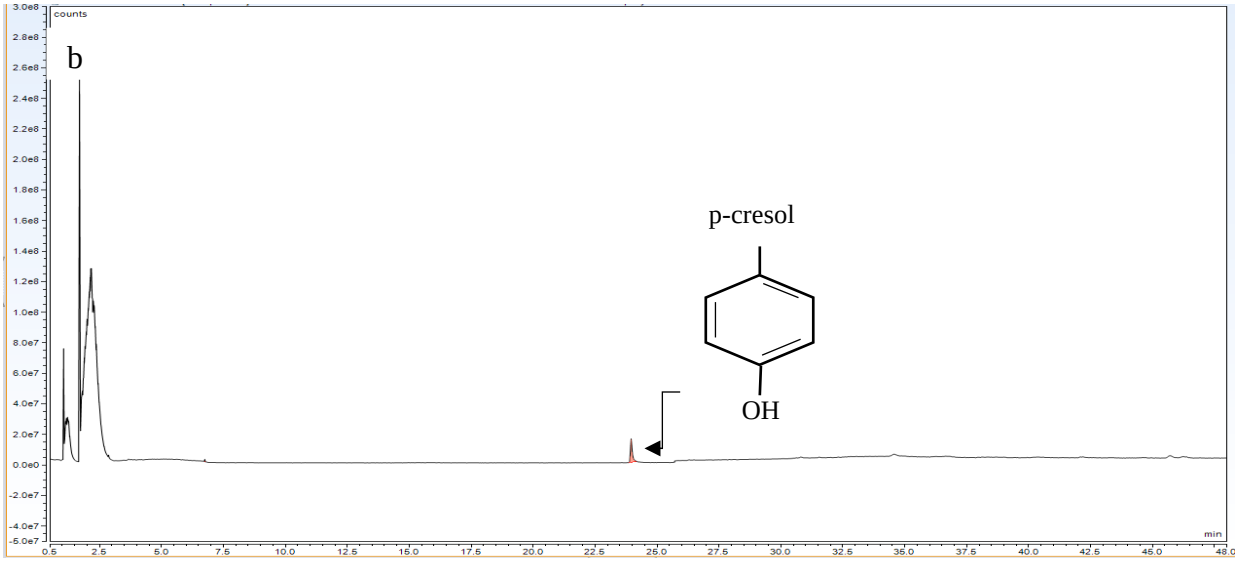
counts
b
p-cresol
OH
min

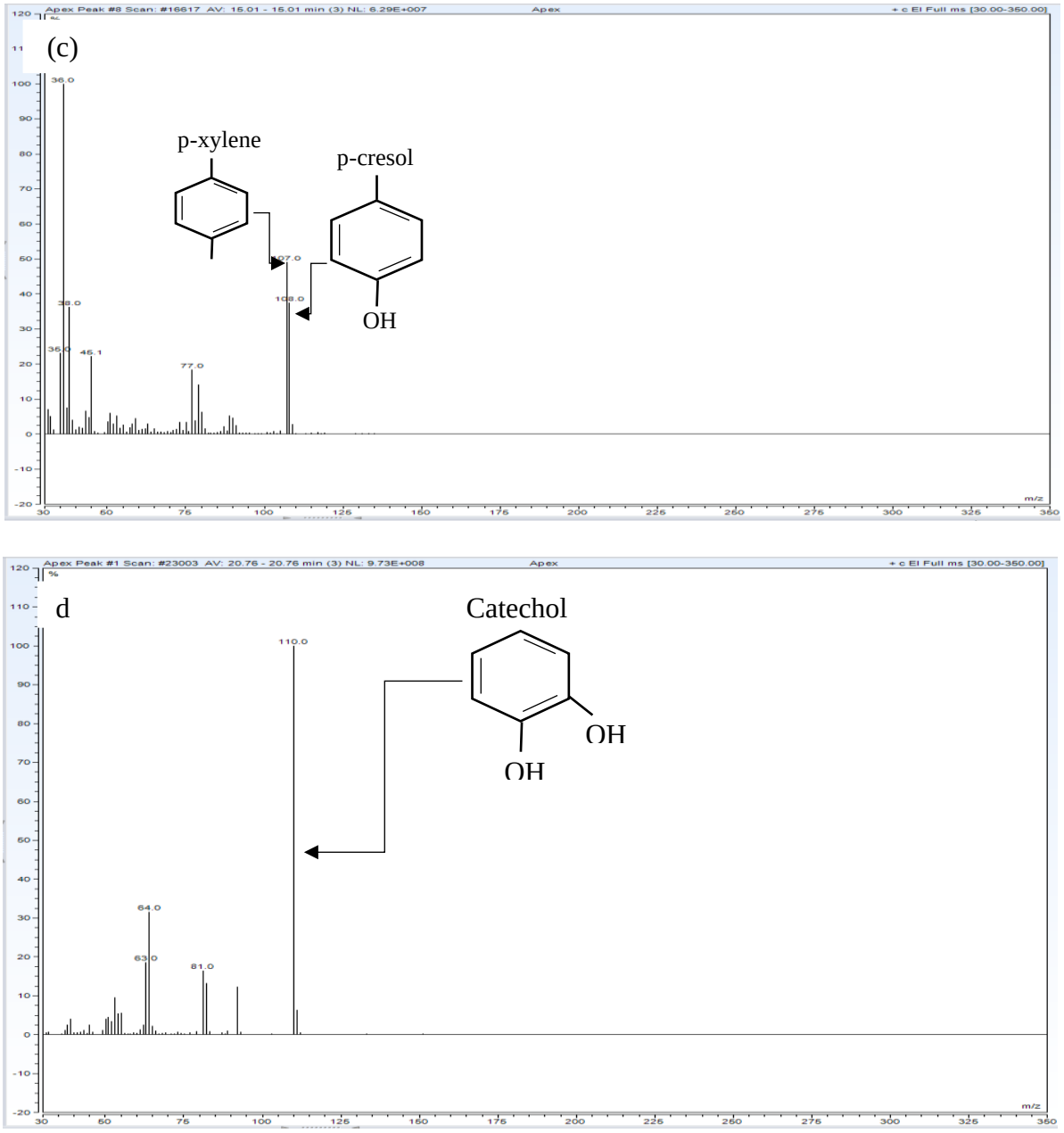

Fig. A6 Mass spectrum for central intermediates. a) presence of p-cresol and benzoic acid in the p-xylene metabolic system, b) accumulation of p-cresol in the p-xylene metabolic system and; c,d) Gas-chromatographic profiles of the p-xylene metabolic and co-metabolic system

APPENDIX B. Supplementary information of section 3.2.

1- RNA extraction and cDNA synthesis

Total RNA was extracted from all experiments by the RNA total Kit (BioBasic Inc, Canada) and was treated with Thermo Scientific DNase I (RNase-free) to remove plasmid/genomic DNA. Total RNA was quantified at 260 nm and 280 nm with NanoDrop 2000 spectrophotometer (Thermo Scientific). Then, the same amount of total extracted RNA (100ng) was used to synthesize cDNA with Prime Script ^{TM} RT reagent kit and random hexamer primers (Takara Bio Inc, Japan). The quality of cDNA synthesis was assessed by agarose gel electrophoresis with DNA-safe stain after PCR amplification. For each PCR reaction, a negative control (without DNA template) was performed to check possible DNA contamination (Fig. B1). Thermal cycling of PCR was 94°C for 5 min for initial denaturation, followed by 30 cycles of 94°C, 1 min; 60°C, 1 min; 72°C, 1 min; then one more 72°C for 5 min to allow trimming of incomplete polymerizations.

Table B1. Growth characterization of isolated strains at different temperatures

Substrate	Growth (at 5°C) [a]			Growth (at 15°C) [a]			Growth (at 30°C) [a]		
	S2TR-01	S2TR-09	S2TR-20	S2TR-01	S2TR-09	S2TR-20	S2TR-01	S2TR-09	S2TR-20
Benzene	+	+	+	+	+	+	-	-	-
Toluene	±	+	±	+	+	+	-	-	-
Ethylbenzene	±	±	±	±	±	±	-	-	-
Xylene	-	+	-	-	+	±	-	-	-

[a] +, Good growth; ±, poor growth; -, no growth.

Table B2. Temperature profile in Real-time PCR

Steps		Temperature	Time for each step	Cycle
Initial Denaturation		95°C	5min	1
PCR	Denaturation	95°C	15sec	40
	Annealing	60°C	20sec	
	extension	72 °C	20sec	
Melt Curve		57 to 95 °C (raising by 0.3 °C)	15sec for each step	1

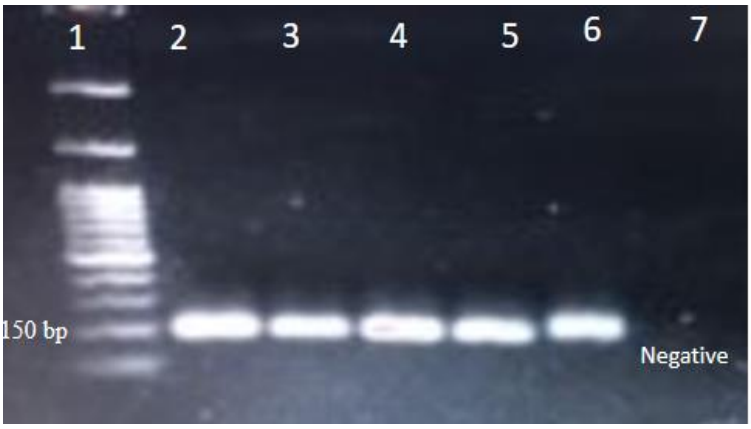

Fig. B1. Amplification of 16srRNA PCR in 2% agarose gel electrophoresis in lanes 2 to 6, Lane 1 resents the DNA ladder, Lane 7 resents negative control (amplified sample without DNA template) for PCR reaction.

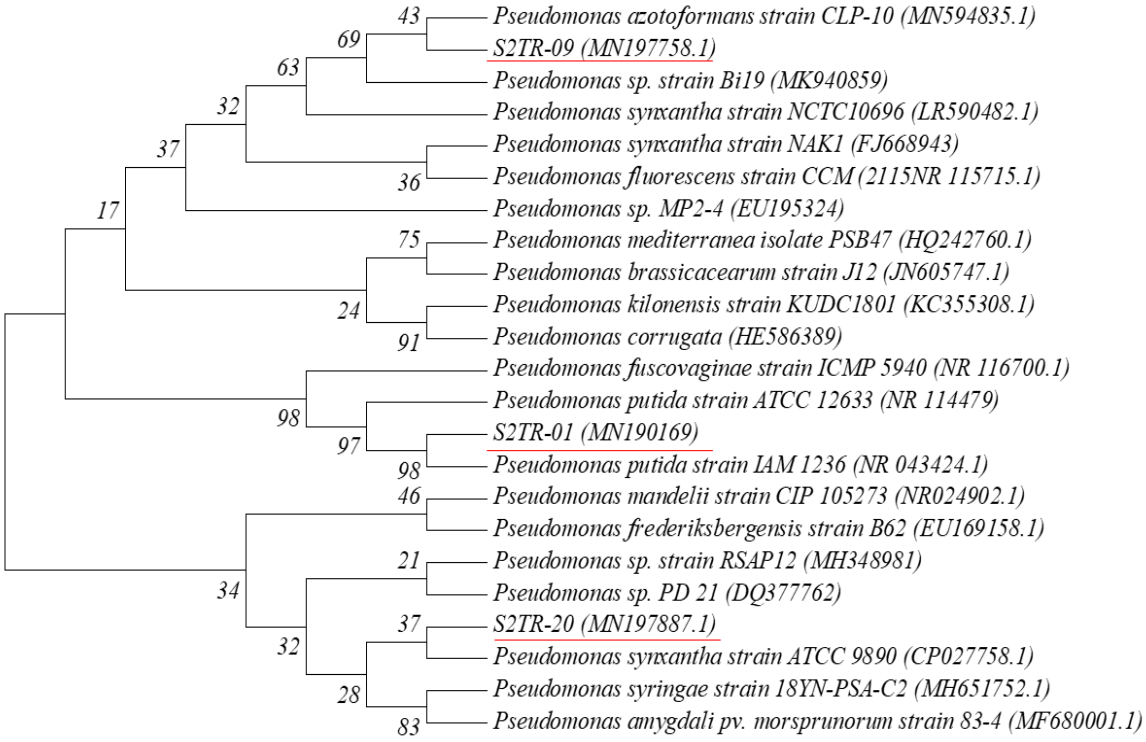

Fig. B2. Phylogenetic tree of S2TR-01, S2TR-09, and S2TR-20 (red underline) and other related bacterial genera**.** Bootstrap values are shown from 1,000 replicates. GeneBank accession numbers for the 16S rRNA sequence are shown in the parenthes

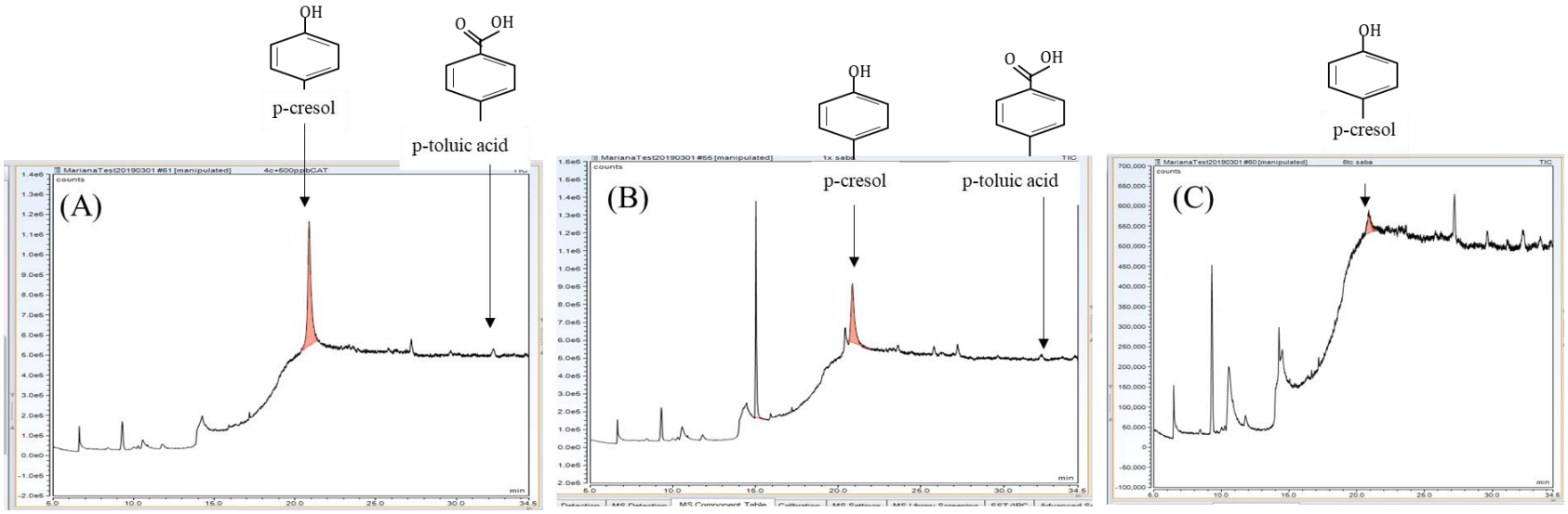

Fig. B3. Mass spectra of key intermediates in the presence of p-xylene A: mass spectrum of the media in presence of *P. putida* S2TR-01; B: spectra of p-xylene biodegradation system in presence of *P. synxantha* S2TR-20; C: spectra of p-xylene biodegradation system in presence of *P. azotoformans* S2TR-09

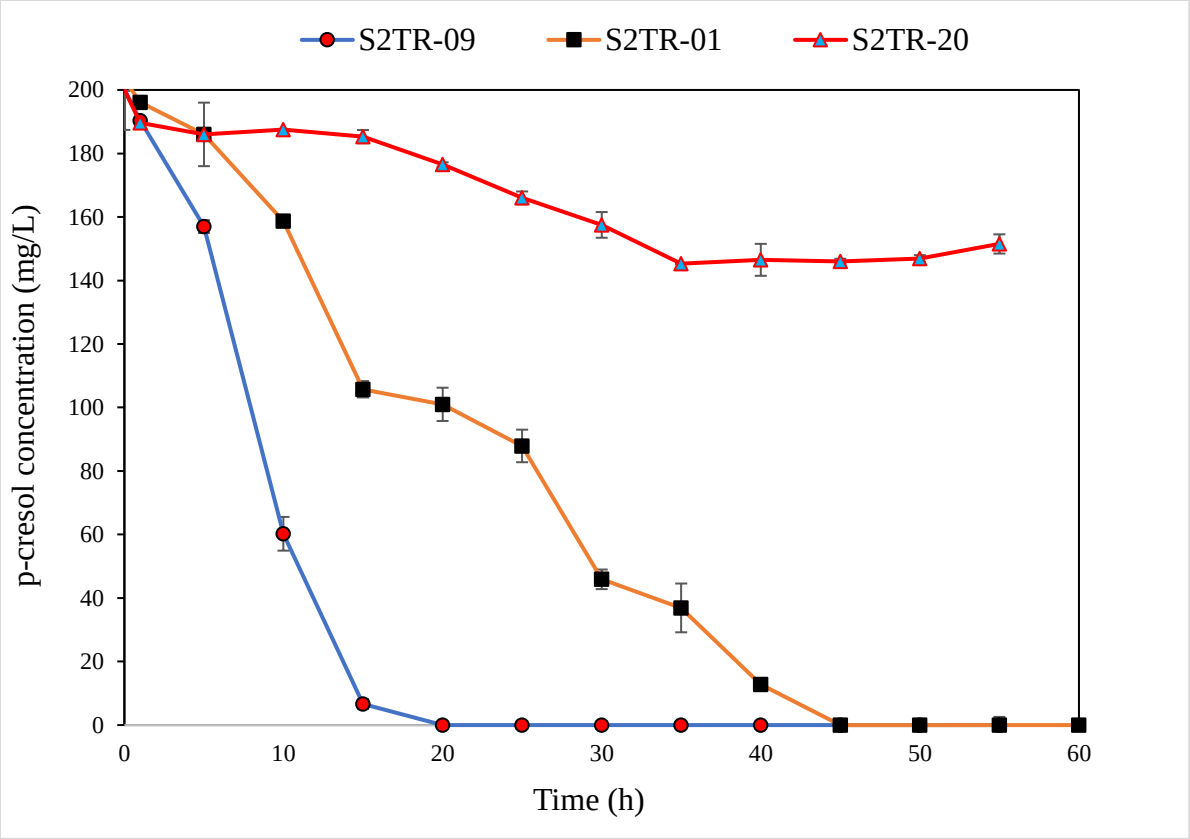

Fig. B4. p-cresol biodegradation by *P. putida* S2TR-01, *P. azotoformans* S2TR-09, and *P. synxantha* S2TR-20 with an initial concentration of 200 mg/L.

APPENDIX C. Supplementary information of section 4.1.

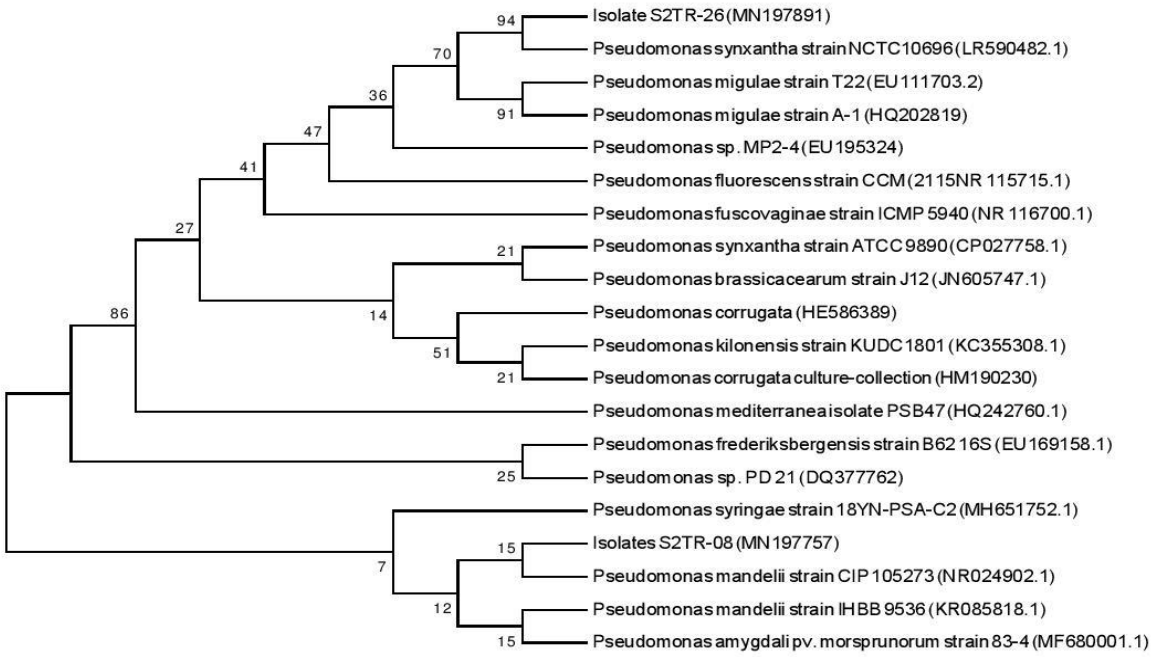

Fig. C1. Phylogenetic tree of S2TR-08 and S2TR-26 and other related bacterial genera**.** Bootstrap values are shown from 1,000 replicates. GeneBank accession numbers for the 16S rRNA sequence are shown in the bracket.

Table C1. Biochemical characteristics of isolates S2TR-08 and S2TR-26 and *Pseudomonas putida* (ATCC 33015). W, White; +, positive; -, negative

Biochemical characteristics	S2TR-08	S2TR-26	*Pseudomonas putida* (ATCC 33015)
Color of colony	W	W	W
Motility	+	+	+
Growth at 37 ˚C	-	-	+
Growth at <10 ˚C	+	+	-
Catalase	+	+	+
H_2S production	-	-	-
Urease	+	-	-

Indole test	+	-	-
Gelatinase	-	-	-
Citrate	+	+	+
Acid production from Glucose	-	-	-
Acid production from lactose	-	-	-
Acid production from sucrose	-	-	-

Table C2. Primers used in this study

Target gene	**Encoded Protein**	**Sequence (5′- > 3′)**	**Length (bp)**	**GC (%)**	**T_m (°C)**	**Amplicon size (bp)**
16S rRNA	16S ribosomal RNA	F: CGGAATTACTGGGCGTAAAG R: TCTACGCATTTCACCGCTAC	20	50	60	149
xylM	xylene monooxygenase	F: AATGTCTCGGTTCGGATCAC R: AGTGGTGTGCCAACTCTTCC	20	50	60	114
xylE	catechol 2,3-dioxygenase	F: CTTCAAGGTGACCGACGATG R: GGTGTACTCCTTCTCGGCATAG	20 22	57 54	60	172
catA-I	catechol 1,2-dioxygenase	F: CCGAGATGAAGAAGTGCACG R: CCCAGTCCGAGTTCAACCTG	20	55	60	177

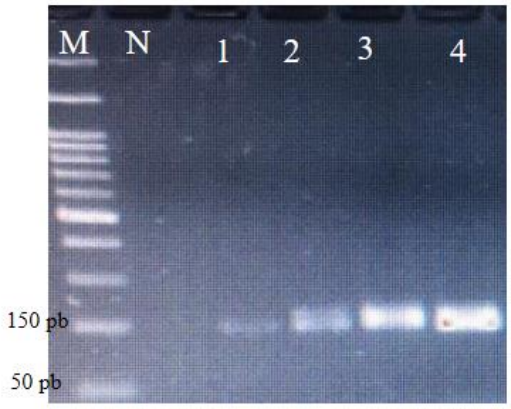

Fig. C2. 16s rRNA amplification, (M) The PCR Marker, (N) negative control; without cDNA template, Lanes (1-4) isolated bacteria

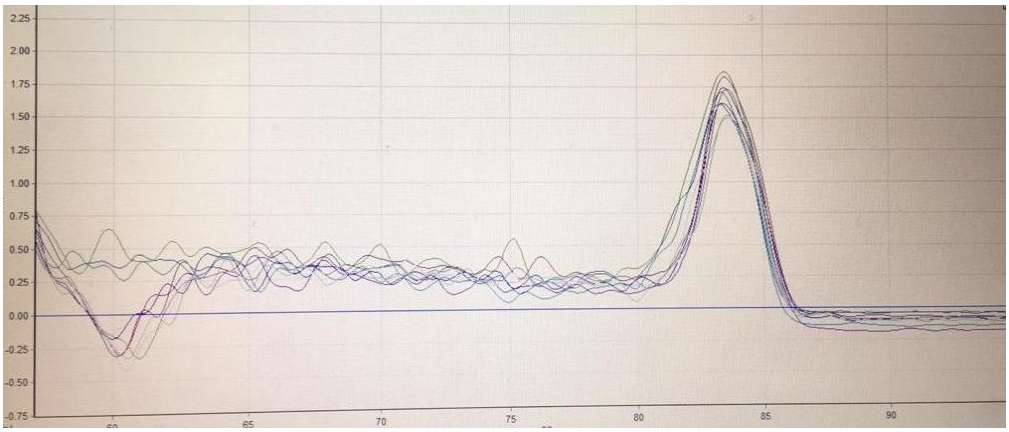

Fig. C3. Melting peaks of the qRT-PCR reactions.

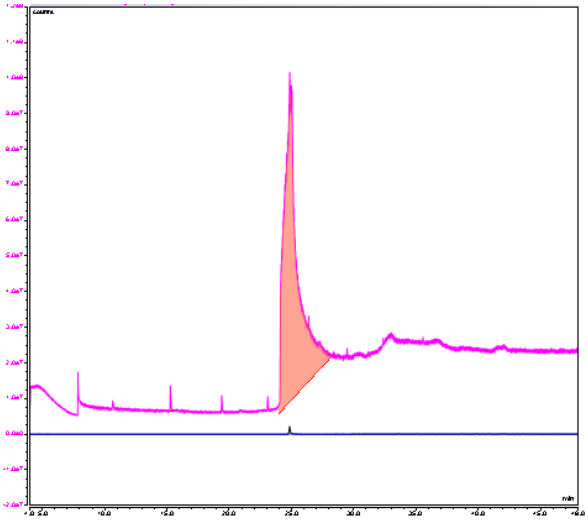

Fig. C4. Full scan mass detection to determine the products formed by the action of xylene monooxygenase. The accumulation of p-cresol with a molecular weight of 108.13 was detected.

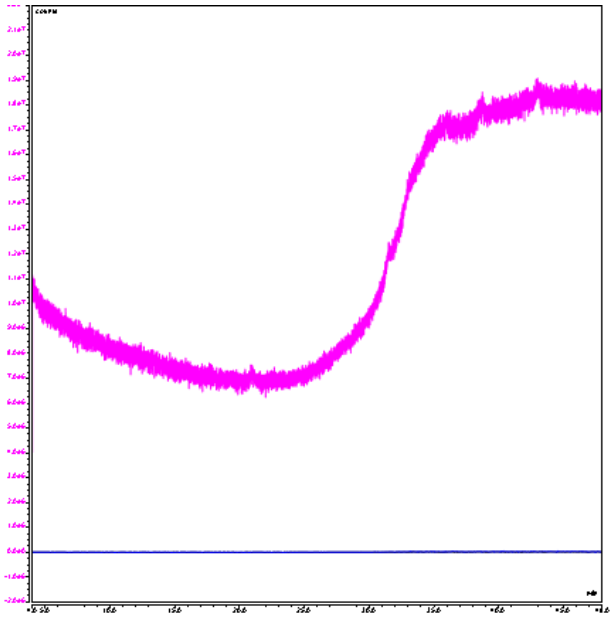

Fig. C5. Full scan mass detection to determine the products formed by the action of catechol 2, 3-dioxygenase on bioconversion products. Inert the final products were detected.

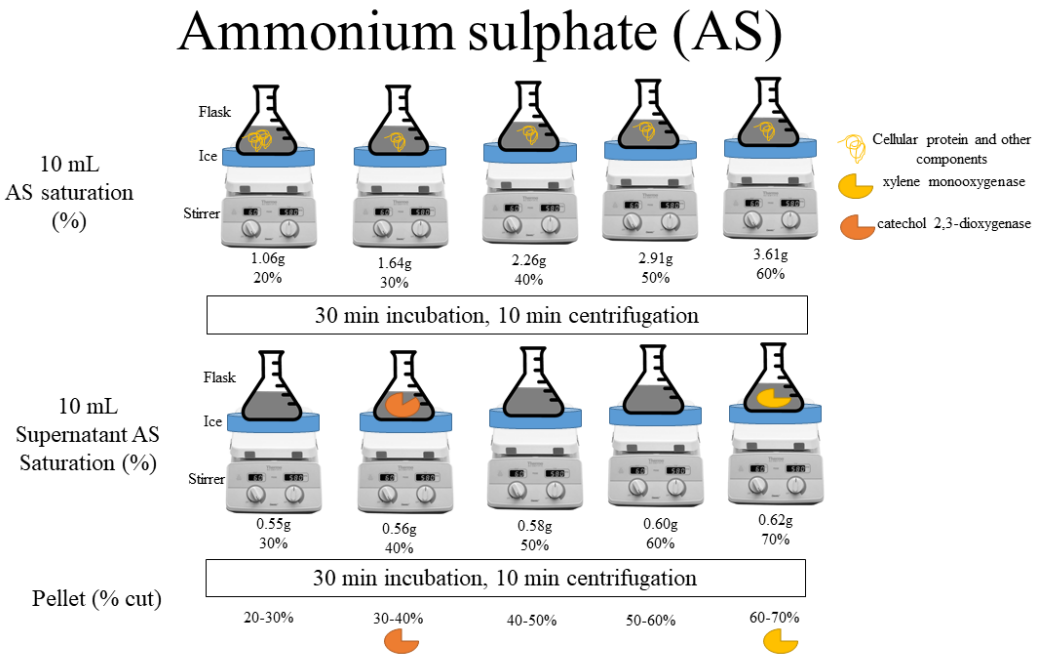

Fig. C6. Ammonium sulfate precipitation procedure for partial enzyme purification

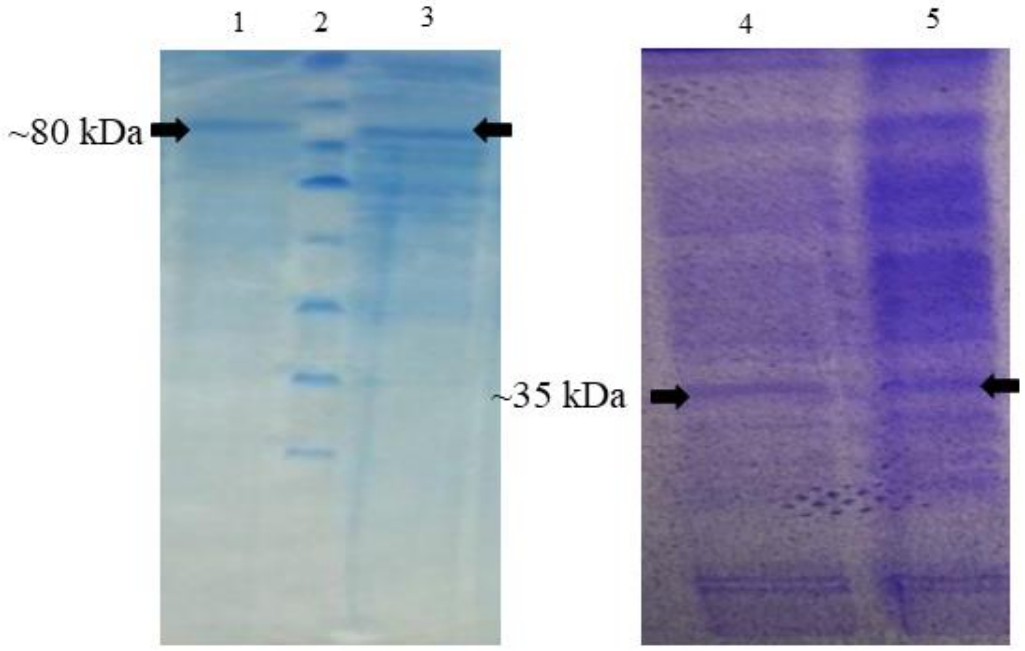

Fig. C7. SDS-PAGE analysis of crude cell extracts of *P. synxantha* S2TR-26 (Lane 1) and *P. mandelii* S2TR-08 (Lane 5). Lane 2: Protein marker latter, Lane 3: partially purified xylene monooxygenase from *P. synxantha* S2TR-26 (~80 kDa), Lane 4: partially purified catechol 2, 3-dioxygenase from *P. mandelii* S2TR-08 (~35 kDa).

Table C3. Specific enzyme activity of crude enzymes and partially purified enzymes in different concentration of ammonium sulphate.

xylene monooxygenase from *P. synxantha* S2TR-26 (U/mg)						**Catechol 2,3-dioxygenase from *P. mandelii* S2TR-08 (U/mg)**					
Crude	20%	30%	40%	50%	60%	Crude	20%	30%	40%	50%	60%
10.15	ND	ND	ND	0.1	49.83	11.07	ND	56.41	ND	ND	ND

Table C4. Proteins concentration and enzyme activities in cocktails of xylene monooxygenase and catechol 2, 3-dioxygenase

	1:1	**1:1.5**	**1:2**	**1.5:1**	**2:1**
Protein (mg/L)	48.5	56.0	68.2	69.8	75.6
xylene monooxygenase (U/mg)	10.2	10.4	10.5	16.4	22.1
Catechol 2, 3-dioxygenase (U/mg)	10.9	17.2	21.3	10.4	11.2

APPENDIX D. Supplementary information of section 4.2.

Enzymes production

Before inoculation for enzyme production, each bacterium was cultured in Tryptic Soy Broth (TSB) at 15±1°C and 150 rpm. Cell concentration was measured by optical density at 600 nm (OD600) and a correlation was obtained between OD600 value and the number of viable bacteria by counting colony-forming units (CFU). Each OD600 value corresponds to 1×10^8 of viable *P. synxantha* and 0.9×10^8 of viable *P. mandelii*.

The enzyme production was carried out in 250 mL serum bottles containing 50 mL of MSM supplemented with 18 g/Lcrustacean waste, 2 g of soy peptone, and 200 mg/L of p-xylene. This concentration was selected based on our previous results that showed 200 mg/L of p-xylene can highly induce the expression of the encoding genes for involved enzymes to compare to 50 and 100 mg of p-xylene (Miri et al. 2021). Crustacean waste and soy peptone were used as a source of calcium and proteins that can promote bacterial growth at a lower cost compared to the standard medium such as tryptic soy broth (Brzeszcz and Kaszycki 2018). Total concentration 2×10^8 cell/mL of fresh culture inoculated to the medium and incubation was performed at 15±1°C on a rotary shaker (150 rpm). Monocultures of *Pseudomonas synxantha* S2TR-26 and *Pseudomonas mandelii* S2TR-08 were established as controls to compare the total protein and enzyme activity. After 24h of incubation, the culture was centrifuged at 3810 *x* g for 20 min. Then, the pellet was collected and washed twice with phosphate buffer (pH 7.2) and then re-suspended in the same buffer then ultrasonicated at 22-30 kHz frequencies for 10 min. (Branson Ultrasonics Corporation, Danbury, CT, USA) to extract intracellular enzymes (Kadri et al. 2018).

Soil characteristics

Grain size distribution and characteristics of the soil are summarized in Table S3. The size of particles between 250 µm and 2 mm was used for column tests. The soil samples were homogenized and dried at 60°C for 24h to remove the moisture.

Table D1. Physico-chemical properties of the soil from a contaminated site.

Physico-chemical properties

pH		6.5±0.5
Porosity		0.29± 0.08
Moisture content		13.6±0.5 (% dry weight)
Water holding capacity		71±2 (%)
Total carbon		2.6±0.3 (%)
Nitrogen		0.2± 0.1 (%)
Soil type	Gravel	25.0 (%)
	Sand	64.8 (%)
	Silt	8.3 (%)
	Clay	0.1 (%)
	Colloids	1.8 (%)

Table D2. Size analysis of soil (Standard method form (ASTM 2007))

Diameter (mm)	50	37.5	25	19	9.5	4.75	2	0.425	0.075	0.0289	0.0169	0.0121	0.0086	00.42	0.0018
Passing (%)	100	100	100	100	100	75	42	20	10.2	8.4	3.6	2.2	1.9	1.8	1.7

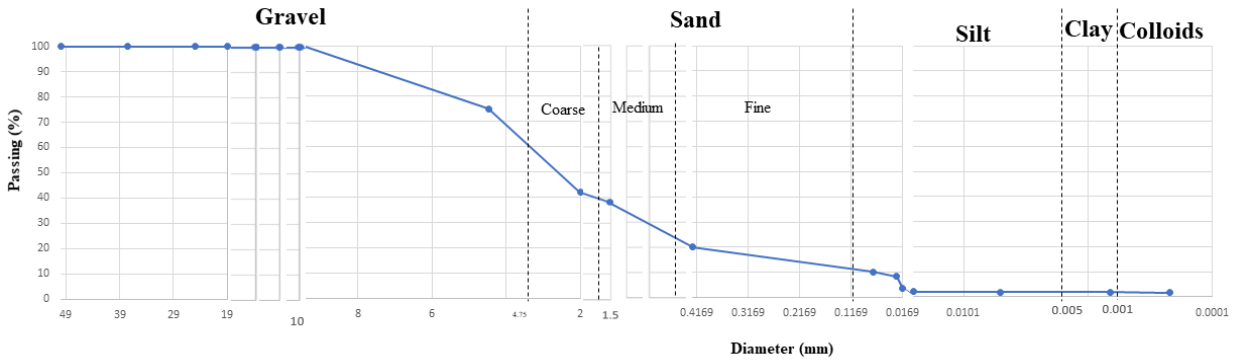

Fig. D1. Particle-size analysis of soil

Basic characteristics of the soil, such as zeta potential, and FTIR analysis were determined by standard methods. The surface charge of soil particles was studied using zeta-sizer Nano ZS (Malvern Instrument Inc., UK). The Fourier transform infrared (FT-IR) spectroscopic analyses were recorded in the range of 400–4000 cm^{-1} using a Nicole IS50 FT-IR Spectrometer (Thermo Scientific, USA) in attenuated total reflectance (ATR) mode with 8 cm^{-1} resolution as reported elsewhere.

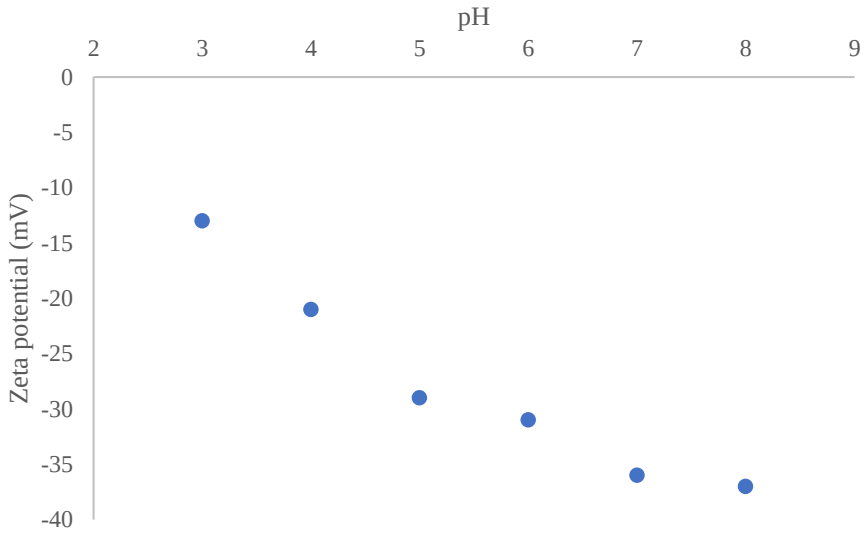

Figure. D2. Zeta potential of soil samples as a function of pH

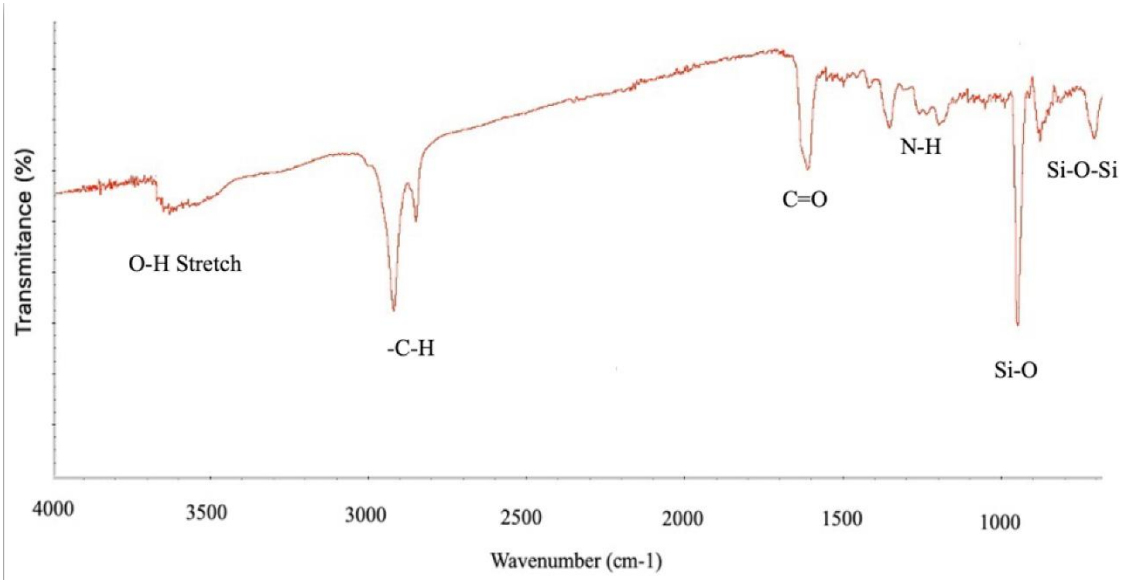

Figure. D3. FTIR of mineral soil samples

Soil column set-up

Tubes were clamped between Teflon end reservoirs and stainless-steel endplates. To avoid particle losses, one stainless-steel mesh was inserted at both the inlet and outlet ends of the column, and two Vitton© O-rings were used to seal the cylinder with the endplates.

Column packing and water saturation were carried out according to Martel and Gélinas (Martel and Gelinas 1996). Briefly, dry packing was carried out using pouring discrete soil portions (with a spoon) into the column and then mechanically compact them with a plunger. The soil portions were deposited in layers of 1 cm and each layer was artificially contaminated with p-xylene using a micropipette of 100 µL to a final concentration of 10,000 mg/kg of soil. To ensure hydraulic connectivity between the layers, lightly scarifying the soil surface (0.5 cm of each layer) was carried out after compaction and before the addition of another layer. This procedure was repeated several times until the top of the soil column was reached (Gilbert et al. 2014). The bulk density of the soil after packing was 1.8 ±0.02 g/cm^3. The columns were saturated with water overnight, following the injection of CO_2 at a pressure of 4 psi to remove entrapped air for complete water saturation. As CO_2 is a water-soluble gas, its bubbles can quickly dissolve in water. The soil columns were allowed to saturate with deaerated water (approximate 5 pore volume) using a peristaltic pump (2 mL/min) from bottom to top to eliminate CO_2. Polyethylene tubes were used for the inflow and outflow of the aqueous solutions.

Table D2. Characterization and initial condition of the soil column experiment

Soil column No.	Column volume (cm^3)	Soil density in column [(1)] (g/cm^3)	Soil intrinsic permeability (m^2)	Pore volume (cm^3)	Hydraulic conductivity (K_w)
1	140.39	1.88	7.5-9.2×10^{-13}	50±0.5	1.3×10^{-6}
2	139.37	1.79		49±0.5	1.4×10^{-6}
3	141.41	1.71		50±0.5	2.4×10^{-6}
4	140.39	1.72		50±0.5	2.2×10^{-6}
5	139.36	1.82		49±0.5	1.5×10^{-6}
6	140.39	1.78		50±0.5	2.3×10^{-6}
7	139.36	1.90		49±0.5	2.4×10^{-6}
8	139.36	1.84		50±0.5	2.5×10^{-6}
9	139.36	1.90		50±0.5	1.6×10^{-6}
10	139.36	1.81		49±0.5	2.9×10^{-6}

11	140.39	1.70		50±0.5	1.7×10^{-6}

(1) Soil density was selected based on site soil density ranging 1.7-1.9 g/cm^3.

Table D3. Parameters of the Freundlich adsorption isotherm model for the enzyme (Low-level concentration of enzyme solutions; X/10) and p-xylene individually (K_{fi}, n from Eq. (5)) and as a mixture (*aij* from Eq.(6))

	Enzyme 1	Enzyme 2	p-xylene
K_f	0.82	0.65	1.53
n	0.99	0.83	1.65
R^2	0.91	0.98	0.94
a_{i1}	1	-	-0.35
a_{i2}	-	1	-0.43
a_{i3}	-	-	1

1 and 2 enzymes, 3 p-xylene

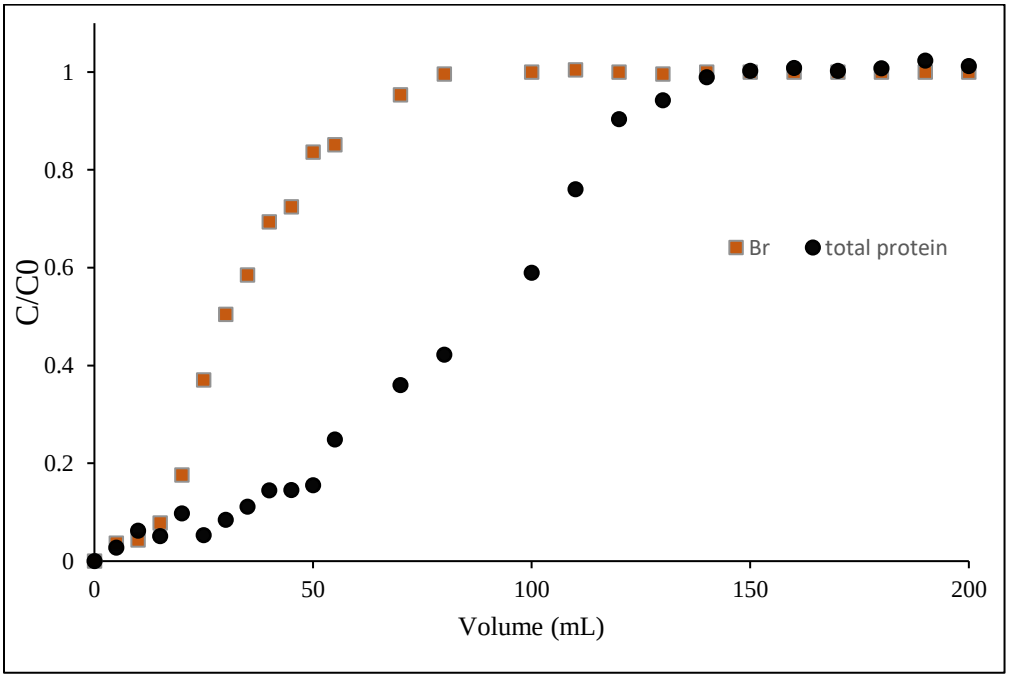

Fig. D4. Relative concentration on the breakthrough curve for trace element (Br^-) and total protein in the effluent sample during enzyme injection.

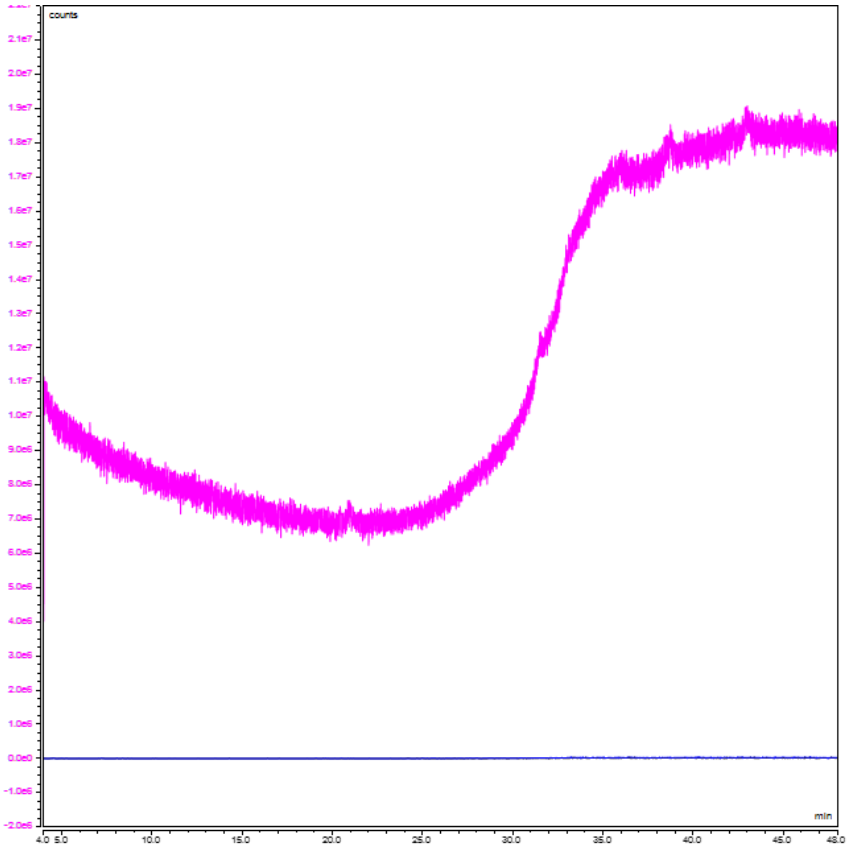

Fig. D5. Full scan mass detection to determine the products of enzymatic biodegradation. The inert final products were detected.

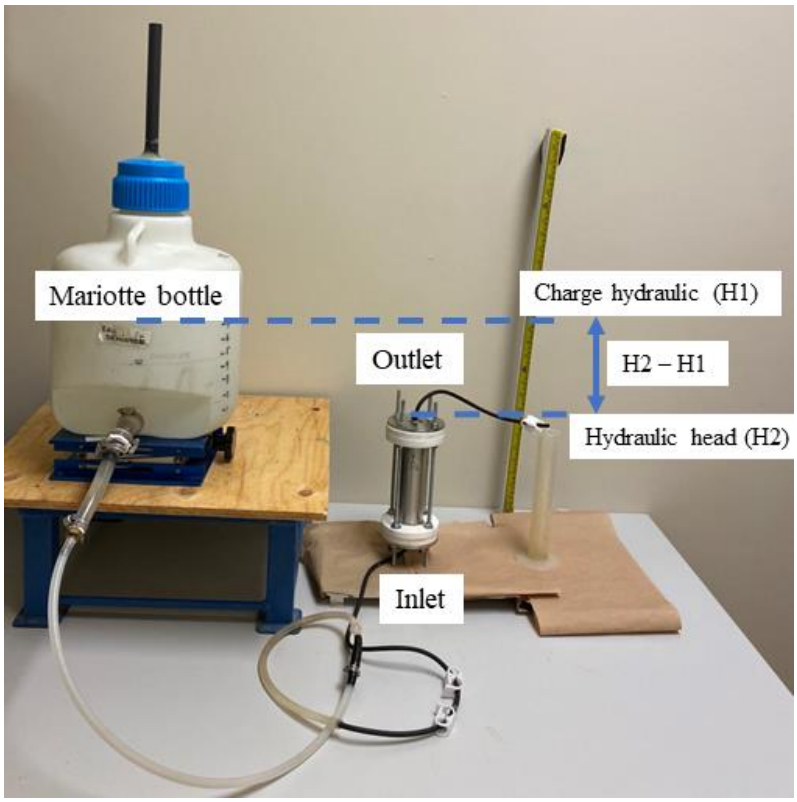

Fig. D6. Hydraulic conductivity measurement set up

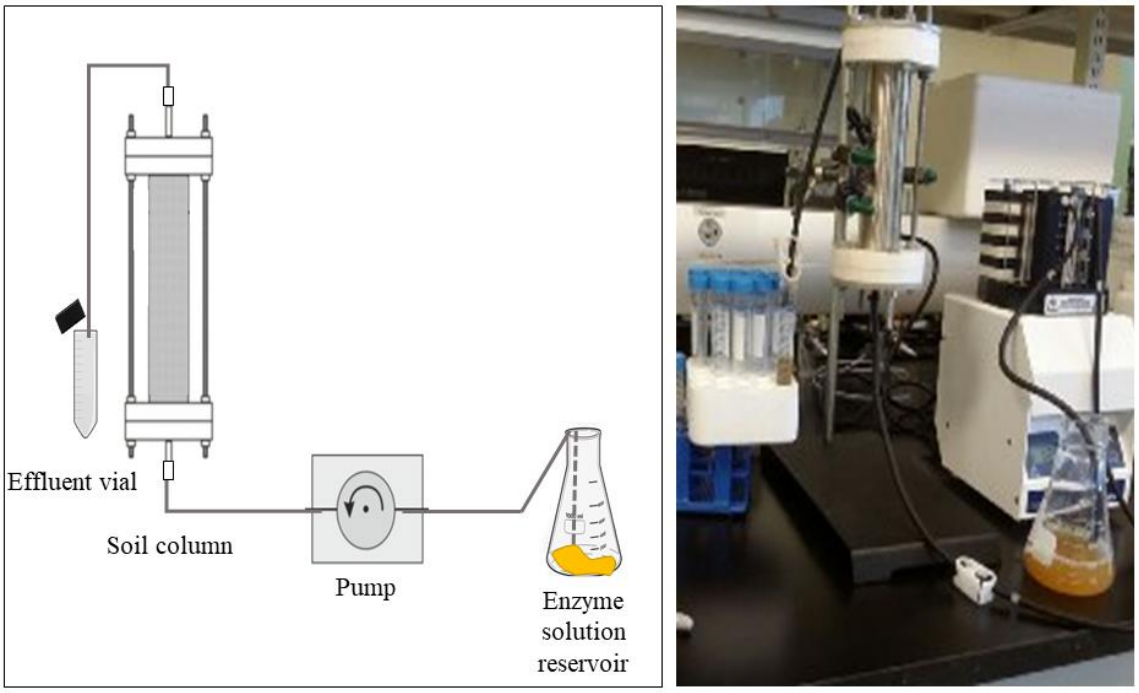

Fig. D7. Enzyme injection set-up

Proteomics sample preparation

The mini S-Trap kit (100-300µg) was used according to the manufacturer's instructions with some modifications. Briefly, 250 µg of protein was reduced using 30 mM TCEP (final concentration) at 60˚C for 15 min and alkylated with 1M IAA at room temperature for 1 h in a dark environment. 12.5% phosphoric acid was added to the samples and mixed with S-trap binding buffer (100 mM TEAB in 90% methanol, pH 7.1). Then the sample mixture was transferred into S-Trap microcolumns and centrifuged at 4000 g until all solution was passed through. The columns were washed with S-trap binding buffer three times and 25 µL of Trypsin/Lys-C buffer with 50 mM TEAB and trypsin (25:1 of protein: trypsin) was added to the columns and incubated at 47˚C, 1h. The resulting peptides were eluted by elution basic buffer (50 mM TEAB), acidic buffer (0.1% formic acid in water) and organic buffer (0.1% formic acid in 80% acetonitrile). The resulting peptides were dried at 45˚C and resuspended in 0.2% formic acid in water.

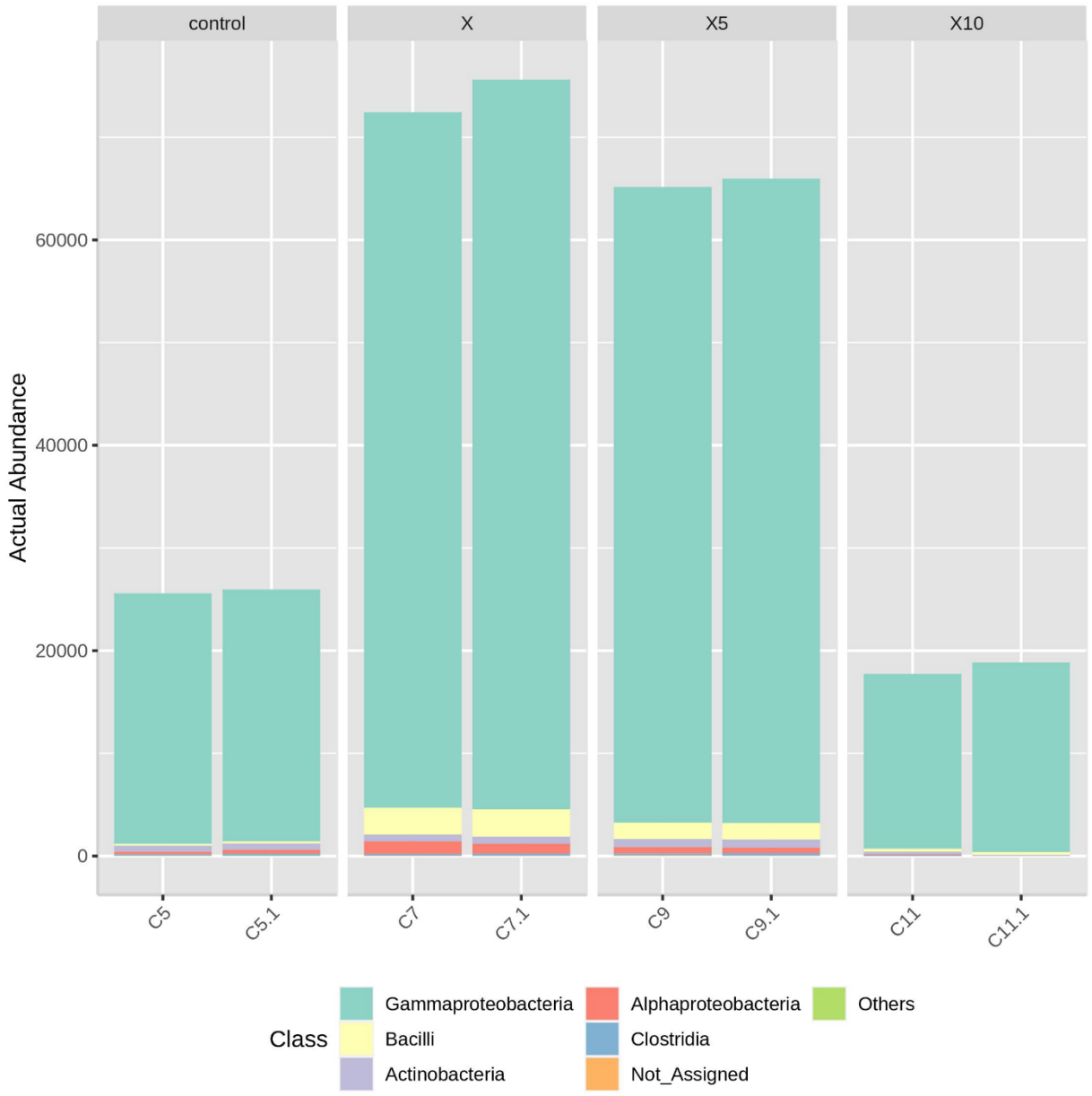

Fig. D8. Class-level comparison of the microbial community.

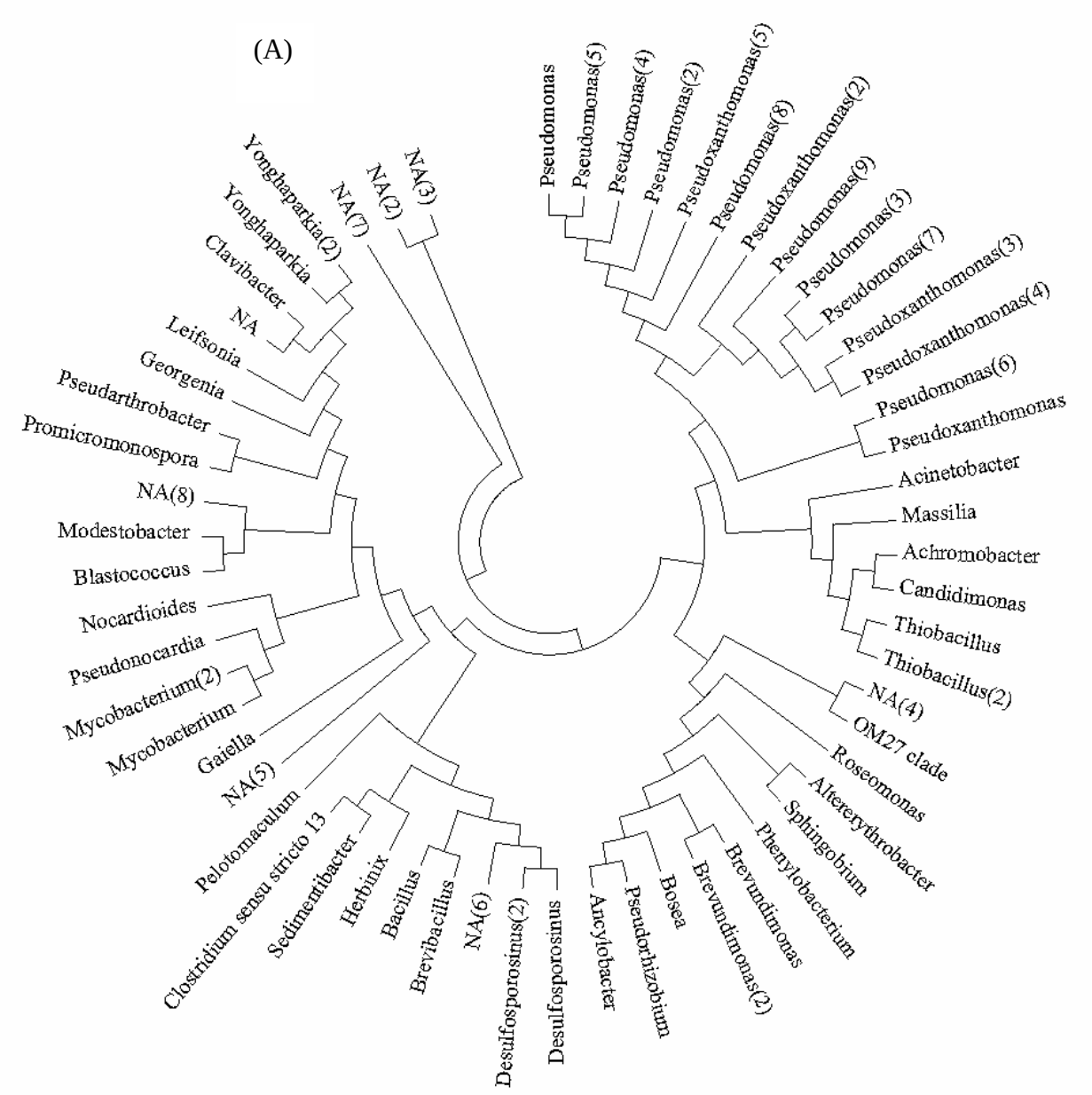
(A)
Pseudomonas
Pseudomonas(5)
Pseudomonas(4)
Pseudomonas(2)
Pseudoxanthomonas(5)
Pseudomonas(8)
Pseudoxanthomonas(2)
Pseudomonas(9)
Pseudomonas(3)
Pseudomonas(7)
Pseudoxanthomonas(3)
Pseudoxanthomonas(4)
Pseudomonas(6)
Pseudoxanthomonas
Acinetobacter
Massilia
Achromobacter
Candidimonas
Thiobacillus
Thiobacillus(2)
NA(4)
OM27 clade
Roseomonas
Altererythrobacter
Sphingobium
Phenylobacterium
Brevundimonas(2)
Bosea
Pseudorhizobium
Ancylobacter
Desulfosporosinus
Desulfosporosinus(2)
NA(6)
Brevibacillus
Bacillus
Herbinix
Sedimentibacter
Clostridium sensu stricto 13
Pelotomaculum
NA(5)
Gaiella
Mycobacterium
Mycobacterium(2)
Pseudonocardia
Nocardioides
Blastococcus
Modestobacter
NA(8)
Promicromonospora
Pseudarthrobacter
Georgenia
Leifsonia
NA
Clavibacter
Yonghaparkia
Yonghaparkia(2)
NA(7)
NA(2)
NA(3)

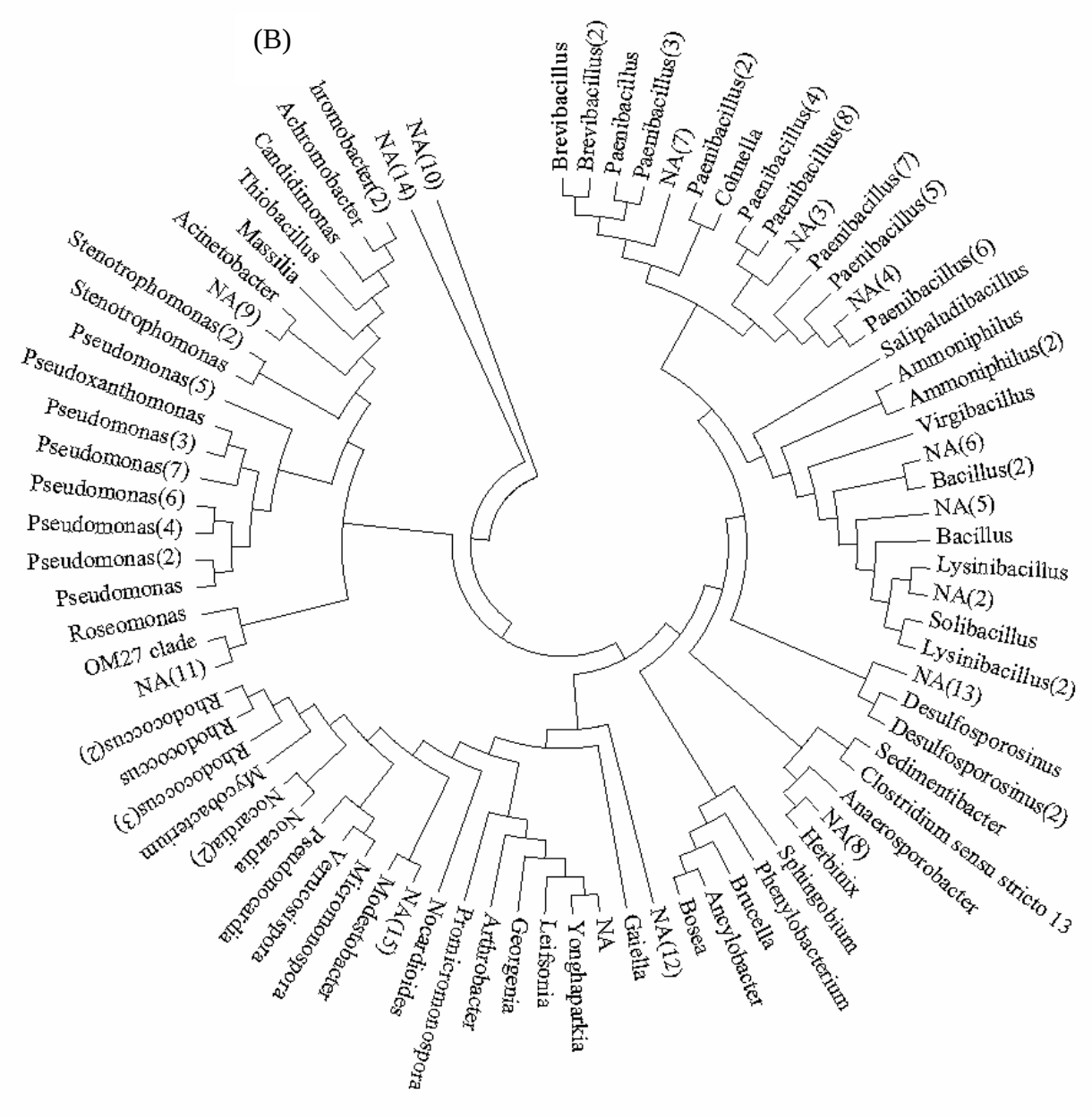
(B)
Brevibacillus
Brevibacillus(2)
Paenibacillus
Paenibacillus(3)
NA(7)
Paenibacillus(2)
Cohnella
Paenibacillus(4)
Paenibacillus(8)
NA(3)
Paenibacillus(7)
Paenibacillus(5)
NA(4)
Paenibacillus(6)
Salipaludibacillus
Ammoniphilus
Ammoniphilus(2)
Virgibacillus
NA(6)
Bacillus(2)
NA(5)
Bacillus
Lysinibacillus
NA(2)
Solibacillus
Lysinibacillus(2)
NA(13)
Desulfosporosimus
Desulfosporosimus(2)
Sedimentibacter
Clostridium sensu stricto 13
Anaerosporobacter
NA(8)
Herbinix
Sphingobium
Phenylobacterium
Brucella
Ancylobacter
Bosea
NA(12)
Gaiella
NA
Yonghaparkia
Leifsonia
Georgenia
Arthrobacter
Promicromonospora
Nocardioides
NA(15)
Modestobacter
Micromonospora
Verrucosispora
Pseudonocardia
Nocardia
Nocardia(2)
Mycobacterium
Rhodococcus(3)
Rhodococcus
Rhodococcus(2)
NA(11)
OM27 clade
Roseomonas
Pseudomonas
Pseudomonas(2)
Pseudomonas(4)
Pseudomonas(6)
Pseudomonas(7)
Pseudomonas(3)
Pseudoxanthomonas
Pseudomonas(5)
Stenotrophomonas
Stenotrophomonas(2)
NA(9)
Acinetobacter
Massilia
Thiobacillus
Candidimonas
Achromobacter
Achromobacter(2)
NA(14)
NA(10)

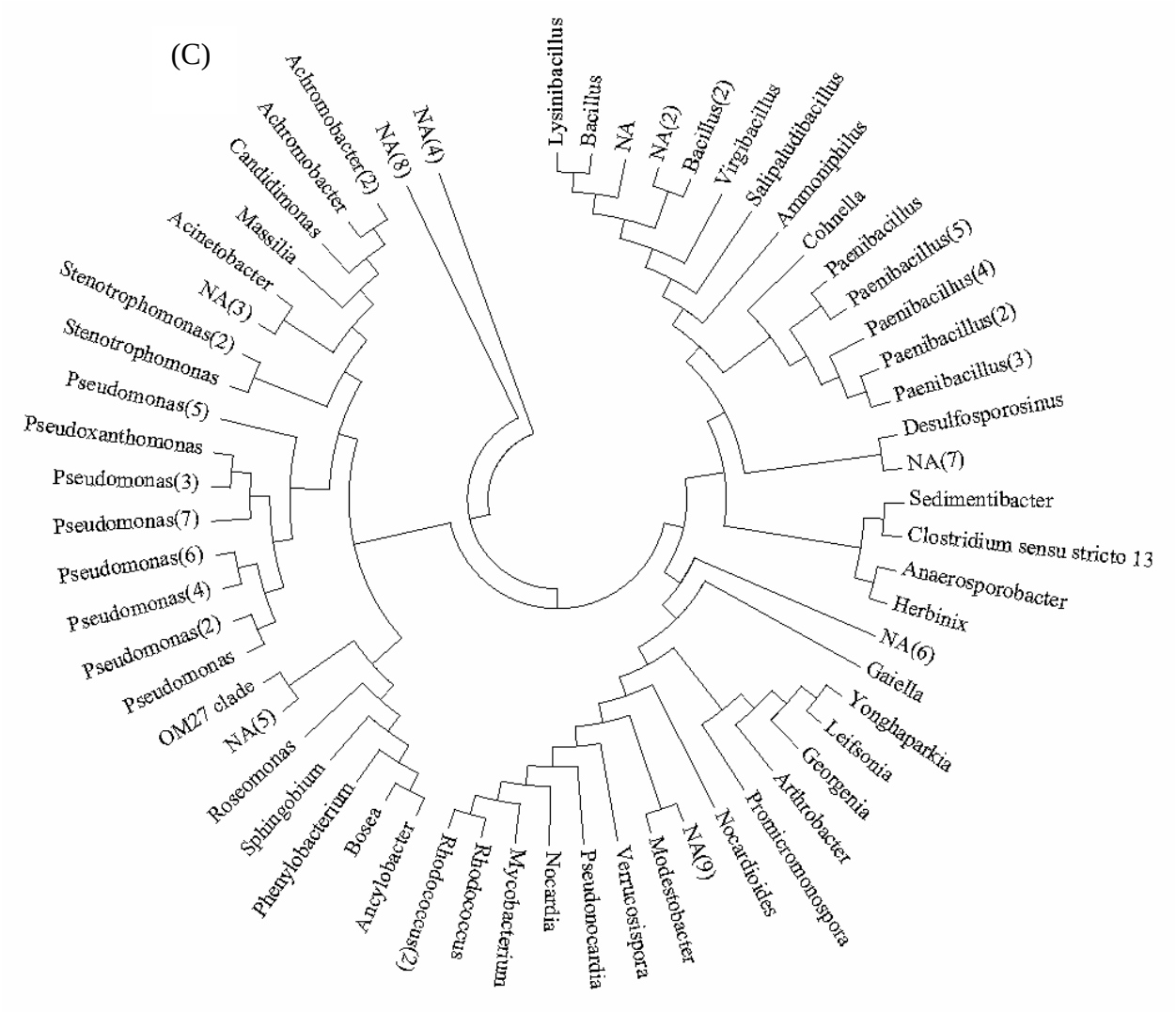
(C)
Lysinibacillus
Bacillus
NA
NA(2)
Bacillus(2)
Virgibacillus
Salipaludibacillus
Ammoniphilus
Cohnella
Paenibacillus
Paenibacillus(5)
Paenibacillus(4)
Paenibacillus(2)
Paenibacillus(3)
Desulfosporosinus
NA(7)
Sedimentibacter
Clostridium sensu stricto 13
Anaerosporobacter
Herbinix
NA(6)
Gaiella
Yonghaparkia
Leifsonia
Georgenia
Arthrobacter
Promicromonospora
Nocardioides
NA(9)
Modestobacter
Verrucosispora
Pseudonocardia
Nocardia
Mycobacterium
Rhodococcus
Rhodococcus(2)
Ancylobacter
Bosea
Phenylobacterium
Sphingobium
Roseomonas
NA(5)
OM27 clade
Pseudomonas
Pseudomonas(2)
Pseudomonas(4)
Pseudomonas(6)
Pseudomonas(7)
Pseudomonas(3)
Pseudoxanthomonas
Pseudomonas(5)
Stenotrophomonas
Stenotrophomonas(2)
NA(3)
Acinetobacter
Massilia
Candidimonas
Achromobacter
Achromobacter(2)
NA(8)
NA(4)

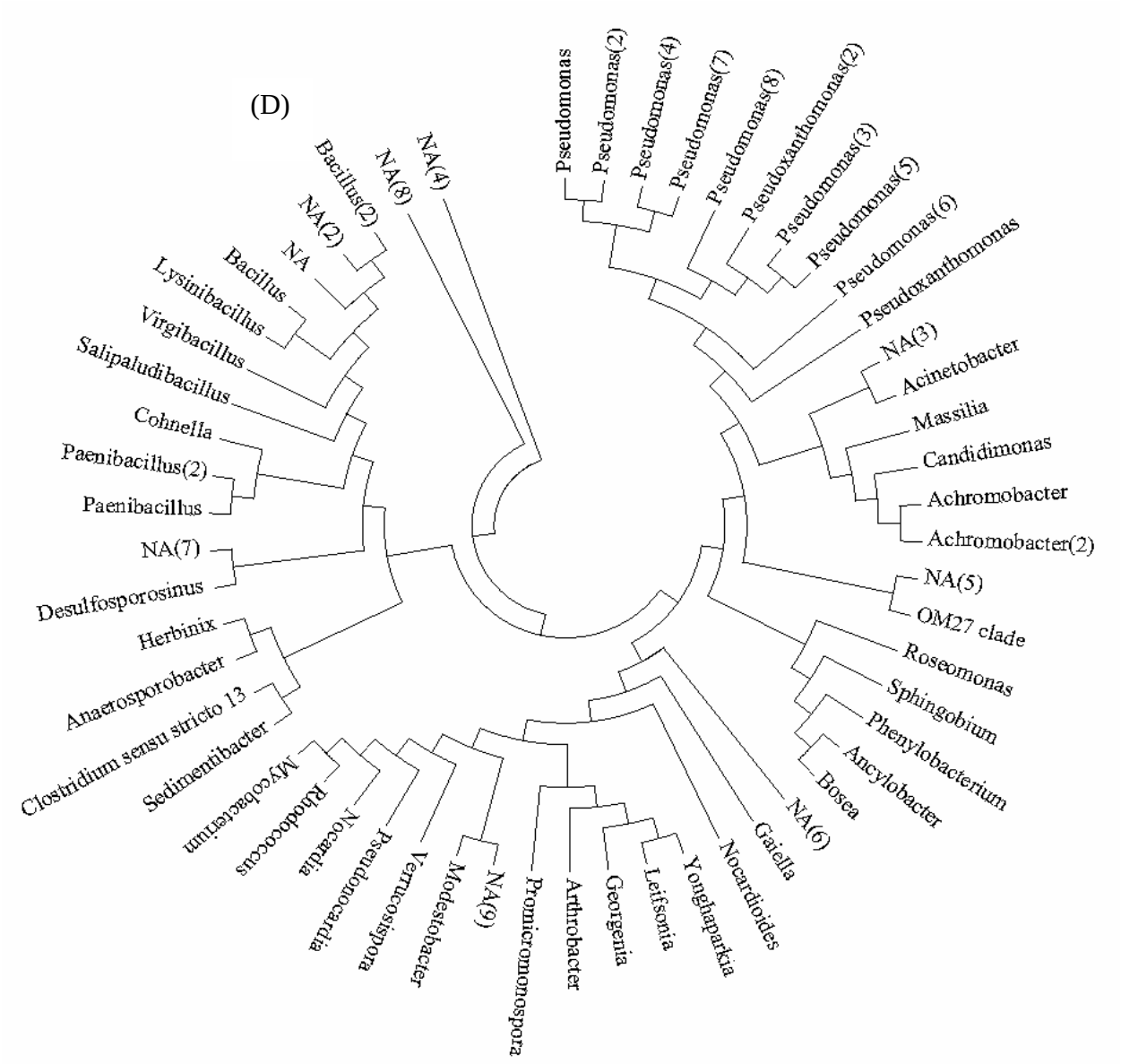
(D)
Pseudomonas
Pseudomonas(2)
Pseudomonas(4)
Pseudomonas(7)
Pseudomonas(8)
Pseudoxanthomonas(2)
Pseudomonas(3)
Pseudomonas(5)
Pseudomonas(6)
Pseudoxanthomonas
NA(3)
Acinetobacter
Massilia
Candidimonas
Achromobacter
Achromobacter(2)
NA(5)
OM27 clade
Roseomonas
Sphingobium
Phenylobacterium
Ancylobacter
Bosea
NA(6)
Gaiella
Nocardioides
Yonghaparkia
Leifsonia
Georgenia
Arthrobacter
Promicromonospora
NA(9)
Modestobacter
Verrucosispora
Pseudonocardia
Nocardia
Rhodococcus
Mycobacterium
Sedimentibacter
Clostridium sensu stricto 13
Anaerosporobacter
Herbinix
Desulfosporosinus
NA(7)
Paenibacillus
Paenibacillus(2)
Cohnella
Salipaludibacillus
Virgibacillus
Lysinibacillus
Bacillus
NA
NA(2)
Bacillus(2)
NA(8)
NA(4)

Fig. D9. The phylogenetic diversity of the microbial community,(A) untreated soil, (B) treated soil with enzyme X, (C) treated soil with enzyme X/5, (D) treated soil with enzyme X/10.

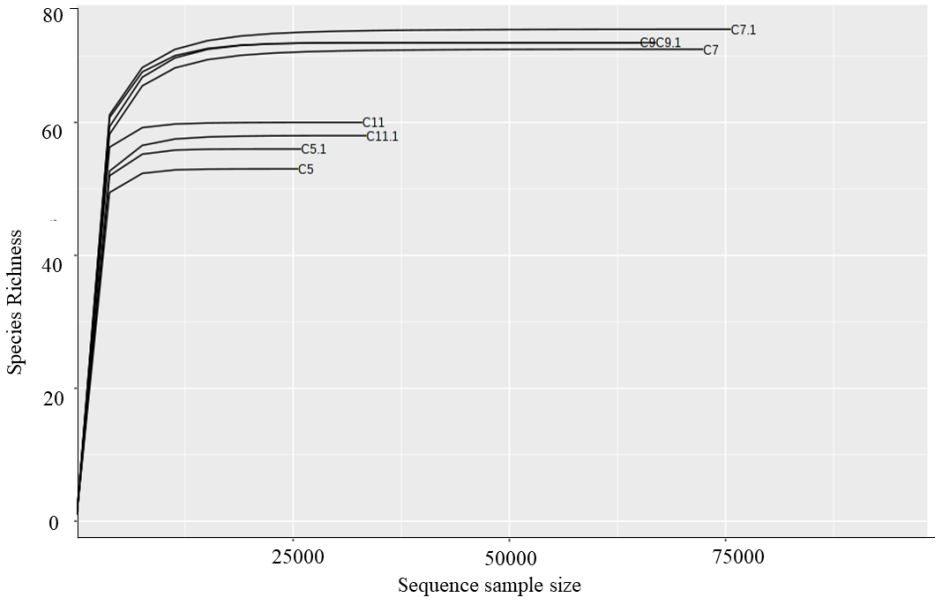

Figure. D10. Refraction curve, C5 and C5-1 (control group; untreated soil and it's replicate), C7 and C7-1 (treated soil with enzyme X and its replicate), C9 and C9-1 (treated soil with enzyme X/5 and its replicate) C11, C11-1 (treated soil with enzyme X/10 and its replicate).

APPENDIX E. Supplementary information of section 5.1.

Characterization of seafood waste residues:

The exact composition of seafood wastes varies with species (shells of shrimp, crab, prawn, lobster, and krill), seasons and many other factors.

Factor	Value
moisture content	~40%
mineral content	41-50%
protein content	35-40%

Determination of diffusion effects in immobilized enzymes

Table E1. List of the calculated k_p and k_r values for toluene using Eq.(9) and (10)

Constants	Value
D_o	8.6×10^{-6}
ε	0.65
λ	0.03
$k_p\,(\lambda)$	0.941
$k_r\,(\lambda)$	0.888
D_e	4.6×10^{-6}

Phylogenetic analysis of isolated strain

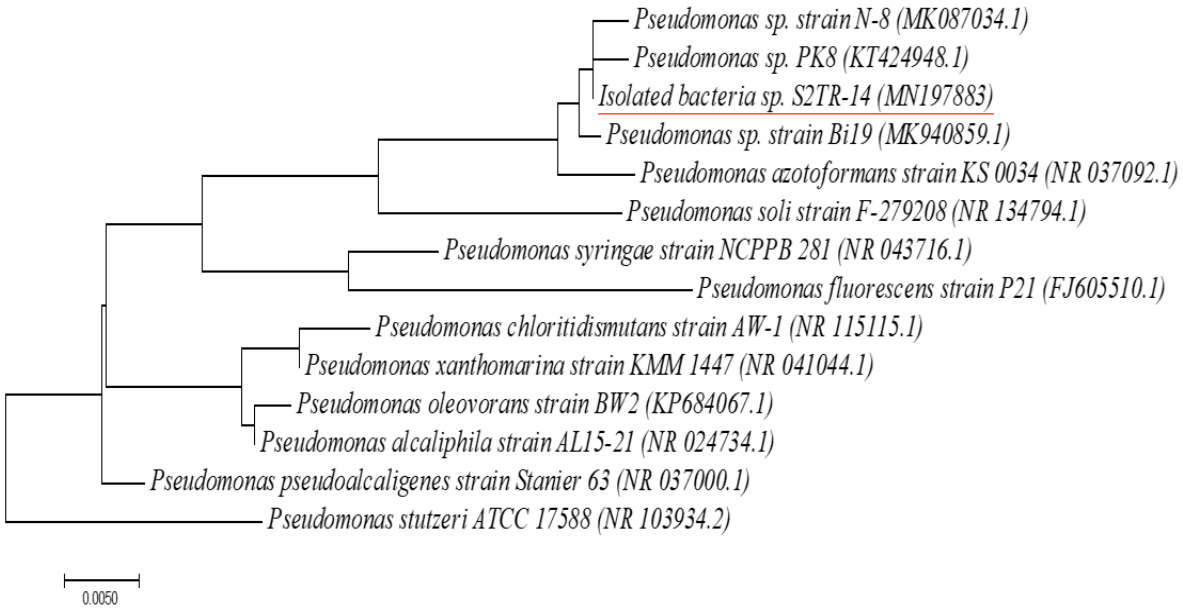

Fig. E1. Neighbor-joining phylogenetic tree of S2TR-14 and some members of the genus *Pseudomonas* based on their 16S rRNA sequence**.** GeneBank accession numbers for the 16S rRNA sequence are shown in the parentheses.

leaching of proteins from for micro and nano biochar-chitosan matrices

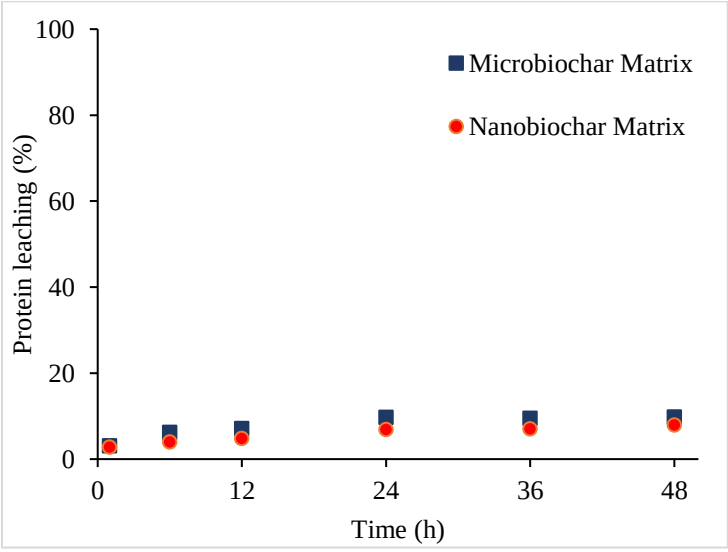

Fig. E2. Percentage protein leaching along the time for micro and nano biochar-chitosan matrices

BTEX biodegradation of contaminated groundwater sample (48h)

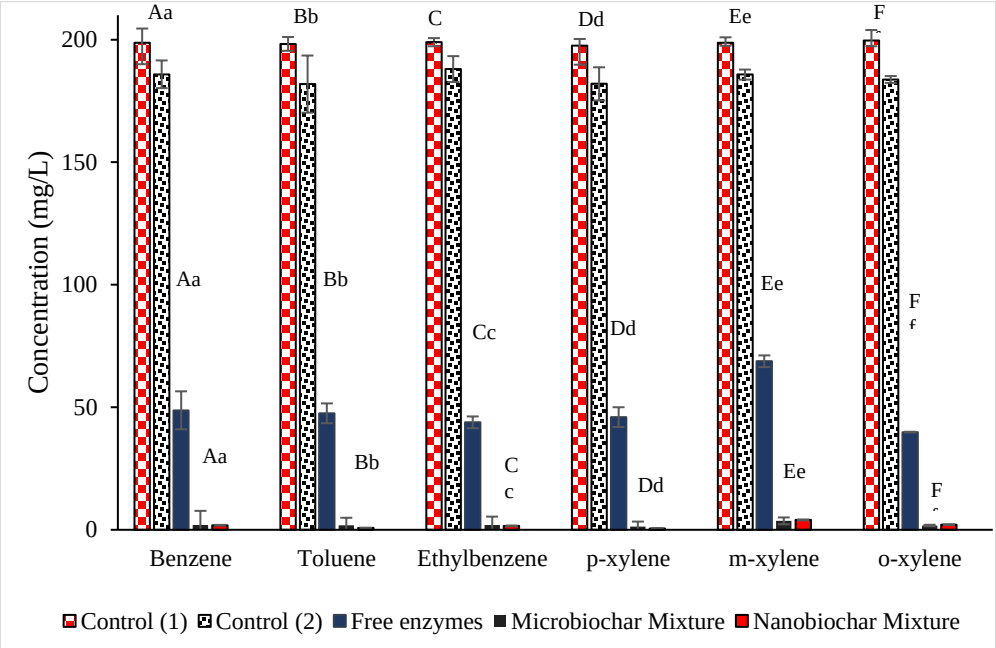

Fig. E3. Biodegradation of BTEX by free and immobilized enzymes on micro and nano biochar-chitosan matrices after 48h incubation, control (1) samples contained groundwater and BTEX without the addition of any enzymes and matrices, the control (2) samples contained groundwater and BTEX with deactivated enzymes immobilized on biochar-chitosan matrices. Capital letters (A-F) indicated the significant difference between the control samples and test samples. Small letters (a-f) indicated the significant difference between the free enzyme sample and immobilized enzymes. The difference of control samples (1 and 2) was not significant and the control (2) sample was used as a control group for comparison with test groups in statistical tests. For Microbiochar and Nanobiochar that were not statistically significant, the letters were not shown. The significance level was 0.05.

APPENDIX F. Supplementary information of section 5.2.

Table F1. Important factors and associated levels for the Box-Behnken design of experiment.

Factors	Levels		
	-1	0	+1
Magnetic particle%, w/v	1	3.5	6
Chitosan %, w/v	0	3.5	6
Glutaraldehyde %, v/v	0	0.55	1
Enzyme %, v/v	1	5	12

Table F2. Proteins identified using LC-MS/MS

MW [kDa]	Best Blast Hit	# Unique Peptides	Contaminant	Protein FDR Confidence	% Coverage
35.1	Extradiol ring-cleavage dioxygenase	5	FALSE	High	31
41.5	Toluene o-xylene monooxygenase oxygenase subunit TouA	6	FALSE	High	35
18.4	Bacterioferritin	4	FALSE	High	16
6.8	Translational regulator CsrA	2	FALSE	High	11
8.5	Acyl carrier protein	1	FALSE	High	9
25.8	Phosphoglycerate kinase	2	FALSE	High	8
40.1	Chaperone protein DnaJ	1	FALSE	High	8
65.9	Copper resistance protein A	2	FALSE	Medium	7
22	50S ribosomal protein L3	1	FALSE	High	6
24.2	50S ribosomal protein L1	1	FALSE	High	6
21.8	Alkyl hydroperoxide reductase C	1	FALSE	High	6
50	ATP synthase subunit beta	3	FALSE	High	5
43.2	Elongation factor Tu	2	FALSE	High	5
40.7	Phosphoglycerate kinase	3	FALSE	High	5

77.3	Elongation factor G	2	FALSE	High	5
20.6	Alkyl hydroperoxide reductase C	1	FALSE	High	25
28.2	30S ribosomal protein S2	1	FALSE	High	14
20	50S ribosomal protein L5	2	FALSE	Medium	4
155.4	DNA-directed RNA polymerase subunit beta'	4	FALSE	High	24
39.2	Aminomethyltransferase	1	FALSE	Medium	3
47.6	Citrate synthase	2	FALSE	High	3
48.9	Uncharacterized protein	1	FALSE	Medium	3
71.9	Transketolase	2	FALSE	High	3
57.8	60 kDa chaperonin	2	FALSE	High	3
45.7	Isocitrate dehydrogenase [NADP]	2	FALSE	High	3
96	Chaperone protein ClpB	2	FALSE	High	13
47	Transcription termination factor Rho	2	FALSE	High	2
75.3	Polyribonucleotide nucleotidyltransferase	3	FALSE	High	2
44.9	Serine hydroxymethyltransferase	2	FALSE	High	2
37.3	DNA-directed RNA polymerase subunit alpha	2	FALSE	High	2
62.1	30S ribosomal protein S1	1	FALSE	High	2
48.9	Biotin carboxylase	1	FALSE	High	2
68.7	Chaperone protein DnaK	1	FALSE	High	11
103.4	Aconitate hydratase	1	FALSE	High	1
154.5	DNA-directed RNA polymerase subunit beta	1	FALSE	High	1
102.9	Protein translocase subunit SecA	1	FALSE	High	1
18.4	Bacterioferritin	4	FALSE	High	16
6.8	Translational regulator CsrA	1	Contaminant	High	11
8.5	Acyl carrier protein	1	FALSE	High	29
25.8	30S ribosomal protein S3	2	FALSE	High	8
40.1	Chaperone protein DnaJ	1	FALSE	High	8
65.9	Copper resistance protein A	1	FALSE	Medium	7
22	50S ribosomal protein L3	2	FALSE	High	6
24.2	50S ribosomal protein L1	1	FALSE	High	6
21.8	Alkyl hydroperoxide reductase C	1	FALSE	High	16
50	ATP synthase subunit beta	3	FALSE	High	25

43.2	Elongation factor Tu	2	FALSE	High	15
40.7	Phosphoglycerate kinase	3	FALSE	High	5
77.3	Elongation factor G	2	FALSE	High	5

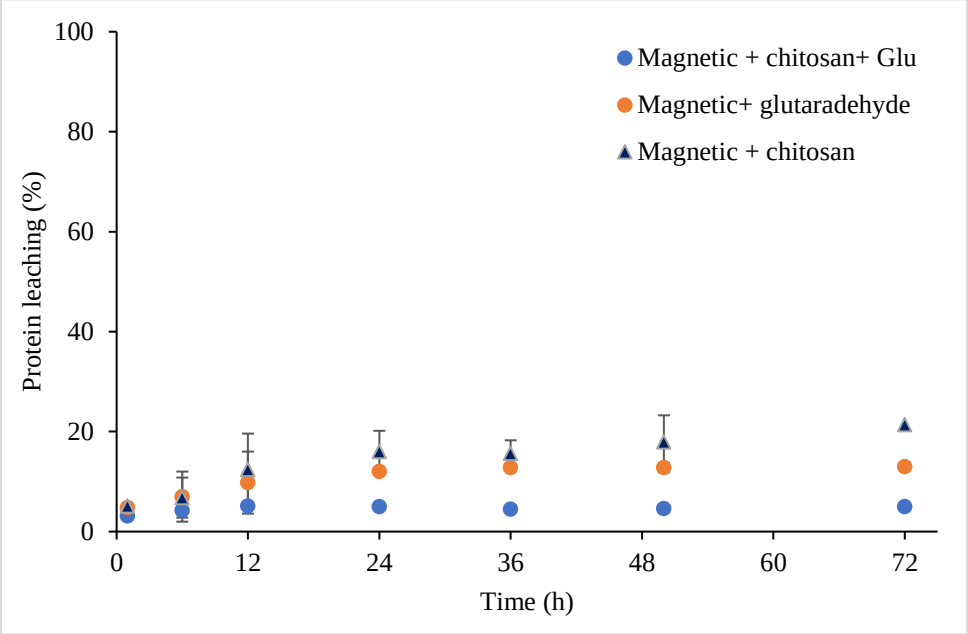

Fig. F2. Percentage protein leaching along the time for immobilized enzymes on Magnetic particles with/without chitosan and glutaraldehyde

Table F3. Experimental response on the effect of four parameters, such as magnetic particles, chitosan, glutaraldehyde, and enzyme concentrations on immobilization yield

RunOrder	Magnetic particles	Chitosan	Glutaraldehyde	Enzyme	immobilization yield
1	3.5	3.5	1.00	1.0	29.8750
2	3.5	1.0	0.55	10.0	79.2950
3	1.0	3.5	0.55	10.0	68.7800
4	3.5	1.0	0.55	1.0	25.7750
5	6.0	3.5	0.55	10.0	76.9300
6	1.0	3.5	0.55	1.0	11.8900
7	3.5	6.0	0.10	5.5	31.2600
8	3.5	3.5	0.10	1.0	11.1550
9	3.5	6.0	1.00	5.5	35.5200
10	1.0	1.0	0.55	5.5	63.1050
11	3.5	6.0	0.55	1.0	11.1050
12	1.0	3.5	0.10	5.5	28.9050
13	3.5	3.5	0.10	10.0	77.7700

14	3.5	3.5	0.55	5.5	51.4000
15	6.0	3.5	0.55	1.0	24.6250
16	6.0	3.5	0.10	5.5	50.3150
17	3.5	3.5	0.55	5.5	54.5150
18	3.5	1.0	1.00	5.5	43.9900
19	1.0	3.5	1.00	5.5	40.2150
20	3.5	6.0	0.55	10.0	48.7150
21	6.0	3.5	1.00	5.5	44.9350
22	6.0	6.0	0.55	5.5	61.6950
23	1.0	6.0	0.55	5.5	14.0950
24	3.5	1.0	0.10	5.5	85.9950
25	3.5	3.5	1.00	10.0	67.4050
26	3.5	3.5	0.55	5.5	53.1800
27	6.0	1.0	0.55	5.5	49.2400
28	2.0	2.0	0.50	10.0	91.8750
29	2.0	0.0	1.00	10.0	59.2950
30	2.0	2.0	0.00	10.0	68.7800
31	2.0	0.0	0.00	10.0	55.7750
32	2.0	0.0	0.00	5.0	66.9300
33	2.0	0.5	0.10	12.0	59.1500
34	2.0	1.0	0.05	10.0	61.5448